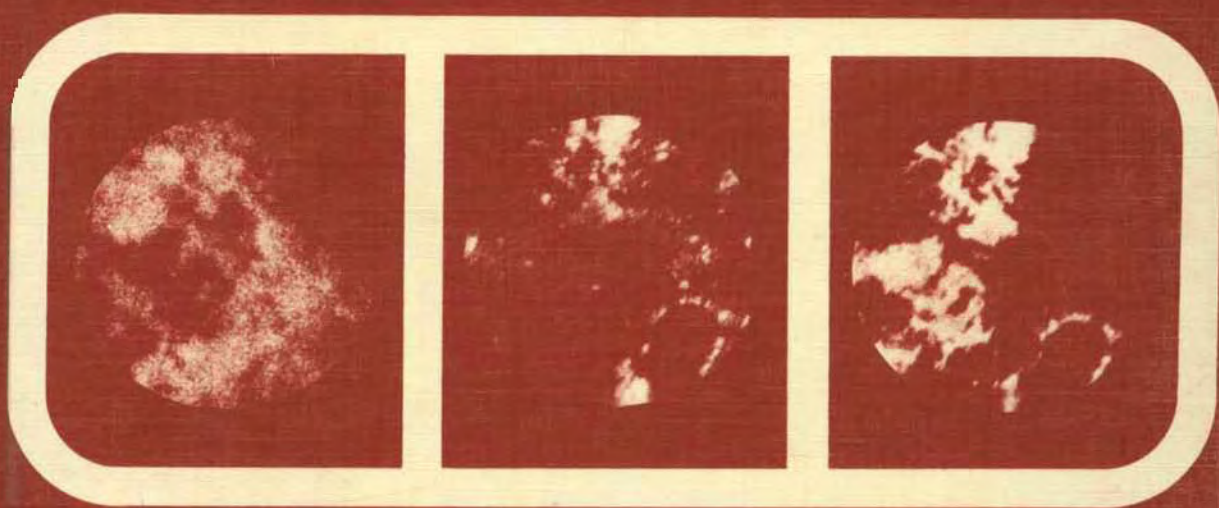


E.B.A. BISDOM AND J. DUCLOUX
(EDITORS)

SUBMICROSCOPIC STUDIES OF SOILS



DEVELOPMENTS IN SOIL SCIENCE 12

Developments in Soil Science 12

SUBMICROSCOPIC STUDIES OF SOILS

Further Titles in this Series

1. I. VALETON
BAUXITES

2. IAHR
FUNDAMENTALS OF TRANSPORT PHENOMENA
IN POROUS MEDIA

3. F.E. ALLISON
SOIL ORGANIC MATTER AND ITS ROLE IN
CROP PRODUCTION

4. R.W. SIMONSON (Editor)
NON-AGRICULTURAL APPLICATIONS OF SOIL SURVEYS

5A. G.H. BOLT and M.G.M. BRUGGENWERT (Editors)
SOIL CHEMISTRY. A. BASIC ELEMENTS

5B. G.H. BOLT (Editor)
SOIL CHEMISTRY. B. PHYSICO-CHEMICAL MODELS

6. H.E. DREGNE
SOILS OF ARID REGIONS

7. H. AUBERT and M. PINTA
TRACE ELEMENTS IN SOILS

8. M. SCHNITZER and S.U. KHAN
SOIL ORGANIC MATTER

9. B.K.G. THENG
FORMATION AND PROPERTIES OF CLAY-POLYMER COMPLEXES

10. D. ZACHAR
SOIL EROSION

11A. L.P. WILDING, N.E. SMECK and G.F. HALL (Editors)
PEDOGENESIS AND SOIL TAXONOMY. I. CONCEPTS AND
INTERACTIONS

Developments in Soil Science 12

SUBMICROSCOPIC STUDIES OF SOILS

EDITED BY

E.B.A. BISDOM

Netherlands Soil Survey Institute, Wageningen, The Netherlands

and

J. DUCLOUX

Université de Poitiers, Laboratoire de Pédologie, Poitiers, France

Reprinted from the journal:
Geoderma, Vol. 30, Nos. 1–4



ELSEVIER

Amsterdam—Oxford—New York—Tokyo 1983

ELSEVIER SCIENCE PUBLISHERS B.V.
1 Molenwerf
P.O. Box 211, 1000 AE Amsterdam, The Netherlands

Distributors for the United States and Canada:

ELSEVIER SCIENCE PUBLISHING COMPANY INC.
52, Vanderbilt Avenue
New York, N.Y. 10017

ISBN 0-444-42195-5 (Vol. 12)
ISBN 0-444-41882-7 (Series)

© Elsevier Science Publishers B.V., 1983

All rights reserved. No part of this publication may be reproduced, stored in a retrieval system or transmitted in any form or by any means, electronic, mechanical, photocopying, recording or otherwise, without the prior written permission of the publisher, Elsevier Science Publishers B.V., P.O. Box 330, 1000 AH Amsterdam, The Netherlands

Printed in The Netherlands

PREFACE

This special issue of *Geoderma* is the result of the work of members of the "International Working-Group on Submicroscopy of Undisturbed Soil Materials (IWGSUSM)". The papers are from the second workshop of IWGSUSM, organized in 1981 by J. Ducloux at the University of Poitiers, France; the symposium on "Submicroscopy of Undisturbed Soil Materials" organized in 1981 by M.L. Thompson in Atlanta, Georgia, U.S.A. during the annual meeting of the Soil Science Society of America, and work done in 1982. The papers mainly concern in situ electron microscopic studies of materials in thin sections of soils and of unimpregnated soil constituents in peds. Ion microscopy is discussed in one paper.

The plan to start IWGSUSM originated in 1975, but it was 1979 before E.B.A. Bisdom could write the first circular letter. By this time sufficient new submicroscopic techniques had been tested to allow detailed studies of soil constituents in thin sections. One of the problems, then and now, is however, that the costs of using electron microscopes, ion microscopes, laser microprobe mass analyzers, etc. are rather high and that the interpretation of data can be intricate. Consequently, an international organization was founded to assess the significance of projects and to start cooperative efforts. Such cooperation between specialized laboratories should facilitate the study of intricate problems. Various specialists joined IWGSUSM, i.e. soil micromorphologists, soil physicists, soil chemists, engineers in soil mechanics, geologists, geographers, biologists, etc. The first results of three cooperative research projects, i.e. on soil pollution, the characterization of organic matter in Vertisols, and the effects of the application of sewage sludge and pig slurry on surface crusts of cultivated soils are discussed.

The first workshop of IWGSUSM was organized by E.B.A. Bisdom in 1980 at the Netherlands Soil Survey Institute, Wageningen, The Netherlands. A book *Submicroscopy of Soils and Weathered Rocks* contains papers presented at this workshop plus introductory articles on techniques and instruments used in submicroscopy, and review articles which discuss in situ submicroscopic work done in soil science. The present special issue of *Geoderma*, which will also appear as a book in the series "Developments in Soil Science", gives various technical papers and practical applications of submicroscopy in soil science. Some papers discuss purely submicroscopic subjects, whereas submicroscopy is used in other papers as one of a number of techniques.

Most submicroscopic studies start by using the light microscope to investigate soil constituents in thin sections and unhardened soil peds. Such work is usually done by soil micromorphologists and specialists in, for example, soil mechanics. Soil physicists are attracted by this type of in situ work because by using the combination of light microscopy and submicroscopy it can be seen where transported soil particles have been deposited in the soil profile — especially under controlled experimental con-

ditions — and data on very fine and larger pores (voids) can be collected by using an image analyzer to study the porosity in micrographs obtained by light microscopy and electron microscopy. The soil chemist, who usually works with wet chemistry and disturbed bulk samples, is attracted by the in situ microchemical results obtained from dry samples by various submicroscopic techniques. Amorphous, poorly crystalline and clayey materials in thin sections will usually be of interest for the microanalysis of chemical elements

Submicroscopy is a young field of soil science which can help different specializations by giving various types of in situ information. IWGSUSM was an independent organization until the end of 1982 and will form part of the "Subcommission on Soil Micromorphology" of the "International Society of Soil Science" in 1983. Colleagues who are interested in the submicroscopic work of IWGSUSM can contact the secretary E.B.A. Bisdom, or the organizers of sister organizations outside Western Europe, i.e., S. Zauyah (Asia), C.B. Wells (Australia and New Zealand), M.L. Thompson (Canada and USA), T. Tursina (Eastern Europe) and J.J. de Oliveira (Latin America).

Assistance in the preparation of this volume was given by the Technical Staff of the Netherlands Soil Survey Institute.

E.B.A. Bisdom and J. Ducloux

SUBMICROSCOPIC STUDIES OF SOILS

edited by

E.B.A. BISDOM and J. DUCLOUX

Editorial Committee:

A. BOEKESTEIN, P. CURMI, C. JEANSON, C. FOX, S. LEDIN, P.J. LOVELAND,
P. SMART, G. STOOPS, M.L. THOMPSON, and C.B. WELLS

CONTENTS

Preface	V
List of abbreviations	IX

Cooperative Research Projects

Submicroscopy and chemistry of heavy-metal-contaminated precipitates from column experiments simulating conditions in a soil beneath a landfill E.B.A. Bisdom, A. Boekestein (Wageningen, The Netherlands), P. Curmi (Rennes, France), P. Lagas (Leidschendam, The Netherlands), A.C. Letsch (Petten, The Netherlands), J.P.G. Loch (Leidschendam, The Netherlands), R. Nauta (Eindhoven, The Netherlands) and C.B. Wells (Glen Osmond, S.A., Australia)	1
Characterization of in situ organic matter constituents in vertisols from Argentina, using submicroscopic and cytochemical methods — First report S. Stephan (Bonn, F.R. Germany), J. Berrier (Versailles, France), A.A. De Petre (Tezanos Pinto, E.R., Argentina), C. Jeanson (Brunoy, France), M.J. Kooistra (Wageningen, The Netherlands), H.W. Scharpenseel and H. Schiffmann (Hamburg, F.R. Germany)	21
Changes in surface structure (crusting) after application of sewage sludge and pig slurry to cultivated agricultural soils in northern Italy M. Pagliai (Pisa, Italy), E.B.A. Bisdom (Wageningen, The Netherlands) and S. Ledin (Uppsala, Sweden)	35

Submicroscopic Techniques

Etched thin sections for coupled optical and electron microscopy and micro- analysis L.D. Norton, J.M. Bigham, G.F. Hall, and N.E. Smeck (Columbus, Ohio, U.S.A.)	55
Microradiography as a submicroscopic tool L.R. Drees and L.P. Wilding (College Station, Texas, U.S.A.)	65
STEM-EDXRA and SEM-EDXRA investigation of iron-coated organic matter in thin sections with transmitted, secondary and backscattered electrons E.B.A. Bisdom (Wageningen, The Netherlands), R. Nauta and B. Volbert (Eindhoven, The Netherlands)	77
Variations in backscattered electron(BSE) images with a Scanning Electron Microscope(SEM) as applied to mineral grains and excrements in a podzol, to precipitates on a water-tube filter and to bauxite E.B.A. Bisdom, F. Thiel (Wageningen, The Netherlands), B. Volbert and J. Jackman (Eindhoven, The Netherlands)	93
Quantitative analysis of trace and major elements in thin sections of soils with the secondary ion microscope(Cameca) E.B.A. Bisdom, S. Henstra (Wageningen, The Netherlands), H.W. Werner, P.R. Boudewijn, W.F. Knippenberg, H.A.M. de Grefte (Eindhoven, The Netherlands), J.M. Gourgout and H.N. Migeon (Courbevoie, France)	117

Applied Submicroscopy

Effect of potassium on soil structure in relation to hydraulic conductivity Y. Chen, A. Banin and A. Borochovit (Rehovot, Israel)	135
Lightmicroscope and submicroscope observations of salts in marine alluvium (India) M.J. Kooistra (Wageningen, The Netherlands)	149
An optical, scanning electron microscopic and microanalytical study of cementation in some podzols W.J. McHardy and L. Robertson (Aberdeen, Great Britain)	161
Calcium-dominated organans in Humic Podzols from the Hudson and James Bay Lowlands of Ontario, Canada R. Protz (Guelph, Ontario, Canada)	171
SEM and light microscopic observations of minerals in bog-ores of the Belgian Campine G. Stoops (Gent, Belgium)	179
Submicroscopic characterisation of phosphatic and sesquioxidic nodules of some soils of the "Chaco Deprimido" (Argentina): preliminary results H.J.M. Morrás (Castelar, Argentina)	187
Characteristics and significance of composite particles derived from a Colombian andosol profile P.A. Riezebos and W.J. Lustenhouwer (Amsterdam, The Netherlands).	195
SEM-EDXRA investigation of tubular features and iron nodules in lateritic soils from Malaysia S. Zaayah (Serdang, Selangor, Malaysia) and E.B.A. Bisdom (Wageningen, The Netherlands).	219
Fabric sequences as related to genetic processes in two Alberta soils S. Pawluk (Edmonton, Alta., Canada)	233
Scanning electron microscopy of engineering soils K. Collins (Glasgow, Strathclyde, Great Britain)	243
SEM-EDXRA studies of precipitates which clogged a water-tube filter E.B.A. Bisdom and A. Jongerius (Wageningen, The Netherlands)	253

Applied Submicroscopy and Image Analysis

Quantimet 720 analysis of porosities in backscattered electron scanning images made with different photo-techniques D. Schoonderbeek, F. Thiel, and E.B.A. Bisdom (Wageningen, The Netherlands).	271
The characterization of microporosity in a ploughpan by submicroscopic and Quantimet techniques A. Jager, O. Boersma and E.B.A. Bisdom (Wageningen, The Netherlands).	277
The development of soil porosity in experimental sandy soils with clay admixtures as examined by Quantimet 720 from BESI and by other techniques J. Chrétien (Dijon, France) and E.B.A. Bisdom (Wageningen, The Netherlands).	285
The characterization of the shape of mineral grains in thin sections of soils by Quantimet and BESI E.B.A. Bisdom and D. Schoonderbeek (Wageningen, The Netherlands)	303
Porosity measurements and form analysis of mineral grains in thin sections from oil-gas reservoir rocks using Quantimet 720 and BESI E.B.A. Bisdom (Wageningen, The Netherlands), H.A. van Adrichem Boogaert (Haarlem, The Netherlands), G. Heintzberger, D. Schoonderbeek and F. Thiel (Wageningen, The Netherlands).	323
Subject Index	339

LIST OF ABBREVIATIONS

AES	Auger Electron Spectroscopy
BE	Backscattered Electrons
BESI	Backscattered Electron Scanning Images
BLE	Bombardment-induced Light Emission
BSE	= BE
EDAX	= EDXRA
EDS	Energy-Dispersive Spectroscopy (Spectrometer) = EDXRA
EDX	= EDXRA
EDXRA	Energy Dispersive X-ray Analysis (Analyzer)
EELS	Electron Energy-Loss Spectrometry
ELS	= EELS
EMA	Electron Microprobe Analysis (Analyzer) = EPMA
EMP	Electron Microprobe analysis, i.e. EDXRA(EDX) and WDXRA (WDX)
EPMA	Electron Probe Micro-Analysis(Analyzer) = EMA
ESCA	Electron Spectroscopy for Chemical Analysis
HEIS	High Energy Ion Scattering = RBS
IMMA	Ion Microprobe Mass Analysis (Analyzer)
ISS	Ion Scattering Spectrometry = LEIS
LAMMA	Laser Microprobe Mass Analysis (Analyzer) = LMP
LEIS	Low Energy Ion Scattering = ISS
LMP	Laser Microprobe analysis = LAMMA
LOES	Laser Optical Emission Spectrometry
LTA	Low Temperature Ashing
MFD	Multi-Function-Detector
OES	Optical Emission Spectrometry
OTM	Optical Transmission Microscopy
PIXE	Particle Induced X-ray Emission
RBS	Rutherford Backscattering Spectrometry = HEIS
SAM	Scanning Auger Microprobe
SE	Secondary Electrons
SEI	Secondary Electron Images
SEM	Scanning Electron Microscope (Microscopy)
SIMS	Secondary Ion Mass Spectrometry (Spectrometer)
SSMS	Spark Source Mass Spectrometry
STEM	Scanning Transmission Electron Microscope (Microscopy)
TEELS	Transmission Electron Energy Loss Spectrometry
TEM	Transmission Electron Microscope (Microscopy)
WDS	Wavelength Dispersive Spectroscopy = WDXRA
WDX	= WDXRA
WDXRA	Wavelength Dispersive X-ray Analysis (Analyzer)
XPS	X-ray Photoelectron Spectroscopy
XRD	X-Ray Diffraction
XRF	X-Ray Fluorescence spectrometry

This Page Intentionally Left Blank

COOPERATIVE RESEARCH PROJECTS

This Page Intentionally Left Blank

SUBMICROSCOPY AND CHEMISTRY OF HEAVY-METAL-CONTAMINATED PRECIPITATES FROM COLUMN EXPERIMENTS SIMULATING CONDITIONS IN A SOIL BENEATH A LANDFILL

E.B.A. BISDOM¹, A. BOEKESTEIN², P. CURMI³, P. LAGAS⁴, A.C. LETSCH⁵, J.P.G. LOCH⁶, R. NAUTA⁶ and C.B. WELLS⁷

¹ *Netherlands Soil Survey Institute, P.O. Box 98, 6700 AB Wageningen (The Netherlands)*

² *Technical and Physical Engineering Research Service, 6700 AJ Wageningen (The Netherlands)*

³ *INRA, Laboratoire de Science du Sol, 65 Route de St Brieuc, 35042 Rennes, Cedex (France)*

⁴ *National Institute for Water Supply, 2060 AD Leidschendam (The Netherlands)*

⁵ *Energy Research Foundation, 1755 ZG Petten (The Netherlands)*

⁶ *Philips, Application Laboratory-Electron Optics, Industrial Equipment Division, Building TQ 111-p, Eindhoven (The Netherlands)*

⁷ *CSIRO, Private Bag No. 2, Post Office, Glen Osmond, S.A. 5064 (Australia)*

(Accepted for publication February 17, 1983)

ABSTRACT

Bisdom, E.B.A., Boekestein, A., Curmi, P., Lagas, P., Letsch, A.C., Loch, J.P.G., Nauta, R. and Wells, C.B., 1983. Submicroscopy and chemistry of heavy-metal-contaminated precipitates from column experiments simulating conditions in a soil beneath a landfill. *Geoderma*, 30: 1–20.

The first results of a cooperative research project of IWGSUSM (International Working-Group on Submicroscopy of Undisturbed Soil Materials) are discussed. Wet chemistry of heavy metals which precipitated during column experiments, simulating conditions in a soil beneath a landfill, was studied. To compare these data of bulk chemistry with in situ microchemistry of the same heavy metals, thin sections were made. Using the normal technique of impregnation, problems are encountered in the hardening process. However, if gamma radiation is used, an absorbed dose of 5Mrad (50 kGy) was sufficient to harden the polyester resin.

The first thin sections of the upper 30 cm of a sandy column have now been studied with SEM-EDXRA (scanning electron microscope—energy dispersive X-ray analysis) and initial quantification was tried out using EMA (electron microprobe analysis) and SEM-WDXRA (scanning electron microscope—wavelength dispersive X-ray analysis). The first results demonstrate that the heavy-metal-containing cutans (coatings on the walls of voids and on the surfaces of mineral grains) are brown and black when studied with the light microscope. The brown ones contain the smallest amounts of heavy metals and the black ones the largest amounts. Coatings of polluted precipitate are usually only present on part of the larger mineral grains; they can be concentrated in small bands, whereby smaller grains are often completely coated, or occur isolated on the surface of a small number of grains. Brown cutans also often contain fragments of black cutans. The distribution of Fe, Ni, Cu, Zn and Pb is extremely heterogeneous. Often this heterogeneity is already present in measurements of precipitates on the surface of one mineral. This indicates a

rather extreme variety in composition of the pollutants, even on a microscale, and emphasises that submicroscopic techniques are certainly necessary to obtain detailed in situ information. The use of a step by step approach and the acquisition of numerous data should eventually allow a good understanding of the processes at work. STEM (scanning transmission electron microscope) — EDXRA measurements at magnifications larger than $\times 10,000$ are of considerable help.

INTRODUCTION

The National Institute for Water Supply of the Netherlands has done research, using laboratory columns, on the behaviour of heavy metals beneath landfills, viz. in soil and groundwater. The study was carried out at the request of the Netherlands Ministry of Health and Environmental Protection. The results of these physicochemical investigations will eventually be used for soil protection measures. The Netherlands Soil Survey Institute sampled the columns and studied the precipitates with light microscopy and sub-microscopy in thin sections. Other organizations joined the cooperative research project at a later stage.

The first steps to quantify the polluted precipitates in thin sections, were done with SEM-EDXRA. Subsequently, EMA (electron microprobe analysis) and SEM-WDXRA (scanning electron microscopy — wavelength dispersive X-ray analysis) were carried out using virtually the same material in different thin sections prepared from the same sample. To obtain analyses at magnifications larger than $\times 10,000$, STEM-EDXRA (scanning transmission electron microscopy — energy dispersive X-ray analysis) was done. Such very high magnifications are important because SEM-EDXRA (scanning electron microscopy — energy dispersive X-ray analysis) has a maximum magnification of $\times 10,000$ (Bisdorf et al., 1975, 1976).

The present samples were taken from the upper 30 cm of one of three experimental columns, viz. a column filled with calcareous dune sand. Hardening of the samples raised considerable problems, presumably because of similar heavy metals in pollutant and catalyst used for the hardening of the plastic. At present a new method has been introduced at the Netherlands Soil Survey Institute which allows the hardening of the samples using gamma radiation (cf. below).

This paper must be regarded as a first approximation showing an in situ picture of an intricate problem which can only be solved by combining knowledge and techniques of various disciplines. A great deal of attention has been given here to the results of column experiments which simulate conditions in a soil beneath a landfill (Loch et al., 1981; Lagas and Loch, 1981). Mathematical models (Van Eijkeren and Loch, 1981) are being developed to describe the transport of polluted materials in soils.

The column experiments were initiated to test the results of earlier research of the landfill Ambt-Delden in the Province of Overijssel, The Netherlands. Wet chemistry had demonstrated that the presence of fatty acids in

leachates from the landfill affected the behaviour of heavy metals. Consequently, column experiments were set up in which leachates were applied both with and without fatty acids but always with the heavy metals iron, nickel, copper, zinc and lead. Various interesting results were obtained with the experimental approach which lasted seven months. Control of the experiments was enhanced by periodic sampling and analysis of the soil solution at several depths in the columns.

MATERIALS AND METHODS

Experimental set-up

Experimental columns were made of grey polythene with a length of 140 cm and a diameter of 18 cm (Fig. 1). Five tap-points were made in the wall of a column at 20 cm intervals (Lagas and Loch, 1981). A perforated polythene tube of 18 cm length penetrated from each tap point into the column. These perforated tubes were positioned alternatively perpendicular to each other. The percolation rate was 1.6 cm day^{-1} (Loch et al., 1981).

A total of 3 columns were percolated with this leachate, viz. the column with calcareous dune sand, one with the same sand and dispersed fine clay, and the third with sand and clay aggregates. The clay aggregates had a dia-

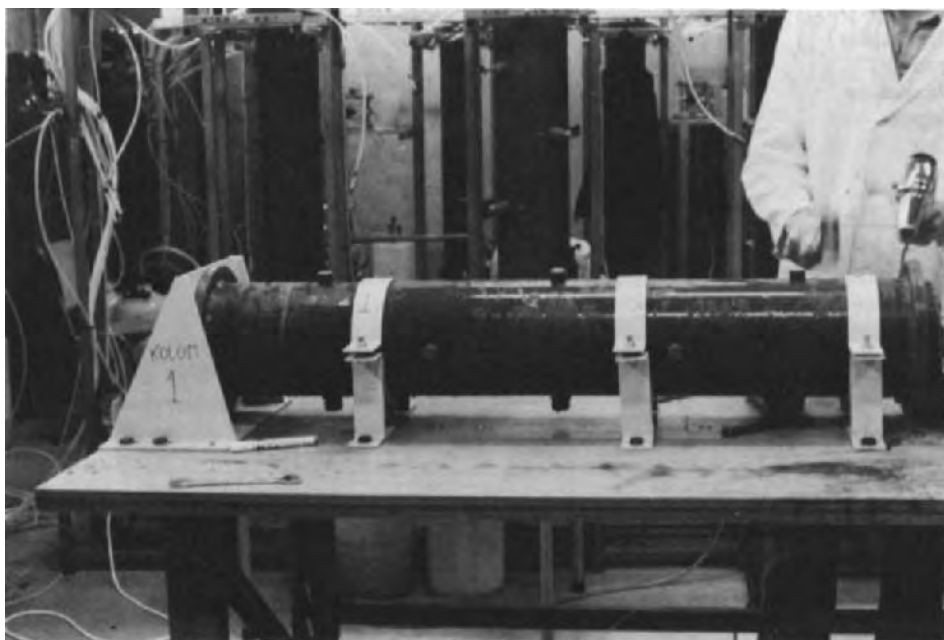


Fig. 1. Experimental column 1 with calcareous sandy material and polluted precipitates. Five tap-points and the position of the associated polythene tubes, which cross the polythene column at 90° to each other, are discernable.

meter of 2 to 4 cm. The sand/clay ratio of the columns with clay was 10 : 1. The column from which the present thin sections were derived was treated with synthetic landfill leachate without fatty acids.

Composition of the input solution

The leachates applied to the columns are similar to the actual leachate at the Ambt-Delden landfill. In these experiments the methanogenic phase in a landfill (cf. Hoeks, 1978) was simulated by using leachates without fatty acids, containing the same heavy metals as the Ambt-Delden leachate (Lagas and Loch, 1981; Loch et al., 1981). This leachate was synthesized and its composition is indicated in Table I.

TABLE I

Composition of the input solution used in the experiments (g/l)

Ascorbic acid	1.8
Chloride	9.2
Sulphate	2.0
Total carbonate	0.18
Sodium	1.6
Potassium	0.8
Ammonium	0.7
Calcium	1.6
Magnesium	0.49
Iron	1.40
Manganese	0.055
Copper	0.064
Zinc	0.065
Lead	0.208
Nickel	0.059

During the experiment ascorbic acid was added as a redox buffer in order to keep the redox potential of the solution low. The pH of the pore water was 5.7 during the experiment and a redox potential of 150 mV could be maintained. The concentrations of Fe, Zn and Mn in the input solution were substantially higher. This high concentration of heavy metals was chosen to allow a comparison of the behaviour of the metals and to obtain measurable concentrations in the percolate.

The reasoning for synthesizing a percolate with this composition was mainly to obtain a known and constant composition of the leachate in the laboratory. Percolate from the field was not acceptable because production and composition of percolate in a landfill is not constant.

Analysis of percolates and solid materials

The procedure used for the chemical analysis of soil solution (percolate) and the results have been described by Lagas and Loch (1981). Percolation

was terminated after seven months. The soil material in the columns was drained to field capacity and subsequently frozen. The sampling for chemical analysis of the solid materials was done every 5 cm. Sand and clay aggregates were sampled separately. Separate samples were also taken for XRD analysis.

Soluble salts and exchangeable adsorbed cations of the solid materials were extracted with a 0.5 M BaCl₂-solution (Loch et al., 1981). Subsequently, the precipitated and strongly adsorbed forms of the metals and other cations were extracted with 0.1 N HCl. Metal concentrations in the extracts were determined by atomic absorption spectroscopy.

The preparation of thin sections and the use of gamma radiation to harden the polyester resin

Plastic impregnated samples, taken from the column with calcareous dune sand (Figs. 2 and 3) and other types, raised considerable problems or were impossible to harden with the method described by Jongerius and Heintzberger (1975); a procedure commonly used for the preparation of thin sections of soils. Recent experiments with gamma radiation at the Netherlands Soil Survey Institute to harden the present samples, proved that this could be done in two days if the absorbed dose was 5 Mrad (50 kGy) or more.

The gamma radiation is obtained from a plate-shaped source in which a number of bars with Cobalt-60 are placed in a rack. Each bar is able to provide 1,000 Curies ($37 \cdot 10^{12}$ Bq) or more, depending on the type of installa-

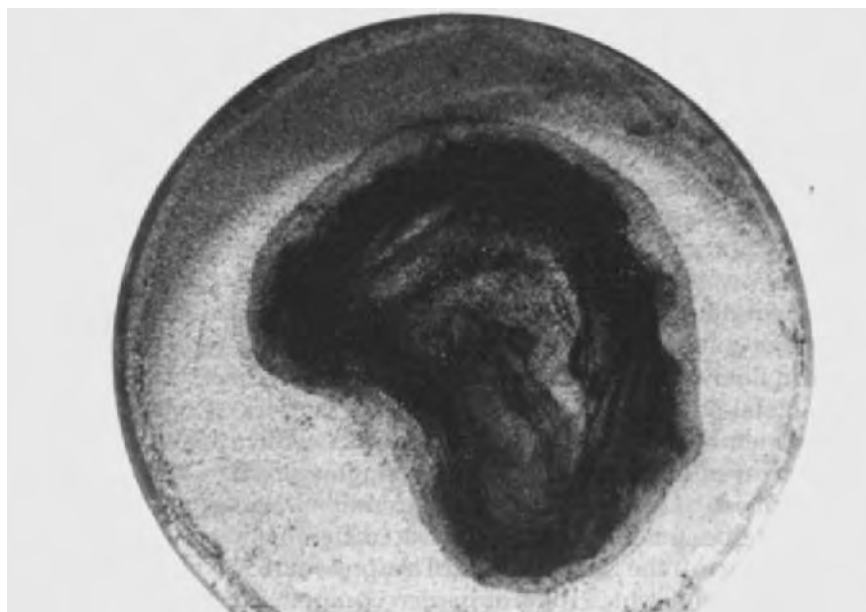


Fig. 2. Rings of predominantly black polluted precipitate just after defrosting of the column.

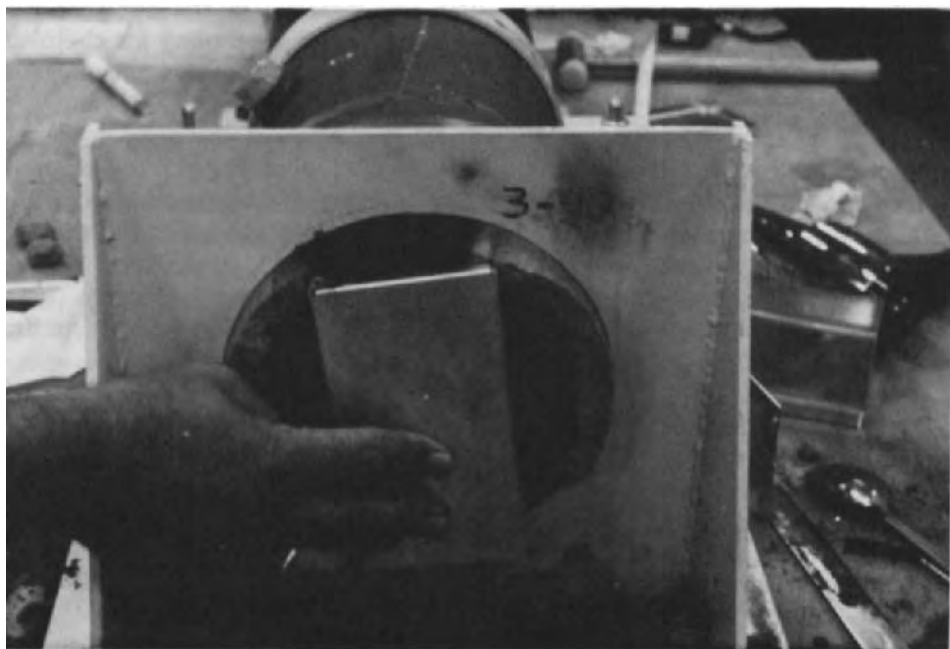


Fig. 3. A $15 \times 8 \times 5$ cm metal sample box was used for sampling the tube which had a diameter of 18 cm. The box penetrated 5 cm into the polluted sand and will allow the preparation of a thin section with 15 cm length and 8 cm width.

tion used. The best way to operate with success is to use the “train” principle whereby samples move several times past the radiation source with intermittent rest-periods of an hour or more.

The gamma irradiation method was also used for samples of the Netherlands Soil Survey Institute and of the International Soil Museum which had not hardened in the past. Most of the samples hardened sufficiently for the preparation of thin sections. Further tests should be made, however, to obtain detailed knowledge on possibilities to harden various types of soil samples using plastics and gamma radiation. Samples from which the monostyrene or acetone diluter of the polyester resin have been removed, can thus be hardened quickly. Such samples include those of saline and volcanic soils plus heavy metal-polluted and oil-impregnated samples. The impression is that the new method also gives harder samples in which the soil material is less easily destroyed and which carries less grinding powder. Additional tests will be performed to get an idea of the complete range of possibilities, amongst which the possibility to work at different temperatures during gamma irradiation of the soil samples. The present tests also proved that pieces of thin sections, which did not harden completely, do so upon gamma irradiation.

TRANSPORT AND RETENTION OF HEAVY METALS IN THE SOIL — RESULTS

Former results

A number of results from earlier work are of importance for the present interpretation of analytical data obtained from the column experiments. Clay minerals play a major role in the retention of heavy metals transported through a soil or experimental column. Such ions are usually present at very low concentrations when adsorption takes place on colloidal surfaces and under these conditions a very low reversibility of the process is possible because of preferential adsorption by chemical bonding (Harmsen, 1977).

Soil organic matter, especially humic and fulvic acids, can also adsorb heavy-metal cations. This adsorption and that on oxides and hydroxides of Mn, Fe and Al is of a chemical nature (Bar-Yosef et al., 1975).

The mobility of copper in soils is usually very low. Strong complexation of copper with soil humic acid has been reported (Sposito et al., 1976). If sulphides of heavy metals can form in the leachate of the landfill, they may precipitate in the underlying soil profile.

Under equilibrium conditions (Lagas and Harmsen, 1980) and when fatty acids are present in a concentration of 0.3 mol/l, heavy metals in the soil can be present in larger percentages than monovalent positively charged, uncharged and negatively charged complexes. The effect is that the precipitation and adsorption of the metals as cations is severely reduced.

Results of the column experiments

Precipitation of iron, nickel, copper, zinc and lead was demonstrated. Breakthrough curves (Lagas and Loch, 1981) indicated that copper and lead remained predominantly in the columns. Physicochemical processes are thought to be responsible for the retainment of copper and lead.

Iron, nickel and zinc percolated through the columns together with sulphate at the start of the experiment. After six to eight weeks the nickel, zinc, iron and sulphate concentrations decreased in the percolate. Apparently, sulphate-reducing bacteria triggered the precipitation of iron, nickel and zinc in the form of sulphides. There was probably not enough sulphide to precipitate all the iron as FeS. Possibly Cu and Pb were also precipitated as sulphides.

Further physicochemical information on the behaviour of metals in the columns during experiments will be discussed in a follow-up paper at the 1982 workshop of IWGSUSM in Paris. By then a great deal of the distribution of Fe, Ni, Cu, Zn, Pb and S over column one will also have been studied, together with some of the other columns using light microscopy and sub-microscopy. This distribution, measured by SEM-EDXRA-WDXRA, STEM-EDXRA and EMA, can then be compared with chemical measurements of bulk water samples and light microscopic observations.

Results of submicroscopic and light microscopic studies of precipitates

Only the upper part, viz. the top 30 cm, of one column with calcareous dune sand has so far been examined with SEM-EDXRA (Bisdom et al., 1981a, Bisdom, 1983). The middle sample, at a depth from 15 to 20 cm, was also analysed by EMA, SEM-WDXRA and STEM. The other two samples came from depths 0–5 cm and 25–30 cm.

Light microscopy

Light microscopic observations demonstrated that only very little precipitate (grain cutans, coatings) was present on the surface of the mineral grains and on the wall of pores in the upper 5 cm of the experimental column. Carbonate was hardly found in the upper 5 cm. Precipitates were abundantly present at a depth of 15–20 cm and carbonate was still virtually absent. Both polluted precipitates and separate carbonate grains were found at a depth of 25–30 cm in the column.

Detailed information on the distribution of the pollutants with depth will follow in a later paper when more samples have been hardened and prepared into thin sections. So far, light microscopy has demonstrated the presence of two types of cutans in the samples, viz. black and brown ones. The colours of the samples in the columns, immediately after sampling, were predominantly black in a reductive environment. During preparation of the samples oxidation of some of them took place. Colour changes were observed during the drying and treatment of samples, e.g. from black to green and brown.

After preparation of thin sections only brown and black cutans or mixtures of them were observed with the light microscope in pores and on the surface of mineral grains. The brown polluted material was predominantly isotropic which usually indicated poorly crystalline or amorphous materials. The black cutans remained black under crossed polarizers and no further information was obtained with transmitted light.

Bands with brown and black cutans were found in the lower two thin sections. Mixtures of the two types of cutans were frequently present between such bands. No special position of black and brown material has yet been found in mixed cutans and grain cutans. Even on the surface of one mineral grain very heterogeneous mixtures of black and brown cutanic polluted material could be found, often with diffuse boundaries. Only one light microscopic micrograph is shown (Fig. 4) of different types of cutans because they become similar in appearance when printed in black and white. To obtain additional information on the nature and composition of the precipitates, submicroscopy was used, viz. SEM-EDXRA, SEM-WDXRA, EMA and STEM-EDXRA.

SEM-EDXRA

EDXRA analysis of the brown and black cutans indicated that black cutans (Fig. 5) contained S, Fe, Ni, Cu, Zn and Pb, whereas less elements

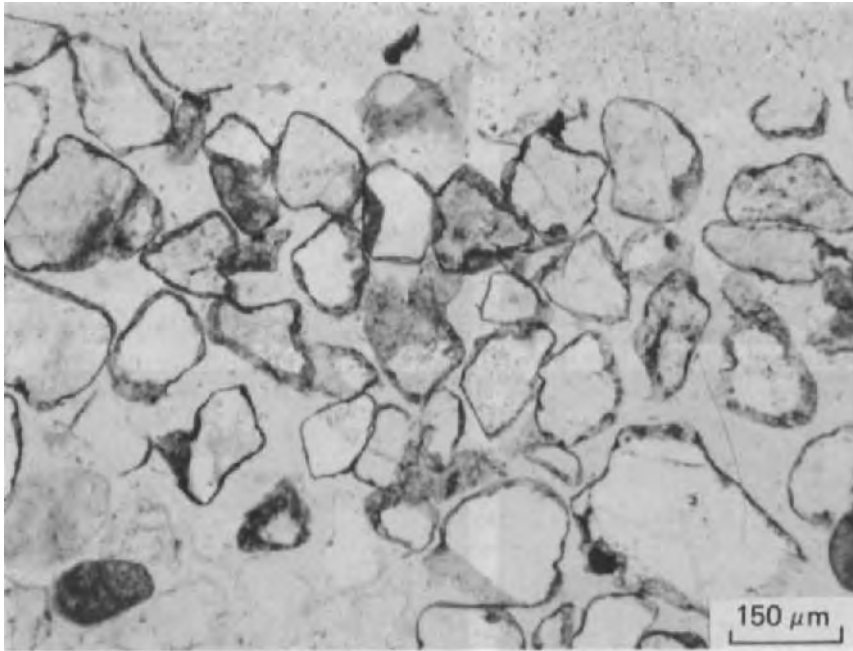


Fig. 4. Brown cutans (polluted precipitates) in pores and on the surface of mineral grains. Black cutans (coatings) and mixed brown and black cutans are similar in appearance when printed in black and white. Plane polarized light.

were found in the brown cutans, i.e. usually S, Fe and Ni (Bisdorn et al., 1981a; Bisdorn, 1983). When a mixture of brown and black cutans occurred, the number of elements increased in such precipitates. Apart from these elements Al, Si, Cl, K and Ca were also found. Al and Si are constituents of the soil and were not present in the fluids used in this experiment. Measurements of such elements in point analyses indicate therefore either a protrusion of the mineral grain at a shallow level underneath the cutan or the presence of the Al and Si in clay minerals, microcrystalline materials or amorphous substances.

Cutans having a very irregular distribution of heavy metals may show this in BESI (Bisdorn and Thiel, 1981). They usually represent mixtures of black and brown cutanic materials. Experience has shown that poorly crystalline and amorphous materials may cause problems in BESI (backscattered electron scanning images) portrayal of materials in thin sections. This is probably also the case for the predominantly brown cutanic materials which usually raise problems in BESI-portrayal. This electron microscopic behaviour would support the light microscopic analysis of isotropic amorphous brown cutanic materials in thin sections. It also indicates that BESI portrayal of mixed brown and black cutanic materials mainly concerns the black material.

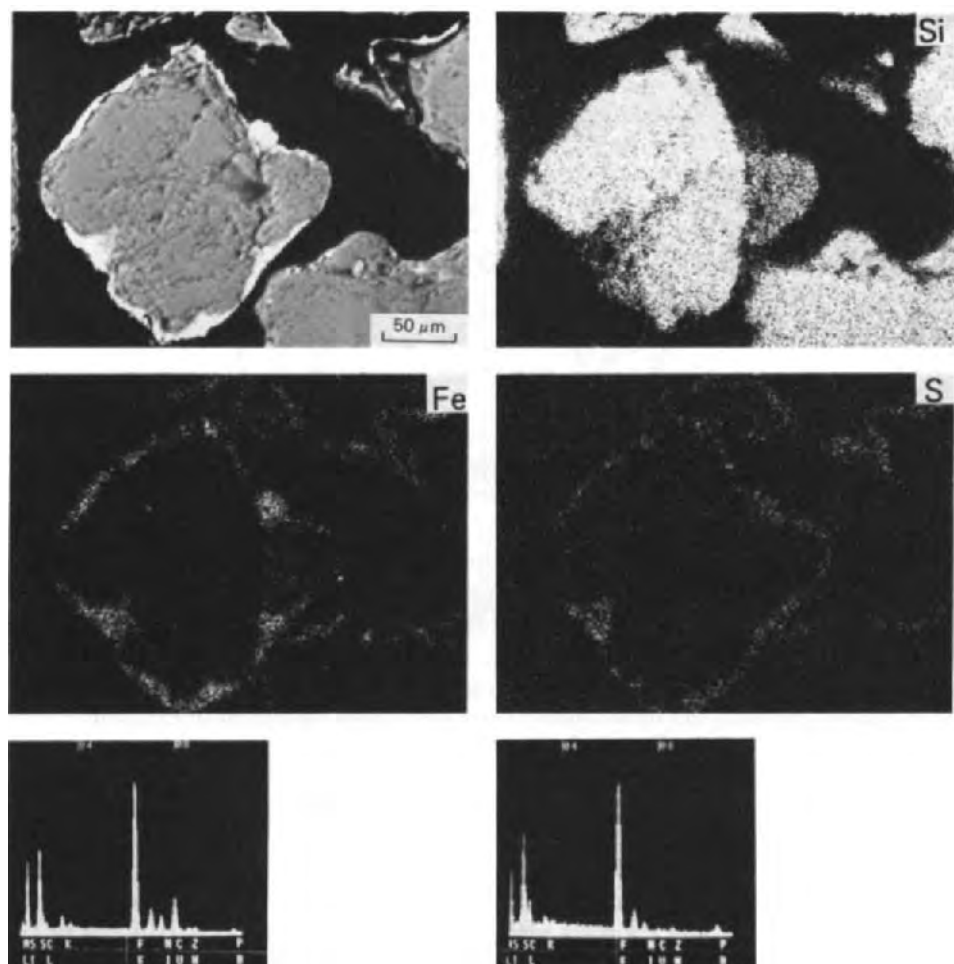


Fig. 5. SEM-EDXRA of a black heavy-metal-contaminated cutan on the surface of quartz grains and in the periphery of pores. The first image gives a backscattered electron scanning image (BESI). Concentrations of white in the three X-ray images give the distribution of Si, S and Fe in the precipitate and minerals. Point analyses indicate the presence of heavy metals such as Fe, Ni, Cu, Zn and Pb and variability of these elements in the precipitate present on one mineral grain.

A special case of the effects of pollutants from a landfill on soil components is given in Fig. 6. It is a shell fragment consisting of aragonite which shows precipitation of pollutants both on its surface and internally. Both black and brown pollutants are found in the shell in the form of discontinuous concentric rings. Absorption of the pollutants by the aragonite probably occurred along very small pores, cleavages and dislocations, because no larger microcracks were detected in the shell with BESI or with secondary electron

images (SEI). A larger number of point analyses were made in six evenly spaced traverses over the width of the shell fragment, including precipitates on the periphery of the shell fragment. They indicated that microchemical differences could exist in one concentric ring.

The adsorption of pollutants by carbonate and sometimes in the cracks of quartzes indicate that minerals may store polluted substances for longer or shorter times. This will probably be in smaller quantities than storage by clays or organic matter, but may be a factor when reclamation of polluted soils is planned.

EMA and SEM-WDXRA

Electron microprobe analysis (EMA) and scanning electron microscopy-wavelength dispersive X-ray analysis (SEM-WDXRA) were done on the thin section from 15 to 20 cm depth to obtain semi-quantitative microchemical analysis results with the help of a number of standards. No definite figures can be given here, however, because of the extreme heterogeneity which could be present in one cutan. These semi-quantitative analyses demonstrated the presence of somewhat more heavy metals than SEM-EDXRA did in the brown cutans, viz. less than one weight per cent for Ni, Cu, Zn and Pb. The Fe was present in much larger quantities than the other heavy metals in the brown cutans, viz. from 12 to 17 wt.%. The distribution of these elements and of Al, Si and S is given in the X-ray images of Fig. 7. Part of the brown cutan is vaguely recognisable around the blackish quartz grain in the absorbed electron image made with EMA (Cameca MS 46).

The black cutans comprise much more Cu (up to 15 wt.%) than the brown cutans according to some analyses. Pb can be present up to 3 wt.%, while Ni and Zn usually stay below 1 wt.%. Fe is somewhat higher than in the brown cutans, viz. up to 19 wt.%. The amount of sulphur was also higher in the black cutans than in the brown ones, but has only been measured so far with SEM-WDXRA. Only a part of the black cutan, which extends between two mineral grains which are not visible on the micrograph, is visible in black in the absorbed electron image of Fig. 8. The real width of the cutan is portrayed in the white band of the X-ray image of Fe. Apart from the heavy metals Fe, Ni, Cu, Zn and Pb, X-ray images of Si and S are also given.

To obtain microanalytical results which include the quantification of trace elements in the cutans, one should use ion microscopy (Bisdorn et al., 1977, 1983; Henstra et al., 1980, 1981). Another method, which gives no quantitative results at present but which can indicate the presence of trace elements, is laser microprobe mass analysis (Bisdorn et al., 1981b). So far, however, none of these techniques has been used in this cooperative research project.

STEM-EDXRA

The scanning transmission electron microscope—energy dispersive X-ray analyzer (STEM-EDXRA), a Philips EM 400T, was used to study microvaria-

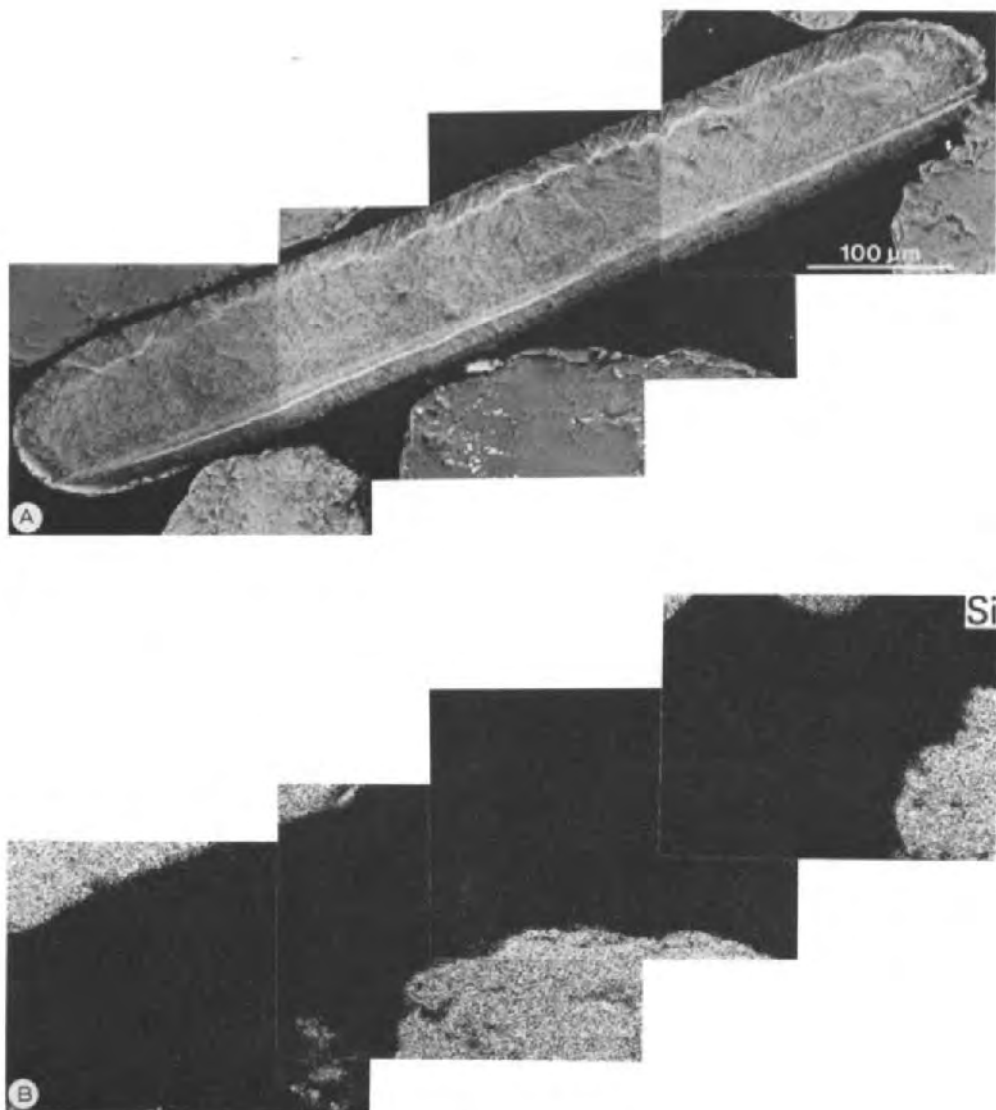
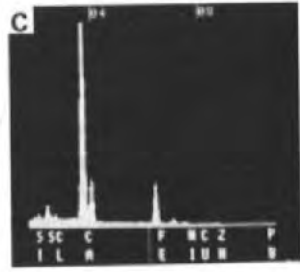
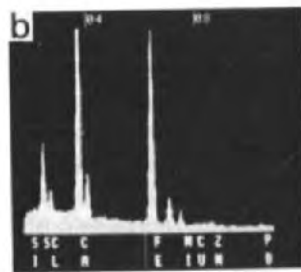
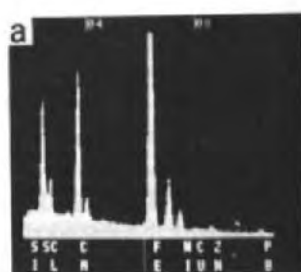
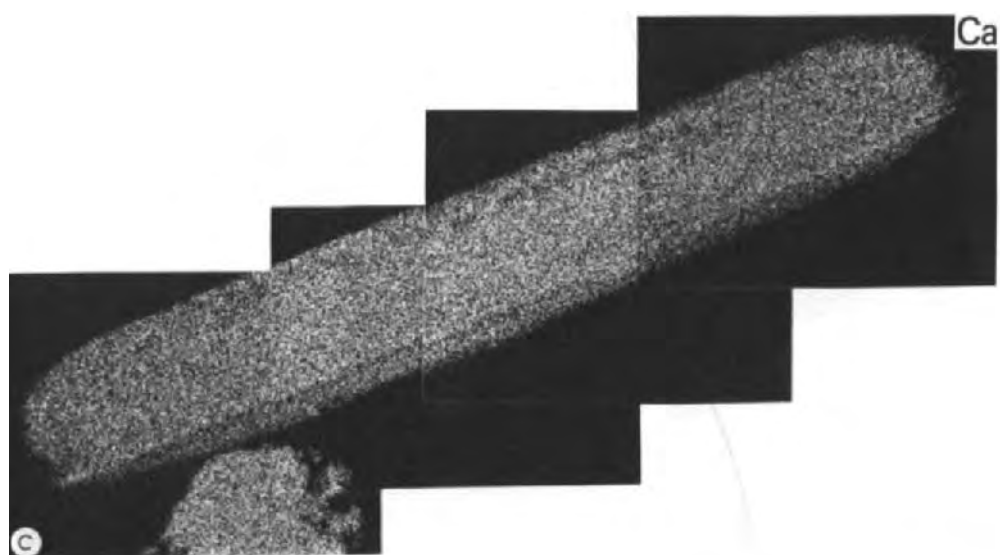


Fig. 6. BESI of shell fragment with surrounding fragments of mineral grains, the other parts of which are situated outside the micrograph. X-ray images of Si, Ca and Fe. Various point analyses to illustrate compositional differences in the discontinuous concentric bands of polluted material which invaded the shell fragment.



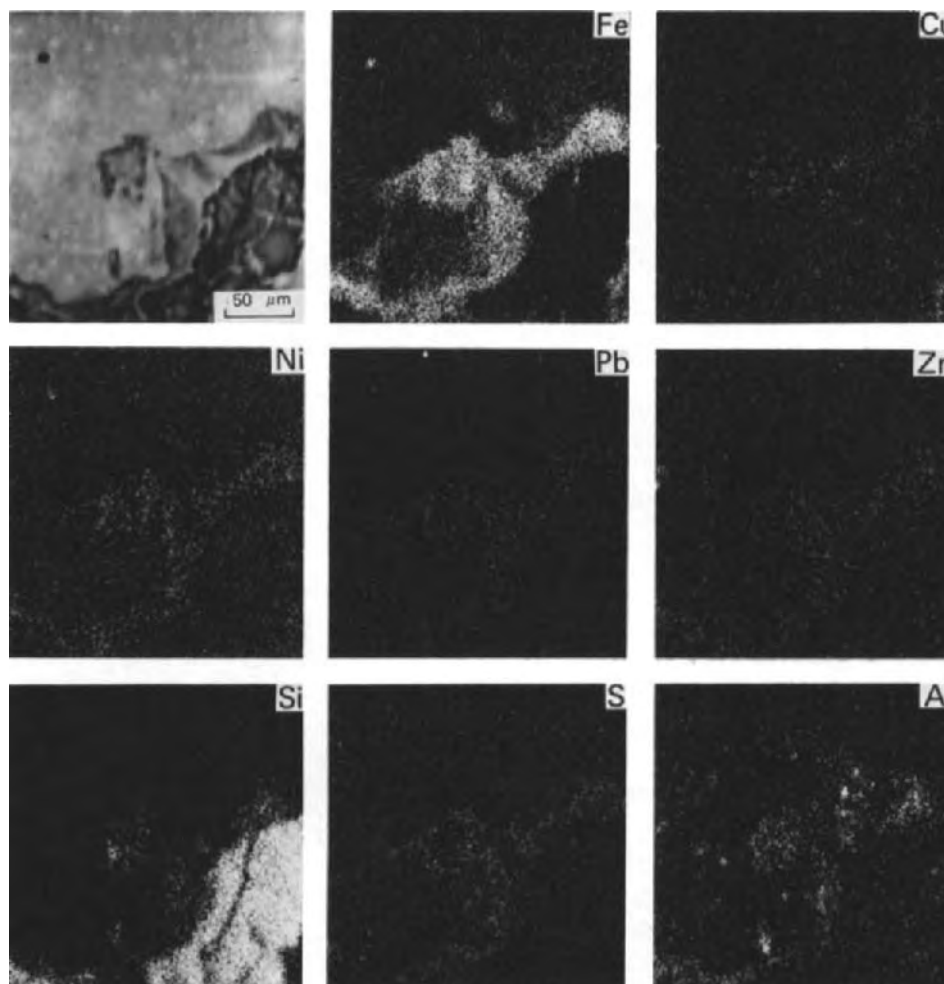


Fig. 7. EMA of a brown cutan. The cutan is vaguely present on the surface of a mineral grain in the absorbed electron image. X-ray images of Fe, Ni, Cu, Zn and Pb (polluting heavy metals), S, Al and Si were made.

tions in chemical elements in a black cutan (Fig. 9). This can be done at higher magnifications than the $\times 10,000$ possible with SEM-EDXRA. In the present case good micrographs stopped at a magnification of $\times 25,000$, becoming vague at higher ones. A number of point analyses, two of which are shown in Fig. 9, were made in the black cutan at $\times 25,000$ and demonstrated peaks of predominantly Fe and Ni for the heavy metals. The peaks for Cu, Zn and Pb were very small but present. Other elements were Al, Si, S, Cl, K and Ca. The peak of Si, to the right of the small Al-peak, is not indicated due to computer programming and insufficient space for the symbol of the

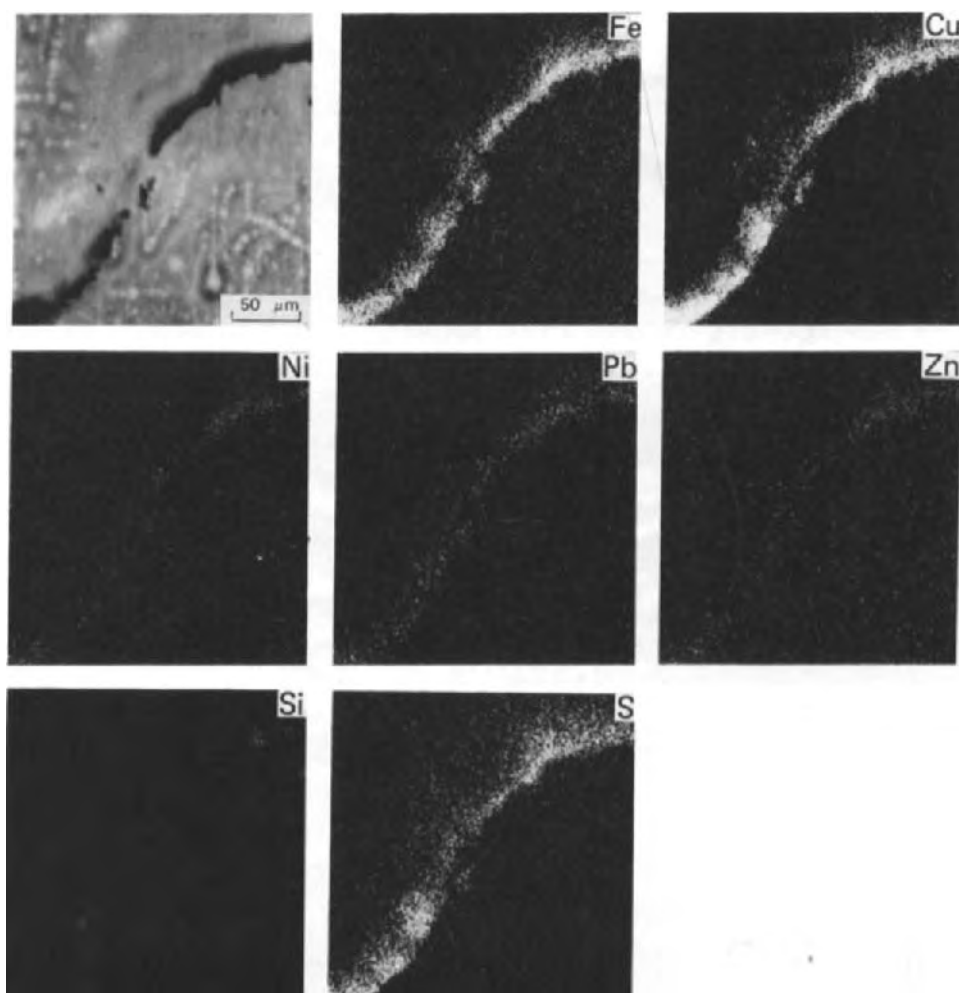


Fig. 8. EMA of a black cutan in a void which extends between two mineral grains that are not visible in the absorbed electron image. X-ray images of Fe, Ni, Cu, Zn, Pb, S and Si.

element. The totality of peaks showed a similar configuration for all point analyses and height differences of the peaks for the individual elements in the four points were small.

XRD

To obtain an idea whether crystallised forms are also present in the black and brown cutans, the precipitate was concentrated for XRD (X-ray diffraction) analysis (Breeuwsma and Balkema, 1981). Most of the loose samples contained PbS (galena) while FeS (mackinawite) was represented in the largest number of samples. No crystallised forms of Cu, Zn and Ni were found

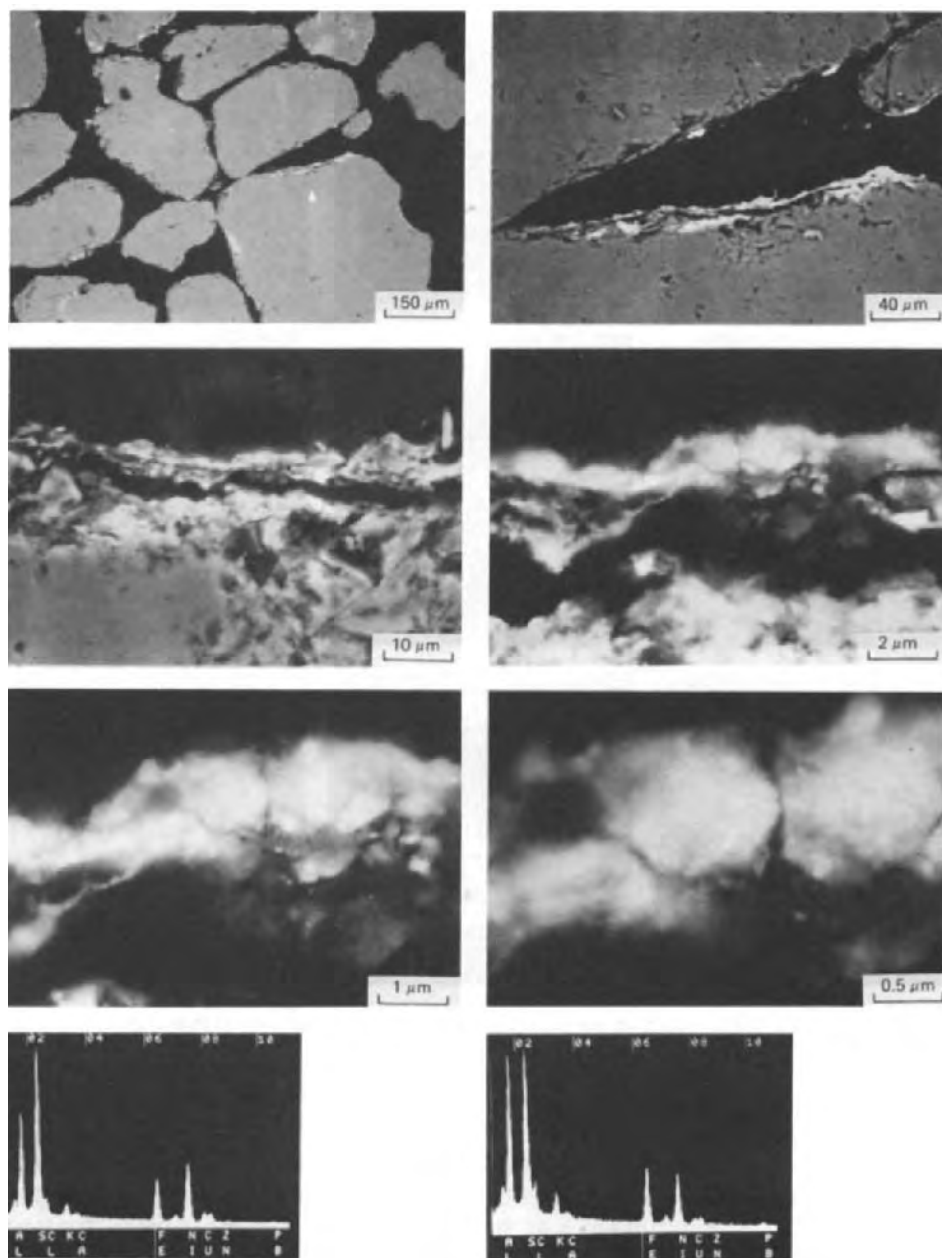


Fig. 9. STEM-EDXRA of a black cutan on the surface of a quartz grain. BESI at various magnifications up to $\times 25,000$. At $\times 12,500$ and $\times 25,000$ small particles can be discerned in predominantly poorly crystalline and amorphous polluted precipitate. Point analyses show that Fe and Ni were the dominant heavy metals in this precipitate, with less Cu, Zn and Pb. Other elements in the black cutan were Al, Si, S, Cl, K and Ca.

with XRD analysis. The reason why PbS formed and no CuS, ZnS and NiS, was because of the possibility to incorporate the small Cu^{2+} , Zn^{2+} and Ni^{2+} ions in the FeS lattice whilst the Pb^{2+} ion was too large and therefore combined with S to galena. This explanation may be applicable to a number of cases but the real picture seems to be somewhat more complicated according to light microscopic and submicroscopic analysis. For example, Cu can be found in some samples in such quantities that they are comparable to the quantity of iron. Consequently, not all the copper can be stored in the FeS lattice under such circumstances. Also, the existence of black and brown cutans, with differences in composition, cannot be established with XRD analysis. The same is true for microchemical analysis of poorly crystallised and amorphous materials, when only studied with XRD-techniques. The strength of the latter technique is, however, that we get significant information about the identity of the crystallised forms in the pollutants.

XRD analysis showed that galena and mackinawite can be found in the cutans and grain cutans of polluted material which precipitated on mineral grains and in voids. The micrographs in Fig. 9 indicate that small crystallites are possibly present in the black cutans at magnifications of $\times 12,500$ and $\times 25,000$. Such microcrystallites, after concentration procedure to obtain sufficient material, are probably the PbS and FeS found by Breeuwsma and Balkema (1981) with XRD analysis. Under natural conditions these microcrystallites are embedded in poorly crystallised and amorphous materials as indicated by light microscopy and submicroscopy.

Discussion

When the chemical elements in the brown and black cutans are compared, SEM-EDXRA analysis indicated that S was present in both cutans and less heavy metals in the brown cutans. SEM-WDXRA and EMA analysis demonstrated that virtually all chemical elements found in the black cutans can also be present in the brown ones. SEM-EDXRA only found Fe and Ni in the sample at a depth of 15–20 cm in the experimental column (Bisdom et al., 1981a; Bisdom, 1983). It was indicated, however, that more sensitive techniques could also possibly show the presence of Cu, Zn and Pb in the brown cutans. This was indeed the case with SEM-WDXRA and EMA, but the brown cutans retained less heavy metals than the black ones. Light microscopic observations have indicated that mixtures of brown and black cutans also exist. This probably indicates a genetic relation between the brown and black cutans. The isolated black flecks usually had a composition similar to that of black cutans, whereas the surrounding or adjacent brown materials showed the common composition with less heavy metals. This mixed occurrence of black and brown material in one cutan is thought to indicate that the black cutans possibly represent a brown cutan in which the crystallisation of heavy-metal sulphides has occurred to a degree at which FeS and PbS formed. The black colour of the cutan could then be explained by the presence of considerable quantities of very small crystallites of FeS and PbS in the cutanic material.

Finally, something must be said about the other elements which can be measured in black and brown cutans, viz. Al, Si, Cl, K and Ca. These elements are not found by XRD analysis but frequently measured with sub-microscopic techniques. Various possibilities exist to explain the presence of these elements. The one chosen for the moment implies that the elements possibly represent minute quantities of clay minerals and microcrystalline materials in the black cutans especially, or form part of the poorly crystalline and amorphous material of black and brown cutans.

CONCLUSIONS

In the column experiments the conditions were similar to those of the methanogenic phase in the landfill. Metal sulphides precipitated in the column and thin sections from the upper 30 cm were made for in situ analysis of the precipitates (cutans). This was done with light microscopy, SEM-EDXRA-WDXRA, EMA and STEM-EDXRA. It gave in situ information on the microchemistry and on the constituents of grain cutans (coatings) and cutans on the walls of voids. These data could be compared with the ones from XRD done on bulk samples after concentration of the pollutants to obtain sufficient material for analysis. XRD indicated the presence of FeS (mackinawite) and PbS (galena), while wet chemical and submicroscopical analysis found, in addition, Cu, Zn, Ni and S.

Some of the Cu, Zn and Ni may be incorporated in the FeS lattice, but the Cu concentrations in the cutans were sometimes too high. Consequently, CuS could possibly also form if crystallisation takes place in such minor quantities that the amount of material is too small for XRD analysis. The same may be true of ZnS and NiS but in still smaller quantities than CuS. A lot of poorly crystallised and amorphous material is usually present in both types of cutans as indicated by light microscopy and submicroscopy.

Brown cutans were usually isotropic when observed with the light microscope and did not give good quality BESI (backscattered electron scanning images) or secondary electron images (SEI). With the EMA the brown cutan became vaguely visible using an absorbed electron image (Fig. 7). This indicates a poorly crystalline or amorphous state of the material. The brown cutans had less heavy metals than the black ones as far as quantity is concerned. Not all the brown cutans had Cu, Zn and Pb but Fe and Ni could usually be found together with S.

Black cutans exhibited small particles when analysed with the EM 400T, an apparatus which can operate as a SEM, TEM and STEM coupled with EDXRA at low and very high magnifications. These particles were interpreted as probably being the minerals galena and mackinawite in the form of microcrystalline material which coloured the cutan black. Apart from the PbS and FeS minerals, the black cutans also contained Ni, Zn and Cu in minor quantities but frequently a little more than was present in the brown cutans. Only Fe reached 12–17 wt.% in the brown cutans, while Ni, Cu, Zn

and Pb stayed below 1 wt.%. Iron in the black cutans could be 18 wt.%, copper up to 15 wt.% and lead 3 wt.%. Ni and Zn remained below 1 wt.% in the black cutans. Black cutans were interpreted as being a further stage in cutan development than brown ones because they exhibit crystallised very small materials and can be present as flecks in a brown cutan with very vague boundaries between brown and black substances. In the black cutans, however, a lot of poorly crystallised and amorphous materials is still visible when observed at high magnifications of $\times 25,000$ or more.

The polluted heavy-metal-containing solutions were also observed to invade a shell fragment and to form virtually concentric and continuous bands. The composition of the precipitate in the shell is similar to that found in black and brown cutans, and, like these, can be extremely heterogeneous over microdistances in the same band. Such measurements can only be made with submicroscopic techniques for *in situ* analysis.

Future submicroscopic and light microscopic investigations will concentrate on the manner in which cutans (coatings, precipitates) are distributed in the three columns, i.e. with respect to mineral grains, clays and voids (pores). These data will help to develop mathematical models to describe the transport of polluted materials in soils. *In situ* analysis of the chemical elements in the cutans will be compared with physicochemical data obtained from percolates and solid soil materials.

REFERENCES

- Bar-Yosef, B., Posner, A.M. and Quirk, J.P., 1975. Zinc adsorption and diffusion in goethite. *J. Soil Sci.*, 26: 1–21.
- Bisdom, E.B.A., 1981. Light microscopic and submicroscopic analysis of thin sections of soils. *Agron. Abstr.*, p. 196.
- Bisdom, E.B.A., 1983. *In situ* microanalysis of man-made precipitates in soil beneath a landfill and on the surface of a water-tube filter. In: R. Hallberg (Editor), *Environmental Biogeochemistry. 5th International Symposium on Environmental Biogeochemistry*, 1981, Stockholm. *Ecol. Bull.*, 35: 547–553.
- Bisdom, E.B.A. and Thiel, F., 1981. Backscattered electron scanning images of porosities in thin sections of soils, weathered rocks and oil-gas reservoir rocks using SEM-EDXRA. In: E.B.A. Bisdom (Editor), *Submicroscopy of Soils and Weathered Rocks. 1st Workshop of the International Working-Group on Submicroscopy of Undisturbed Soil Materials (IWGSUSM) 1980*, Wageningen. Centre for Agricultural Publishing and Documentation (Pudoc), Wageningen, pp. 191–206.
- Bisdom, E.B.A., Henstra, S., Jongerius, A. and Thiel, F., 1975. Energy-dispersive X-ray analysis on thin sections and unimpregnated soil material. *Neth. J. Agric. Sci.*, 23(4): 113–125.
- Bisdom, E.B.A., Henstra, S., Hornsvelde, E.M., Jongerius, A. and Letsch, A.C., 1976. Wavelength and energy dispersive X-ray microanalysis with EMA and SEM-EDXRA on thin sections of soils. *Neth. J. Agric. Sci.*, 24(4): 209–222.
- Bisdom, E.B.A., Henstra, S., Jongerius, A., Brown, J.D., von Rosenstiel, A.P. and Gras, D.J., 1977. Light and heavy element detection in thin sections of soils with the ion microprobe mass analyzer (IMMA). *Neth. J. Agric. Sci.*, 25(1): 1–13.
- Bisdom, E.B.A., Heintzberger, G. and Lagas, P., 1981a. SEM-EDXRA measurements on thin sections of heavy metal contaminated soil samples from column experiments. In:

- W. van Duijvenbooden, P. Glasbergen and H. van Lelyveld (Editors), *Quality of Groundwater. Proceedings of an International Symposium, Noordwijkerhout, 1981. Studies in Environmental Science, Vol. 17. Elsevier, Amsterdam, pp. 489–493.*
- Bisdom, E.B.A., Henstra, S., Jongerius, A., Heinen, H.J. and Meier, S., 1981b. Chemical element detection in thin sections of soils with the laser microprobe mass analyzer (LAMMA 500). *Neth. J. Agric. Sci.*, 29(1): 23–36.
- Bisdom, E.B.A., Henstra, S., Werner, H.W., Boudewijn, P., De Grefte, H.A.M., Knippenberg, W.F., Gourgout, J.M. and Migeon, H.N., 1983. Quantitative analysis of trace and other elements in thin sections of soils with the secondary ion microscope (Cameca). *Geoderma*, 30: 117–134 (this issue).
- Breeuwsma, A. and Balkema, W., 1981. Mineralogisch onderzoek naar de precipitatie van zware metalen in percolatieproeven met vuilstortwater. Report No. 1593. Netherlands Soil Survey Institute, Wageningen, The Netherlands, 23 pp.
- Harmsen, K., 1977. Behaviour of heavy metals in soil. *Agric. Res. Rep.* 866. Centre for Agricultural Publishing and Documentation (Pudoc), Wageningen, 171 pp.
- Henstra, S., Bisdom, E.B.A., Jongerius, A., Morgan, A.E., Werner, H.W. and De Grefte, H.A.M., 1980. Quantitative analysis on thin sections of soils by secondary ion mass spectrometry. In: P. Brederoo and V.E. Cosslett (Editors), *Electron Microscopy 1980. Proceedings of the 7th European Congress on Electron Microscopy including the 9th International Conference on X-ray Optics and Microanalysis, The Hague, Vol. 3. Analysis. Seventh European Congress on Electron Microscopy Foundation, Leiden, pp. 224–225.*
- Henstra, S., Bisdom, E.B.A. and Boekestein, A., 1981. Submicroscopic techniques for in situ microchemical analysis of soils, III. Destructive techniques. In: E.B.A. Bisdom (Editor), *Submicroscopy of Soils and Weathered Rocks. 1st Workshop of the International Working-Group on Submicroscopy of Undisturbed Soil Materials (IWGSUSM) 1980, Wageningen. Centre for Agricultural Publishing and Documentation (Pudoc), Wageningen, pp. 55–65.*
- Hoeks, J., 1978. Biochemische afbraakprocessen bij composteren en storten van vaste afvalstoffen. ICW-Nota 1103, Wageningen, 15 pp.
- Jongerius, A. and Heintzberger, G., 1975. Methods in soil micromorphology. A technique for the preparation of large thin sections. *Soil Surv. Pap.*, 10. Netherlands Soil Survey Institute, Wageningen, 48 pp.
- Lagas, P. and Harmsen, K., 1980. Complexering van zware metalen in vuilstortpercolaat (Delden). RID-Report CBH 80-01. National Institute for Water Supply, Leidschendam, 43 pp.
- Lagas, P. and Loch, J.P.G., 1981. Column experiments on the behaviour of heavy metals in soil. RID-Mededeling, 81-2. National Institute for Water Supply, Leidschendam, 96 pp.
- Loch, J.P.G., Lagas, P. and Haring, B.J.A.M., 1981. Behaviour of heavy metals in soil beneath a landfill; results of model experiments. In: W. van Duijvenbooden, P. Glasbergen and H. van Lelyveld (Editors), *Quality of Groundwater. Proceedings of an International Symposium, Noordwijkerhout, The Netherlands, 1981. Studies in Environmental Science, Vol. 17. Elsevier, Amsterdam, pp. 545–555. (Also in: Sci. Total Environ., 21 (1981): 203–213.)*
- Sposito, G., Holtzclaw, K.M. and Baham, J., 1976. Analytical properties of the soluble, metal-complexing fractions in sludge-soil mixtures 2. Comparative structural chemistry of fulvic acid. *Soil Sci. Soc. Am. J.*, 40: 691–697.
- Van Eijkeren, J.C.H. and Loch, J.P.G., 1981. Modellering van Bodemverontreiniging. RID Jaarverslag. In press.

CHARACTERIZATION OF IN SITU ORGANIC MATTER CONSTITUENTS IN VERTISOLS FROM ARGENTINA, USING SUBMICROSCOPIC AND CYTOCHEMICAL METHODS — FIRST REPORT

S. STEPHAN¹, J. BERRIER², A.A. DE PETRE³, C. JEANSON⁴, M.J. KOOISTRA⁵,
H.W. SCHARPENSEEL⁶ and H. SCHIFFMANN⁶

¹ *Institut für Bodenkunde der Universität Nussallee 13, 5300 Bonn (F.R.G.)*

² *C.N.R.A., Département de Science du Sol, Etoile de Choisy, Route de Saint-Cyr,
78000 Versailles (France)*

³ *Facultad de Ciencias Agropecuarias, Universidad Nacional de Entre Ríos, Tezanos
Pinto, E.R. (Argentina)*

⁴ *C.N.R.S., Muséum National d'Histoire Naturelle, 4 Avenue du Petit Chateau, 91800
Brunoy (France)*

⁵ *Netherlands Soil Survey Institute, P.O. Box 98, 6700 AB Wageningen (The Netherlands)*

⁶ *Ordinariat für Bodenkunde der Universität, Von-Melle-Park 10, 2000 Hamburg (F.R.G.)*

(Accepted for publication February 17, 1983)

ABSTRACT

Stephan, S., Berrier, J., De Petre, A.A., Jeanson, C., Kooistra, M.J., Scharpenseel, H.W. and Schiffmann, H., 1983. Characterization of in situ organic matter constituents in vertisols from Argentina, using submicroscopic and cytochemical methods — First report. *Geoderma*, 30: 21–34.

The investigation of residence, alteration and circulation of soil organic matter is an ideal problem for integrated research including microscopy and submicroscopic methods. The subject of the present study is an argillic Pelludert of Argentina. The organic matter in this soil shows an unexpectedly steep gradient of ¹⁴C age. Below 25 cm the frequency of microscopic organic features decreases rapidly. Only few types are present at greater depth. Features produced by faunal activity, as well as brown to black areas of different composition have been investigated with SEM-EDXRA. The main subjects of laser-induced mass spectra were dark grains of few microns diameter which abound in the fine mass. Some spectra are presented and discussed. Further investigations are planned in order to demonstrate how submicroscopy, associated to the physico-chemical methods, can contribute to the knowledge and to the comprehension of the genesis of Vertisols.

INTRODUCTION

The investigation of soil organic matter (O.M.) by bulk analysis is reaching the limits of usefulness. Further work may be expected to use in situ determinations as well as the isolation of individual organic constituents (plant,

animal, fungal, bacterial and derived products) which show interesting chemical composition and turnover behaviour. Our intention is not to replace bulk analysis but to supplement it in order to increase our knowledge of soil organic matter and improve our interpretation of soil processes. The investigation of residence times, alteration and circulation of O.M. is an ideal problem for integrated research using microscopic and submicroscopic methods.

The subject of our work is a Vertisol of the Yerua series (PNUD, FAO, INTA, 1967), an Argillic Pelludert with a gilgai relief of 5 m crest to crest distance, situated in the Entre Rios province of Argentina at 58° 25'W 31° 26'S on a slight slope, 30 m above sea level. The soil has been formed from a Quaternary clay-rich marl; the annual precipitation is approximately 1000 mm and the mean annual temperature is about 19°C. The dominating factor, however, is the high clay content, with a preponderance of smectite, some illite and traces of kaolinite. Fig. 1 presents some conventional data obtained from samples of the gilgai trough. We emphasise the high swelling capacity shown by a COLE value of up to 0.16.

DEPTH cm	GRAIN SIZE DISTRIBUTION (1)				pH	O.M. % (2)	C/N	COLE	CaCO ₃ % (3)	COLOUR moist (4)	TEXTURE (5)	SLICKEN- SIDES (6)	INTER- SECTING SLICKEN- SIDES (6)	CaCO ₃ MODULE (6)	Fe-Mn CON- CRETION (6)
	a	b	c	d											
13					6.1	4.6	12		0	10 YR 2/1	p,P	1	0	0	2
40					6.3	4.1	11	0.16	0	10 YR 2/1	P,Pr	3	3	0	2
80					6.5	4.1	12	0.16	0	10 YR 3/1	Pr,W	3	3	1	2
100					7.2	2.2	10	0.14	6	10 YR 3/2	Pr,W	3	3	3	2
140					7.2	1.4	9	0.16	7	7.5 YR 4/2	Pr,W	2	0	3	2
					7.4	0.5	9		7	7.5 YR 5/4	C some Pr, W, P	1	0	3	2

Fig. 1. Analytic data of the Yerua pedon. (1) grain size distribution: a = 0–2 μ m, b = 2–20 μ m, c = 20–50 μ m, d = 50 μ m–2 mm; (2) organic matter; (3) carbonate noted as CaCO₃; (4) Munsell scale; (5) p = subpolyhedrons, P = polyhedrons, Pr = prisms, W = wedges; C = coherent; (6) 0 = absent, 1 = trace to 3 = many.

MATERIAL

Bulk analysis and some microscopic work was done on air-dried material collected in 1979. Other in situ investigations, including some more micro-morphological work have been made on small, undisturbed samples collected in 1980, freeze-dried in Argentina and distributed to the various laboratories.

RESULTS

Carbon dating of the O.M. (Table I)

The ^{14}C analysis (Scharpenseel and Pietig, 1968/69; Scharpenseel, 1972) produced an unexpectedly steep age gradient. The sample from only 15–30 cm gives an age of 1100 years, and the age rises to more than 4000 years at 75–90 cm, despite evidence of swelling and shrinking as well as faunal activity including a number of earthworm holes visible on the wall.

TABLE I

Carbon dating of O.M.

Depth (cm)	Age (LIBBY) years before present
0–15	0* ¹
15–30	1120 \pm 60
30–45	2320 \pm 60
45–60	2610 \pm 70
60–75	2890 \pm 70
75–90	4140 \pm 90
90–105	3760 \pm 70

*¹ ^{14}C contents 107 \pm 1% of the modern standard

Micromorphology

Thin sections from air-dried, impregnated samples (Altemüller, 1974) of the 1979 material were investigated in order to estimate the number of distinct organic features (Table II). The results agree quite well with the carbon dating data. Below a certain depth only 3 types of organic feature can be recognized, and these do not allow any further differentiation.

The freeze-dried samples were taken at depths of 0–5, 20–25, 40–45 and 60–65 cm, respectively. They were processed as described by Jongerius and Heintzberger (1975) and show the same basic composition at every depth. The soil matrix has an aseptic fabric, and all samples contain small brown to black rounded areas up to 50 μm in diameter which are definitely of differ-

PLATE I

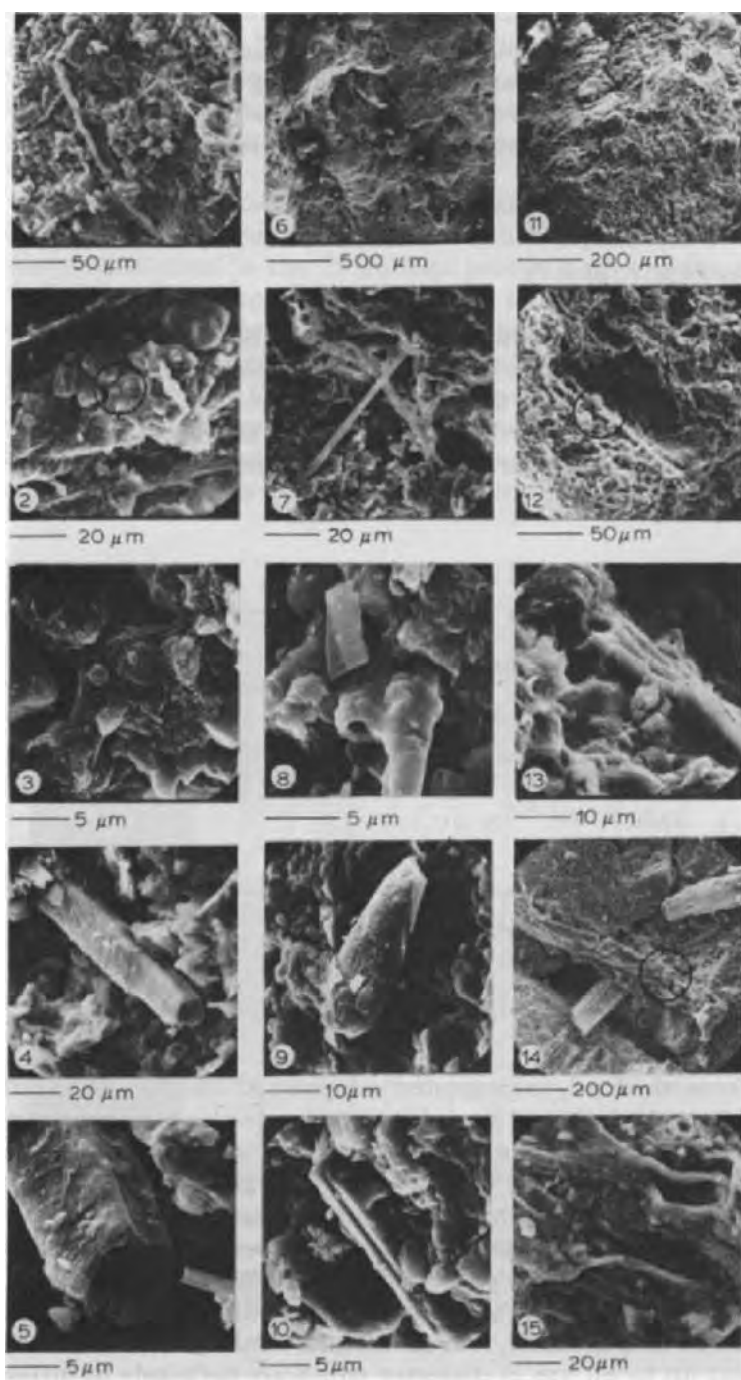


TABLE II

Organic soil constituents in thin sections; values from 1 (=traces) up to 5 (= abundant)

	Depth (cm)						
	5—10	25— 30	55— 60	85— 90	120— 125	137— 142	150— 155
Roots containing cellulose	3	3	1	—	—	—	—
Root remnants without cellulose	2	2	1	—	—	—	—
Fruits and seed grains	1	—	—	—	—	—	—
Fungus sclerotia	2	—	—	—	—	—	—
Faecal pellets	3	2	1	—	—	—	—
Dark particles of 2—6 μ m size	5	5	5	3	3	3	3
Dark particles smaller than 2 μ m	5	5	5	3	3	3	3
Suberine, cutine, chitine etc.	3	2	3	2	2	3	1

ent composition. Below 40 cm there is some evidence of current clay illuviation processes. The influence of the fauna is important above 25 cm, but is of minor influence below that depth. The fauna is responsible for the production of a relatively small number of primary voids, for the fragmentation of O.M., for the mixing of organic and mineral materials in their alimentary canals, and for the transport of organic and mineral particles within the soil. As a result of the faunal activity the humus form of the topsoil is a mull. The quantity of O.M. in the form of faecal pellets decreases rapidly with depth; below 25 cm the void system is mainly determined by physical processes, and only few of the voids are produced by roots or soil fauna.

PLATE I

Mineral material and organo-mineral complexes in a Vertisol, investigated with SEM-EDXRA.

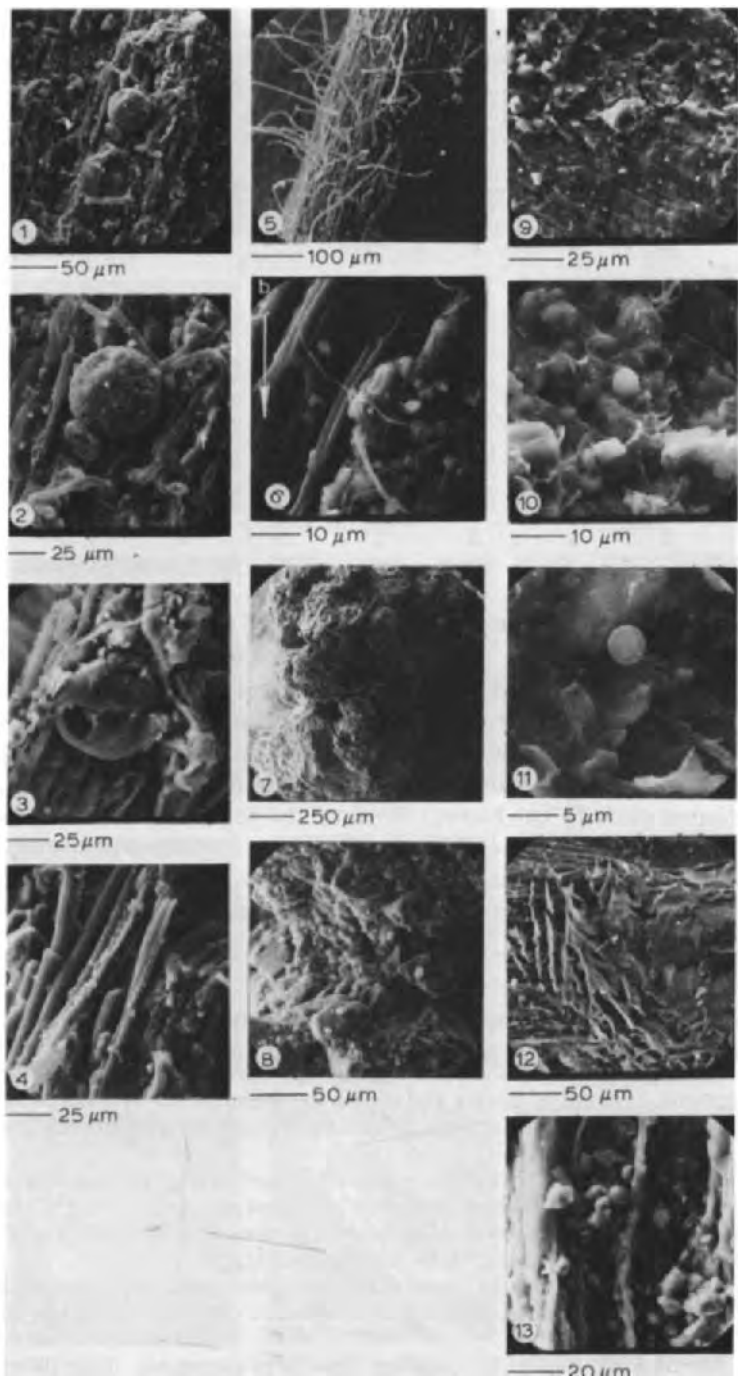
1—5. A₁ horizon, 0—4.5 cm depth: 1. polyhedral aggregates associated with roots; 2. aggregates on a root fragment; 3. detail of 2, clay and silt particles connected by amorphous substance; 4. diatom (very clear Si peak with EDXRA) in contact with argillic particles; 5. detail of 4.

6—10. B₁₁ horizon, 20—24.5 cm depth: 6. poorly individualized aggregates, absence of roots, presence of numerous pores; 7. fungus filaments in a pore; 8. jointed fungus filament in contact with clay particles, fragment of a diatom; 9. thecamoeba, Si, Al, Ca, Ti; 10. numerous long minerals, amphiboles (?), Si, Fe, Ca, Ti, Na, Mg.

11—13. B₁₂ horizon, 40—44.5 cm depth: 11. poorly individualized aggregates, absence of roots, numerous nodules; 12. clay cutans, very numerous and of different thickness; 13. detail of 12.

14—15. B₁₂ horizon, 60—64.5 cm depth: 14. jointing cuneiform aggregates, plant debris with or without visible cell structure; 15. detail of 14, plant debris covered with amorphous substance comprising mineral particles.

PLATE II



SEM-EDXRA investigation

The submicroscopic investigation of three superficial horizons permits to characterize: the microstructures; O.M., its alteration and association with minerals; micro-organisms or the traces of their activity (Jeanson, 1981). It refines in this way the knowledge and comprehension of the pedogenetic mechanisms.

The well separated subpolyhedral microaggregates of the A horizon impart a certain fragility to this material (Plate I, 1). At certain depth however, the aggregates are hardly individualized and the microstructures more compact (Plate I, 6, 11, 14).

The abounding plant fragments in the A horizon are only slightly decomposed with clearly visible cells (Plate II, 1–3). Anyhow, they are colonized by fungus mycelium throughout the A and B₂₁ horizon (Plate II, 4, 5), and the cell walls suffered by fungus lysis and subsequent lysis by bacteria (Plate II, 6), changing the cell walls into a fine-lamellated amorphous substance (Plate II, 10–12). In the B₂₂ horizon there are spheric bodies of 4–8 μm diameter near the well decomposed plant debris, and the hypothesis can be made that they have been derived from the cell material after the cell walls have been decomposed. They bear a notable resemblance to certain brown products of the same shape and size, which are visible by TEM in certain humus forms.

Micro-organisms occur frequently in the superficial horizons and are often associated with organic matter. In the A horizon the fungus mycelium is frequently accompanied with protozoa and thecamoebae which have exogenic thecae consisting of mineral grains of the environment (Plate II, 1–3). There are also thecamoebae and diatoms in contact with minerals (Plate I, 4, 5, 9). Traces of the activity of earth-consuming organisms are well visible till more than 20 cm depth in the compact B₂₁ horizon. There are pores of 100 μm diameter (Plate I, 6) and ovoid aggregates of 300 μm length and 200 μm width (Plate II, 7, 8). From size, shape, nature and arrangement of the

PLATE II

Organic matter and microorganisms in a Vertisol, investigated by SEM-EDXRA.

1–4. A₁ horizon, 0–4.5 cm: 1. surface of a decomposing plant fragment, cell structure poorly visible, numerous fungus filaments and thecamoebae; 2. detail of 1, clay skin of a thecamoeba, ϕ 60 μm ; 3. fresh plant fragment with very clear cell structure, absence of mycelium, broken thecamoeba, ϕ 60 μm ; 4. strongly decomposed plant fragment, no plant cell visible, combined, jointed fungus filaments.

5–8. B₁₁ horizon, 20–24.5 cm: 5. mycelium forming a very dense network on a plant fragment; 6. detail of a plant cell wall, bacterial lysis (b)?; 7. cluster-shaped accumulation of subspheric aggregates, dejections of enchytreids or collembolae?; 8. detail of 7, contact of two aggregates.

9–12. B₂₂ horizon, 40–44.5 cm: 9. completely decomposed plant fragment, diffuse cell structure; 10. detail of 9; 11. spheric body, brown substance? ϕ 4 μm ; 12. lamellated amorphous substance.

13. B₂₂ horizon, 60–64.5 cm, plant fragment with mineral cutan.

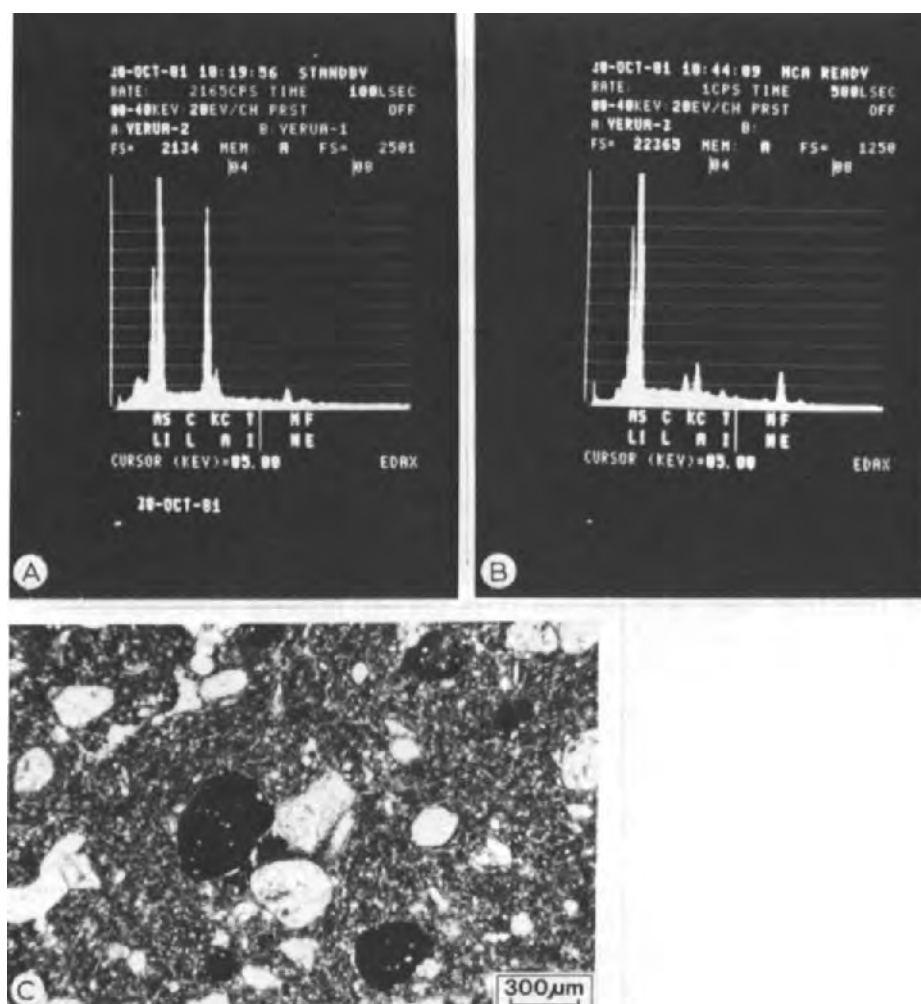


Fig. 2. Two EDXRA point analyses (A and B) of different dark-coloured areas (B21 horizon, 20–24.5 cm depth). C. Rounded, dark-coloured nodules with sharp external boundaries, embedded in the groundmass (plane polarized light).

aggregates, the hypothesis is deduced that they are dejections of enchytreides (small earthworms) or collembolae (apterygote insects). This needs, however, to be proved by field observations and cultures in the laboratory.

The accumulation of substances may be investigated, too. In all samples there are small brown to black rounded areas up to 0.5 mm diameter. These have different chemical compositions and several origins are possible: humifying fragments of organic matter, faecal pellets, soil matrix material or O.M. impregnated with iron and/or manganese, weathered minerals or mineral aggregates. Some of these brown/black areas have been examined with SEM-

EDXRA. As shown by Fig. 2, most of them consisted of a clay-rich material containing various quantities of manganese and/or iron.

Laser-induced mass spectra

One of the more modern methods for characterising unknown substances is mass spectrometry. It is developing into an appropriate tool for the investigation of soil organic matter (W. Flaig, pers. comm., 1982), and examples of mass spectrograms of ions produced by pyrolysis of different soil materials have already been produced for several characteristic soils (Halma et al., 1979). Ions from individual particles of microscopic size may be induced, however, by both argon or oxygen ions (SIMS) or by a laser beam (LAMMA). Mass spectroscopy of laser-induced ions from small (about 1 μm) parts of thin sections is practicable with the LAMMA 500 machine of the Leybold-Heraeus Co. as mentioned by Henstra et al. (1981) and Bisdom et al. (1981).

The samples were placed in sandwich grids and investigated at carefully prepared edges. The analysis of some of the spectra (Figs. 3, 4) indicates that certain particles can be differentiated, but more spectra are needed to confirm this. As the intensities cannot be compared with standards, and only are appointed to five peak heights in the figures, there is no quantitative evaluation possible. Heinen et al. (1979) characterises spectra from certain types of organic and inorganic compounds, but the interpretation of individual mass numbers seems to be rather difficult when applied to more complicated systems. In the text which follows, numbers in brackets are mass numbers observed.

Cation mass spectra (Fig. 3)

In the soil matrix of Vertisols, there are striking dark grains about 3 μm in size. Some of the larger ones look like organic remnants, but there also seem to be transitions to sesquioxide accumulations. The mass spectra of these various grains are of course quite different. In spectrum 44 Mn (55) is important whereas Fe (56) has a high peak in 61 and also contributes to the spectra in 43 and 28. In diagrams 43, 44, 28, 55 and 61 an ion with mass number (57) most probably represents some component of organic matter, as do (60) in 65, (89) in 44 and (26) in spectrum 65.

Comparing these ions together with Al (27) and the quite weak peak of Si^+ , which always gives a rather small signal, one can distinguish between relatively pure O.M. particles represented by spectrum 65, particles with predominantly inorganic compound such as 61 and mixed materials linked together by absorption.

Two Fe-Mn nodules have been investigated in order to obtain comparable spectra of true sesquioxide materials, here represented by spectrum 32. At

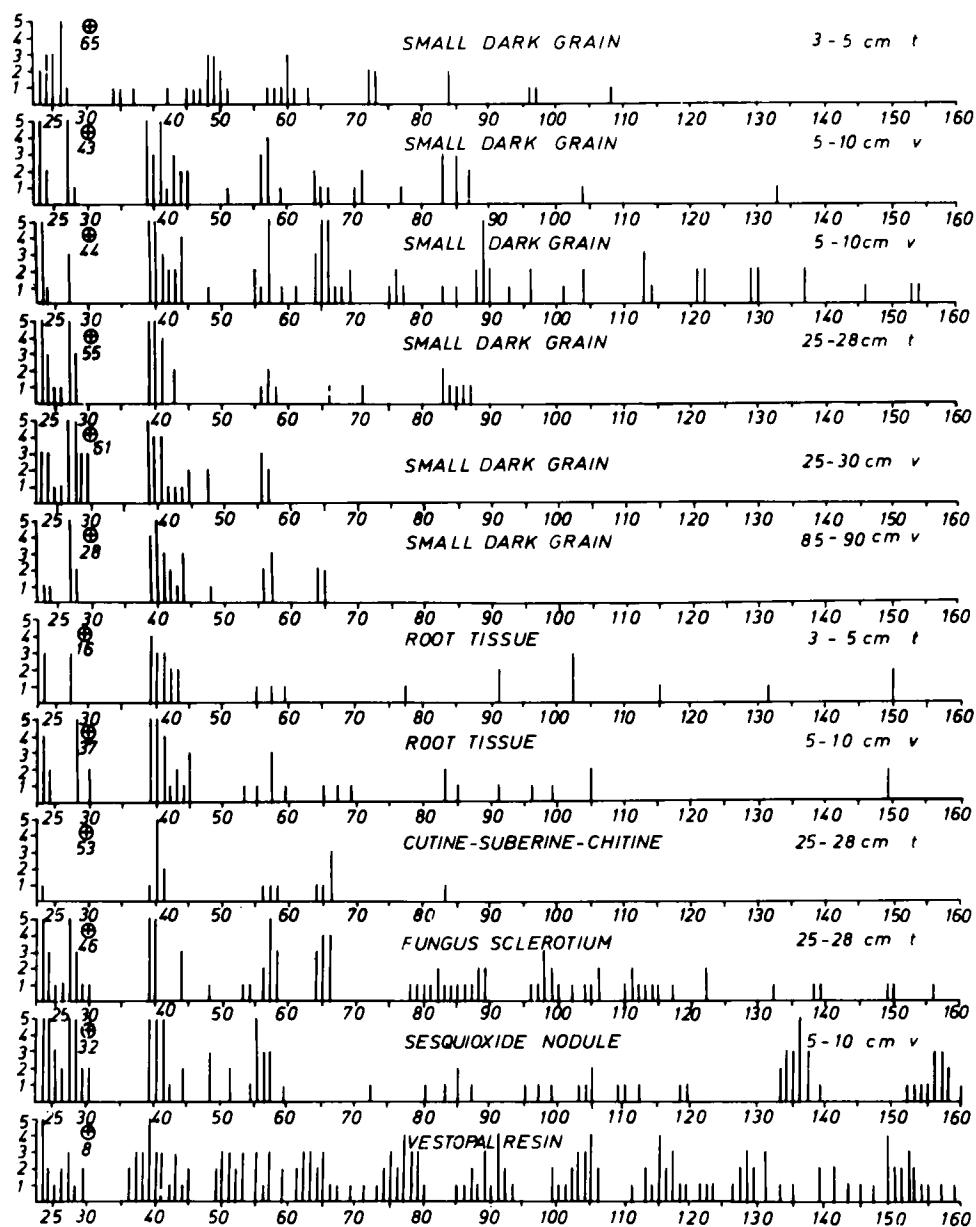


Fig. 3. Laser-induced cations. *t* = gilgai top, *v* = gilgai valley. Horizontal scale, mass numbers; vertical scale, strength of signal: 1 = up to 3, 2 = 4–9, 3 = 10–39, 4 = 40–69, 5 = at least 70 units recorded.

the point analysed, Mn exceeds Fe. Assuming that the peak at mass number (28) is due to Si, then besides the usual high Al peak, there is also a strong peak due to Si. There are also, however, organic compounds in the nodule,

e.g. the masses arranged around (136) and (157) as well as the ions (26) and (57) already mentioned. We are not sure whether the peak (48) is from an organic compound or from Ti.

Spectrum 8 represents the resin with which the samples have been impregnated. It is possible to recognise spectra due to resin-contaminated materials by comparison with this spectrum. It is proved by this that the resin is usually confined to the pore space, as is already known from micromorphological observations. In this spectrum, as well as in other spectra of high molecular weight substances, mass numbers appear in groups of at least three consecutive peaks arranged round a maximum, features also visible at higher mass numbers than those shown here. In spectrum 8 one of these groups is arranged round (105), the mass number of styrene + H. The differences between the individual mass maxima could not be interpreted unequivocally. A mass difference of 1 points to single H differences, whereas a difference of 2 is given by different redox states of (multi-)chinone-hydrochinone systems. Both cases mentioned are easy to detect. Features like these also appear in mass spectra of fungal material, root tissues, some of the small grains and as is clearly evident, in that of the sesquioxide nodule.

Anion mass spectra

The negative ions are dominated by organic substances. These may be due to the acid groups which are so abundant in the O.M. of soils. Moreover, single atoms mainly form cations, and the oxides exhibit various stages of oxidation. In the sesquioxide nodule, spectrum 30, MnO (71) exceeds Mn (55) and MnO₂ (87), and FeO (72) exceeds Fe (56) and FeO₂ (88). The mass numbers (63) and (79) may belong to PO₂ and PO₃, respectively. They

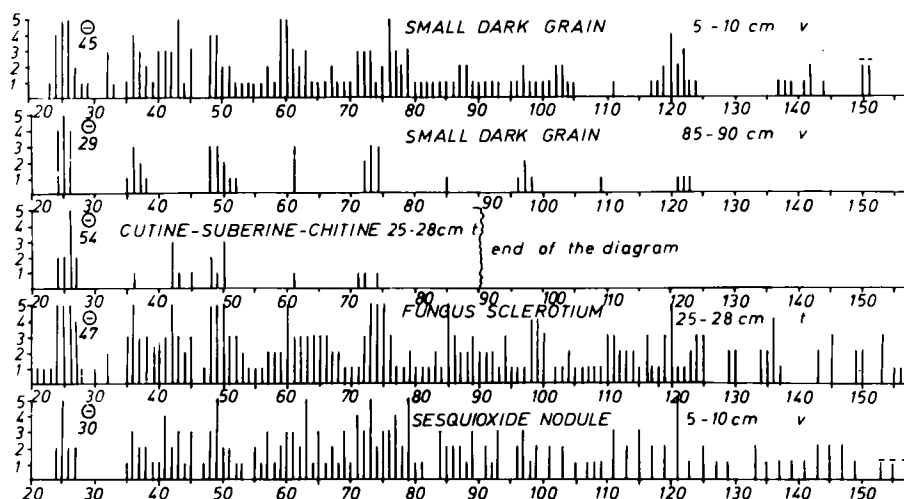


Fig. 4. Laser-induced anions. For the legend see Fig. 3.

produce strong peaks in the case of this sesquioxide nodule, as well as in the spectrum 45 which belongs to one of the dark grains.

There are more identifications which are not yet firmly established but which are tentatively submitted to illustrate the situation. Both SiO_2 and CO_3 have the same mass number (60). The presence of both compounds can be established in spectrum 45 by the appearance of SiO_3 (77) and HCO_3 (45). As in the positive spectra, Si (28) is quite inconspicuous. (43) seems to belong to AlO, and O_2 and S overlap at mass number (32).

As with the cations, the negative spectra show that the dark grains have various quite different compositions. The grain from a depth of 85–90 cm produces a much simpler spectrum than that from 5–10 cm depth, but this may not be general. The fungal sclerotium, spectrum 47, generates an exceptionally large number of different ions, and the negative spectrum also shows a high proportion of O.M. in the sesquioxide nodule.

DISCUSSION

The Yerua soil as a true Pelludert with gilgai relief, intersecting slickensides, dark colours and a very high swelling capacity certainly undergoes swelling and shrinking which, together with an obviously high biological activity are thought to produce complete homogenisation of at least the upper 80 cm. However, the morphological and chemical differentiation of the soil profile does not seem to permit more than a very slow recent soil mixing, and the idea of a fast and complete vertical rearrangement is clearly disproved by the differentiation of the minimum O.M. age as indicated by ^{14}C dating (Table I).

The main problem is to connect these high ^{14}C values with the visible incorporation of O.M. which could not be inactive for thousands of years. The high age might reflect the accumulation of a special form of O.M., of very high residence time, well protected by the clay matrix and only incorporated at very low rates, at least after the pool has been saturated. The main part of O.M., however, is quite short-living (Scharpenseel, 1975).

As a consequence, the farmers must make all efforts to preserve the humus contents of these soils.

The most constant elements of the micromorphologic distinct organic features (Table II) are abounding dark grains of a size up to $6\text{ }\mu\text{m}$ and some suberin-like material. The nature of the dark particles is variable without any possibility of a clear differentiation. This may point to a more complicated structure of these grains. Some bodies look like organic detritus, others are based on sesquioxides, and even true sesquioxide nodules contain organic substances, as mentioned. The shape of a grain of course belongs to a distinct sesquioxide particle or plant debris, respectively; but the chemical nature and reactivity might be influenced, and sometimes governed, by a number of adsorbed substances.

FURTHER INVESTIGATIONS

The members of the team are now completing the investigations presented in this paper and performing some additional experiments. As the methods usually used by Foster (1981) have proved to be unsuitable for the samples from Yerua, alternative techniques are being tried. Conventional humus investigations and some special experiments remain to be done, but the team is hopeful that it will be able to present a more complete report at the Paris meeting.

ACKNOWLEDGEMENTS

We thank Dr. Heinen of Leybold-Heraeus Co., Köln for his introduction to and help with the LAMMA instrument, and Dr. R.C. Foster of CSIRO, Glen Osmond who revised the main part of the manuscript.

REFERENCES

- Altemüller, H.J., 1974. Mikroskopie der Böden mit Hilfe von Bodendünnschliffen. Handbuch der Mikroskopie in der Technik, Band 4, Teil 2. Umschau-Verlag, Frankfurt, pp. 309–367.
- Bisdorn, E.B.A., Henstra, S., Jongerius, A., Heinen, H.J. and Meier, S., 1981. Chemical element detection in thin sections of soils with the Laser Microprobe Mass Analyzer (LAMMA 500). *Neth. J. Agric. Sci.*, 29: 23–36.
- Foster, R.C., 1981. Localization of organic materials in situ in ultrathin sections of natural soil fabrics using cytochemical techniques. In: E.B.A. Bisdorn (Editor), *Submicroscopy of Soils and Weathered Rocks. 1st Workshop of the International Working-Group on Submicroscopy of Undisturbed Soil Materials (IWGSUSM)*, 1980, Wageningen, pp. 309–317.
- Halma, G., Miedema, R., Posthumus, M.A. and Van de Westeringh, W., 1979. Characterization of soil types by pyrolysis-mass spectrometry. *Agrochemica*, 22: 372–382.
- Heinen, H.J., Meier, S., Vogt, H. and Wechsung, R., 1980. Laser induced mass spectrometry of organic and inorganic compounds with LAMMA. Paper. 8th Triannual International Mass Spectrometry Conference, Oslo, 1979, 21 pp.
- Henstra, S., Bisdorn, E.B.A. and Boekestein, A., 1981. Submicroscopic techniques for in situ microchemical analysis of soils, III. Destructive techniques. In: E.B.A. Bisdorn (Editor), *Submicroscopy of Soils and Weathered Rocks. 1st Workshop of the International Working-Group on Submicroscopy of Undisturbed Soil Materials (IWGSUSM)*, 1980, Wageningen, pp. 55–65.
- Jeanson, C., 1981. Structuration du sol par la faune terricole. Incidences sur les concentrations organo-minérales. In: *Colloques internationaux du C.N.R.S. No. 303, Migrations organo-minérales dans les sols tempérés*. Paris, pp. 113–123.
- Jongerius, A. and Heintzberger, G., 1975. *Methods in Soil Micromorphology. A Technique for the Preparation of Large Thin Sections*. Netherlands Soil Survey Institute, Wageningen, 49 pp.
- PNUD, FAO, INTA, 1976. *Suelos y erosion de la provincia de Entre Ríos*. Copied manuscript, 2nd ed., EERA del INTA Paraná, 2 Vol., 168 pp.

- Scharpenseel, H.W., 1972. Natural radiocarbon measurements on humic substances in the light of carbon cycle estimates. In: *Proceedings of the International Meeting on Humic Substances*, Nieuwershuis, 1972. Pudoc, Wageningen, pp. 281—292.
- Scharpenseel, H.W., 1975. Relativer und Sukzession von Fraktionen der organischen Bodensubstanz. *Mitt. Dtsch. Bodenk. Ges.*, 22: 453—466.
- Scharpenseel, H.W. and Pietig, F., 1968/69. Einfache Boden- und Wasserdatierung durch Messung der ^{14}C - oder Tritiumkonzentration. *Geoderma* 2: 273—289.

CHANGES IN SURFACE STRUCTURE (CRUSTING) AFTER APPLICATION OF SEWAGE SLUDGE AND PIG SLURRY TO CULTIVATED AGRICULTURAL SOILS IN NORTHERN ITALY

M. PAGLIAI, E.B.A. BISDOM and S. LEDIN

C.N.R. — Institute for Soil Chemistry, 78-Pisa (Italy)

Netherlands Soil Survey Institute, 6700 AB Wageningen (The Netherlands)

Department of Soil Sciences, Swedish University of Agricultural Sciences, S-75007 Uppsala 7 (Sweden)

(Accepted for publication February 17, 1983)

ABSTRACT

Pagliai, M., Bisdom, E.B.A. and Ledin, S., 1983. Changes in surface structure (crusting) after application of sewage sludge and pig slurry to cultivated agricultural soils in northern Italy. *Geoderma*, 30: 35–53.

The first results of a cooperative research project on changes in cultivated agricultural topsoils after treatment with sewage sludge and pig slurry are discussed for a silty clay soil (Vertic Xerochrept) and a sandy loam soil (Typic Psammaquent). Such changes are expressed in the surface structure, including crusts, of the soils and have a direct effect on their fertility. To measure these changes, special attention was paid to porosity characteristics; especially increases in porosity after application of organic manures to agricultural soils with crusting problems. Light microscopy, SEM-EDXRA (scanning electron microscopy — energy dispersive X-ray analysis) and Quantimet (electro-optical image analysis) were applied and allowed quantitation and visualisation of pores. Initial results clearly demonstrate that the porosity of the topsoil increased after treatment with urban refuse or pig slurry and that crusting decreased.

INTRODUCTION

This cooperative research project of IWGSUSM (International Working Group on Submicroscopy of Undisturbed Soil Materials) was started to determine the effect of the application of livestock effluents and sewage sludges on the structure of Italian soils with crusting problems. Soil crusting in cultivated soils is one of the most dangerous phenomena in Italy both from an agronomic and a soil erosion point of view. The main effects of a soil crust are: reduction of water infiltration, increase in run-off, reduction of gas exchange between the soil and atmosphere, and interference with seed germination.

Many authors have studied the structure and the mechanism of formation of soil crusts (McIntyre, 1958; Evans and Buol, 1968; Epstein and Grant, 1973; Falayi and Bouma, 1975; Pagliai and La Marca, 1979; Pagliai et al.,

1981b; Jongerius, 1981). According to the mechanism of formation, two types of crusts can be distinguished, i.e. those formed as a result of raindrop impact (structural crusts), and those formed by translocation of fine particles and their deposition at a certain distance from their original location (depositional crusts) (Chen et al., 1980).

The principal reason for crust formation in cultivated soils is poor stability of soil aggregates upon which the impact of raindrops causes detachment of constituents. The instability of aggregates is higher the lighter the texture of the soil and the lower its organic matter content. This small amount of organic matter is caused by a severe shortage of manure and by intensive cultivations which replaced the traditional farming rotations. Moreover, heavy rainfall followed by a strong and dry wind is normal in the Po area of northern Italy and the decomposition rate of organic matter is high in the Italian climate. For these reasons, sources of organic matter had to be found, i.e. livestock effluents and sewage sludges in which the organic matter accounts for about 50% of the sludge dry matter. The area with intensive cultivation is increasing in Italy and due to a severe shortage of manure, the use of sewage sludge and pig slurry has become increasingly popular.

This study has been carried out with an in situ investigation of unhardened soil peds and crusts by SEM (scanning electron microscope) and by examination of soil materials in thin sections with the light microscope, SEM-EDXRA (scanning electron microscope — energy dispersive X-ray analyzer) and Quantimet 720 (electro-optical image analyzer). Special attention was paid to the upper 5 cm of the soil, especially to porosity changes related to the application of manure and sewage sludge.

The present paper is the first of a series. Only some of the samples have been examined with all techniques so far, viz. the upper part of a silty clay soil — treated with 300 m³/ha of pig slurry — by light microscopy, SEM-EDXRA and Quantimet; and a sandy loam soil — treated with compost of anaerobic sludge and the organic fractions (20–80%) of urban refuse (CANS in Table I) — by light microscopy and Quantimet. Samples of control plots of both soils were also investigated with the light microscope and Quantimet.

EXPERIMENTAL PLOTS AND SAMPLING

Two soils with a strong tendency to form surface crusts were chosen for experiments with pig slurry and sewage sludge. A silty clay soil (Vertic Xerochrept) and a sandy loam soil (Typic Psammaquent) were planted with corn in May 1980. Pig slurry was applied in June to the silty clay, about one month after the corn was sown, whereas the sewage sludge had been ploughed into the sandy loam before May 1980.

This experiment with silty clay soils was carried out on four plots of 1 ha each. 1 ha represented the control of the Vertic Xerochrept and the other 3 ha were treated with different amounts of pig slurry. 1 ha of the silty clay soil received 100 m³, a second 200 m³ and the third experimental plot 300

m³ of livestock effluent. Surface samples of the Vertic Xerochrept were taken at the end of September.

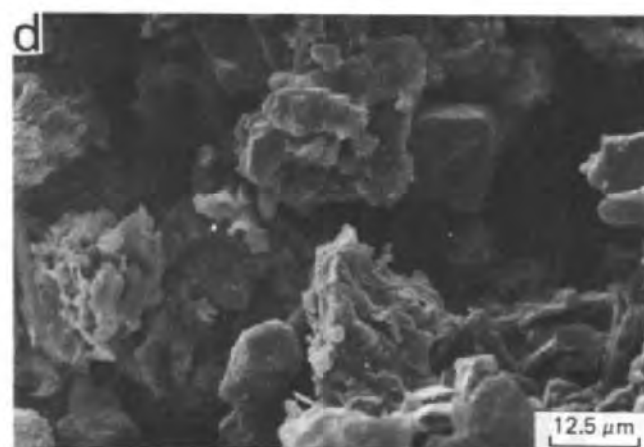
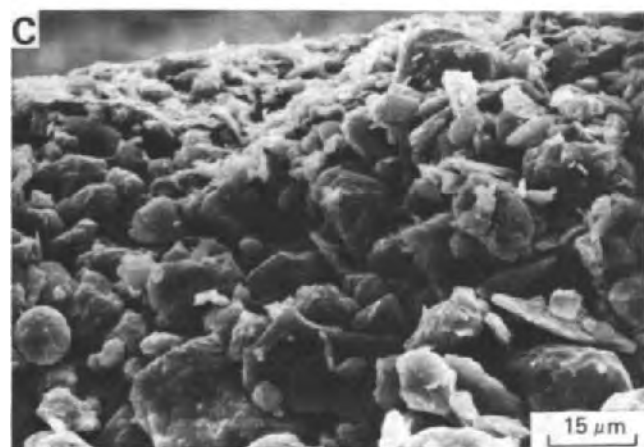
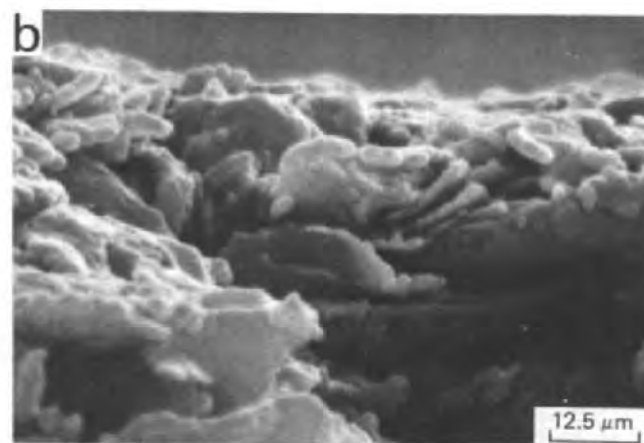
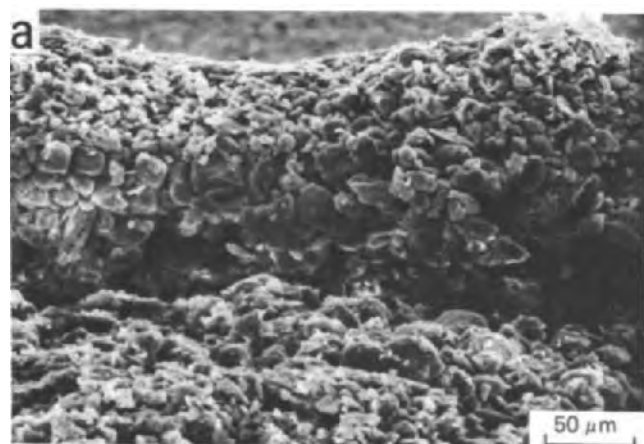
The experimental plots on the sandy loam soil (Typic Psammaquent) were each 500 m². Six of these plots were studied, viz. one control plot, four plots which were given different types of sewage sludge, and one plot that was treated with manure. The four sewage sludges differed in composition and were applied in quantities that were equivalent to 50 tons/ha of manure on an organic carbon basis. The four sludges consisted of aerobic sludge (AS), anaerobic sludge (ANS), a compost of aerobic sludge and the organic fraction (40–60%) of urban refuse (CAS), and a compost of anaerobic sludge and the organic fraction (20–80%) of urban refuse (CANS). The sixth plot was treated with manure (M). Surface samples of the sandy loam soil were taken four months after the application of the sewage sludges, i.e. at the beginning of September.

SEM STUDY OF UNHARDENED SOIL MATERIAL

A scanning electron microscope (SEM) study was made of small pieces of the uppermost part of the silty clay soil which was treated with 300 m³/ha pig slurry. The secondary electron images (SEI) of pieces of the treated soil were compared with pieces of the crust of the control soil, i.e. in and below the dense part of its surface crust. The pieces of soil were attached to stubs with silver, coated with gold to give conductivity to the insulating material and studied by SEM. To obtain the right position of the soil pieces on the stubs these were oriented with the help of stereo microscope and examined with a Jeol 25S3 scanning electron microscope.

A surface sample of the control plot was broken with pliers to observe the microstructure of the crust (Fig.1). Three microlayers were distinguishable (Fig.1a), viz. a very thin top part, a middle part which was much thicker, and a lower part of which only the upper section and surface is portrayed in the foreground. These three microlayers had different compositions. The top part was comprised of fine clayey particles (Fig.1b) which were arranged in platy and other structures. Silt-sized particles were dominant in the middle microlayer of the crust which was rather clean and fairly free from adhering clay particles (Fig.1c). A mixture of coarser and finer particles is distinguishable in the lower part of the crust (Fig.1d).

The crust had formed on nearly horizontal soil surfaces and the following mechanism of crust formation could be envisaged. Raindrop impact is believed to be the principal force in the formation of this type of crust which was called structural crust in the introduction. The raindrops, when hitting the very top of the soil, separate the finest particles from the silt and sand which may also move over short distances. The smallest particles such as single clay minerals, somewhat larger entities and organic materials, are kept in a dispersed state as long as the rain continues. Water fills every pore and stands a few millimetres above the surface of the soil because the



infiltration rate is so low that accumulation of water takes place. When the rain stops, the finest material sediments on top of the silt and sand particles. These coarser particles function as a filter and do not allow small particles to follow the downward movement of percolating water. When the soil dries, all particles are brought closer together and kept that way by attraction forces and in the dry state these will affect the clay particles strongest. Small particles can be brought very close to each other and Van der Waal's forces will be active; the formation of cation bridges and edge-surface attraction is also possible. As long as the crust is dry the short range attraction forces will remain active.

When 300 m³/ha pig slurry is put onto the silty clay soil, SEM micrographs show that crust formation will continue and that the process as such remains the same. However, straw fragments (Fig.2a), pig hairs (Fig.2b) and other organic materials are able to break up the crust (Fig.2c). The results can be compared with secondary electron images (SEI) of the crust in the control soil, a top view of which is given at the same magnification in Fig.2d.

To allow a continuous view of the upper 0.6 mm of the crust in the control plot, a photo-montage was made (Fig.3). The very thin top part with fine clayey material is somewhat less expressed than in Fig.1c and maximally a few microns thick. It is underlain by the relatively clean middle part of the crust up to about 0.15 mm depth. This microlayer of silt-sized particles, without many adhering clay particles, is followed by the lower part of the studied crust in which a mixture of particles occurs.

LIGHT MICROSCOPY OF THIN SECTIONS

Undisturbed soil samples were taken from the upper 5 cm of a Vertic Xerochrept (silty clay soil) and of a Typic Psammaquent (sandy loam soil). At sampling time, in September, the soils were so dry that further shrinkage was almost negligible. Both the control samples and the samples treated with pig slurry (silty clay soil) or sewage sludge (sandy loam soil) were air-dried at room temperature. Samples were subsequently impregnated and made into thin sections.

The larger part of the upper 5 cm of both soils is portrayed in Figs.4 and 5 (Vertic Xerochrept) and Figs. 6—9 (Typic Psammaquent). Samples treated with organic material are shown in Figs. 5 and 9.

Fig.1. SEM micrographs of unimpregnated crust of the control plot on silty clay. The fine clayey material of the Vertic Xerochrept is only a few microns thick at the surface (a). Detail of the fine clayey material (b). The very thin surface part of the crust is underlain by relatively clean silty particles (c). A mixture of silt and clay can be found in the lower part of the crust (d).

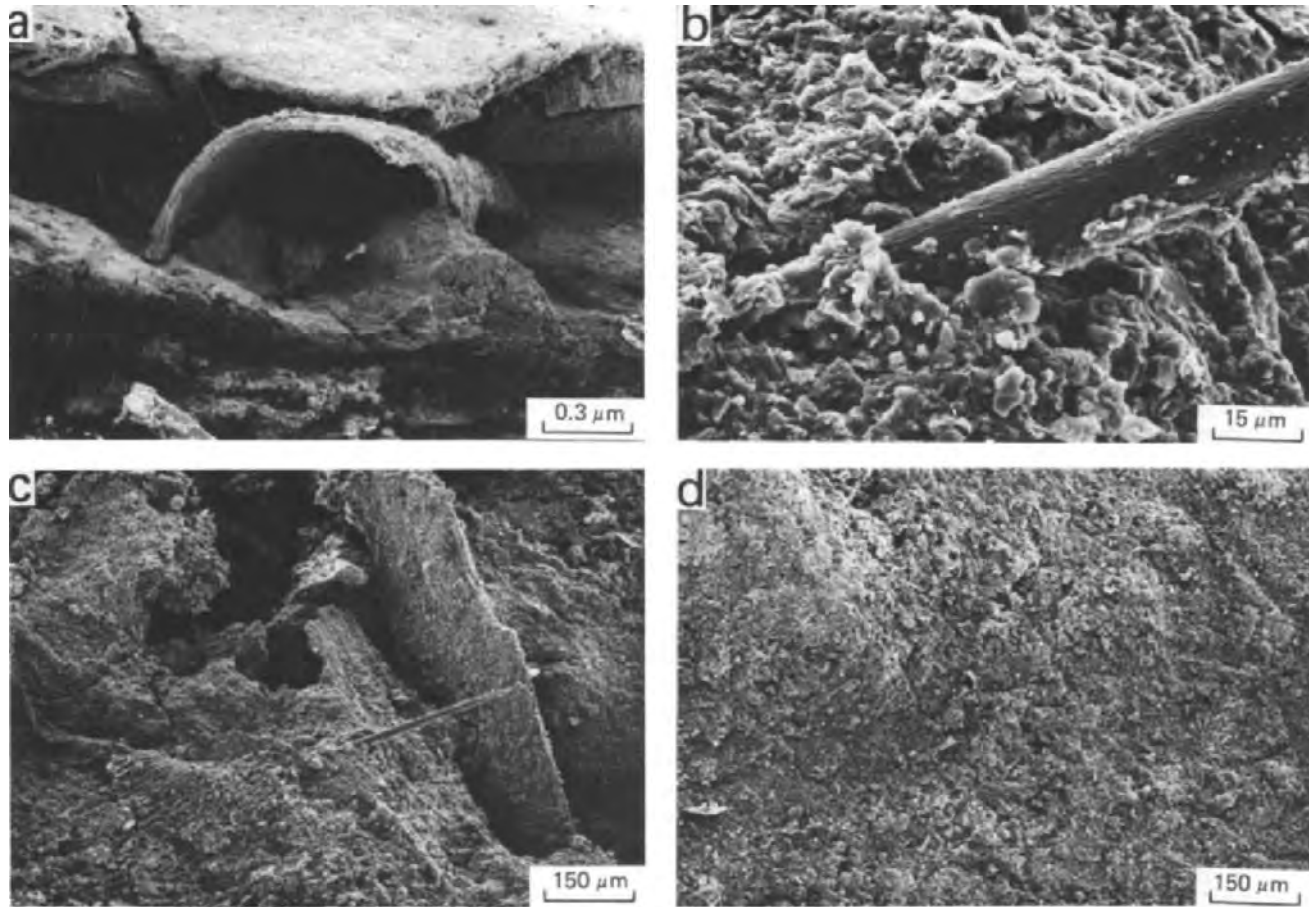


Fig.2. SEM micrograph of a straw fragment (a) and a pig hair (b). The broken crust of the silty clay soil after treatment (c) and before (d).

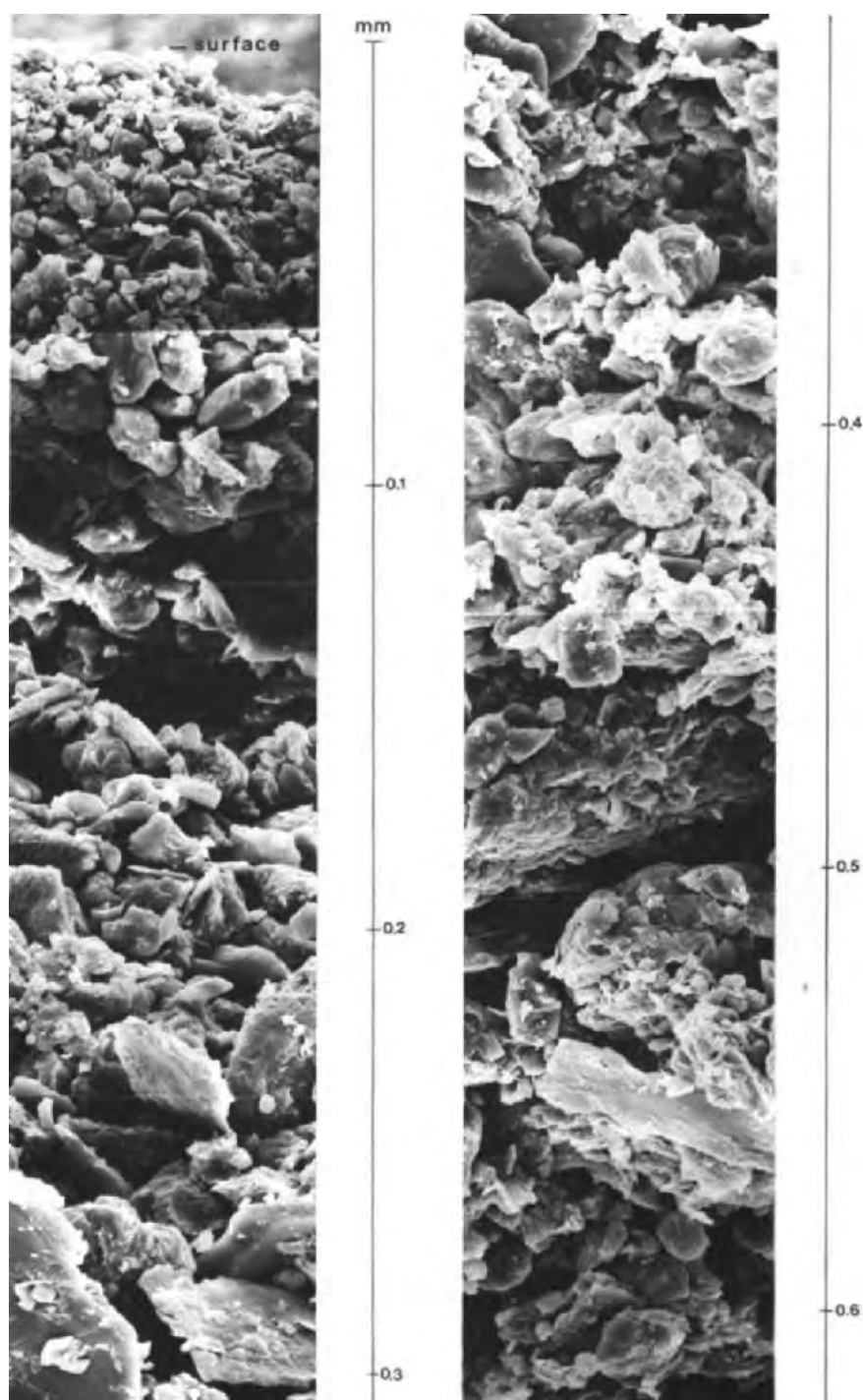


Fig.3. SEM view of about 0.6 mm crust. The same differentiation as given in Fig. 1 can be discerned, viz. a very thin surface layer, rather clean silt underneath, and a mixture of silt and clay particles below 0.15 mm depth. Untreated soil.

LIGHT MICROSCOPY OF THE SILTY CLAY SOIL

No continuous very thin top part is distinguishable in the surface crust of the Vertic Xerochrept in Fig. 4 at this small magnification. The same part of the crust, however, was clearly indicated on SEI taken by SEM (Fig.1) and proved to be a few microns thick. A pronounced platy structure (Fig.4) is present in the control plot of the silty clay soil as indicated by the sub-horizontal fractures. Some orientation of the soil particles was seen with crossed polarizers at the top of the soil and adjacent to the horizontal fractures.

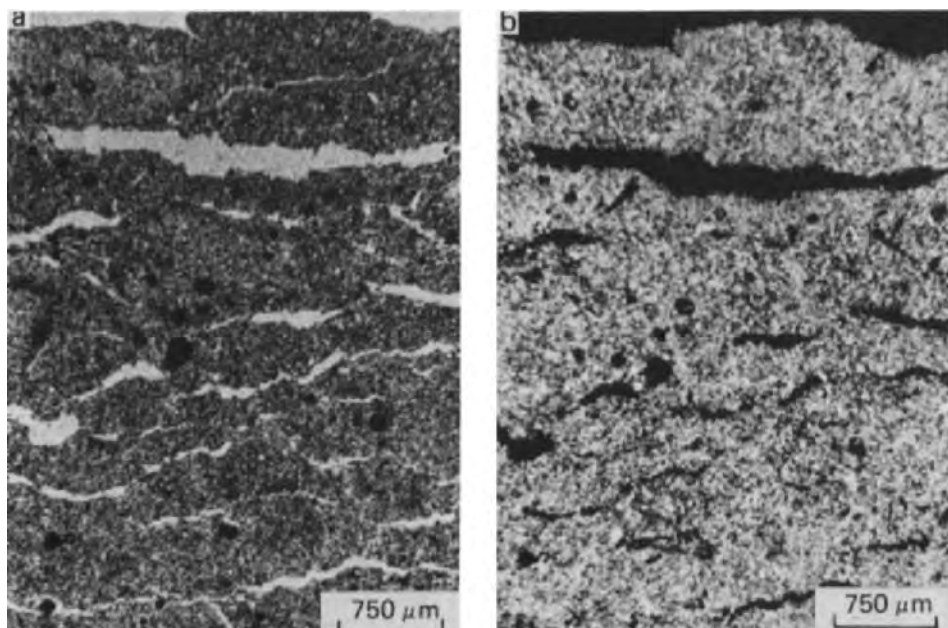


Fig.4. Platy structure in untreated silty clay crust of a Vertic Xerochrept. Differences in structure are difficult to establish at this small light microscopic magnification. Plane polarized light (a) and crossed polarizers (b).

A representative area of a thin section from soil treated with 300 m³/ha of pig slurry is shown in Fig.5. Compared with the untreated soil, a significant increase in porosity was discernable. This was thought to be the case after land spreadings of pig slurry but has now been visualised. Usually, all the large pores had an irregular shape. The adhesion of soil particles to organic materials seemed evident. Cracks and microcracks were also formed in the thin crust and these are of importance for improved water infiltration.

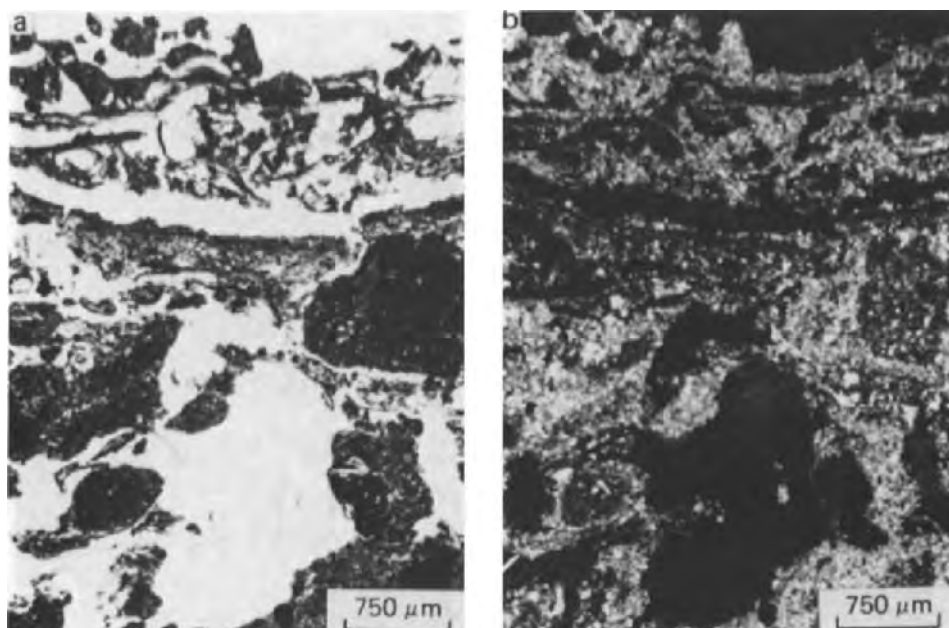


Fig. 5. The silty clay crust of Fig.4 was broken after treatment with pig slurry and considerable macroporosity developed. Plane polarized light (a) and crossed polarizers (b).

LIGHT MICROSCOPY OF THE SANDY LOAM SOIL

Light microscopy of the Typic Psammaquent shows more variability in structure than the silty clay soil. A certain microlayering can be observed in Fig.6, starting with coarser material and ending with clayey material at the top and at the end of a cycle of sedimentation. On the present surface of the soil, just above the latest sedimented clay lammella, the start of a new sedimentation cycle can be discerned and is indicated by a microlayer of sandy material. A small gully-like structure is present in the lower half of Fig.6a.

The topography of the soil surfaces in the experimental plots is virtually flat and it has been indicated above that the impact of raindrops is considered to be the main force that separates the soil particles in poorly stable aggregates. Fig.6, however, demonstrates that small-scale sedimentation processes also do occur in furrows and puddles. Entrapped air may be present below a surface sealing of muddy material, and vesicles can form (Fig. 7). In this case, carbon dioxide liberated by biological activity from organic material added to the soil, may play a role in the formation of vesicles. Such vesicles can collapse at deeper levels (Fig.7a) or remain intact (Fig.8). One difference between the bottom part of the two figures is the presence of a clay lammella in Fig.8 and its absence in Fig.7. It should be noted

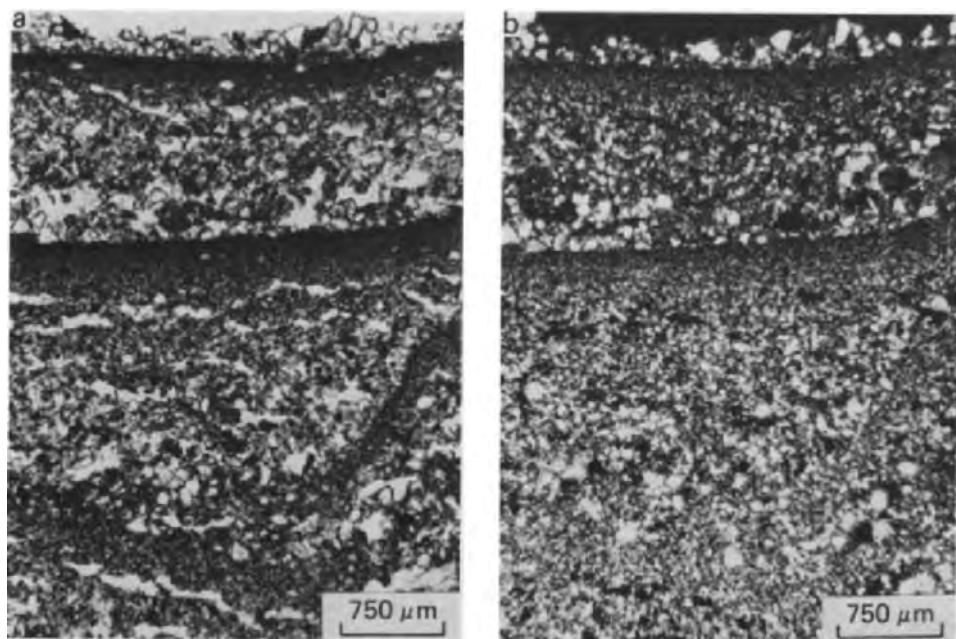


Fig.6. Two undisturbed layered crusts in sandy loam of an untreated Typic Psammaquent. A new cycle is started at the surface with the deposition of sandy material. Near the bottom of the micrograph there is a gully-like structure, a possible origin of which is described in the text. Plane polarized light (a) and crossed polarizers (b).

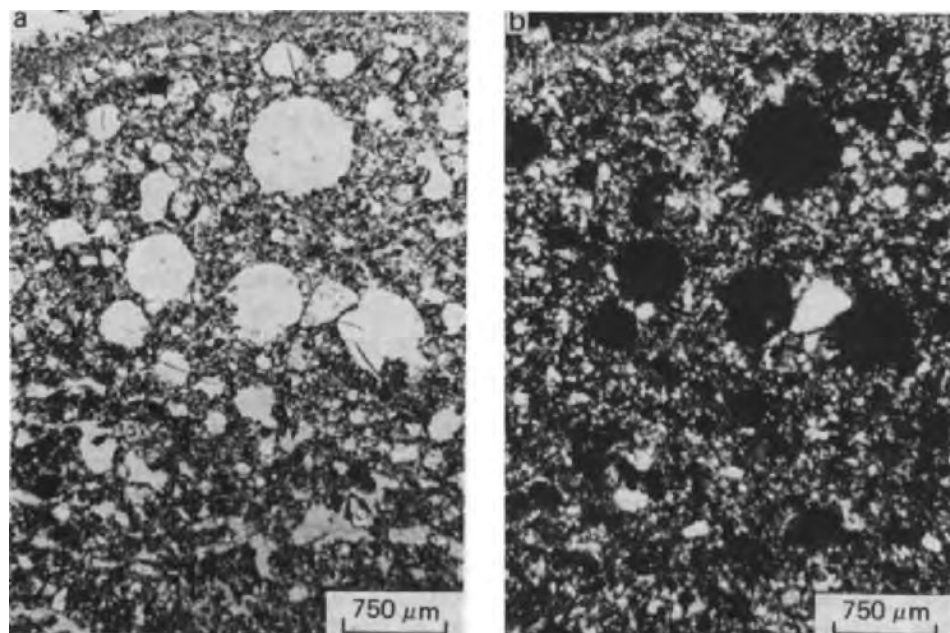


Fig.7. Vesicles and sealing-layer in sandy loam. Collapsed vesicles at the bottom of the micrograph. Plane polarized light (a) and crossed polarizers (b). Untreated Typic Psammaquent.

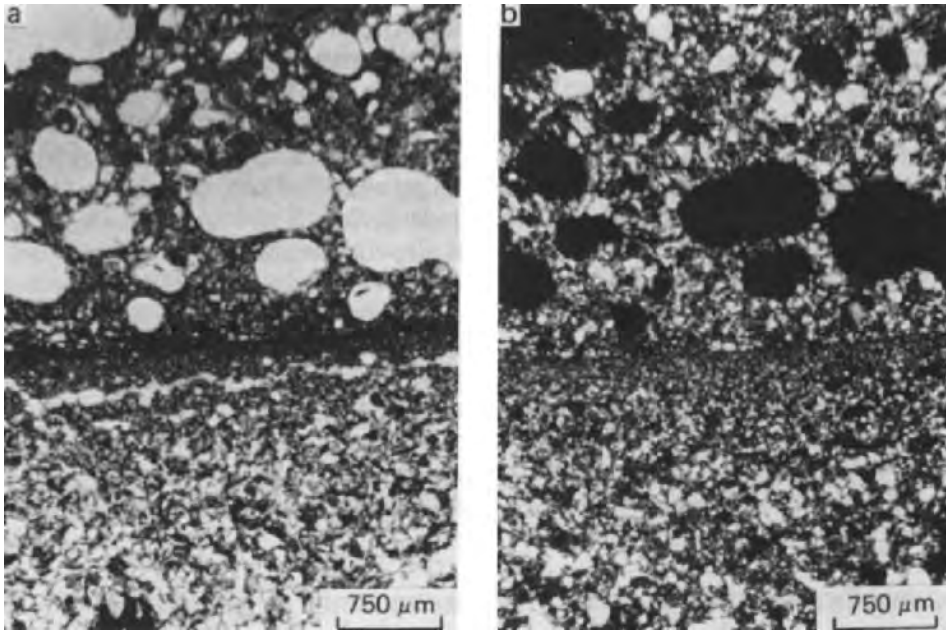


Fig.8. Uncollapsed vesicles in Typical Psammaquent. These are present above a clay lamella in the centre of the micrograph. Plane polarized light (a) and crossed polarizers (b). Untreated soil.

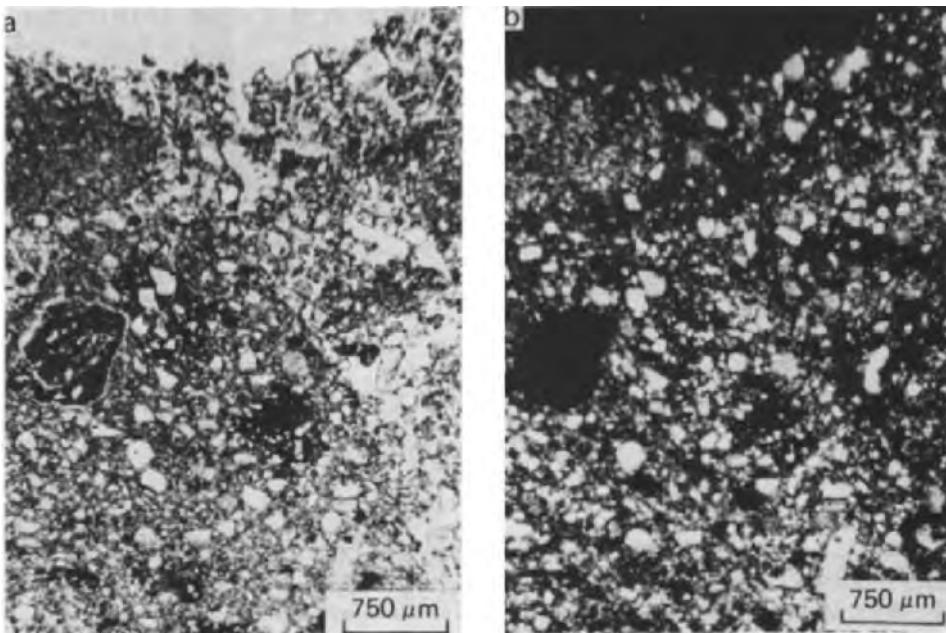


Fig.9. Sandy loam of a Typical Psammaquent treated with sewage sludge. Macro-porosity is mainly visible in the form of vertical cracks or channel-shaped pores. Plane polarized light (a) and crossed polarizers (b).

that Miller (1971) and Kemper and Miller (1974) regard the presence of vesicles in the topsoil as an indication of an unstable and transitory structure helped by a poor stability of soil aggregates.

The other types of pores in Figs.6—8 are often elongated in a subhorizontal direction. These pores have irregular walls. The elongated pores are well expressed underneath the lammellae with fine soil material in Figs.6 and 8, while they also occur at the bottom part of Fig.7. A special type of pore, related to the collapse of vesicles, is also discernable in the latter figure.

When the sandy loam was treated with sewage sludge (Fig.9) considerable changes occurred in the surface part of the Typic Psammaquents. Part of the centre of the silty clay crust on the surface of the soil and the silty layer underneath have newly formed pores. Channel-type pores are, for example, visible at the right hand side of Fig.9b. These pores could also be observed in the field and are therefore regarded as predominantly natural ones. Frequently, however, such channel-type pores or cracks are regarded as artificial, caused by drying during sample preparation or by movements during sampling.

QUANTIMET MEASUREMENTS OF THE LARGER PORES IN THIN SECTIONS

Larger pores, with diameters larger than 30 μm , were measured in the upper 5 cm of the silty clay soil and the sandy loam soil using combined light microscopic and Quantimet techniques. These techniques were described by Jongerius (1974, 1975), Jongerius et al. (1972, 1979), Ismail

TABLE I

Effect of treatments on porosity of the soil surface layer (0—5 cm); data are the means of three and five replications, respectively for the silty clay soil and for the sandy loam soil

Treatments	Rounded pores (%)	Irregular pores (%)	Elongated pores (%)	Total porosity (%)
<i>Silty clay soil</i>				
Control	0.3	2.8	6.7	9.8 (± 1.1)
300 m ³ /ha of pig slurry	3.0	18.7	9.4	31.1 (± 2.3)
<i>Sandy loam soil</i>				
Control	2.4	8.2	7.3	17.9 (± 1.6)
CANS	1.2	20.5	11.4	33.1 (± 1.2)

CANS stands for: Compost of anaerobic sludge and the organic fraction of urban refuse (20—80%). The quantity applied was equivalent to 50 tons/ha of manure on an organic carbon basis.

Numbers between parentheses represent the standard error.

(1975) and Murphy et al. (1977a, b). Such Quantimet measurements of porosities in thin sections were correlated by Bouma et al. (1977, 1979) with the saturated hydraulic conductivity of heavy clays.

Quantimet measurements are usually necessary to characterise pore systems in thin sections. Some of the results of such measurements are given in Table I for the silty clay and sandy loam soil, i.e. porosity characteristics of the upper 5 cm of the control plots and of treated plots. Although this is a rather rough approach to porosity measurements, the table serves to illustrate some differences between the porosities of the control and treated plots. These measurements will be refined when more thin sections become available and submicroscopic imaging can be used on a larger scale, i.e. backscattered electron scanning images (BESI) which are measured by Quantimet (Bisdorn and Thiel, 1981; Jongerius and Bisdorn, 1981).

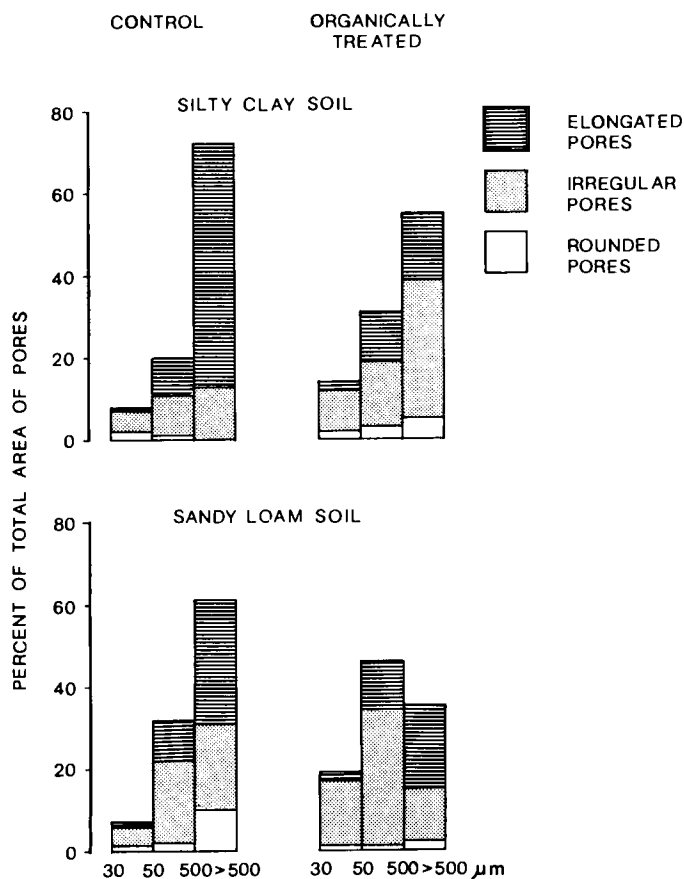


Fig.10. Distribution of the size and shape of pores larger than 30 μm before and after treatment with organic matter.

The total porosity of the studied micrographs, made with a light microscope, was determined by Quantimet and shape groups of pores distinguished, viz. rounded, irregular and elongated pores. Such shape groups can be found by measuring the area (A) and the perimeter (Pe) of the pores and by working with A/Pe^2 ratios. Rounded pores have $A/Pe^2 > 0.04$, irregular pores A/Pe^2 from 0.04 to 0.015, and elongated pores have $A/Pe^2 < 0.015$ (Bouma et al., 1977). The pores of each shape group were subsequently subdivided into three size classes, viz. 30–50 μm , 50–500 μm and $> 500 \mu\text{m}$ (Fig.10). This was done for rounded and irregular pores according to the equivalent pore diameter, whereas the width, calculated from area and perimeter data, was used for elongated pores.

In the present study only preliminary results of Quantimet measurements can be given. The measurements confirm that plots treated with organic debris have a higher porosity than control plots. The total porosity increased from 9.8% (control plot) to 31.1% (plot treated with 300 m^3/ha of pig slurry) in the Vertic Xerochrept and from 17.9% (control plot) to 33.1% (plot treated with anaerobic sludge and urban refuse) in the Typic Psammaquent (Table I).

The treated plots contained less pores larger than 500 μm than the control plots (Fig.10), whereas the number of pores smaller than 500 μm increased in the size classes 30–50 μm and 50–500 μm . Quantimet measurements also indicated that the decrease in pores larger than 500 μm was principally given by the reduction of elongated pores with respect to the control. This means that the organic fertilizers were able to reduce cracks which originated by shrinkage (Pagliai et al., 1981a). When rounded pores of Table I are compared with percentages of rounded pores in Fig.10, it is shown that large rounded pores occur mainly in plots of the silty clay soils which were treated with pig slurry, whereas they were present in the control plot of sandy loam soils. The percentage of irregular pores increased in all organically treated plots with one exception; pores larger than 500 μm in the sandy loam soil treated with sewage sludge.

BACKSCATTERED ELECTRON SCANNING IMAGES OF POLISHED BLOCKS AND THIN SECTIONS

Backscattered electron scanning images (BESI) were made of one sample-block of silty clay treated with 300 m^3 of pig slurry. This block represented the upper 5 cm of a Vertic Xerochrept of which the surface crust had become broken and more porous. The present BESI micrographs only represent a few examples of what can be done with this submicroscopic technique on polished blocks and thin sections. High quality micrographs can be obtained of various materials and porosities (Bisdorn and Thiel, 1981). With this technique one can easily obtain images of such quality that even pores with a diameter smaller than 0.1 μm become measurable by Quantimet (Jongerijs and Bisdorn, 1981). If in situ microchemical analysis is also neces-

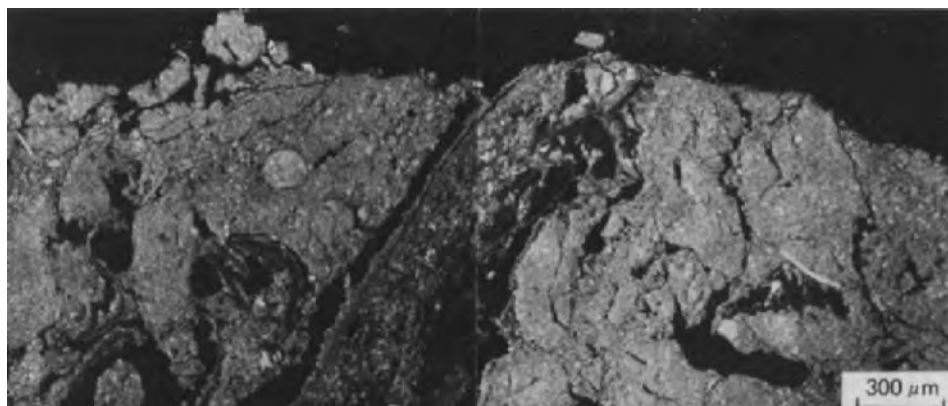


Fig.11. Backscattered electron scanning image (BESI) of the silty clay crust treated with pig slurry. Organic matter may take up a position which breaks the crust.

sary, a number of submicroscopic techniques are available (cf. review articles by Bisdorf, 1981a, b).

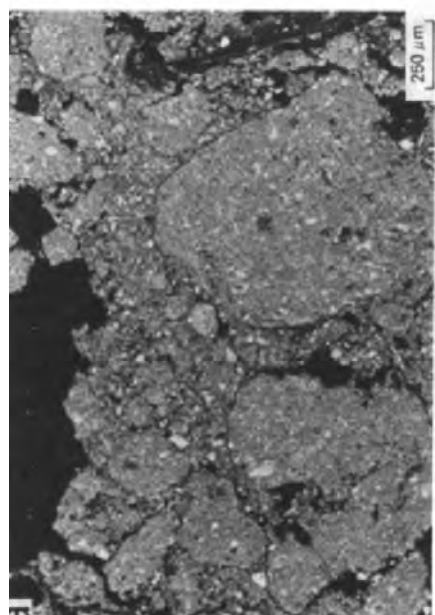
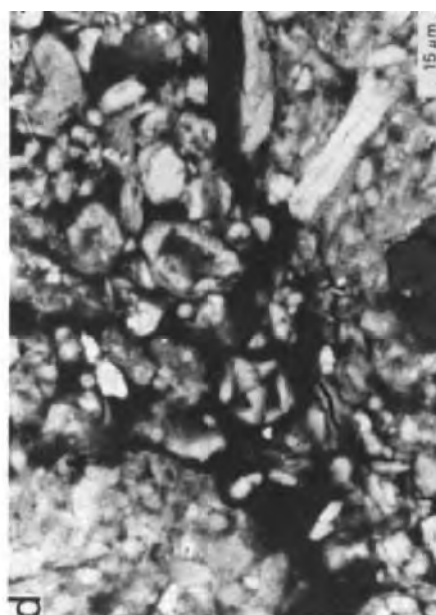
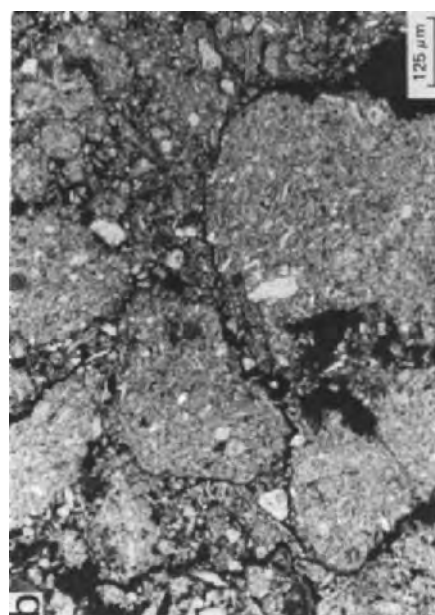
The present sample-block forms part of a series of which thin sections are currently being made. These allow microscopic and submicroscopic visualisation of the effects of crust formation and destabilisation processes, if present. For the moment only a few micrographs are given of the surface of the loosened crust (Fig.11), of part of the former crust at various magnifications (Fig.12), and of pig slurry which was found 2 to 3 cm below the surface of the Vertic Xerochrept (Fig.13). These and other BESI images indicate that the organically treated crust is very heterogeneous in a horizontal and vertical direction.

CONCLUSIONS

Light microscopy, electron microscopy and Quantimet 720 were used to study the behaviour of surface crusts of Vertic Xerochrepts and Typic Psammaquents in experimental plots from Italy before and after treatment with pig slurry and sewage sludge. Only the initial part of our cooperative research project has been completed and therefore only first results are discussed in this paper.

SEM observation of unhardened pieces of untreated crust from the silty clay soil demonstrated that the upper 0.6 mm of the 5 cm thick surface crust could be subdivided into three microlayers. The uppermost microlayer was comprised of clayey material and was only a few micrometres thick. The underlying silty microlayer was about 0.15 mm thick. The lower microlayer consisted of a mixture of predominantly silt and clay. The microlayers are thought to have formed as a result of raindrop impact and the effects of wetting and drying of the soil together with small-scale sedimentation processes.

Light microscopy of the 5 cm thick surface crust of the sandy loam soil demonstrated the existence of various cycles of sedimentation. Each cycle



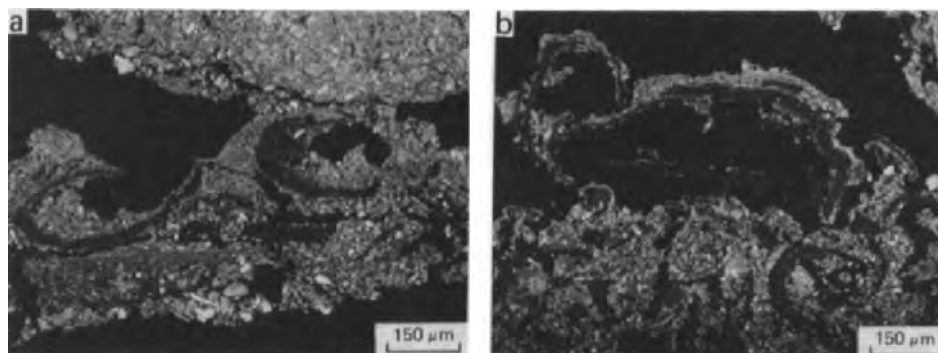


Fig.13. Pig slurry (a) and (b) has also been found some centimetres below the surface. A variety of forms in the organic matter are indicated by BESI.

started with coarser material and ended with clayey material. Microlayering, although observed by SEM, was far less present in silty clay soil. Sub-horizontal fractures indicated the presence of platy structures in the crusts of Vertic Xerochrepts.

Porosity changes, going from untreated to treated plots, can be observed on micrographs from light microscopy or electron microscopy. The attention is mainly attracted by larger pores and cracks but it is hard to obtain good insight into the total porosity if no Quantimet techniques are involved. As a consequence mistakes can be made. In the present case only rough Quantimet measurements are involved because additional thin sections must be prepared for combined BESI and Quantimet investigation. It is clear, however, that the increased porosity, after treatment of the soil crust with organic matter, could be documented by Quantimet and light microscopy. Pores larger than $500\text{ }\mu\text{m}$ decreased in number after treatment of the crust, largely because of a reduction in elongated pores. The percentage of irregular pores increased in most organically treated plots.

Future research will concentrate on the study of all samples with more emphasis on submicroscopic techniques to supply backscattered electron scanning images for Quantimet measurement of capillary and larger pores. More secondary electron images will also be made of unhardened soil materials in treated and untreated crusts. When all thin sections are ready in the three laboratories, more light microscopic information will also become available. The combination of the three techniques will allow better insight into the effects of different organic materials on crust formation, especially on porosity development.

Fig.12. BESI of the crust of a Vertic Xerochrept treated with pig slurry (a). Some organic fragments of pig slurry are visible. Microporosity can also be studied by Quantimet if the black pores are measured in micrographs (b) to (d).

REFERENCES

- Bisdom, E.B.A., 1981a. A review of the application of submicroscopic techniques in soil micromorphology, I. Transmission electron microscope (TEM) and scanning electron microscope (SEM). In: E.B.A. Bisdom (Editor), *Submicroscopy of Soils and Weathered Rocks*. 1st Workshop of the International Working-Group on Submicroscopy of Undisturbed Soil Materials (IWGSUSM) 1980, Wageningen. Centre for Agricultural Publishing and Documentation (Pudoc), Wageningen, pp. 67–116.
- Bisdom, E.B.A., 1981b. A review of the application of submicroscopic techniques in soil micromorphology, II. Electron microprobe analyzer (EMA), scanning electron microscope — energy dispersive X-ray analyzer (SEM-EDXRA), laser microprobe mass analyzer (LAMMA 500), electron spectroscopy for chemical analysis (ESCA), ion microprobe mass analyzer (IMMA), and the secondary ion microscope (SIM). In: E.B.A. Bisdom (Editor), *Submicroscopy of Soils and Weathered Rocks*. 1st Workshop of the International Working-Group on Submicroscopy of Undisturbed Soil Materials (IWGSUSM) 1980, Wageningen. Centre for Agricultural Publishing and Documentation (Pudoc), Wageningen, pp. 117–162.
- Bisdom, E.B.A. and Thiel, F., 1981. Backscattered electron scanning images of porosities in thin sections of soils, weathered rocks and oil-gas reservoir rocks using SEM-EDXRA. In E.B.A. Bisdom (Editor), *Submicroscopy of Soils and Weathered Rocks*. 1st Workshop of the International Working Group on Submicroscopy of Undisturbed Soil Materials (IWGSUSM) 1980, Wageningen. Centre for Agricultural Publishing and Documentation (Pudoc), Wageningen, pp. 191–206.
- Bouma, J., Jongerius, A., Boersma, O., Jager, A. and Schoonderbeek, D., 1977. The function of different types of macropores during saturated flow through four swelling soil horizons. *Soil Sci. Soc. Am. J.*, 41(5): 945–950.
- Bouma, J., Jongerius, A. and Schoonderbeek, D., 1979. Calculation of saturated hydraulic conductivity of some pedal clay soils using micromorphometric data. *Soil Sci. Soc. Am. J.*, 43(2): 261–264.
- Chen, Y., Tarchitzky, J., Brouwer, J., Morin, J. and Banin, A., 1980. Scanning electron microscope observations on soil crusts and their formation. *Soil Sci.*, 130(1): 49–55.
- Epstein, E. and Grant, W.J., 1973. Soil crust formation as affected by raindrop impact. In: *Ecological Studies*, 4. *Physical Aspects of Soil Water and Salts in Ecosystems*, pp. 195–201.
- Evans, D.D. and Buol, S.W., 1968. Micromorphological study of soil crusts. *Soil Sci. Soc. Am. J.*, 32: 19–22.
- Falayi, O. and Bouma, J., 1975. Relationships between the hydraulic conductance of surface crusts and soil management in a Typic Hapludalf. *Soil Sci. Soc. Am. J.*, 39: 957–963.
- Ismail, S.N.A., 1975. Micromorphometric soil-porosity characterization by means of electro-optical image analysis (Quantimet 720). *Neth. Soil Surv. Inst.*, Wageningen, *Soil Surv. Pap.*, 9: 104 pp.
- Jongerius, A., 1974. Recent developments in soil micromorphology. In: G.K. Rutherford (Editor), *Soil Microscopy*. *Proceedings of the Fourth International Working-Meeting on Soil Micromorphology*, Kingston, 1973. The Limestone Press, Kingston, Ont., pp. 67–83.
- Jongerius, A., 1975. Micromorphometric soil analysis by means of Quantimet 720. In: *Fortschritte der quantitativen Bildanalyse, Vorträge des IMANCO-Symposiums*, pp. 161–185.
- Jongerius, A., 1981. Micromorphological applications in agricultural research. *International Working-Meeting on Soil Micromorphology*. London, 1981. In press.

- Jongerius, A. and Bisdorf, E.B.A., 1981. Porosity measurements using the Quantimet 720 on backscattered electron scanning images of thin sections of soils. In: E.B.A. Bisdorf (Editor), *Submicroscopy of Soils and Weathered Rocks*. 1st Workshop of the International Working-Group on Submicroscopy of Undisturbed Soil Materials (IWG-SUSM) 1980, Wageningen. Centre for Agricultural Publishing and Documentation (Pudoc), Wageningen, pp. 207–216.
- Jongerius, A., Schoonderbeek, D. and Jager, A., 1972. The application of the Quantimet 720 in soil micromorphology. *The Microscope*, 20: 243–254.
- Jongerius, A., Schoonderbeek, D. and Bouma, J., 1979. Micromorphometric image analysis of flow patterns in swelling clay soils. In: *Proceedings of the Quantimet-Symposium on Advances of Quantitative Image Analysis*. *Microsc. Acta*, Suppl., 3: 115–120.
- Kemper, W.D. and Miller, D.E., 1974. Management of crusting soils: some practical possibilities. In: J.W. Cary and D.D. Evans (Editors), *Soil Crusts*. Agric. Exp. Sta., Univ. Ariz., Tech. Bull., 214: 1–6.
- McIntyre, D.S., 1958. Soil splash and the formation of surface crusts by raindrop impact. *Soil Sci.*, 85: 261–266.
- Miller, D.E., 1971. Formation of vesicular structure in soil. *Soil Sci. Soc. Am. J.*, 35(4): 635–637.
- Murphy, C.P., Bullock, P. and Turner, R.H., 1977a. The measurement and characterisation of voids in soil thin sections by image analysis, I. Principles and techniques. *J. Soil Sci.*, 28(3): 498–508.
- Murphy, C.P., Bullock, P. and Biswell, K.J., 1977b. The measurement and characterisation of voids in soil thin sections by image analysis, II. Applications. *J. Soil Sci.*, 28(3): 509–518.
- Pagliai, M. and La Marca, M., 1979. Micromorphological study of soil crusts. *Agrochimica*, 23(1): 16–25.
- Pagliai, M., Guidi, G., La Marca, M., Giachetti, M. and Lucamente, G., 1981a. Effect of sewage sludges and composts on soil porosity and aggregation. *J. Environ. Qual.* In press.
- Pagliai, M., La Marca, M. and Lucamente, G., 1981b. Micromorphological investigation of the effect of sewage sludges applied to soil. *International Working Meeting on Soil Micromorphology*, London, 1981. In press.

This Page Intentionally Left Blank

SUBMICROSCOPIC TECHNIQUES

This Page Intentionally Left Blank

ETCHED THIN SECTIONS FOR COUPLED OPTICAL AND ELECTRON MICROSCOPY AND MICRO-ANALYSIS¹

L.D. NORTON, J.M. BIGHAM, G.F. HALL, and N.E. SMECK

Department of Agronomy, The Ohio State University, Columbus, Ohio (U.S.A.)

(Accepted for publication February 17, 1983)

ABSTRACT

Norton, L.D., Bigham, J.M., Hall, G.F., and Smek, N.E., 1983. Etched thin sections for coupled optical and electron microscopy and micro-analysis. *Geoderma*, 30: 55–64.

Coupled use of optical transmission microscopy and SEM–EDXRA in the study of soil thin sections initially proved difficult because of problems in differentiation of mineral grains and impregnating medium with the secondary electron detector of the SEM. It was also difficult to locate the same small micromorphological features with both techniques, especially when the feature was hidden below the surface of the thin section. A procedure was developed that included selective dissolution (etching) of the impregnating medium and is presented here. After etching, many micromorphological features could be more easily recognized and those immediately below the surface were partially exposed. Application of the procedure proved useful in analyzing bridging plasma too small to identify by optical transmission microscopy that connected silt grains in fragipan horizons.

INTRODUCTION

Optical transmission microscopy (OTM) is a highly refined tool for acquiring two-dimensional optical data from soil thin sections; however, much additional information is often hidden in the 30 μm thickness of the standard thin section. The scanning electron microscope (SEM) offers great depth of field and is capable of supplementing OTM analyses with three-dimensional electron optical data. Unfortunately, the impregnating resin in soil thin sections severely restricts the retrieval of such information. The secondary electron detectors employed on most SEM's provide a colorless image of the thin section surface with little difference in gray-scale between soil fabric and impregnating medium. The featureless surface of the polished thin section makes discrimination of many micromorphological features with SEM difficult and information on the third-dimension attain-

¹ The material presented here was given in part before Division S–5 of the Soil Science Society of America Meetings, December 3, 1981 in Atlanta, Georgia (USA).

able only with specialized equipment. Certainly, procedures whereby micromorphological features in soils could be studied in thin section by OTM and then with enhanced relief by SEM would be of considerable value (Jenkins, 1981).

In a pedologic study involving loess-derived soils with fragipans, micromorphological examination of thin sections at magnifications of 250 X revealed that the fragipans contained plasma connecting silt grains. The arrangement and size of these plasmic bodies did not facilitate identification by light optical techniques (i.e., refractive index, birefringence, interference figures, or dispersion). Therefore, a methodology was developed whereby optical techniques and SEM-EDXRA could be coupled to observe and analyze these and various other micromorphological features in thin section and also observe part of the third dimension.

Similar approaches have been employed by McKeague and Wang (1980) to successfully determine that Al complexed with organic matter was the bonding agent in ortstein horizons of New Brunswick soils, and by McKeague and Protz (1980) to show that Si, Fe, and Al were all present in variable amounts in the cementing material of duripans in British Columbia. In this study, the incorporation of an etching procedure involving partial selective dissolution of the impregnating medium was found to be extremely useful.

After etching, overlapping magnifications of the OTM and SEM facilitated locating and observing the same features with both instruments, and EDXRA added further information on the elemental composition and distribution of elements in the soil fabric. The complementary nature of these techniques (Wilding and Geissinger, 1973) enabled the optical and chemical properties of exposed bridges between skeleton grains in the fragipan to be determined. The main emphasis of this article is to describe the method used and to provide examples related to our study.

MATERIALS AND METHODS

Oriented peds taken from excavated soil pits were dried at 95°C prior to impregnation with Scotchcast #3 epoxy resin using a method similar to that described by Innes and Pluth (1970). The two parts of the resin heated to 95°C were mixed immediately prior to impregnation of the soil at 4 mm Hg pressure. Vacuum was maintained until bubbling ceased. The impregnated samples were cured at 95°C overnight, cooled, cut into blocks, and 5 × 7.5 cm polished thin sections prepared.

After polishing to near 30 μm the thin sections were left uncovered. During observation with OTM a temporary cover slip was applied with refractive oil. Areas of interest on the thin sections were noted, and approximately a 1 cm^2 area was removed by cutting an outline around the area and gently lifting from the glass slide with a razor blade. The specimen was uniquely shaped in order to maintain the known orientation. After rem-

oval from the glass slide the subsections were still quite durable, but were handled with care to avoid dislodging skeletal grains or cracking the fabric.

Selective removal of the impregnating resin was accomplished by placing the specimen in a beaker containing methylene chloride and slowly swirling for approximately 2 minutes at room temperature. The solution was then poured off and the film gently washed with acetone to remove the methylene chloride. Dissolution with methylene chloride constituted our etching in which only part of the epoxy resin was removed from the thin section.

The specimens were mounted for SEM-EDXRA by a method similar to that described by Bisdom et al. (1976) and McKeague and Wang (1980). Prior to mounting, the specimens were photographed under reflected, plane-polarized, and cross-polarized light at low magnifications. Various micro-morphological features of interest were photographed at successively higher magnifications to provide images for helping to locate them with the SEM. The specimen was attached to a Cambridge style SEM stub and vacuum coated with 50 nm carbon. The samples were observed and analyzed on a JEOL JXA-35 SEM with an EDAX-9100 computerized X-ray spectrometer or on a Cambridge stereoscan with an ORTEC 6200 X-ray spectrometer.

RESULTS AND DISCUSSION

Discussion of the procedure

Problems encountered in sample preparation, locating areas of interest, and differentiation of soil material with the secondary electron image of the SEM were overcome by the described procedure. Scotchcast #3 resin was used as the impregnating medium because it is stable under vacuum and the electron beam of the SEM (Innes and Pluth, 1970), while yielding only very low intensity peaks for Na and Cl with EDXRA. Removal of the thin section from the glass slide eliminated the possibility of obtaining background X-rays through holes in the thin section, especially when the sample was etched and elemental Si mapping was performed. The etched specimens were noticeably more fragile after etching but after mounting to the SEM stub, no special precautions were required as with Low Temperature Ashing (LTA) (Jenkins, 1981). The etching procedure greatly improved the usefulness of the specimens for secondary electron observation by creating relief and exposing internal surfaces (Fig. 1). Likewise, where polished mineral surfaces remained after etching, EDXRA could be performed without interferences created by surface roughness. Mineral grains that could be identified using petrographic techniques could then be analyzed with EDXRA to obtain spectra representative for the species. The use of transmitted and reflected light images of the specimen at overlapping magnifications greatly enhanced the usefulness of the SEM-EDXRA as a powerful tool in this type of micromorphological study. As an example, Fig. 2

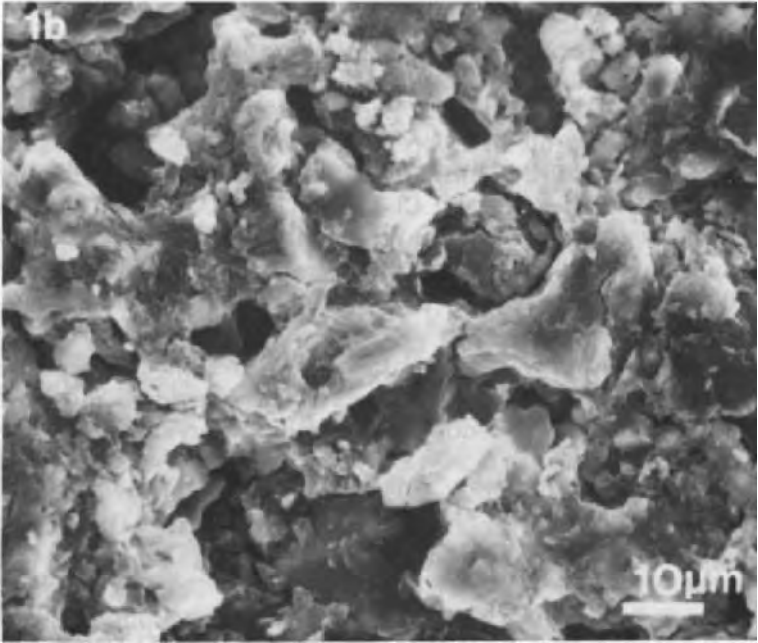
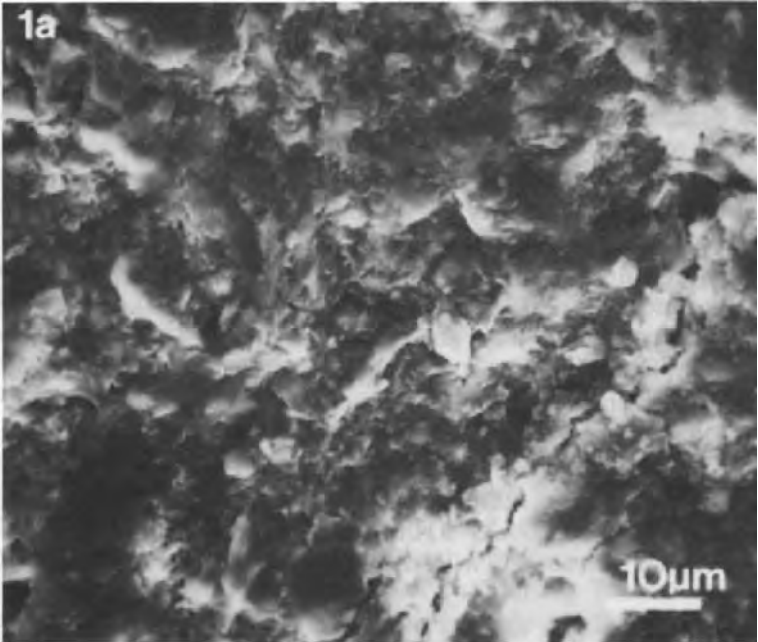


Fig.1. Secondary electron images of unetched (a) and etched (b) thin sections from a fragipan horizon of a Hosmer soil.

illustrates the various images of a simple void argillan truncated at the interface of a fragipan prism interior and a vertical eluvial seam.

The procedure employed was not extremely time consuming and did not restrict observations with OTM, either before or after application of SEM-EDXRA. If an area of interest was found on the SEM the specimen could be washed free of the conductive coating, remounted on a glass slide and reanalyzed with OTM. Such cognitive use of the two types of observations proved very effective in analyzing the bridging material occurring in fragipans found in loess. A possible disadvantage is that heating of some soils to 95°C could considerably alter their fabrics through desiccation. However, comparative studies involving replicate unheated samples impregnated with methylmethacrylate thinned with styrene revealed only slightly more desiccation of the fabrics with heating than air-drying. Unfortunately, the etching procedure is probably only applicable to mineral soils low in organic matter since both methylene chloride and acetone may solubilize some organic constituents.

Application of SEM-EDXRA to the study of fragipans

A fragipan (modified from *L. fragilis* brittle, and pan: meaning brittle pan) is a dense soil layer that is brittle when moist and very hard when dry. Fragipans severely restrict plant root profusion in soils and thereby limit agricultural productivity. They also reduce the suitability of soil for many engineering and urban uses. Although fragipans are geographically extensive their genesis remains obscure. The source of their brittleness has been widely studied and has generally been attributed to weak cementation by one or more soil components (Grossman and Carlisle, 1969). However, there is still no consensus regarding composition of the cementing material.

OTM examination of the fragipan horizons from a loess derived Hosmer soil (fine-silty, mixed, mesic, Typic Fragiudult; Soil Survey Staff, 1975) revealed isotropic to highly birefringent plasma bridging silt grains at magnifications greater than 250 \times (Fig. 3). The plasmic bodies were too small to yield interference figures or to identify with other optical techniques. Since the bridges could not be identified by conventional OTM, SEM-EDXRA was used to locate and analyze the composition of the material.

Qualitatively, the composition of mineral grains and major micromorphological features in the fragipan horizon were easily determined by EDXRA of the polished, pedestal-like surfaces in the thin section. Plasma separations of clay occurred mainly around skeleton grains, which was reasonable since it was determined that the fragipan had skeletal plasmic fabric (Brewer, 1976) from optical techniques (Fig. 3). The plasma separations were characterized by small desiccation cracks and by EDXRA spectra that exhibited roughly a 2:1 ratio of Si:Al peak heights with substantial but variable peaks for K, Ca and Fe. The spectra were very similar to those

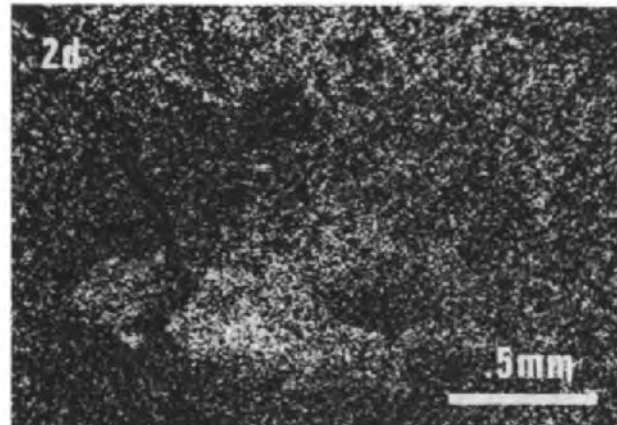
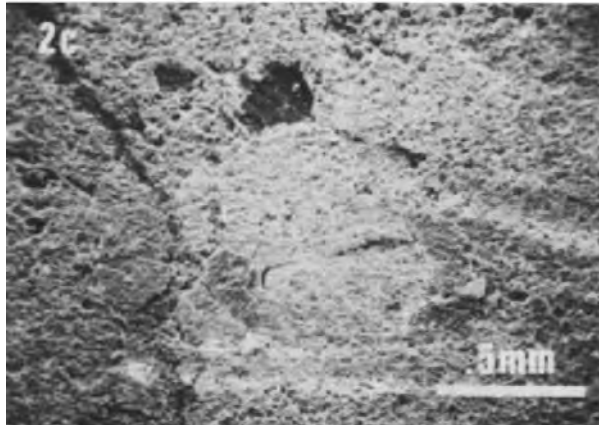
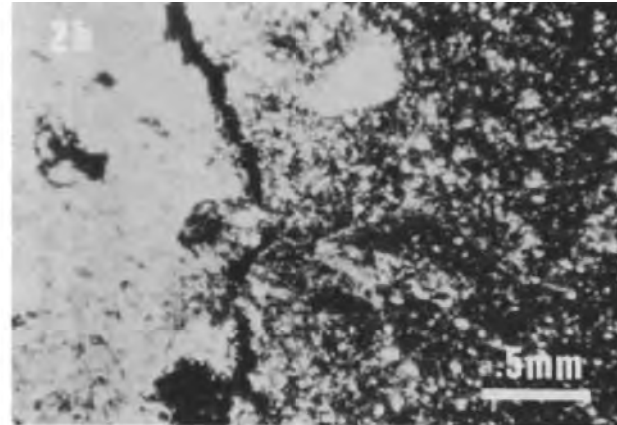
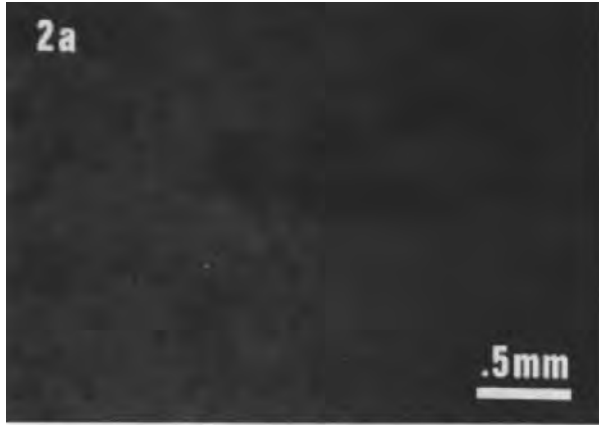


Fig.2. Reflected light micrograph (a), cross-polarized light micrograph (b), secondary electron image (c), and an iron distribution map (d) of a void argillan truncated at the interface of the fragipan interior and a vertical eluvial seam from a Hosmer soil.

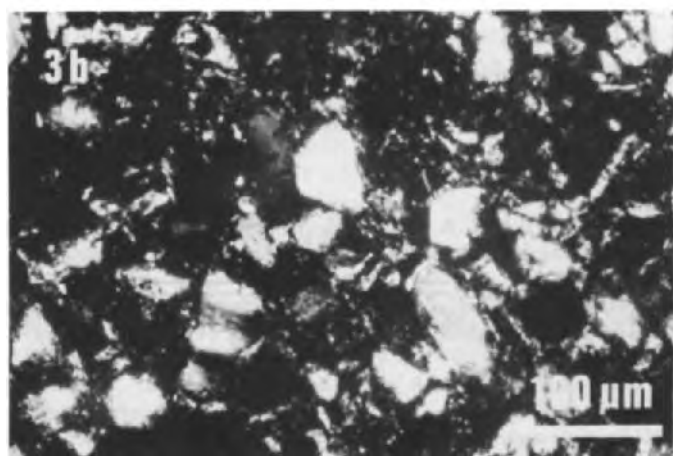
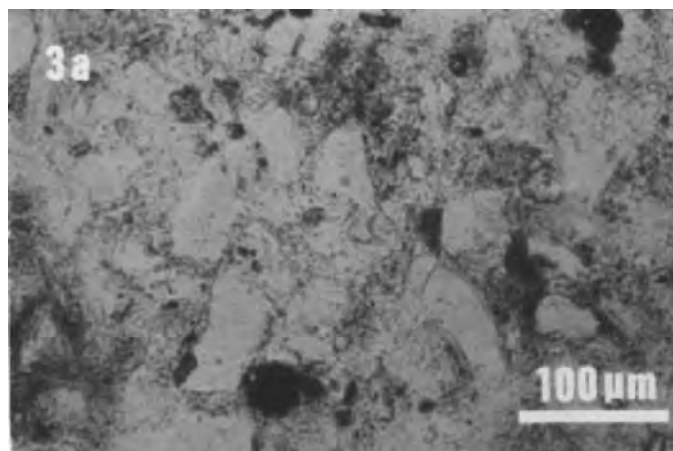


Fig.3. Plane-polarized (a) and cross-polarized (b) light micrographs of soil fabric from the interior of a fragipan prism from a Hosmer soil developed in loess illustrating plasma bridging skeleton grains.

for large argillans and papules that could be differentiated on the basis of their texture and conductance under the SEM.

After etching, mineral grains were easily recognized at magnifications greater than $200\times$; at magnifications of $250\text{--}2000\times$ small features forming bridges between silt grains could be seen in the fragipan. These bridges were conspicuous in that they did not appear to be cracked due to desiccation as were the argillans and other plasma separations. The bridges could also be found between grains of differing composition. Fig. 4 is an example of such a case and Fig. 5 illustrates the EDXRA spectra at points *a*, *b*, and

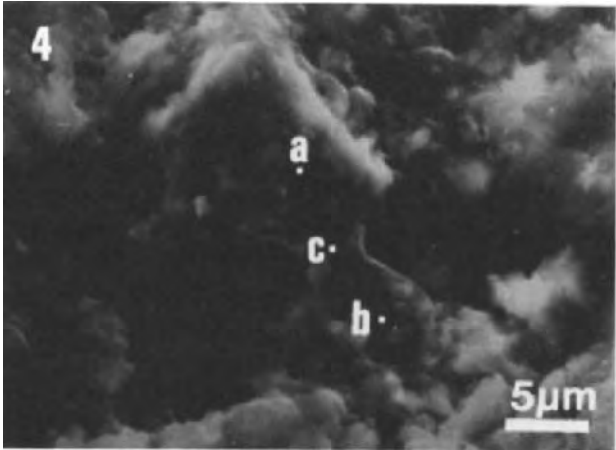


Fig.4. Secondary electron image of a silicate bridge in the fragipan of a Hosmer soil showing locations of EDXRA spectra at points *a*, *b*, and *c*.

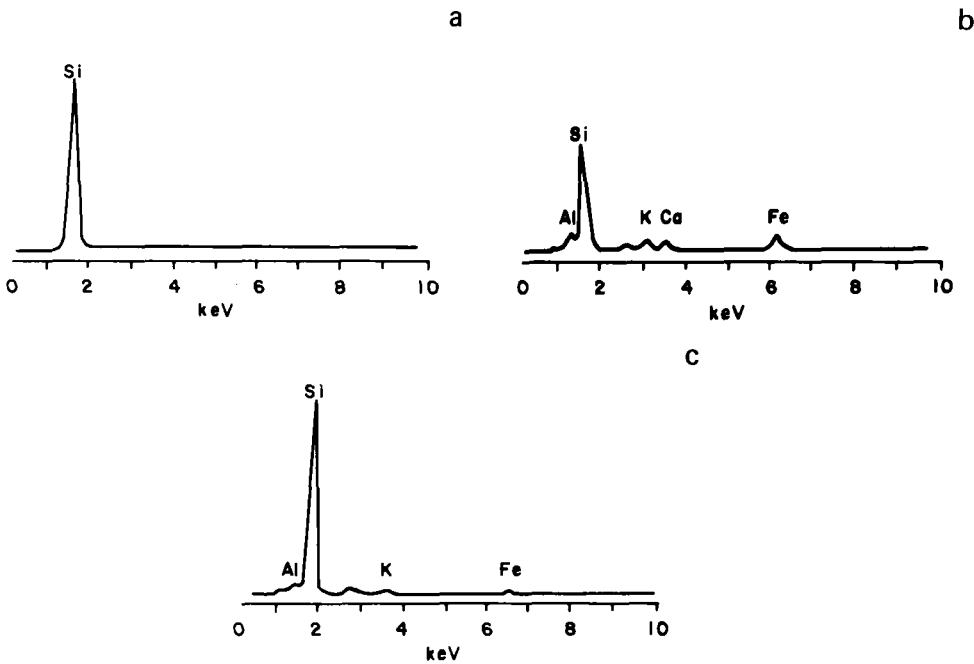


Fig.5. EDXRA spectra from the corresponding points *a*, *b*, and *c*, on Fig.4.

c, on Fig. 4. The upper grain was identified as being quartz while the lower grain is probably a feldspar. The EDXRA spectrum of the bridging material (Fig. 5c) was very characteristic for other bridges observed in the fragipan. These features always contained a large Si peak with smaller peaks for

Al, K and Fe. The spectrum, if the Si peak was not so intense, would closely resemble the spectra from argillans observed in large papules and cutans. Possibly, the bridges have some silicate clay incorporated in them. The high Si content of the bridges was a characteristic feature; however, the Al content was somewhat variable. The variability may be due to differing amounts of exchangeable Al associated with clay, or to Al-interlayering of clay minerals; however, after considering data from an infrared spectroscopic study of the soils (Norton, 1981), both Si and Al probably occur in the structure of a poorly crystallized hydrous oxide occurring in the bridges. It is possible that these bridges are the source of brittleness in the fragipan.

CONCLUSION

The advantages of the technique described were that the same specimen could be observed interchangeably with OTM and SEM-EDXRA and that very little additional effort was required to make the transition from conventional OTM to SEM-EDXRA observation. The etching and the use of OTM photographs made the location and identification of soil features much easier than with non-etched samples.

REFERENCES

- Bisdom, E.B.A., Henstra, S., Jongerius, A. and Thiel, F., 1975. Energy dispersive X-ray analysis on thin sections and unimpregnated soil material. *Neth. J. Agric. Sci.*, 23: 113–125.
- Bisdom, E.B.A., Henstra, S., Hornsvelt, E.M. and Jongerius, A., 1976. Wavelength and energy dispersive microanalysis with EMA and SEM-EDXRA on thin sections of soils. *Neth. J. Agric. Sci.*, 24:209–222.
- Brewer, R., 1976. *Fabric and Mineral Analysis of Soils*. R.E. Krieger Publishing, Huntington, N.Y., 482 pp.
- Grossman, R.B. and Carlisle, F.J., 1969. Fragipan soils of the eastern United States. *Adv. Agron.*, 21: 237–239.
- Innes, R.P. and Pluth, D.J., 1970. Thin section preparation using an epoxy impregnation for petrographic and electron microprobe analysis. *Soil Sci. Soc. Am. Proc.*, 34: 483–485.
- Jenkins, D.A., 1981. The transition from optical microscopic to scanning electron sub-microscopic studies on soils. In: E.B.A. Bisdom (Editor), *Submicroscopy of Soils and Weathered Rocks*. 1st Workshop of the International Working-Group on Submicroscopy of Undisturbed Soil Materials (IWGSUSM) 1980, Wageningen. Centre for Agricultural Publishing and Documentation, Wageningen, pp. 163–172.
- McKeague, J.A. and Protz, R., 1980. Cement of duric horizons, micromorphology and energy dispersive analysis. *Can. J. Soil Sci.*, 60:45–52.
- McKeague, J.A. and Wang, C., 1980. Micromorphology and energy dispersive analysis of ortstein horizons of podzolic soils from New Brunswick and Nova Scotia, Canada. *Can. J. Soil Sci.*, 60:9–21.
- Norton, L.D., 1981. *Loess Distribution and Pedogenesis of Loess-Derived Soils in East-Central Ohio*. Unpublished Ph.D. dissertation, Ohio State University, Columbus, Ohio, 230 pp.

Soil Survey Staff, 1975. Soil Taxonomy: A Basic System of Soil Classification for Making and Interpreting Soil Surveys. U.S. Dep. Agric., Handbook Number 436. U.S. Govt. Print. Off., Washington, D.C., 754 pp.

Wilding, L.P. and Geissinger, H.D., 1973. Correlative light optical and scanning electron microscopy of minerals: A methodology study. J. Sediment. Petrol., 43:280—286.

MICRORADIOGRAPHY AS A SUBMICROSCOPIC TOOL

L.R. DREES and L.P. WILDING

Department of Soil and Crop Sciences, Texas A&M University, and Texas Agricultural Experimental Station, College Station, Texas 77843 (U.S.A.)

(Accepted for publication February 17, 1983)

ABSTRACT

Drees, L.R. and Wilding, L.P., 1983. Microradiography as a submicroscopic tool. *Geoderma*, 30: 65–76.

Contact X-ray microradiography is a microscopic application of conventional radiography. The resulting in situ shadow images on fine-grained photographic film can be viewed under the light microscope up to 500 \times without loss of detail or depth of focus distortions. Differential absorbance of X-rays by the sample offers a non-destructive means of examining the internal phases of a specimen which may be obscured in light transmission or SEM microscopy. Such phases include voids, nodules, concretions, occluded minerals, lithorelicts, and other chemical segregations. Microradiography is an especially convenient tool because of minimum sample preparation and the small investment cost for camera fabrication to existing X-ray equipment.

INTRODUCTION

Radiographic principles and procedures remain essentially unchanged since the discovery of X-rays by Wilhelm Conrad Röntgen in 1895. X-ray radiography is currently employed in many scientific endeavors. It is used widely in the geological and paleontological fields. Two excellent books that review these applications are Bouma (1969) and Krinitzsky (1970).

In soil materials, only limited application has been made of radiography. Carbajal et al. (1966, 1969) used microradiography of thin sections to study the distribution of various elements and mineral phases in the soil profile. More recently, Rogaar and Thiadens (1975) used radiography to examine the natural pore structure in soils. Earthworm burrows and their shapes and contents have also been investigated using radiography (Rogaar and Boswinkel, 1978).

Microradiography has proven to be a useful interface between light-optical and SEM techniques for analysis of occluded mineral phases in vegetative tissues of grasses and tree leaves. For example, light-optical and SEM micrographs of biogenic opal isolated from soils and vegetative com-

ponents have been reported previously (Wilding and Drees, 1971, 1973, 1974; Wilding et al., 1977). Many of these isolates are fragmented and difficult to relate to in situ sites of localization. The X-ray microradiograph technique has served a vital role in this linkage and provides the only known means to directly visualize the distribution of these occluded phases.

THEORY

Contact-microradiography is a submicroscopic technique for examining the internal phases of a specimen which may not be identified by microscopic or other techniques because of opaqueness, sample thickness or lack of resolution. Such phases include voids, nodules, concretions, occluded minerals, lithorelicts, and other chemical segregations within the specimen. X-rays impinging on the sample are differentially absorbed by occluded chemical phases within the sample. Absorption of X-rays within the sample reduces the intensity of the primary beam by an amount equal to:

$$I = I_0 e^{-(\mu/\rho)\rho X} \quad (1)$$

where I_0 = intensity of radiation incident on the sample, I = intensity of transmitted radiation after passing through a sample of thickness X , μ/ρ = mass absorption coefficient (cm^2/g) determined by chemical composition and wavelength of radiation being absorbed, and ρX = mass per unit area of sample thickness X with density ρ .

Since mass absorption coefficients are dependent on wavelength, intensity ratios may be maximized by selecting radiation wavelengths which will maximize differences between the absorption coefficients of the matrix and occluded phases. Table I illustrates the advantages of using specific wavelengths to optimize image contrast. Differential chemical composition can be noted by changes in image contrast when exposure is made with different monochromatic X-ray sources. For example, iron oxide nodules or concretions appear lighter on radiography film than quartz when Cu-irradiation is used (Table I). The inverse is true if Cr-irradiation is used. Carbajal et al. (1969) effectively used different radiation wavelengths to identify iron and manganese concentrations in soil thin sections.

CONTACT MICRORADIOGRAPHY

Contact microradiography is a submicroscopic technique to record a shadow image at unity magnification on a fine-grained photographic emulsion (Fig. 1). The resulting image is then viewed with a light microscope at magnifications up to 500 \times without significant loss of detail. With the availability of high-resolution films and plates (> 2000 lines/mm) that exhibit very fine grain-size and thin emulsion (< 5 μm), it is possible to obtain high-resolution images at magnifications up to 500 \times with contact microradiography. Because the photographic emulsion is very thin, depth of

TABLE I

Numerical difference in mass-absorption coefficients between common soil minerals and quartz for selected radiations*¹

Absorbing material	Radiation		
	Cr (2.29 Å)	Fe (1.937 Å)	Cu (1.54 Å)
SiO ₂ (quartz)	0.0	0.0	0.0
Al ₂ O ₃	-15.6	-6.0	-3.9
Fe ₂ O ₃	-20.8	-9.7	+195.6
CaCO ₃ (calcite)	+111.2	+68.2	+40.7
TiO ₂ (rutile)	+263.3	+169.2	+98.2
KAlSi ₃ O ₈ (orthoclase)	+37.1	-28.7	+13.8
NaAlSi ₃ O ₈ (albite)	-9.0	-2.0	-1.8
CaAl ₂ Si ₂ O ₈ (anorthite)	+48.0	+34.2	+17.9
KAl ₃ Si ₃ O ₁₀ (OH) ₂ (muscovite)	+18.6	+16.1	+7.8

*¹ Negative values yield images darker than quartz while positive values yield images lighter than quartz. The greater the difference, the greater the image contrast to quartz.

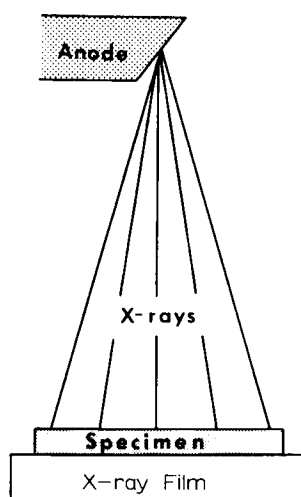


Fig. 1. Schematic view and geometric relationship of basic components for contact-micro-radiography.

focus is not a problem in viewing microradiographs. By exposing the sample at slightly different angles, microradiography is also suitable for stereographic images (Hamblin, 1962; Rogaar and Thiadens, 1975).

X-ray projection radiography is an alternate method which requires the sample to be placed close to a point-focus X-ray source. An enlarged shadow image is then obtained depending on the source-sample to sample-film ratio.

Fine details of microfossils have been reported by Jongbloed and Porrenga (1968) using this technique. X-ray projection radiography does have its limitations in requiring specialized equipment to obtain a point source of X-rays. Such equipment is not generally available to micromorphologists. This technique also poses problems with image edge distortion due to the finite dimensions of the X-ray source.

Optimum image contrast in contact microradiography is usually obtained with a monochromatic X-ray source. White continuous radiation may be used if tube voltages are kept sufficiently low to produce longer wavelengths. The X-ray source may be a commercial apparatus designed for radiography. However, an X-ray generator associated with X-ray diffraction equipment is usually more readily available and convenient. Microradiography cameras are easily fabricated to fit a powder camera track of a diffractometer (Schmidt, 1952). Fig. 2 illustrates schematically one of two cameras built by the present authors and mounted on a camera track of a Philips Diffractometer. This arrangement has several advantages for microradiography:

- (1) The powder camera track permits quick and accurate alignment of radiography camera.
- (2) The X-ray tubes designed for powder camera usually have smaller spot focusing that favors optimum resolution.
- (3) The diffractometer tube towers generally have built-in safety shutters and filter monochrometers.
- (4) The microradiography camera usually does not interfere with other simultaneous diffractometer uses.

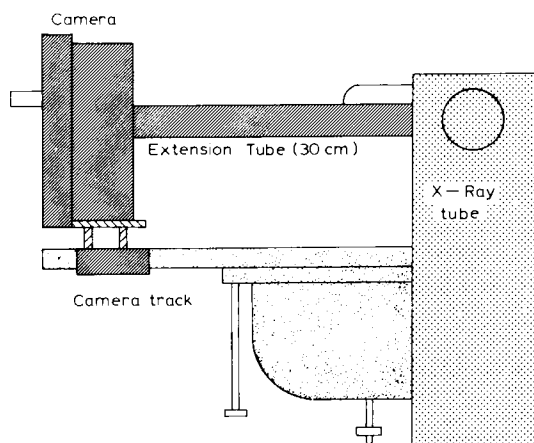


Fig. 2. Schematic view of a microradiography camera mounted on a powder camera track of a Philips X-ray diffractometer.

X-ray tube voltages can be adjusted to reduce the harder white radiation while maintaining a high intensity of the characteristic radiation. Tube

voltages in the range of 20–40 kV with 10–20 mA are common for micro-radiography purposes. The authors generally use 20 kV and 10 mA Ni K β filtered Cu-radiation. Excellent results have been achieved using emulsion-coated glass slides (Kodak Spectroscopic Plates, Type 649-0) and sheet film cut to size (Kodak High Resolution Film, S0-343).

Close physical contact between sample and film is necessary for maximum resolution and enlargement. Positive contact during long exposure eliminates distortion resulting from room or equipment vibrations. Sample-film contact is most conveniently achieved by a vacuum cassette film holder. The cassette consists of a metal base with a recessed area milled to accommodate the photographic film. An outer perimeter and cross channels have been milled slightly deeper to allow vacuum distribution to the film via a side or back vacuum port (Fig. 3).

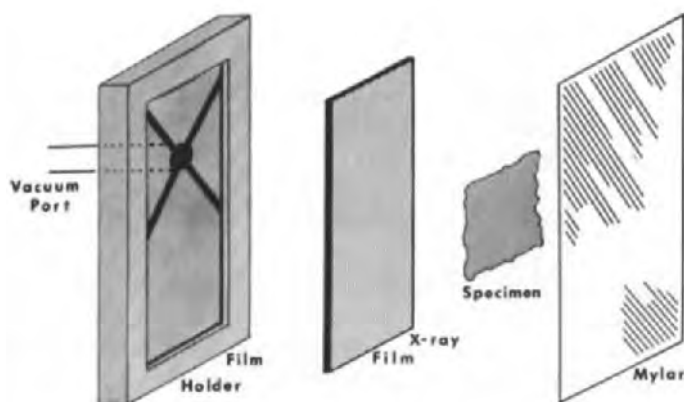


Fig. 3. Basic components of the vacuum cassette for contact-microradiography. The lead-backed film holder is designed to accept Kodak Spectroscopic Plate, 649-0. The cassette fits into a radiation-proof and light-tight camera illustrated in Fig. 2.

In practice, photographic film is placed into the machined recess, emulsion side up, and the sample placed on top of it. A flexible X-ray transparent sheet is then placed over the sample (Fig. 3). The sheet is of sufficient size to cover the sample and overlap the perimeter of the cassette. When vacuum is applied, the sheet presses the sample firmly against the film. In some instances, however, it may be desirable to place a small thin sheet of non-absorbing mylar between the sample and film to protect the emulsion from scratches, moisture, or other physical or chemical contamination.

Mylar serves as an ideal sheeting material; it is strong, flexible and X-ray transparent. However, if the cassette must be transported from the dark-room where it is loaded, to the X-ray source in a lighted room, an opaque sheeting is necessary. Plastic sheeting containing chlorine or other elements that are highly absorbent of soft X-rays must be avoided. Black paper may also be used to keep out light, but caution should be exercised because some

paper has internal structural components which may be recorded on the photographic film.

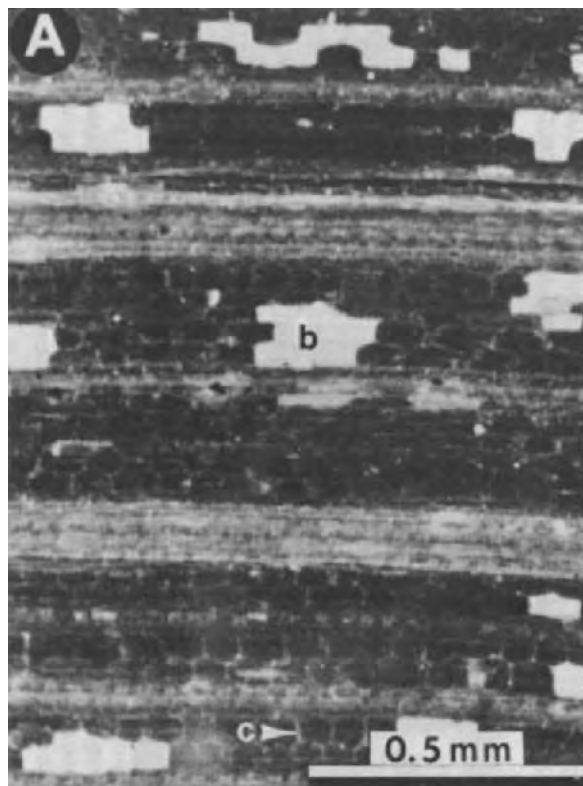
Focal distances between X-ray source and the sample commonly range from 8 to 30 cm. Longer focal lengths reduce edge distortions and blurring of boundaries, which is especially important if the sample must be placed a small distance from the film or the sample is thick. However, longer focal lengths result in greater absorption of softer X-rays in the air path. If the focal distance is short, sample thickness is most critical. For practical purposes, exposure time (intensity of X-rays) follows an inverse square relationship with distance, except for long focal distances where air absorption becomes a significant factor. Exposure times are not given here since they depend on film speed, focal distance, wavelength, tube voltage, tube current, and filters. Exposure guides can easily be constructed for each set of conditions.

Caution is advised in constructing a radiographic camera. Every precaution should be taken to ensure that there is no leakage of X-rays around ports or through the back. Lead shields should be used behind the film to reduce backscattering and X-ray transmission through the camera. Exposure monitoring of the camera is advised while in use.

APPLICATIONS

Host mineral inclusions as cellular infillings are evident in a wide variety of vegetative material including grasses and tree leaves (Fig. 4). Although the mineralogy of the cellular infillings cannot be identified from microradiography, previous X-ray diffraction and light optical analysis, the authors have identified biogenic opal (Wilding and Drees, 1974), and calcium oxalates. These cellular inclusions generally conform to the shape of the individual host cell and are concentrated along conductive vesicles (Fig. 4). In tree leaves (Fig. 4B) the larger discrete white images are calcium oxalate crystals. Darker laminated gray tones within conductive elements are biogenic opal and cellulose fibers. In the blades of grass (Fig. 4A), the white areas are completely silicified bulliform cells or partially silicified incrustations of cell walls. Lighter and darker parallel bands represent variable degrees of silicification in midrib sections of the blades. Weakly or partially silicified cell wall elements are evident in the microradiographs (Fig. 4). These cell walls usually fragment when biogenic opal is extracted by ashing or acid digestion (Fig. 5). Although the SEM micrograph yields significant information about the structure and configuration of silicified cell walls (Fig. 5), the X-ray microradiograph (Fig. 4) more clearly shows their continuity and relationship to the plant tissue as a whole. Precise zones of silicification can be directly observed in situ without pretreatment modifications.

Fig. 4. X-ray microradiography of grass blades and tree leaves. A. Big bluestem (*Andropogon gerardi*); B. Aspen poplar (*Populus tremloides*). Note: *b* = silicified bulliform cells; *c* = silicified cell walls; *o* = calcium oxalate crystals; *e* = silica- and cellulose-impregnated conductive elements. Both micrographs at same magnification.



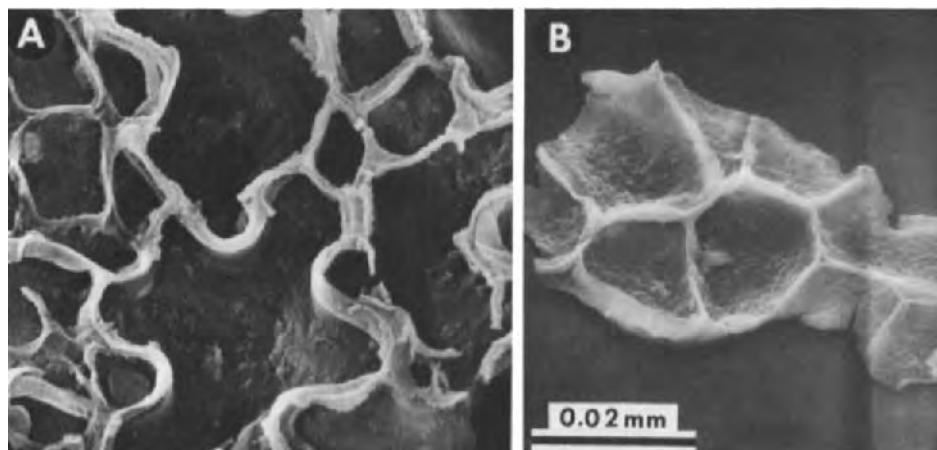


Fig. 5. Scanning electron micrographs of silicified cell walls: A. Fragment isolated from sugar maple (*Acer saccharum*); B. Fragment from forest soil isolate. Both micrographs at same magnification.

Contact microradiography has special utility in identifying the fine structure of soil fabric in thin sections. Many features are not clearly resolved in plane-polarized or cross-polarized optical microscopy. Plasma aggregate units, their size and arrangement in thin sections are often more clearly resolved in microradiographs. This is attributed to differential X-ray absorption as a consequence of chemical, mineralogical, textural and/or cementation compositional effects. Specimen variations coupled with very thin film emulsion reduce the depth of focus and increase apparent resolution and image sharpness. Increased resolution is illustrated in Fig. 6 where the definition of two mica flakes is much enhanced in the microradiograph

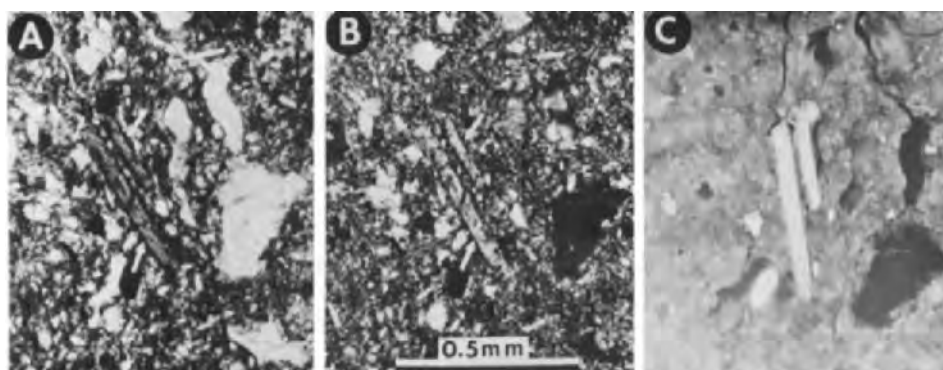


Fig. 6. Photomicrographs of soil thin section showing mica flakes. A. Plane-polarized light; B. Cross-polarized light. Arrows in A and B point to flakes exhibiting higher X-ray absorbance in microradiograph (C). All micrographs at same magnification.

versus either plane or polarized light microscopy. It is probable that the resolution for these skeleton grains in the microradiograph is enhanced relative to the s-matrix because they contain iron oxides or other elements that have a higher relative mass absorption coefficient for Cu-irradiation (Table I).

Lithorelicts composed of quartz and K-feldspar phases are observed in Fig. 7. Under cross-polarized light optics (Fig. 7A), it is difficult to distinguish these minerals because optical phenomena of untwinned K-feldspars are similar to quartz and some of the grains of both minerals are at extinction. It is easier and more accurate to distinguish these mineral phases by microradiography (Fig. 7B) where feldspars appear lighter than quartz due to higher relative mass absorption coefficients (Table I). These gray-tone image contrasts are suitable for quantification using advanced automated image analysis systems.

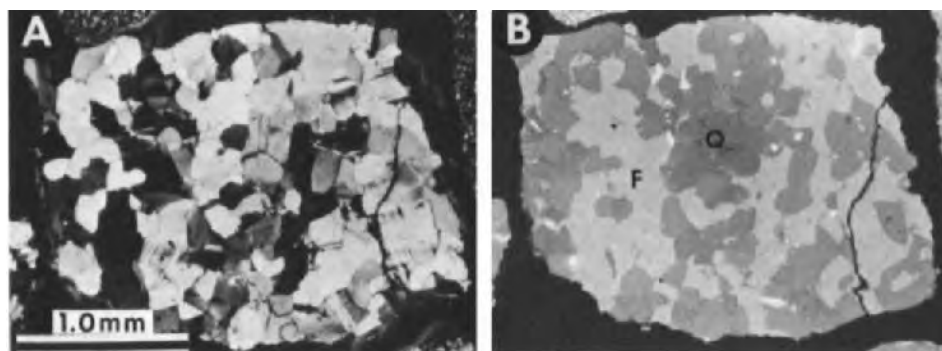
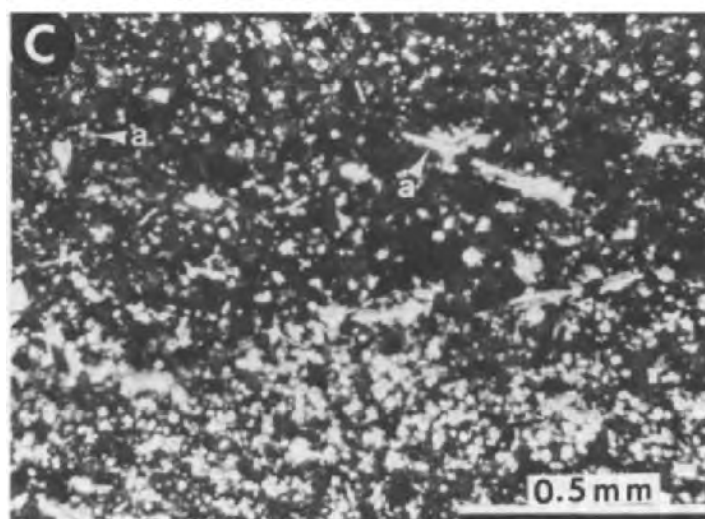
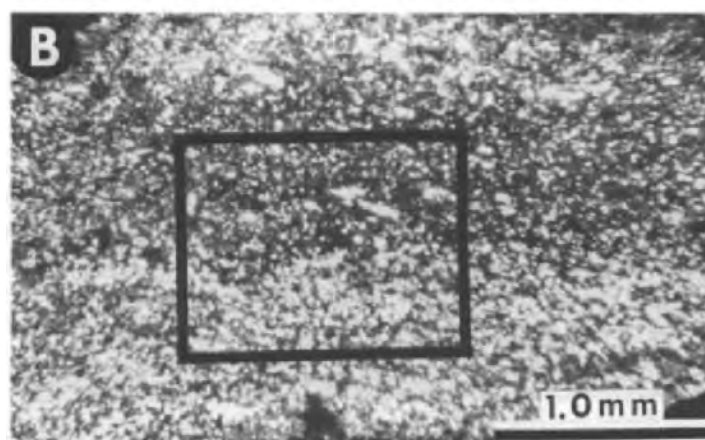
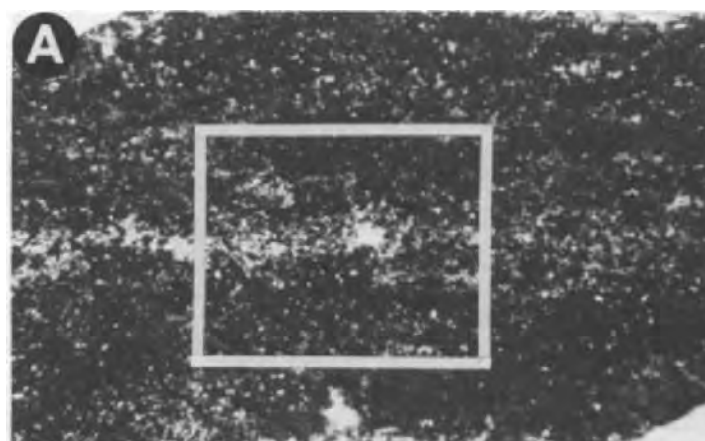


Fig. 7. Thin section of soil lithorelict composed of quartz and feldspar. A. Cross-polarized light, B. X-ray microradiograph showing image contrast differences for quartz (Q) and feldspar (F).

Microradiography can also be effectively used to observe opaque or thick specimens that prohibit light transmission. Fig. 8A illustrates such an example in a thin section where a nearly opaque shale lithic yields little fabric or compositional information when observed under plane-polarized light. In contrast, Fig. 8B illustrates a microradiograph of this same specimen with greater fabric resolution. Fig. 8C is an enlargement of a select field in Fig. 8B that clearly depicts the arrangement of plasma aggregates.

Thin sections of organic soils are often so strongly pigmented with organic matter that the occluded detrital grains are mostly obscured. Microradiographs have proven useful to ascertain the relative abundance of inorganic phases. In some organic sections, macropores are also better defined.



CONCLUSIONS

X-ray microradiography is a useful submicroscopic tool to complement optical and electron microscopy. It permits direct image analyses of components that are obscured by occlusion within host materials and thus cannot be viewed by transmitted-light microscopy or by SEM. This technique particularly lends itself to thin sections where it often enhances fabric and compositional information. In thin sections, voids, plasma aggregates and their distributions may be clearly differentiated from anisotropic components at extinction. Internal structure and compositional attributes of detrital grains and vegetative tissues may also be obtained without prior preparation or sample destruction. In most instances, specimens examined by X-ray microradiography may be examined by other microscopic techniques with direct image comparison.

X-ray microradiography may be a convenient additional tool to most mineralogical laboratories because of its small investment cost for camera fabrication and adaptability to existing X-ray equipment.

REFERENCES

- Bouma, A.H., 1969. *Methods for the Study of Sedimentary Structures*. Wiley-Interscience, New York, N.Y., 458 pp.
- Carbajal, H., Vicente, J.G. and Voltz, M.K., 1966. La microradiografía de contacto aplicada al estudio de la micromorfología de suelos. *Anal. Edafol. Agrobiol. (Madrid)*, 25: 491–503.
- Carbajal, H., Benayas, J., Vicente, J.G. and Alonso, J.J., 1969. Contact-microradiography as applied to the distribution of iron and manganese in thin sections of Mediterranean brown soil. *Geoderma*, 3: 133–145.
- Hamblin, W.K., 1962. X-ray radiography in the study of structures in homogeneous sediments. *J. Sediment. Petrol.*, 32: 133–145.
- Jongebloed, W.L. and Porrenga, D.H., 1968. Microradiography and X-ray microscope in geology. *Geol. Mijnb.*, 47: 435–442.
- Krinitzsky, E.L., 1970. *Radiography in the Earth Sciences and Soil Mechanics*. Plenum Press, New York, N.Y., 163 pp.
- Rogaar, H. and Boswinkel, J.A., 1978. Some soil morphological effects of earthworm activity; field data and X-ray radiography. *Neth. J. Agric. Sci.*, 26: 146–160.
- Rogaar, H. and Thiadens, R.A.H., 1975. X-rays applied to the study of the pore structure in soils. *Neth. J. Agric. Sci.*, 23: 321–333.
- Schmidt, R.A.M., 1952. Microradiography of microfossils with X-ray diffraction equipment. *Science*, 115: 94–95.
- Wilding, L.P. and Drees, L.R., 1971. Biogenic opal in Ohio soils. *Soil Sci. Soc. Am. Proc.*, 35: 1004–1010.
- Wilding, L.P. and Drees, L.R., 1973. Scanning electron microscopy of opaque opaline forms isolated from forest soils in Ohio. *Soil Sci. Soc. Am. Proc.*, 37: 647–650.

Fig. 8. Thin section of nearly opaque shale lithorelict: A. Plane-polarized light; B. X-ray microradiography of same field illustrating enhanced resolution; C. Magnification of square area in A and B showing individual plasma aggregates (a).

- Wilding, L.P. and Drees, L.R., 1974. Contributions of forest opal and associated crystalline phases to fine silt and clay fractions of soils. *Clays Clay Miner.*, 22: 295—306.
- Wilding, L.P., Smeck, N.E. and Drees, L.R., 1977. Silica in soils: quartz, cristobalite, tridymite, and opal. In: J.B. Dixon and S.B. Weed (Editors), *Minerals in Soil Environments*. Soil Sci. Soc. Am., Madison, Wisc., pp. 471—552.

STEM-EDXRA AND SEM-EDXRA INVESTIGATION OF IRON-COATED ORGANIC MATTER IN THIN SECTIONS WITH TRANSMITTED, SECONDARY AND BACKSCATTERED ELECTRONS

E.B.A. BISDOM¹, R. NAUTA² and B. VOLBERT²

¹ *Netherlands Soil Survey Institute, P.O. Box 98, 6700 AB Wageningen (The Netherlands)*

² *N.V. Philips, Application Laboratory—Electron Optics, TQ-III-p, 5600 MD Eindhoven (The Netherlands)*

(Accepted for publication February 17, 1983)

ABSTRACT

Bisdom, E.B.A., Nauta, R. and Volbert, B., 1983. STEM-EDXRA and SEM-EDXRA investigation of iron-coated organic matter in thin sections with transmitted, secondary and backscattered electrons. *Geoderma*, 30: 77–92.

Experiments have been carried out with STEM-EDXRA (scanning transmission electron microscope—energy dispersive X-ray analyzer) and SEM-EDXRA (scanning electron microscope—energy dispersive X-ray analyzer) on thin sections with thicknesses of about 5 μm and 20 μm , respectively.

Common thin sections with a thickness of about 20 μm , were analysed with the Philips SEM 505 and the Jeol-JSM-35C. Such thick preparations only allow near-surface imaging with secondary and backscattered electrons plus microchemical analysis up to $\times 10\,000$. The beam spot of the Philips EM 400T/ST, which can operate as a STEM-SEM-TEM with EDXRA, can be made smaller than is possible with the other two machines which were specifically built as SEM-instruments. Consequently, microchemical analysis could be performed at magnifications of more than $\times 10\,000$. Indications are that analysis at $\times 50\,000$ with EDXRA gave additional elements to those measured with SEM-EDXRA at $\times 10\,000$. In this manner near-trace-element quantities become measurable.

Investigation of 5 μm thick thin sections was mainly done with the Philips EM 400T/ST in the SEM-EDXRA and STEM-EDXRA mode. In this experiment the thin section was thinned maximally by normal grinding processes and subsequently removed in small pieces from the object glass together with the plastic used for mounting. These pieces were then placed in a copper grid and studied close to their surfaces with SEM-EDXRA and in the transmission mode with STEM-EDXRA. The use of TEM-EDXRA was not possible because this requires ultrathin sections of about 1 μm thickness. Even when the plastic, used for mounting the soil material on the object glass, is replaced by dissolvable material, the 5 μm thick thin section would still be a few microns thick. No diamond knife or ion thinning technique, used for the preparation of ultrathin sections of soft soil materials such as organic matter and clay, was applied in this study.

INTRODUCTION

Modern soil microanalysis of thin sections is often performed with SEM-EDXRA (scanning electron microscope—energy dispersive X-ray analysis) and EMA (electron microprobe analysis) (Bisdom et al., 1975, 1976; Bisdom, 1981a, b; Boekestein et al., 1981). Such microchemical analysis of soil material, however, frequently stops at magnifications which are insufficient for the study of very small soil particles, viz. at about $\times 10\,000$ for the microanalysis of chemical elements. Secondary electron images (SEI) and backscattered electron scanning images (BESI) can be obtained — dependent on the soil material being studied — at higher magnifications but such micrographs are no longer supported by microchemical *in situ* information.

There are instruments, such as the Philips EM 400T/ST, which are able to perform microchemical analysis in thin sections at magnifications of more than $\times 10\,000$. This is due to smaller beam spot diameters than are present in normal SEM instruments which were also used in the present study. Ideally, thin sections should always be ultrathin or about $1\ \mu\text{m}$ thick. This would allow the microchemical investigations of individual small soil components and give some idea of the composition of small masses of the smallest soil particles. In practice, however, the preparation of ultrathin sections is still difficult except of relatively soft soil materials such as organic matter and rather pure clays. Such ultrathin sections were made and studied with TEM by Bresson (1981) and Foster (1981).

The pieces of thin section in the copper grid were also studied in the SEM-EDXRA mode of the scanning transmission electron microscope (EM 400T/ST). Similar materials were investigated in thin sections mounted on the object glasses by SEM-EDXRA (Jeol-JSM-35C). In this manner, some control of the microchemical measurements of the EM 400T/ST was obtained. Both backscattered and secondary electron images were made close to the surface of the thin section using the Philips SEM 505 and EM 400T/ST. Such pictures could be compared with STEM-EDXRA micrographs made with transmitted electrons which passed a piece of thin section that was about $5\ \mu\text{m}$ thick. This thickness was obtained by maximal grinding of the soil material until it was virtually gone, and keeping the plastic layer, used for mounting on the object glass, intact. The technique is rapid and could be used to find out whether ion thinning, a process which takes much longer, is necessary for a certain research problem or not.

MATERIALS AND METHODS

The soil material used in these experiments is iron-coated organic material from peat of a sandy Typic Humaquept with bog iron ore. Processing of the peaty material to a thin section was done according to methods described by Jongerius and Heintzberger (1975). Usually, these are mammoth-sized thin

sections of 15×8 cm which are $15 \mu\text{m}$ to $25 \mu\text{m}$ thick. For the present analyses, much smaller thin sections are used, viz. of about 3.5×2.5 cm and the same thickness as the mammoth one. The surface of these thin sections was studied using specific SEM instruments, viz. the Jeol-JSM-35C and the Philips SEM 505. Pieces of the small thin sections were also maximally ground and taken from the object glass at about $5 \mu\text{m}$ thick. They were subsequently inserted in a copper grid for inspection with the Philips EM 400 T/ST scanning transmission electron microscope in both the SEM and STEM mode.

To obtain some insight into the microchemistry and morphology of iron-coated organic material, SEM-EDXRA was done with a Jeol-JSM-35C using an ECON windowless detector for the detection of chemical elements down to carbon at a magnification of about $\times 10\,000$ (Bisdorn et al., 1975). The morphology of the material in the thin section was also studied in the backscattered electron mode. This is possible with a backscattered electron detector of the semi-conductor type which comprised two solid-state detectors (Bisdorn and Thiel, 1981). No satisfactory backscattered electron scanning images (BESI) could be obtained from the iron-coated organic material and it was decided to do tests with other detector systems as well.

The Multi-Function-Detector (MFD) system of the Philips SEM 505, which was described by Volbert (1981) and in short in Bisdorn et al. (1983, this issue), uses four detectors for the registration of backscattered electrons. This results in a good detector efficiency. Imaging can start at $\times 10$ and frequently stops at $\times 10\,000$ or more depending on the type of soil material. The four detectors allow the production of high-quality micrographs, even of difficult soil materials such as the present ones. So far, experiments with soil materials indicate that BESI are obtainable with a SEM (SEM 505) and are frequently comparable to those of a Scanning Transmission Electron Microscope (EM 400T/ST) in the BSE (backscattered electron)-mode, an instrument which has a smaller beam spot diameter and a different backscattered electron detector system. Consequently, the step from the conventional SEM (SEM 505) to the STEM (EM 400T/ST) in the BSE-mode, was rather simple although the SEM worked with about $20 \mu\text{m}$ thick thin sections and the STEM with about $5 \mu\text{m}$ thick ones.

The Philips EM 400T/ST (T stands for twin lens and ST for scanning transmission) has been used for investigating iron-coated organic material at low and very high magnifications. The instrument can be used as a SEM-EDXRA, STEM-EDXRA and TEM-EDXRA as discussed in the introduction. Only SEM-EDXRA and STEM-EDXRA modes were used on the approximately $5 \mu\text{m}$ thick thin sections made by maximal grinding of the thin section at one side. This gives a type of wedge shape going from the common thickness of about $20 \mu\text{m}$ for light microscopy to $5 \mu\text{m}$ for transmitted electron microscopy. All thicknesses can be studied with SEM-EDXRA of the EM 400 T/ST but only the thinnest parts of the wedge with STEM-EDXRA. If the thin sections could be made about $1 \mu\text{m}$ thick, the work could also be done with the TEM-EDXRA mode of the STEM.

RESULTS

BSE and SE imaging by SEM 505

BESI of iron-coated organic material in peat are shown in Fig. 1. As is the case with light microscopy, the morphology and details on structure and fabric of the soil materials may change considerably with the magnification in submicroscopy. Shortly, what is not visible at low magnifications may become recognizable at higher ones. This is illustrated in backscattered electron scanning images of Figs. 1 and 2, viz. in the BSE (A+B) mode. These micrographs were made with the four detectors of the MFD (multi-function-detector) system (Volbert, 1981; Bisdorf et al., 1983) and just underneath the surface of a 20 μm thick thin section.

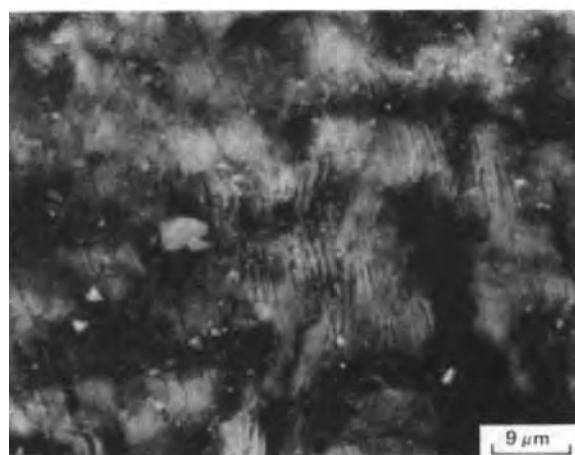
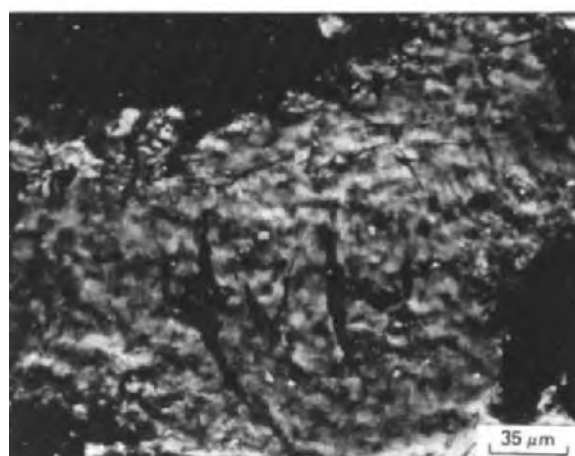
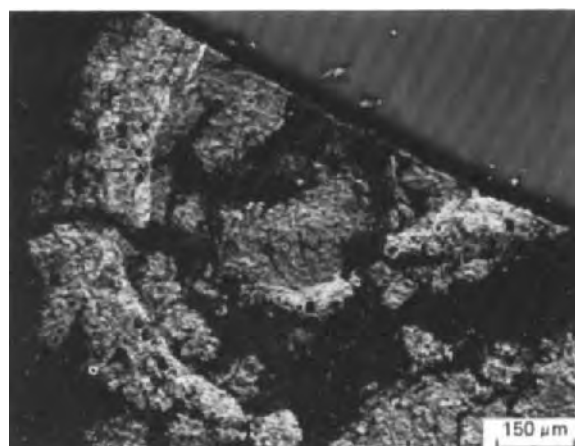
No orientations are visible at a low magnification in Fig. 1, i.e., in the central part of the micrograph with a bar scale of 200 μm ($\times 50$ on the original micrograph). The next figure at $\times 200$ shows a weak lamellar orientation which becomes evident at $\times 500$ (micrograph with bar scale of 20 μm). This orientation occurs in organic material which is covered and impregnated with iron hydroxide. The iron hydroxide is usually poorly crystallized or amorphous but goethite is locally present. The poorly crystallized nature of the iron hydroxide is demonstrated best in the BSE (A+B) image of Fig. 2 at $\times 2000$. Such poorly crystallized and amorphous materials do not usually allow backscattered electron imaging at much higher magnifications.

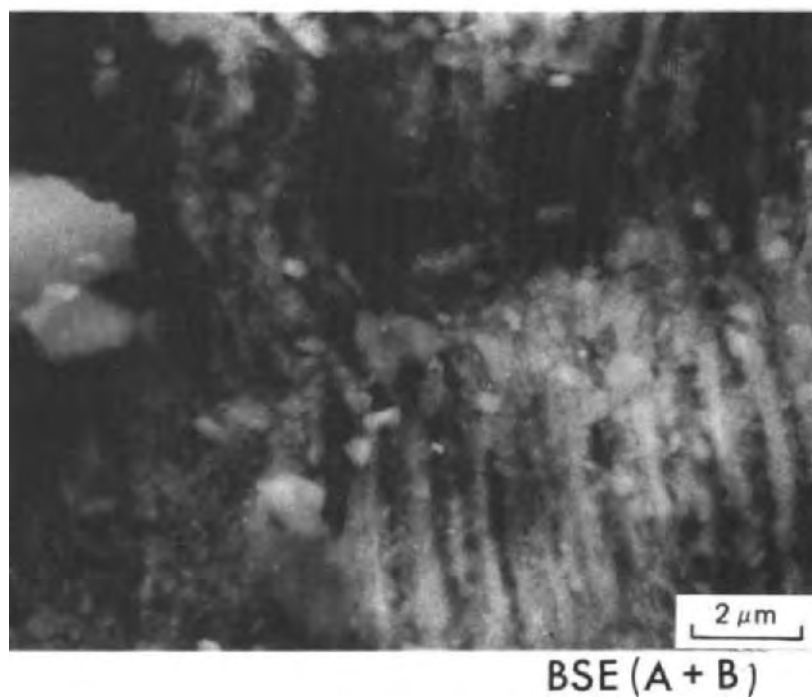
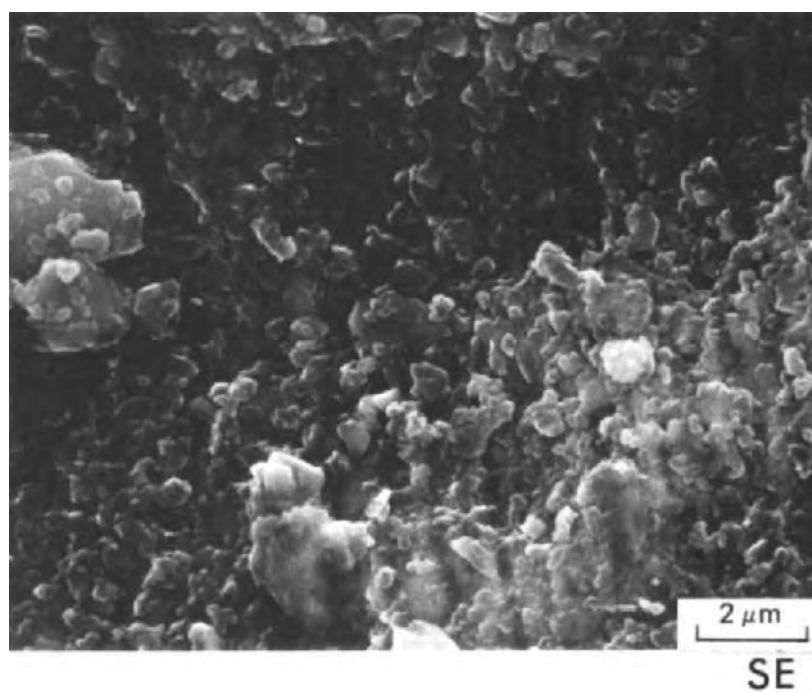
A secondary electron (SE) image is also given in Fig. 2 to allow a comparison of the results of SE and BSE techniques when applied to iron-coated organic material. Lineation is visible in the SE image but much better and more "naturally" developed orientation is present in the BSE (A+B) image of Fig. 2. This example also demonstrates that backscattered electrons give images which come from a shallow depth, estimated to be from 1 μm to 5 μm beneath the surface of the thin section. The SE-image, at 30 keV primary electron energy, comes from a shallower depth near to the surface of the thin section. This secondary electron image gives the impression that smearing of the soil material occurred during polishing of the soft constituents. Such polishing effects are no longer visible in the BSE-mode.

STEM imaging and STEM-EDXRA analysis by EM 400T/ST

When iron-coated organic material was studied with the Philips EM 400 T/ST (Figs. 3 to 6), maximally thinned and hand-polished specimens of

Fig. 1. BESI (backscattered electron scanning image) of iron-coated organic material in peat from a sandy Typic Humaquept ($\times 50$ to $\times 500$). Structure in the peat fragment becomes clearly visible at $\times 500$ magnification. Enlargements with the SEM 505 are made from central parts of preceding micrographs. BSE means backscattered electrons. The highest BSE (A + B) magnification of the studied soil material is shown in Fig. 2.

**BSE (A+B)**



about 5 μm thickness were placed in a copper grid after removal from the object glass. Subsequently, the copper grid was placed in a sample holder which in turn was inserted into the STEM. A series of submicroscopic techniques thus become possible, of which only a few have been used in this study, viz. the SEM-EDXRA mode at 20 keV to study close-to-surface material in the thin section (Figs. 3 and 4), and the STEM-EDXRA mode at 120 keV to investigate the total thickness of 5 μm in the transmission mode (Figs. 5 and 6).

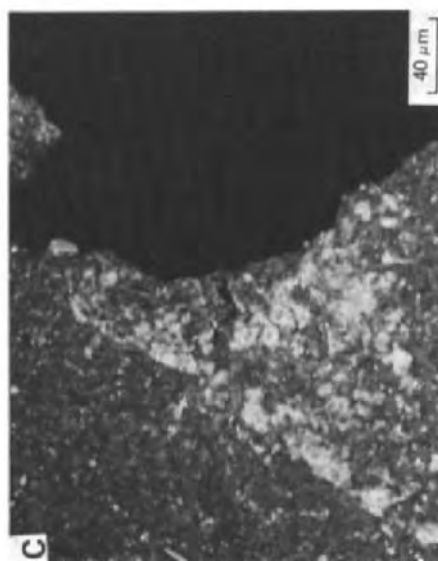
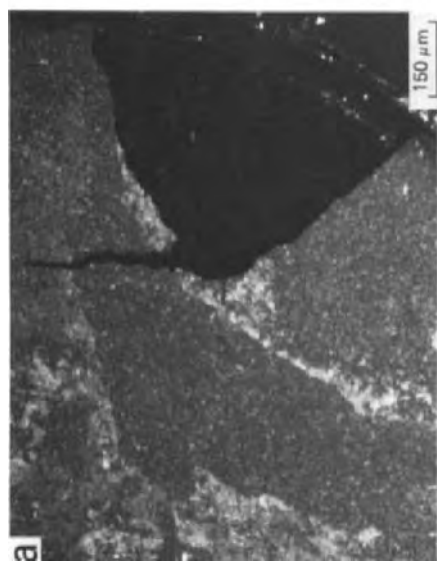
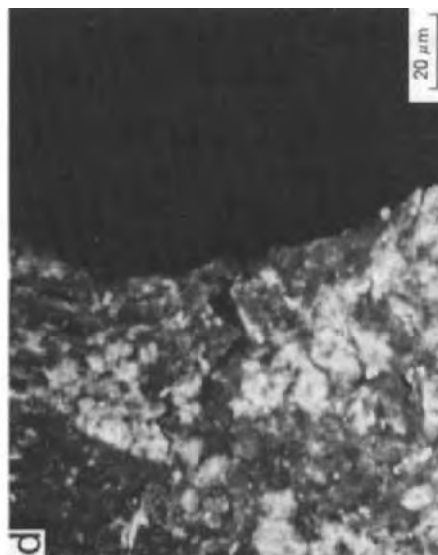
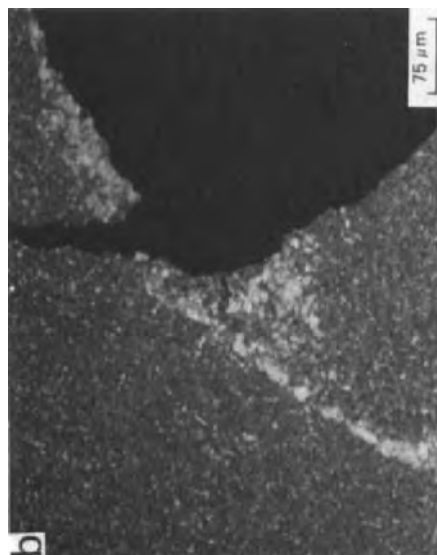
The LM (low-magnification) scanning mode at 20 keV was used to obtain micrographs at $\times 100$ to $\times 800$ magnifications (Fig. 3). The LM SEM mode uses the condenser lens as the probe-forming lens and images were made from backscattered electrons. The ring in the right hand corner of the micrograph with a bar scale of 100 μm was caused by the sample holder. The white of the four photos in Fig. 3 indicates the presence of iron-containing compounds in the peaty materials.

The images of Fig. 4 were made in a SEM mode whereby the standard objective lens was used as the probe-forming lens. This operational mode allows imaging with backscattered electrons at higher magnifications than the LM SEM mode of Fig. 3. To allow a comparison with the LM SEM mode, magnifications were started at $\times 800$. The maximum magnification was reached at $\times 6400$ using backscattered electrons.

To allow a comparison of SEM and STEM modes of operation, STEM was started at $\times 3200$ and followed by an image of $\times 6400$. The latter two micrographs can be compared with the last two in Fig. 4 and are the beginning of a series of STEM images in Figs. 5 and 6. It is clear that there is a great deal of difference between the SEM (close-to-surface) and STEM (transmission) mode of operation of the EM 400T/ST and in the results obtained. STEM gives the best imaging near the edges of a thin section or where the soil material borders on a pore or artificial crack caused by charging and heating of the soil sample. This is understandable because the thin sections are thinnest at such places.

Bright-field imaging was done with the STEM mode of operation in Figs. 5 and 6. Imaging was started at $\times 3200$ and finished at $\times 50\,000$ in Fig. 6. Due to the number of micrographs made, the results of one example are spread over two figures. The channel which runs more or less horizontally, in the micrographs with magnifications $\times 3200$, $\times 6400$ and $\times 12\,500$ in Fig. 5, has been enlarged artificially after charging and heating. All micrographs in Figs. 5 and 6 show that some details can be discerned but that these studies need EDXRA for chemical identification purposes.

Fig. 2. The difference between secondary electron (SE) and BSE images made with the SEM 505 ($\times 2000$). The structure in the BSE (A + B) image, obtained from 1 to 5 μm depth in the thin section, is clearly discernable. The SE image comes from a shallower depth in the thin section and gives only little information on structure in the iron-coated organic material.



Point-analyses with STEM-EDXRA were made at $\times 50\,000$ in black and grey coloured microareas of the soil matrix in Fig. 6. Even at this scale some variety in chemical elements could be discerned, especially in the peaks of Al and Si. Another important result was the possibility of measuring P, Ca and Cu in the four analyses. Such elements were not detected with a conventional SEM-EDXRA such as the JSM-35C and the SEM 505. This is due to the higher primary electron energy of STEM-EDXRA which allows microchemical analyses at larger depths than in the SEM apparatus used for scanning electron microscopy of surfaces only. The detection of minute quantities of P, Ca and Cu in the thin section is important because this could indicate that STEM-EDXRA work can be done *in situ* on near-trace-element quantities at large magnifications. The reliability of such measurements becomes even better, however, if ultrathin samples can be measured because less soil material is then available below the surface of the specimen. The added possibility, using a Scanning Transmission Electron Microscope to investigate chemical elements at magnifications larger than $\times 10\,000$, is important for the study of thin sections and ultrathin sections because such microvariety is frequently present in many soils.

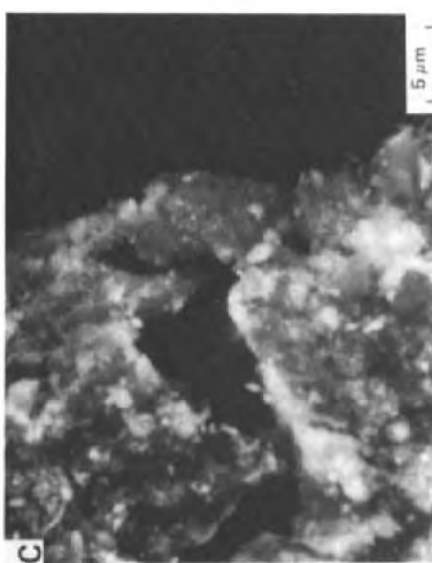
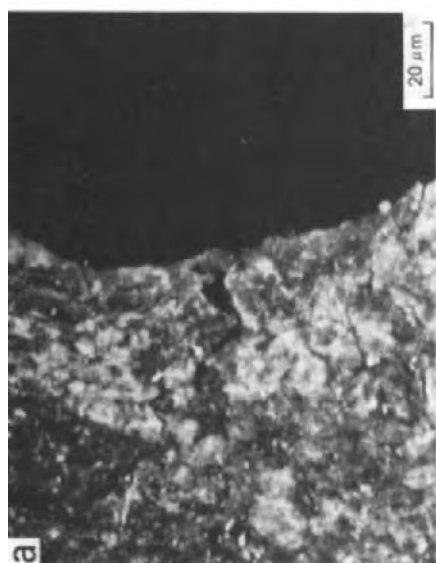
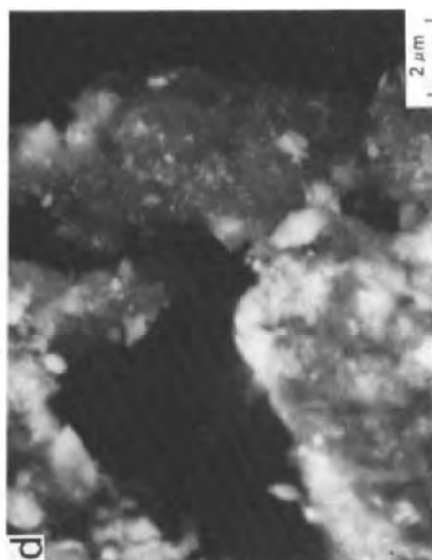
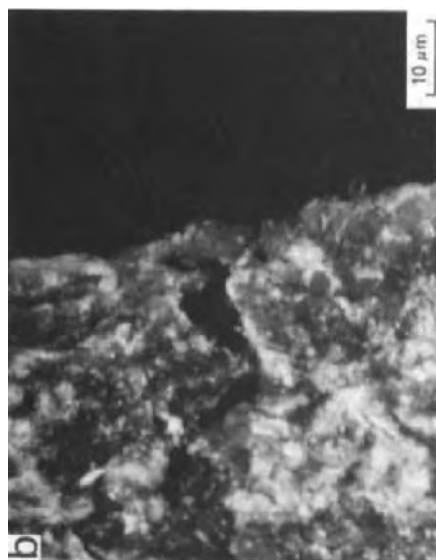
CONCLUSIONS

SEM-EDXRA analysis with a conventional SEM (JSM-35C or SEM 505) allows a quick inventarisation of predominantly the heavier chemical elements in a thin section up to magnifications of $\times 10\,000$. Experiments with iron-coated organic material from peat have shown that this can be done at much higher magnifications with an instrument such as the EM 400T/ST which can operate as a SEM, STEM and TEM combined with EDXRA equipment.

For this particular material a maximal magnification for EDXRA analysis was reached on a $5\,\mu\text{m}$ thick thin section using the STEM-EDXRA mode of the EM 400T/ST. Indications are that elements like P, Ca and Cu, which were not measured with conventional SEM-EDXRA point-analyses at $\times 10\,000$, represent near-to-trace-element quantities analysed by STEM-EDXRA at $\times 50\,000$. As a consequence, STEM-EDXRA investigation can be used in cases where insufficient microchemical detail is obtained during SEM-EDXRA, SEM-WDXRA (scanning electron microscopy—wavelength dispersive X-ray analysis) or EMA (electron microprobe analysis).

Other elements measured were Al, Si, Fe and Cl. Chlorine was indicated only once with STEM-EDXRA. The quantity of Al and Si could vary significantly in the four point-analyses. Considerable iron was present. The

Fig. 3. Low-magnification scanning mode at 20 keV with the EM 400T/ST ($\times 100$ to $\times 800$). Operation as a SEM (scanning electron microscope) on iron-coated organic material from peat without orientation. White areas contain larger quantities of iron compounds than grey ones. This figure is continued in Fig. 4 with another mode of operation using the same instrument.



elements Al, Si and Fe were also found with a conventional SEM and represent major elements in the iron-coated peaty material. Even at larger magnifications, also reached by conventional SEM-EDXRA in machines specifically built for scanning electron microscopy (JSM-35C and SEM 505), STEM-EDXRA analysis may be of importance because of the higher accuracy which can be obtained.

The quality of the microchemical analysis would be even better if the 5 μm thick thin section could become ultrathin. For this, ion thinning or cutting with a diamond cutter are necessary. In practice, however, such methods are only applied to relatively pure and soft soil materials such as clays and organic matter. The more common soil materials are, however, mixtures of harder and softer substances from which it is difficult to obtain ultrathin sections. Ion thinning can be a good method, but preparation, in order to guarantee the necessary very small thickness of about 1 μm , is often difficult. As a consequence, TEM-EDXRA work on such ultrathin sections could possibly be started with the examination of thicker samples with STEM-EDXRA.

The present experiments indicate that STEM-EDXRA work can only be done on or near the boundary of soil material and voids where the sample is thinnest. It therefore becomes necessary to make future samples thinner than 5 μm to obtain results in the middle of the soil matrix as well as in cases where no voids are present. The simplest way seems to be to replace the plastic used for mounting on the object glass by dissolvable material. In this way, the 5 μm thick thin section would become about 3 μm thick. Polishing of both sides of the thin section should be done to guarantee minimal thickness differences. In practice, however, such parallelism will be difficult to obtain between the surfaces of the thin section due to hardness differences of the soil constituents. Microthickness differences will therefore remain.

Backscattered electron imaging was done with three instruments, viz. the Jeol-JSM-35C, the Philips SEM 505 and the Philips EM 400T/ST. The first two instruments were built for SEM work, whereas the latter machine can operate in SEM, STEM and TEM modes. All these instruments offer possibilities of obtaining backscattered electron scanning images (BESI). In the present case the SEM stopped at $\times 2000$ magnification and the Scanning Transmission Electron Microscope in the BSE-mode at $\times 6400$. A lot of detail on the structure and fabric of soil materials can be obtained in this way, especially because BESI contain information from a somewhat greater

Fig. 4. SEM mode of the EM 400T/ST at 20 keV ($\times 800$ to $\times 6400$). The smallest magnification used in this mode has a somewhat better resolution than the last micrograph in Fig. 3 which was also taken at $\times 800$. Orientations remain absent. Very fine threads are barely visible in the central pore. These indicate breakage of the thin section material at such sites followed by dislocation. Such movements were caused by charging and heating of the soil material at 120 keV in the STEM mode, of micrographs which are given in Figs. 5 and 6.

depth in the thin section than the secondary electron images, a depth which is not affected by polishing. Another advantage of BESI is the portrayal of iron accumulations in white without needing to make X-ray images of the element to find its distribution over the thin section. The positioning of line scans and point analyses for microchemical information therefore becomes easier with BESI.

Due to the very high accelerating voltage of 120 keV in STEM, instead of the 20 keV in LM SEM and other SEM modes, pieces of thin section in the copper grid may break. At such surfaces the thin section may be thinner than normal and therefore interesting for transmitted electron study by STEM. The best way to study small soil particles will be by TEM-EDXRA using ultrathin sections. As long as these are still difficult to make, it seems reasonable to use thicker thin sections and to study them by STEM-EDXRA. In this manner the edges of 5 μm thick maximally ground thin sections and 3 μm thick thin sections of which the layer used for mounting has been removed could play a role in transmitted electron microscopy. The ideal remains, however, a technique which allows the easy preparation of ultrathin sections of all kinds of soil materials. This is not only because of EDXRA measurements but also to allow in situ electron diffraction of individual soil minerals. The possibility to study ultrafabric and ultrastructure in ultrathin sections also indicates the necessity of their regular manufacturing to obtain a basic insight into soil environments. The machines are ready to help us but better preparation techniques for ultrathin sections must be found.

Fig. 5. STEM (scanning transmission electron microscopy) bright-field imaging at 120 keV with the EM 400T/ST ($\times 3200$ to $\times 25\,000$). Transmitted electron micrographs were made of the same iron-coated organic material as was present in the last two images of Fig. 4. The very fine threads in the pore of Fig. 4, caused by charging and heating, have now become easy to observe and exhibit a certain topography. Small soil fragments are distinguishable in the soil matrix.

Fig. 6. STEM bright-field imaging with the EM 400T/ST (Figs. 6a and 6b) and EDXRA (energy dispersive X-ray analysis) of the same material as in Fig. 5 at $\times 50\,000$ and under similar conditions (Figs. 6c to 6f). Overlap is present in Figs. 6a and 6b, with Fig. 6b starting about halfway across Fig. 6a, i.e., point-analysis *e* (Fig. 6e) therefore also lies in Fig. 6a, while number 4 is situated at the lower boundary of Fig. 6a. Point analyses *c-f* of Fig. 6b are given in the same order in Figs. 6c to 6f. EDXRA point analyses at $\times 50\,000$, measured with the EM 400T/ST in the STEM-EDXRA mode, seemed to give additional chemical elements to those measured at $\times 10\,000$, the highest magnification for EDXRA analysis with a SEM (i.e., JSM-35C or SEM 505) used for scanning electron microscopy of surfaces only.

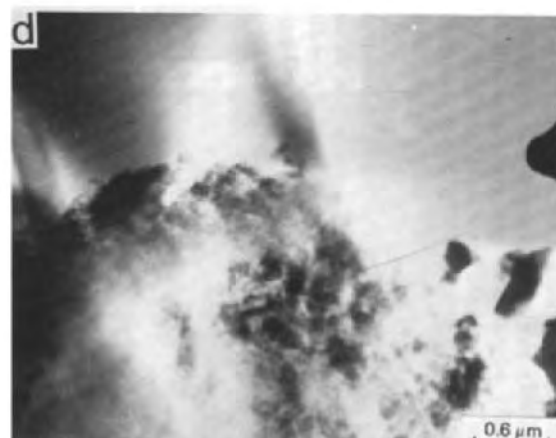
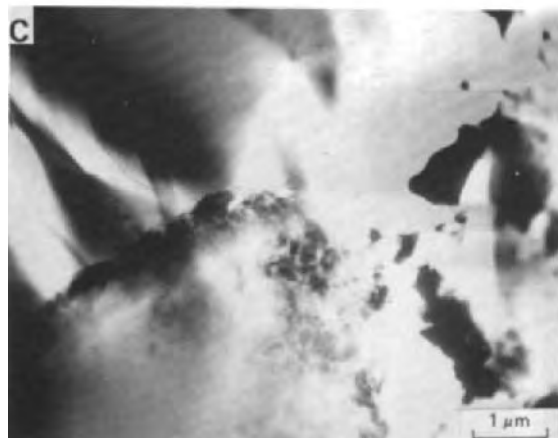
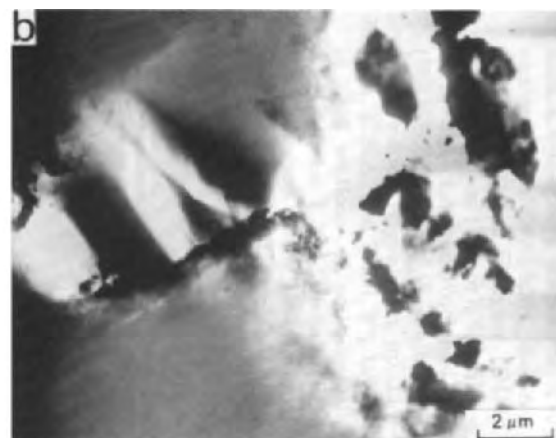
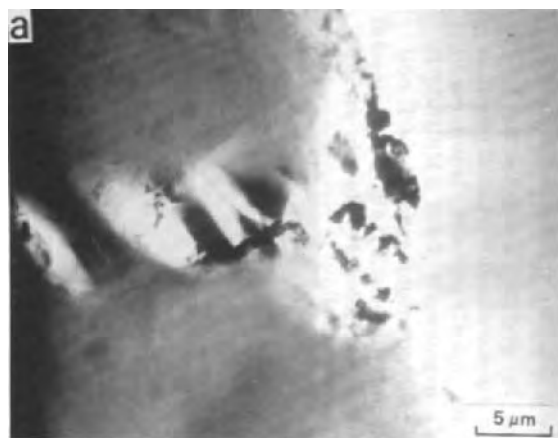


Fig. 5. Legend on p. 88.

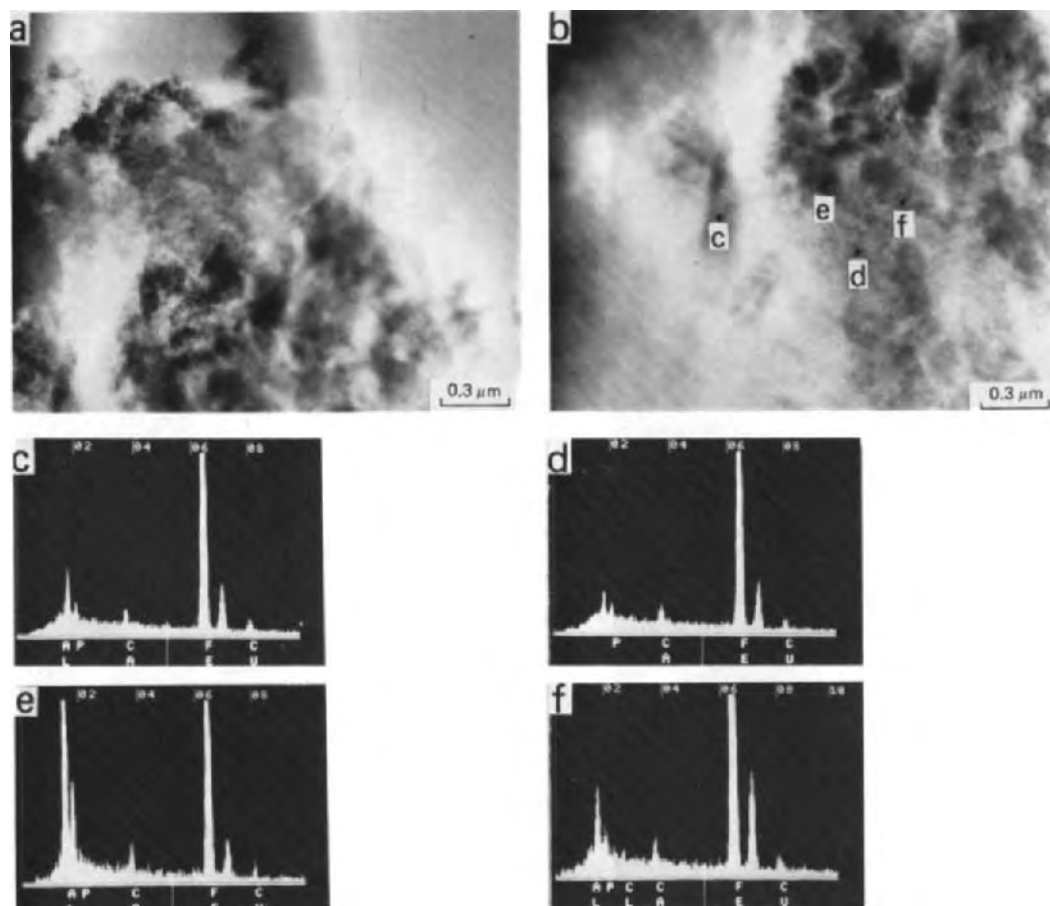


Fig. 6. Legend on p. 88

REFERENCES

- Bisdom, E.B.A., 1981a. A review of the application of submicroscopic techniques in soil micromorphology, I. Transmission electron microscope (TEM) and scanning electron microscope (SEM). In: E.B.A. Bisdom (Editor), *Submicroscopy of Soils and Weathered Rocks*. 1st Workshop of the International Working-Group on Submicroscopy of Undisturbed Soil Materials (IWGSUSM), 1980, Wageningen. Centre for Agricultural Publishing and Documentation (Pudoc), Wageningen, pp. 67–116.
- Bisdom, E.B.A., 1981b. A review of the application of submicroscopic techniques in soil micromorphology, II. Electron microprobe analyzer (EMA), scanning electron microscope-energy dispersive X-ray analyzer (SEM-EDXRA), laser microprobe mass analyzer (LAMMA 500), electron spectroscopy for chemical analysis (ESCA), ion microprobe mass analyzer (IMMA), and the secondary ion microscope (SIM). In: E.B.A. Bisdom (Editor), *Submicroscopy of Soils and Weathered Rocks*. 1st Workshop of the International Working-Group on Submicroscopy of Undisturbed Soil Materials (IWGSUSM), 1980, Wageningen. Centre for Agricultural Publishing and Documentation (Pudoc), Wageningen, pp. 117–162.
- Bisdom, E.B.A. and Thiel, F., 1981. Backscattered electron scanning images of porosities in thin sections of soils, weathered rocks and oil-gas reservoir rocks using SEM EDXRA. In: E.B.A. Bisdom (Editor), *Submicroscopy of Soils and Weathered Rocks*. 1st Workshop of the International Working-Group on Submicroscopy of Undisturbed Soil Materials (IWGSUSM), 1980, Wageningen. Centre for Agricultural Publishing and Documentation (Pudoc), Wageningen, pp. 191–206.
- Bisdom, E.B.A., Henstra, S., Jongerius, A. and Thiel, F., 1975. Energy-dispersive X-ray analysis on thin sections and unimpregnated soil material. *Neth. J. Agric. Sci.*, 23 (4): 113–125.
- Bisdom, E.B.A., Henstra, S., Hornsvelde, E.M., Jongerius, A. and Letsch, A.C., 1976. Wavelength and energy dispersive X-ray microanalysis with EMA and SEM-EDXRA on thin sections of soils. *Neth. J. Agric. Sci.*, 24 (4): 209–222.
- Bisdom, E.B.A., Thiel, F., Volbert, B. and Jackman, J., 1983. Variations in backscattered electron scanning images with the Philips SEM 505 as applied to mineral grains and excrements in a podzol, to precipitates on a water-tube filter and to bauxite. *Geoderma*, 30: 93–116 (this issue).
- Boekestein, A., Henstra, S. and Bisdom, E.B.A., 1981. Submicroscopic techniques for in situ microchemical analysis of soils, I. Non-destructive techniques, 1. In: E.B.A. Bisdom (Editor), *Submicroscopy of Soils and Weathered Rocks*. 1st Workshop of the International Working-Group on Submicroscopy of Undisturbed Soil Materials (IWGSUSM), 1980, Wageningen. Centre for Agricultural Publishing and Documentation (Pudoc), Wageningen, pp. 29–44.
- Bresson, L.M., 1981. Etude ultramicroscopique d'assemblages plasmiqes sur lames ultra-minces de sols réalisées par bombardement ionique. In: E.B.A. Bisdom (Editor), *Submicroscopy of Soils and Weathered Rocks*. 1st Workshop of the International Working-Group on Submicroscopy of Undisturbed Soil Materials (IWGSUSM), 1980, Wageningen. Centre for Agricultural Publishing and Documentation (Pudoc), Wageningen, pp. 173–189.
- Foster, R.C., 1981. Localization of organic materials in situ in ultrathin sections of natural soil fabrics using cytochemical techniques. In: E.B.A. Bisdom (Editor), *Submicroscopy of Soils and Weathered Rocks*. 1st Workshop of the International Working-Group on Submicroscopy of Undisturbed Soil Materials (IWGSUSM), 1980, Wageningen. Centre for Agricultural Publishing and Documentation (Pudoc), Wageningen, pp. 309–317.

- Jongorius, A. and Heintzberger, G., 1975. Methods in soil micromorphology. A technique for the preparation of large thin sections. Neth. Soil Surv. Inst., Wageningen, Soil Surv. Pap., 10: 48 pp.
- Volbert, B., 1981. Verbesserung der topographischen Information durch Ueberlagerung von Sekundärelektronen (SE) - und invertiertem Rückstreuielektronen (BSE) - Signal. Beiträge Elektronenmikroskopische Direktabbildung und Analyse von Oberflächen (EDO), Innsbruck, 14: 325—330.

VARIATIONS IN BACKSCATTERED ELECTRON (BSE) IMAGES WITH A SCANNING ELECTRON MICROSCOPE (SEM) AS APPLIED TO MINERAL GRAINS AND EXCREMENTS IN A PODZOL, TO PRECIPITATES ON A WATER-TUBE FILTER AND TO BAUXITE

E.B.A. BISDOM¹, F. THIEL², B. VOLBERT³ and J. JACKMAN³

¹ *Netherlands Soil Survey Institute, P.O. Box 98, 6700 AB Wageningen (The Netherlands)*

² *Technical and Physical Engineering Research Service, 6700 AJ Wageningen (The Netherlands)*

³ *N. V. Philips, Application Laboratory-Electron Optics, TQ-III-p, 5600 MD Eindhoven (The Netherlands)*

(Accepted for publication February 17, 1983)

ABSTRACT

Bisdom, E.B.A., Thiel, F., Volbert, B. and Jackman, J., 1983. Variations in backscattered electron (BSE) images with a Scanning Electron Microscope (SEM) as applied to mineral grains and excrements in a podzol, to precipitates on a water-tube filter and to bauxite. *Geoderma*, 30: 93–116.

The results of experiments on various materials in thin sections, using a Scanning Electron Microscope with a secondary electron detector and four backscattered electron detectors, are discussed. The Multi-Function-Detector (MFD) system for backscattered electrons allows the observation of the 'real' topography in a thin section with the SE-BSE mode and is also able to give good information on the contrasts in materials (atomic contrasts) with the BSE (A+B) mode. Various other possibilities are also present with this system, e.g. the study of soil materials over different depths below the surface of a thin section. Of considerable interest is the possibility to start the investigation of thin sections at $\times 10$ magnification without the loss of part of the picture on the display screen or micrograph. As a consequence, interpretational steps from the field observations to light microscopy and submicroscopy will most probably become easier in the near future. Maximum magnifications using the BSE-signal were dependent on the type of analysed material, but were usually significantly higher than with older backscattered electron detector systems.

INTRODUCTION

Backscattered electron scanning images (BESI), called backscattered electron (BSE) images in this paper, of soil materials were introduced by Bisdom and Thiel (1981) and macro- and microporosities measured from them by Quantimet (Jongerijs and Bisdom, 1981). The instrument used to make BSE images was a SEM with a backscattered electron detector of the semi-

conductor type, comprising two solid state detectors. A lot of experience was gained with this machine by studying materials of soils, weathered rocks and oil—gas reservoir rocks. BSE micrographs of materials in thin sections were of a much better quality than SE (secondary electron) micrographs, especially up to magnifications of about $\times 4000$. The maximal magnification was rather dependent on the type of material being investigated and often stopped below $\times 1000$. BSE images allow structure and fabric analyses of soil materials in thin sections at such magnifications. Of special interest to us was the possibility of studying soil porosity of all kinds of materials because the Quantimet could measure pores in BSE micrographs.

A newer type of instrument allows different modes of operation using BSE and SE detectors. The results on the portrayal of materials and porosities are discussed below.

MATERIALS AND METHODS

Soil material, occurring in the A horizon of a podzol from The Netherlands, was studied with a SEM 505 equipped with a Multi-Function-Detector (MFD) consisting of four backscattered electron detectors and the common secondary electron detector (Jackman, 1980). Such horizons often show a combination of mineral and organic materials in micro-areas of a thin section. BSE perform especially well on soil and other materials with heavier chemical elements (Bisdorn and Thiel, 1981). This means that difficulties arise when the lighter elements in organic material must be portrayed with BSE due to the small BSE coefficient. These should appear blackish if only elements like H, C, N and O are involved. In practice, however, Fe and other elements are also often present in the organic tissues and images are obtained, even with BSE, because of these heavier elements. There is also the possibility of working with a combination of BSE and SE detectors, or with the SE detector alone, to study materials on or near to the surface of a thin section (Volbert, 1981).

A precipitate on a copper water-tube filter (courtesy of the Dune Water Works, The Hague, The Netherlands) was studied with the MFD system of the Philips SEM 505. A separate paper on this precipitate, with BSE and microchemical information, is also presented in this issue (Bisdorn and Jongerius, 1983). This was done with the Jeol-JSM-35C equipped with an EDAX 9100 system using an ECON windowless detector for the detection of chemical elements with a low atomic number. The BSE detector was of the semiconductor type, comprising two solid state detectors. Some of the micrographs in this paper can be compared with those in the paper by Bisdorn and Jongerius (1983).

Bauxite from Surinam (courtesy International Soil Museum, Wageningen, The Netherlands) was the third material analysed by the MFD system. Similar material of the same sample has already been investigated with secondary ion mass spectrometry (SIMS) and quantification done in an area of about

300 μm diameter (Henstra et al., 1980). The bauxite showed considerable variation in the composition of micro-areas and was studied for its trace and major elements with the Cameca IMS 300 (Henstra et al., 1981). Such analyses can now be done quantitatively from a micro-area with a diameter of 1.5 μm with the Cameca IMS 3F (Bisdorf et al., 1983a). In the present case, the occurrence of gibbsite crystals and fluidal structures with a high Al content were studied with backscattered electrons.

A few technical details of the MFD system are given. Four backscattered electron detectors are connected by fibre optics to two photomultiplier/pre-amplifier combinations which can be placed outside the specimen chamber (Jackman, 1980). Each of the four backscattered electron detectors of the MFD system is fitted with phosphor of the optimal thickness for 30 keV electrons, and an Al-layer suitable for operation down to 5 keV. Secondary electrons lack the energy to penetrate the Al-layer and consequently only backscattered electrons are recorded by a scintillator. The impact of backscattered electrons on the detector produces photons of visible light conducted by the fibre optics to the photomultiplier tube. By replacing the phosphor of the BSE-detector by a light-gathering lens which focuses on the fibre optics bundle, cathodoluminescence detection is possible depending on the type of soil material being investigated.

Optical switches which connect the fibre optics of two BSE-detectors to one of two photomultiplier tubes allow the rapid switching of detection modes and any combination of the four signals coming from the detectors through the fibre optics to the photomultiplier tubes can be chosen. The result is that rotation of the sample can be simulated without movement of the analysed material itself due to changes in illumination of the sample. BSE-detectors can be compared with light sources which illuminate the specimen. Working with one active BSE-detector therefore causes strong shadowing effects, four active detectors (homogeneous illumination) reduce the shadowing, material contrast is optimised.

Two backscattered electron detectors (scintillators), indicated as detector A in Fig. 1, can be combined to a signal A, and the other two scintillators (detector B) to a signal B. The central part of the sample in Fig. 1 has a higher atomic number (A.N.) than the remainder of the sample. The signal height is larger if the sample is tilted towards detector A or B. An intermediate signal height is reached for the flat part of the sample, as indicated by backscattered electron signals A or B in Fig. 1. Surfaces which tilt away from the detectors, give the same signal as the flat parts of the remainder of the sample with a lower atomic number. If both detectors are used, signals A + B give material contrast and signals A-B topographic contrast, as indicated in a schematic way in Fig. 1.

In our studies we used signals A+B or A-B, and the secondary electron (SE) detector. The effects of signal mixing (A+B), (A-B) and SE-BSE, are discussed below with the results. It will be shown that the separation of different contrasts is possible, viz. material and topographic contrasts in soil

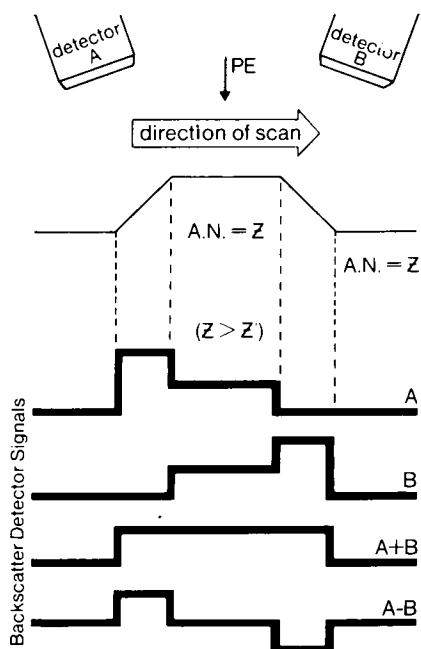


Fig. 1. MFD-scintillators can give signals A, B, A+B and A-B. Each of these signals gives a certain type of information of which the backscattered electron signal, BSE (A+B), is very useful for thin section studies (material contrast). The BSE (A-B) signal results in topographic contrast.

material present in the A-horizon of a podzol and in precipitates which clog the filter of a water tube. The possibility of observing the studied materials of the thin section on TV-rate images was of considerable help in this work. This means that the whole display screen is illuminated simultaneously due to the very fast reaction time of the detector system.

RESULTS

Soil material in the A-horizon of a podzol

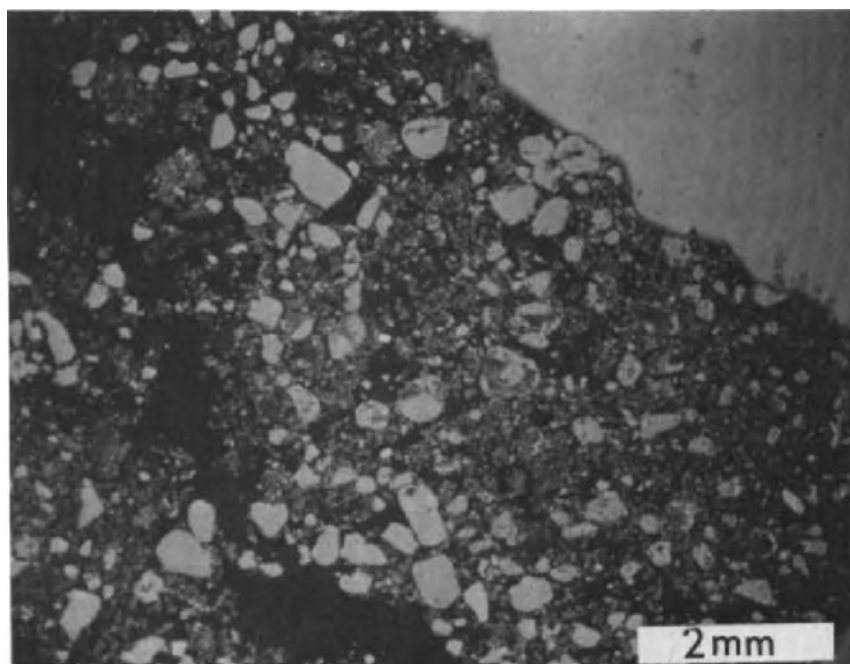
A view of the analysed material in the A horizon of a podzol is shown in Fig. 2. The white grains are predominantly quartz in various size classes, whereas the greyish material and the small included mineral fragments constitute excrements. The micrograph of Fig. 2 was made with all four scintillators (A+B), which give uniform illumination in the light optical analogues and optimal material contrast without topography. The same results are obtained in the BSE (A+B) mode of Figs. 3 and 4.

If only two scintillators (BSE-detectors) A or B are used, the illumination effects can be seen in Fig. 3. BSE (A) and BSE (B) show shadowing or topographic effects, whereby certain particles seem to rise from the micrograph

in one photo and form holes in the other. If the position of the detector (light source) is known, it can be decided if the surface detail is a hole or not. Such effects can be used in special studies but were of little interest to our investigation.

Imaging of the topography of a multi-compositional rough specimen can be done in the BSE-mode by subtracting the signal of two scintillators (B) from the signal of the other two scintillators (A) as illustrated in Fig. 1. This BSE (A-B) mode, however, can result in the wrong interpretation of the specimen's topography due to an artefact called pseudotopography which occurs at high primary electron (PE)-energies. This pseudotopography is caused by anisotropic backscattering of the BSE at the material boundaries (Volbert, 1981).

An example of a BSE(A-B) image at 30 keV primary electron energy is given in Fig. 5. This information depth is deeper than the SE and SE-BSE images taken at the same and high acceleration voltage. SE-BSE images are considered to approach the real topography best at the surface of the thin section and to have a smaller information depth than the SE-signal due to suppression of the BSE-information in the secondary electron signal. The use of the Multi-Function-Detector in the Philips SEM 505 allows the generation



BSE (A+B)

Fig. 2. Low magnification image of soil material in the A horizon of a podzol. All the used signals have been indicated underneath the micrographs. Enlargements in Figs. 3 to 8 are from the central part of this figure.

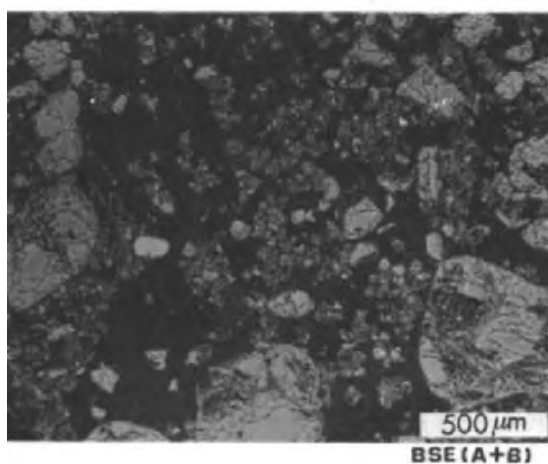
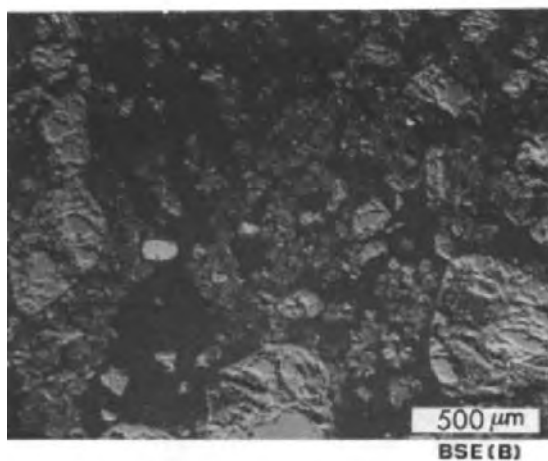
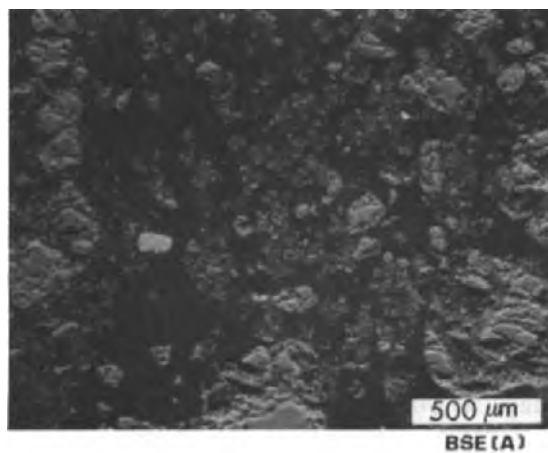
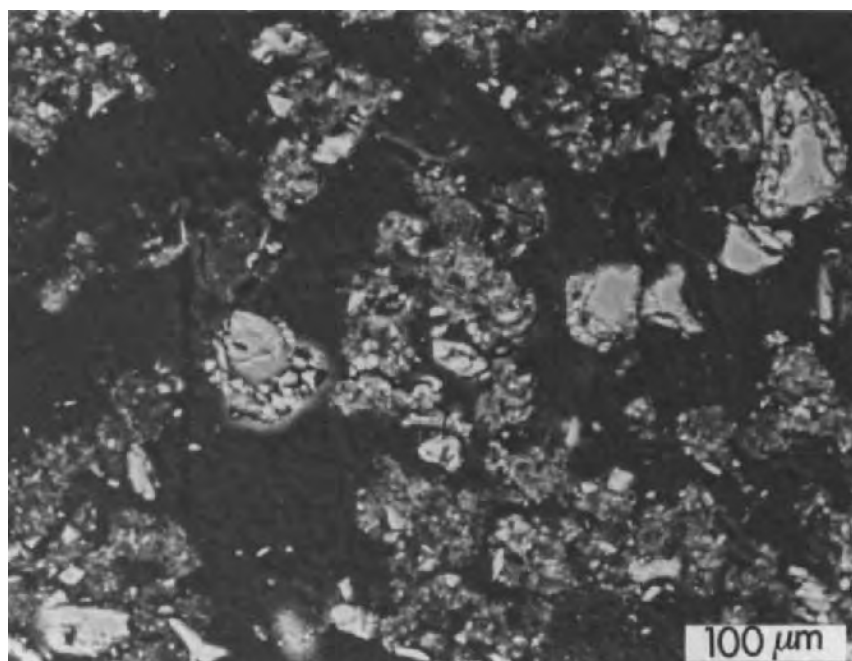


Fig. 3. Shadowing effects in the BSE (A) and BSE (B) modes. Optimal material contrast in the BSE (A+B) mode. Minerals and mineral fragments in excrements are whitish to grey and organic matter with or without heavier chemical elements greyish to black.



BSE (A+B)

Fig. 4. Detail of Fig. 3 in which the smaller mineral fragments inside the excrements become more visible. Larger minerals, predominantly quartz grains, were already visible in Fig. 3.

of (SE-BSE) signals at both high and low primary electron energies. The best topographic contrast in Fig. 5 is given by SE-BSE, whereas the best material contrast is found in the BSE (A+B) mode. Of major importance for most of the submicroscopic studies on thin sections is the material contrast BSE (A+B) which can started at low magnifications of about $\times 10$ (Fig. 2) and may continue to $\times 1000$ and $\times 30\,000$ (Figs. 6 – 8) depending on the type of soil material.

The difference between SE and BSE (A+B) signals at high primary electron energies is clearly demonstrated in the higher magnifications of the materials in excrements of Figs. 6 – 8. The SE-image shows a mixture of depth and surface information and the BSE-image only depth information. The BSE (A+B) mode gives images at a greater depth than the SE-signal. Usually, depth of analysis with backscattered electrons is greatest in organic materials and lower in mineral grains due to the different penetration depth of the PE. Images from pores usually come from a maximum depth of about $5\,\mu\text{m}$, whereas this is commonly $1\,\mu\text{m}$ to $3\,\mu\text{m}$ depth for backscattered electrons in mineral grains. As already explained above, however, depth of analysis with BSE depends not only on the type of soil material analysed but also on the acceleration voltage used. Of practical importance is the fact that high pol-

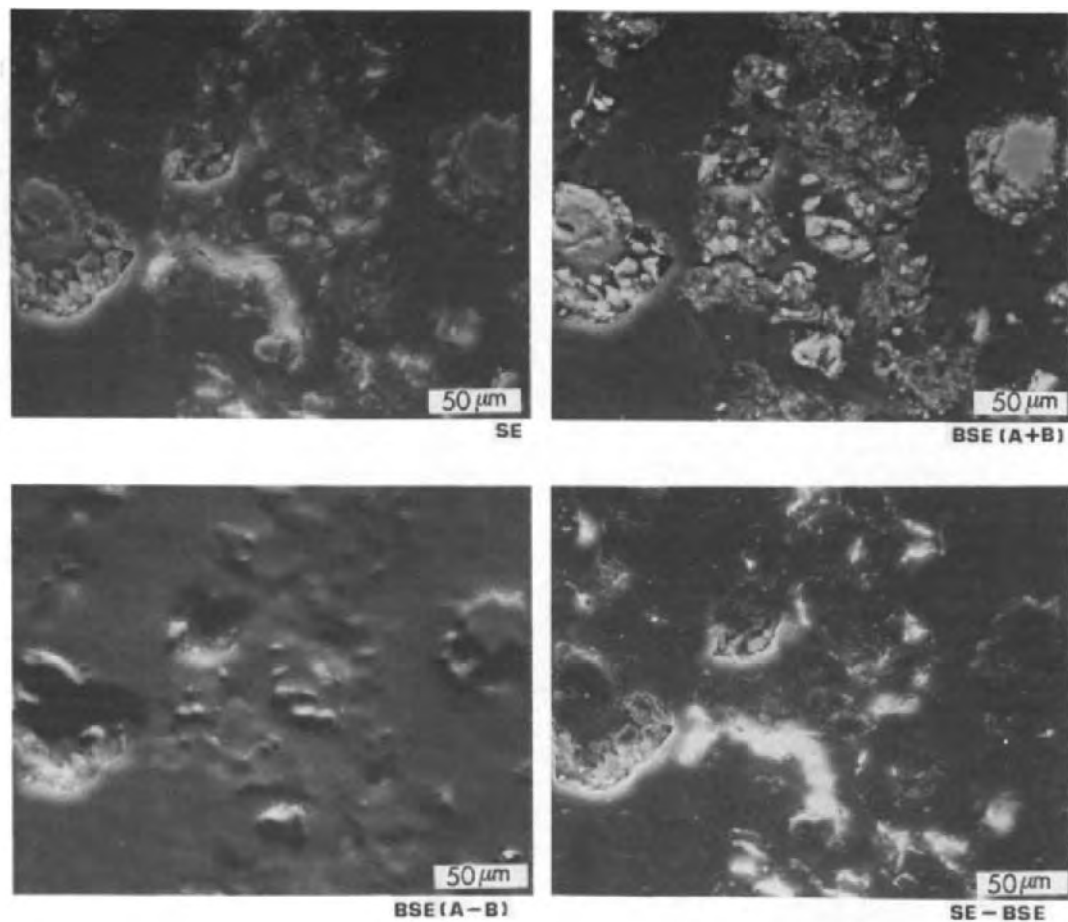


Fig. 5. Mixing of various signals, including the secondary electron (SE) signal. The SE signal gives a mixture of depth and surface information; the BSE (A+B) signal an optimal material contrast; the BSE (A-B) signal pseudotopography; and the SE-BSE signal the 'real' topography.

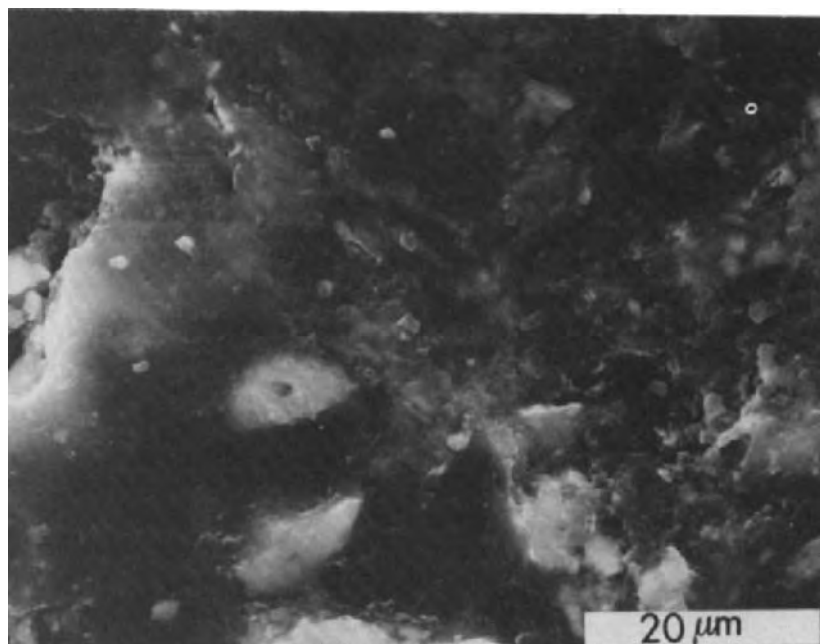
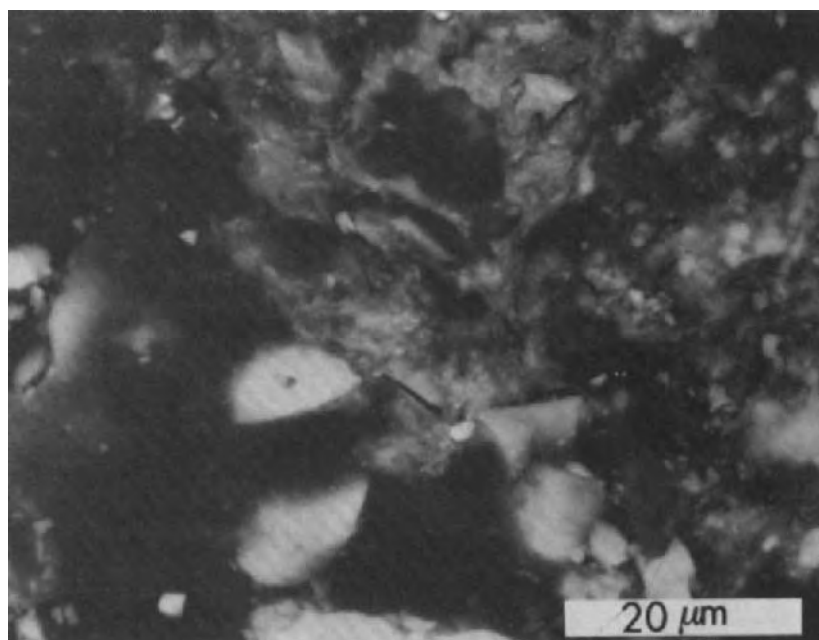
**SE****BSE (A+B)**

Fig. 6. Enlargement of the central part of Fig. 5. The BSE (A+B) signal gives information about a somewhat deeper depth below the surface of the thin section than the SE image. The BSE (A+B) mode provides a clear picture from some 1 μm to 5 μm depths, whereas smearing effects due to polishing are visible in the SE image.

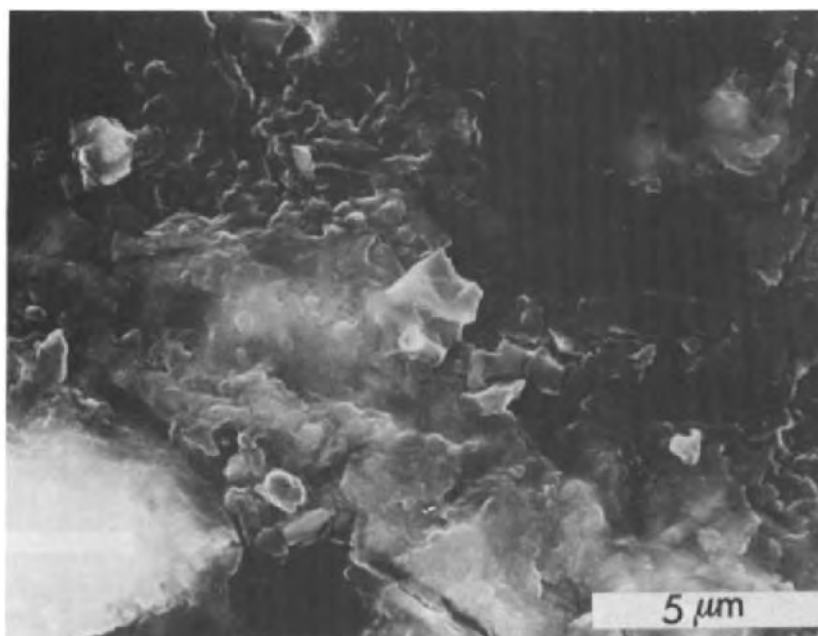
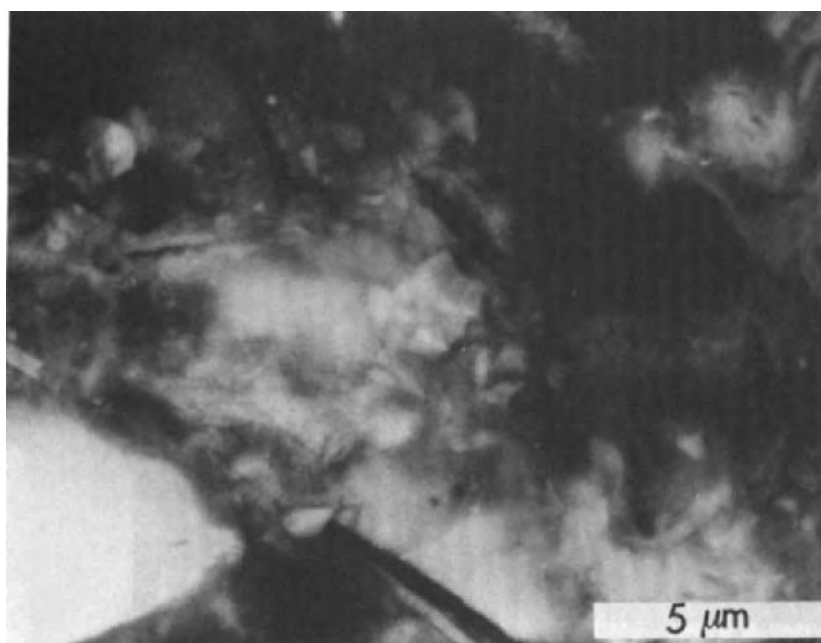
**SE****BSE (A+B)**

Fig. 7. Particles which are very small in Fig. 6 (central part), are more easily recognisable in this figure. Information concerning the material in the soil matrix can be obtained.

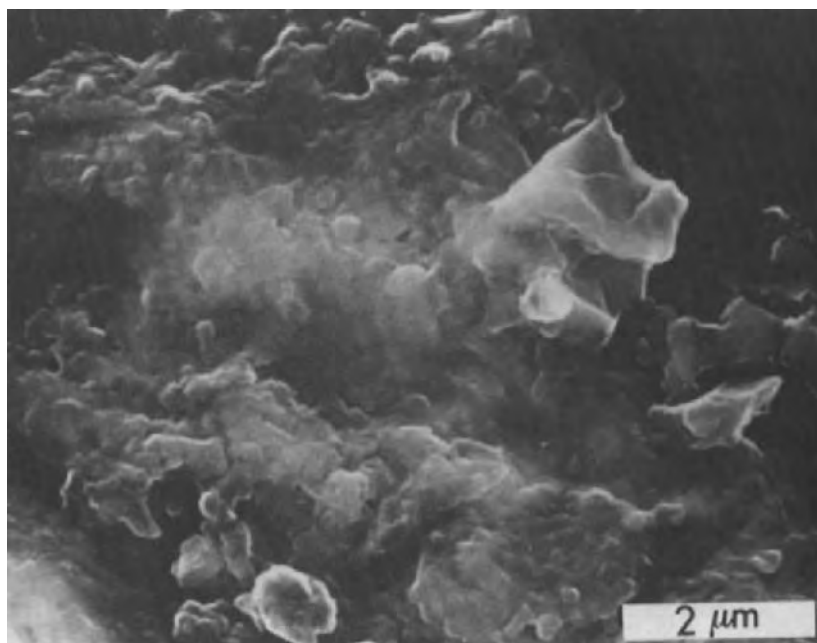
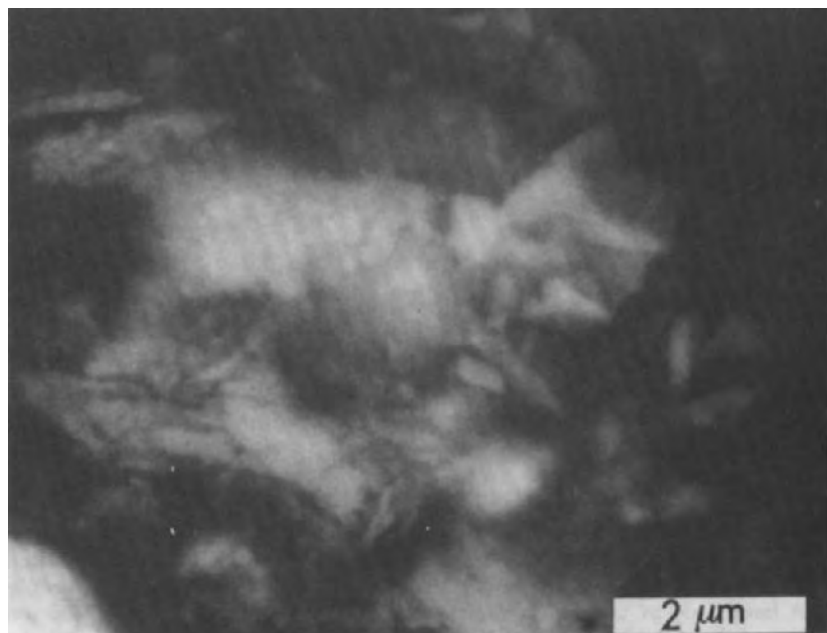
**SE****BSE (A+B)**

Fig. 8. Maximal enlargement of the central part of Fig. 7. The SE image is still of a good quality but the BSE (A+B) image is at its maximum magnification. The maximal enlargements with BSE are very dependent on the type of soil material and the instrument used.

ishing of the thin section surface is not really necessary for BSE (A+B) imaging but is better when other modes are also used and absolutely essential when the topographic contrast is investigated using the SE-BSE mode (Fig. 5).

An important asset of the use of the SE mode is the possibility of obtaining higher magnifications than with BSE. This is observable in Figs. 7 and 8 where the BSE (A+B) images are becoming unsharp at higher magnifications, whereas SE images are still offering detail at the same magnifications and larger. SE-imaging is often used for the portrayal of organic matter in thin sections, whereas BSE-imaging is theoretically unsuitable. In practice, however, heavier chemical elements can be present on or in the organic tissue and BSE-imaging becomes possible. This is also the case with the organic matter in the A horizon of the podzol (Figs. 5 — 8) and consequently BSE (A+B) images could be made of both organic materials and minerals.

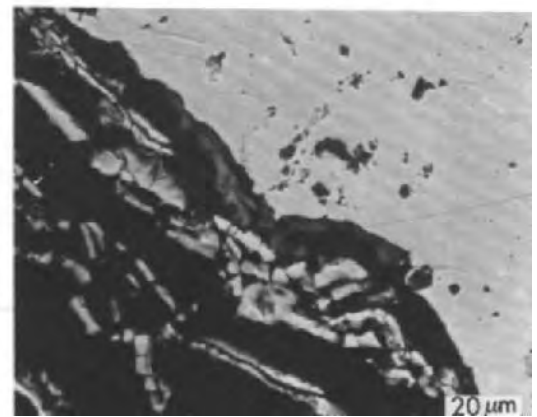
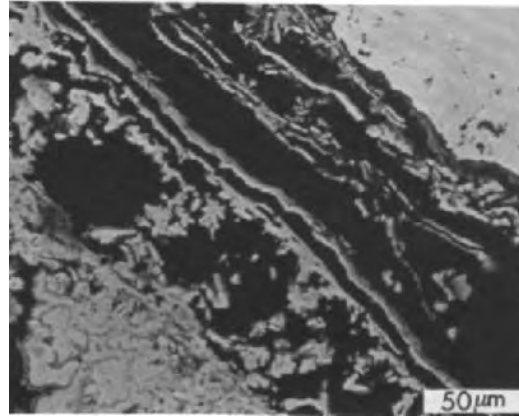
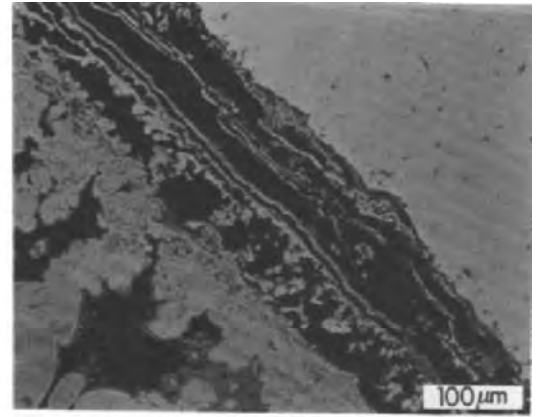
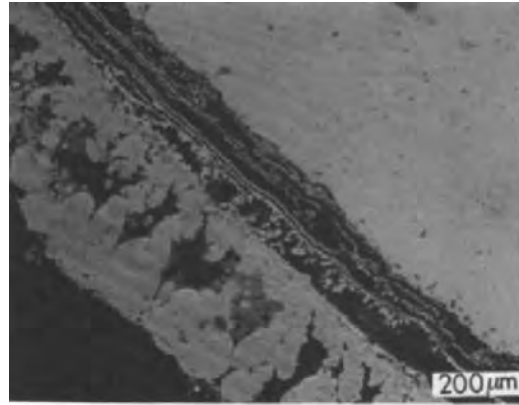
Precipitates on a water-tube filter

Only the more technical details of the Philips SEM 505 imaging of precipitates on and corrosion of a water-tube filter are discussed here. A separate paper in this issue, by Bisdom and Jongerius (1983), discusses some of the processes studied by light microscopy and SEM-EDXRA, viz. a Jeol-JSM-35C (SEM) equipped with an energy dispersive X-ray analysis system. Some of the results of the imaging with both machines can be compared.

A view of the precipitate and part of the copper filter is shown in Fig. 9, i.e. the BSE (A+B) mode. The corroded filter can be seen in the upper right position of the images. Exfoliated and weathered pieces of the copper tube are recognisable going towards the middle of the micrograph followed by precipitates that end on the lower left hand side of the photo. In the micrograph with a bar scale of 20 μm , only the Cu-filter and exfoliated-weathered pieces of the tube are portrayed. Maximal magnification with BSE (A+B) is reached in Fig. 10.

Different operational modes are illustrated in Figs. 11 and 12. The materials in these figures are the same as those in Fig. 10. Shadowing effects with two scintillators (BSE-detectors) A or B are given in Fig. 11. It is clearly demonstrated that the BSE (A) mode of operation gives a picture which is different from the BSE (B) mode due to the different directions of illumination. A complete range of different operational systems is given in Fig. 12 whereby BSE (A+B) gives the material contrast and SE-BSE the 'real' topo-

Fig. 9. Precipitates on a water-tube filter and corrosion of the copper filter. Details on the corrosion of the filter are shown in Figs. 10 — 13 and details on the precipitate in Figs. 14 — 15. Exfoliated platelets and small pieces of the original filter can be seen at the upper right hand side of the micrographs with bar scales of 100 μm and 200 μm . Towards the lower left of the images whitish precipitates have settled onto the exfoliated platelets and show a number of growth patterns with intermittent pores that are locally partly or wholly filled with greyish deposits.



BSE (A+B)

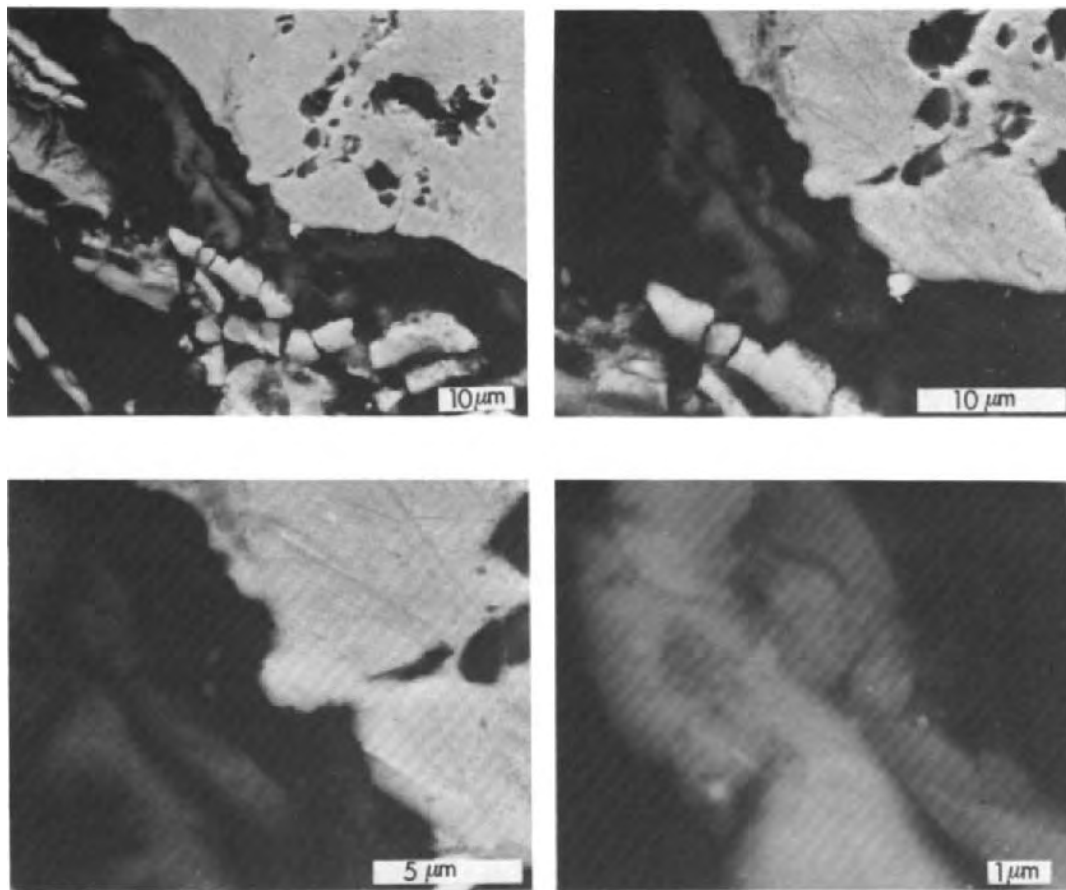


Fig. 10. Detail of the central part of the BSE (A+B) micrograph with a 20 μm bar scale in Fig. 9. The depth of information below the surface of the thin section has become somewhat larger.

BSE (A+B)

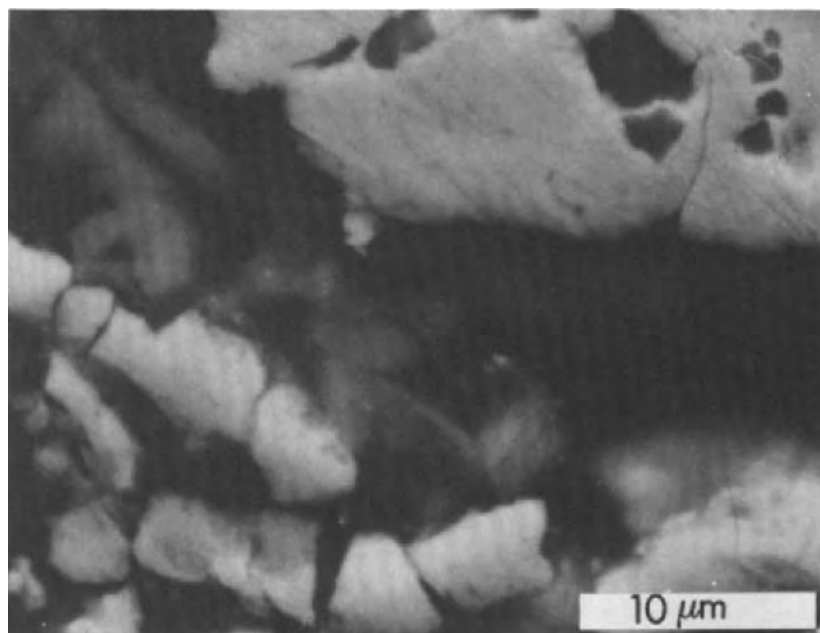
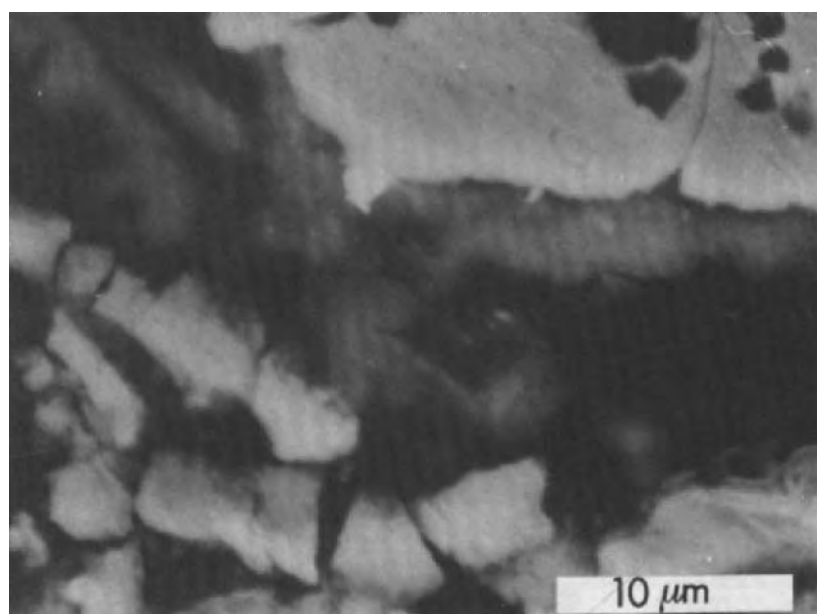
**BSE (A)****BSE (B)**

Fig. 11. Shadowing effects if only two backscattered electron detectors are used in the A or B mode (compare Fig. 12).

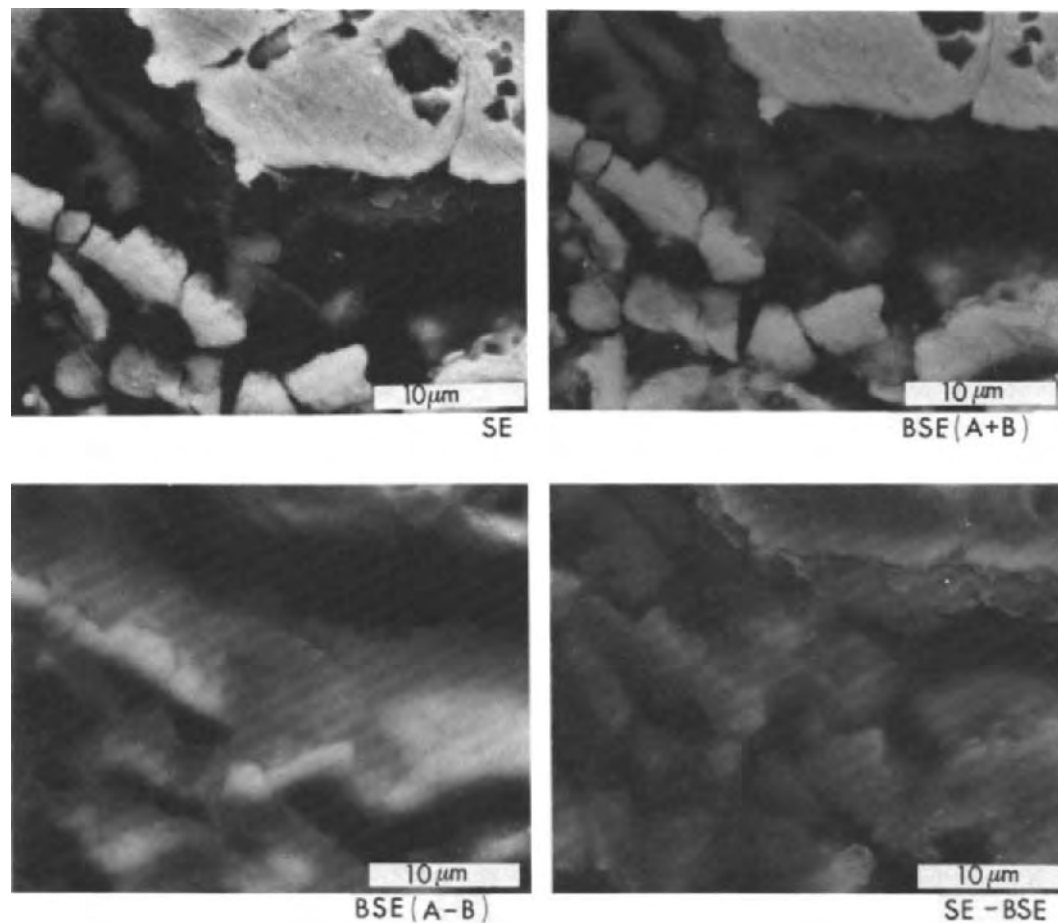


Fig. 12. Four other modes of operation on the same material as in Fig. 11. A mixture of depth and surface information in the SE image; an optimal material contrast in the BSE (A+B) image; pseudo-topography in the BSE (A-B) image; and the SE-BSE signal which gives the 'real' topography.

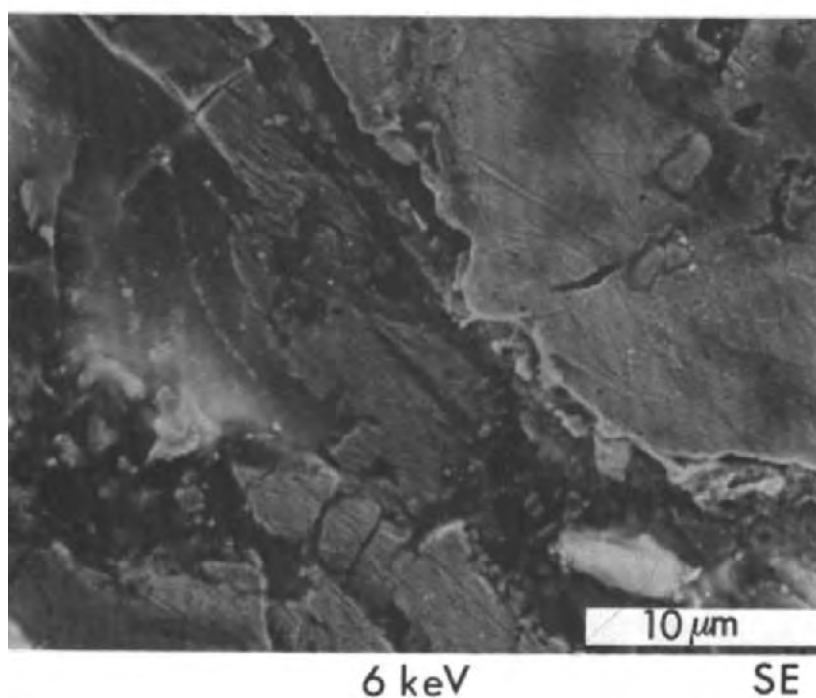
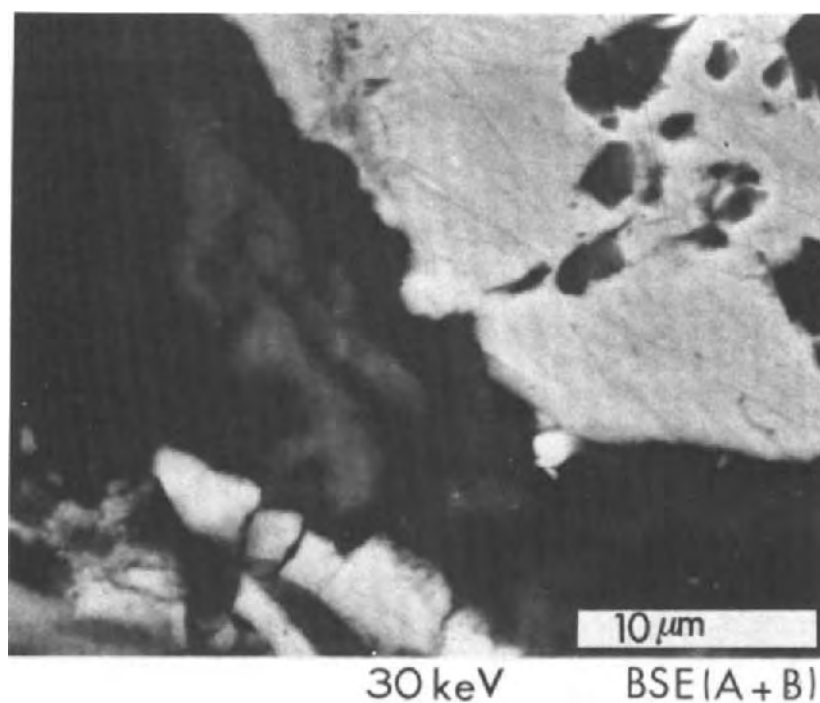
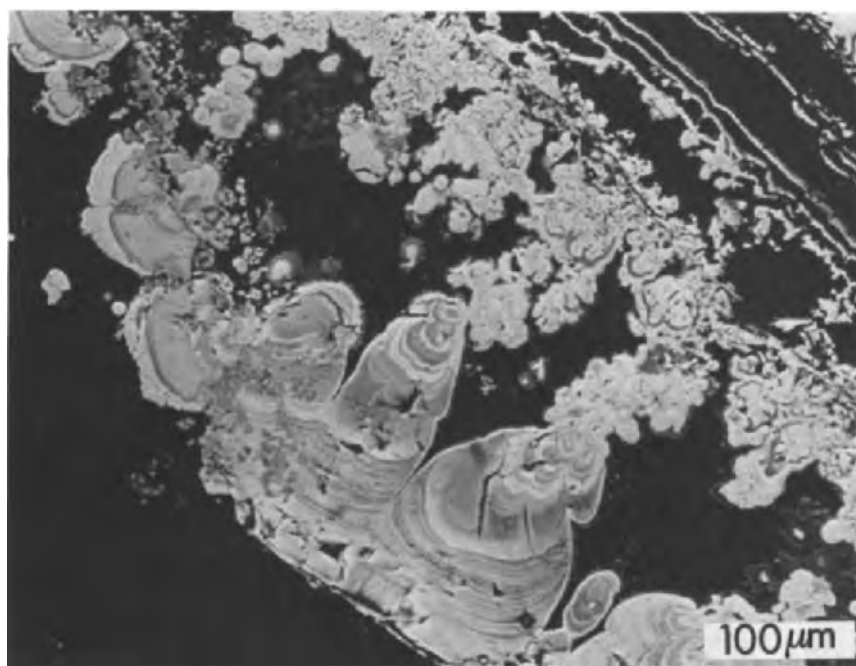


Fig. 13. SE image made at a low primary electron energy of 6 keV. The micrograph at 6 keV gives nearer-to-surface information than the BSE (A+B) image made at a high primary electron energy of 30 keV.

graphic contrast. Figs. 9 to 12 were all made with a primary electron energy of 30 keV. When this acceleration voltage becomes smaller imaging of the surface with SE is easier (Fig. 13). This is clear if the SE image in Fig. 13, taken at 6 keV, is compared with the BSE (A+B) image made with 30 keV acceleration voltage. The SE image of Fig. 13 also represents nearer to surface information than the SE image of Fig. 12 taken at 30 keV. The 'real' topographic contrast, however, is given in the SE-BSE mode (Fig. 12) at both high and low primary electron energies.

The BSE (A+B) micrographs of Figs. 14 and 15 show the precipitate on the corroded copper filter at various magnifications. All photos were taken at 30 keV acceleration voltage. The middle part of Fig. 14 is enlarged in Fig. 15. The structure of a 'crystallising' iron, sulphur and copper containing compound (Bisdorn and Jongerius, 1983) is visible in Fig. 15. The rings in the precipitate are partly composed of branching fibres that form a dendritic pattern.



BSE (A+B)

Fig. 14. Precipitates and some exfoliated platelets of the copper filter. Rings and bands can be discerned in the precipitate.

Bauxite

BSE images of Al concentrations in bauxite from Surinam are shown in Figs. 16 and 17. The composition of this material was tested with SEM-

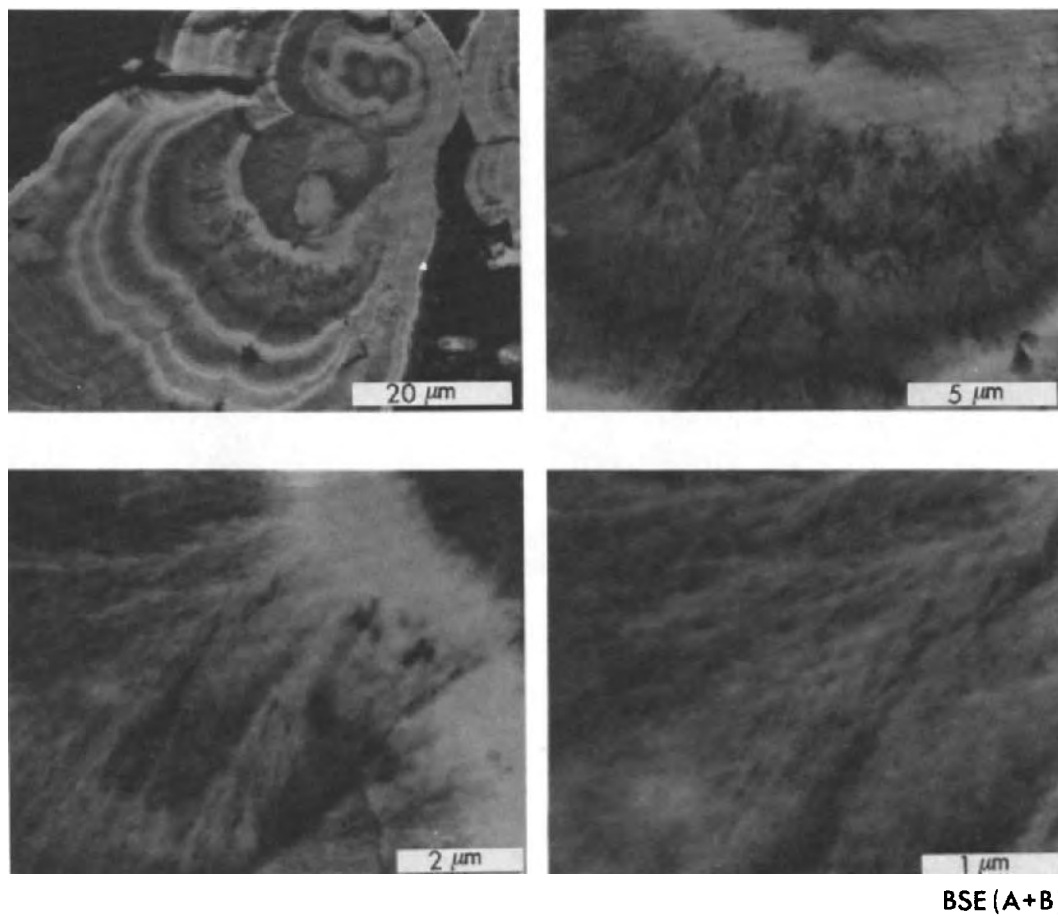


Fig. 15. The internal structure of the rings can be massive or exhibit a dendritic pattern.

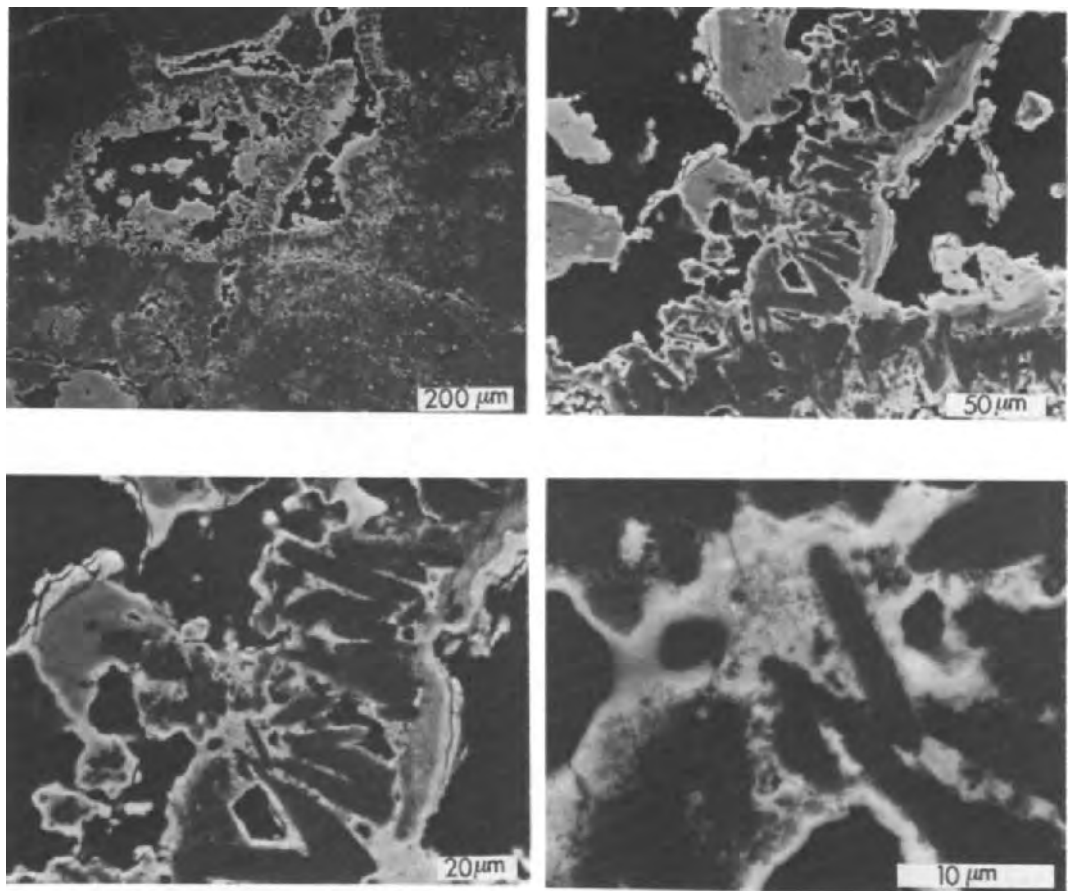


Fig. 16. Various magnifications of lath-shaped and blackish gibbsite crystals. The gibbsite minerals are surrounded by whitish to grey amorphous material high in aluminium. Most of the gibbsite crystals are associated with pore systems in which they had sufficient space to crystallize and grow.

BSE (A+B)

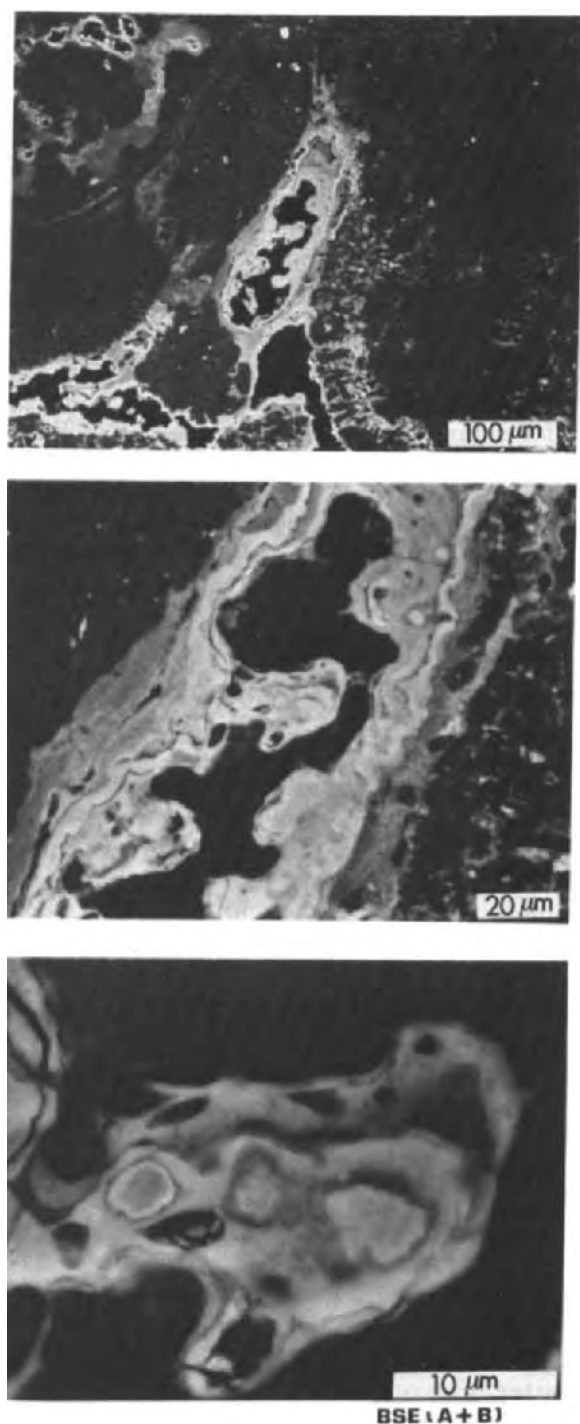


Fig. 17. Fluidal structures of whitish to grey mainly amorphous material with a high aluminium content in a pore. Well crystallized gibbsite, forming a gibbsan, is present in the pore of the upper micrograph.

EDXRA (scanning electron microscopy — energy dispersive X-ray analysis) and ion microscopy (Henstra et al., 1980).

The micrograph with a 200- μm bar scale in Fig. 16 shows the general area in which gibbsite crystals have grown, viz. associated with a void system and surrounded by a red and yellow coloured matrix when viewed in the light microscope. The Al content of this matrix was considerable and Fe reached the highest concentration in the red coloured matrix.

The area in which the gibbsite crystals grew, viz. associated with the pores, was predominantly white when viewed with the light microscope and highest in Al content according to submicroscopic analyses. The blackish crystals, in the micrographs with bar scales of 50, 20 and 10 microns of Fig. 16, grew in an amorphous substance in which no microstructure could be discerned by either light microscopy or submicroscopy. This is illustrated best in Fig. 17. Pieces of bauxite were also viewed with STEM (scanning transmission electron microscope), viz. the Philips EM 400T/ST. This instrument allows examination of the bauxite at even higher magnifications than the Philips SEM 505, but even here no microstructures were observed.

CONCLUSIONS

Backscattered electron scanning images have been made of mineral grains and excrements in a podzol, of precipitates on a water-tube filter and of bauxite. It has been demonstrated that the material contrast is portrayed best in the BSE (A+B) mode of operation. The best 'real' topographic contrast, giving an impression of the actual surface of the thin section, was obtained in the SE-BSE mode of operation. The SE-BSE mode can give a good image of the surface of a thin section at high and low primary electron energies, whereas the BSE (A+B) mode gives subsurface information at high acceleration voltages of 30 keV.

The maximum magnification possible with the BSE-signal is strongly dependent on the type of soil material being investigated in the thin section and varies from about $\times 1000$ to $\times 30\,000$ with the Philips SEM 505. The minimum magnification is about $\times 10$ and a picture of the whole display screen is still possible at such low magnification. Consequently, the range of investigation possibilities using BSE is considerable, especially if the instrument is also equipped with EDXRA and WDXRA (wavelength dispersive X-ray analysis) for microchemical analysis for in situ identification of soil particles.

BSE can be used to study microfabric and microstructure of materials in thin sections. The possibility to examine both at low and high magnifications will facilitate interpretation of the results and interpretation into field observations. The combination of field studies, light microscopy and submicroscopy will therefore allow a better understanding of processes which take place in soil profiles. This is especially so because BSE studies are not only possible with soil materials but also with pores (Bisdorf and Thiel, 1981) which can also be studied by Quantimet (Jongerijs and Bisdorf, 1981).

The high quality of the micrographs is basically the result of the Multi-Function-Detector (MFD) system, which can be used in combination with a secondary electron (SE) detector system. The possibility to simulate the rotation and illumination of the soil sample is of much practical help during studies. No significant cathodoluminescence was found in the present samples, but this could be of importance for other types of micromorphological studies.

The totality of possibilities offered by a SEM with all the different information carriers (signals) will have significant implications for present and future micromorphological research of materials in thin sections and loose soil materials. The results of studies in thin sections can be correlated with those obtained in the SEM-EDXRA, STEM-EDXRA and TEM-EDXRA-modes at very high magnifications when ultrathin sections can be prepared (Bresson, 1981; Bisdom, 1981; Bisdom et al., 1983b). Apart from these techniques several other submicroscopic methods have been introduced for in situ microchemical element analysis, e.g. EMA (electron microprobe analyzer), LAMMA (laser microprobe mass analyzer) and SIM (secondary ion microscopy) (Bisdom, 1981).

REFERENCES

- Bisdom, E.B.A., 1981. A review of the application of submicroscopic techniques in soil micromorphology, II. Electron-microprobe analyzer (EMA), scanning electron microscope-energy dispersive X-ray analyzer (SEM-EDXRA), laser microprobe mass analyzer (LAMMA 500), electron spectroscopy for chemical analysis (ESCA), ion microprobe mass analyzer (IMMA), and the secondary ion microscope (SIM). In: E.B.A. Bisdom (Editor), *Submicroscopy of Soils and Weathered Rocks*. 1st Workshop of the International Working-Group on Submicroscopy of Undisturbed Soil Materials (IWGSUSM) 1980, Wageningen. Centre for Agricultural Publishing and Documentation (Pudoc), Wageningen, pp. 117–162.
- Bisdom, E.B.A., 1982. Microchemical analysis in thin sections of soils. International Working-Meeting on Soil Micromorphology, August 17th–21st, 1981, London. In press.
- Bisdom, E.B.A. and Thiel, F., 1981. Backscattered electron scanning images of porosities in thin sections of soils, weathered rocks and oil-gas reservoir rocks using SEM-EDXRA. In: E.B.A. Bisdom (Editor), *Submicroscopy of Soils and Weathered Rocks*. 1st Workshop of the International Working-Group on Submicroscopy of Undisturbed Soil Materials (IWGSUSM) 1980, Wageningen. Centre for Agricultural Publishing and Documentation (Pudoc), Wageningen, pp. 191–206.
- Bisdom, E.B.A. and Jongerius, A., 1983. SEM-EDXRA studies of precipitates which clogged a water-tube filter. *Geoderma*, 30: 253–270.
- Bisdom, E.B.A., Henstra, S., Werner, H.W., Boudewijn, P., De Grefte, H.A.M., Knippenberg, W.F., Gourgout, J.M. and Migeon, H.N., 1983a. Quantitative analysis of trace and other elements in thin sections of soils with the secondary ion microscope (Cameca). *Geoderma*, 30: 117–134.
- Bisdom, E.B.A., Nauta, R. and Volbert, B., 1983b. STEM-EDXRA and SEM-EDXRA investigation of iron-coated organic material in thin sections with transmitted, secondary and backscattered electrons. *Geoderma*, 30: 77–91.

- Bresson, L.M., 1981. Etude ultramicroscopique d'assemblages plasmiques sur lames ultraminces de sols réalisées par bombardement ionique. In: E.B.A. Bisdorn (Editor), *Submicroscopy of Soils and Weathered Rocks. 1st Workshop of the International Working-Group on Submicroscopy of Undisturbed Soil Materials (IWGSUSM) 1980*, Wageningen. Centre for Agricultural Publishing and Documentation (Pudoc), Wageningen, pp. 173–189.
- Henstra, S., Bisdorn, E.B.A., Jongerius, A., Morgan, A.E., Werner, H.W. and De Grefte, H.A.M., 1980. Quantitative analysis on thin sections of soils by secondary ion mass spectrometry. In: P. Brederoo and V.E. Cosslett (Editors), *Electron Microscopy, 1980. Proceedings of the 7th European Congress on Electron Microscopy including the 9th International Conference on X-ray Optics and Microanalysis, The Hague, 1980, Vol. 3: Analysis*, pp. 224–225.
- Henstra, S., Bisdorn, E.B.A. and Boekestein, A., 1981. Submicroscopic techniques for in situ microchemical analysis of soils, III. Destructive techniques. In: E.B.A. Bisdorn (Editor), *Submicroscopy of Soils and Weathered Rocks. 1st Workshop of the International Working-Group on Submicroscopy of Undisturbed Soil Materials (IWGSUSM) 1980*, Wageningen. Centre for Agricultural Publishing and Documentation (Pudoc), Wageningen, pp. 55–65.
- Jackman, J.J., 1980. New scanning electron microscope depends on multifunction detectors. *Ind. Res. Dev.*, 22(6): 115–120.
- Jongerius, A. and Bisdorn, E.B.A., 1981. Porosity measurements using the Quantimet 720 on backscattered electron scanning images of thin sections of soils. In: E.B.A. Bisdorn (Editor), *Submicroscopy of Soils and Weathered Rocks. 1st Workshop of the International Working-Group on Submicroscopy of Undisturbed Soil Materials (IWGSUSM) 1980*, Wageningen. Centre for Agricultural Publishing and Documentation (Pudoc), Wageningen, pp. 207–216.
- Volbert, B., 1981. Verbesserung der topographischen Information durch Ueberlagerung von Sekundärelektronen (SE) — und invertiertem Rückstreuelektronen (BSE) — Signal. *Beiträge Elektronenmikroskopische Direktabbildung und Analyse von Oberflächen (EDO)*, Innsbruck, 14: 325–330.

QUANTITATIVE ANALYSIS OF TRACE AND MAJOR ELEMENTS IN THIN SECTIONS OF SOILS WITH THE SECONDARY ION MICROSCOPE (CAMECA)

E.B.A. BISDOM¹, S. HENSTRA², H.W. WERNER³, P.R. BOUDEWIJN³,
W.F. KNIPPENBERG³, H.A.M. de GREFFE³, J.M. GOURGOUT⁴ and H.N. MIGEON⁴

¹ *Netherlands Soil Survey Institute, P.O. Box 98, 6700 AB Wageningen (The Netherlands)*

² *Technical and Physical Engineering Research Service, P.O. Box 356, 6700 AJ Wageningen (The Netherlands)*

³ *Philips Research Laboratories, 5600 MD Eindhoven (The Netherlands)*

⁴ *Cameca, B.P. 6, 92403 Courbevoie Cédex (France)*

(Accepted for publication February 17, 1983)

ABSTRACT

Bisdorn, E.B.A., Henstra, S., Werner, H.W., Boudewijn, P.R., Knippenberg, W.F., De Grefte, H.A.M., Gourgout, J.M. and Migeon, H.N. Quantitative analysis of trace and major elements in thin sections of soils with the secondary ion microscope (Cameca). *Geoderma*, 30: 117–134.

A series of experiments have been performed for a number of years to obtain quantitative microchemical analysis by secondary ion microscopy of materials in thin sections of soils. The first successful quantification was obtained from an area with a diameter of 300 μm in bauxite and done with an IMS 300 at Philips Research Laboratories. Such an area, however, is frequently too large for most soil samples which are extremely heterogeneous even on a microscale. A second generation IMS 3F was tested for soils at the Cameca factory in Paris. This instrument allows the quantification of trace and major elements of soil constituents in a spot with 1.5 μm diameter, using a computer program developed by Philips Research Laboratories. Calcite and clay from a Petrocalcic Xerochrept were used for this test. Ion spectra, ion images and linear traverses were made giving information on the nature and distribution of both major and trace elements. The possibility of investigating a larger number of chemical elements simultaneously in linear traverses is of considerable help in the study of thin sections. Various submicroscopic and other techniques are discussed to give some insight into the position of ion microscopy amongst these.

INTRODUCTION

Ion microscopy can be regarded as an advanced form of submicroscopic research of materials in thin sections of soils. This technique can be used if other forms of analyses have already been done. Such analyses may include wet chemistry or beam techniques which require more soil material than is necessary for most of the submicroscopic techniques.

Submicroscopy of thin sections is preceded by light microscopy, by which a number of questions cannot be solved. The next step is the choice of in-

strument to be used for in situ analysis to solve these questions. For soil scientists such a choice is usually restricted to electron microscopy with or without equipment for microchemical analysis; the lightest elements and trace elements cannot be determined by this type of analysis.

A preliminary knowledge of the microchemistry of the materials under study is frequently obtained with SEM-EDXRA (scanning electron microscope — energy dispersive X-ray analyzer). When an EMA (electron microprobe analyzer) or a SEM-WDXRA (scanning electron microscope — wavelength dispersive X-ray analyzer) are used one can obtain semi-quantitative or quantitative data on most elements present in concentrations above trace element level (Bisdom, 1981).

Ion microscopy is necessary for in situ microchemical investigation of all chemical elements and trace elements in a thin section. The first experiments were done with an ion microprobe mass analyzer (IMMA) (Bisdom et al., 1977). These tests gave ion images of hydrogen and allowed the detection of both major and trace elements. However, no quantification program for soil materials was available at that time.

Experiments with the laser microprobe mass analyzer (LAMMA 500) also allowed the detection of ions from thin sections by using the laser beam in grazing incidence and from the edges of the piece of thin section inward; a method which was called laser milling (Bisdom et al., 1981; Henstra et al., 1981). However, the amount of sample analysed was significant in these thicker samples. Ideally, the thin section should be ultra thin giving a much smaller microvolume for analysis when shot through. Quantification is not yet possible with the LAMMA 500.

Experiments with the Cameca ion microscope started in 1977 at the Biophysical Laboratory of the University of Paris in Créteil, France. The team consisted of P. Galle and A. Quettier of this laboratory and J.M. Gourgout of Cameca. Work was done with the IMS 300 on pieces of thin section. Charging problems were significant and no accurate results could be obtained.

In 1978 H.W. Werner of Philips Research Laboratories invited the first two authors for experiments with a Cameca IMS 300. A conductive and round tantalum plate, with a 400 μm diameter orifice in the centre, took care of the charging problem. Together with A.E. Morgan and H.A.M. de Grefte, quantitative analysis was performed on a piece of thin section from bauxite with 300 μm diameter (Henstra et al., 1980). Wet chemical and optical emission spectroscopy data were provided by the analytical department of Philips Research Laboratories. To evaluate the concentration of the elements from the measured secondary ions set free during sputtering of the thin section, computer programs made by H.W. Werner, J. v.d. Berg and A.E. Morgan were used (Werner, 1974; Morgan and Werner, 1977a, b, 1978). The 300 μm diameter of the analysed area in the thin section, however, was too large for the study of most soil materials because of their heterogeneity even on a microscale.

In 1980, a visit was made to the Cameca factory in Paris. Quantitative analysis was done with the new Cameca IMS 3F ion microscope in a spot with $1.5\ \mu\text{m}$ diameter using computer programs by H.W. Werner and A.E. Morgan. These data were afterwards screened by H.W. Werner and P.R. Boudewijn.

W.F. Knippenberg included a section on the comparison of data from wet chemical analysis and analyses by beam techniques. Wet chemical methods are often used at Philips Research Laboratories before secondary ion mass spectroscopy (SIMS) is started. A section on various instrumental techniques for bulk, thin film and microanalysis was inserted by H.W. Werner to illustrate the place of ion microscopy.

INSTRUMENT

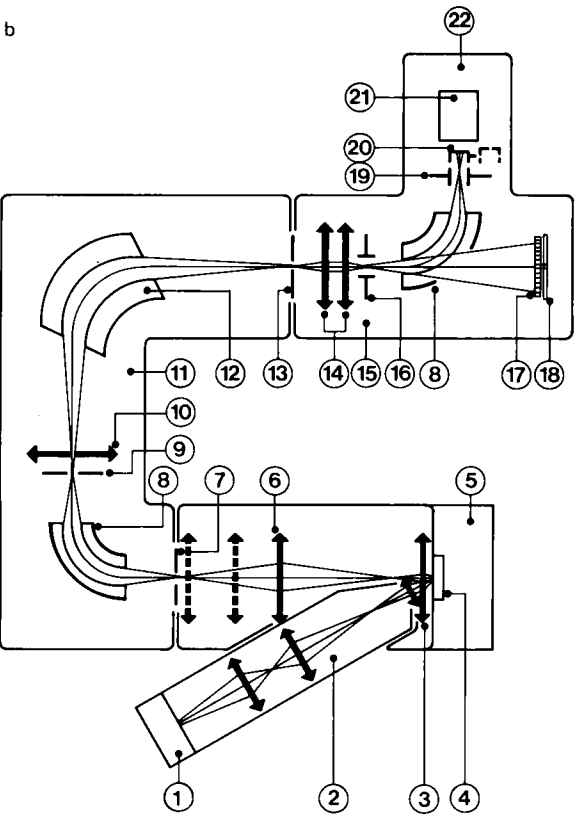
A secondary ion mass spectrometry (SIMS) analysis is accomplished by bombarding the surface of a solid sample with a beam of energetic ions. Due to the impact of these primary ions, atoms from the near-surface region of the sample will be sputtered away. Depending on the primary ion energy, the incident angle and the nature of the primary ions a fraction of the sputtered particles will be charged. These secondary ions (positive or negative) are collected and analysed according to their mass-to-charge ratio in a mass spectrometer, thereby providing qualitative and quantitative information about the elemental composition of the near-surface region of the sample.

Previous experiments were carried out with the ion microprobe mass analyzer, IMMA (Bisdorf et al., 1977) and the ion microscope Cameca IMS 300 (Henstra et al., 1980). The present investigations were performed with a second generation SIMS instrument, the Cameca IMS 3F (Fig. 1a), which is a direct imaging secondary ion microscope. Fig. 1b shows a schematic diagram of the instrument. The primary ions are supplied by a duoplasmatron ion source capable of producing O_2^+ , N_2^+ , Ar^+ and O^- ions. These primary ions are accelerated to energies ranging from 5 to 20 keV; an ion optical column containing three electrostatic lenses focuses the ion beam to small diameter; the diameter on the sample varies from $200\ \mu\text{m}$ to $1.5\ \mu\text{m}$. Deflection plates enable steering of the primary beam for localized spot analysis and rastering for high-quality depth profiling.

In contrast to ion microprobe instruments, which require rastering of a focused primary beam to obtain ion images, the Cameca instrument uses ion optical concepts with direct imaging; the lateral resolution ($0.5\ \mu\text{m}$) is controlled by the secondary ion optics rather than the primary beam diameter.

The secondary ions are extracted by a high extraction field and focused onto the entrance slit of the mass spectrometer; for a given mass resolution the overall transmission of the spectrometer can be optimized by means of a transfer optics as a function of the analysed sample area.

The mass spectrometer is double focusing resulting in a combination of high transmission with high mass resolving power. The mass range extends from 1 to 250 amu (atomic mass units).



The mass-analysed secondary ions are detected by a Faraday cup or an electron multiplier in the pulse-counting mode, thus providing a high dynamic range and high sensitivity.

In the ion microscope mode, ion images are obtained by a microchannel-plate electron multiplier and a fluorescent screen; the images can be viewed using a binocular microscope, or photographed with a 35 mm camera.

Quantitative information about the sample composition cannot be obtained in the ion microscope mode, the electron multiplier must be used to measure the secondary ion currents. Consequently, the lateral resolution in quantitative microspot analysis is determined by the primary ion beam diameter ($\geq 1.5 \mu\text{m}$).

Several operational modes of the instrument are available: e.g., mass spectrum, depth profiling, step scanning of sample and isotopic analysis.

Quantitative analysis

Direct quantitative analysis by SIMS is complicated by the large variations in ion yield found from one element to another and, for a particular element, from one matrix to another. Quantification with an uncertainty of a few per cent can only be accomplished after calibration using standard samples of similar composition. In many cases, however, preparation of such standards is impossible and other methods of quantification of SIMS results must be used.

One method is based upon the local thermal equilibrium model (LTE model) of secondary ion emission proposed by Anderson and Hinthorn (1973) whereby concentrations can be specified in general to within an accuracy of a factor of 2–3. Although the physical basis of the model is questionable, results on a variety of samples have shown that quantitative interpretation of SIMS measurements is possible (Morgan and Werner, 1977a, 1978; Morgan, 1980).

According to the LTE model the sample compositions can be estimated directly from the secondary ion currents using the equation:

$$C_M = K I_{M^+} M^{1/2} [Z_{M^+}(T_i)/Z_{M^+}(T_s)] \exp(E_M/kT_i)$$

where C_M is the atomic concentration of an element M in the sample, K is an element-independent constant (Henstra et al., 1980), I_{M^+} is the measured secondary ion current corrected for isotopic abundance and M is the mass

Fig. 1. The Cameca IMS 3F ion microscope (a) and schematic diagram (b). 1 ion gun; 2 = primary column; 3 = immersion lens; 4 = specimen; 5 = specimen chamber; 6 = transfer optics; 7 = entrance slit; 8 = electrostatic analyzer; 9 = energy slit; 10 = image transfer lens; 11 = spectrometer; 12 = electro-magnet; 13 = final slit; 14 = projection lenses; 15 = projection, display and detection system; 16 = deflector; 17 = channel-plate; 18 = fluorescent screen; 19 = deflector; 20 = remote controlled Faraday cup; 21 = electron multiplier; 22 = detection system.

number of the isotope monitored. $Z_{M^0}(T_i)$ and $Z_{M^+}(T_i)$ are the electronic partition functions of the neutrals M^0 and M^+ ions at temperature T_i , respectively. E_M is the first ionization potential of M , k is the Boltzman constant and T_i (ionization temperature) is a matrix-dependent fitting parameter.

For a quantitative analysis knowledge of T_i is required. This parameter can be derived if the concentrations of one or more elements in the investigated sample are known (internal standard method) or from suitable, standard samples since samples of a given matrix have similar T_i values (Morgan and Werner, 1977a, 1978). In the case of complex matrices T_i can be estimated on a proportional basis from the values of the constituent components (Morgan, 1980).

Obtaining the data for the partition functions and E_M from the literature, and given the value of T_i , quantitative interpretation of SIMS results can be made both for major and trace elements.

EXAMPLE OF THIS METHOD

Calcite from a carbonate sample with clay inclusions of a Petrocalcic Xerochrept from southern Spain was taken for the experiment with the Cameca IMS 3F. The distribution pattern of calcite and clay may vary significantly in the thin section which was made from a plastic-hardened sample using the method described by Jongerius and Heintzberger (1975). This may give some difficulty at the start of the work because localisation with the ion microscope is not easy for soil samples. The following procedure was therefore chosen. A micrograph of the thin section was made with the petrographic microscope before the piece of thin section was removed from the object glass for insertion in and analysis with the ion microscope. The latter instrument can make ion images similar to X-ray images in electron microscopy. These ion images can be used for localization purposes, i.e. the distribution pattern of the chemical elements in the ion images allow localization of the area of analysis and of the larger soil components in the micrograph made with the petrographic microscope. An extra orientation mark forms the tantalum plate which surrounds the area to be analysed. The tantalum plate is used to counteract charging.

Ion microscopy offers operational modes which can be compared with those of electron microscopy, i.e. images, line scans and point analyses can also be made. Images are now called ion images, line scans are also indicated as step scan analysis and point analyses have the same name.

Ion spectra

Positive and negative ion spectra can be made of areas which can differ in diameter. During our experiment, predominantly positive secondary ion spectra were made of areas with diameters of 150 μm , 60 μm , 25 μm and 8 μm . Spectra were also obtained from spots with a diameter of 1.5 μm .

A positive secondary ion spectrum of an area with 150 μm diameter in calcite is given in Fig. 2. A large number of positive ions is indicated: H, Li, B, C, O, Ca, Na, Mg, Al, Si, K, Ca, Ti and Cr, as well as the molecular ions CaO , Ca_2O and Ca_2O_2 . This wealth of elements, including trace elements, in calcite seems to suggest that some of the elements have been derived from clay inclusions found in the carbonate. X-ray diffraction demonstrated that montmorillonite, palygorskite and kaolinite were the dominant clay minerals.

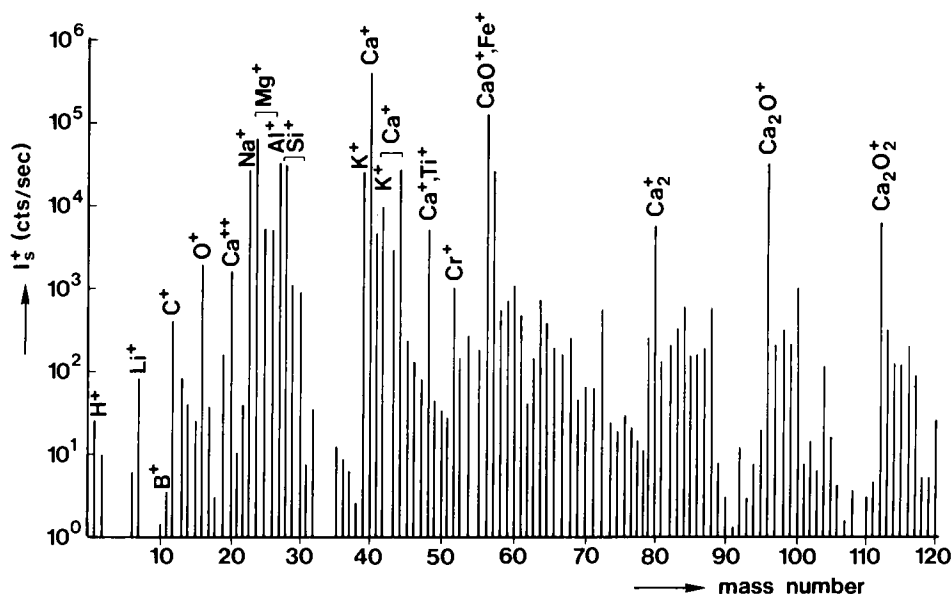


Fig. 2. Positive secondary ion spectrum of calcite. Analysed area ϕ 150 μm .

Ion images

Ion images can be made of trace and major elements due to high count rates and good peak to background ratios. Of special interest is the high mass resolving power of the Cameca IMS 3F which allows the separation of elemental and molecular ions which occur at the same mass number. Not only the diameter of the field used for secondary ion imaging can be changed but also the mass resolving power. As a consequence it is possible to investigate the soil sample in different modes.

The first example are ion images from calcite (CaCO_3) investigated with a mass resolving power $M/\Delta M$ of 300 (Fig. 3). Positive secondary ion images are given of ^1H , ^{23}Na , ^{24}Mg , ^{28}Si , ^{39}K , ^{40}Ca , ^{48}Ti and ^{52}Cr . The ion images were made with various exposure times ranging from half a second for calcium to thirty seconds for titanium and chromium. The calcium is present

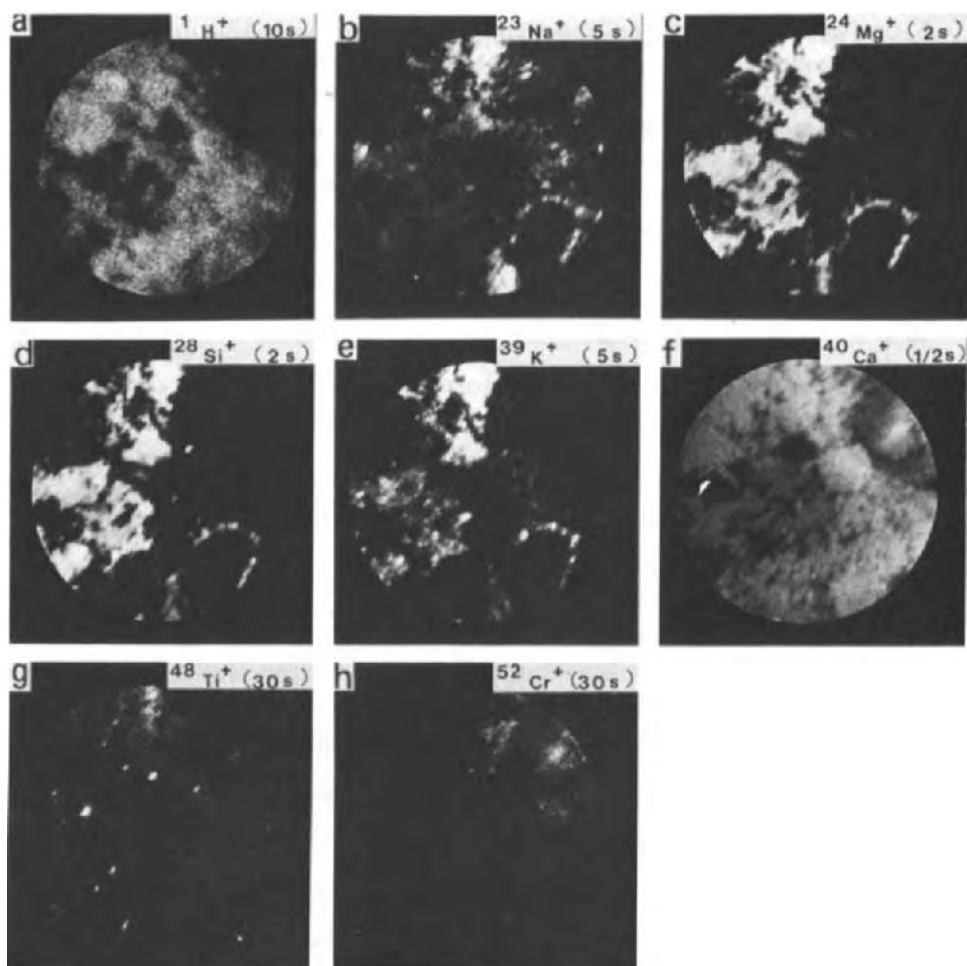


Fig. 3. Positive secondary ion images of some elements present in calcite. Mass resolving power $M/\Delta M = 300$. Field of view $\phi = 150 \mu\text{m}$.

over virtually the whole image; the sodium, magnesium, silicon and potassium are represented in similar distribution patterns over the calcite; the titanium and chromium are concentrated in a few areas; hydrogen is present over a larger part of the sample and probably indicates the presence of plastic which was used for hardening of the sample. No obvious distribution relation is present between hydrogen and other ions in the images. It is therefore postulated that ions other than hydrogen may also be associated with the calcite and not only with plastic.

The second example concerns the distinction between ${}^{56}\text{CaO}$ and ${}^{56}\text{Fe}$ positive ions. Mass interference of CaO and Fe occurs because both have 56 amu (atomic mass units). To solve this problem, an instrument is neces-

sary which has a high mass resolving power. The Cameca IMS 3F is able to obtain a good result (Fig. 4) by increasing the mass resolving power $M/\Delta M$ to 5000. Consequently, different distribution patterns can be recognized for ^{56}CaO and ^{56}Fe in the images.

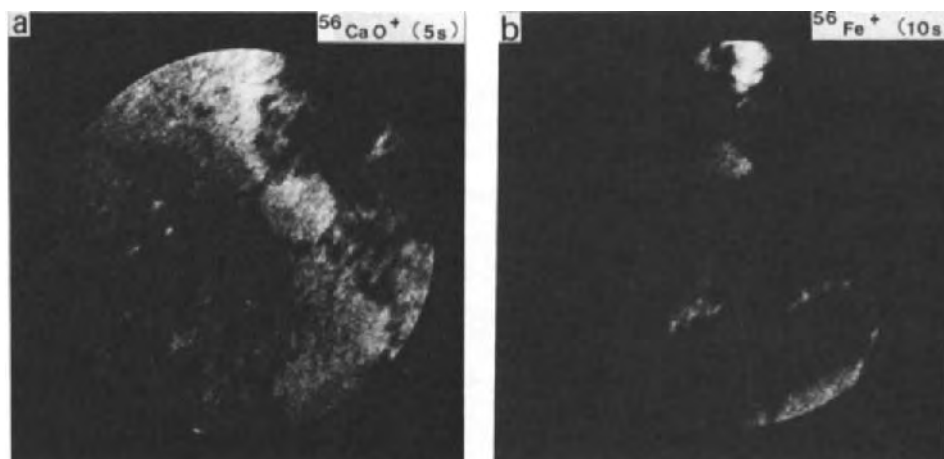


Fig. 4. Positive secondary ion images of Fe and CaO present in calcite. Mass resolving power $M/\Delta M = 5000$. Field of view $\phi = 150 \mu\text{m}$.

The third and last example of ion images was made from a sample with calcite and clay (Fig. 5). Positive secondary ion images are given of ^{23}Na , ^{24}Mg , ^{27}Al , ^{28}Si , ^{39}K , ^{40}Ca , ^{48}Ti and ^{52}Cr . Exposure times varied from half a second for calcium to thirty seconds for potassium, titanium and chromium. These ion images indicate that calcite is mainly concentrated in the northwest part of the images and clay in the southeast. Potassium is the only element found in the whole image. The calcite part of the image contained sodium, titanium and chromium besides calcium, whereas the clay part had predominantly aluminium and silicon. To obtain more insight into the distribution and quantity of chemical elements, a line scan was made.

Line scan or step scan analysis

Line scanning is also called step scan analysis in ion microscopy because it is done in steps which involve 50 point analyses along a line AB (Fig. 6). The elements can be scanned simultaneously, up to ten elements with the present computer capacity. Only the elements Mg, Si, Ca and Al are portrayed in Fig. 6 for readability reasons. Ti and Na were also scanned and these elements had low count rates varying between 10^0 and 10^1 cts/sec in both calcite and clay.

Clay is present near point A of Fig. 6. The amount of clay is at a maximum up to 4 steps in the direction of point B and thereafter gradually de-

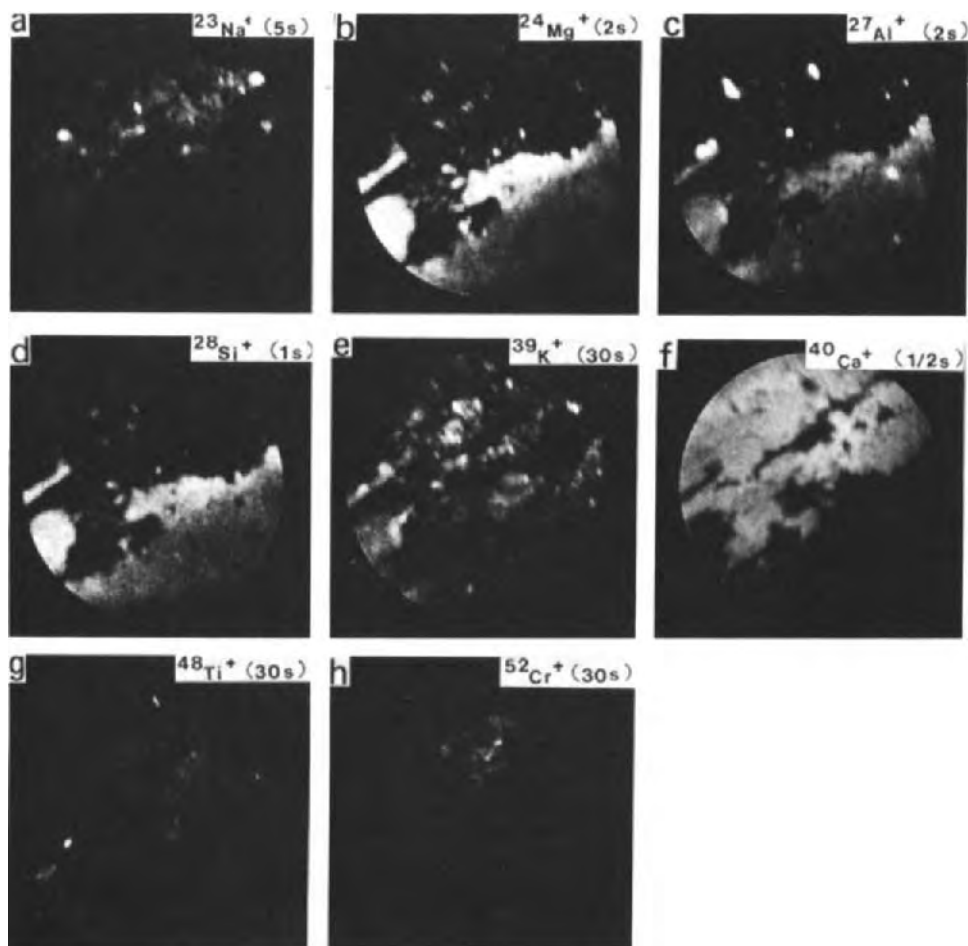


Fig. 5. Positive secondary ion images of some elements present in a sample with calcite and clay. Mass resolving power $M/\Delta M = 300$. Field of view $\phi = 150 \mu\text{m}$.

creases in quantity up to about 8 steps from A. Calcite is dominant in the other part of the line scan.

Ion images of Ca and Mg in Fig. 6 are the same as in Fig. 5 and were used to indicate the position of line AB. Minor differences in distribution patterns of chemical elements may occur because the sample is very slowly eroded during analysis. The fifty point analyses of the line scan indicated that Mg, Si, Ca and Al are present and give about 10^3 cts/sec in the clay fraction. The number of counts for calcium in the calcite is not much higher than measured in clay, whereas the figure is much lower for Mg, Si and Al. To obtain some insight into the quantity of individual elements in point analyses, calculations were done with a computer.

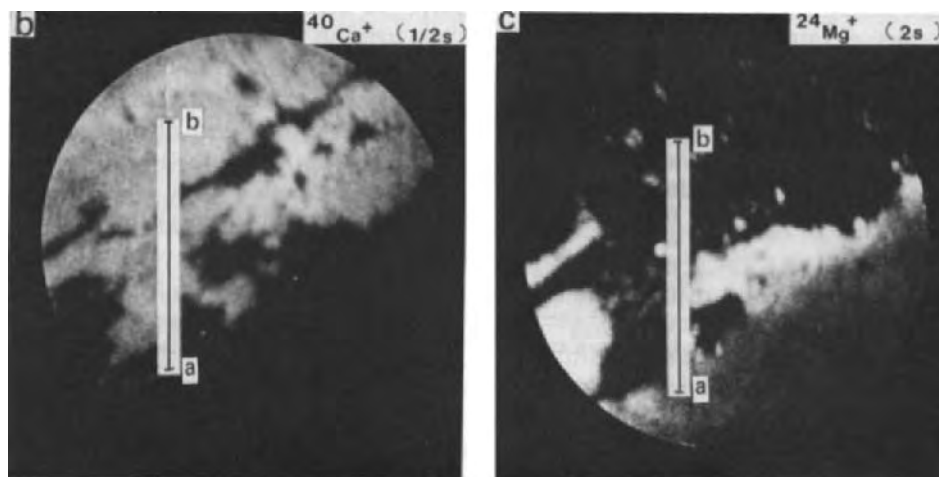
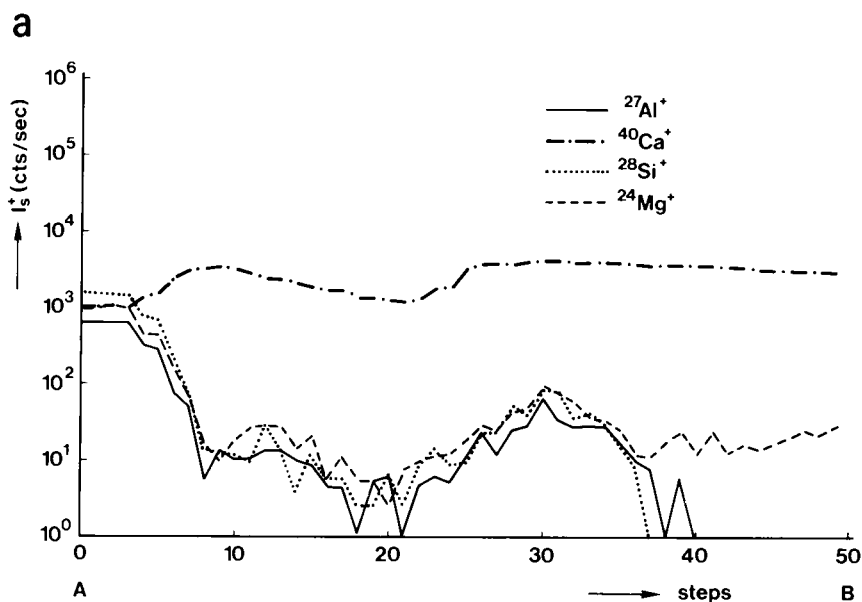


Fig. 6. Step scan analysis along the line AB in secondary ion images of Ca and Mg from a sample with calcite and clay (cf. Fig. 5). The diameter of the primary ion beam is $1.5\ \mu\text{m}$.

Point analyses

Point analyses were done in a spot with $1.5\ \mu\text{m}$ diameter in both calcite and clay. Quantification of data was possible using the procedure described in the section on quantitative analysis. A quantitative SIMS analysis of the elements in calcite is given in Table I and of clay in Table II. All elements other than Ca are present in small quantities in the calcite. The clay of Table

TABLE I
Quantitative SIMS analysis of calcite

Element	Calculated concentration (atomic per cent)
Ca	19.17
Na	0.07
Mg	0.30
Al	0.11
Si	0.27
K	0.01
Ti	0.07

Calculated concentrations have been summed to a substance fraction of atoms of 20%.

TABLE II
Quantitative SIMS analysis of clay inclusions in calcite

Element	Calculated concentration (atomic per cent)
Ca	0.05
Na	0.02
Mg	3.33
Al	4.49
Si	28.23
K	0.02
Ti	0.04
Cr	<0.01
Fe	0.66

Calculated concentrations have been summed to a substance fraction of atoms of 36.85%.

II had Mg, Al and Si as the principal elements. The results indicate that even trace elements can be measured quantitatively in point analyses of soil samples. As was explained, however, electron microscope techniques should help to obtain a preliminary insight into the quantity of chemical elements which are represented above trace element quantity in the sample. Wet chemical and other techniques for the research of bulk samples can also be used. These are described briefly below together with a number of other submicroscopic techniques for in situ investigation of materials in thin sections.

WET CHEMICAL ANALYSIS AND ANALYSIS BY BEAM TECHNIQUES

A characteristic of wet chemical bulk analysis is its mono-element sequential mode of operation: after dissolution of the sample, sometimes followed

by extraction procedures, each element is determined under optimized non-compromise conditions. For the determination, instrumental detection techniques are usually used, each with specific detection limits. Well above the detection limit quantitative determinations can be performed with accuracies better than 0.1% (Knippenberg, 1974). To be able to perform these operations in a rational way a semiquantitative instrumental survey analysis, e.g. by optical emission or X-ray spectrometry, usually precedes wet chemical analysis.

Because of the high accuracy obtainable, wet chemical analysis is used in the analysis of standard samples for purely instrumental techniques like the beam techniques.

The analysis yields an average value of the composition of the analysed mass. One distinguishes methods of macro-, micro-, or ultra-microanalysis depending on whether the analysed samples involve amounts of material in the order of 100 mg, 100 μg or 100 ng, respectively. Sampling of these amounts can be performed mechanically, chemically or by sputtering techniques. Even in cases where the amount of material available would allow macroanalysis, microanalysis is often preferred to check on homogeneity and to reach a better statistical evaluation. The reproducibility of the beam techniques is rather high (order of %) so that both the homogeneity of the standard samples and the heterogeneity of the investigated sample can be checked. The information volume of the beam techniques can be some orders of magnitude smaller than the "information volume" of the sample investigated in practice by wet chemical analysis; the absolute detection limit may be of the same order of magnitude.

INSTRUMENTAL TECHNIQUES FOR BULK, THIN FILM AND MICROANALYSIS

A large number of sophisticated instrumental techniques for chemical analysis is available at present wherewith — contrary to wet chemistry — a multi-element analysis can be carried out simultaneously. The speed of the analysis is thereby increased significantly. The detectable elements — in particular when mass spectrometric methods (SSMS or SIMS; cf. Table III) are used — range from hydrogen to uranium.

A distinction must be made between methods for bulk analysis and for thin film and microanalysis (Werner, 1982/83): in bulk analytical methods, such as spark source mass spectrometry, optical emission spectroscopy and X-ray fluorescence (cf. Table IV), 10 to 50 mg of sample is used per analysis corresponding to a large probed volume ($2 \cdot 10^9$ to $10^{10} \mu\text{m}^3$ per analysis). Bulk analytical methods obviously give the average chemical concentration of the probed volume.

In thin film and microanalysis information about the distribution (one-, two- and three-dimensional) of the elements in the sample is needed. In that case methods with small information depths and widths must be used. With respect to information depth two groups can be distinguished. Group (a) has

TABLE III

Abbreviations of instrumental techniques for chemical analysis

AES	Auger Electron Spectroscopy
BLE	Bombardment-induced Light Emission
EELS	Electron Energy-Loss Spectrometry (=ELS)
EMP	Electron Microprobe analysis, used in two modes viz. Energy Dispersive X-ray analysis (EDX) and Wavelength Dispersive X-ray analysis (WDX)
ESCA	Electron Spectroscopy for Chemical Analysis
HEIS	High Energy Ion Scattering = RBS
ISS	Ion Scattering Spectrometry = LEIS
LAMMA	Laser Microprobe Mass Analysis = LMP
LEIS	Low Energy Ion Scattering = ISS
LMP	Laser Microprobe Analysis = LAMMA
LOES	Laser Optical Emission Spectrometry
OES	Optical Emission Spectrometry
PIXE	Particle Induced X-ray Emission
RBS	Rutherford Backscattering Spectrometry = HEIS
SAM	Scanning Auger Microprobe
SEM	Scanning Electron Microscopy
SIMS	Secondary Ion Mass Spectrometry
SSMS	Spark Source Mass Spectrometry
STEM	Scanning-Transmission Electron Microscope
TEM	Transmission Electron Microscope
TEELS	Transmission Electron Energy Loss Spectrometry
XPS	X-Ray Photoelectron Spectroscopy
XRF	X-ray Fluorescence Spectrometry

an information depth of maximally 3 nm, such as in SIMS, AES, ESCA, LEIS, BLE (cf. Table V). Depth profiles are obtained using these methods (with the exception of HEIS) by continuous bombardment of the sample with an ion beam; the sample is thereby sputtered with a constant erosion rate. By tuning the instrument to one or several elements and recording the corresponding signals as a function of time (depth) depth profiles are obtained. In HEIS a depth profile is obtained without the need to sputter the sample (Werner, 1980, 1982/83). Depth resolutions down to about 3 nm can be achieved with group (a) methods.

Group (b) (cf. first column in Table V) has an information depth of about 1 μm or is limited by the sample thickness. With LOES and LAMMA the material is evaporated by the laser beam. Depth profiles analogous, as were described under (a) for sputtering, can be obtained. The depth resolution is about 1 μm .

The detection limit in thin film and microtechniques is between some per cent down to the ppm and even to the ppb range (Table V, 2nd column). The lateral resolution (Table V, 3rd column) is in the micron and submicron range; with analytical electron microscopy it can even be 5 nm. This lateral resolution allows inclusions with the above mentioned dimensions to be

TABLE IV

Comparison between bulk and thin film-analytical methods

Bulk-analytical methods

Spark source mass spectrometry

Bulk analysis mode: sample consumption 10—50 mg per analysis, probed volume^{*1} = $2 \cdot 10^{-9}$ — $10^{10} \mu\text{m}^3$. Thin film analysis mode: 1 spark gives crater of typically $50 \mu\text{m}$ diameter \times $1 \mu\text{m}$ depth approximately 10^3 craters/analysis, equivalent to 2 mm^2 eroded surface \times $1 \mu\text{m}$ depth \approx probed volume $\approx 2 \cdot 10^6 \mu\text{m}^3 \approx 10 \mu\text{gr}$.^{*1}

Optical (atomic) emission spectrometry

Sample consumption: 10 mgr/analysis \approx probed volume^{*1} = $2 \cdot 10^9 \mu\text{m}^3$.

X-ray fluorescence, XRF

Exposed area $A_b = 10 \text{ cm}^2$; information depth $\leq 10 \mu\text{m}$. \approx probed volume = $10^{10} \mu\text{m}^3$; no sample consumption.

*Several modes of thin-film analytical methods^{*1}*

Type of analysis:

Spatial extension:

Remark:

Point (micro) analysis

0-dimensional

Extension of probed volume V in any direction $\leq \mu\text{m}$; probed volume $\approx \mu\text{m}^3$.

Surface (monolayer) analysis

Probed volume = exposed area (1 mm^2) \times information depth ($\leq 1 \text{ nm}$) = $10^3 \mu\text{m}^3$.

Depth analysis

Thickness of analysed layer between 5 nm and $10 \mu\text{m}$; depth resolution, $\Delta z \geq 2 \text{ nm}$, both z -dependent and z -independent (see text).

one-dimensional

Line scan

Analysis of surface composition along predetermined line.

(Element) imaging of surface

two-dimensional

Imaging by means of scanning-beam or optical system; lateral resolution: typically 100 nm — $1 \mu\text{m}$.

Combination of depth analysis and imaging

three-dimensional

^{*1} Assuming a sample density of 5 gr/cm^3 .

TABLE V

Selected analytical features of the different methods

	Information depth	Detection limit (fractional concentration* ¹)	Lateral resolution	Element range
(a) AES	0.4–2.5 nm	10 ⁻³	0.1–3 μm	≥ Li
ESCA	1–3 nm	10 ⁻²	15 μm–1 nm	≥ He
LEIS	0.3–1 nm	10 ⁻³	100 μm	≥ Li
HEIS	3–10 ³ nm	10 ¹² –10 ¹⁵ /cm ²	1–3 μm	≥ C
SIMS	0.3–1 nm	100 ppm (bulk)	0.1–1 μm	(M _X > M _{substrate})
BLE	0.3–1 nm	10 ⁻⁵ % = 0.1 ppm	100 μm	≥ H
(b) LAMMA	0.1–1 μm	< 0.1 ppm-ppb	≈ μm	H-U
LOES	0.2–1 μm	10 ⁻³	10 μm	69 elements
SEM-EDX	≈ μm	10 ⁻³	1 μm	> Na
EMP-EDX	≈ μm	10 ⁻³	1 μm	> Na
TEM-EDX	≈ sample thickness (≈ 100 nm)	10 ⁻³	≈ 5 nm	> Na
EELS-TEM	≈ sample thickness (≈ 100 nm)	< 10 ⁻³	≈ 5 nm	> B, C
PIXE	≈ μm	0.1–10 ppm	3–1000 μm	> Na

*¹ Unless otherwise stated.

analysed, a feature that may turn out to be most important for further chemical analysis of soil materials in the micron and nanometer range.

CONCLUSIONS

During earlier experiments with the ion microscope, a Cameca IMS 300 was used to obtain quantitative data from secondary ions sputtered from an area in the thin section with 300 μm diameter. The present experiment was done with a second generation ion microscope, the Cameca IMS 3F. This instrument allowed quantification of soil material in a spot with 1.5 μm diameter. Such point analyses can be used well in soil micromorphology because they even allow quantification of trace elements in thin sections of materials which vary in composition over micron-distances.

Electron microscopy, EMA (electron microprobe analysis) and SEM-WDXRA (scanning electron microscope – wavelength dispersive X-ray analysis) allow the investigation of most elements quantitatively when not present as trace elements. Ion microscopy is able to analyse all elements, including hydrogen, and gives data on trace elements. If research interests include trace elements, electron microscopy should therefore be followed by ion microscopy.

In the present experiment with calcite and clay, a wealth of chemical elements were analysed. Such information may be difficult to compare with data obtained by electron microscopy and light microscopy because no such detail on in situ microchemistry has been encountered so far. Consequently, only tentative interpretations are allowed. In the present case, it seems that some of the elements, analysed with the Cameca IMS 3F in the calcite, have been derived from clay inclusions. Light microscopy, electron microscopy and ion microscopy seem to indicate that such elements may have been emplaced in the calcite during the replacement of clay.

Ion microscopy will usually represent a final stage of in situ soil research. Quantification of the chemical elements in soil materials will not be easy, even if computer programs are available. It will remain necessary to include other techniques based on in situ research of thin sections or on bulk analysis of pre-treated and disturbed samples. Several of these techniques have been indicated briefly in this paper and should allow some insight into analytical possibilities and the position of ion microscopy. So far, only a few of the most promising instruments have been tested on soil materials in thin sections. However, with ion microscopy, it will be possible to investigate a large number of problems in soil micromorphology in the required detail. Such detail may be of importance for the study of thin sections from the natural soil environment and for the investigation of samples derived from physicochemical experiments.

REFERENCES

- Anderson, C.A. and Hinthorne, J., 1973. Thermodynamic approach to the quantitative interpretation of sputtered ion spectra. *Anal. Chem.*, 45: 1421–1438.
- Bisdom, E.B.A., 1981. A review of the application of submicroscopic techniques in soil micromorphology, II. Electron microprobe analyzer (EMA), scanning electron microscope-energy dispersive X-ray analyzer (SEM-EDXRA), laser microprobe mass analyzer (LAMMA 500), electron spectroscopy for chemical analysis (ESCA), ion microprobe mass analyzer (IMMA), and the secondary ion microscope (SIM). In: E.B.A. Bisdom (Editor), *Submicroscopy of Soils and Weathered Rocks*. 1st Workshop of the International Working-Group on Submicroscopy of Undisturbed Soil Materials (IWGSUSM) 1980, Wageningen. Centre for Agricultural Publishing and Documentation (Pudoc), Wageningen, pp. 117–162.
- Bisdom, E.B.A., Henstra, S., Jongerius, A., Brown, J.D., Von Rosenstiel, A.P. and Gras, D.J., 1977. Light and heavy element detection in thin sections of soils with the ion microprobe mass analyzer (IMMA). *Neth. J. Agric. Sci.*, 25 (1): 1–13.
- Bisdom, E.B.A., Henstra, S., Jongerius, A., Heinen, H.J. and Meier, S., 1981. Chemical element detection in thin sections of soils with the laser microprobe mass analyzer (LAMMA 500). *Neth. J. Agric. Sci.*, 29 (1) 23–36.
- Henstra, S., Bisdom, E.B.A., Jongerius, A., Morgan, A.E., Werner, H.W. and De Grefte, H.A.M., 1980. Quantitative analysis on thin sections of soils by secondary ion mass spectrometry. In: P. Brederoo and V.E. Cosslett (Editors), *Electron Microscopy 1980. Proceedings of the 7th European Congress on Electron Microscopy including the 9th International Conference on X-ray Optics and Microanalysis*, The Hague. Seventh European Congress on Electron Microscopy Foundation, Leiden, 1980. Vol. 3. Analysis, pp. 224–225.

- Henstra, S., Bisdorn, E.B.A. and Boekestein, A., 1981. Submicroscopic techniques for in situ microchemical analysis of soils, III. Destructive techniques. In: E.B.A. Bisdorn (Editor), *Submicroscopy of Soils and Weathered Rocks*. 1st Workshop of the International Working-Group on Submicroscopy of Undisturbed Soil Materials (IWGSUSM) 1980, Wageningen. Centre for Agricultural Publishing and Documentation (Pudoc), Wageningen, pp. 55–65.
- Jongerius, A. and Heintzberger, G., 1975. Methods in soil micromorphology. A technique for the preparation of large thin sections. *Neth. Soil Surv. Inst., Soil Surv. Pap.*, 10: 48 pp.
- Knippenberg, W.F., 1974. Inorganic chemical analysis. *Philips Techn. Rev.*, 34 (11/12): 298–304.
- Morgan, A.E., 1980. An alternative to the relative sensitivity factor approach to quantitative SIMS analysis. *Surf. Interface Anal.*, 2: 123–133.
- Morgan, A.E. and Werner, H.W., 1977a. Test of a quantitative approach to secondary ion mass spectrometry on glass and silicate standards. *Anal. Chem.*, 49: 927–931.
- Morgan, A.E. and Werner, H.W., 1977b. Semiquantitative analysis by secondary ion mass spectrometry. *J. Micros. Spectros. Electron.*, 2: 285–290.
- Morgan, A.E. and Werner, H.W., 1978. Semiquantitative analyses by secondary ion mass spectrometry using one fitting parameter. *Mikrochim. Acta (Wien)*, 11: 31–50.
- Werner, H.W., 1974. Theoretical and experimental aspects of secondary ion mass spectrometry. *Vacuum*, 24: 493–505.
- Werner, H.W., 1980. Modern methods for thin film and surface analysis. In: P. Brederoo and V.E. Cosslett (Editors), *Electron Microscopy 1980. Proceedings of the 7th European Congress on Electron Microscopy including the 9th International Conference on X-ray Optics and Microanalysis*, The Hague. Seventh European Congress on Electron Microscopy Foundation, Leiden, 1980. Vol. 3. Analysis, pp. 200–207.
- Werner, H.W., 1982/83. The application of beam and diffraction techniques for thin film and surface micro-analysis. In: H. Oechsner (Editor), *Thin Film Analysis*. Springer-Verlag, Berlin.

APPLIED SUBMICROSCOPY

This Page Intentionally Left Blank

EFFECT OF POTASSIUM ON SOIL STRUCTURE IN RELATION TO HYDRAULIC CONDUCTIVITY

Y. CHEN, A. BANIN and A. BOROCHOVITCH

*The Seagram Center for Soil and Water Sciences, The Hebrew University of Jerusalem,
PO Box 12, Rehovot, 76100 (Israel)*

(Accepted for publication February 17, 1983)

ABSTRACT

Chen, Y., Banin, A. and Borochovitch, A., 1983. Effect of potassium on soil structure in relation to hydraulic conductivity. *Geoderma*, 30: 135–147.

The effect of exchangeable K^+ on soil structure and permeability has been studied. A loamy sand, a light clay and a heavy clay soil were leached with solutions adjusted to potassium adsorption ratios (PAR) of 0.0, 0.72, 3.74 and ∞ . Exchangeable K^+ percentage (EPP) and hydraulic conductivity (HC) were measured on the leached soils. SEM observations on undisturbed soil samples were used to evaluate changes in soil structure and pore size.

EPP values for the three soils ranged as follows: 0.8–1.3, 5.5–9.2, 16.0–21.0 and 58.0–76.0 for PAR's of 0.0, 0.72, 3.74 and ∞ , respectively. HC increased slightly (20%) up to EPP values of about 20% for the loamy sand and heavy clay soil, while a decrease in HC corresponding to any increase of EPP was observed for the light clay soil. This soil was richer in illite and also exhibited higher affinity for K^+ . At the highest EPP values (58.0–76.0) HC of the three soils decreased to about 20% of the values measured for the Ca^{2+} saturated soils.

SEM observations were performed and Ca^{2+} saturated soils compared with the K^+ enriched ones. Ca^{2+} treated loamy sand exhibited discrete clay aggregates located in the spaces between sand particles or attached to them. K^+ enrichment resulted in the formation of a dense network of clay microaggregates filling up the pore space. The micro-aggregate structure of the two Ca^{2+} clay soils changed to a dense layer composed of much smaller particles following K^+ enrichment. Pores were mostly smaller than 10 μm in the K^+ soil compared to several tens of microns in the Ca^{2+} form.

SEM observations and the fact that clay content did not vary with depth suggest that dispersion of clay microaggregates and their rearrangement in situ were the major mechanisms involved in HC reduction, rather than long-range clay migration and the formation of a clay enriched layer with impeded drainage.

INTRODUCTION

Soil permeability is recognized as a major factor in soil management. The effect of the exchangeable cation species on soil permeability with particular emphasis on the deleterious effects of Na^+ vs. ($Ca^{2+} + Mg^{2+}$) are well

documented (e.g. U.S. Salinity Laboratory Staff, 1954; Quirk and Schofield, 1955). Fewer reports on K^+ effects on soil permeability have been published and results seem to vary or conflict, possibly due to differences in soil mineralogy and sample preparation procedures. Generally, soil permeability relates to exchangeable cations in the following order: $Ca \cong Mg > K > Na$. However, differences in the relative values of permeability have been reported: $Mg > K > Na$ (Reeve et al., 1954); $Ca > Mg > K = Na$ (Quirk and Schofield, 1955); $Ca > K > Na$ (Gardner et al., 1959); $NH_4 = K > Na$ (Martin and Richards, 1959); and $Ca = Mg > K > Na$ (clay loam) and $Ca > Mg > K = Na$ (clay) (Ahmed et al., 1969). In contrast, some researchers report larger aggregates of greater stability in K^+ -saturated soils than in those saturated with divalent cations: $K > Ca = Mg > Na$ (Cecconi et al., 1963); $K > Ca$ (Ravina, 1973); suggesting that K^+ in the exchange sites has favorable effects on soil permeability.

The major mechanisms involved in the decreases in permeability due to monovalent exchangeable cations are swelling, dispersion and clay migration which affect the hydraulic conductivity (HC) of the soil (Quirk and Schofield, 1955). The relative importance of these mechanisms is a matter of controversy. Chen and Banin (1975) suggest that clay dispersion, detachment of clay from sand particles and their rearrangement in situ are the major mechanisms responsible for reduction in HC in sodic sandy soils. Clay dispersion resulting in aggregate destruction was found to be the major mechanism causing HC reduction in a sodic clay soil (Chen and Banin, 1975). On the basis of these observations, it has been suggested that short- and long-range clay migration can be distinguished (Chen, 1975; Chen and Banin, 1975). According to these investigators, in situ clay particle rearrangement following aggregate destruction and resulting pore-size reduction is considered as short-range migration, whereas the downward movement of clay, which often leads to the formation of an impeded layer, is considered as long-range migration.

Since K^+ is a major nutritional element for plants, enrichment of K^+ in the exchange sites due to fertilizer practice can be expected. Heavy K^+ fertilizer application is a common practice in greenhouse agriculture and leads to soil exchangeable K^+ levels which are much greater than those of field soils. The purpose of this study was, therefore, to investigate the effects of K^+ on the permeability of soils commonly used for greenhouse agriculture in Israel.

MATERIALS AND METHODS

Soils

A loamy sand, a light-clay and a heavy-clay soil were sampled at Rehovot, Timorim and Yagur, respectively, in Israel. These soils pose permeability problems when used as greenhouse soils. Chemical and physical properties of the field soils were determined as follows: cation exchange capacity (CEC)

and adsorbed cation species by displacement with 1 *N* sodium acetate and 1 *N* ammonium acetate, respectively (U.S. Salinity Laboratory Staff, 1954); particle-size analysis by the hydrometer method (Van der Watt, 1966); organic matter by a wet-combustion method (Black et al., 1965); and CaCO₃ content by a calcimeter method (Black et al., 1965). The mineralogical composition of the clay fraction was determined using methods described by Gal et al. (1974).

The potassium adsorption ratio (PAR) was calculated as:

$$\text{PAR} = K/[(\text{Ca} + \text{Mg})/2]^{1/2} \quad (1)$$

where *K* and (*Ca* + *Mg*) are the corresponding ions concentrations in meq/l. Gapon's constant (*K_G*) was calculated as:

$$K_G = [K/(\bar{\text{Ca}} + \bar{\text{Mg}})]/\text{PAR} \quad (2)$$

where *K*, $\bar{\text{Ca}}$ and $\bar{\text{Mg}}$ are the quantities of the corresponding exchangeable cations in meq/100 g soil.

Hydraulic conductivity measurements on soils equilibrated to required exchangeable K⁺ percentage (EPP).

The soils were air-dried, crushed and sieved through a 2 mm sieve. PVC pots (2.8 l capacity) were used as permeameters (McNeal and Reeve, 1964). The pot-permeameter and the HC measurement system and procedure are described by Chen and Banin (1975).

Leaching solutions were prepared by dissolving chloride salts of K⁺ and Ca²⁺ to give PAR values of 0, 0.72, 3.74 and ∞ at K⁺ + Ca²⁺ concentrations of either 1 *N* or 0.02 *N*. To prevent microbial growth in the soil 50 ppm of HgCl₂ were added to the leaching solutions. The compositions of the leaching solutions are given in Table I. The treatments were designated as K₁, K₂, K₃ and K₄ corresponding to increasing PAR values of the leaching solutions.

Leaching was initiated by applying the solution to the top of the soil and flooding the surface until a head of about 4–6 cm of solution was established. The solution level was thereafter maintained at this level by use

TABLE I

Compositions of the leaching solutions

Treatment	PAR	K ⁺ concentration (meq./l)		Ca ²⁺ concentration (meq./l)	
		0.02 <i>N</i>	1 <i>N</i>	0.02 <i>N</i>	1 <i>N</i>
K ₁	0.00	0.00	0.00	20.00	1000.00
K ₂	0.72	2.14	15.80	17.86	984.20
K ₃	3.74	8.85	80.20	11.15	919.80
K ₄	∞	20.00	1000.00	0.00	0.00

TABLE II

Origin and characteristics of soil samples

Soil location	Soil texture class	Moisture contents of air-dried soils (%)	Cation exchange capacity (meq./100 g)	Exchangeable cations (meq./100 g)				Exchangeable potassium percentage (%)	CaCO ₃ (%)	Particle-size analysis (%)			Organic matter (%)
				K	Na	Mg	Ca			clay	silt	sand	
Rehovot	loamy sand	2.0	10.9	0.2	0.2	1.5	9.0	2.2	2.6	13.8	1.3	85.0	0.7
Timorim	light clay	5.9	34.5	2.0	0.5	9.4	22.6	5.8	15.8	40.0	16.2	43.8	2.1
Yagur	heavy clay	8.4	53.7	0.9	0.7	15.4	36.7	1.6	12.5	48.7	25.0	26.3	3.7

of Mariot-bottles. The leaching was thus conducted under saturated conditions at a gradient of 1.3–1.5 cm/cm.

Soils were equilibrated by passing 20 l of the 1 *N* solution followed by 10 l of the 0.02 *N* solution. HC measurements were performed toward the end of the leaching process while the 0.02 *N* solutions were passing through the soil. After equilibration and HC measurements, excess solution was allowed to drain out and soil samples taken for CEC, exchangeable cation species determination, and SEM observations. CEC was also determined on soil sections of the K_4 treatments at depths of 0–5, 5–10 and 10–14 cm as a measure for the possible formation of a clay-rich layer.

SEM observations

The total depth of the saturated soil in the pot was sampled using a 2.5-cm internal diameter cork borer. The sampler with soil was submerged in liquid nitrogen, which rapidly froze the wet soil. The sample was released by rubbing the outside of the tube to warm it. The frozen soil core was then sheared parallel to its axis by applying pressure with a pair of pliers, exposing a fresh undisturbed soil surface normal to the top of the cylinder. The frozen sample was glued using Duco cement onto an aluminum stub with the exposed surface facing upward, freeze-dried, and coated with carbon and gold. A Jeol model JSM 35 C scanning electron microscope was used to obtain micrographs at magnifications of $\times 160$ and $\times 1600$.

RESULTS AND DISCUSSION

Properties of the soils

Chemical and physical properties of the three soils studied are presented in Table II. Soil texture varied from loamy sand to heavy clay (International Society of Soil Science classification). Properties related to clay contents such as moisture content of air-dried soils and CEC, vary accordingly. CaCO_3 content is small in the sandy soil and much greater for the clayey soils. The organic matter content is very small in the sandy soil and somewhat greater in the light clay. The exchangeable K^+ percentage of the natural soils does not exceed 5.8%.

The mineralogical properties of the soils are presented in Table III. Montmorillonite comprises the major fraction followed by kaolinite. Illite which is of special interest due to its K^+ fixation properties, comprises about 10% of the sandy loam and heavy clay soils and 16% of the light clay soil.

Exchangeable cation species and capacity

General. Exchangeable K^+ contents and percentages, CEC and K_G of the leached soils are summarized in Table IV. EPP values for a given PAR treat-

TABLE III

Mineralogical composition of the clay fraction

Soil location	Illite (%)	Montmorill. (%)	Kaolinite (%)	Free oxides (%)					CaCO ₃ (%)
				SiO ₂	Fe ₂ O ₃	Al ₂ O ₃	MnO ₂ ($\times 10^{-4}$)	total	
Rehovot	10	56	26	1.9	4.2	0.4	3	6.5	1.5
Timorim	16	47	19	2.6	2.2	0.3	4	5.1	13.5
Yagur	11	58	17	2.7	2.3	0.4	2	5.4	9.0

ment differed somewhat among the soils, possibly due to differences in their illite content. In each soil K_G decreased with increase of PAR and of EPP due to saturation of the K^+ -preferring sites. The data show that CEC values for the various PAR treatments within a single soil did not differ significantly. However, some reduction in CEC due to K^+ fixation took place in soils treated with solutions of $PAR = \infty$. This is confirmed by comparing CEC-data of the field soils (Table II) with those of the soils treated with solutions of $PAR = \infty$ (Table IV).

TABLE IV

Exchangeable K^+ , CEC, EPP and K_G of the leached soils (means of triplicates)

Soil location	Treatment	Solution PAR	Exchangeable K (meq./100 g)	CEC (meq./100 g)	EPP (%)	K_G (l/mole) ^{1/2}
Rehovot	K_1	0.00	0.1	11.0	0.8	∞
	K_2	0.72	0.6	11.0	5.5	2.57
	K_3	3.74	1.9	11.6	16.0	1.61
	K_4	∞	6.0	10.7	58.0	0.51
Timorim	K_1	0.00	0.4	33.6	1.3	∞
	K_2	0.72	3.1	33.7	9.2	4.48
	K_3	3.74	7.2	34.8	21.0	2.28
	K_4	∞	23.4	29.9	76.0	1.17
Yagur	K_1	0.00	0.4	52.9	0.8	∞
	K_2	0.72	3.4	54.1	6.4	3.02
	K_3	3.74	10.8	51.4	21.0	2.25
	K_4	∞	39.4	50.6	71.0	0.91

Measurements of CEC as a function of soil depth in the permeameter, for the K_4 treatments showed the following ranges (data in meq./100 g): Rehovot 10.3–10.7; Timorim 29.9–30.2; and Yagur 49.9–50.6. These data show that the clay contents (assessed by CEC) are practically constant with depth, suggesting that long-range clay migration and the formation of an impeded clay layer did not take place.

Effect of potassium on hydraulic conductivity. Relative HC data (HC of the K_1 treatment for each soil taken as 1.0) are plotted against EPP in Fig. 1. The curves for the Yagur and Rehovot soils are similar, both exhibiting HC increase up to EPP of about 20% and a steep decrease in HC with further increase of EPP. The Timorim soil responds differently to an EPP increase, HC decreasing with any increase in EPP. Small EPP-effects on soil permeability thus seem to be different among the soils and relate to structural or compositional factors which are not well understood at this time. It seems that at small EPP's K^+ may have positive effects on HC in some soils, possibly due to interlayer adsorption on illite resulting in the stabilization of microaggregates. The differences in response of the various soils could not be correlated with any of their measured chemical or mineralogical properties. We therefore feel, that further research is required to elucidate K^+ effect on soils at low EPP's. However, large EPP values produced deleterious effects in the three soils studied. Moreover, in one of the soils in this study (Timorim) EPP values below 25% resulted in soil deterioration.

Of interest is a comparison of the effect of Na^+ (Chen and Banin, 1975) with that of K^+ . The loamy sand in the two studies originates from very close locations, belong to the same soil type and differ somewhat in clay contents. The light-clay soil from Timorim in this study resembles the Kefar Menachem soil (Chen and Banin, 1975). Timorim and Kefar Menachem soils belong to the same soil type and resemble in clay

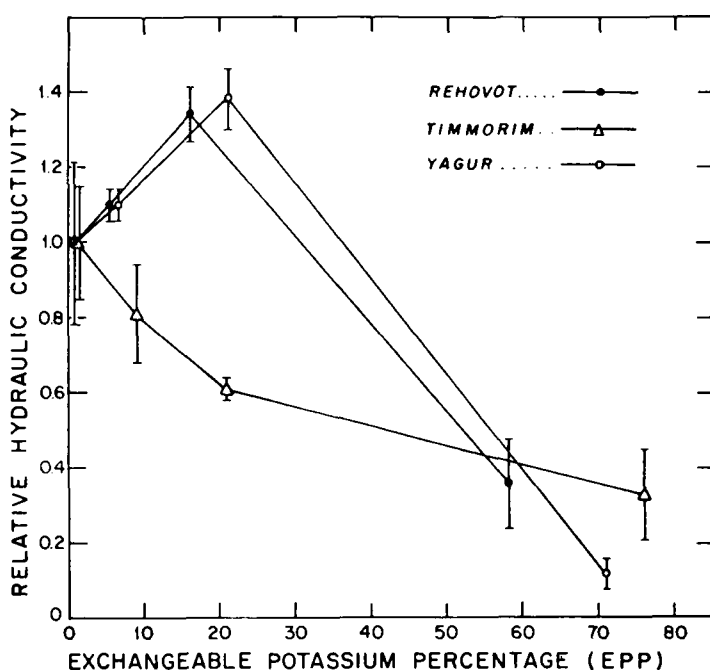


Fig. 1. Relative hydraulic conductivity vs. EPP (average \pm standard deviation).

mineralogy, CaCO_3 content and other chemical properties. Whereas 15% of exchangeable Na^+ reduced HC by 80% (relative HC = 0.2), 60%-75% of exchangeable K^+ were required to cause a similar reduction suggesting that the deleterious effect of potassium is less than that of sodium. This is in accord with earlier reports (Reeve et al., 1954; Brooks et al., 1956; Gardner et al., 1959; Ahmed et al., 1969).

SEM observations. SEM observations on the effect of increased exchangeable K^+ percentage on soil fabric are presented in Figs. 2–4. Only the two extreme treatments, K_1 and K_4 , are presented for each soil. Sand particles coated and interspersed with clay material can be seen in the low-magnification micrographs of the sandy soil (Rehovot: Fig. 2). The Ca^{2+} -treated soil (K_1) shows discrete, rounded clay aggregates in the pore space between the much larger sand particles, but most of the clay microaggregates are attached to sand particles. Pores as large as $100\text{ }\mu\text{m}$ can be seen. Potassium-enrichment (K_4) resulted in the formation of a dense continuous network of clay particles filling the pore space between the sand particles, thus reducing the average pore size. The higher magnification shows discrete clay aggregates coating the sand particles in the Ca^{2+} soil, whereas a large number of small aggregates forming a network are seen on the K_4 micrograph.

In the two clay soils the low-magnification micrographs show a continuous mass of fine material mixed with larger particles, with no obvious difference between the Ca^{2+} soil and the K^+ enriched one. However, at the higher magnification the dispersion effects of the adsorbed K^+ are seen. In the Timorim Ca^{2+} soil (Fig. 3) discrete microaggregates are seen with pores of $5\text{--}10\text{ }\mu\text{m}$ in size between them. In the K^+ enriched soil many small clay aggregates are seen, causing a reduction in the average pore size to $0.5\text{--}2\text{ }\mu\text{m}$. Very similar changes were found in the Yagur clay soil (Fig. 4). These changes in particle arrangement and pore-size distribution correspond well with the HC changes and must be due to high K^+ enrichment.

The number of published investigations of SEM studies on K^+ affected soils is small, and it is thus difficult to draw comparisons with our work. Ravina (1973) presented SEM micrographs of Ca^{2+} and K^+ saturated clay fractions extracted from a Grumusol. Preparation methods were destructive and air-drying was applied after the K^+ enrichment and prior to the SEM observations. Ravina (1973) concluded that more points of contact between particles could be seen in the K^+ saturated clay and, therefore, a coarser structure formed. This is not in accord with our observations. We believe that the preparation procedures of the soils are of major importance. Therefore, we studied samples which were undisturbed and not allowed to air-dry once leaching had started.

Chen and Banin (1975) showed the effects of Na^+ on soil structure which were similar to those of K^+ although more extreme, albeit the effect of Na^+ appeared at a much lower monovalent exchangeable ion percentage (10–16%). It appears that the degree of structural damage in soils con-

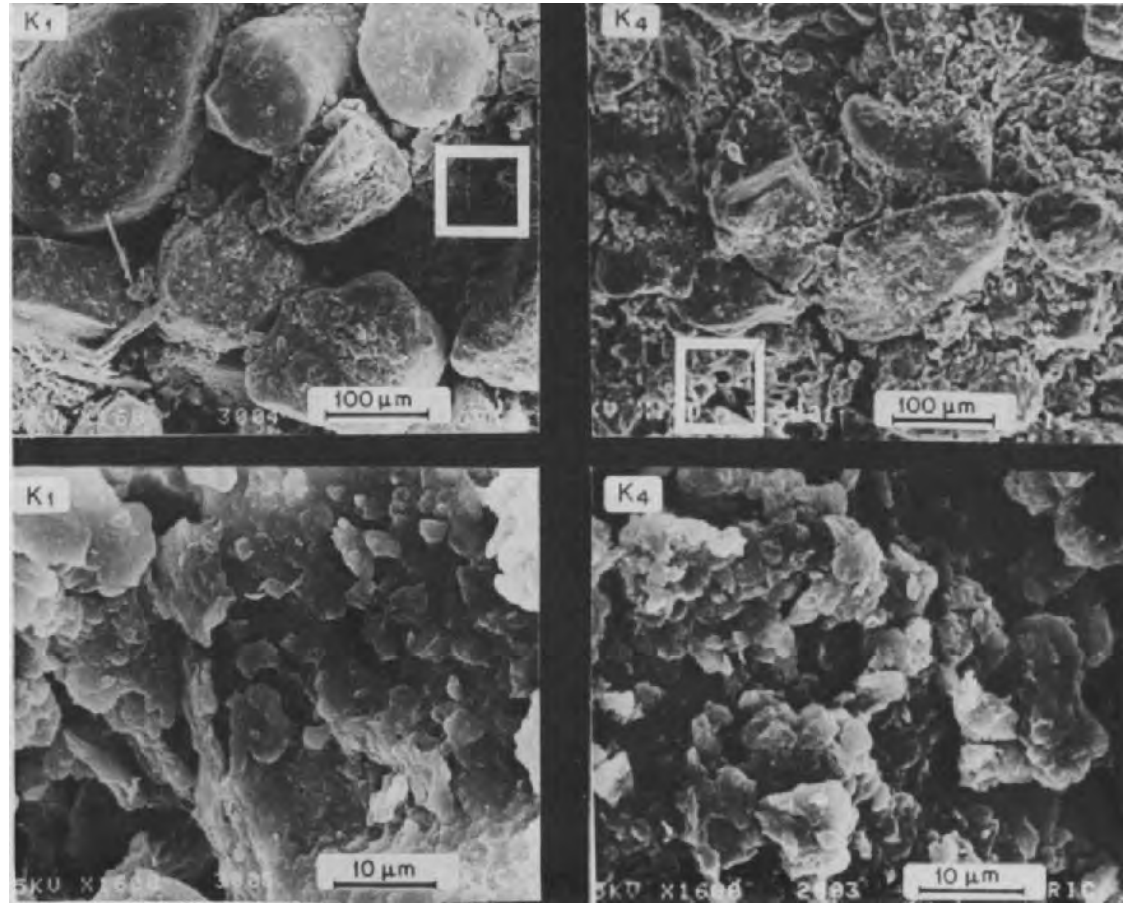


Fig. 2. SEM micrographs of a sandy soil (Rehovot) at EPP values of 1% (K₁) and 58% (K₄). White inserts in the top figures are enlarged in the bottom ones.

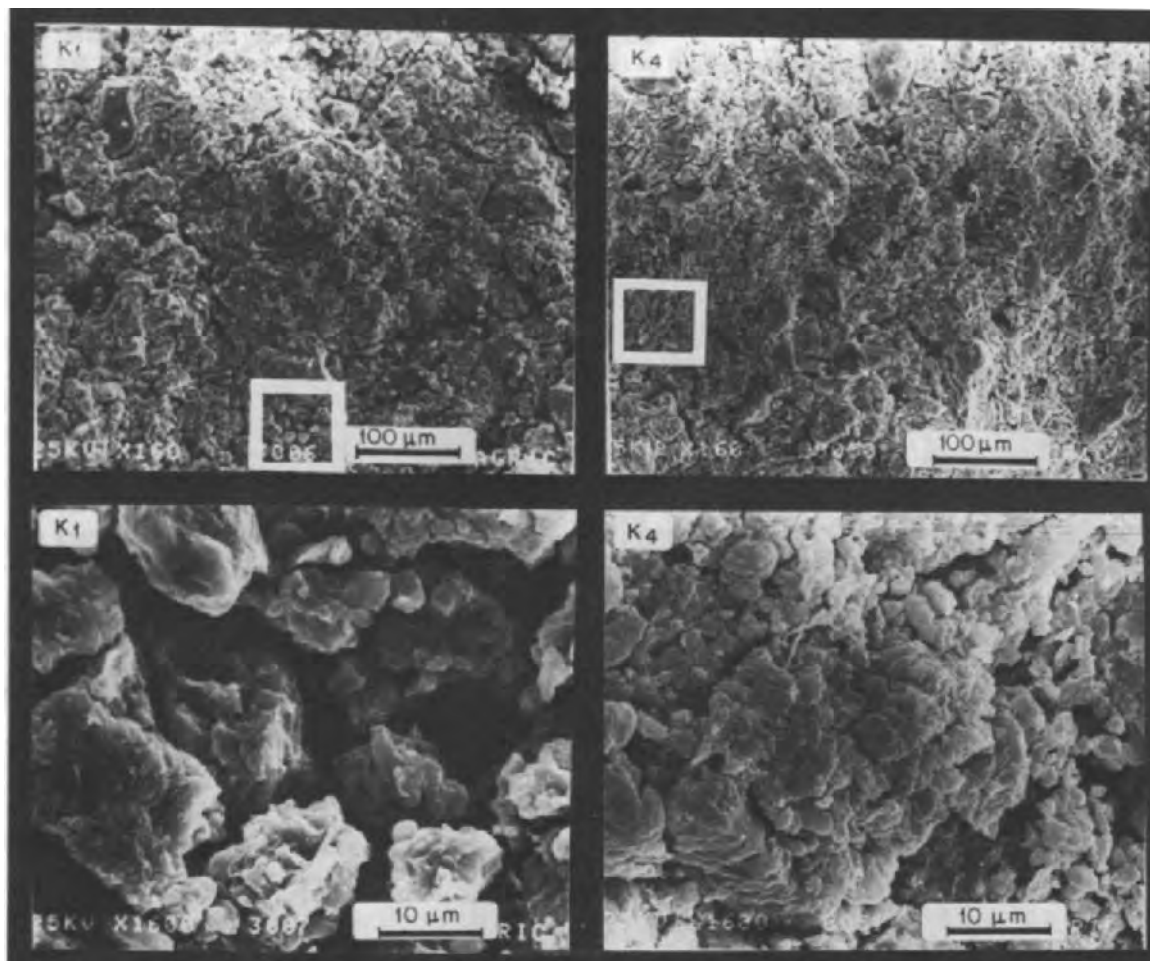


Fig. 3. SEM micrographs of a light-clay soil (Timorim) at EPP values of 1% (K_1) and 76.1% (K_4). White inserts in the top figures are enlarged in the bottom ones.

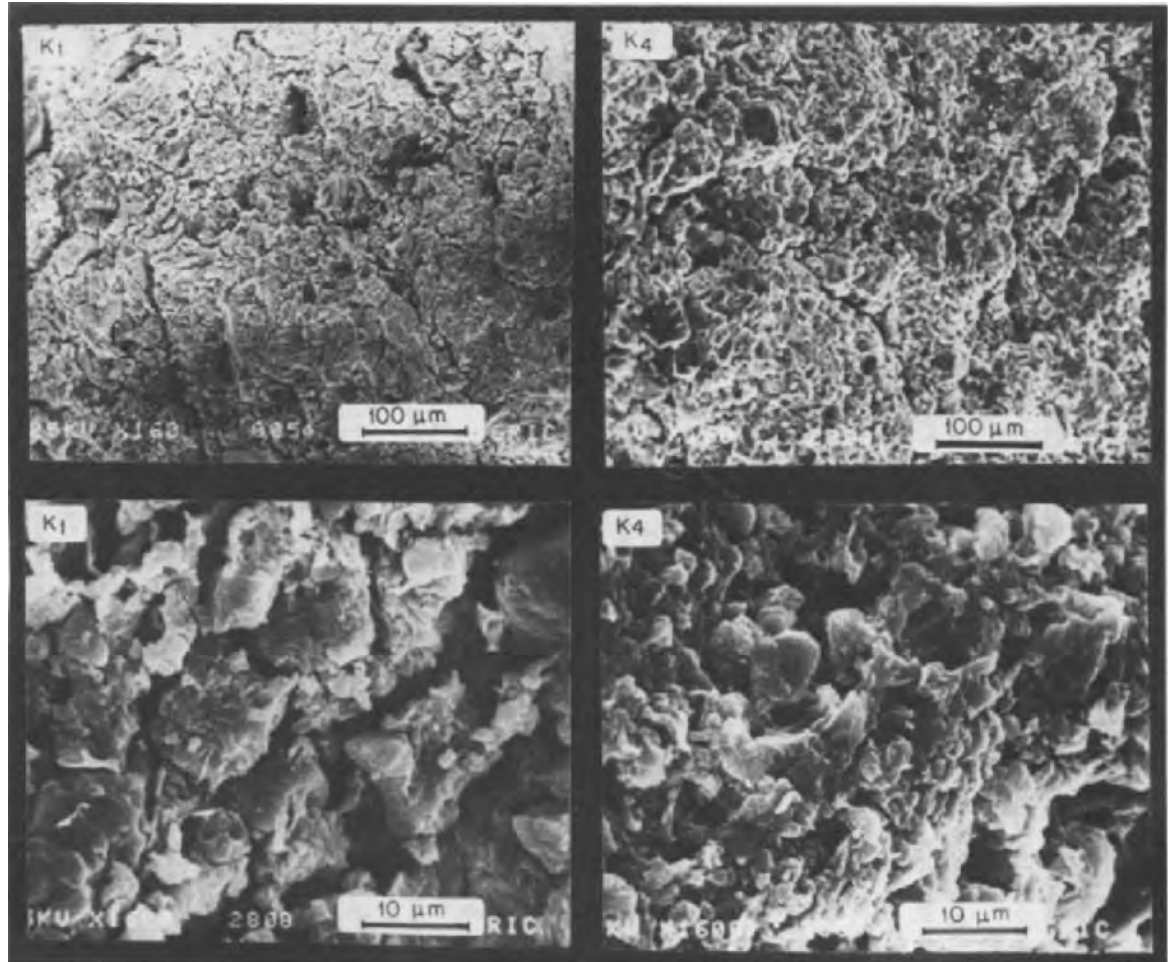


Fig. 4. SEM micrographs of a heavy-clay soil (Yagur) at EPP values of 1% (K_1) and 71% (K_4) and at two magnifications.

taining 60–75% exchangeable K^+ is comparable with that occurring with 10–16% exchangeable Na^+ .

Bisdorn (1981) in his review article on the application of submicroscopic techniques in soil micromorphology has emphasized the importance of SEM as a tool to improve understanding of soil structure and soil–water relationships. This work provides SEM evidence for structural changes due to exchangeable K^+ and illustrates the mechanism involved at high EPP's. Our observations strengthen the hypothesis of Chen and Banin (1975) that dispersion of the fine soil fraction (mostly clay aggregates) and its rearrangement in situ to form a dense network of particles with smaller pores between them is the major mechanism for HC reduction, rather than massive clay migration and the formation of an impermeable layer.

REFERENCES

- Ahmed, S., Swindale, L.D. and El-Swaify, S.A., 1969. Effects of adsorbed cations on physical properties of tropical black earths, 1. Plastic limit, percentage stable aggregate and hydraulic conductivity. *J. Soil Sci.*, 21: 255–268.
- Bisdorn, E.B.A., 1981. A review of the application of submicroscopic techniques in soil micromorphology, I. Transmission electron microscope (TEM) and scanning electron microscope (SEM). In: E.B.A. Bisdorn (Editor), *Submicroscopy of Soils and Weathered Rocks*. Center for Agricultural Publishing and Documentation, Wageningen, pp. 67–116.
- Black, C.A., Evans, D.D., White, J.L., Ensminger, L.E. and Clark, F.E. (Editors), 1965. *Methods of Soil Analysis*. Am. Soc. Agron., Madison, WI, Monogr., 9, 1349–1353; 1393–1396.
- Brooks, R.H., Bower, C.A. and Reeve, R.C., 1956. The effect of various exchangeable cations upon the physical conditions of soils. *Soil Sci. Soc. Am. Proc.*, 20: 325–327.
- Cecconi, S., Salazar, A. and M. Martelli, M., 1963. The effect of different cations on the structural stability of some soils. *Agrochimica* 7: 185–204.
- Chen, Y., 1975. Evaluation of montmorillonite behavior and particle structure as a model for swelling and flow impediment in soils. Ph.D. Thesis, The Hebrew University of Jerusalem.
- Chen, Y. and Banin, A., 1975. Scanning electron microscope (SEM) observations of soil structure changes induced by sodium-calcium exchange in relation to hydraulic conductivity. *Soil Sci.*, 120: 428–436.
- Gal, M., Ravikovitch, S. and Amiel, A.J., 1974. Clay mineral distribution and origin in the soil types of Israel. *J. Soil Sci.*, 25: 79–89.
- Gardner, W.R., Mayhugh, M.S., Goertzon, J.O. and Bower, C.A., 1959. Effect of electrolyte concentration and ESP on diffusivity of water in soils. *Soil Sci.*, 88: 270–274.
- Martin, J.P. and Richards, S.J., 1959. Influence of exchangeable H, Ca, Na, K and NH_4 at different H levels on certain physical properties of soils. *Soil Sci. Soc. Am. Proc.*, 23: 335–338.
- McNeal, B.L. and Reeve, R.C., 1964. Elimination of boundary-flow errors in laboratory hydraulic conductivity measurements. *Soil Sci. Soc. Am. Proc.*, 28: 713–714.
- Quirk, J.P. and Schofield, R.K., 1955. The effect of electrolyte concentration on soil permeability. *J. Soil Sci.*, 6: 163–178.
- Ravina, I., 1973. The mechanical and physical behavior of Ca-clay soil and K-clay soil. *Ecol. Stud.*, 4: 131–140.

- Reeve, R.C., Bower, C.A., Brooks, R.H. and Gschwend, F.B., 1954. A comparison of the effects of exchangeable Na^+ and K^+ upon the physical conditions of soils. *Soil Sci. Soc. Am. Proc.*, 18: 130—132.
- U.S. Salinity Laboratory Staff, 1954. *Diagnosis and Improvement of Saline and Alkali Soils*. USDA Handbook 60, pp. 100—101.
- Van der Watt, H.V.H., 1966. Improved tables and a simplified procedure for soil particle analysis by hydrometer method. *S. Afr. J. Agric.*, 9: 911—916.

This Page Intentionally Left Blank

LIGHTMICROSCOPE AND SUBMICROSCOPE OBSERVATIONS OF SALTS IN MARINE ALLUVIUM (INDIA)

M.J. KOOISTRA

Stichting voor Bodemkartering (Stiboka), Wageningen (The Netherlands)

(Accepted for publication February 17, 1983)

ABSTRACT

Kooistra, M.J., 1983. Lightmicroscope and submicroscope observations of salts in marine alluvium (India). *Geoderma*, 30: 149–160.

In samples from a salt-affected Indian soil series, a curly stem-like salt efflorescence occurred. Unimpregnated soil material and thin sections from these samples, prepared in two different ways, were studied with lightmicroscopy and submicroscopy. The samples came from the Dandi soil series, classified as Halaquepts (Soil Survey Staff U.S.D.A., 1975), which occur extensively on marine alluvium in the semi-arid parts of Gujarat (India). In the unimpregnated samples, several habits of halite (massive crusts, cubical forms, thin threads and curly stem-like forms) were determined with SEM–EDXRA. In large thin sections (8 × 15 cm) covered with a thin glass slide, which could only be studied under a lightmicroscope, no halite was observed. However, another salt of unknown composition, not observed in unimpregnated soil material, was detected. In addition, in small thin sections (2 × 3 cm) with highly polished surfaces, remnants of halite could be observed under the lightmicroscope. With submicroscopy the presence of halite was confirmed and the unknown salt was proved to be a habit of gypsum. This gypsum forms roughly circular shapes, that have diameters varying between 80–200 μm , cracked surfaces and diffuse extinction patterns under crossed polarizers. It occurs along void walls, often in association with halite and in the fine-grained groundmass near voids. Halite occurs along void walls and as angular grains in coarse-grained laminae. The habit of the gypsum observed and the curly stem-like halite on the unimpregnated soil material, have not previously been reported in the literature. The habits of halite need not all be pedogenetic; though the gypsum, a much less soluble salt, probably is pedogenetic. Techniques of preparing thin sections must be improved for the further study of easily soluble salts in soils.

INTRODUCTION

The micromorphology of a large number of Indian benchmark soils was analysed and interpreted in The Netherlands*. Some of these soils were salt-affected. Undisturbed soil samples from one of the salt-affected soil

*Co-operation between the Indian National Bureau of Soil Survey and Land Use Planning and The Netherlands Soil Survey Institute/International Soil Museum.

series (Dandi) showed a special kind of salt efflorescence on void-walls. The morphology, composition and occurrence of salts in these samples was studied in unimpregnated soil samples, and in thin sections, using light-microscope and submicroscope techniques.

MATERIAL

The soil materials showing the salt efflorescence were derived from the Dandi series, classified as Halaquepts, saline phases of Ustochrepts (Soil Survey Staff U.S.D.A., 1975). Halaquepts occur extensively in the semi-arid parts of southern and eastern Gujarat, one of the western coastal states of India, and are represented by the Dandi series (Murthy et al., 1980). These soils are formed in marine alluvium in shallow basins. The soils are deep, slowly permeable, dark greyish brown, fine textured and have columnar and prismatic structures in the B horizon. The pH is usually mildly to moderately alkaline, electrical conductivities vary, but are high, and the exchangeable sodium exceeds 50% (Murthy et al., 1982). The samples were derived from uncultivated soils near the coast.

METHODS

For the preparation of thin sections, blocks measuring $8 \times 15 \times 5$ cm were taken from undisturbed soil material. These samples were air-dried, impregnated with a plastic, hardened, sawn, mounted on glass slides and ground into sections $15 \mu\text{m}$ thick, according to the method described by Jongerius and Heintzberger (1975). The sections were subsequently coated with a thin layer of plastic of the same composition as the one used for mounting, and were covered by a thin glass slide.

While the samples were drying, a curly stem-like salt efflorescence was observed on void walls. A few pieces of soil material with these salts were removed and kept unimpregnated.

Small thin sections measuring approximately 2×3 cm were prepared from the hardened blocks taken from a number of key areas near voids and in the groundmass. The surface of these sections was not covered by a glass slide but was polished. The polishing was done on a disc rotating at a speed of approximately 50 rpm, covered by a polishing cloth and using diamond polishing compound pastes first of $3 \mu\text{m}$ and then $1 \mu\text{m}$. The resulting thin sections were $15 \mu\text{m}$ thick and had the highly polished surface essential for good-quality SEM pictures.

All thin sections were studied under a lightmicroscope. The small thin sections with polished surfaces and the pieces of unimpregnated soil material with the salt efflorescence were examined under a scanning electron microscope (SEM), equipped with a backscattered electron (BE) detector and an energy dispersive X-ray analyzer (EDXRA).

RESULTS

The results are presented below in the following order: (1) submicroscope data on the salt efflorescence in unimpregnated soil material; (2) light-microscope data on salts in large and small thin sections; and (3) submicroscope data on salts in small thin sections.

Submicroscope data on the salt efflorescence in unimpregnated soil material

Several morphologies of salts were observed with the SEM: massive crusts, cubical forms, thin threads with diameters of up to a few microns and the curly stem-like forms (see Fig. 1). No specific occurrence can be given. All forms were encountered to a depth of 90 cm, the maximum depth from which samples were obtained.

The stem-like forms were abundant. They often consisted of a number of thin threads, 5–15 μm in diameter, that coalesced to form a broad, thin, elongated, curly band up to several mm long (Fig. 1b). The results from the EDXRA analyses showed that the morphologies invariably consisted of Na and Cl (Fig. 1c) and must be halite.

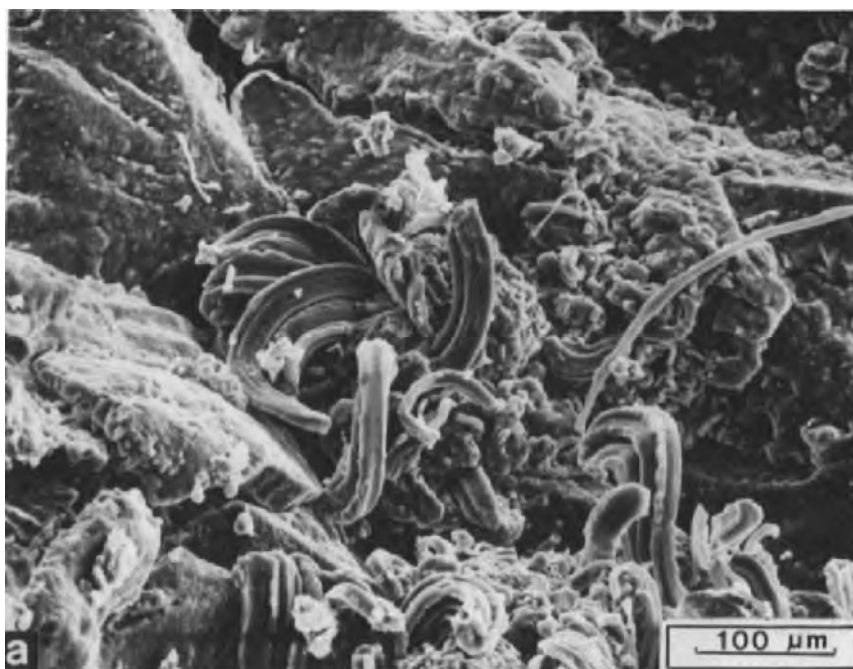


Fig. 1a. Legend on p. 152.

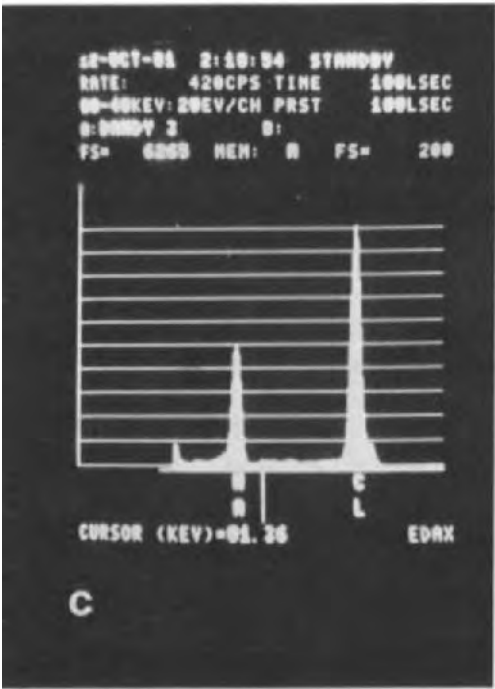
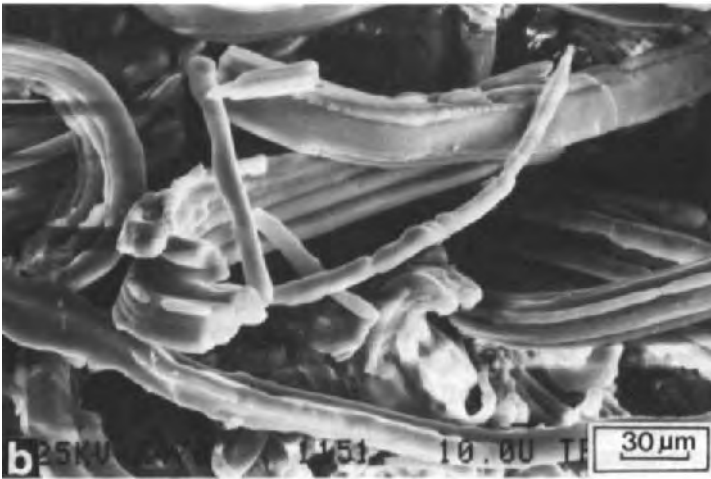


Fig. 1. General view (SEI) of a surface crust (a), detail (SEI) of the curly stem-like material (b), and an EDXRA point-analysis of this material (c) in unimpregnated soil material.

Lightmicroscope data on salts in large and small thin sections

Large thin sections. These thin sections were carefully studied for the presence of salts. In voids and in the groundmass colourless, optically isotropic halite could not be detected with certainty. In some of the voids, thin accumulations of predominantly fine-grained soil material with some larger mineral grains, occurred along the walls. No halite could be detected with certainty in and around this material either. In the large thin sections, however, another kind of salt was observed. In plain light loose, very thin accumulations of soil material, roughly circular in shape and varying between 80–200 μm in diameter were discerned. No internal structure, colour or relief could be detected. Under crossed polarizers this material was greyish-white and had a diffuse extinction pattern (Fig. 2). This type of salt

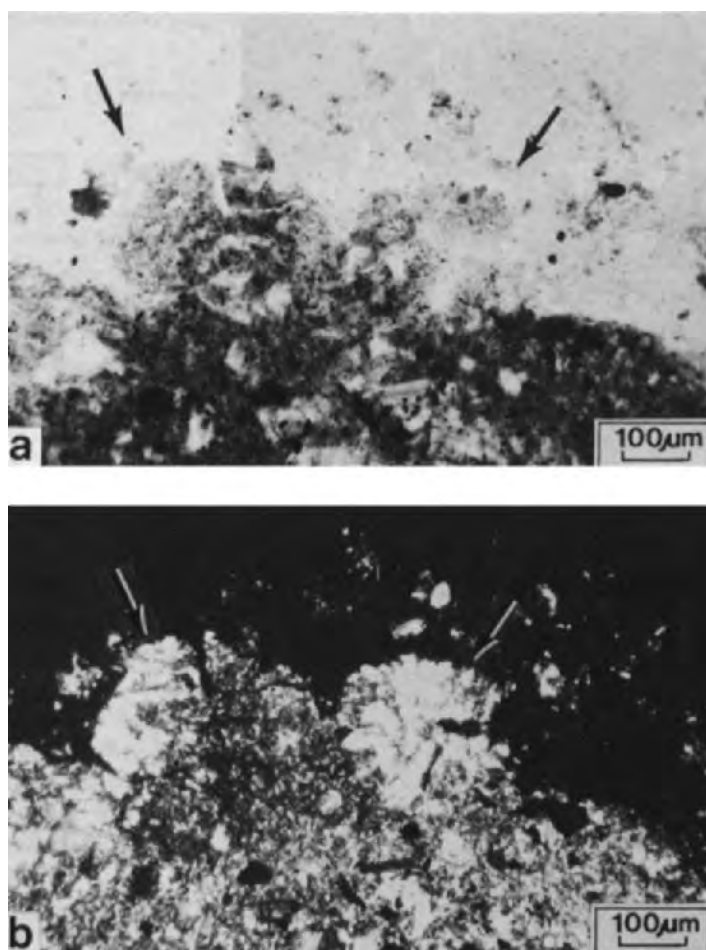
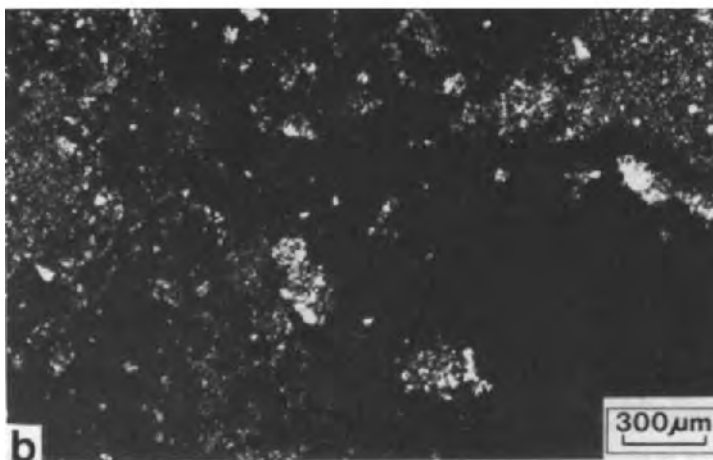
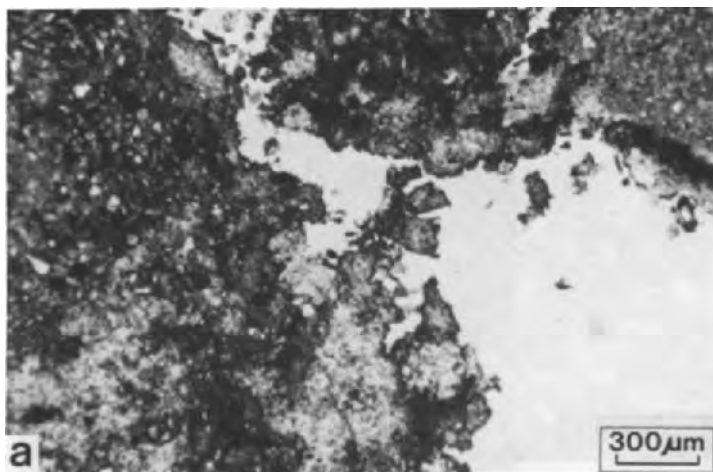


Fig. 2. Circular shapes of gypsum (arrowed), occurring along a void wall. Large, covered, thin section: a. plain light; b. crossed polarizers.

occurred in voids near the walls, often in association with the above-mentioned thin accumulations of predominantly fine-grained soil material and locally in the groundmass near voids, restricted to clay-rich material.

Small uncovered thin sections. In contrast with the large thin sections, in the small uncovered thin sections, colourless, optically isotropic material, showing rectangular cleavage patterns was observed locally. This material may be halite. It occurred locally as a kind of surface crust along the walls of voids and was present together with other mineral grains in some sandy sedimentary laminae. Under crossed polarizers, the optical isotropy of these grains caused these sandy sedimentary laminae to appear to have an open packing. In the large thin sections sandy sedimentary laminae with this open packing were also observed, but the presence of salt crystals was not proved.



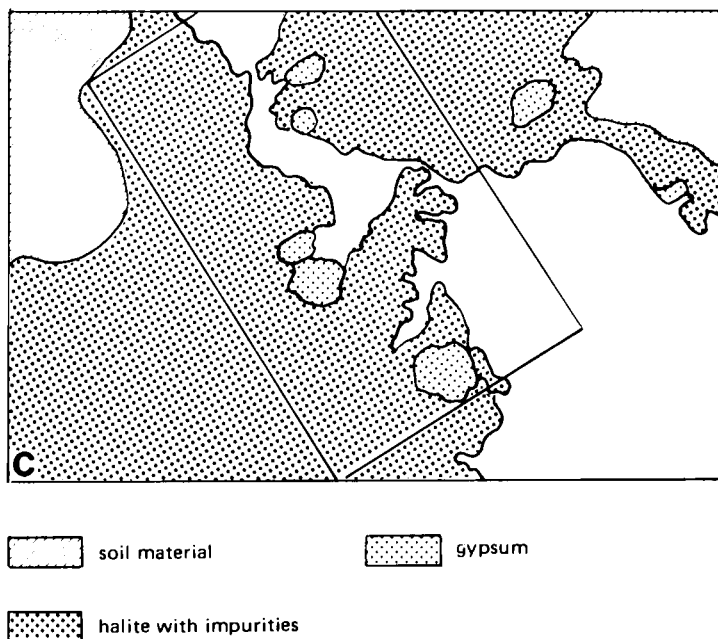


Fig. 3. Salt accumulation along void walls. Small, uncovered thin section: a. plain light; b. crossed polarizers; c. explanation (inset framework Fig. 4).

The roughly circular shaped salt detected in the large thin sections, was also observed in the small thin sections and yielded additional information. In plain light the surface of this salt generally had a cracked pattern and when present in voids it was often embedded in the surface crusts formed by the halite-type of salt observed in the small thin sections (Fig. 3).

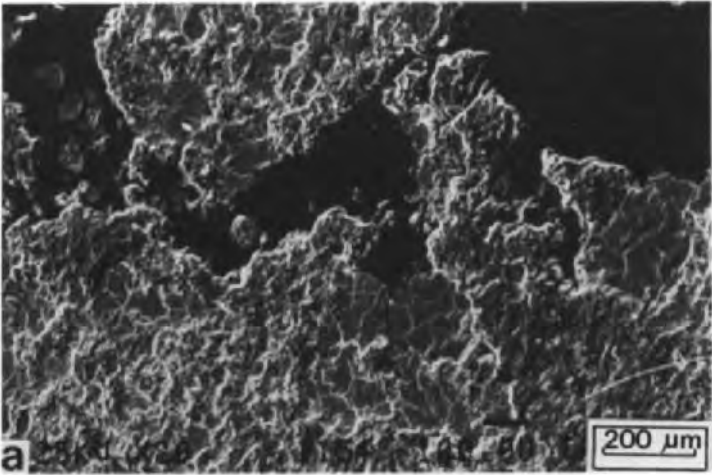
Submicroscope data on salts in small thin sections

Both types of salts detected in the small thin sections were studied with submicroscopy.

The salt type that was colourless and optically isotropic under the light-microscope was recognizable in secondary electron images (SEIs). But it could not be seen in backscattered electron scanning images (BESIs: see Fig. 4, a and b). BESIs indicate the chemical composition and variation of the object under study. The reason that the colourless, optically isotropic material was not represented in BESIs could be that only lighter elements are present in this salt. EDXRA point-analyses of this material showed that Na, Mg, Al, Si, Cl, K, Ca and Ti were present in slightly varying quantities. A typical point-analysis is given in Fig. 4c. In voids where the lightmicroscopy and submicroscopy showed no other material to be present other than plastic, only Cl was distinctly measured in point-analyses. The same results,

SEIs, BESIs and point-analyses, were obtained from the grains of salt material present in coarser-grained laminae.

The other type of salt observed both in the large and small thin sections was clearly visible in the SEIs and BESIs (Fig. 4, a and b). This salt appeared to be composed mainly of Ca and S and was therefore a habit of gypsum. Fig. 5 shows an SEI and X-ray images of Ca and S of one of the gypsum accumulations.



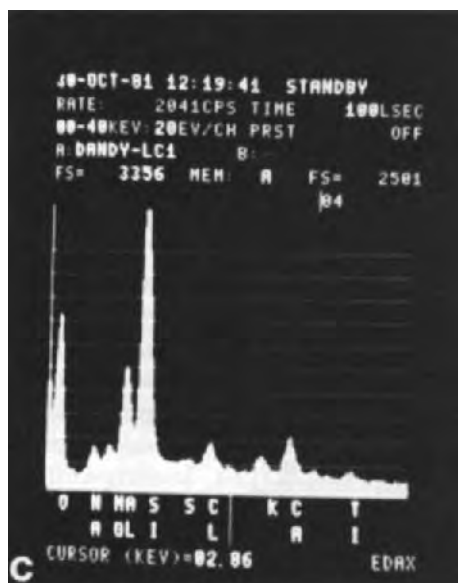


Fig. 4. Part of the salt accumulation along void walls of Fig. 3: a. scanning electron image; b. backscattered electron scanning image; c. EDXRA point-analysis of the zone containing halite.

DISCUSSION OF THE DATA

On the walls of voids in the dried samples, halite was present in various habits. In Eswaran et al. (1980) the morphologies of halite in soils revealed by SEM are discussed. These authors reported that massive crusts and cubical forms occurred in salic horizons and on the floors and walls of profile pits.

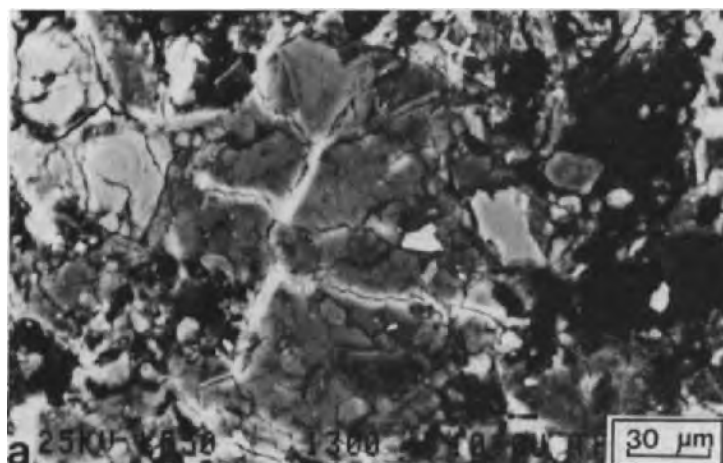


Fig. 5a. Legend on p. 158.

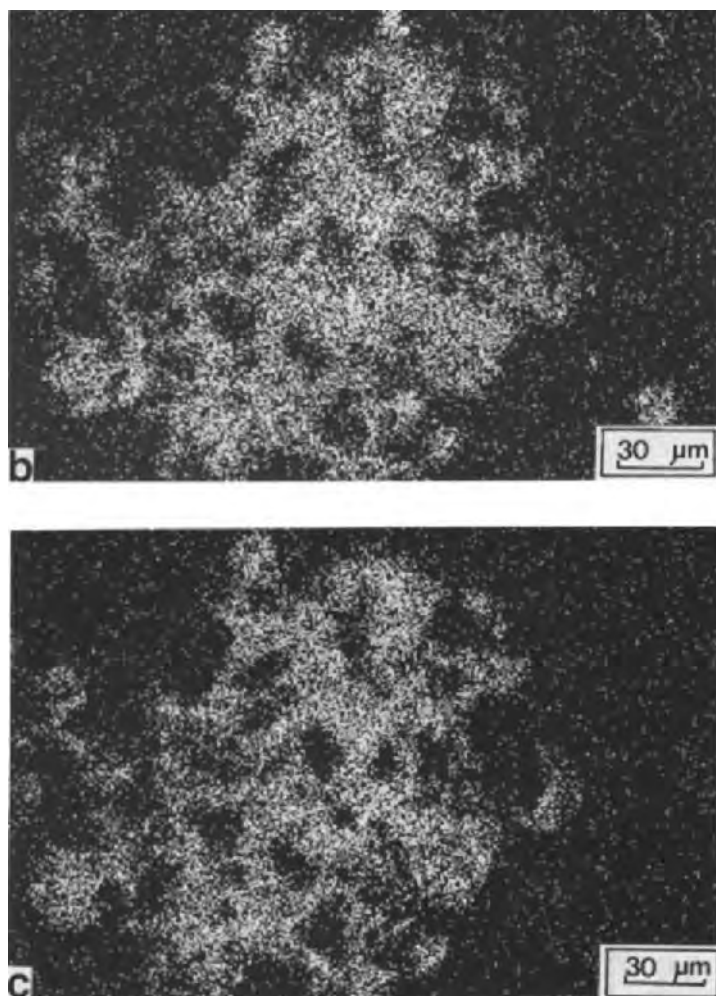


Fig. 5. A gypsum accumulation: a. scanning electron image; b. X-ray image of Ca; c. X-ray image of S.

The cubical, hexahedral, halite crystals occurred only rarely in soils. The stem-like halite habit observed in the Dandi series of soils differs from the fibres mentioned in Eswaran et al. (1980): the individual threads are smaller, the cross-section is more circular and the way individual threads coalesce differs. This type of halite has not previously been described in the literature. The fibres mentioned by Eswaran et al. occurred in salt crusts at the surface; the curly stem-like halite was found in dried soil material from below the surface. No other types of salts were detected in the salt efflorescence. After impregnation the halite was no longer detectable in the large thin sections covered by thin glass slides. But in the small thin sections,

halitic material could be traced with light-microscopy and submicroscopy. This material was not only composed of Na and Cl but also included clay and some other soil material. The latter two materials were visible in the large thin sections as loose accumulations of usually fine-grained soil material, which are impurities of the halite. During impregnation some of the halite dissolved. The Cl measured in the hardened plastic was probably derived from dissolved halite. It is not clear why remnants of this salt were observed under the light microscope in uncovered thin sections with polished surfaces. The low hardness of saline material may reduce its resistance to polishing, resulting in slightly etched surfaces that mark its occurrence.

In addition to halite, a second type of salt, not detected in the dried unimpregnated samples, occurred in the large and small thin sections. This salt, which generally occurred in circular shapes, is a form of gypsum and occurred locally embedded in the halite crusts along the walls of voids and in fine-grained soil material near voids. Gypsum commonly occurs as lenticular crystals in soils. In Hanna and Stoops (1976) a kind of feather-like gypsum is described; in Stoops et al. (1978) rosette-like aggregates of gypsum prisms are described. These two habits of gypsum are most related to the gypsum identified in the Dandi series, but are different. The Dandi habit of gypsum has not been described in the literature. The diffuse extinction patterns may result from crystal splitting which is visible in the cracked surfaces, and results from small impurities in the crystals (Grigor'ev, 1961).

CONCLUSIONS

As well as carbonates, which could be unequivocally determined under a light microscope, halite and gypsum also occurred to a depth of 90 cm in the soils of the Dandi series under study. The halite and gypsum could only be determined with submicroscopy. The habits of the halite observed are not necessarily pedogenetic. It is unknown whether precipitation habits of salts, especially of halite, formed during drying in the laboratory are the same as those formed under natural conditions. Gypsum is a much less soluble salt and the habit and occurrence observed are likely to be present in nature too. Before the habits and occurrence of fairly soluble salts (which are very important in salt-affected soils used for agriculture) can be studied further, techniques of impregnation and sample preparation must be improved. New methods will have to be developed. Polishing the surface of thin sections, instead of covering them with a thin glass slide, seems to enhance the visibility of halite in light microscopy.

REFERENCES

- Eswaran, H., Stoops, G. and Abtahi, A., 1980. SEM morphologies of halite (NaCl) in soils. *J. Microsc.*, 120 (3): 343-352.

- Grigor'ev, D.P., 1961. Ontogony of Minerals. IPST, Jerusalem.
- Hanna, F.S. and Stoops, G., 1976. Contribution to the micromorphology of some saline soils of the North Nile Delta in Egypt. *Pedologie*, 26 (1): 55—73.
- Jongerius, A. and Heintzberger, G., 1975. Methods in soil micromorphology. A technique for the preparation of large thin sections. *Soil Surv. Pap.*, 10. Neth. Soil Surv. Inst., Wageningen.
- Murthy, R.S., Hirekerur, L.R. and Bhattacharjee, J.C., 1980. The taxonomy of salt-affected soils of the Indian subcontinent. *International Symposium on Salt-Affected Soils*, Karnal, 1980, pp. 67—76.
- Murthy, R.S., Hirekerur, L.R., Deshpande, S.B. and Venteka Rao, B.V. (Editors), 1982. *Benchmark Soils of India. Morphology, Characteristics and Classification for Resource Management*. Natl. Bur. Soil Surv. and Land Use Planning (ICAR), Nagpur, India.
- Soil Survey Staff SCS, U.S.D.A., 1975. *Soil Taxonomy. A Basic System of Soil Classification for Making and Interpreting Soil Surveys*. U.S. Gov. Print. Off., Washington, D.C.
- Stoops, G., Eswaran, H. and Abtahi, A., 1978. Scanning electron microscopy of authigenic sulphate minerals in soils. In: M. Delgado (Editor), *Proc. 5th Int. Working Meeting on Soil Micromorphology*, Granada, pp. 1093—1113.

AN OPTICAL, SCANNING ELECTRON MICROSCOPIC AND MICROANALYTICAL STUDY OF CEMENTATION IN SOME PODZOLS

W.J. McHARDY and L. ROBERTSON

The Macaulay Institute for Soil Research, Craigiebuckler, Aberdeen (Great Britain)

(Accepted for publication February 17, 1983)

ABSTRACT

McHardy, W.J. and Robertson, L., 1983. An optical, scanning electron microscopic and microanalytical study of cementation in some podzols. *Geoderma*, 30: 161–170.

The nature of a strongly cemented horizon occurring in a soil profile at Lochend Farm on the shores of Loch Leven has been investigated by optical and scanning electron microscopy and electron probe microanalysis, and comparisons have been made with more weakly cemented B_h horizons of two other podzol profiles developed on sands and gravels. Under the optical microscope the monomorphic organic coatings present on skeleton grains in the cemented horizons of all three profiles appear similar. Of the elements detectable by microanalysis, Al is dominant in all the coatings whereas a low Fe and relatively high Ca content is characteristic only of the Lochend material.

INTRODUCTION

Scanning electron microscopy (SEM) and electron probe microanalysis have been used in several studies on soil morphology. Lynn and Grossman (1970) and McHardy and Birnie (1975), among others, have examined specific parts of the soil fabric. Gillespie and Protz (1972) used micromorphology and electron probe microanalysis in the study of two residual soils and, more recently, Qureshi et al. (1978) have studied the distribution of phosphorus within the soil fabric using electron probe microanalysis. In several papers, (e.g., Eswaran, 1971; Eswaran and Raghu Mohan, 1973) SEM observations have been directly correlated with observations made by optical microscopy. Indeed in SEM studies of soils, it is important to make such correlations and comparisons, since scanning electron micrographs of soils tend to have limited significance on their own.

The main problem with SEM studies of undisturbed soil materials is that individual clay-size grains and their inter-relationships can only be resolved at very high magnifications, at which only a few square microns can be examined and photographed at any one time: in order to get an overall picture of the specimen many fields of view have to be examined and these may differ widely in appearance. Also the large depth of field, characteristic of the SEM,

is not always an advantage since it can further complicate interpretation. Stereo-pairs can greatly assist with interpretation and are very desirable but, unless the relevant sophisticated SEM equipment is available, they can only be studied in retrospect. It would be useful to regard SEM of soils as an extension of conventional optical micromorphology but, although there is good overlap in the magnification ranges, the widely differing preparation techniques required, present problems.

Optical microscopy of soil materials has reached an advanced stage. A wealth of micromorphological data derived from examination of soil thin sections using the polarising microscope has been accumulated and much of it can be interpreted with varying degree of certainty in terms of soil forming processes. In some of the more detailed soil classification systems micromorphological criteria are essential in defining diagnostic horizons. The question arises as to how the soil thin section, so meticulously prepared and examined, can be utilized for SEM studies. Since the thin section consists of a flat polished surface, three-dimensional morphological detail is not readily obtained unless a combination of BE and SE techniques described by Bisdom et al. (1983) or the low temperature ashing technique described by Price and Jenkins (1980) is used; where an X-ray analysis accessory, either energy-dispersive spectroscopy (EDS) or wavelength dispersive spectroscopy (WDS) is available, however, it is possible to obtain analytical data on optically observed features.

The potential of this approach has been explored by an investigation of the nature of the cementing material present in B_h horizons of three Scottish podzols.

MATERIALS AND METHODS

The three soil profiles used in this study are from Lochend Farm, Fife (NGR NO 183/005), Culbin Forest, Morayshire (NGR NJ 026/638) and Windyhills, Aberdeenshire (NGR NJ 799/399). According to the U.S. Department of Agriculture Soil Survey Staff (1975) all three profiles are Spodosols and can be assigned to either the Humod or Aquod sub-order.

The Lochend Farm site differs from the other two in that it is located within 1.5 km of the present shore-line of Loch Leven, a stretch of water that has been artificially drained within historical times with subsequent lowering of the water level. The profile is developed on water-laid sands and gravels derived mainly from Upper Old Red Sandstone sediments and lavas. Five horizons can be differentiated in the profile. The upper horizon, A_p, is a very dark brown 10YR 2/2 fine sandy loam with coarse to medium subangular blocky structure, which changes sharply at 21 cm into AE, a dark reddish brown (5YR 3/2 and 2.5/2) weakly cemented loamy sand. At 26 cm there is a diffuse and irregular boundary with the B_h horizon, a black (5YR 2.5/1) gritty sandy material, which is strongly cemented and almost impossible to dig with a spade, and at 42 cm a very sharp change occurs into C₁, a greyish

brown to dark greyish brown (10YR 4/2-3/2) silty sand with dark reddish brown streaks (5YR 3/2) containing old root material. There is a further sharp change at 60–70 cm into C₂, a dark reddish brown (5YR 3/3) gritty sand with no apparent structure.

The profile from Culbin Forest has been described in detail elsewhere (Soil Survey of Scotland, 1962). This profile is a buried humus podzol developed in blown sand over raised beach gravels. Humus-iron cementation is a feature of the B_h horizon.

The profile from Windyhill is a podzol developed on Pliocene gravels. Within the loose lower part of this profile there occur rather erratically and at varying depths sandy layers cemented by translocated humic material.

Undisturbed soil samples were collected from the cemented horizons of the three profiles using boxes 75 × 55 × 45 mm in size. The samples were freeze-dried, vacuum-impregnated with polyester resin (BK 17449) and thin sections were prepared for examination by a polarising microscope. Photomicrographic records were made of relevant areas in the thin sections after which they were cut out, mounted on SEM stubs and coated with 20 nm of carbon. At an early stage it was noted that during SEM examination the glass disc on which the thin section was mounted made a significant contribution to the Si X-ray signal. This was overcome by using Canada balsam rather than polyester resin as a mounting medium, since after optical examination the Canada balsam could be dissolved with Inhibisol (a commercial cleaning fluid based on trichloroethylene), the thin section removed from the glass support slide and cleaned ultrasonically prior to SEM study.

The SEM and microanalysis work was carried out using a Cambridge Scientific Instruments S4 stereoscan equipped with a wavelength dispersive X-ray spectrometer and a Link Systems energy-dispersive X-ray analyzer.

RESULTS AND DISCUSSION

Lochend profile

The most characteristic features observed in thin sections prepared from the strongly cemented horizon were well developed isotropic monomorphic grain coatings (De Coninck et al., 1973) as in Fig. 1, a and b and pelletal polymorphic aggregates as in Fig. 1c. Fig. 1d is a scanning electron micrograph of the same field of view as shown in Fig. 1c. The numbers 1–4 on Fig. 1d indicate small areas which have been analyzed qualitatively using the energy dispersive X-ray analysis system, and the spectra for 1, 2 and 4 are given in Fig. 1e. Area 1 is in the embedding resin and the spectrum from this area shows only a small Si-peak. Most of the primary mineral grains are quartz: an X-ray spectrum (not shown in Fig. 1e) from area 3 has only a large Si-peak. The particle labelled 2 is not quartz, however, as it contains, in addition to Si, Al and K a little Na, Mg, Ti and Fe. Both its chemical composition and appearance under the optical microscope are consistent with it being a piece

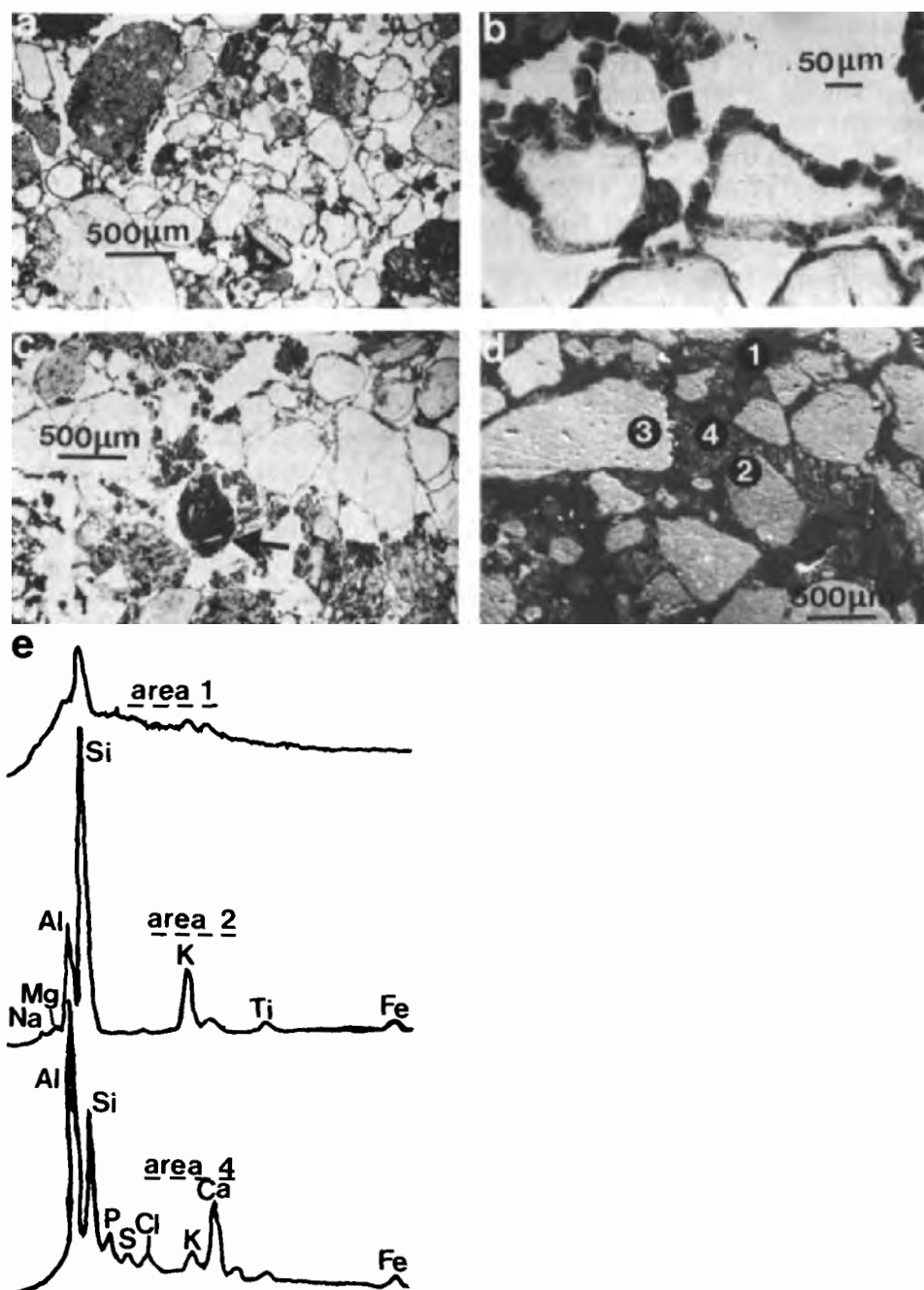


Fig. 1. Lochend profile. (a) Plane-polarized light micrograph showing strongly developed isotropic monomorphic grain coatings. (b) Area in centre of (a) at higher magnification. (c) Plane-polarized light micrograph showing pellety aggregates of cementing material. (d) Scanning electron micrograph of roughly the same field of view as (c). In the SEM the specimen is viewed at an angle of 45° which causes foreshortening of the image. Thus it is not possible to match the SEM image exactly with the light micrograph. (e) X-ray spectra from positions 1, 2 and 4 marked on Fig. 1d.

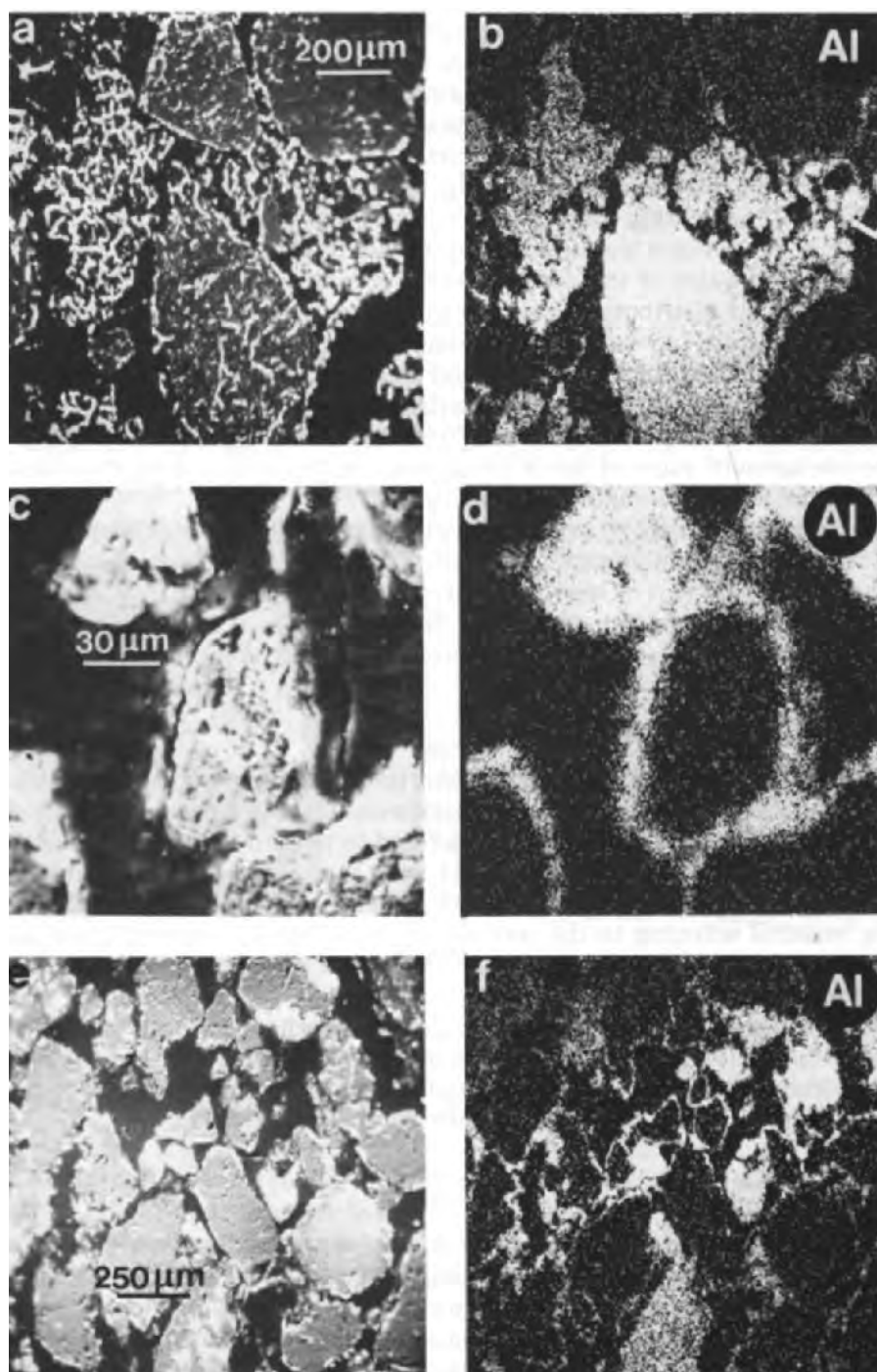


Fig. 2. Lochend profile. Scanning electron micrographs (a, c and e) and corresponding Al distribution images (b, d and f) of (a) the area of pelleted material depicted in Fig. 1c, (c) a single coated grain and (e) a region of continuous coatings at low magnification.

of lava. It is this particle that appears dark grey (arrowed) in the optical micrograph (Fig. 1c). The spectrum from the brown pellety material, area 4, shows that Al is the predominant constituent with Si, Ca and a little Fe. There are also small distinct peaks representing P, S, Cl and K. A scanning electron micrograph of, roughly, the central area of Fig. 1d (Fig. 2a) and the corresponding Al distribution image (Fig. 2b) show the pellety aggregates to be rich in Al. The coating material surrounding the sand grain in the centre of Fig. 2c is very clearly defined by the Al distribution image (Fig. 2d) and the continuous nature of the coatings at lower magnification (Fig. 2e) is obvious from the Al distribution image (Fig. 2f) of the same field. The pellety aggregates appear to have almost the same Al content as the coatings. With the WDS system used for the distribution images of Fig. 2, a high beam current is necessary to get a measurable quantity of X-rays and this considerably degrades the secondary electron image (Boekstein et al., 1981). The high peak-to-background ratio of the WDS system, on the other hand, does give much superior elemental distribution images.

From optical microscopy these cementing materials are described as isotropic monomorphic/polymorphic organic matter. X-ray microanalysis shows that the Al content is very high. A significantly high Ca but relatively low Si and Fe content is characteristic. The P, S and Cl content is presumably associated with the organic part of the aluminium organic complex.

Culbin profile

Optical examination of soil thin sections prepared from the cemented material shows grain coatings similar in appearance to those from the cemented Lochend material. Because the coatings tended to be thin and the grains were mostly quartz, it was difficult to detect with the microprobe anything except Si even at the edge of the grains. However, it was possible to study the coating material adhering to the walls of holes vacated by sand grains during the ultrasonic cleaning of the section (Fig. 3, a and c). In Fig. 3a the approximate area of analysis giving the X-ray spectrum in Fig. 3b is ringed. This spectrum shows a very high Al:Si ratio, an intermediate Fe peak and small peaks for P, S, Cl, K and Ca. In Fig. 3c a piece of coating material (ringed) is more clearly visible on the inward sloping wall of another hole. The X-ray spectrum (Fig. 3d) from this area is similar to that in Fig. 3b.

Windyhills profile

Optical microscopy of thin sections of the cemented horizon from this profile again showed similar grain coatings (Fig. 4a). The scanning electron micrograph (Fig. 4b) shows a hole (arrowed) in the section previously occupied by a sand grain. A scanning electron micrograph of part of the pore wall at higher magnification (Fig. 4c) and the accompanying Al, Si and Fe distribution images (Fig. 4, d-f) show that the coating material clearly contains

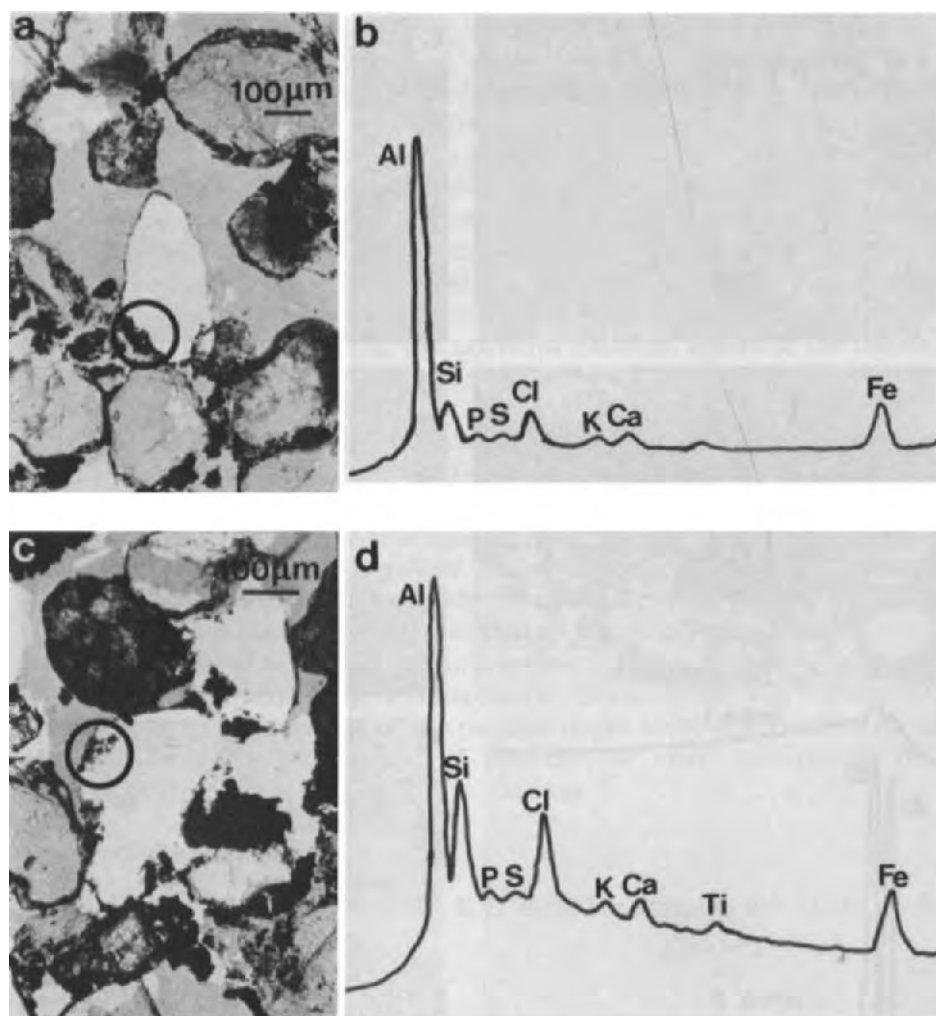


Fig. 3. Culbin profile. (a) Plane-polarized light micrograph of a thin section from the cemented B_h horizon. (b) X-ray spectrum from area ringed in Fig. 3a. (c) Plane-polarized light micrograph showing pore vacated by a sand-grain. (d) X-ray spectrum from wall of pore with coating material, ringed in Fig. 3c.

Si and some Fe as well as Al. Allowing for the fact that the spectrum from area 1 (Fig. 4c) is that for the embedding resin and is included merely for comparison, X-ray spectra (Fig. 4g) show a variation of composition within the coating. For example at area 2 on Fig. 4c the Al peak is slightly smaller than the Si peak whereas at area 3 it is twice the size and the general pattern of the spectrum is more akin to that of the Lochend pellet material. This implies that in the coating there is a mixture of clay mineral and an aluminium organic complex.

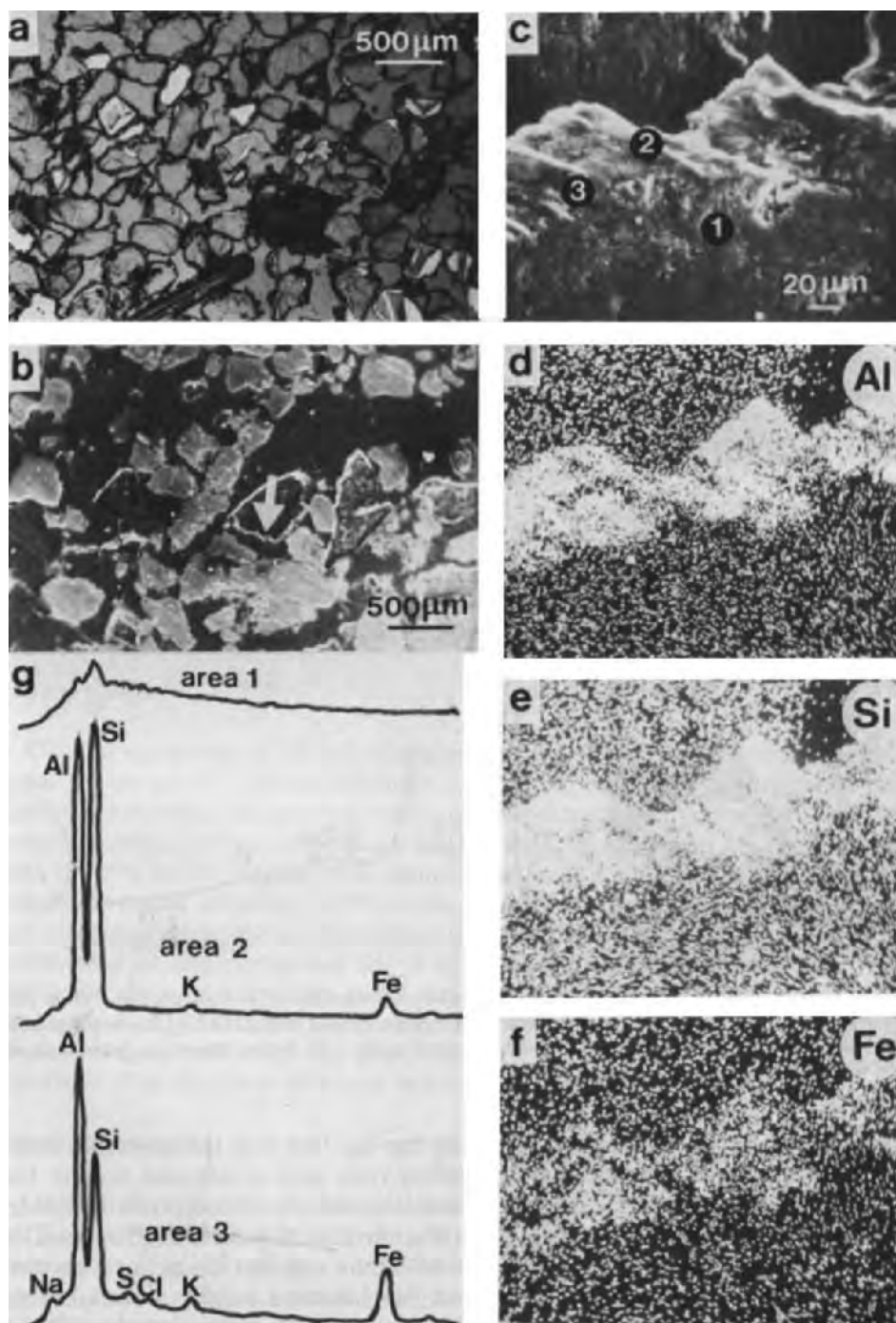


Fig. 4. Windyhills profile. (a) Plane-polarized light micrograph of a thin section of the cemented B_h horizon. (b) Scanning electron micrograph showing a pore vacated by a sand grain. (c) Magnified scanning electron micrograph of the wall of the pore in centre of Fig. 4b with corresponding Al, Si and Fe X-ray distribution images (d, e and f). (g) X-ray spectra from areas 1, 2 and 3 marked on Fig. 4c.

DISCUSSION

The strong cementation in the Lochend profile has been compared with weaker cementation in the B_h horizon of two other podzols. Optical microscopy shows monomorphic organic coatings which appear similar for all three profiles although they are best developed and thickest in the Lochend material. X-ray microanalysis of the coatings shows some similarities, but also, perhaps more significantly, some differences. Of the elements detectable by X-ray analysis Al is dominant in all the coatings but a low Fe and relatively high Ca content is characteristic only of the Lochend material. P, S and Cl are consistently detectable in the Lochend coatings, less so in the others and these elements may have some correlation with the nature and amount of the organic part of the complex.

This approach to the study of coatings is not unique. Bisdorn and Jongerius (1978) have used a combined SEM-microanalysis technique in a study of the nature of cutans in which they concluded that where organic matter is present it may conceal a heterogeneous distribution of other compounds. Robin and De Coninck (1978) have described similar coatings in the cemented B horizons of podzols developed on sandy parent material in the Paris Basin, and Van Ranst et al. (1980) have demonstrated the association of organic matter with aluminium in cemented spodic B horizons.

More work on this subject is necessary. In particular, the organic matter occurring in other horizons of the profiles ought to be analysed for comparison and X-ray analysis should, if possible, be made quantitative for the amount of aluminium present in the coatings.

ACKNOWLEDGEMENT

The authors wish to thank Mr. E.L. Birse for bringing the site at Lochend Farm to their attention.

REFERENCES

- Bisdorn, E.B.A. and Jongerius, A., 1978. SEM-EXDRA and/or IMMA analysis of cutans, an indurated horizon and clayified roots in thin sections of some Dutch soils. In: M. Delgado (Editor), *Soil Micromorphology. Proceedings of the 5th International Working Meeting on Soil Micromorphology, Granada, 1977*. University of Granada, Spain, pp. 741–756.
- Bisdorn, E.B.A.; Thiel, F., Volbert, B. and Jackman, J., 1983. Variations in backscattered electron (BSE) images with a Scanning Electron Microscope (SEM) as applied to mineral grains and excrements in a podzol, to precipitates on a water-tube filter and to bauxite. *Geoderma*, 30: 93–116.
- Boekestein, A., Henstra, S. and Bisdorn, E.B.A., 1981. Submicroscopic techniques for in situ microchemical analysis of soils, 1. Non-destructive techniques. In: E.B.A. Bisdorn (Editor), *Submicroscopy of Soils and Weathered Rocks. 1st Workshop of the International Working-Group on Submicroscopy of Undisturbed Soil Materials (IWGSUSM), 1980, Pudoc, Wageningen*, pp. 29–44.

- De Coninck, F., Righi, D., Maucorps, J. and Robin, A.M., 1973. Origin and micromorphological nomenclature of organic matter in sandy spodosols. In: G.K. Rutherford (Editor), *Soil Microscopy. Proceedings of the 4th International Working Meeting on Soil Micromorphology*, Kingston, 1973. The Limestone Press, Kingston, Ont., pp. 263–280.
- Eswaran, H., 1971. Electron scanning studies of the fabric of fracture surfaces. *Soil. Sci. Soc. Am. J.*, 35: 787–790.
- Eswaran, H. and Raghu Mohan, N.G., 1973. The microfabric of petroplinthite. *Soil Sci. Soc. Am. J.*, 37: 79–82.
- Gillespie, J.E. and Protz, R., 1972. The micromorphology and electron microprobe analysis of two residual soils, one developed on granite, the other on marble, in Peterborough county, Ontario. *Can. J. Soil Sci.*, 52: 79–89.
- Lynn, W.C. and Grossman, R.B., 1970. Observations of certain soil fabrics with the scanning electron microscope. *Soil. Sci. Soc. Am. J.*, 34: 645–648.
- McHardy, W.J. and Birnie, A.C., 1975. Scanning electron microscope studies of a surface water gley. *J. Soil. Sci.*, 26: 426–431.
- Price, F. and Jenkins, D.A., 1980. Removal of resin from standard soil thin-sections by low temperature ashing as a means of following transmitted optical by scanning electron microscopy. *Clay Minerals*, 15: 309–315.
- Qureshi, R.A., Jenkins, D.A. and Davies, R.I., 1978. Electron probe microanalytical studies of phosphorus distribution within soil fabric. *Soil Sci. Soc. Am. J.*, 42: 698–703.
- Robin, A.M. and De Coninck, F., 1978. Micromorphological aspects of some podzols in the Paris Basin. In: M. Delgado (Editor), *Soil Micromorphology. Proceedings of the 5th International Working Meeting on Soil Micromorphology*, Granada, 1977. University of Granada, Spain, pp. 1019–1050.
- Soil Survey of Scotland, 1962. *Handbook of a Soil Survey Field Meeting*, Inverness. Macaulay Inst. Soil Res., Aberdeen.
- U.S. Department of Agriculture Soil Survey Staff, 1975. *Soil Taxonomy — a Basic System of Soil Classification for Making and Interpreting Soil Surveys*. Gov. Print. Off., Washington, D.C.
- Van Ranst, E., Righi, D., De Coninck, F., Robin, A.M. and Jamagne, M., 1980. Morphology, composition and genesis of argillans and organans in soils. *J. Microsc.*, 120: 353–361.

CALCIUM-DOMINATED ORGANANS IN HUMIC PODZOLS FROM THE HUDSON AND JAMES BAY LOWLANDS OF ONTARIO (CANADA)

RICHARD PROTZ

Department of Land Resource Science, University of Guelph, Guelph, Ont. N1G 2W1 (Canada)

(Accepted for publication February 17, 1983)

ABSTRACT

Protz, R., 1983. Calcium-dominated organans in Humic Podzols from the Hudson and James Bay Lowlands of Ontario (Canada). *Geoderma*, 30: 171–177.

The SEM-EDXRA analysis of cutans within five Humic Podzolic soils derived from calcareous sands and gravels revealed the presence of Ca-dominated organans. It is postulated that organic matter saturated by H and Al is translocated through the Ae-horizon and precipitated within the Bh horizon in the presence of calcareous material. Weathering of the calcareous material within the Bh horizon results in the partial replacement of the H and Al in the organans by Ca.

INTRODUCTION

Developmental sequences of Podzolic soils formed under black spruce (*Picea mariana* (Mill.) B.S.P.) and lichen (dominantly *Cladina rangiferina* (L.) Harm) vegetation within the Hudson and James Bay Lowlands of Ontario have been reported by Protz (1982). It was shown that a Humic Podzol develops on coarse textured calcareous beach ridges before the evolution of Humo-Ferric Podzol (terminology of the Canada Soil Survey Committee, 1978). The Bh horizons of the Humic Podzols had large amounts of organic matter (from 6 to 25 percent) but low amounts of Na-pyrophosphate-extractable Fe and Al. Initial work indicated the organic matter in the Bh horizons was Ca-saturated. In previous studies of chemical compositions of cutans of Canadian soils none were found to be dominated by Ca (Brewer et al., 1973; McKeague and Protz, 1980; McKeague and Wang, 1980; McKeague, 1981).

The purpose of this paper is to report the SEM-EDXRA results which indicate the presence of Ca-dominated organans in Humic Podzols and to suggest the genetic process by which they form.

MATERIALS AND METHODS

The field soil sampling procedures used are described in Protz (1982). The particle-size distribution, organic matter, pH, CaCO_3 equivalent, pyrophosphate-extractable Fe and Al analyses were made following procedures outlined by McKeague (1978). Exchangeable cations (Al, Ca, Mg, H, K and Na), were determined using the Ag-Thiourea extraction procedure of Pleysier and Juo (1980). Impregnation of undisturbed samples followed procedures outlined by McCarrick and Protz (1978). The SEM-EDXRA analyses were made using a JEOL JSM-35C Scanning Electron Microscope with a Tracor X-ray detector and a TN-2000 Data System. Thin sections were coated with Au-Pd for analyses using 15KV.

RESULTS AND DISCUSSION

Thin sections from five Humic Podzols were studied. Organans coated all sand grains within the Bh horizon (Fig. 1). These grains consisted of quartz, feldspar and calcite as well as sandstone and limestone fragments. The organans were reddish-orange in color and are similar to those in Bhc horizons of Ortstein soils reported by McKeague and Wang (1980). A backscattered electron image of the organans (Fig. 2a) shows their fractured nature due to drying before impregnation. The X-ray image of Si (Fig. 2b) indicates the

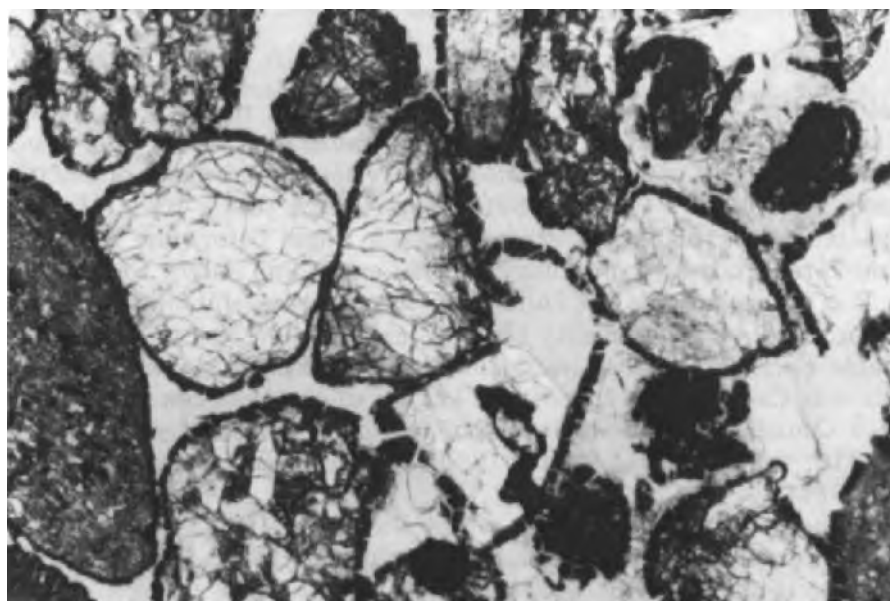


Fig. 1. Ca-dominated organans coating all sand grains within a Bh horizon of a Humic Podzol. Plane polarized light (55 \times).

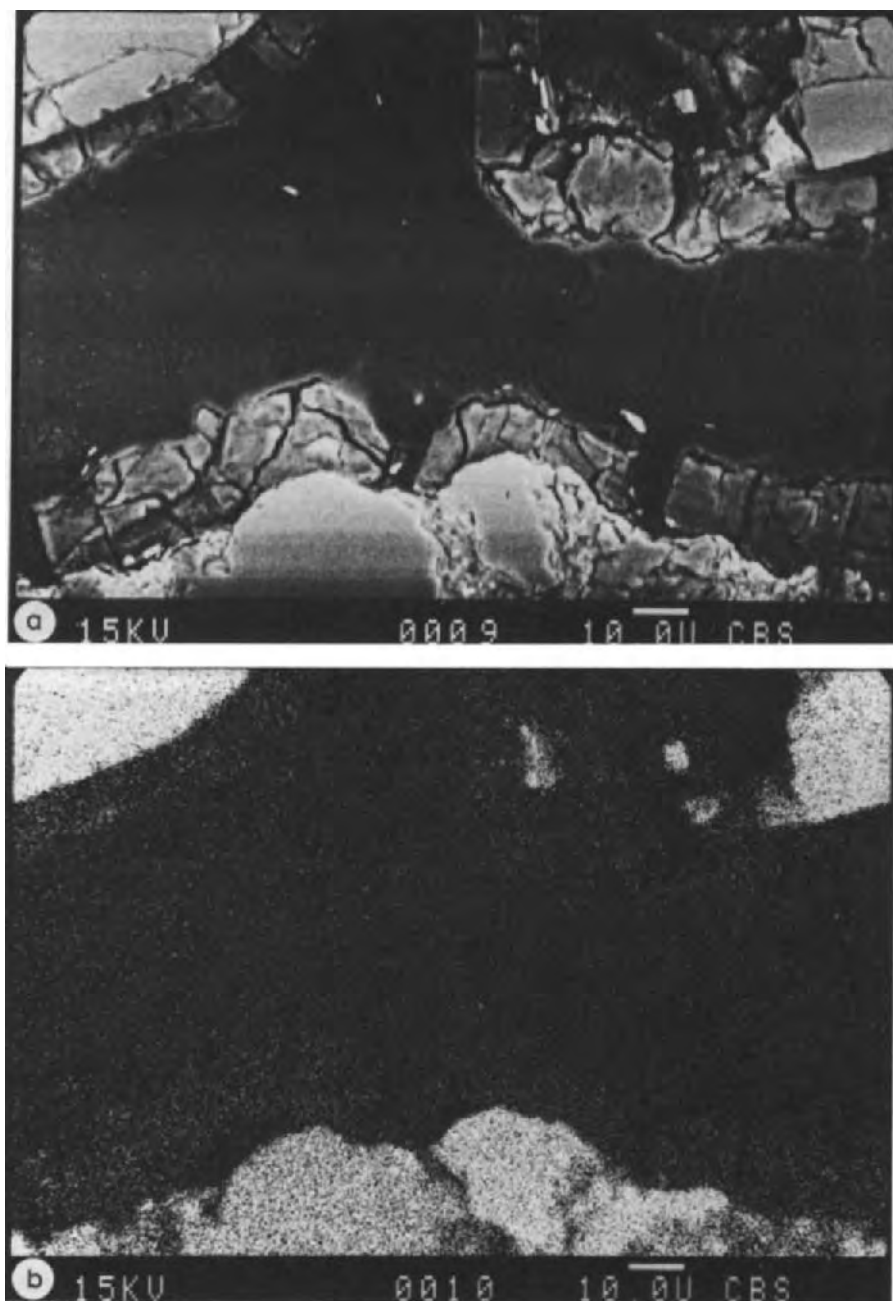


Fig. 2. a. Backscattered electron scanning image of a typical Ca-dominated organan. b. X-ray image of Si. c. X-ray image of Al. d. X-ray image of Ca. e. X-ray image of Fe. f. Representative X-ray spectrum of a Ca-dominated organan.

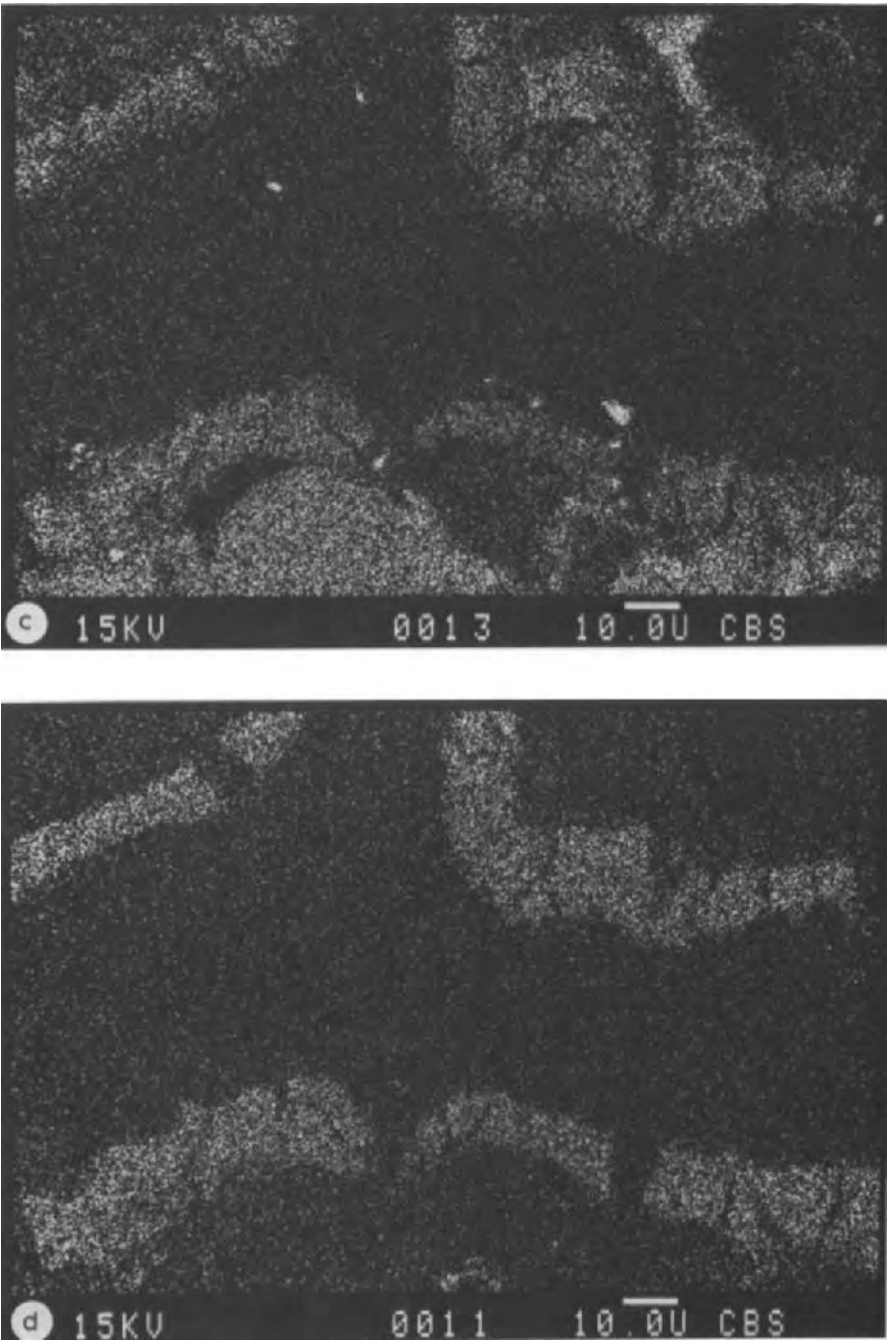
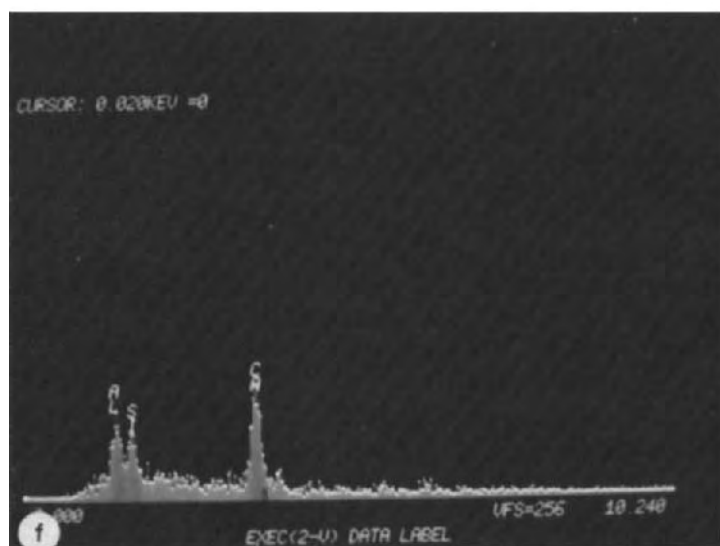


Fig. 2 (continued).



presence of some silicon within the organans. Al in Fig. 2c is present in feldspar grains and within organans. The X-ray image of Ca (Fig. 2d) isolates the Ca-dominated organans from the covered mineral grains. The presence of a minimal amount of Fe in the organans is demonstrated in Fig. 2e. A typical EDXRA spectrum of a Ca-dominated organan is shown in Fig. 2f.

To establish the variation in elemental composition of organans, twenty spots were examined by SEM-EDXRA. The mean, standard deviation and variance of the relative amounts of Si, Ca, Al and Fe within these twenty spots are given in Table I. The average Si: Ca: Al: Fe ratios are 4: 13: 6: 1 within these organans.

TABLE I

Mean, standard deviation and variance of relative amounts of Si, Ca, Al and Fe in twenty spots of calcium-dominated organans in the Bh horizon of Humic Podzols

Statistic	Si	Ca	Al	Fe
Mean	0.123	0.566	0.268	0.042
Std. dev.	0.092	0.116	0.096	0.020
Variance	0.008	0.013	0.009	0.000

As the black spruce (*Picea mariana* (Mill.) B.S.P.) and lichens (dominantly *Cladina rangiferina* (L.) Harm) mature, the organic surface is thickened on the calcareous sand and gravels. This results in the dissolution of calcareous mineral material resulting in an increase in the void space, the leaching of Ca and Mg from the solum and the formation of thin Ae horizons (Protz, 1982). Through this acid horizon organic materials can move mechanically because of increased void size and faunal activity. Bal (1970) has stated that faunal excrements as large as 30 μm could be transported in a coarse textured Podzol. Ugolini et al. (1977) have shown that organic particles containing traces of aluminum, iron, silicon and sulfur migrated from the upper A and B to lower horizons. Dispersed organic matter can also move in suspension.

De Coninck (1980) has suggested two different mechanisms for the formation of two types of spodic horizons. In loose spodic horizons an excess of polyvalent cations are present which immobilize potentially mobile organic substances formed during the breakdown of plant remains. In cemented spodic horizons the polyvalent cations have been previously removed and mobile organic substances migrate downward to depths of higher ionic concentrations, to drier soil material. In the Ae horizons of four of the five soils studied, the sum of exchangeable Al and H was greater than the sum of exchangeable Ca and Mg. Within the Bh horizons of all five soils, exchangeable Ca and Mg were much higher than Al and H.

The acidic organic material is precipitated on all sand grains and as such holds water around grains. Under this moist condition the calcareous material in the Bh horizon dissolves releasing Ca to saturate the organans. The original H- and Al-saturated organic matter thus becomes Ca-saturated.

The age of the organic matter within the Bh horizons of four Humic Podzols has been determined by ^{14}C analyses. The dates range from 940 ± 80 years B.P. to 4470 ± 120 years B.P. Therefore it can be said that these Ca-

dominated organans formed within 1000 years of beach ridge development and may have persisted for 3500 years in the Hudson and James Bay Lowlands of Ontario.

CONCLUSIONS

Calcium-dominated organans exist in Bh horizons of Humic Podzols according to EDXRA measurements in soils derived from coarse textured calcareous deposits under black spruce and lichen vegetation. The Bh horizons have been formed within 1000 years after beach ridge development and have persisted for the last 3500 years.

ACKNOWLEDGEMENTS

I gratefully acknowledge: NSERC Grant No. A-3547, O.M.A.F. Program 39 and D.S.S. contract No. 05479-00097 for financial support; the Laboratory of the Ontario Institute of Pedology for many of the analyses; Mr. Cameron Ackerly for assistance with the SEM-EDXRA portion of this study; Dr. Leo Bal and Martin Shipitalo for commenting on an earlier draft of this manuscript, and Sheree Henry for typing this manuscript.

REFERENCES

- Bal, L., 1970. Morphological investigation in two moder — humus profiles and the role of the soil fauna in their genesis. *Geoderma*, 4: 5—36.
- Brewer, R., Protz, R. and McKeague, J.A., 1973. Microscopy and electron microprobe analysis of some iron-manganese pans from Newfoundland. *Can. J. Soil Sci.*, 53: 349—361.
- Canada Soil Survey Committee, 1978. The Canadian System of Soil Classification. Res. Branch, Can. Dep. Agric. Publ., 1646; 164 pp.
- De Coninck, F., 1980. Major mechanisms in formation of spodic horizons. *Geoderma*, 24: 101—128.
- McCarrick, T. and Protz, R., 1978. The effects of soil composition upon three acrylic soil impregnating resins. *Commun. Soil Sci. Plant Analysis*, 9: 955—962.
- McKeague, J.A. (Editor), 1978. Manual on soil sampling and methods of analysis: Can. Soc. Soil Sci., 212 pp.
- McKeague, J.A. and Wang, C., 1980. Micromorphology and microprobe analysis of ortstein horizons of podzolic soils from New Brunswick and Nova Scotia, Canada. *Can. J. Soil Sci.*, 60: 9—21.
- McKeague, J.A. and Protz, R., 1980. Cement of duric horizons, micromorphology and energy dispersive analysis. *Can. J. Soil Sci.*, 60: 45—52.
- McKeague, J.A., 1981. SEM-EDXRA as an extension of light microscopy in soil characterization and genesis studies. In: E.B.A. Bisdom (Editor), *Submicroscopy of Soils and Weathered Rocks*. Pudoc, Wageningen, pp. 277—282.
- Pleysier, J.L. and Juo, A.S.R., 1980. A single extraction method for measuring exchangeable cations and effective CEC in soils with variable charges. *Soil Sci.*, 129: 205—211.
- Protz, R., 1982. Development of podzolic soils in the Hudson Bay and James Bay Lowland, Ontario. *Naturaliste Can.*, 109: 501—510.
- Ugolini, F.C., Dawson, H. and Zachara, J., 1977. Direct evidence of particle migration in the soil solution of a Podzol. *Science*, 198: 603—605.

This Page Intentionally Left Blank

SEM AND LIGHT MICROSCOPIC OBSERVATIONS OF MINERALS IN BOG-ORES OF THE BELGIAN CAMPINE*

G. STOOPS

Laboratory for Mineralogy, Petrography and Micropedology, Krijgslaan 281, 9000-Gent (Belgium)

(Accepted for publication February 17, 1983)

ABSTRACT

Stoops, G., 1983. SEM and light microscopic observations of minerals in bog-ores of the Belgian Campine. *Geoderma*, 30: 179–186.

Soft bog-ore deposits are frequently present in alluvial soils of the Nete Valley, Province of Antwerp, Belgium. A profile was studied consisting of four layers of which the upper three were analyzed with the light microscope and SEM (scanning electron microscope). The top layer consisted mainly of clay and fragmented diatom shells. Isotropic Fe-oxihydrates and radiating goethite needles were present in the underlying limonitic layer. Siderite and vivianite were found in the third layer, the former often present in the wall of root channels, whereas the latter was frequently found within the channels. Vivianite was also found associated with decaying roots or alone inside root channels. Pyrite framboids were also found in the lower part of the profile.

The presence, close to each other, of different minerals such as goethite, pyrite, siderite and vivianite cannot be explained by macroenvironmental mineral equilibria alone. It requires the existence of different microenvironments which can vary in time and place. The study of such microenvironments, however, requires additional in situ microchemical submicroscopic techniques.

INTRODUCTION

A research project on soft bog-ore deposits of the Belgian Campine is currently in progress. These deposits are frequently observed in alluvial soils of the Nete Valley in the Province of Antwerp, Belgium. A typical profile was exposed in these deposits and results of preliminary investigations are reported here. The profile had a high groundwater level and all horizons were oversaturated. Four layers could be distinguished: a greyish, clayey topsoil of 20 cm thickness with “rust” coated channels; a 20 cm thick limonite rich

*Contribution to the research program: “Weathering and neosynthesis in relation to soil genesis”. Fonds voor Kollektief Fundamenteel Onderzoek — Belgium.

The material presented here was given in part before Division S-5 of the Soil Science Society of America Meetings, December 3, 1981 in Atlanta, Georgia, U.S.A.

greyish-yellow layer with orange-yellow mottles; a vivianite-rich layer of 30 cm, which after oxidation consisted of alternating bluish flecks (vivianite) and white veins and tubes (siderite); and layered alluvial deposits starting at a depth of 70 cm in the profile. The present study gives data on the upper three layers.

METHODS

Large undisturbed soil blocks were impregnated with polyester resin for thin section preparation following drying by acetone replacement (Fitzpatrick, 1980). These thin sections were studied with the light microscope. Undisturbed clods, which were not hardened, were investigated with a binocular microscope, which allowed subsampling for SEM studies. Samples for SEM study were mounted with collodion on aluminium stubs, coated with gold and examined with a Cambridge Stereoscan (Stoops and De Mets, 1970). Mineralogical determinations were confirmed by XRD-analyses, using a Gandolfi camera.

Results

The clayey surface layer of the bog-ore profile was sampled between 10 and 15 cm depth. It is characterised by a porous microstructure in which rust-coated channels, occasionally containing roots, dominate in the thin section. The greyish fine fraction consists mainly of small opaline bodies (phytoliths and diatoms) and clay. SEM showed that much of the fine fraction comprises fragments of diatoms (Fig. 1).

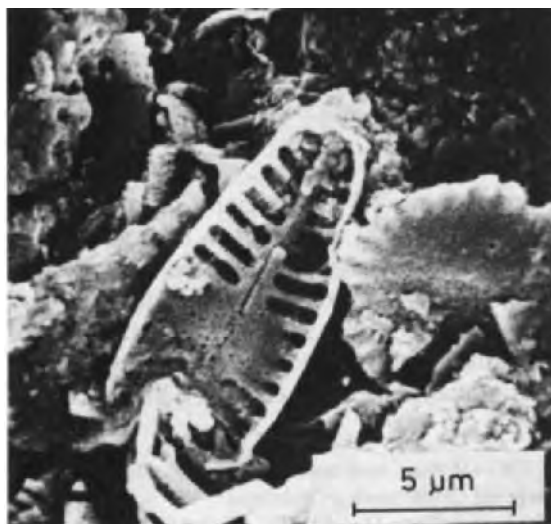


Fig. 1. Fragments of diatom shells and clay in the groundmass of the surface horizon (SEM).

The underlying limonitic layer was sampled between 20 and 30 cm. It has a porous microstructure with many root channels. The sample consists of alternating greyish and brownish zones. The small greyish zones are similar to those of the topsoil, whereas the larger brownish zones exhibit dark reddish-brown, compact, structureless isotropic domains and yellowish to brownish bands of goethite.

The brownish bands consist of weakly birefringent, length-slow goethite fibres (first order grey up to yellow) forming a radiating pattern perpendicular to the walls of voids. Sometimes several layers could be distinguished in thin sections (Fig. 2). Similar goethite coatings were observed by Eswaran (1972) in an Ultisol from Nicaragua.

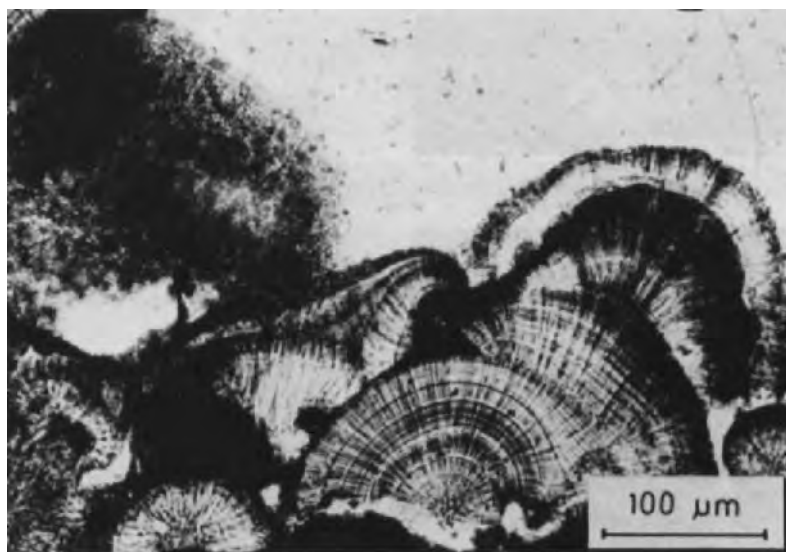


Fig. 2. Fan-like goethite coating on the wall of a pore in the limonitic layer. Polarised light.

SEM of the seemingly structureless isotropic limonitic material did not reveal structure at higher magnifications, although numerous shrinkage cracks could be seen (Fig. 3). The radiating goethite fibres could be distinguished, however, and are about $1.6 \mu\text{m}$ thick (Fig. 4). Orientation of the fibres perpendicular to the wall of pores was also found in the clods (Fig. 5a) as was layering of the goethite (Fig. 5b). Such surfaces of goethite coatings have the aspect of a micropore filter (Fig. 5c). Apparently individual entities of radiating fibrous goethite leave intermittent spaces during growth.

The upper part of the vivianite and siderite containing layer was sampled between 40 cm and 50 cm and the lower part between 60 cm and 70 cm. The very heterogeneous upper part has a porous microstructure sometimes disturbed by shrinkage fissures in zones that are rich in organic material.

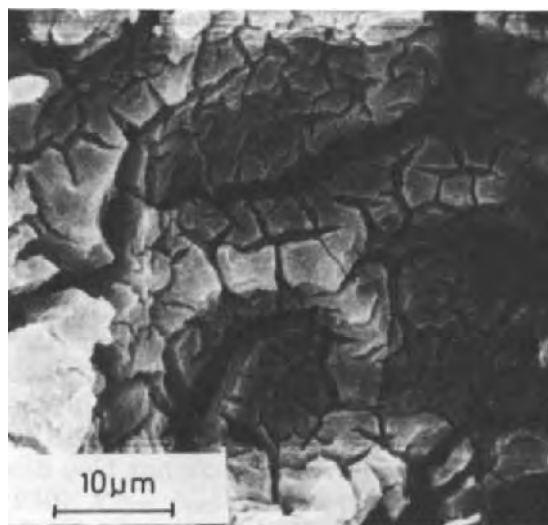


Fig. 3. Amorphous iron oxihydrates in limonitic layer with shrinkage cracks (SEM).

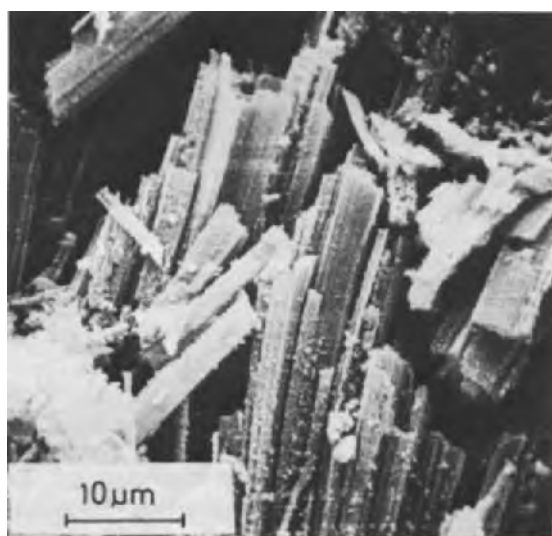


Fig. 4. Goethite needles in fan-like goethitic coating (SEM).

Most frequently, the groundmass in thin sections consists of a yellowish, isotropic clay with very few coarse detrital grains. Siderite spherulites with a diameter of 20–25 μm occur subcutaneously on the root channels. Their radial fabric is evidenced by the orthogonal extinction cross seen under crossed polarizers. Vivianite is present in the channels as a blue, fine, granular mass, sometimes mixed with root-residues (Fig. 6).

SEM studies of the soft bog-ore did not give clear morphological charac-

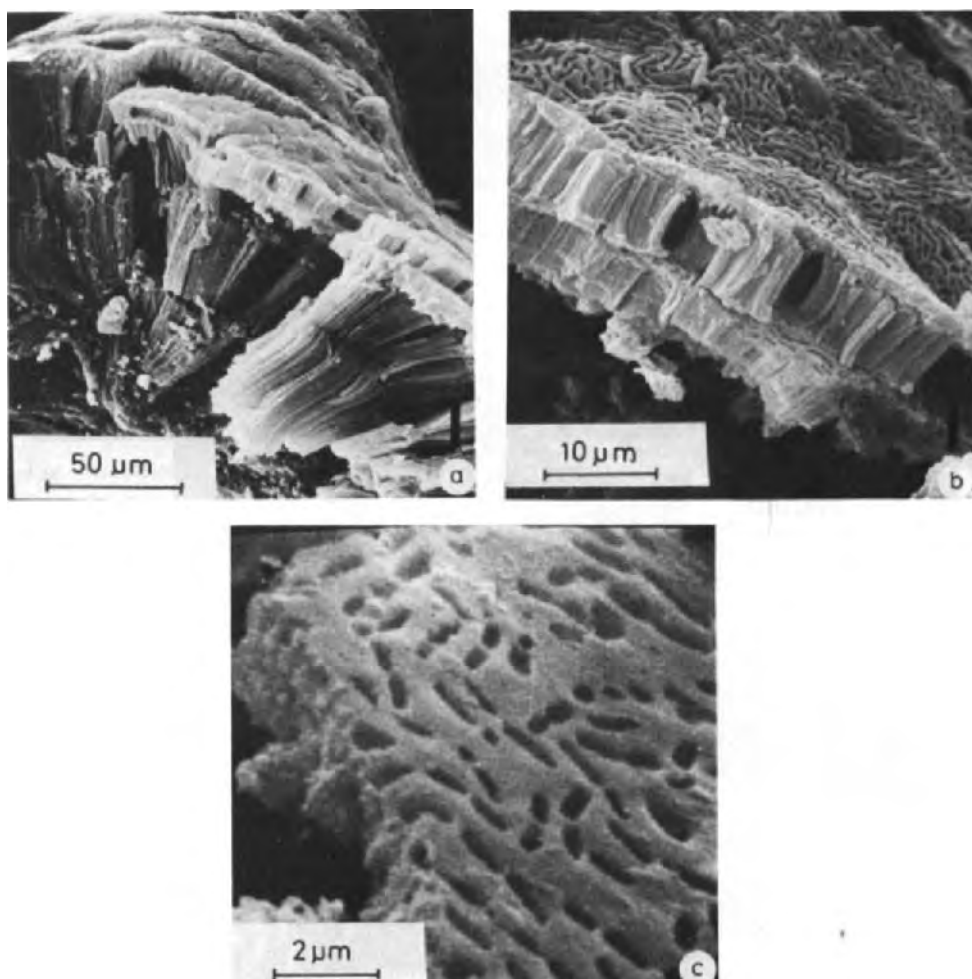


Fig. 5. Goethite coatings on the walls of pores in the limonitic layer: a) coating of radiating goethite needles; b) layered goethite; and c) topography of the surface of a goethite coating (SEM).

teristics of the subcutaneous siderite spherulites. In a sample of hard bog-ore from the same area optically comparable, but cutaneous siderite deposits were observed. These grains seem to be composed of a parallel growth of rhombohedral crystals (Fig. 7). The fine grained vivianite of the soft bog-ore was observed as irregular lathlike crystallites (Fig. 8).

The lower part of the vivianite- and siderite-containing layer is still porous in thin section, with channels and packing pores. A brownish, isotropic organic substance with recognizable cell structures dominated strongly over the coarse detrital grains, (quartz and glauconite). Siderite is less frequent than in the upper part of this layer. Vivianite sometimes occurs as relatively large,

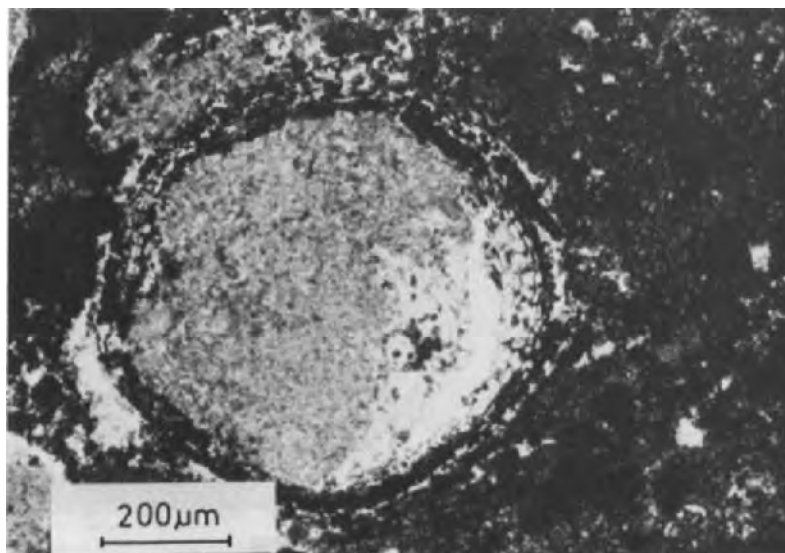


Fig. 6. Root remnant in soft bog-ore, partly filled with fine granular vivianite and partly surrounded by siderite. Polarised light.

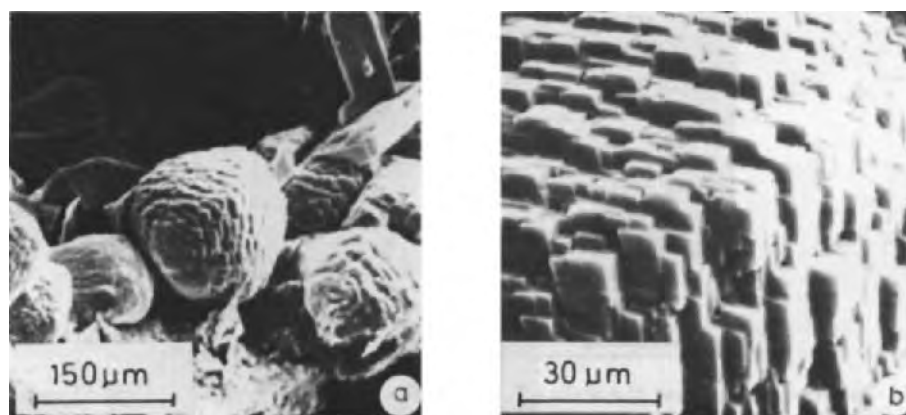


Fig. 7. Siderite: a) siderite spheres covering the wall of a pore in a hard bog-ore; b) detail of the central sphere (SEM).

200 μm long, lathlike crystals on organic matter. It forms frequently radiating aggregates but is found in most cases as infillings of fissures and channels, surrounded by siderite spherulites. In some places pyrite framboids were observed between siderite spherulites.

CONCLUSIONS

A sequence of a number of minerals was observed in a soft bog-ore in the Nete Valley, Province of Antwerp, Belgium. Field studies established four

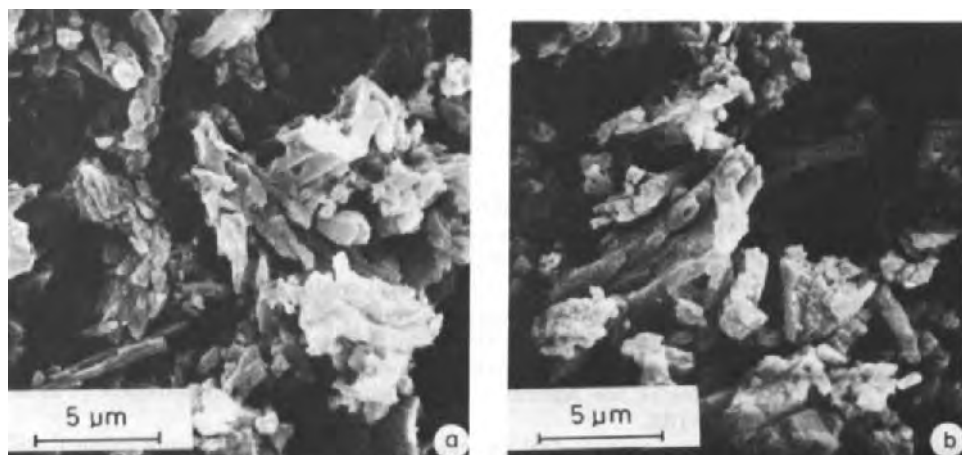


Fig. 8. Anhedronal and elongated granular vivianite in a root channel; a) and b) (SEM).

layers, viz. a clayey surface layer, a limonitic layer, a layer containing vivianite and siderite, and layered alluvial deposits below a depth of 70 cm.

Light microscopy allowed the identification of phytoliths and diatoms in the clayey layer. Both goethite fibres and structureless isotropic domains with iron oxihydrates were present in the reddish-brown zone of the limonitic layer. Siderite and vivianite were distinguished in the third layer. Vivianite was often associated with organic material, whereas siderite occurred subcutaneously to root channels. Pyrite framboids were also recognised in this layer.

SEM observations of the same material in unhardened clods of soil helped to establish the morphology of various minerals at both lower and higher magnifications. In this manner *in situ* observations made with the light microscope in thin sections could be compared with SEM data on loose materials.

The above data indicate that goethite, siderite, vivianite and pyrite have formed in the soft bog-ore. All of these may crystallise near to each other in the lower part of the profile. Such crystallisation cannot be explained by macroenvironmental mineral equilibria alone. This indicates that various microenvironments with different conditions must exist and have existed beside each other; even in these profiles with a high groundwater table. It also emphasizes that further *in situ* studies of these micro-environments require microchemical analyses with a number of submicroscopic techniques such as described by Bisdom (1981), especially EMA (electron microprobe analysis) and SEM-WDXRA (scanning electron microscopy-wavelength dispersive X-ray analysis).

ACKNOWLEDGEMENTS

Dr. F. De Coninck, Dr. E. Van Ranst and Dr. R. Vochten are thanked for providing the undisturbed samples. Mr. Bohain of the Laboratory of Elec-

tron Microscopy of the State University of Ghent is thanked for his assistance.

REFERENCES

- Bisdorn, E.B.A., 1981. A review of the application of submicroscopic techniques in soil micromorphology, II. Electron microprobe analyzer (EMA), scanning electron microscope-energy dispersive X-ray analyzer (SEM-EDXRA), laser microprobe mass analyzer (LAMMA 500), electron spectroscopy for chemical analysis (ESCA), ion microprobe mass analyzer (IMMA), and the secondary ion microscope (SIM). In: E.B.A. Bisdorn (Editor), *Submicroscopy of Soils and Weathered Rocks*. 1st Workshop of the International Working-Group on Submicroscopy of Undisturbed Soil Materials (IWGSUSM) 1980, Wageningen. Centre for Agricultural Publishing and Documentation (Pudoc), Wageningen, pp. 117–162.
- Eswaran, H., 1972. Micromorphological indicators of pedogenesis in some tropical soils derived from basalts from Nicaragua. *Geoderma*, 7: 15–31.
- Fitzpatrick, E.A., 1980. *The Micromorphology of Soils*. Department of Soil Science, University of Aberdeen, 186 pp.
- Stoops, G. and De Mets, M., 1970. Scanning elektronenmikroskopie toegepast in de bodemmikromorfologie. *Natuurwet. Tijdschr.*, 52: 10–16.

SUBMICROSCOPIC CHARACTERISATION OF PHOSPHATIC AND SESQUIOXIDIC NODULES OF SOME SOILS OF THE “CHACO DEPRIMIDO” (ARGENTINA): PRELIMINARY RESULTS

HECTOR J.M. MORRAS

I.N.T.A., Centro de Investigaciones de Recursos Naturales, Castelar (Argentina)

(Accepted for publication February 17, 1983)

ABSTRACT

Morrás, H.J.M., 1983. Submicroscopic characterisation of phosphatic and sesquioxidic nodules of some soils of the “Chaco Deprimido” (Argentina): preliminary results. *Geoderma*, 30: 187–194.

In this paper two examples are presented of the investigation by submicroscopic techniques, of particular problems in the characterisation and analysis of various pedological features in soils of the “Chaco Deprimido”.

The first concerns nodules seen in an alluvial soil. The techniques established their phosphatic composition and identified them as small bone fragments which are undergoing alteration.

The second relates to study of sesquioxidic nodules and cutans in solodised soils and planosols, and shows them to have a dominantly manganiferous composition; this result enables one to make certain interpretations concerning the physicochemical conditions essential for the formation of such pedological features.

INTRODUCTION

Microscopic studies of some soil profiles of the “Chaco Deprimido” already yielded considerable data concerning their composition and organisation. Thus, the skeleton and plasma components as well as the various pedological features were already identified and interpreted at the scale of optical microscopy. Subsequently, particular pedological features as well as isolated mineral fractions were the object of ultramicroscopic observations and elemental microanalysis, which yielded results of great interest in relation to the interpretation of the composition and genesis of these soils (Morrás, 1978b, 1980, 1981a, b; Morrás et al., 1982).

Additionally, studies are currently in progress to characterise the sesquioxidic concentration and certain phosphatic nodules seen in soils of this region. The preliminary results obtained by means of submicroscopic techniques are presented below.

MATERIALS AND METHODS

The "Chaco Deprimido" region is characterised by halomorphic soils developed on loessoid sediments mainly formed by minerals of volcanic origin. For the most part, according to the criteria of "Soil Taxonomy" (U.S.D.A., 1975), the soils are Mollisols and Alfisols with natric horizons. Some of these soils have an albic horizon which is characteristic of solodic soils and planosols. In certain parts of the landscape one also finds soils of alluvial origin which are relatively weakly developed.

Nodules, shown to be phosphatic, were found and studied in one of the latter soil profiles (Fluvent). On the other hand, dark sesquioxidic segregations, usually considered to be ferri-manganiferous in micromorphological descriptions, were studied in samples from soils with an albic horizon (a Natraqualf, a Natrustalf and an Argialboll).

These pedological features were studied by optical and electron microscopy of both massive samples and thin sections of the soils. The submicroscopic analyses were made with a wavelength-dispersive X-ray spectrometer (WDXRA) attached to a scanning electron microscope, SEM (Camebax). With this instrument it is possible to make morphological observations as well as semi-quantitative elemental analyses in the form of elemental distribution images, concentration profiles (traverses) and point-analyses. Some SEM-observations were made also with a JEOL-JEM 32 instrument.

RESULTS AND DISCUSSION

Characterisation of phosphatic nodules in the alluvial soil

Macroscopic examination of this soil had revealed yellowish-white nodules ca. 2 mm in diameter which resemble certain kinds of calcareous nodules in appearance. However, two things led one to suspect that the nodules have a different composition.

Firstly, chemical analysis of the soil showed an abnormally large phosphorus content — both total and extractable (Olsen's P). In Table I one can compare the values obtained for this soil (profile 10) with those for a Nat-

TABLE I

Total and extractable phosphorus contents for the Fluvent and Natrustalf (P_2O_5 , $\mu\text{g/g}$ dry soil)

Profile	Horizon	Total P	Extractable P
No. 10	A1	25,000	20,600
(Fluvent)	IIC	1,500	1,200
No. 79	A1	250	34
(Natrustalf)	B3	500	32

rustalf typical of this region (profile 79). Secondly, examination of soil thin sections revealed features which, from their morphology, orange colour in plain light and isotropy in polarised light, resemble phosphatic material of biological origin seen in other soils (Morrás, 1978a).

Therefore, discrete nodules in this profile were separated into two groups depending on the state of their surfaces: (1) generally smooth surface, (2) rougher surface and of a more altered appearance.

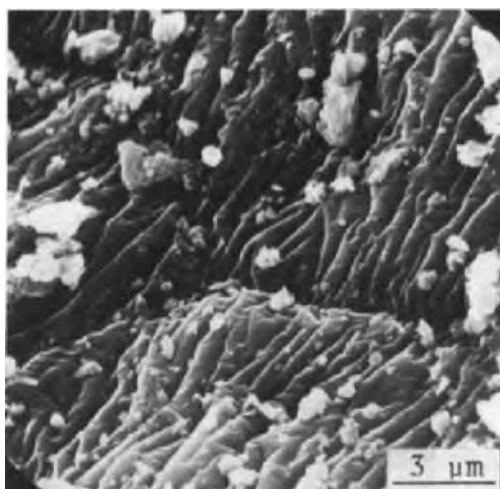


Fig. 1. SEM image of “unaltered nodules” showing their biological structure (bone fragments).

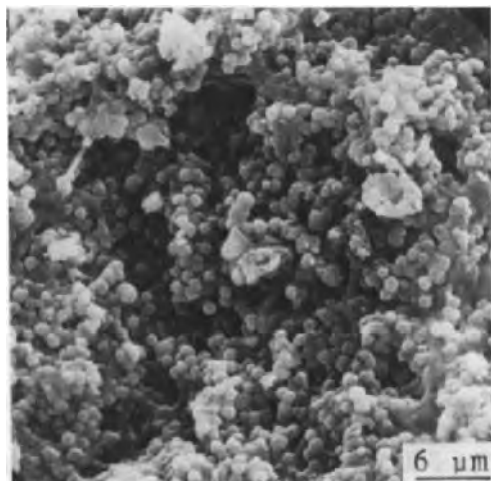


Fig. 2. Fragments of “altered” bone characterised by modification of their surface structure and the appearance of pelley aggregates. Secondary electron image.

Examination of the first group of nodules by SEM revealed certain biological structures similar to those in bone fragments (Fig. 1). In contrast, the nodules of the second group contain numerous aggregates in the form of small pellets (Fig. 2), developed on a similar framework to that seen in the preceding nodules. This morphology could result from the alteration of the original bone tissue, with concomitant formation of minerals of different composition.

In addition to morphological evidence, which already indicated origin and composition of these soil nodules, preliminary microprobe analyses confirmed the predominance of phosphorus and calcium, accompanied by lesser amounts of silicon, aluminium, potassium and magnesium. Analyses by WDXRA caused significant damage to the analysed nodules, making quantitative analysis difficult; use of an energy-dispersive spectrometer (EDS) should overcome this problem.

Characterisation of sesquioxide segregations in the solodic soils and the planosols

Optical microscopic examination of these soils showed the presence of sesquioxides both in the form of glaeboles (nodules, concretions) and as cutans. In transmitted light these features are, in general, dark brown, sometimes with a reddish tint, suggesting a basically manganiferous composition with, perhaps, some iron.

The distribution and morphological nature of these features differs, depending on the horizon under consideration: in the A1 horizons sesquioxides are rare or absent, but in the lower part of the A2 they are present

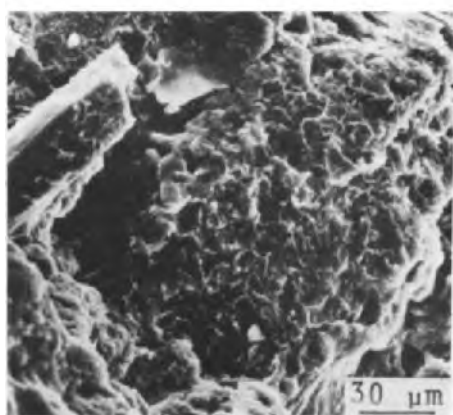


Fig. 3. Manganiferous coating (todorokite ?) on the surface of a soil aggregate from an Argialboll. Secondary electron image.

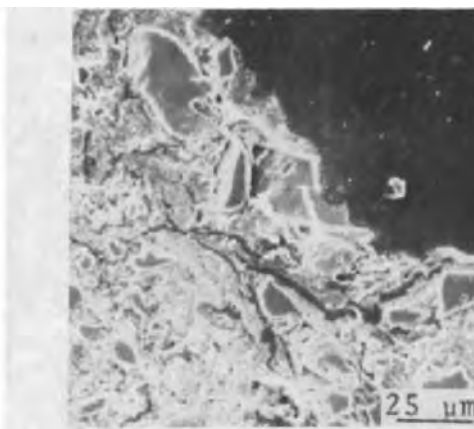


Fig. 4. Secondary electron image of a sesquioxidic neocutan in a soil thin section from an Argialboll.

in some cutans; in the upper part of the B horizon they are common and in the form of cutans, neocutans and irregularly shaped nodules, whereas in the middle and lower parts of the B horizon they are found mainly as irregular or, more rarely, rounded nodules.

Observation by SEM of undisturbed soil aggregates showed that the sesquioxide coats have a specific morphology. They are characterised by the development of reticulated platelets which project from the sample surface (Fig. 3). This crystal habit has been described often for todorokite (a complex manganiferous material) (Aubry and Pomerol, 1976).

In addition, microanalysis of some sesquioxidic cutans and neocutans has delimited their composition more precisely. For example, the secondary electron image of one such cutan is seen in Fig. 4. In the greyish matrix, fine veins of darker hue stand out, which can be taken to indicate the separation of a particular element or phase.

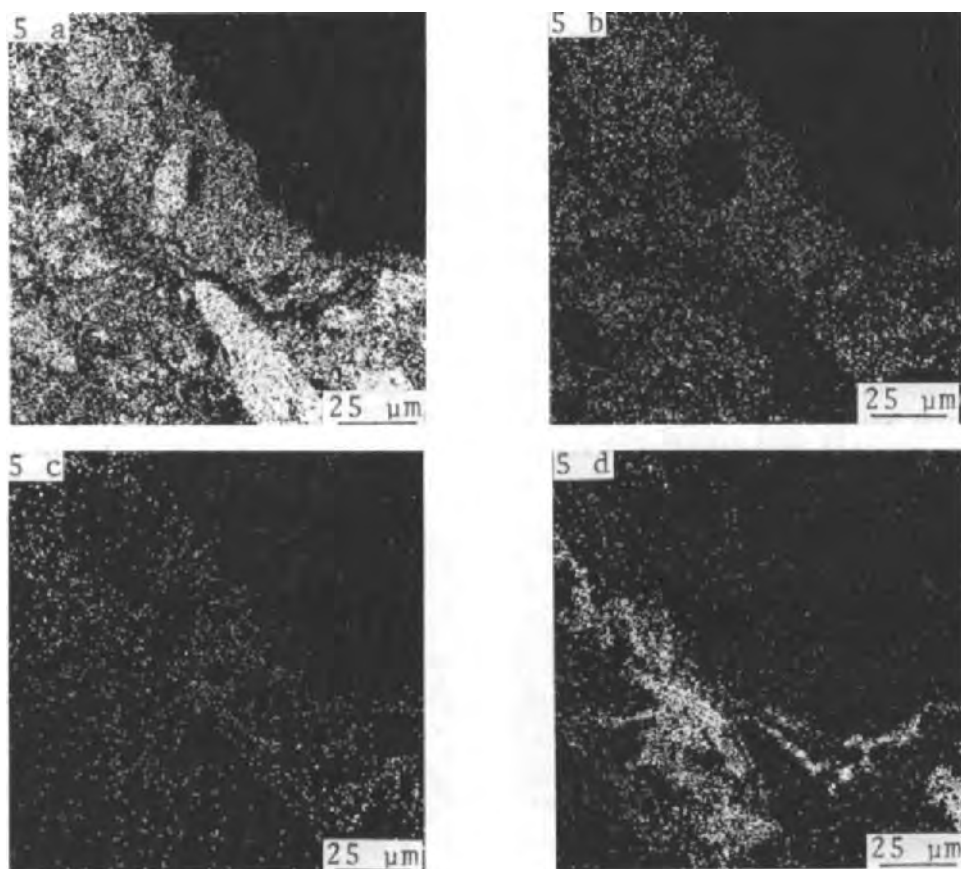


Fig. 5. Elemental analysis distribution images of the neocutan in Fig. 4. (a) Si; (b) Al; (c) Fe, this element seems to be most abundant near the void surface associated with some clay domains; (d) Mn, concentrated in the dark veins of Fig. 4.

The distribution images of silicon (Fig. 5a) and aluminium (Fig. 5b) give evidence of the relative distribution of the quartzose/glassy skeleton, and aluminosilicate plasma. Iron (Fig. 5c) appears to be associated with the fine fraction of the soil, with a concentration layer towards the aggregate surface associated with some of the clay domains. In contrast, manganese (Fig. 5d) is clearly concentrated in the dark veins mentioned above.

On the other hand, traverses with the microprobe of a siltargillan, an argillan plus sesquioxides and a neosesquan (Figs. 6 and 7) show both the segregation of iron and manganese and the greater proportion of the latter. In the non-oriented regions of the siltargillan, iron, associated with clay, seems to be more abundant than manganese; in contrast, in the oriented clay (which is illustrated by the multiple peaks of Si, Al, K and Fe) with secondary sesquioxide staining, manganese appears to be dominant.

The analyses show that manganese is the principal component of, and is almost solely confined to, the more abundant, dark sesquioxide accumulations, whilst iron is confined to the rarer reddish pockets. The results agree with those of other writers who also established the separation of ferruginous and manganiferous phases, as well as the lack of correlation between the contents of the two elements in concretions, in different kinds of soils (e.g. Childs, 1975; Childs and Leslie, 1977).

Thus, from these results, it seems possible to infer that the physico-chemical conditions in these solodised solonetztes and planosols favour the mobilisation and segregation of manganese to the exclusion of iron. The latter must remain immobile and eventually migrate in association with the other soil components such as clay and organic matter.

In this context, it is worth remembering that manganese compounds are much more readily reduced, and thus more susceptible to mobilisation than iron compounds (Van Schuylenborgh, 1973). Consequently, this may signify that, in the profiles studied, extreme reducing conditions do not occur

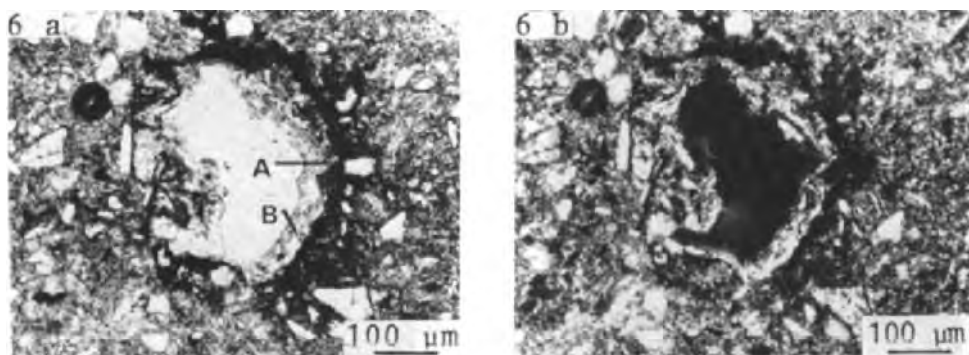


Fig. 6. (a) A siltargillan (a mixture of clay and fine silt grains) and a neosesquan from an Argialboll. The lines A (see Fig. 7) and B (not given in Fig. 7) correspond to microanalytical traverses across these features. Light microscope (plane-polarized light). (b) The same field of view (cross-polarized light).

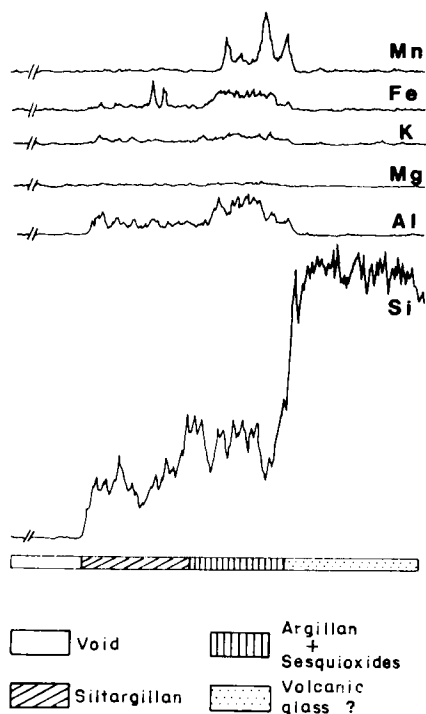


Fig. 7. Relative distribution of various elements (Mn, Fe, K, Mg, Al and Si) along traverse A of Fig. 6.

in spite of the surface waterlogging that periodically affects them, and which is one of the principal factors in the development of these kinds of soils (Morrás, 1979).

Conversely, a larger oxidation potential or the typical high pH of these sodic soils, may provide the Eh–pH conditions necessary for the precipitation and accumulation of manganese.

Further analyses should enable one both to complete this investigation and refine the initial interpretations, by attempting to relate more closely the chemical and mineralogical nature of these manganiferous accumulations to the conditions necessary for their genesis.

CONCLUSIONS

In this work, the utilisation of SEM and WDXRA techniques helped to clarify two particular problems. Firstly, it was possible to establish the phosphatic composition of some nodules found in alluvial soils and to identify them as small bone fragments which are undergoing alteration. Secondly, sesquioxidic concentrations in some surface hydromorphic soils were shown to be composed almost exclusively of manganese, while iron is absent or scarce.

In this respect, the two cases discussed here exemplify the possibilities offered by submicroscopic techniques for the clarification of numerous problems (frequently impossible to resolve by other means), as well as opening up new avenues of research. The pursuit of these studies of the soils of the "Chaco Deprimido" has, in this way, resulted in a more sure and a more detailed understanding of their chemical and mineralogical characteristics, assisting as it does in defining the pedogenic mechanisms which have participated in the evolution of the different kinds of soils of this region.

ACKNOWLEDGEMENTS

The author is grateful to Dr. P. Loveland (Rothamsted Experimental Station, England) for his kind assistance in the translation of this paper into English.

REFERENCES

- Aubry, M. and Pomerol, B., 1976. Les néoformations manganifères dans la craie du Bassin de Paris. Discussion sur l'origine du manganèse. C.R. Acad. Sci. Paris., Sér. D, 283: 1261—1264.
- Childs, C., 1975. Composition of iron-manganese concretions from some New Zealand soils. *Geoderma*, 13: 141—152.
- Childs, C. and Leslie, D., 1977. Interelement relationships in iron manganese concretions from a catenary sequence of yellow grey earth soils in loess. *Soil Sci.*, 123(6): 369—376.
- Morrás, H., 1978a. Phosphatic nodules from a soil profile of Santa Fe Island, Galapagos. In: M. Delgado (Editor): *Micromorfología de Suelos*. Proceedings of the 5th International Working Meeting on Soil Micromorphology, Granada, pp. 1007—1018.
- Morrás, H., 1978b. Contribution à la connaissance pédologique des "Bajos Submeridionales" (Province de Santa Fe, Argentine). Influence de l'environnement sur la formation et l'évolution des sols halomorphes. Thèse, Université de Paris, 7, 184 pp.
- Morrás, H., 1979. Discussion sur les mécanismes de pédogenèse des planosols et d'autres sols apparentés. *Sci. Sol*, 1: 57—68.
- Morrás, H., 1980. La utilización integrada de técnicas microscópicas y microanalíticas en el estudio de los constituyentes del suelo. In: *Actas IX Reunión Argentina de la Ciencia del Suelo*, Paraná (Argentina), pp. 1165—1176.
- Morrás, H., 1981a. Characteristics and composition of some cutans and glaeboles of probable artificial origin. In: *Proceedings of the 6th International Working Meeting on Soil Micromorphology*, London. In press.
- Morrás, H., 1981b. Morphological and analytical properties of degraded argillans from A2 horizons of solodic planosols. In: *Proceedings of the 6th International Working Meeting on Soil Micromorphology*, London. In press.
- Morrás, H., Robert, M. and Bocquier, G., 1982. Caractérisation minéralogique de certains sols salsodiques et planosodiques du "Chaco Deprimido" (Argentine). *Cah. ORSTOM, sér. Pédol.*, 19(2): 151—169.
- U.S.D.A., 1975. Soil Taxonomy. A basic system of soil classification for marking and interpreting soil surveys. Handbook No. 436, 754 pp.
- Van Schuylenborgh, J., 1973. Sesquioxide formation and transformation. In: E. Schlichting and U. Schwertmann (Editors), *Pseudogley and Gley*. Verlag Chemie, pp. 93—102.

CHARACTERISTICS AND SIGNIFICANCE OF COMPOSITE PARTICLES DERIVED FROM A COLOMBIAN ANDOSOL PROFILE

P.A. RIEZEBOS and W.J. LUSTENHOUWER

Laboratory of Physical Geography and Soil Science, University of Amsterdam, Dapperstraat 115, 1093 BS Amsterdam (The Netherlands)

Netherlands Organization for the Advancement of Pure Research (ZWO), De Boelelaan 1085, 1081 HV Amsterdam (The Netherlands)

(Accepted for publication February 17, 1983)

ABSTRACT

Riezebos, P.A. and Lustenhouwer, W.J., 1983. Characteristics and significance of composite particles derived from a Colombian andosol profile. *Geoderma*, 30: 195–217.

Composite particles, frequently observed in sand and coarse silt from laboratory-treated andosol materials, have been collected at eight levels in an andosol profile near Guasca (Colombia) and studied by microscopic, SEM and electron microprobe techniques. The particles appear to be made up of a varying number of fine sand- to clay-sized grains of various shape and nature, cemented together by an optically isotropic material of allophanic composition. Plots of the chemical parameters of this cement against depth reveal a zonal arrangement of major and minor elements. A stratified arrangement is also shown by petrographic features of the light- and heavy-mineral fractions of the associated sample material, and by the fabric of small undisturbed lumps from depths between the eight levels.

The composite particles are obviously the product of allophane-generating sites in surficial layers containing unstable solids as volcanic glass and minerals. Although in this study the particles have been investigated in the form of artificial fragments, more or less similar ones will originate under natural conditions. It is argued that their occurrence as sand- and silt-sized individuals in natural erosion products, and thus also in aggradational soils, must drastically affect chemical soil parameters, when obtained by wet chemical analysis of bulk samples.

INTRODUCTION

Routine-microscopic observations of sand-sized material from andosols developed from surficial volcanic ashes on the Sabana de Bogotá (Colombia), reveal the frequent occurrence of composite particles. Apparently their stability was sufficiently large to resist disintegration during common laboratory pretreatments.

Since in volcanic soils various types of composite particles may be found, ranging from actual rock fragments to aggregates the discrete components of which are held together by unlike charges only, their characteristics were studied more closely.

Examination of grain mounts and thin sections of different size fractions showed one particular type to be dominant. This type could not be classed among rock fragments (fresh or altered) nor among glassy fragments containing phenocrysts.

When mechanical forces are applied, they are rather easily reduced, although the impression has been gained that there is a variation in firmness. Ultrasonic treatment during 30 min of a 32–50 μm size fraction, e.g., showed a rather low susceptibility of the particles to disintegration. After sieving over a 32 μm sieve, the treated material lost about half of its weight only.

Additional microscopic investigation of undisturbed lumps from these soils often suggested that pulverising actions as carried out during the laboratory pretreatment would easily result in a high number of individual composite particles of different size and shape. If these composite particles can originate in this way, it also means that they must be a rather usual constituent of natural soil erosion products.

In discussing the genesis of Indonesian volcanic soils at altitudes above 1300 m, Mohr and Van Baren (1954) already mentioned probably this kind of composite particles. They denominated the mechanism producing them “mountain granulation” and the products formed “pseudo sands”.

Present-day geomorphological research is often focussed on the unravelling of the various erosional processes. Hence it was decided to investigate their properties in one single soil profile, to find out whether this knowledge might be of use to increase our judgement in landscape dynamics.

EXPERIMENTAL

Site and general setting of the profile

The profile is situated about 6 km east of the village of Guasca (Fig. 1) along the road to Sueva on a westward facing slope at an elevation of 2805 m (T. van der Hammen, oral communication, 1981), Van der Hammen collected the profile in brass containers and made it available for investigation. Jungerius denominated the soil horizons (see Fig. 12).

According to Botero (1972) soils occurring in this area must be classified as Andic Humitropepts and Andic Cryumbrepts. The profile developed in the Qal unit (Anonymous, 1969) belonging to the Sabana Formation of middle and late Quaternary age. The Qal unit is described as a fine-grained fluvio-lacustrine deposit with glacially derived detrital material. Field evidence, however, shows that the deposit is covered by or highly mixed with volcanic ashes. As a result soil profiles have been developed in pure tephra or in a mixture of ashes and non-volcanic material.

From numerous studies (Van der Hammen et al., 1973; Van Geel and Van der Hammen, 1973; Correal and Van der Hammen, 1977; Van der Hammen, 1978; Dueñas-J., 1977) it has become clear that deposition of

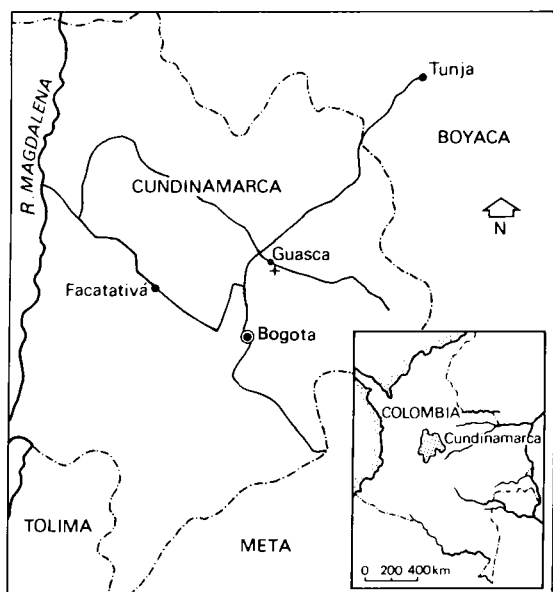


Fig. 1. Map showing the location (+) of the Guasca soil profile.

volcanic ashes on the Sabana de Bogotá has been a frequently repeated event. The investigation of a core from the Laguna de Fuquene area just north of the Sabana de Bogotá showed that deposition must have occurred at least fifteen times during the last 45,000 years (Riezebos, 1978). This study also indicates that these tephra are crystal-vitric ashes with glass contents varying between 25 and 60 grain percentages in the 50–75 μm fractions. On the basis of the mineralogical composition two “types” could be distinguished. The first type contains mainly micas and amphiboles as heavy minerals, while the bulk of the heavy minerals in the second one consists of amphiboles and pyroxenes. The latter type of ashes has probably been deposited after ca. 20,000 yr BP.

Two wet and two dry seasons with an annual rainfall varying between 700 and 900 mm can be distinguished in the Guasca Valley. The annual precipitation in the Eastern Cordilleras, east of the Guasca Valley, varies between 1800 and 2200 mm and seems to be concentrated in the period May–August (Botero, 1972). Hence the amount and distribution of precipitation on the soil profile must have been highly influenced by the altitude and aspect of its topographic position. The mean annual temperature at the soil location must be 11–12°C, calculated according to Van der Hammen (1963).

Treatment of the sampled material

From eight levels of the profile (0–5, 25–30, 50–56, 94–100, 144–150, 190–195, 207–215 and 243–250 cm depth) material was sampled.

Usually the preliminary treatment is directed on the disintegration of the material and the removal of particle coatings, organic and colloidal material, in order to obtain an accurate size distribution of the primary particles.

As this study mainly focusses on the composite particles, the common treatment with acid or alkaline digestion was omitted. After being suspended in demineralized water, the soil material was pulverised by gentle rubbing. Only a H_2O_2 (30%) treatment was applied in order to remove as much as possible the organic matter. The peroxide treatment, however, was stopped after 60 h, because the suspensions remained active.

After washing and drying the material was separated in different particle size fractions by sieving ($> 32 \mu\text{m}$). Subsequently the heavy minerals in the size fractions 50–75, 75–105, 105–150 and 150–210 μm were separated by using bromoform (s.g. 2.89) and their weight percentages determined. The remaining "light" mineral fractions were used for the study of the composite particles.

From several other depths (11–12, 46–47, 82–87, 134–136, 154–156, 195–200, 220–222 and 238–241 cm), undisturbed soil fragments for the preparation of thin sections were taken, in order to examine the soil fabric.

Methods

In addition to the petrological microscope, a SEM (Mark II Cambridge Instruments) was used for the morphological study of the composite particles. Individual specimens collected by handpicking using a binocular magnifier (Bausch and Lomb) were mounted on an aluminum stub with aluminum paint, and subsequently sputter-coated with gold in a vacuum evaporator under continuous rotation of the sample holders. For the examination of the fabric of the composite particles a SEM (type JSM-35C) was applied after embedding in an artificial resin, sectioning, polishing and coating specimens collected by handpicking.

Because of the intimately associated constituents in the composite particles and our incompetence to separate them properly, aqueous suspensions of sand fractions (mineral/distilled water ratio $\cong 1:40$) were subjected for 1.5 h to ultrasonic vibration (Engisonic 50 Kc). During vibration water temperature increased to ca. 35°C . After homogenization of the suspension and the required waiting time (Stoke's formula), drops of the suspension containing clay-sized particles of 1 μm and smaller were placed on the aluminum stubs and the water evaporated at 35°C . After gold-sputtering the samples were also examined using the SEM (Mark II).

The close association of the different constituents also forms a considerable drawback for the assessment of their chemical characteristics. Hence for this purpose an in situ microchemical analysing technique (Boekstein et al., 1981) seemed most appropriate. Electron microprobe analyses (Microscan 9, Cambridge Instruments) were carried out. Handpicked composite particles were embedded in artificial resin, sectioned ($\pm 30 \mu\text{m}$),

TABLE I

Standards used for quantitative electron microprobe analyses

Na — jadeite	S — barite	Cr — chromium oxide
Mg — olivine	Cl — halite	Mn — rhodonite
Al — corundum	K — orthoclase	Fe — hematite
Si — diopside	Ca — diopside	Ni — nickel oxide
P — apatite	Ti — ilmenite	

polished and carbon-coated. For quantitative analyses the standards listed in Table I were used. Percentages were corrected (ZAF-corrections) by an on-line computer program provided by the manufacturer.

RESULTS

Morphology and fabric of the composite particles

The particles show in general a subangular to rounded shape (Fig. 2). At higher magnifications, however, their outlines are often very irregular, showing sometimes a frayed appearance. This is evidently more clear in thin sections than in grain mounts (Fig. 3). The irregularity of the particle edges is occasionally effected by protruding inclusions, but the scanning

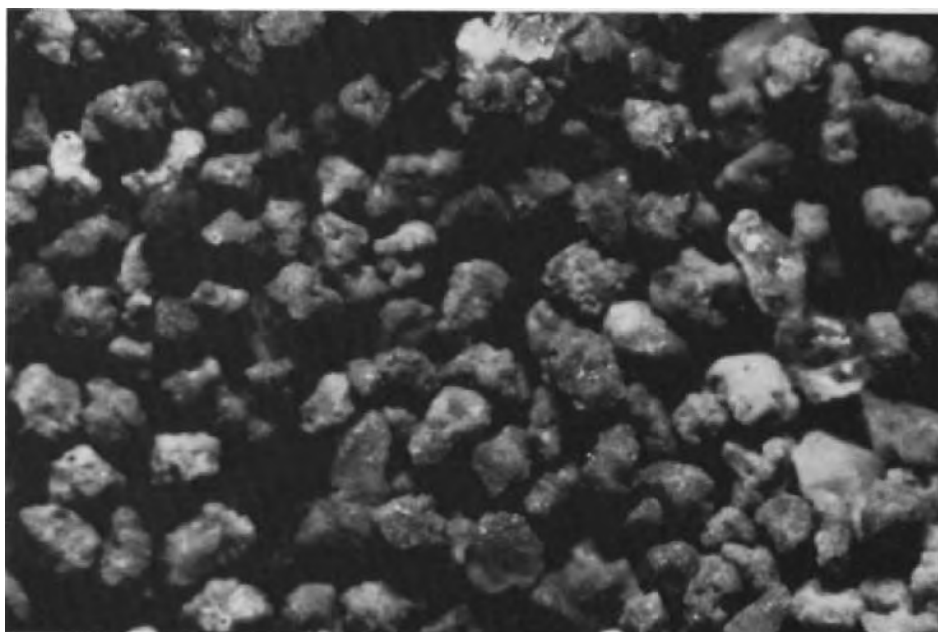
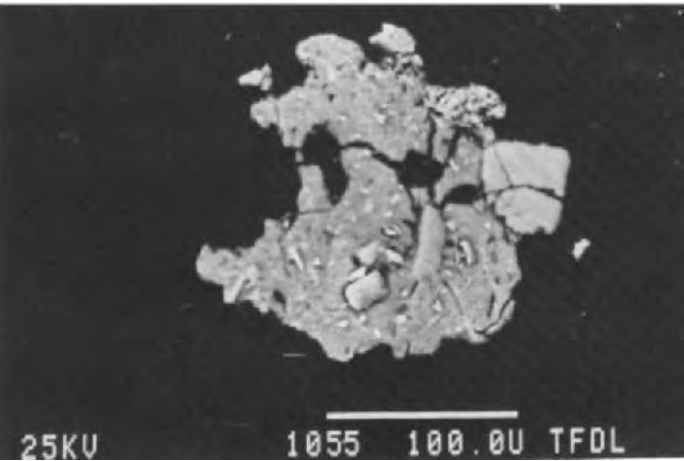
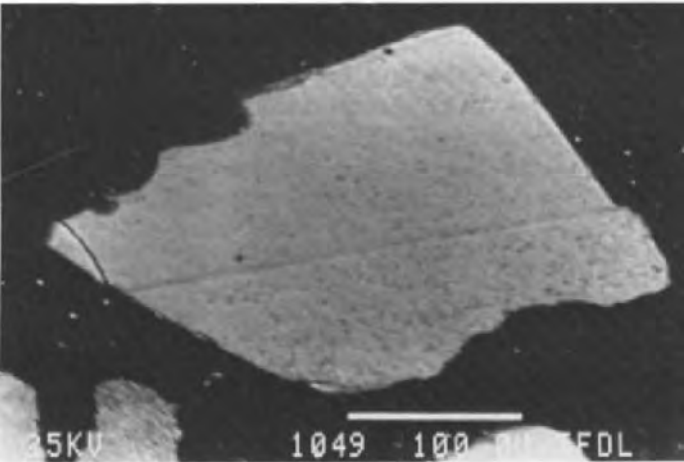
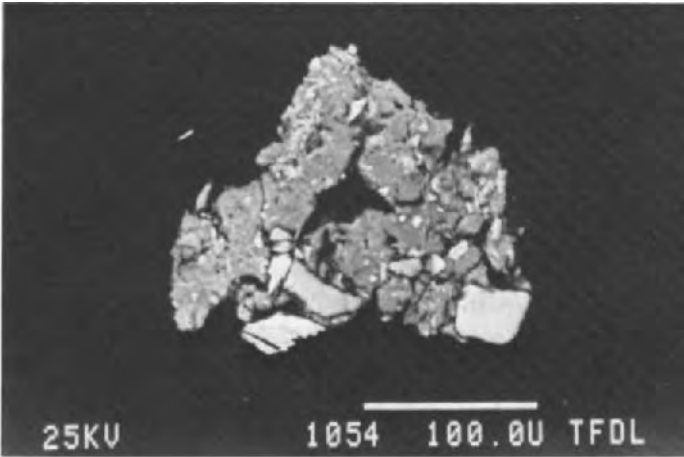


Fig. 2. Photomicrograph of the light-mineral fraction (105–150 μm) from level V of the Guasca soil profile (see Fig. 11).



electron micrographs (Figs. 3 and 4) testify, that crevices and cavities starting at the particle surface contribute more substantially to the irregular surface.

Angular specimens have been observed, but mainly in level I (0–5 cm depth) where they were largely outnumbered, however, by subangular and rounded particles. The surface irregularity of the rounded particles mostly leads, especially under low magnifications, to mammillated shapes. Only once, a local coating with a plain gel-like material has been noticed.

Especially the thin sections show the composite particles to be made of optically isotropic and anisotropic materials. Only the angular specimens mainly found in level I appeared mostly to consist of isotropic material only (Fig. 3). So actually the denomination “composite” particle is not completely justified. As the latter are far in the minority the use of the adjective will be continued. Moreover, X-ray powder analysis performed on the clay fraction of a number of angular composite particles, collected by handpicking and subsequently crushed, yielded an X-ray pattern with clear lines of quartz and cristobalite. Further, very weak 14 and 7 Å reflections were recorded.

As is illustrated in the micrographs of Figs. 3 and 4 the isotropic component envelopes and cements particles of different size, shape and nature. Their number may vary per composite particle. Idiomorphic shapes are not uncommon.

The frequent occurrence of biolites or opal phytolites among the included particles supports the suggestion that the inclusions have been incorporated by the isotropic constituent. Fretted outlines of optically anisotropic and isotropic (glass, biolites) inclusions may be interpreted as a sign that these components are still being dissolved.

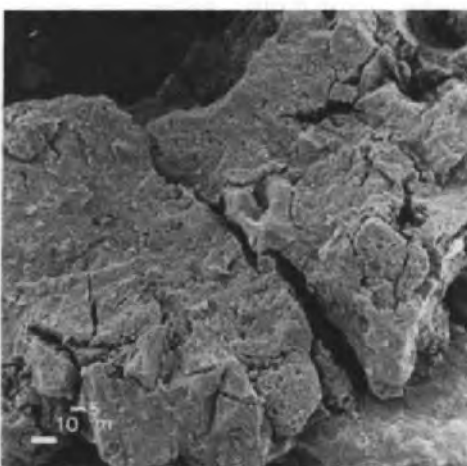
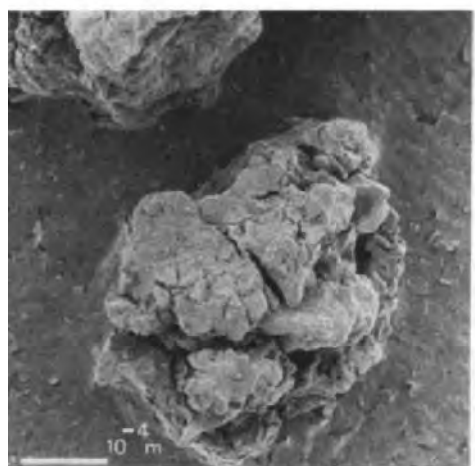
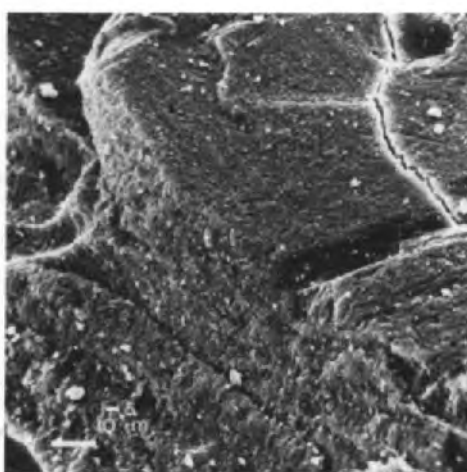
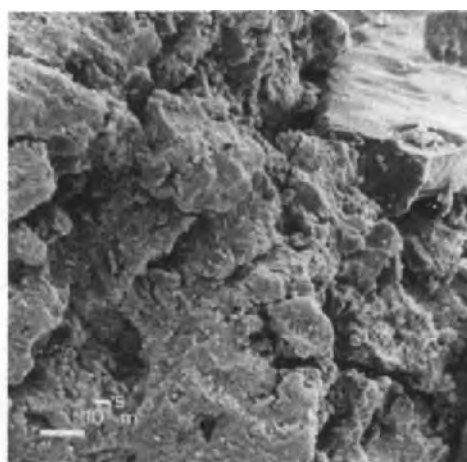
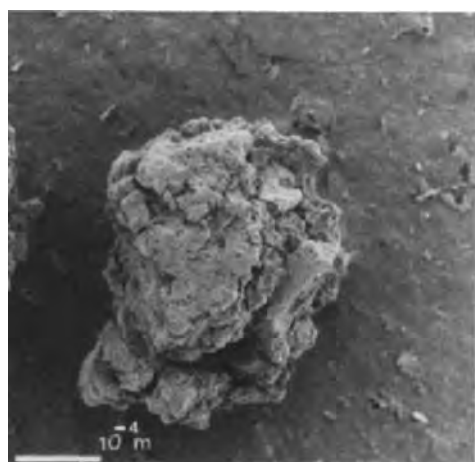
The included crystalline constituents represent in general quartz, feldspars, amphiboles, iron oxide, pyroxenes etc. Among the smallest ones ($< 8 \mu\text{m}$) phyllosilicates seem to dominate. From a genetical point of view, the amorphous, yellow to dark-brown coloured material, by which the other constituents are cemented, seems to be the most interesting component.

The composite particles dominate the light-mineral spectra in the investigated levels; only in level II and III, corresponding with the B2 and BC horizons, their abundance is considerably lowered (see Fig. 12).

Thin-section analysis of associated soil lumps

A careful inspection of the thin sections showed that cutan formation nor plasma separations could be detected at the sampled depths. At the

Fig. 3. Backscattered electron scanning images (BESI) of sectioned and polished composite particles (SEM:JSM-35C). The second one represents an inclusion-free angular specimen from level I of the soil profile (see Fig. 11). Magnification: $\times 525$.



depths above 156 cm, however, small-sized areas could be distinguished deviating from the adjacent S-matrix by colour and/or rather clear boundaries (Fig. 5).

As these areas sometimes exhibit straight and angular boundaries, fail to show a close relationship with channels and joints, have a colour and internal matrix differing from the surrounding S-matrix and have highly variable dimensions, it is hardly possible to interpret them as pedological features (pedotubules, fecal pellets, glaebules, nodules).

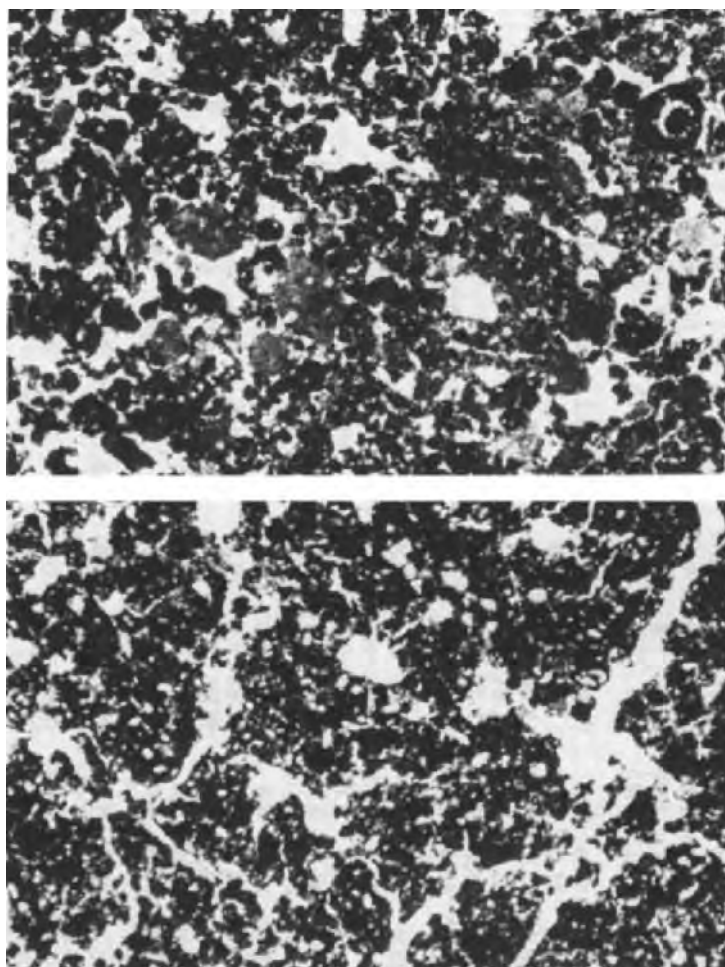


Fig. 5. Photomicrographs showing the fabric at depth of 134–136 cm (upper) and of 195–200 cm (lower) of the soil profile. Magnification $\times 8$.

Fig. 4. Oblique (tilt of the sample holder 45°) scanning electron micrographs of composite particles (SEM: Mark II Cambridge Instruments).

TABLE II

Chemical analyses and calculated $\text{SiO}_2/\text{Al}_2\text{O}_3$ molar ratios of the amorphous cement in a number of composite particles collected from 8 levels of the Guasca soil profile

Level	SiO_2	Al_2O_3	TiO_2	FeO	P_2O_5	MgO	NiO	CaO	Na_2O	K_2O	SO_3	Cl	$\text{SiO}_2/\text{Al}_2\text{O}_3$	Surface analyzed
I (0—5 cm)	32.95	35.05	1.25	12.6	1.85	0.8	—	0.15	0.1	0.2	0.5	0.2	1.59	ca. $3 \times 4 \mu\text{m}$
	28.7	36.0	1.4	12.75	1.9	0.85	n.d.	0.15	0.1	0.15	0.5	0.2	1.35	ca. $20 \times 25 \mu\text{m}$
	18.95	38.35	1.50	11.3	0.55	0.15	—	0.1	0.05	0.15	0.65	0.2	0.80	ca. $20 \times 25 \mu\text{m}$
	21.7	35.1	1.45	13.15	1.3	0.35	—	0.15	0.05	0.1	0.45	0.35	1.05	ca. $3 \times 4 \mu\text{m}$
	24.95	35.15	1.35	10.5	1.55	1.05	—	0.15	0.05	0.1	0.45	0.2	1.20	ca. $3 \times 4 \mu\text{m}$
II (25—30 cm)	25.6	38.6	1.6	10.9	n.d.	0.65	0.15	0.2	0.15	0.1	n.d.	n.d.	1.24	ca. $23 \times 30 \mu\text{m}$
	26.1	41.05	1.65	11.6	n.d.	0.6	0.1	0.15	0.1	0.1	n.d.	n.d.	1.08	ca. $2 \times 3 \mu\text{m}$
	28.05	41.75	1.65	12.05	n.d.	0.6	0.05	0.20	0.05	n.d.	n.d.	n.d.	1.14	ca. $2 \times 2 \mu\text{m}$
	28.85	42.25	1.55	11.07	n.d.	0.7	0.1	0.6	0.15	0.15	n.d.	n.d.	1.16	ca. $2 \times 2 \mu\text{m}$
	28.0	38.55	1.7	11.35	0.95	0.6	0.05	0.15	0.2	0.15	0.3	0.15	1.23	ca. $23 \times 30 \mu\text{m}$
III (50—56 cm)	27.25	38.0	1.6	11.05	0.7	0.75	0.15	0.25	0.15	0.15	0.45	0.15	1.22	ca. $23 \times 30 \mu\text{m}$
	34.6	42.35	1.4	9.5	0.4	0.3	—	0.1	0.1	0.2	n.d.	0.1	1.39	ca. $8 \times 9 \mu\text{m}$
	33.25	38.2	2.0	13.25	1.6	0.9	—	0.2	0.3	0.2	n.d.	0.25	1.48	ca. $8 \times 9 \mu\text{m}$
	33.4	43.1	1.65	8.95	0.25	0.2	—	0.1	0.15	0.15	n.d.	0.2	1.31	ca. $8 \times 9 \mu\text{m}$
IV (94—100 cm)	34.3	41.55	1.3	9.55	0.25	0.25	n.d.	0.1	0.15	0.3	n.d.	0.05	1.40	ca. $6 \times 7 \mu\text{m}$
	15.05	44.65	1.1	7.9	0.2	0.15	—	0.1	—	0.15	0.3	0.2	0.57	ca. $8 \times 9 \mu\text{m}$
	12.7	24.0	0.7	27.65	0.4	0.5	n.d.	0.2	0.25	0.1	0.1	0.25	0.90	ca. $8 \times 9 \mu\text{m}$
	23.55	31.15	0.95	18.45	0.35	1.25	—	0.2	0.05	0.2	0.3	0.25	1.28	ca. $6 \times 7 \mu\text{m}$
	18.25	41.35	1.0	6.6	0.1	0.1	—	0.1	—	0.05	0.15	0.3	0.75	ca. $6 \times 7 \mu\text{m}$
V (144—150 cm)	15.2	52.5	1.75	10.2	0.35	0.15	—	0.05	0.05	0.1	0.35	0.25	0.49	ca. $8 \times 9 \mu\text{m}$
	23.45	40.05	1.65	9.7	0.25	0.2	n.d.	0.1	0.15	0.2	0.25	0.15	0.99	ca. $8 \times 9 \mu\text{m}$
	16.3	38.65	1.8	10.9	0.3	0.15	—	0.1	—	0.1	0.15	0.2	0.72	ca. $32 \times 37 \mu\text{m}$
	16.2	45.65	1.95	16.3	0.3	0.2	—	0.1	0.05	0.1	0.2	0.2	0.60	ca. $8 \times 9 \mu\text{m}$

VI (190—195 cm)	32.15	35.5	1.25	8.6	1.35	1.4	—	0.15	0.05	0.2	n.d.	0.2	1.75	ca. 8 × 9 μm
	35.45	28.85	1.1	7.45	1.0	1.2	—	0.15	0.2	0.45	n.d.	0.2	1.58	ca. 8 × 9 μm
	32.95	35.3	1.45	8.7	1.35	1.5	n.d.	0.15	0.1	0.3	n.d.	0.15	1.51	ca. 8 × 9 μm
	38.95	31.75	1.35	8.8	1.15	1.6	—	0.15	0.1	0.35	n.d.	0.1	1.54	ca. 8 × 9 μm
	34.75	33.95	1.35	8.1	1.15	1.65	n.d.	0.3	0.15	0.3	n.d.	0.2	2.08	ca. 8 × 9 μm
	32.6	31.55	0.95	6.5	0.75	1.1	—	0.1	0.05	0.2	n.d.	0.2	1.58	ca. 8 × 9 μm
	32.55	34.85	1.1	7.55	0.85	1.35	n.d.	0.1	0.05	0.6	n.d.	0.2	2.08	ca. 8 × 9 μm
	28.5	31.9	0.9	6.15	1.1	1.05	n.d.	0.05	0.1	0.45	n.d.	0.2	1.74	ca. 8 × 9 μm
VII (207—215 cm)	31.25	36.55	1.2	7.75	0.45	1.15	—	0.2	0.05	0.4	n.d.	0.1	1.45	ca. 8 × 9 μm
	31.25	32.7	1.15	7.2	0.4	1.65	—	0.4	0.15	0.25	n.d.	0.1	1.62	ca. 8 × 9 μm
	34.05	32.15	0.95	6.6	0.6	1.1	n.d.	0.15	0.05	0.25	n.d.	0.1	1.80	ca. 8 × 9 μm
VIII (243—250 cm)	37.1	31.7	0.95	7.25	—	0.85	0.05	0.25	—	0.25	n.d.	0.1	1.98	ca. 28 × 25 μm
	33.7	35.2	0.9	7.05	0.1	0.75	—	0.3	0.1	0.25	n.d.	0.1	1.62	ca. 10 × 14 μm
	33.9	31.8	1.1	7.4	n.d.	0.7	—	0.15	—	0.2	n.d.	0.2	1.81	ca. 23 × 30 μm

Below the depth of 156 cm, these particular areas were lacking in the thin sections. So, they likely represent pedorelics, incorporated in the matrix of the present soil. Another difference is that above 156 cm the fabric units are in general more rounded while below this depth they are more angular.

Chemical features of the amorphous component

From the 210–300 μm size fractions a number of composite particles was sampled randomly and used for electron probe micro-analyses of the amorphous component. The results and the calculated $\text{SiO}_2/\text{Al}_2\text{O}_3$ molar ratios are presented in Table II.

The results indicate a considerable difference between the investigated levels. Levels I and IV, e.g., display a wide range in the measured abundances of several elements (P_2O_5 , Al_2O_3 , FeO and SiO_2) while the measured range of these elements in other levels, e.g. II and VII, is much more limited.

A conspicuous anomaly is shown by the high Ni content in level II. This relatively high amount of nickel could not be related to any specific inclusion. Commonly such abundances are found in the weathering products

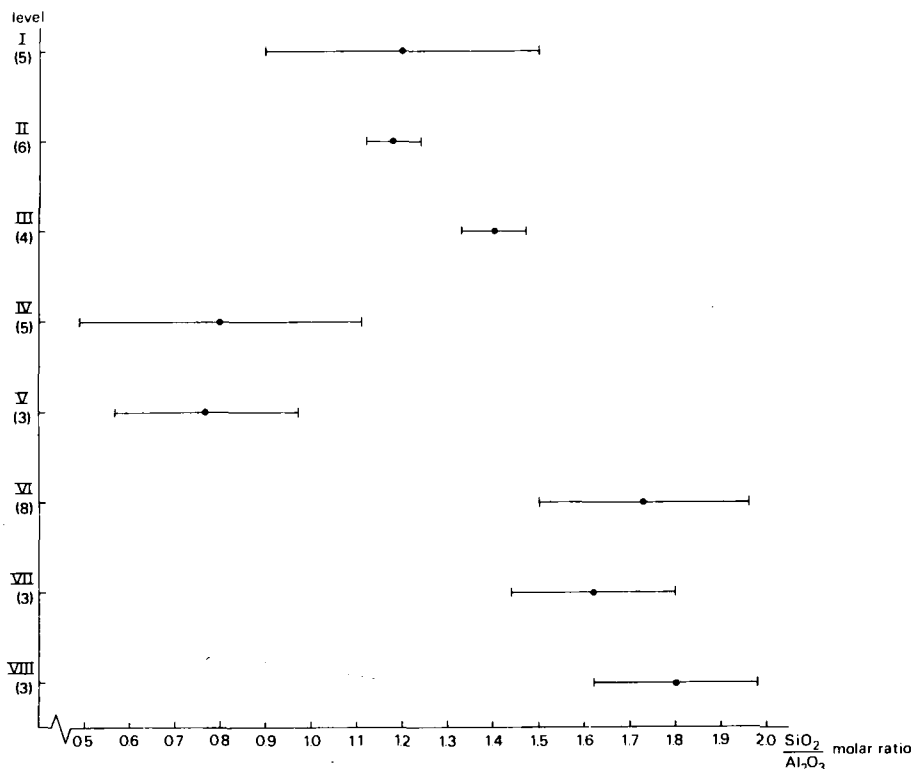


Fig. 6. $\text{SiO}_2/\text{Al}_2\text{O}_3$ molar ratios against depth. Data are from Table II. Black dots indicate average values and bars standard deviations.

of mafic to ultramafic rocks which, however, are unknown in this part of Colombia.

Another notable phenomenon are the relatively high P_2O_5 concentrations in the amorphous component of the measured particles from levels VI and I. The measured values of CaO, Na_2O and Cl do not vary very much.

Fig. 6 gives the arithmetic averages and standard deviations of the SiO_2/Al_2O_3 molar ratios as a function of depth. Figs. 7, 8 and 9 present the values of some measured elements in various plots. They illustrate in several respects the differences between the levels. The SiO_2/Al_2O_3 molar ratio, which varies between 0.49 and 2.08, shows in particular that the amorphous cementing constituent of the composite particles from the levels VIII, VII

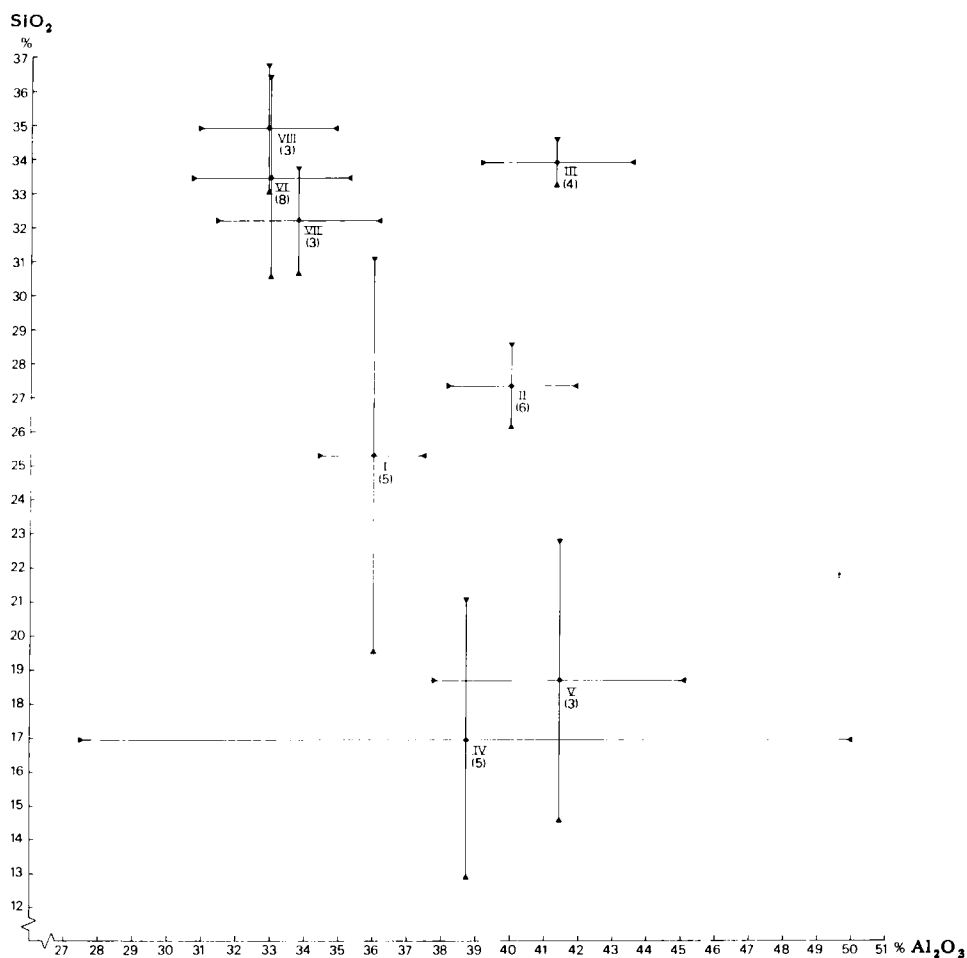


Fig. 7. SiO_2 vs. Al_2O_3 plot. Data are from Table II. Mean values are indicated by black dots, standard deviations by bars. Roman numerals represent the investigated level, number between brackets the number of analyses.

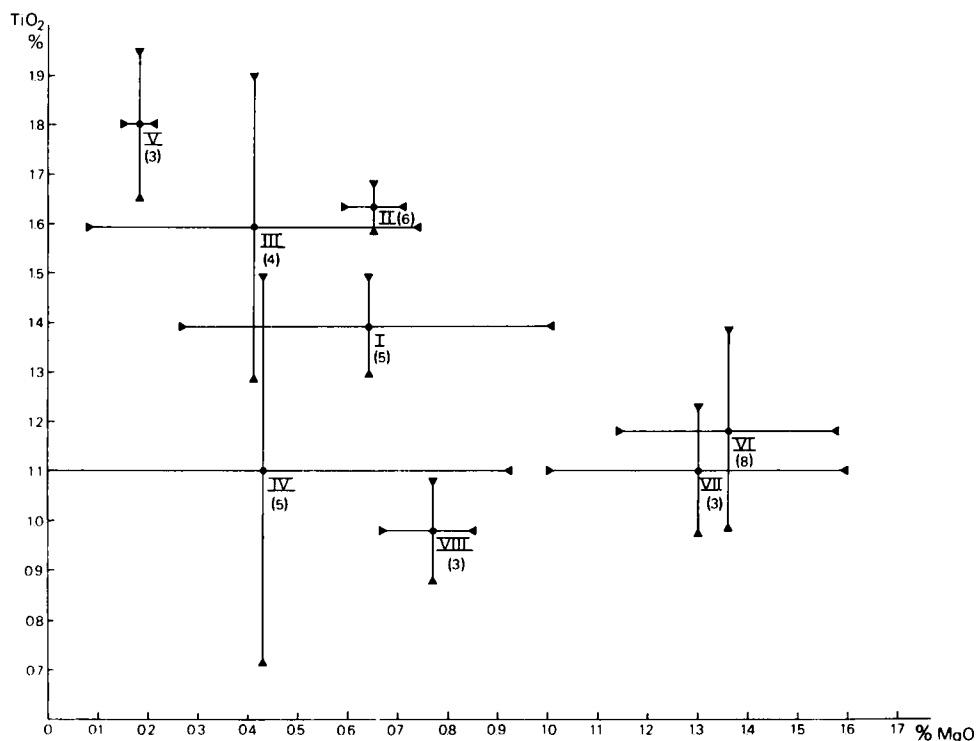


Fig. 8. Plot of TiO₂ vs. MgO (see Fig. 7).

and VI deviates significantly from that in the remaining ones. Further, that among these remaining ones, V and IV can be discriminated from III and II, which mutually also differ significantly.

Morphology of the dispersed amorphous component

Because SEM observations on the surface of composite particles hardly provided information about whether the amorphous component consisted of individual units and if so, of what morphology, it has been assumed that this information might be found by examination of the finest ($< 1 \mu\text{m}$) products obtained by ultrasonic vibration of sand-sized composite particles.

The micrographs (Fig. 10) show that discrete particles seem to be discernable and also that their majority has a spherical shape. Clustering of these spherules can be observed, with themselves and with differently shaped particles. The dimensions of apparently individual spherules seem to vary between ca. 400 and 1000 Å. In view of their abundance, it seems likely that these spherules represent the dispersion products of the amorphous cement.

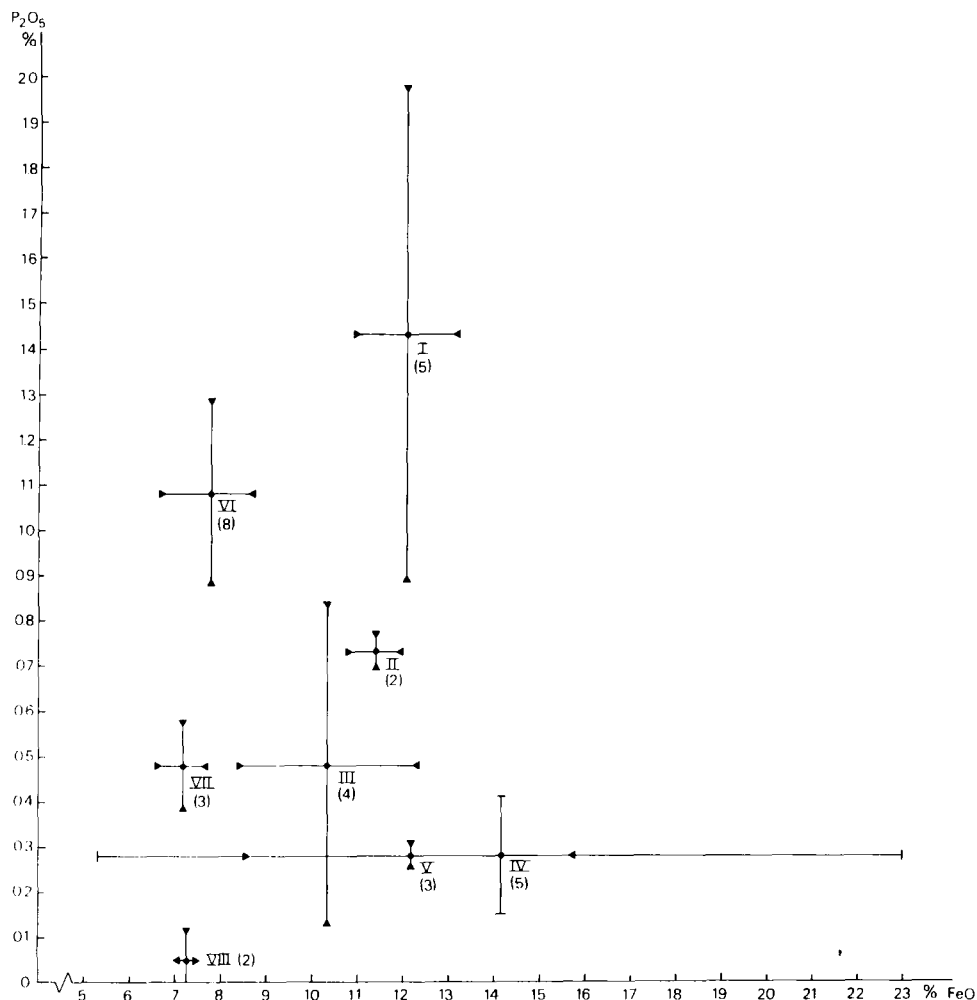


Fig. 9. Plot of P_2O_5 vs. FeO (see Fig. 7).

Compositions of the associated heavy- and light-mineral fractions

For the sake of completeness the mineral compositions of the heavy and light concentrates of the samples from which the composite particles have been studied, were established using the petrological microscope.

These results are summarized in Fig. 11 together with the weight percentages of the heavy concentrates. Only the mineral spectra of the 105–150 μm size fraction are presented, as the other sand-sized fractions show almost similar ratios in their spectra.

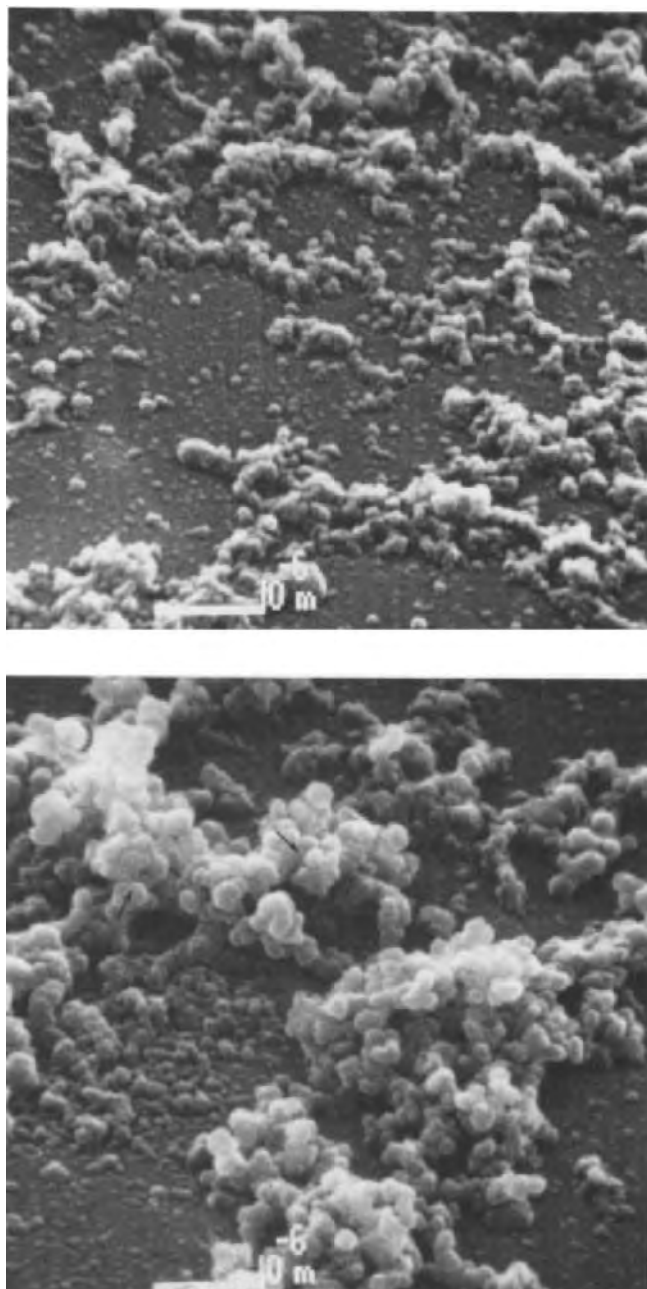


Fig. 10. Oblique (tilt 45°) scanning electron photomicrographs (SEM: Mark II Cambridge Instruments) of the $< 1 \mu\text{m}$ fraction obtained by ultrasonic treatment. In the upper part of the lower micrograph (use magnifying glass) many spheres show a regular arrangement of dagger-shaped protuberances.

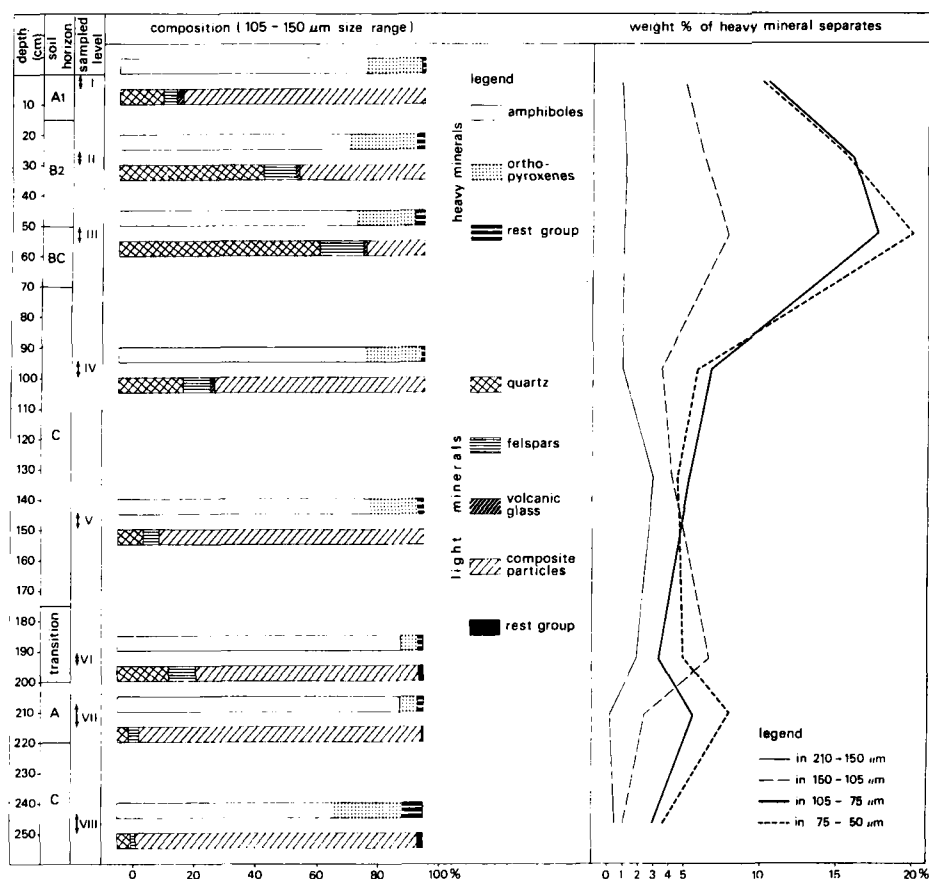


Fig. 11. Summary of various petrographic properties as a function of soil depth.

A discrimination of the sampled levels on the basis of the heavy-mineral composition is not possible. The change shown by the light-mineral compositions in level II and III coincides with a considerable increase of the heavy-mineral weight percentages.

DISCUSSION

Composite particle characteristics

The present observations support the initial supposition that they must be considered as artificially produced fragments of the three-dimensionally connected matrix of the present soil. Subrounded to rounded shapes observed may be co-produced by the peroxide treatment.

Theoretically, however, two "types" of composite particles might be expected to occur in the size fractions obtained from that part of the profile

above a depth of 156 cm: one representing the pedorelics recognized in the thin sections of the soil lumps, and another representing fresh fragments. However, due to the very heterogeneous nature of the composite particles, no reliable criteria for distinction in grain mounts could be defined.

The angular, optically inclusion-free specimens as found in level I (see Fig. 3), are probably artificially produced cutan fragments. In thin sections they exhibit occasionally light and dark banding. Spot analysis of these differently coloured bands in one single particle showed the dark band to contain more FeO and SiO₂ and less Al₂O₃ than the lighter coloured band. A similar correlation in chemical composition and colour depth is apparent when particles with a dark brown cement are compared with specimens having a yellowish brown cement.

Position and function of the amorphous component in the individual composite particles strongly suggest that their existence is exclusively due to this particular constituent. Hence, from a genetical point of view this component seems to be the most intriguing one.

The continuous reactivity of composite particles with H₂O₂ as observed under the microscope testifies that humic substances must form part of the amorphous cement. Very probably these substances have also played a role in its genesis. Because technical facilities to establish their nature and amount in surface areas of a few microns were not available, their possible contribution cannot be discussed.

The first solid phase, originating by precipitation from weathering solutions of primary volcanic minerals and the associated glass, is generally named allophane. This name is used to describe naturally occurring hydrous aluminosilicates ranging rather widely in composition. For its chemical characterization usually the SiO₂/Al₂O₃ molar ratio is applied.

Table II shows that these ratios observed in the isotropic cement vary between 0.49 and 2.08. These values seem to be in agreement with those reported in literature for allophane-like materials of clay sizes (Henmi and Wada, 1976). The question arises, however, whether comparison is completely justified. The latter ratios often have been determined in solutions containing the dissolved components from clays treated by dithionite-citrate (Mehra and Jackson, 1960), and by Na₂CO₃ (Wada and Greenland, 1970), and even in solutions containing completely dissolved clays (Henmi and Wada, 1976).

With exception of nickel, and perhaps sulphur and chlorine, the remaining elements (Table II) have frequently been reported as constituents of allophanes and allophane-like materials (see e.g. Hamblin and Greenland, 1972). The phosphate adsorption capacity of allophane is rather well-documented (see, e.g., Taylor and Wilson, 1979; Parfitt and Henmi, 1980).

Work done during the last decade reveals that allophane consists of morphologically similar particles (Kitagawa, 1971; Wada et al., 1972; Henmi and Wada, 1976; Wada and Wada, 1977; Shoji and Saigusa, 1977; Parfitt and Henmi, 1980, etc.). These particles appear as rings in high-resolution

electron micrographs and are three-dimensionally interpreted as hollow spherules with outside diameters of 35–50 Å.

The SEM observations (Fig. 10) show that the $< 1 \mu\text{m}$ particles separated by ultrasonic vibration from sand-sized composite particles also have predominantly a spherical shape, but the dimensions are considerably larger, approximately varying between 400 and 1000 Å. De Villiers and Jackson (1967) and Cloos et al. (1968, 1969) proposed a structural model of allophane with aluminosilicate cores of 50 Å, being covered with a complex form of hydroxy–aluminum cations. These coverings are thought to play an important role in the phosphate adsorption process. In view of the ability of allophane to adsorb acid organic material of high molecular weight from aqueous solutions (Taylor and Wilson, 1979) it is thinkable that this, to a certain degree, might result in larger dimensions of the spherules. Some of the individual clusters illustrate convincingly (see arrows in Fig. 10) the micromorphological model of allophane micro-aggregates proposed by Kitagawa (1971), only the composing spherules are much greater.

In summary, the data suggest that the amorphous cementing component of the composite particles is of allophane nature. Probably it originated from interstitial waters in surficial layers with dissolving volcanic glass and minerals. Indications pointing to separate phases in this segregation could optically not be recognized. Composition and nature of the parent glass fragments in particular (Kirkman and McHardy, 1980), but also relative proportions of glass and crystalline phases have undoubtedly been important controls in the cement formation. However, in view of the variations in single-element abundances, even in the restricted micro-environment of one level, the precipitation seems hardly to have followed a rigid scheme.

Abundance—depth relationships

Fig. 11 shows that, in terms of light-mineral compositions and in terms of weight percentages of the heavy minerals, the Guasca profile exhibits an evident zonal development. The presence and absence of pedorelics above and below the depth of 156 cm, also point to such a development.

Combining these data the following sedimentary history of the Guasca profile may be framed. A soil developed in volcanic ash (Fig. 11, level VIII and VII) has been covered by material also of volcanic origin. Initially this material came from close by (level VI), but later on, it arrived from other sources, or sources at greater distance because of the presence of “exotic” micropeds above a depth of 156 cm. These soil-derived relics have substantially contributed to this covering (level V and IV). In the further course of this accumulation another change in material occurred, indicated by an increase of the associated heavy-mineral weight percentages, and in the light-mineral fraction by an increase of quartz next to the appearance of minor amounts of volcanic glass (levels III and II). It might be possible that this change has been intensified by contemporaneous or subsequent

differentiation at the depositional surface. The final stage of accumulation is characterized by a decrease of quartz and heavy-mineral weight percentages (level I) and probably represents the present "in transit" surface layer.

It is surprising that this fourfold zonation (levels VIII, VII and VI, levels V and IV, levels III and II, and level I), running more or less concurrently with some soil-horizon boundaries, is confirmed by the chemical features of the allophanic cement in associated composite particles. Certain element abundances allow to recognize this zonation even in greater detail.

Fig. 6 illustrates that the third zone e.g. can be subdivided using the $\text{SiO}_2/\text{Al}_2\text{O}_3$ molar ratio. Corroborative evidence for this are the observed Ni abundances in level II (Table II). The plot of Fig. 7 illustrates the great lack of affinity in terms of silica between the first (levels VIII, VII and VI) and second zone (levels V and IV), suggesting that the allophanic constituent precipitated from different solutions or under completely different conditions.

Also the vertical variability of some minor-element abundances supports the phenomenon of a zonal arrangement. The average Mg content in level VIII is significantly lower than that in levels VII and VI (Fig. 8). This plot also shows that the average Ti abundance in level V is much higher than in level IV. Conspicuous are the high phosphorus abundances recorded in levels VI and I (Fig. 9).

Of vital importance, however, is the question whether the chemical stratification shown by the allophanic constituent of the composite particles at different depths, results from micro-environmental conditions governing at the various depths of the present soil column, or whether it is a reflection of the differences in material supplied.

As signs for cement segregation in distinctly different phases could not be detected, its formation from evaporating interstitial water by co-precipitation of silica and alumina creating Si—O—Al linkages, has to be considered as a continual process occurring as long as moisture is periodically supplied and easily weatherable mineral phases are available. In this view, the wide ranges of some element abundances (Al, Si, Fe, Mg, P and Ti) found at certain levels (see Table II and Figs. 7, 8 and 9) could be accounted for by variations in controlling conditions at a microscale resulting, within one level, in chemically varying cement compositions.

But the significantly different averages of element contents between the levels cannot so easily be explained. Neither can be ignored the agreement in zonal arrangement between the petrographic characteristics and the allophanic cement chemistry of the composite particles.

Hence, it seems that the vertical changes in cement chemistry of the composite particles measured, in the first place are related to the petrographical properties of the associated parent material. But undoubtedly they also reflect the influence of depth-dependent precipitation in the soil column, as is demonstrated by phosphorus (Fig. 9).

Without a systematic *in situ* microchemical analysis of the isotropic component in optically manifest pedorelics and in the adjacent S-matrix areas, it will not be possible to distinguish between the effects of these two contributing factors.

CONCLUDING REMARKS

The composite particles found in sand-sized fractions isolated from Colombian andosol material, constitute another illustration of the fact that dispersion of volcanic soil material and peptization of the associated clay might be a difficult process to effect in the laboratory. Hence grain-size distributions of such materials could be rather unreliable.

The persistency of the original fabric must also have consequences under natural conditions. Andosols on the Sabana de Bogotá have a low bulk density and consist in general for a great deal of water-stable peds being individual natural soil aggregates (Soil Survey Staff, 1951). When their parent materials are continuously moist, they form heavy, smeary clays. Upon drying, however, these peds originate which do not rehydrate easily. As a result these soils have a large storage capacity, which is probably the reason that they can form a protective cover in the landscape.

When these soils are destroyed by erosional processes, these peds and their fragments will initially constitute the erosional products. But in course of time, progressive diminution during transport along the land surface will produce finally sand- and silt-sized aggregates resembling composite particles. At a certain moment these units may even form the bulk of the erosional products.

Soil development in aggradational sites of such landscapes may consequently take place in parent materials rich in composite particles being actually fragments of previous soils. The upper part of the Guasca profile apparently demonstrates such a situation.

It is obvious that chemical parameters obtained by wet chemical analysis of bulk samples from the different horizons of such soils will be of little use for a better understanding of the pedogenetic and weathering processes in a particular site or area, nor will contribute significantly to the development of theories. This applies in particular when the composite particles arrived from several distant places, e.g. by aeolian transport.

The work done on the Guasca profile illustrates that the only way to collect relevant information in order to attack such problems successfully is a.o. a thorough microscopic fabric analysis followed by the use of a sub-microscopic technique for microchemical analysis (Bisdorf, 1981).

ACKNOWLEDGEMENTS

Financial support was supplied by the Netherlands Foundation for the Advancement of Tropical Research (WOTRO). Scanning electron microscope

facilities were provided by the Working Group SEM, University of Amsterdam and by TFDL, Department EM, Wageningen. Electron microprobe facilities were provided by the Free University, Amsterdam, and the WACOM, a working group for analytical geochemistry subsidized by the Netherlands Organization for the Advancement of Pure Research (ZWO).

The authors thank the following persons who assisted with the preparation of the manuscript: Mrs. O.M. Bergmeijer-de Vré, Mrs. M.C.G. Keijzer-v.d. Lubbe and Mr. C. van der Bliek.

REFERENCES

- Anonymous, 1969. Geological Map of Colombia, Sheet K-11, Zipaquira. Instituto Nacional de Investigaciones Geologico-Mineras.
- Bisdorn, E.B.A., 1981. A review of the application of submicroscopic techniques in soil micromorphology, I and II. In: E.B.A. Bisdorn (Editor), *Submicroscopy of Soils and Weathered Rocks*. Pudoc, Wageningen, pp. 67–162.
- Boekestein, A., Henstra, S. and Bisdorn, E.B.A., 1981. Submicroscopic techniques for in situ microchemical analysis of soils, I. Non-destructive techniques 1. In: E.B.A. Bisdorn (Editor), *Submicroscopy of Soils and Weathered Rocks*. Pudoc, Wageningen, pp. 29–44.
- Botero, P.J., 1972. Soils of Guasca-Guatavita (Colombia). Unpublished MSc thesis, Institute for Aerial Survey and Earth Sciences, Enschede.
- Cloos, P., Herbillon, A. and Echeverria, J., 1968. Allophane-like synthetic silico-aluminas. Phosphate adsorption and availability. *Trans. 9th Intern. Congr. Soil Sci.*, II: 733–743.
- Cloos, P., Léonard, A.J., Moreau, J.P., Herbillon, A. and Fripiat, J.J., 1969. Structural organization in amorphous silico-aluminas. *Clays Clay Miner.*, 17: 279–287.
- Correal Urrego, G. and Van der Hammen, T., 1977. Investigaciones Arqueológicas en los Abrigos rocosos del Tequendama. *Bibliotheca Banco Popular*.
- De Villiers, J.M. and Jackson, M.L., 1967. Cation exchange capacity variations with pH in soil clays. *Soil Sci. Soc. Am. Proc.*, 31: 473–476.
- Dueñas-J., H., 1977. Estudio palinológico de los 35 mts. superiores de la sección Targona, Sabana de Bogotá. *Caldasia*, 12: 539–571.
- Hamblin, A.P. and Greenland, D.J., 1972. Mineralogy of soils from the Holocene volcanic areas of southern Australia. *Aust. J. Soil Res.*, 10: 61–79.
- Henmi, T. and Wada, K., 1976. Morphology and composition of allophane. *Am. Mineral.*, 61: 379–390.
- Kirkman, J.H. and McHardy, W.J., 1980. A comparative study of the morphology, chemical composition and weathering of rhyolitic and andesitic glass. *Clay Miner.*, 15: 165–173.
- Kitagawa, Y., 1971. The “unit-particle” of allophane. *Am. Miner.*, 56: 465–475.
- Mehra, O.P. and Jackson, M.L., 1960. Iron oxide removal from soils and clays by a dithionite-citrate system with sodium bicarbonate buffer. *Clays Clay Miner.*, 7: 307–327.
- Mohr, E.C.T. and Van Baren, 1954. *Tropical Soils*. Van Hoeve, The Hague, Bandung — Interscience Publishers, London, New York, 498 pp.
- Parfitt, R.L. and Henmi, T., 1980. Structure of some allophanes from New Zealand. *Clays Clay Miner.*, 28: 285–294.
- Riezebos, P.A., 1978. Petrographic aspects of a sequence of Quaternary volcanic ashes from the Laguna de Fuquene area, Colombia, and their stratigraphic significance. *Quaternary Res.*, 10: 401–424.

- Shoji, S. and Saigusa, M., 1977. Amorphous clay materials in Towada Ando soil. *Soil Sci. Plant Nutr.*, 23: 437–455.
- Soil Survey Staff, 1951. *Soil Survey Manual. Handbook 18.* U.S. Dept. of Agriculture, Wash., D.C., 503 pp.
- Taylor, D.H. and Wilson, A.T., 1979. The adsorption of yeast RNA by allophane. *Clays Clay Miner.*, 27: 261–268.
- Van Geel, B. and Van der Hammen, T., 1973. Upper Quaternary vegetational and climatic sequence of the Fuquene area (Eastern Cordillera, Colombia). *Palaeogeogr., Palaeoclimatol., Palaeoecol.*, 14: 9–92.
- Van der Hammen, T., 1963. Historia de clima y vegetación del Pleistoceno superior y del Holoceno de la Sabana de Bogotá. *Bol. Geol.*, 11: 189–226.
- Van der Hammen, T., 1978. Stratigraphy and environments of the Upper Quaternary of the El Abra corridor and rock shelters (Colombia). *Palaeogeogr., Palaeoclimatol., Palaeoecol.*, 25: 111–162.
- Van der Hammen, T., Werner, J.H. and Van Dommelen, H., 1973. Palynological record of the upheaval of the Northern Andes: a study of the Pliocene and lower Quaternary of the Colombian Eastern Cordillera and the early evolution of its high-andean biota. *Res. Palaeobot. Palynol.*, 16: 1–22.
- Wada, K. and Greenland, D.J., 1970. Selective dissolution and differential infrared spectroscopy for characterization of “amorphous” constituents in soil clays. *Clay Miner.*, 8: 241–254.
- Wada, S. and Wada, K., 1977. Density and structure of allophane. *Clay Miner.*, 12: 289–298.
- Wada, K., Henmi, T., Yoshinaga, N. and Patterson, S.H., 1972. Imogolite and allophane formed in saprolite of basalt on Maui, Hawaii. *Clays Clay Miner.*, 20: 375–380.

This Page Intentionally Left Blank

SEM-EDXRA INVESTIGATION OF TUBULAR FEATURES AND IRON NODULES IN LATERITIC SOILS FROM MALAYSIA

S. ZAUYAH and E.B.A. BISDOM

Soil Science Department, University Pertanian, Serdang, Selangor (Malaysia)

Netherlands Soil Survey Institute, P.O. Box 98, 6700 AB Wageningen (The Netherlands)

(Accepted for publication February 17, 1983)

ABSTRACT

Zauyah, S. and Bisdom, E.B.A., 1983. SEM—EDXRA investigation of tubular features and iron nodules in lateritic soils from Malaysia. *Geoderma*, 30: 219–232.

Tubular features were observed with SEM in unhardened pieces of iron nodules found in some lateritic soils of Malaysia. EDXRA measurements demonstrated that the tubes were coated with predominantly Fe and Al. They probably represent mycelia encrusted as a result of lateritization or ferrallitization processes.

The iron nodules frequently exhibited fluidal structures in backscattered electron scanning images. White areas in the images contained most iron, whilst grey areas of the nodules were composed of predominantly Al, Si, K and Fe, similar to the composition of the soil matrix surrounding the iron nodules. The nodules are interpreted as having formed in clayey material most of which is still present in these features.

INTRODUCTION

Iron nodules are common in many soils of Malaysia. If a soil horizon with such nodules is more than 25 cm thick, the soil is classified as lateritic (Zauyah, 1982). The profile from which the samples under study were taken is situated on a very gentle slope in rolling to undulating terrain. The material in which the soil formed is interpreted as colluvial. Its age is unknown but the soil can be classified as a clayey, oxidic isohypothermic Tropeptic Haplarthox. The horizon in which the nodules with the tubes occur is the B22cn. The profile is well drained, and rubber trees are growing on it.

Loose unimpregnated pieces of these nodules were studied by S. Zauyah with a SEM (scanning electron microscope) and by Miss M. Lai of the electron microscope department of the Pertanian University of Malaysia. Small tubes that often formed a network in pores or at fracture surfaces were detected. Because no EDXRA (energy dispersive X-ray analysis) system was available with the SEM, some loose samples of tube-containing iron nodules were forwarded to E.B.A. Bisdom for microchemical analysis with SEM-EDXRA.

The present study also concerns SEM-EDXRA investigation of plastic-

impregnated polished blocks containing iron nodules embedded in the soil matrix. Various point analyses were made inside the iron nodules and in the soil matrix surrounding them. A considerable number of micrographs were necessary to document and illustrate the matters discussed in this paper.

MATERIALS AND METHODS

Loose unimpregnated pieces of iron nodules and the surfaces of plastic-impregnated nodules were studied with a Jeol-JSM-35C equipped with an EDAX 9100 system with an ECON windowless detector for the detection of chemical elements. This instrument is a follow-up of the Jeol-JSM-U3 scanning electron microscope (SEM) with an EDAX system that consisted of a Si (Li) detector with a 707A-type multichannel analyzer (Henstra et al., 1973; Bisdorf et al., 1975, 1976).

The present study also uses the backscattered electron method (Robinson and Nickel, 1979; Bisdorf and Thiel, 1981). The BE detector used in the Jeol-JSM-35C is of the semiconductor type and comprises two solid state detectors. Details of this technique are given by Bisdorf and Thiel (1981) and also in this second issue of the work of IWGSUSM (International Working-Group on Submicroscopy of Undisturbed Soil Materials). It is important to note that high quality backscattered electron scanning images (BESI) can now be made, and that this technique allows visual detection of some differences in chemical composition between the heavier chemical elements of the images; for example, iron and calcium usually are whitish on BESI, whereas Al and Si are greyish on the micrographs. Such differences in chemical compositions on BESI are subsequently checked with X-ray images and point analyses.

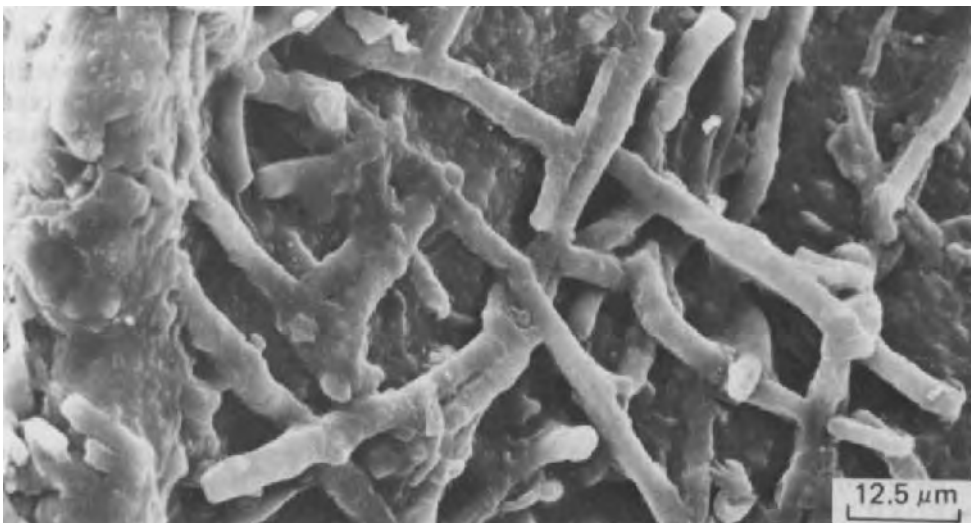


Fig. 1. A network of tubular features, interpreted as mycelia, with a predominantly smooth surface inside an iron nodule.

RESULTS

Tubular features and iron-containing minerals in unhardened iron nodules

Tubular features and iron-containing minerals were studied in unimpregnated iron nodules with SEM-EDXRA. The tubes often formed a network (Fig. 1) inside pores of the iron nodules or on fracture surfaces. SEM demonstrated that the length of the tubes ranged from about 15 μm to about 70 μm , with diameters between 3 and 4 μm . However, exceptions to these figures are rather common because of various degrees of encrustation of the tubes. Both hollow and partly or wholly filled tubes were found.

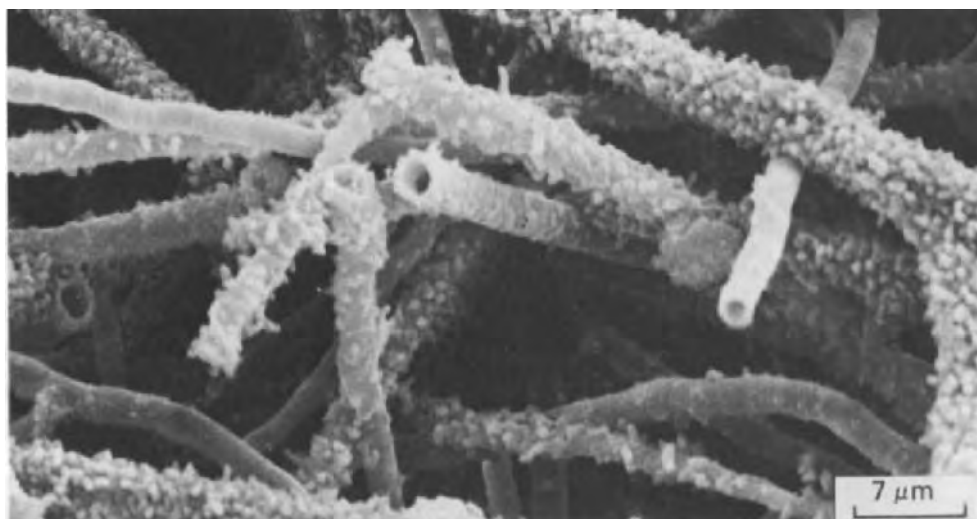


Fig. 2. Small tubes with a rough surface caused by growth of small particles inside an iron nodule.

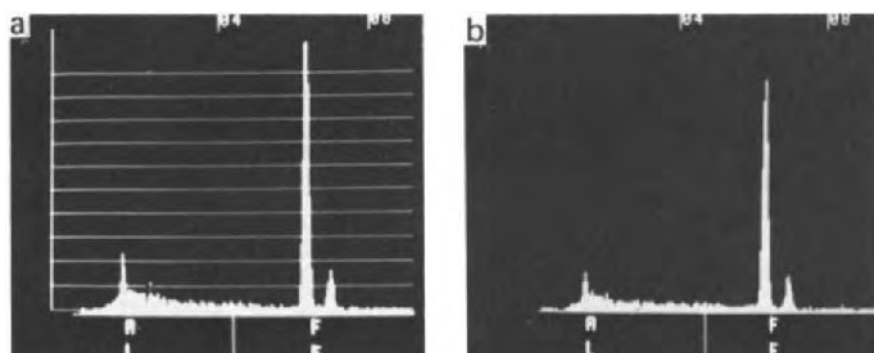


Fig. 3. Point analyses (a and b) showing that Fe and Al are the main constituents of the walls of the small tubes in the iron nodules.

Some of the tubes had a smooth surface (Fig. 1) whereas others were rough because of very small particles attached to the smooth subsurface (Fig. 2). EDXRA measurements indicated that Fe and Al are usually present in the wall of the tubes (Fig. 3). Very small amounts of Si were found especially in point analyses of tubes with an unfavourable position in the SEM for EDXRA analysis, and were probably due to contamination. Often, even when care was taken to position the tubes well for measurement, no Si was recorded.

Goethite (Fig. 4) and hematite (Fig. 5) were present in a number of pores

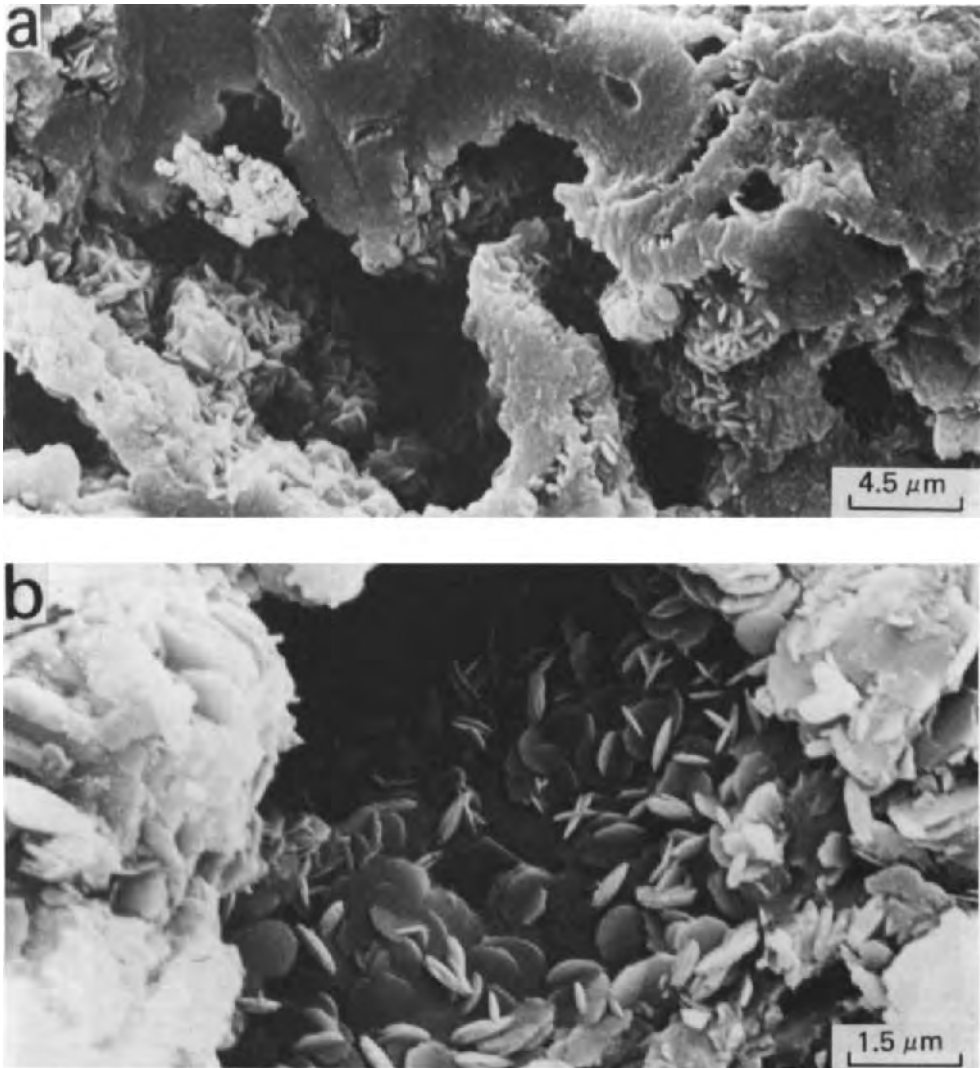


Fig. 4. Lenticular goethite crystals in voids of an iron nodule (a) and goethite in a void at a higher magnification (b).

of the iron nodules. Acicular goethite (Fig. 6) could form cutans (goethans) on the walls of pores, and form a substrate for a network of tubes (Fig. 7) in some cases. Similar micrographs as given in Figs. 4–6 were published by Eswaran et al. (1978) for soils of Malaysia and Zaire.

When not only the vicinity of pores is studied with SEM-EDXRA but the area in between as well, it soon becomes evident that networks of encrusted tubular features can be found here also. In various micro-areas, all the porosity in between the tubular features is gone. EDXRA measurements in these areas give: Fe; Fe plus Al; or Fe, Al, Si and K. Ti was also found locally.

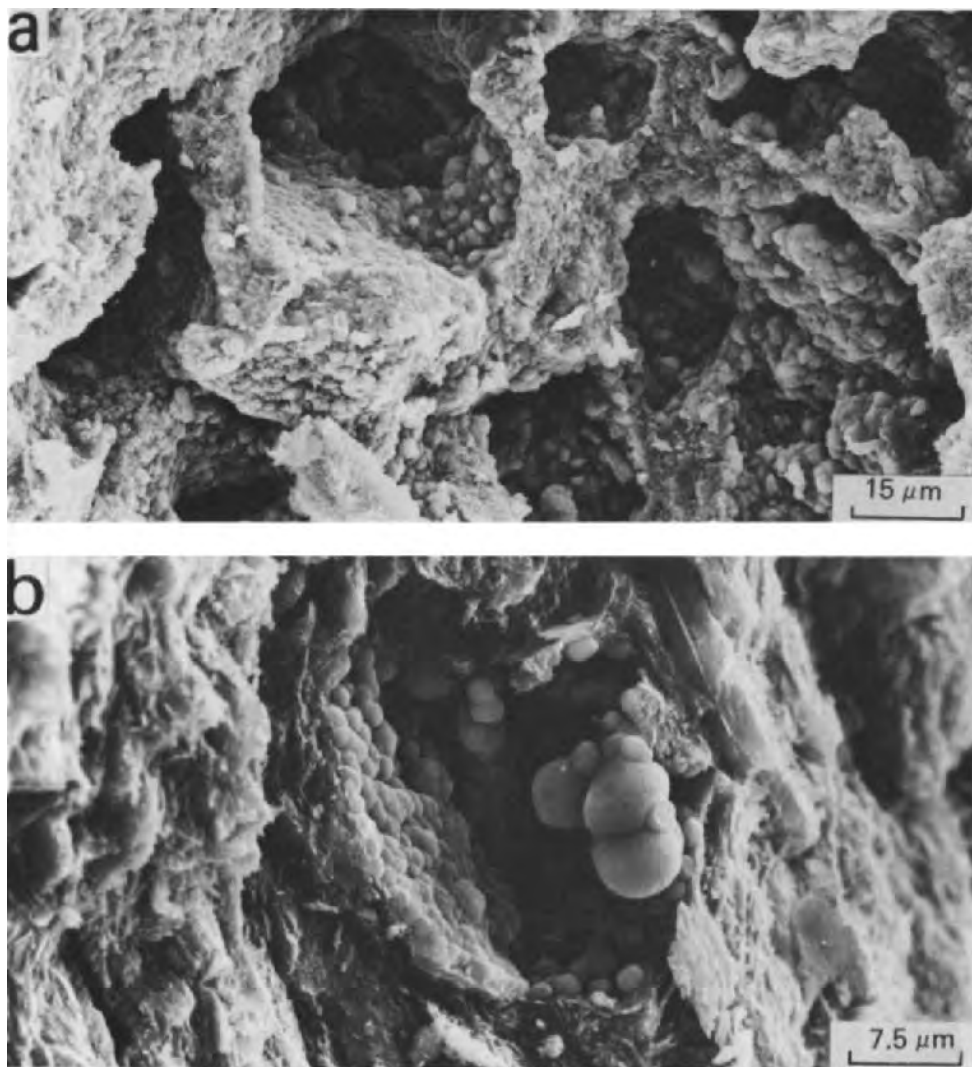


Fig. 5. Rounded grains of hematite (a) in voids of an iron nodule, and hematite in a void at a higher magnification (b).

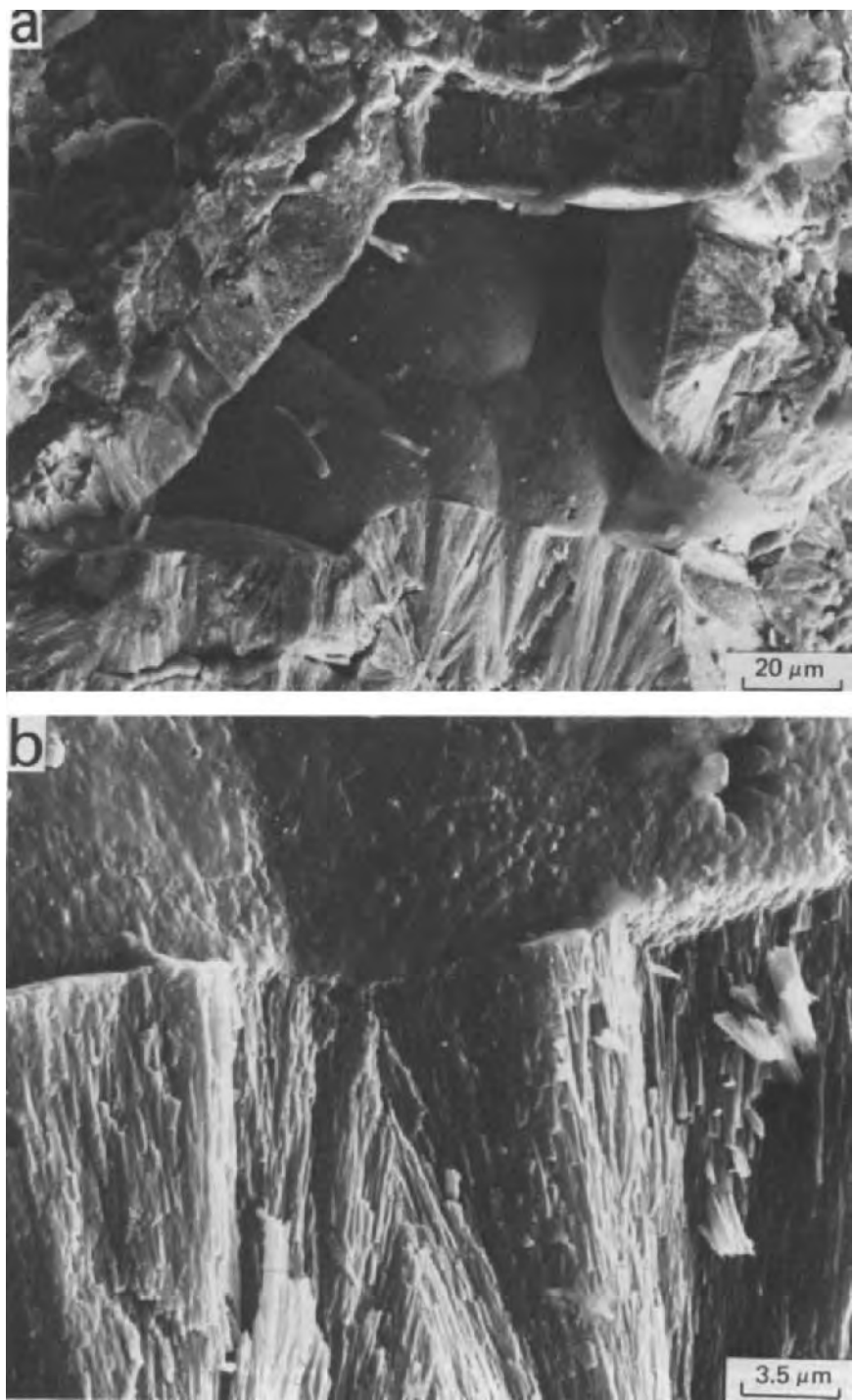


Fig. 6. Acicular goethite in a goethan (a), and detail of the goethan (b).

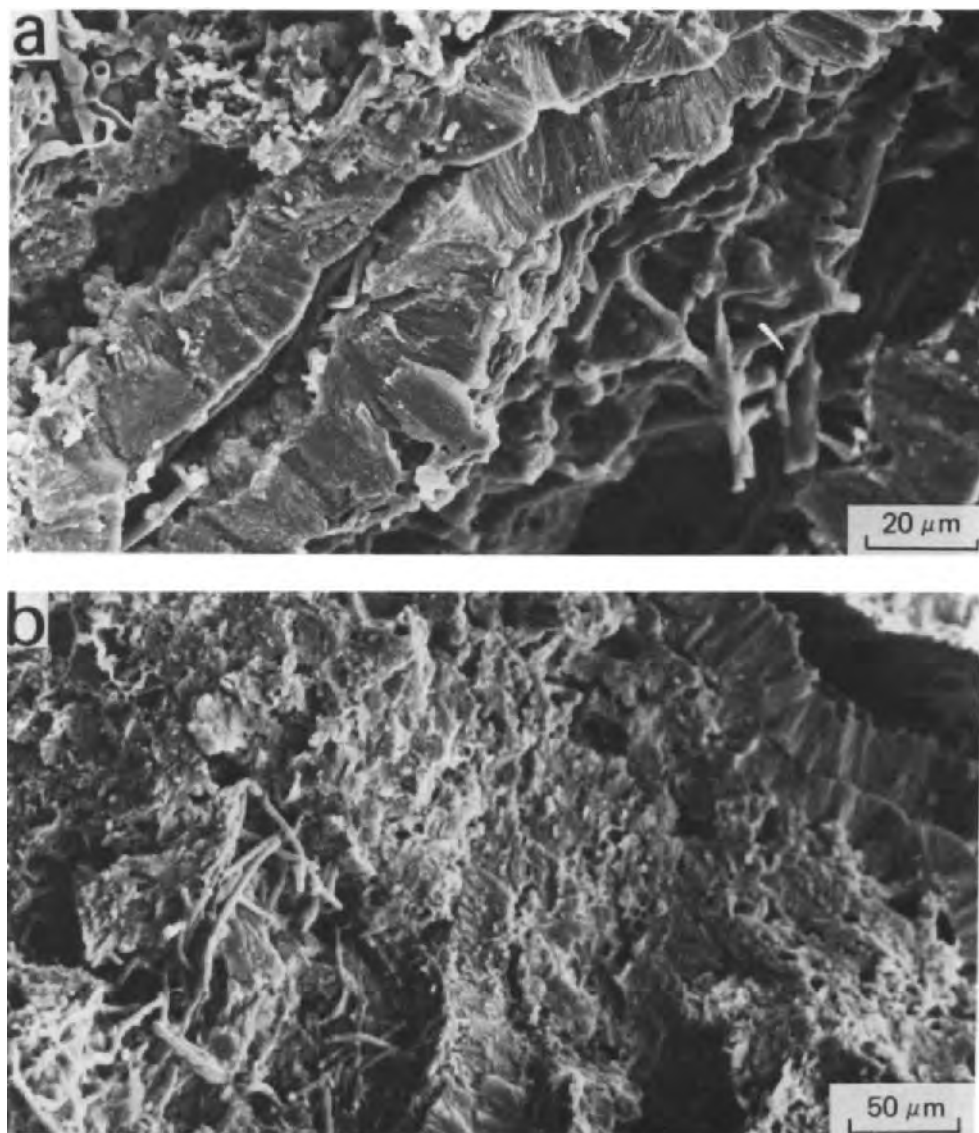
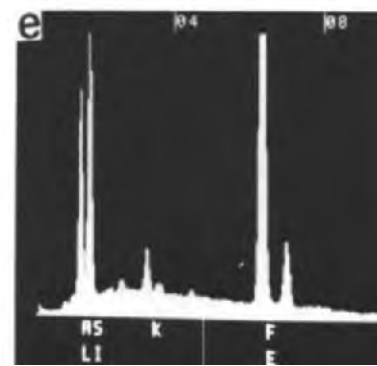
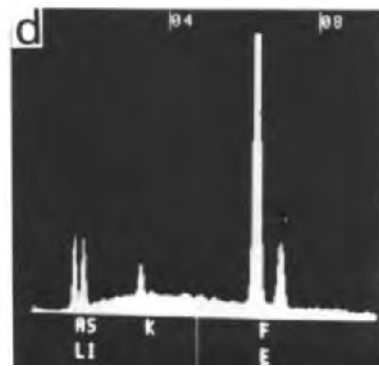
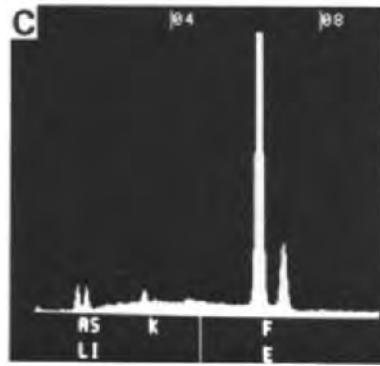
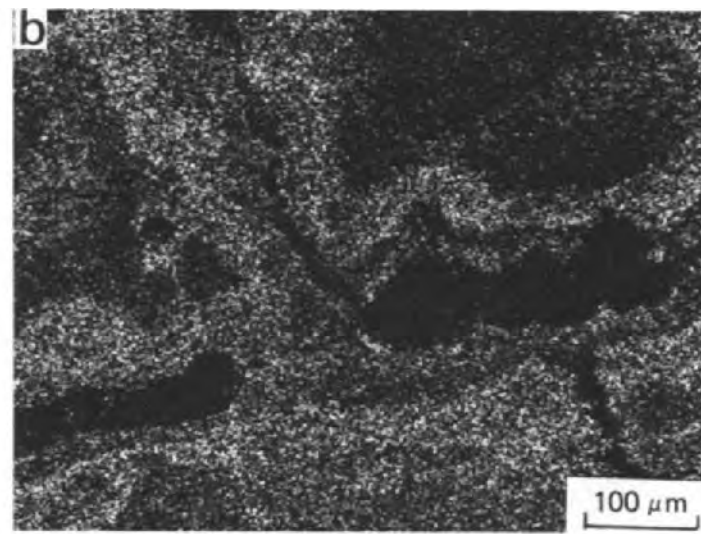
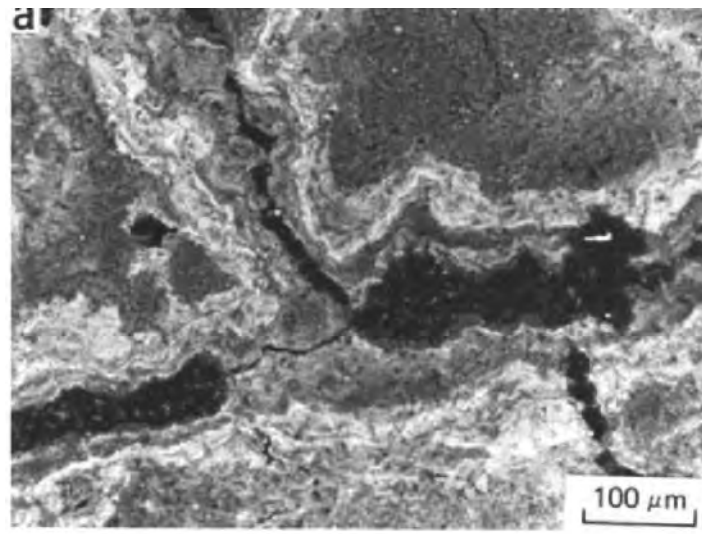


Fig. 7. Acicular goethite of a goethan in an iron nodule with a superimposed network of small tubes (a), and a view showing a complex of goethans and tubular features (b).

Such measurements probably indicate a combination of encrusted tubes and tubes situated in a clayey soil matrix with considerable iron and some extra aluminium. The clay in the iron nodules was found by XRD techniques to be predominantly kaolinite.



Fluidal structures in iron nodules of plastic-hardened polished blocks

Backscattered electron scanning images (BESI) of iron nodules in plastic-hardened polished blocks demonstrated fluidal structures around pores and in the matrix of the nodules (Figs. 8, 9). The whitish colour on BESI is given

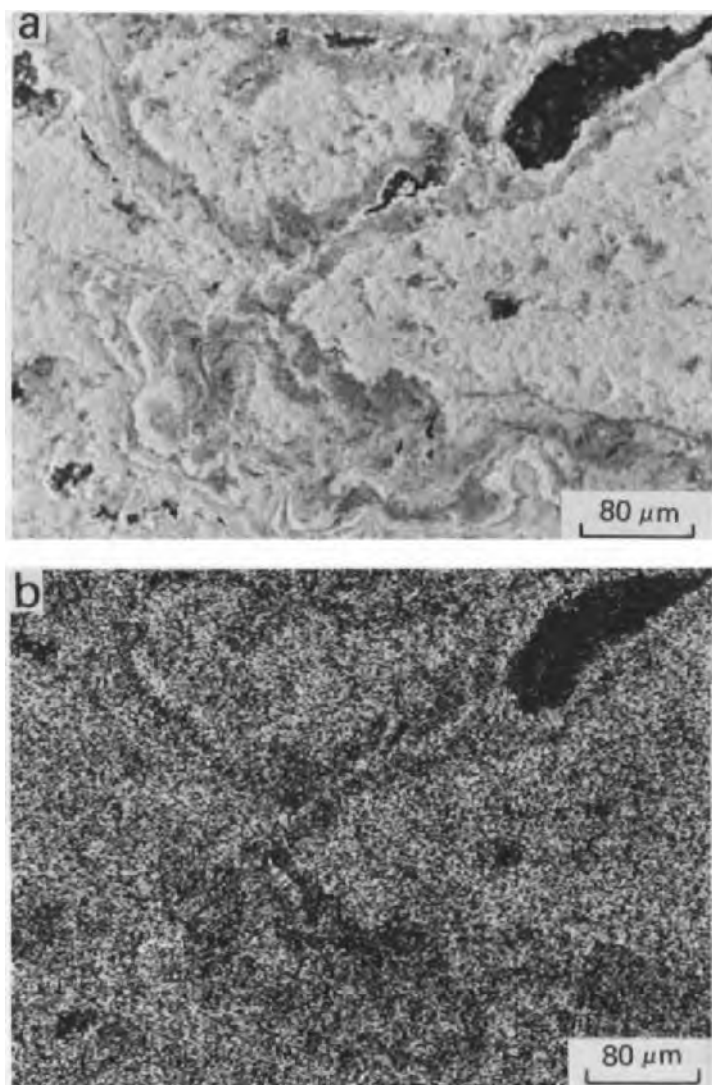


Fig. 9. Fluidal structure in the matrix of an iron nodule (a), and X-ray image of Fe (b).

Fig. 8. Fluidal structure mainly associated with the wall of pores in an iron nodule (a), and X-ray image of Fe (b). Point analyses of a whitish area (c), of an intermediately coloured area with more Al and Si (d), and of a greyish area (e) with the least Fe. An explanation for the height of the Fe peaks is given in the text.

by areas with considerable Fe and only small amounts of Al and Si, according to X-ray images and point analyses (Fig. 10). The greyish areas contain much more Al and Si, and less iron.

If point analyses of the greyish areas in the iron nodules are compared with point analyses of the soil matrix which surrounds the nodules (Fig. 11), a similarity in measurements is evident. Small areas with a higher Fe content are also present in the soil matrix. Titanium is also found in a number of micro-areas.

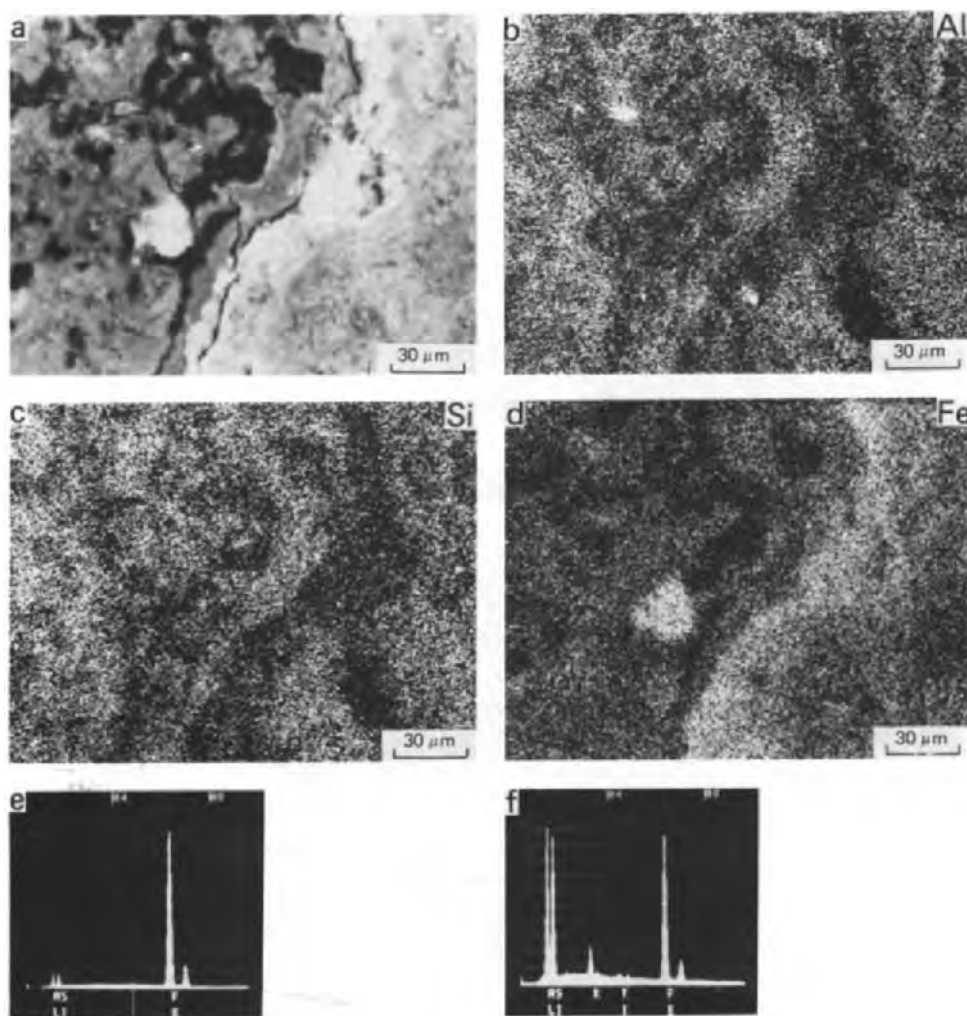


Fig. 10. View of a micro-area in an iron nodule (a). Most of the iron is present in the whitish sites and most of the clay in the greyish sites. X-ray images of Al (b), Si (c) and Fe (d). Point analyses of the whitish area with most Fe (e) and the greyish area with more Al and Si (f).

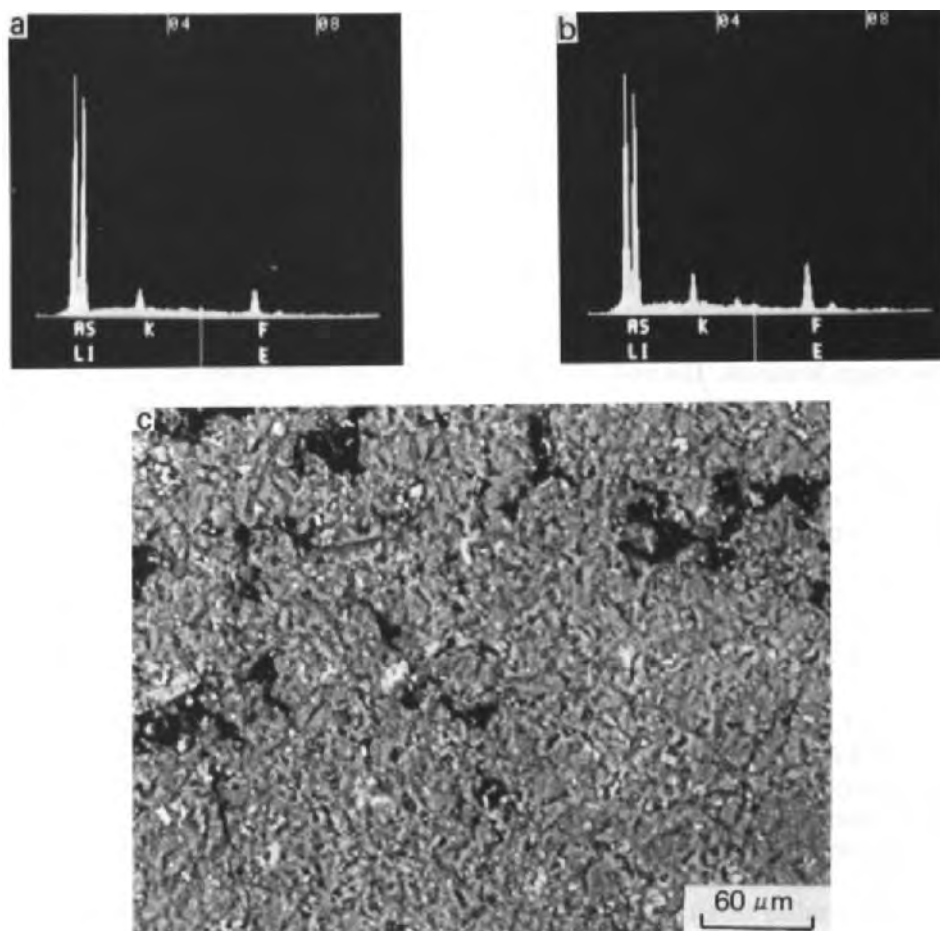


Fig. 11. Point analyses (a and b) of the clay in the soil matrix (c). Al and Si peaks are virtually of the same height and similar in configuration and height to those measured in the greyish area (Fig. 10f) of the iron nodule.

DISCUSSION AND CONCLUSIONS

Tubular features

The tubular features of Figs. 1 and 2 were observed at various magnifications with SEM, and analysed by EDXRA. Interpretation of the tubular features leads to mycelia or fungal hyphae. The composition of the wall of the tubes, i.e. Fe and Al (Fig. 3), and the overall morphology of the network of tubular features, indicate encrustation of the mycelia. This means that a kind of fossilization affected the original fungal hyphae whereby both Fe and Al were deposited. Such a process, in which Si is leached and Fe and Al stay in the profile, is called lateritization or ferrallitization.

The loose iron nodules, which were not hardened with plastic, also demonstrate that Fe can accumulate without Al in the pores (Figs. 4–6), viz. as goethite and hematite. Consequently, processes giving only iron accumulation and those giving both iron and aluminium accumulation were documented to have occurred in the same iron nodule. Apart from physico-chemical reasoning, the relative abundance of Fe with respect to Al may have played a role.

Iron nodules

When the iron nodules are studied in the field with the unaided eye or at low magnifications, the red colour often gives an impression of a homogeneous structure of the nodules. Light microscopy and SEM-EDXRA analysis show, however, that the iron nodules are in reality heterogeneous and have various internal fabrics. Fluidal structures (Figs. 8, 9) and bands of soil materials with different colours (Figs. 8–10) are present in BESI and give a rather complicated picture, the origin of which is not yet completely understood.

Whitish colours in the micrographs are given by accumulations of Fe together with some Al and Si (Figs. 8c and 10e). The greyish areas contain less Fe and more Al and Si (Figs. 8e and 10f). Attention was primarily given to peaks of Al and Si in the point analyses. This was done on a scale whereby the much larger quantities of iron remained at a maximum and showed no visible differences. However, if the vertical scale is changed, or the counts per second for iron are read, the differences in iron content of the analysed points become clear.

A striking feature of the Al and Si peaks in the whitish, greyish and intermediate areas is the equality of height of both peaks. The configuration remains similar in all micro-areas of the iron nodule, although the height is largest for the peaks in the greyish areas and smallest in the iron-containing whitish parts of BESI. When point analyses are made of clayey material which surrounds the iron nodules, similar peaks to the ones in the greyish areas of the iron nodule are obtained (Fig. 11). The interpretation is therefore that the iron nodules were formed in clayey material, most of which is still present, even though affected by weathering processes.

The hypothesis that the kaolinitic clayey material is weathered in and outside the nodules is based on the described equal peak height of Al and Si. This is too high for Al, which, according to experience with SEM-EDXRA measurements on clays in various soils, should be about half that of the peak for Si. Of course, individual clay minerals require TEM (transmission electron microscope) or STEM (scanning transmission electron microscope) analysis for determination at magnifications larger than the $\times 10,000$ possible with SEM-EDXRA. For the moment, however, we may assume that too much Al has been measured in numerous points of the soil matrix and the iron nodules. This could indicate that relative accumulation of Al has occurred and that Si was leached during the weathering of predominantly kaolinitic clay.

Titanium was measured with EDXRA in some micro-areas and is usually an element which is relatively difficult to leach. Potassium was very often measured in point analyses other than those in accumulations of iron minerals and in the crusts of the mycelia. The element is much too common for this lateritic soil, on which rubber trees have been planted. The occurrence of K is therefore explained as a leaching product of fertilizer which has accumulated in the soil profile.

The iron nodules which have been analysed are found in soil material which according to field observation may have colluviated. It is possible that a few of the iron nodules may have been formed before emplacement in the present position. However, in the main, lateritization processes were probably occurring in the soils before colluviation, as they do in the present profiles. The encrustation of the tubular features, which are relatively rare in the studied profiles, probably occurred nearer to the surface before colluviation brought the iron nodules to the present and deeper position in the B22cn horizon. Indications are, however, that encrustation of mycelia or fungal hyphae is also possible in the lateritic soils of today because Fe and Al are still accumulating and Si is leached after weathering of the kaolinitic clay in and outside the iron nodules.

The submicroscopic study of these lateritic soils can be improved considerably if, besides electron microscopy, trace elements could be studied with ion microscopy or laser analysis (Bisdom, 1981). The present rather rough measurements, due to the presence of very small particles in the studied soil material, indicate, however, that in situ microchemical information may help to unravel the processes which occur during lateritization, and to relate the measurements to XRD and wet chemical analyses of pre-treated loose samples.

ACKNOWLEDGEMENTS

The first author thanks the Pertanian University of Malaysia for financial support of part of this study.

REFERENCES

- Bisdom, E.B.A., 1981. A review of the application of submicroscopic techniques in soil micromorphology, II. Electron microprobe analyzer (EMA), scanning electron microscope-energy dispersive X-ray analyzer (SEM-EDXRA), laser microprobe mass analyzer (LAMMA 500), electron spectroscopy for chemical analysis (ESCA), ion microprobe mass analyzer (IMMA), and the secondary ion microscope (SIM). In: E.B.A. Bisdom (Editor), *Submicroscopy of Soils and Weathered Rocks*. 1st Workshop of the International Working-Group on Submicroscopy of Undisturbed Soil Materials (IWGSUSM) 1980, Wageningen. Centre for Agricultural Publishing and Documentation (Pudoc), Wageningen, pp. 117–162.
- Bisdom, E.B.A. and Thiel, F., 1981. Backscattered electron scanning images of porosities in thin sections of soils, weathered rocks and oil-gas reservoir rocks using SEM-EDXRA. In: E.B.A. Bisdom (Editor), *Submicroscopy of Soils and Weathered Rocks*.

- 1st Workshop of the International Working-Group on Submicroscopy of Undisturbed Soil Materials (IWGSUSM) 1980, Wageningen. Centre for Agricultural Publishing and Documentation (Pudoc), Wageningen, pp. 191–206.
- Bisdorn, E.B.A., Henstra, S., Jongerius, A. and Thiel, F., 1975. Energy-dispersive X-ray analysis on thin sections and unimpregnated soil material. *Neth. J. Agric. Sci.*, 23(4): 113–125.
- Bisdorn, E.B.A., Henstra, S., Hornsvelt, E.M., Jongerius, A. and Letsch, A.C., 1976. Wavelength and energy-dispersive X-ray microanalysis with EMA and SEM-EDXRA on thin sections of soils. *Neth. J. Agric. Sci.*, 24(4): 209–222.
- Eswaren, H., Lim, C., Sooryanarayana, V. and Nordin, D., 1978. Scanning electron microscopy of secondary minerals in Fe-Mn glaebules. In: M. Delgado (Editor), *Soil Micromorphology. Proceedings of the 5th International Working Meeting on Soil Micromorphology*, 1980, University of Granada, pp. 851–885.
- Henstra, S., Bisdorn, E.B.A., Jongerius, A. and Thiel, F., 1973. Energy-dispersive analysis on thin sections of soils. First EDAX European users meeting (Liège, September, 1973). *EDAX Editor*, 3(1): 5–6.
- Robinson, B.W. and Nickel, E.H., 1979. A useful new technique for mineralogy: the backscattered-electron/low vacuum mode of SEM operation. *Am. Mineral.*, 64: 1322–1328.
- Zaayah, S., 1982. Micromorphology of some lateritic soils in Malaysia. In: *6th International Working Meeting on Soil Micromorphology*, 1981, London. In press.

FABRIC SEQUENCES AS RELATED TO GENETIC PROCESSES IN TWO ALBERTA SOILS

S. PAWLUK

Department of Soil Science, University of Alberta, Edmonton, Alta. (Canada)

(Accepted for publication February 17, 1983)

ABSTRACT

Pawluk, S., 1983. Fabric sequences as related to genetic processes in two Alberta soils. *Geoderma*, 30: 233–242.

Terminology based on fabric sequences as proposed recently by Brewer (1979) was found useful for describing microfabrics in Alberta soils since it established a basis of study compatible with field morphological descriptions. The recognized fabric sequences were: granic, fragmic, chlamydic, and iunctic. Each sequence represented a continuum of fabric types distinguished on the basis of related distribution between fine and coarse materials.

Attempts have been made to unify specific fabric types within each of the sequences on the basis of material composition and genetic processes. Since soil horizons were pedogenically generated as well, they in turn could usually be characterized by a single dominant fabric sequence. In our studies we found the granic sequence of fabric to characterize mull layers. The fragmic fabric sequence was more common in subsurface horizons of fine texture. The chlamydic fabric sequence was best developed in spodic and argillic horizons of coarse texture. A well developed iunctic sequence was found in moder as well as in coarse textured highly calcareous horizons. Fabric types within each of the recognized sequences were highly variable in time and/or space within their respective horizons.

INTRODUCTION

A problem frequently experienced in micromorphology has been the demonstration of its usefulness for gathering information applicable to other disciplines within the field of soil science. This paper is concerned with its applicability to pedogenetic studies.

Advantage is taken of recent emphasis placed on related distribution between fine and coarse material for describing spatial arrangement in soil fabrics. Brewer (1977) introduced the terms “f-member” and “f-matrix” to explain related distribution between these kinds of material. He defined “f-members” as recognizable entities that may be simple or compound but that occurred as discrete units. In some cases “f-members” were observed to have a particular relationship with finer material referred to as “f-matrix”.

Based on such relationships Brewer, in 1979, introduced terminology for four principal sequences of fabric description, each representing a continuum of fabric types. These were: granic*¹ (granic-granoidic-granoidic porphyric-porphyric); fragmic *² (fragmic-fragmoidic-fragmoidic porphyric-porphyric); chlamydic *³ (orthogranic-chlamydic-plectic-plectic porphyric-porphyric); and iunctic*⁴ (orthogranic-iunctic-iunctic porphyric-porphyric). In many respects this terminology represents an approach similar to that originally proposed by Stoops and Jongerius (1975). In all four sequences, fabric of the porphyric type was shown to dominate as contact among f-members and between f-members and f-matrix increased to a point where f-members appeared to be embedded in the f-matrix.

Terminology based on fabric sequences has proved to be exceedingly useful for describing microfabrics of soils in the Alberta (Canada) region. It provided a basis for study readily compatible with field morphological investigations and permitted a broadening in the range of generalization in fabric description. Furthermore, the fabric types within each of the defined sequences were found to be genetically related and since soil horizons were similarly pedogenically generated, each defined soil horizon was characterized by a single dominant fabric sequence. Thus, it was possible to consider the fabric sequence as a genetically related, single, identifiable characteristic of the soil horizon. When greater detail required recognition of specific zones of fabric type within a soil horizon or subhorizon, the dominance of each fabric type within a specified sequence was considered for further subdivision.

FABRIC SEQUENCES AND SOIL DYNAMICS

Analytical approach

Fabrics were generally dynamic and fabric types readily changed within their respective sequences in response to soil processes and environmental forces. Therefore the detailed characterization of fabric type within sequences included an evaluation within the complete framework of a dynamic soil system and transient tendencies in response to pedogenic forces.

In order to study the dynamic relationships within fabric sequences, it proved useful to monitor a number of site parameters for assessing the mechanisms involved. The dynamic properties monitored were as follows: (1) seasonal soil moisture and heat fluxes; (2) seasonal variability in biological populations and their activity; (3) transport of suspended and dis-

*¹ Discrete unaccommodated simple or compound units of plasma and skeleton grains including pedological features; shows variable packing or coalescence.

*² Discrete accommodated or partially accommodated compound units including pedological features; shows variable packing or coalescence.

*³ Coatings of f-matrix on f-members with variable coalescence to form "bridges".

*⁴ F-matrix shows variable packing in spaces between adjacent f-members.

solved solids with the aid of field gravity lysimeters and canopy collectors; (4) seasonal groundwater flow patterns and water table fluctuations; (5) seasonal changes in pH, redox and pore water salt concentrations; (6) micromorphological changes in fabric type within soil material and parent material cores embedded at different depths in the pedon (used for monitoring pedogenic trends).

The static characteristics and properties recorded were as follows: (1) morphological features; (2) physical, chemical, and mineralogical attributes (3) micromorphological features using microscopic and submicroscopic techniques, using EMA (electron microprobe analyzer), SEM-EDXRA (scanning electron microscope-energy dispersive X-ray analyzer) and XRD (microcamera).

Two fabric sequences, with appropriate model examples are used to demonstrate the relationships that were observed between fabric types and observed dynamics in two Alberta soils. Sampling was carried out in spring, summer and autumn where control for seasonal variability was desired. Soil monoliths ($7 \times 7 \times 80$ cm) were collected and used for the preparation of a continuous array of 5×7 cm thin sections.

Mullgranic sequence

The soil pedon depicted in Fig.1a was representative of the Typic Cryochrept from an alpine site in the Sunshine Basin, Banff, Alberta. The A1 horizon provided an excellent example of the granic sequence found in soils with mull surface layers. In this case it was referred to as the mullgranic sequence. The mullgranic fabric type (Fig. 1b) was readily identifiable within this sequence. The units were largely compound, discrete, packed loosely and comprised of intimately associated organic and mineral matter. Some fecal pellets were also present. These were the f-members; there was no f-matrix present. Zones of mullgranoidic fabric type (Fig. 1c) were also evident. The mull f-members were more closely packed and were partially coalesced. Where strong coalescence between f-members was observed the fabric type approached a vughy porphyric and was considered to be a mullgranoidic porphyric intergrade (Fig. 1d). In some zones distinct compound units were no longer discernable but the forms of coalesced units were generally evident within the f-matrix; this was identified as porphyric fabric (Fig. 1e).

The mullgranic sequence in A1 horizons of Alberta soils had variable expression of fabric types. The proportion of each fabric type and its degree of expression varied seasonally during which time one fabric type could be altered to another within the same sequence. Depending on processes marked shifts in dominance of fabric type had been observed according to the following:

mullgranic \rightleftharpoons mullgranoidic \rightleftharpoons mullgranoidic porphyric \rightleftharpoons porphyric

A number of factors were implicated in these changes and could result

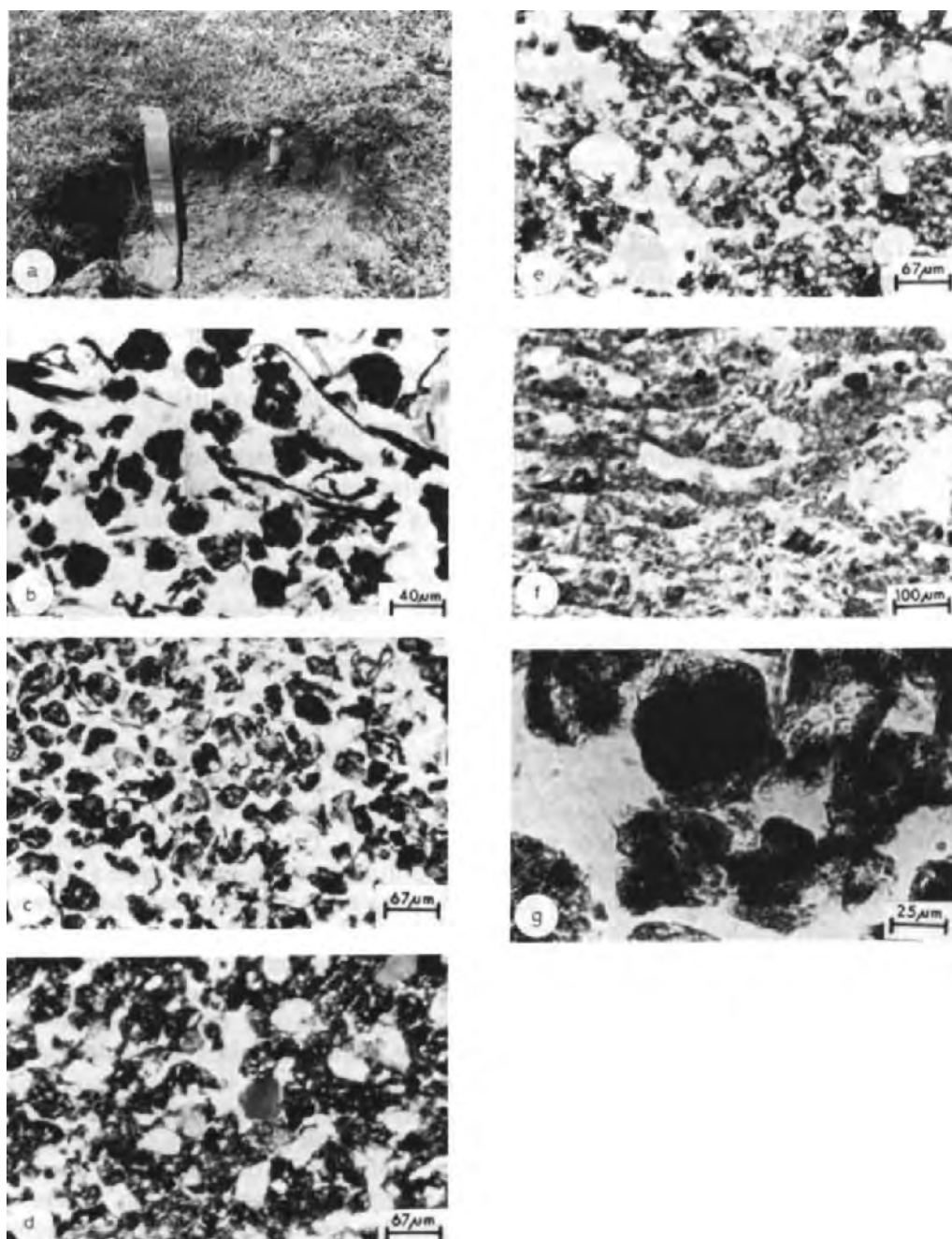


Fig.1. The mullgranitic sequence within the A1 horizon of a Typic Cryochrept: a. section of pedon of a Typic Cryochrept; b. mullgranitic fabric; c. mullgranoidic fabric; d. mullgranoidic porphyric fabric; e. porphyric fabric; f. isobanded granoidic fabric; g. granic units within isobanded granoidic fabric.

in shifts either to the left or right in the sequence. The following were observed to produce shifts to the right; (1) seasonal compaction; (2) raindrop dispersion followed by drying; (3) increase in clay content; (4) waterlogging; (5) some species of earthworms?

Shifts to the left within the mullgranic sequence were produced by the following: (1) increase in soil faunal activity; (2) other biological forces e.g., root exudates; (3) cyclic freezing and thawing; (4) cultivation; (5) wetting and drying.

Seasonal changes in fabric type within the mullgranic sequence were especially obvious for the mull layers of fine texture where mullgranic fabrics dominated in the spring and soils were generally friable.

Porphyric types dominated in the autumn and consistency was much more firm. Spring and autumn freeze-thaw cycles played a major role in moving dominance toward the mullgranic type. Cultivation also produced mullgranic fabric types but the size and shape of f-members were highly irregular and not always well defined. Tillage did not appear to be the best mechanism for producing mullgranic fabrics. Earthworms were also prolific producers of mullgranic fabric types. However, under certain conditions, mullgranoidic porphyric types could form through an overproduction of recalcitrant organic substances.

Major changes in pedogenic forces were shown to produce intergrades to other fabrics not recognized within the sequence. For example, severe compaction accompanied by freeze-thaw resulted in isobanded granoidic intergrades (Fig. 1f). In this case modifying genetic processes were further discerned by utilizing submicroscopic techniques. Some of the mullgranic units (Fig. 1g) appeared as domains of yellowish-brown isotropic gel much like organic plasma with pleistoplasmatic related distribution (Bal, 1973). Other mullgranic units comprised domains of similar appearance but also showed variable anisotropic properties. In order to analyze these domains submicroscopically, cover slips were removed and the slides were sectioned. A section was then polished and carbon-coated for the microprobe. The microprobe used was a Cambridge Geoscan in the C.S.I.R.O. laboratories in Adelaide operated by Dr. K. Norish. The microprobe was equipped with a high-resolution transmitting microscope that permitted accurate identification and centering of the beam. After completion of the microprobe analyses the epoxy-impregnated soil section was peeled away from the glass slide and mounted in a Philips X-ray microcamera with a 60-micron collimator for crystallographic identification.

Analyses for the isotropic domain (Fig. 2) showed a high alumina and low silica content; the main components were amorphous to X-rays. Only weak diffraction lines were evident from small quantities of associated fine-grained quartz. Sodium-pyrophosphate dissolution suggested complexing with humic constituents. This material was believed to constitute a weathering component of the volcanic ash identified in the silt fraction. On the basis of the X-ray diffraction pattern and chemical composition

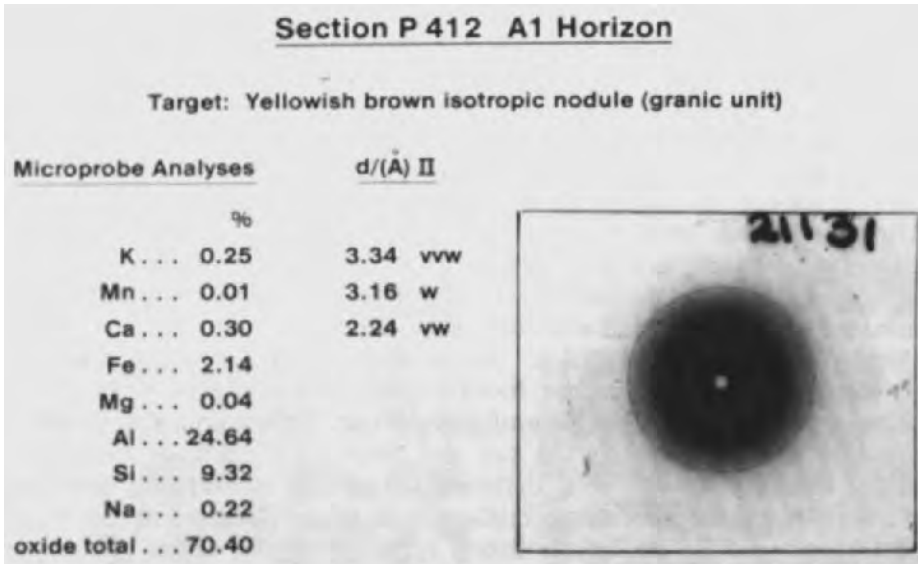


Fig.2. EMA and XRD analyses of yellowish brown isotropic granitic unit from the A1 horizon of the mullgranitic sequence.

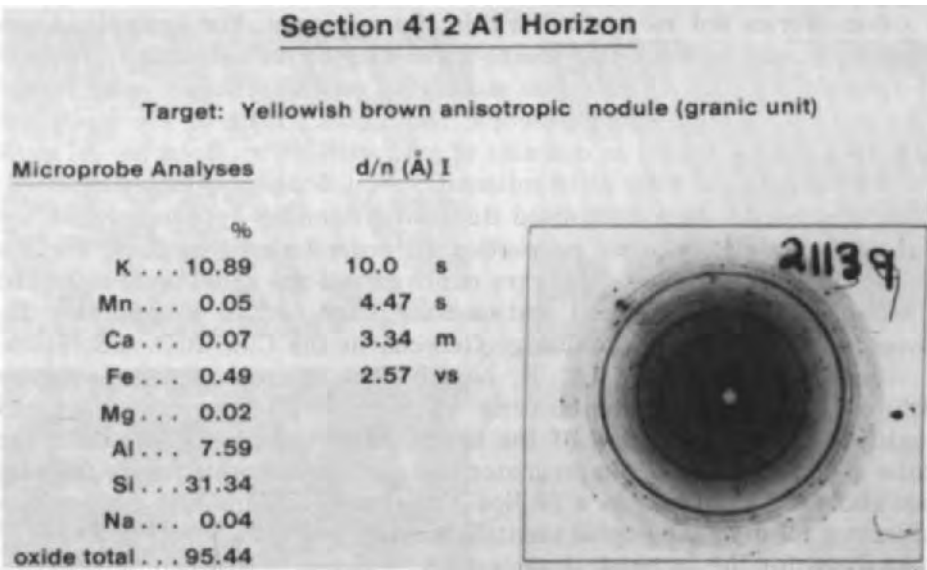
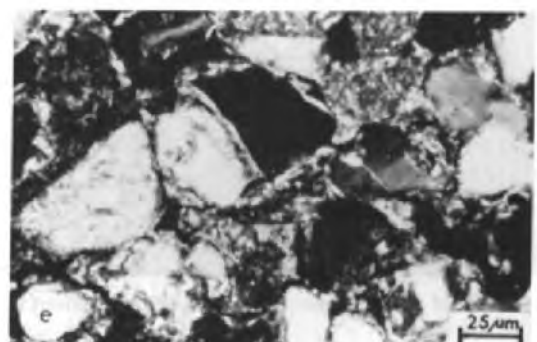
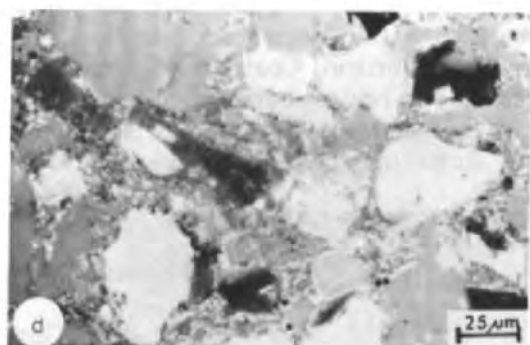
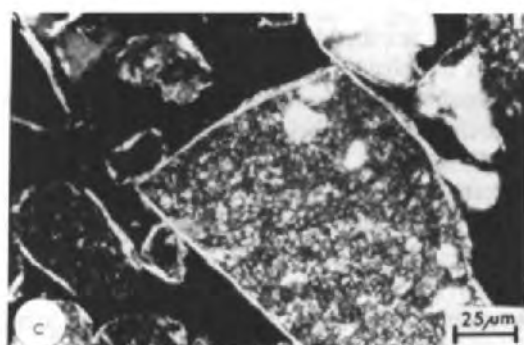


Fig.3. EMA and XRD analyses of yellowish brown anisotropic granitic unit from the A1 horizon of the mullgranitic sequence.

Fig. 4. The chlamydic sequence within the pedon of a Mollic Cryoboralf: a. section of pedon of a Mollic Cryoboralf; b. orthogranic fabric; c. matrichlamydic fabric; d. matri-plectic fabric; e. plectic porphyric fabric.



the anisotropic mullgranic unit (Fig. 3) was readily identified as a domain of micaceous material, dominantly muscovite.

Chlamydic sequence

The chlamydic sequence of fabrics related to the distribution of f-matrix around f-members as coatings and formation of bridges between them (Brewer, 1979). The dynamic relationships between fabric types within this sequence were observed as follows:

orthogranic \Rightarrow matrichlamydic \Rightarrow matriplectic \Rightarrow matriplectic porphyric \Rightarrow porphyric

The fabric sequence was generally characteristic of subsurface horizons in coarse textured soils. All horizons below the A1 of the Mollic Cryoboralf pedon developed from eolian sand, as depicted in Fig. 4a, had microfabrics dominantly within the chlamydic sequence.

Orthogranic fabric types (Fig. 4b) were found in isolated zones within the C horizon. The "ortho" f-members were made up entirely of loosely packed skeleton grains although pedorelicts and lithorelicts were also present. The grains were generally bare in this case or only with thin partial coatings that reflected a minor chlamydic component. Matrichlamydic fabrics (Fig. 4c) characterized the lower eluviated horizon, the transition between the A and B and were also observed in the parent material. The f-matrix was observed as continuous coatings on f-members. While fabrics were similar, differences in composition of f-matrix reflected very different processes within horizons. Matriplectic fabrics (Fig. 4d) dominated in the argillic B horizon. Coatings of f-matrix on the f-members were broadened out to form bridges between closer members.

Although most of the matrix material in the sandy argillic B horizon was illuvial in origin, observed extinction patterns showed lack of uniformity

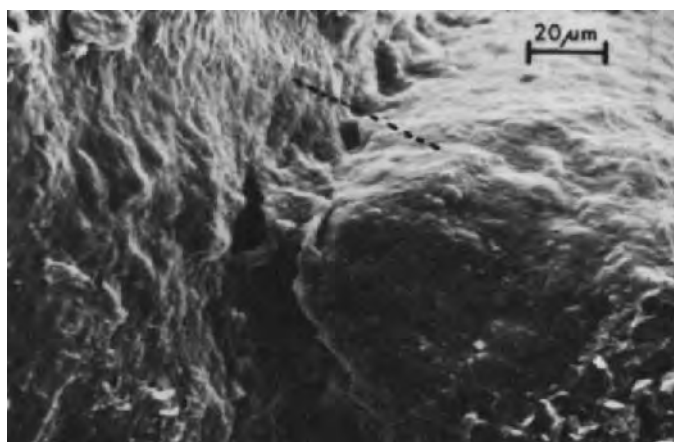


Fig. 5. SEM micrograph showing bimodal orientation for f-matrix in matriplectic fabric.

in orientation and composition. SEM micrograph (Fig. 5) supported bimodal orientation patterns for the f-matrix around and between f-members. It appeared that these fabric types did not originate entirely by thickening of argillans where clays remained oriented parallel to the surface of the f-member. The fact that the clays in the bridges were oriented perpendicular to the surface suggested another mechanism, perhaps withdrawal of moisture from capillary films through evapotranspiration losses.

Line scans made with SEM-EDXRA (Fig. 6) across a matrix bridge between f-members suggested that the plasma comprised a mixture of components with considerable variation in Si/Al/Fe ratios over short distances (in this case 40 microns). The foregoing was supported by lysimeter studies.

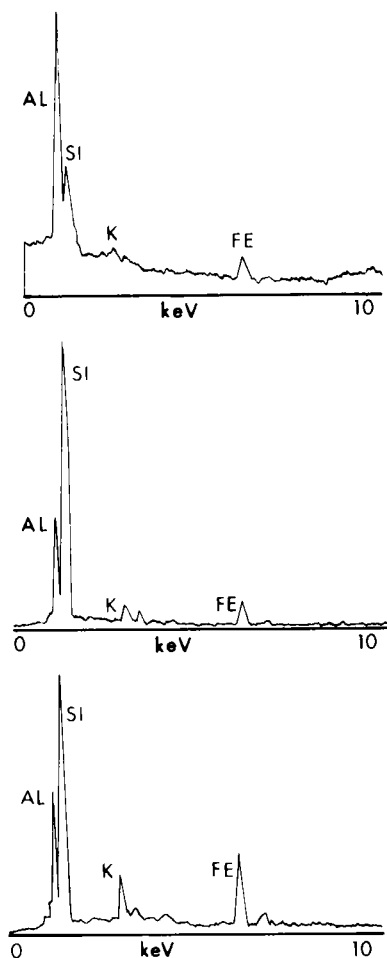


Fig.6. SEM-EDXRA line scans of regions depicted in Fig.5, showing variability in plasma composition over a distance of 40 microns.

Leachates from the eluviated horizon were found to contain significant quantities of amorphous organic matter, iron, and aluminum as well as clay minerals in the colloidal fraction. The separation of constituents within the plasma suggests both podzolization and lessivage contributed to the processes of soil formations, each acting independently.

Plectic porphyric intergrade fabrics (Fig. 4e) were characteristic of horizontal bands within the argillic B horizon. The f-matrix coatings were broad, strongly coalesced and frequently completely filled the voids. In porphyric fabrics the f-members were completely embedded in the f-matrix.

Development of the fabric sequence appeared to reflect particle-size distribution and colloidal transport in the soil. Eluviation resulted in fabrics toward the orthogranic type while illuviation produced fabrics toward the matriplectic porphyric and porphyric types. However, a similar sequence of fabrics was also observed in porous argillaceous sandstones derived through sedimentary processes. Similar related distribution patterns were also shown to be derived through freeze-thaw processes and by wetting and drying.

CONCLUSION

Other sequences of fabric also showed specific relationships between processes and fabric type. Comprehensive studies to discern a better appreciation of the dynamics within these fabric sequences should prove useful in understanding the genesis of the soils and should assist in better planning of their management.

REFERENCES

- Bal, L., 1973. Micromorphological Analysis of Soils. Soil Survey Papers 6. Soil Surv. Inst., Wageningen, 174 pp.
- Brewer, R., 1977. Micromorphology of a euchrozem from Talavera, Queensland. CSIRO Aust. Div. Soils, Div. Rep., 18.
- Brewer, R., 1979. Relationship between particle size, fabric and other factors in some Australian soils. Aust. J. Soil Res., 17: 29—41.
- Stoops, G. and Jongerius, A., 1975. Proposal for a micromorphological classification of soil materials, 1. A classification of the related distributions of fine and coarse particles. Geoderma, 13:189—199.

SCANNING ELECTRON MICROSCOPY OF ENGINEERING SOILS

K. COLLINS

Department of Civil Engineering, University of Strathclyde, George Street, Glasgow, Strathclyde (Great Britain)

(Accepted for publication February 17, 1983)

ABSTRACT

Collins, K., 1983. Scanning electron microscopy of engineering soils. *Geoderma*, 30: 243–252.

Specimen preparation for the scanning electron microscopy of engineering soils is vitally important. The usefulness of critical point drying is assessed on the basis of macroscopic and microscopic data obtained from the critical point drying and the air drying of several natural undisturbed soft clays.

It is emphasised that scanning electron microscopy can play a valuable reconnaissance role, thus providing an indication of the broad character of the soil microfabric, over a wide range of magnification, which aids in the selection of the appropriate programme and methods of quantification.

It is also demonstrated that scanning electron microscopy observations are extremely useful in the interpretation of, and for providing the very necessary background to, quantitative data such as that yielded by optical thin section and mercury porosimetry studies.

INTRODUCTION

The scanning electron microscope (SEM) is an extremely useful tool for studying the microfabric of engineering soils. Several examples are given here in order to give a brief indication of some of the roles which the SEM can successfully fulfil, particularly with regard to combined micromorphological studies.

Consideration, however, is firstly given to some of the advantages and disadvantages of the critical point drying technique applied to wet clays.

CRITICAL POINT DRYING

Prismatic specimens (10 mm × 10 mm × 30 mm) of four natural undisturbed soft sediments were dried by the critical point drying technique and also for comparative purposes by the slow air drying (20°C ambient) method. Shrinkage measurements were made (Table I) and the fabrics of the dried specimens studied using the SEM.

Critical point drying, involved firstly the replacement of the pore water

TABLE I

Shrinkage measurements on critical point and air dried clays

Soil	Approximate volumetric shrinkage (%)		
	Air dried	Critical point dried	
		Direct replacement	Graded replacement
Cemented estuarine silty clay, Ottawa, Canada	36	2	6
San Francisco Bay marine mud, U.S.A.	41	2	8
Cemented lacustrine varved clay, New Liskeard, Canada	30	6	1
Lacustrine clay, New Orleans, U.S.A.	marked	none apparent	not tested

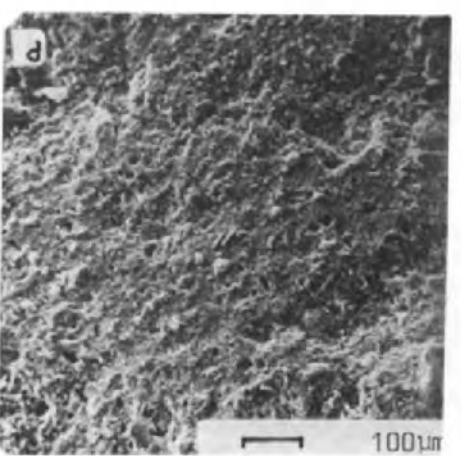
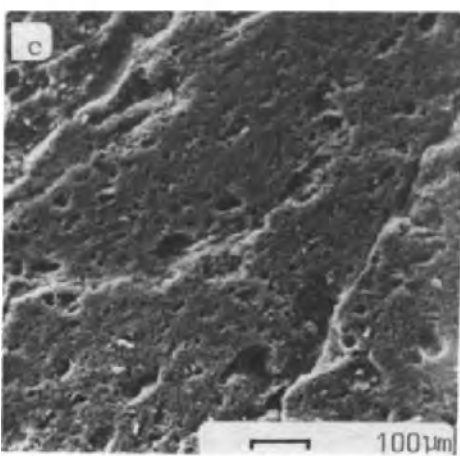
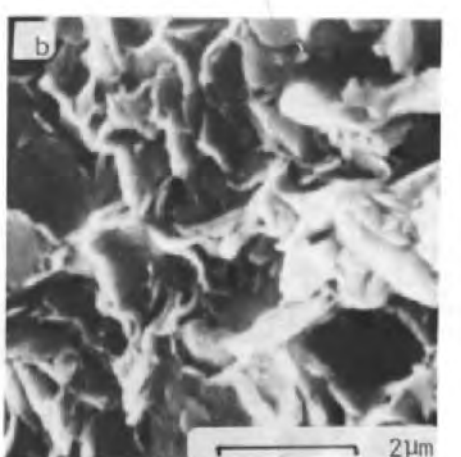
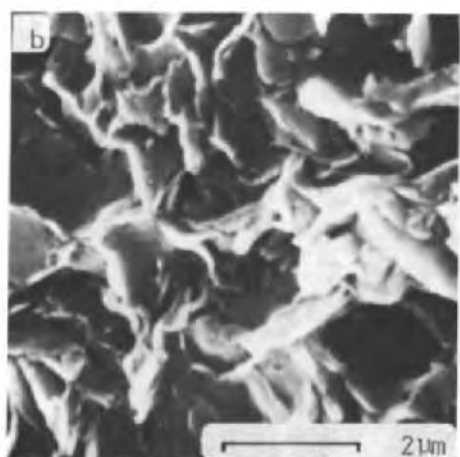
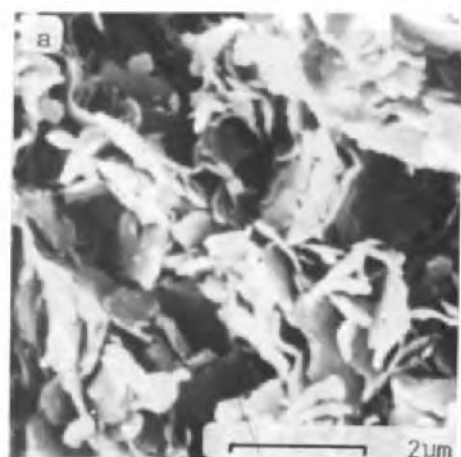
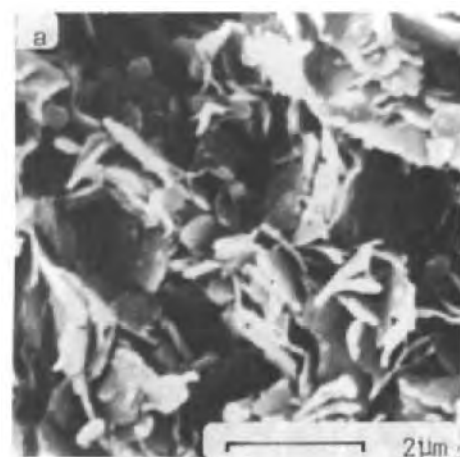
with methanol (both graded and direct replacement methods were used) followed by the replacement of methanol with liquid carbon dioxide, which was then taken to its critical point which occurs at 31°C and 73 atmospheres pressure.

As shown in Table I, volumetric shrinkage was greatly reduced by critical point drying (1–8%) compared to that induced by air drying (30–40%). Visual inspection of the dried specimens, however, showed that some of the critical point dried specimens of each soil were cracked both longitudinally and laterally. Specimens of the uncemented critical point dried clays from San Francisco and New Orleans were particularly fragile and this presented problems in fracturing, mounting and peeling of specimens for the SEM.

SEM observations on the dried specimens indicated that critical point drying had preserved open random clay particle arrangements (Fig. 1a — stereopair), whereas in the case of air drying much denser, though still largely isotropic configurations, were in evidence wherein individual clay particles were not always easily discerned (Fig. 1b — stereopair). It was also clear, however, that unlike air drying the methanol impregnation procedures had induced extensive microcracking in many cases (Fig. 1, c and d). Furthermore, in the case of uncemented critical point dried clays, excessive silt grain removal had occurred during the dry fracturing and fracture surface peeling processes, as evidenced by the apparently extremely porous texture shown in Fig. 1c.

The two stage critical point drying technique therefore, caused minimal shrinkage of soft clays studied and succeeded, it would seem, in preserving

Fig. 1. SEM micrographs of New Orleans clay: (a) clay arrangements, critical point dried — stereopair; (b) clay arrangements, air-dried — stereopair; (c) clay matrix, critical point dried; (d) clay matrix, air-dried.



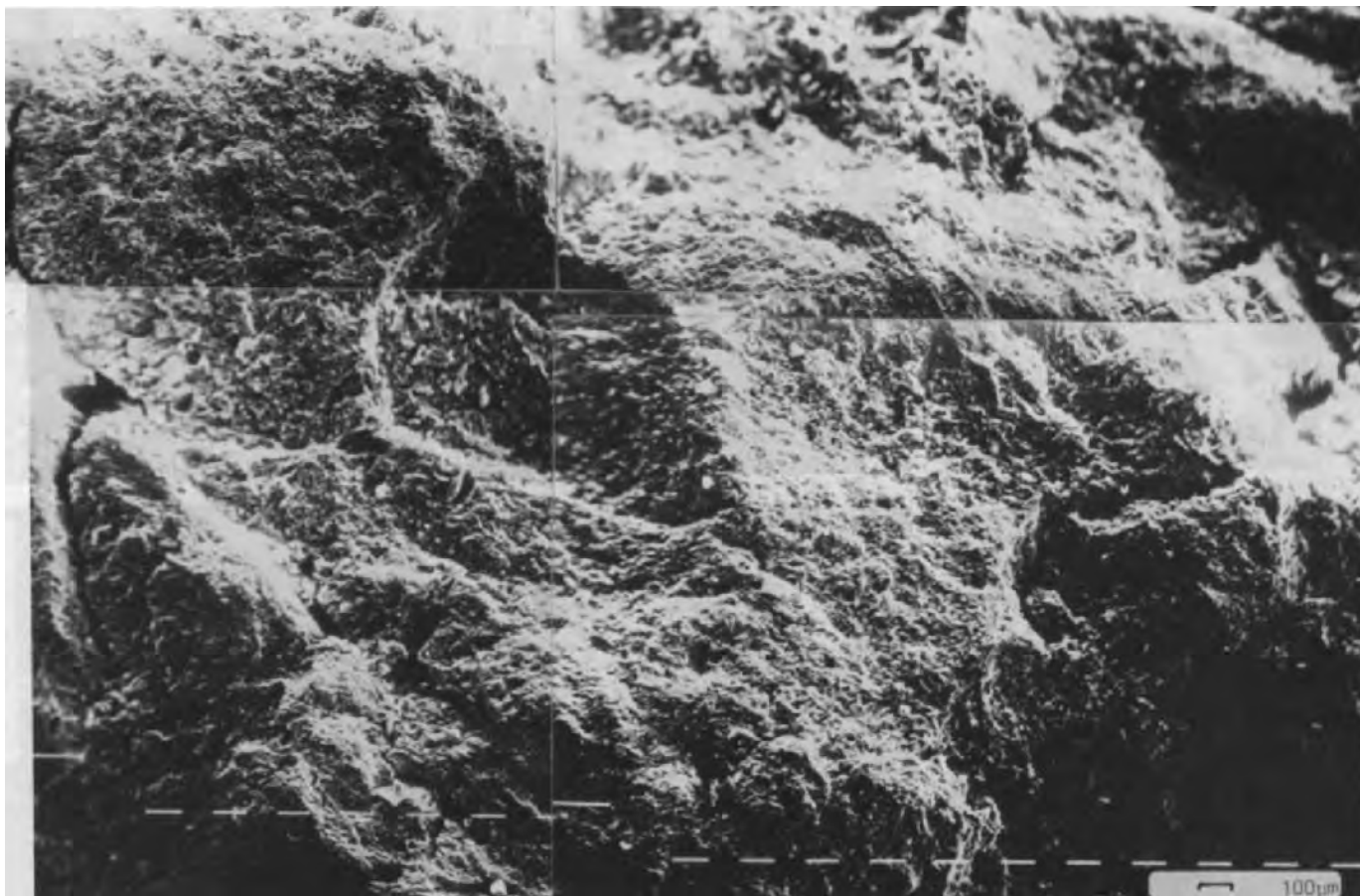


Fig. 2. Portion of SEM montage showing pedal clay fabric in London clay.

open clay particle configurations. On the other hand, it induced extensive macro- and micro-cracking, which is, of course, a serious limitation. The simple air-drying method, while inducing considerable densification, by no means altered totally the overall microfabric character of the natural sediments. Indeed observations of the air-dried specimens served very well to complement those made on the critical point dried specimens.

A RECONNAISSANCE ROLE FOR THE SEM

The SEM in the normal emissive mode can be of immense value in assessing, relatively quickly, the broad character of an engineering soil microfabric over a vast range of magnification from $\times 20$ to $\times 50,000$.

As recommended by Stoops (1974) the first step is to study SEM mounted specimens prior to coating, under the stereomicroscope, to locate features of interest.

The construction of SEM micrograph montages (Fig. 2) is then carried out, initially at low magnifications of $\times 20$ to $\times 80$ with zero tilt (this links well with the stereoscope observations), and subsequently at those higher levels of magnification which seem appropriate. In this way, any fabric heterogeneity or multi-level fabric characteristics can be fully appreciated. Stereopairs (Fig. 3) are also extremely useful, not only as a guard against misinterpretation, but also for gaining a clear impression of the mutual and spatial arrangement of particular fabric features at all levels of magnification.

Using the above approach it is often possible to identify the microfabric features which need to be quantified. For example, Figs. 2 and 3 are SEM observations from an ongoing engineering study of an undisturbed heavily

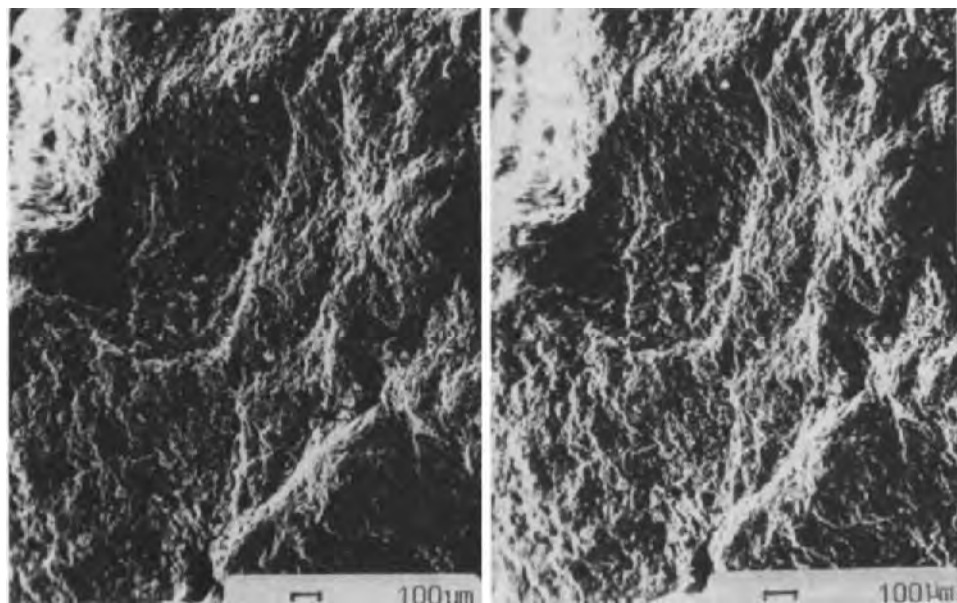


Fig. 3. SEM stereopair of clay peds shown in Fig. 2.

compressed marine clay, which have revealed a pedal fabric. They have also suggested the possibility of preferred orientation of interpedal pores in places, and a variation in the degree and direction of preferred orientation of the clay matrices within the individual peds. It has been decided, therefore, on the basis of these SEM observations, that optical thin section studies should be carried out to study and, if possible to quantify these aspects. In this way the overall microfabric anisotropy could be assessed and related to engineering behaviour.

AN INTERPRETATIVE ROLE FOR THE SEM

SEM observations provide a clearer understanding of the data yielded by quantitative techniques such as optical thin section (birefringence) and mercury porosimetry.

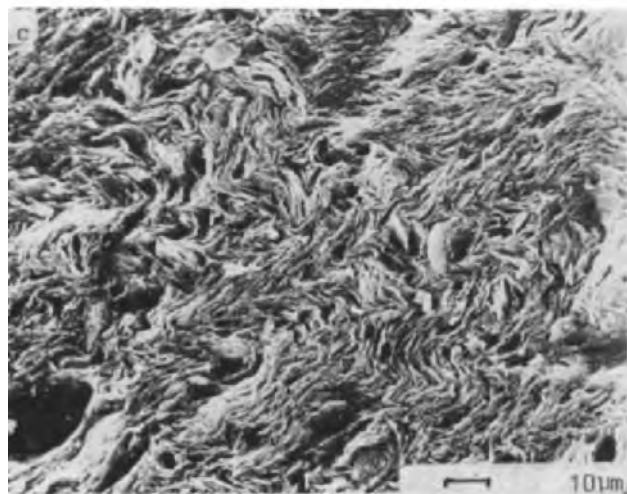
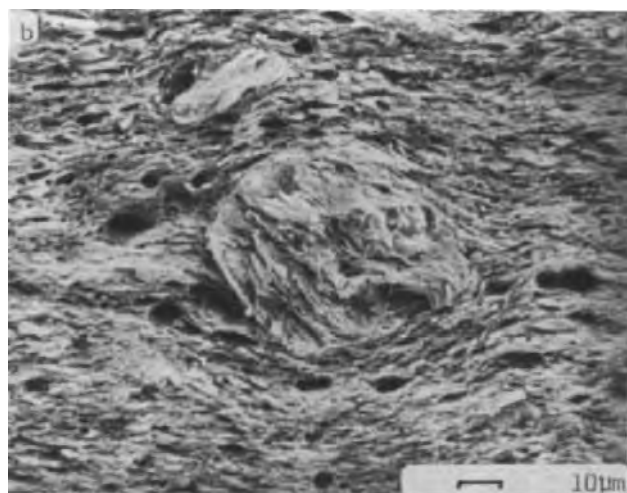
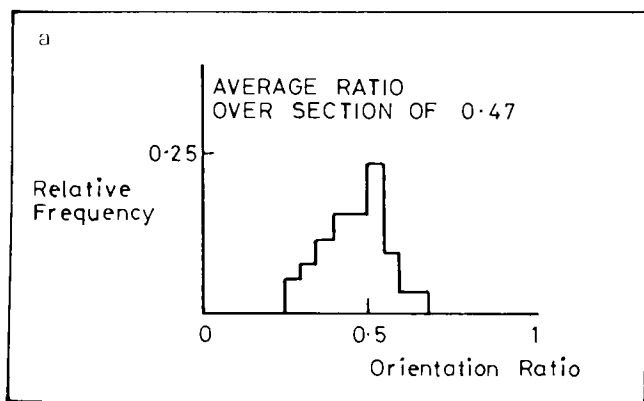
Optical thin section microscopy

Krishnamurthy (1975) studied the fabric of an illite clay compressed from a slurry and sheared. Using crossed nicols he measured an orientation ratio in each case, defined as the ratio of the intensity of illumination at the extinction phase, to the intensity of illumination at the illumination phase, and ratios of unity and zero represent random and perfect clay orientation, respectively (Morgenstern and Tchalenko, 1967). Fig. 4a indicates a medium degree of preferred orientation overall for the undisturbed illite with areas of near perfect orientation as well as highly random zones. SEM observations by the author on the same clay confirmed the existence of near perfect orientation (Fig. 4b) and revealed the turbostratic nature of the random fabric zones (Fig. 4c). The term turbostratic describes the turbulent array of parallel orientated clay platelets (Aylmore and Quirk, 1960). The disruptive influence of clay aggregates (slurry features) which were present in the original slurry and which have survived the compression process, can be clearly seen (Fig. 4b). Fig. 5a indicates that upon shearing, randomness increases over the entire section. This observation was confirmed by the SEM which indicated an increase in the occurrence of turbostratic zones and which also gave a clear insight into the nature of the shear zone which can be seen to be extensive (Fig. 5b) but extremely narrow (2 μm across) and branched in places (Fig. 5c).

Mercury porosimetry

Safiullah (1981) measured the pore size distributions of samples of a silty clay from Glasgow, U.K., compacted to various water contents by the stan-

Fig. 4. Fabric of illite compressed one-dimensionally under 300 kN/m²: (a) optical measurements; (b) SEM micrographs showing clay aggregation and preferred orientation; (c) SEM micrograph showing turbostratic clay.



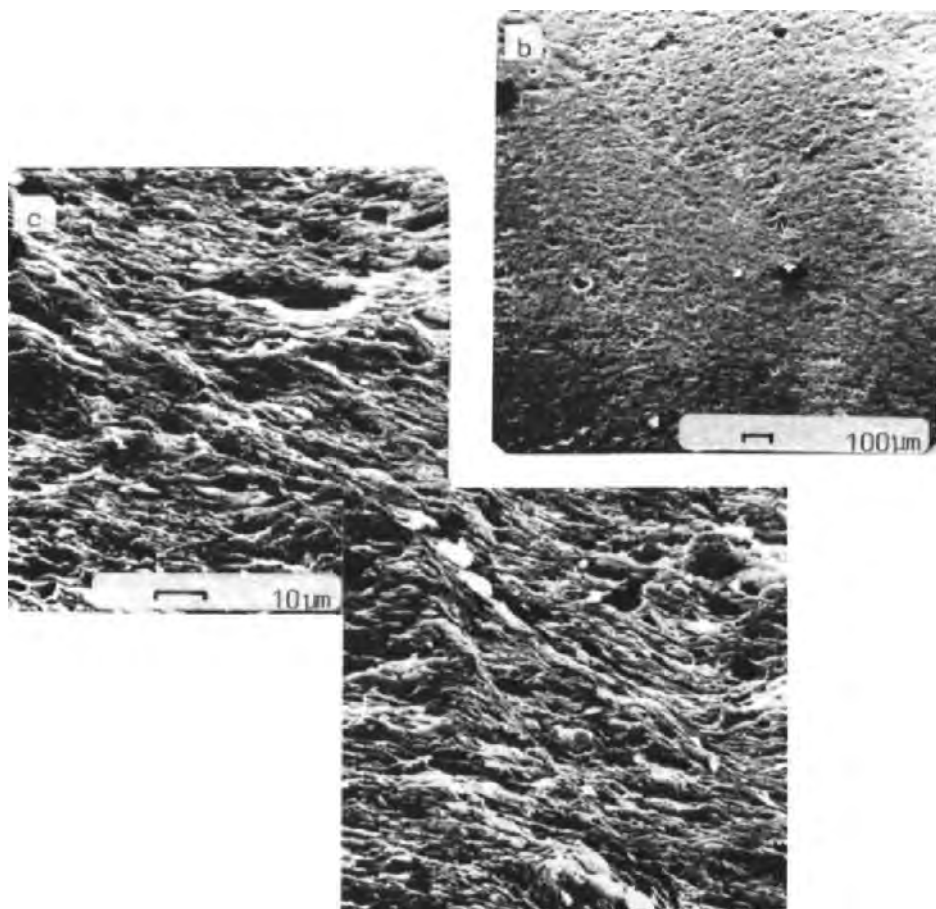
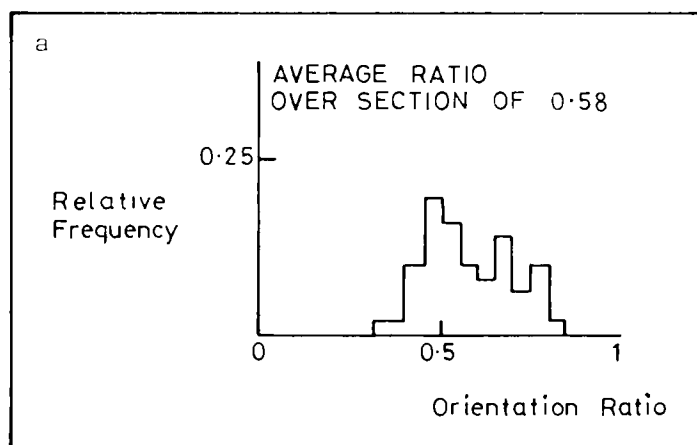


Fig. 5. Fabric of compressed illite sheared under drained plane strain conditions: (a) optical measurements; (b) and (c) SEM micrographs of shear zone.

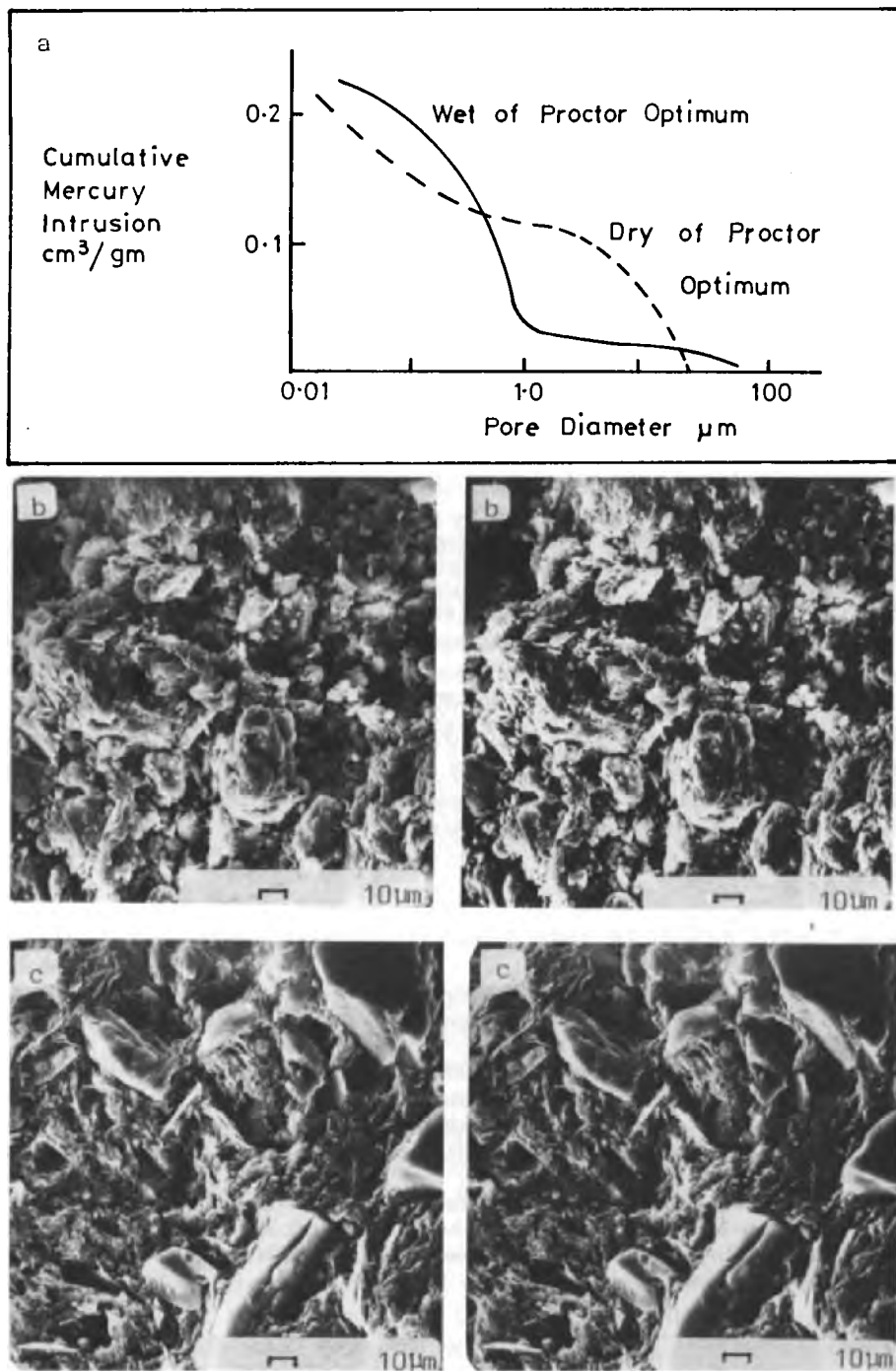


Fig. 6. Fabric of compacted silty clays: (a) mercury porosimetry plots, Glasgow silty clay; (b) SEM stereopair of Luanda silty clay, dry of optimum; (c) SEM stereopair of Luanda silty clay, wet of optimum.

standard Proctor method. The cumulative mercury intrusion curves (Fig. 6a) indicated that the fabrics of the dry and wet side of optimum samples were different with the former showing a bimodal pore distribution. SEM observations showed clearly that this was associated with an aggregated clay fabric and that the small and large modes related to intra-aggregate and inter-aggregate porosity, respectively. This aggregate type fabric can be observed in Fig. 6b which is a stereopair showing the fabric of a silty clay from Luanda, Angola, compacted on the dry side of optimum. By comparison the fabric of the wet side of optimum compacted sample is seen to comprise a uniform clay matrix (Fig. 6c — stereopair).

CONCLUDING REMARKS

Critical point drying reduces shrinkage to a minimum but can often induce cracking and specimen fragility. It is suggested here that any drying technique may introduce artefacts and that therefore as a matter of routine, a number of drying methods should be employed in parallel. For example, critical point drying and air drying can usefully complement one another in the study of soft clays.

SEM observations over a full range of magnification from $\times 20$ to $\times 50,000$, employing montage and stereophotography, can provide a useful basis for a more detailed and possibly quantitative structural analysis using some of the other study techniques available. The SEM can then be employed in parallel with such techniques in order to provide the often very necessary background information which aids in the interpretation of quantitative data from such studies.

REFERENCES

- Aylmore, L.A.G. and Quirk, J.P., 1960. Domain or turbostratic structure in clays. *Nature*, 187: 1046–1048.
- Krishnamurthy, D.N., 1975. *Strength Anisotropy and Fabric Changes During Deformation and Failure of Orientated Clays*. Unpublished Ph.D. thesis, University of Strathclyde, 301 pp.
- Morgenstern, N.R. and Tchalenko, J.S., 1967. Microstructural observations on shear zones from slips in natural clays. *Proc. Geotech. Conf., Oslo*, Vol. 1, pp. 147–152.
- Safiullah, A.M.M., 1981. *Aspects of Engineering Behaviour of Compacted Clays Related to their Pore Size Distribution and Fabric*. Unpublished Ph.D. Thesis, University of Strathclyde, 101 pp.
- Stoops, G., 1974. Optical and electron microscopy. A comparison of their principles and their use in micropedology. In: G.K. Rutherford (Editor), *Soil Microscopy. Proceedings of the 4th International Working-Meeting on Soil Micromorphology*, Kingston, 1973. Limestone Press, Kingston, Ont., pp. 101–118.

SEM-EDXRA STUDIES OF PRECIPITATES WHICH CLOGGED A WATER-TUBE FILTER

E.B.A. BISDOM and A. JONGERIUS

Netherlands Soil Survey Institute, P.O. Box 98, 6700 AB Wageningen (The Netherlands)

(Accepted for publication February 17, 1983)

ABSTRACT

Bisdom, E.B.A. and Jongerius, A., 1983. SEM-EDXRA studies of precipitates which clogged a water-tube filter. *Geoderma*, 30: 253–270.

Light microscopic, submicroscopic and XRD (X-ray diffraction) analyses were done of precipitates which had clogged a water-tube filter. Several zones, mostly consisting of amorphous and poorly crystalline materials, could be distinguished. SEM-EDXRA (scanning electron microscopy — energy dispersive X-ray analysis) indicated that sulphur, copper, iron and zinc were usually represented and that calcium was less common. Light microscopy and XRD indicated the presence of calcite and gypsum.

Corrosion of copper filter segments could be demonstrated by flakes which peeled off, small fragments adjacent to the segments, and a jagged appearance of the edges. A little sulphur was found at the edges of the filter segments together with copper. More sulphur was present in the flakes which, together with copper, formed covellite according to XRD analyses. Rather massive precipitates could be deposited on the disintegrating flakes. Precipitates of younger zones were usually less massive and exhibited a variety of forms.

INTRODUCTION

Precipitates from the surface of a water-tube filter, (courtesy of the Dune Water Works, The Hague, The Netherlands) which was regularly used between 1937 and 1951 to raise water from a reservoir, were studied. The core reached us in 1976 and came from an environment which, according to available well data, was permanently submerged. The tube and the precipitates were photographed immediately after arrival (Fig. 1). Some of the precipitate was subsequently removed in order to observe the build-up of the copper filter itself (Fig. 2).

The central part of the filter was cleaned thoroughly to show the holes in the pipe. The original precipitate, which was coloured brownish yellow to orange-red, is still observable at the top part of the filter. It would seem to be iron hydroxide when observed with the unaided eye. Between this top part and the central part of the filter with holes, one can observe that the entrances to the filter were clogged. The aim of the present study was to investigate the precipitates and to analyse them.

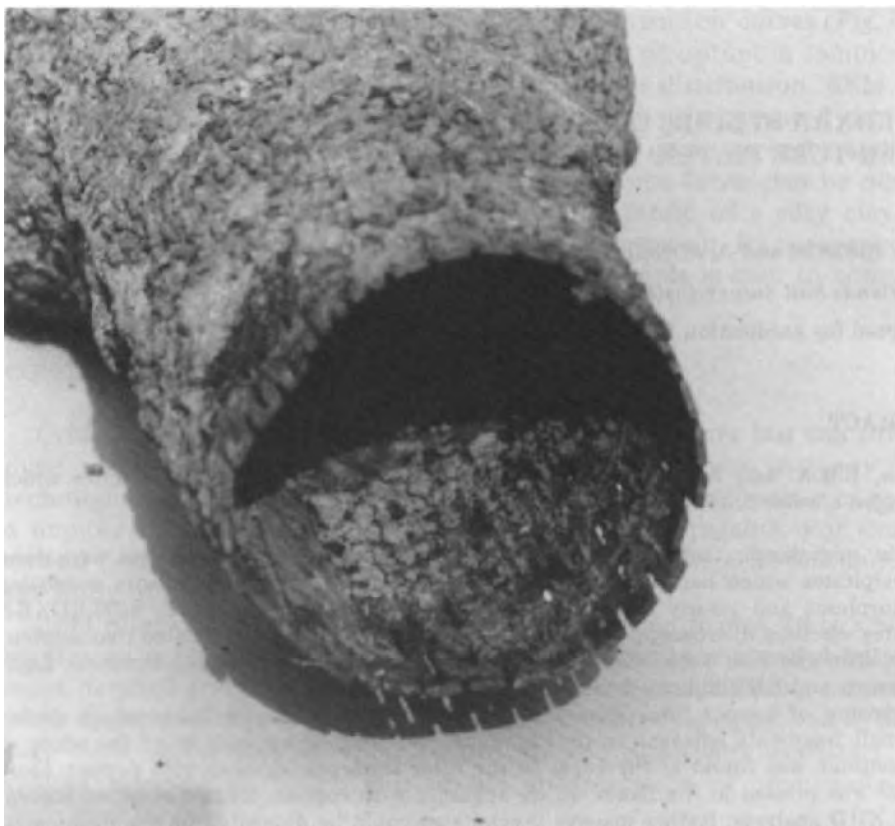


Fig.1. Internal and external precipitates on a water-tube filter. The precipitates have clogged the openings of the filter.

The first results of submicroscopic studies of these precipitates were given in a Dutch report (Bisdom and Jongerius, 1979). Part of a paper on man-made (man-induced) precipitates also discussed some of the present work (Bisdom, 1983).

MATERIALS AND METHODS

The materials studied have been partly described above. The following can be added. The topography of the precipitates on the outside of the tube was irregular, as was the case with precipitates that were deposited inside the tube. The thickness could be 1 cm or more and the uppermost parts of the deposits often formed isolated islands. The outgrowths of precipitates on the external part of the filter could be rather rounded, whereas similar materials inside the tube were sometimes better crystallized. The latter often resembled goethite. It was clear, however, that in situ research



Fig.2. A partly cleaned section of the filter is present in the middle of the photo. No materials were removed from the top part of the tube. Clogged pores can be observed between the two mentioned parts of the water-tube filter.

of undisturbed samples was necessary to obtain more insight into the composition of the precipitates and their relation to the copper filter of the water tube. This was done in the following way.

Thin sections of the metal filter and the precipitates were prepared, following the method described by Jongerius and Heintzberger (1975). Polyester resin was added to the materials to be studied, and thin sections prepared after the samples had hardened. These thin sections were then studied with the light microscope. This indicated that considerable isotropic material was present, i.e. amorphous material and not cubic crystals. Also, various substances seemed to be only poorly crystallized. XRD analyses were done (courtesy Dr. Breeuwsma, Netherlands Soil Survey Institute) and gave, together with light microscopic observations, some idea about the nature of the crystallized materials in the precipitates.

Submicroscopy was applied to study especially the amorphous materials and also to test crystalline materials for their chemical elements. The instrument used was a Jeol-JSM-35C scanning electron microscope with a backscattered electron detector of the semiconductor type. The SEM was equipped with an EDAX 9100 system with an ECON windowless detector for the detection of chemical elements.

RESULTS

General

A schematic drawing was prepared (Fig.3) which gives some idea of the complexity of precipitates on and between the copper filter segments. Five areas are indicated, viz. area a (Fig. 4a) and area b (Fig. 5) in the internal part of the copper filter segment, areas c (Fig. 6a) and d (Fig. 7) externally from the segment, and area e (Fig. 8) between the two filter segments. The quality of the backscattered electron scanning images (BESI) is often not very high at these lower magnifications. This is partly due to high amounts of amorphous materials which are often difficult to portray. The quality of such micrographs can frequently be improved using higher magnifications, by reduction of the shadowing effects and optimization of materials contrast in BESI.

Each of the areas a—e in Fig.3 has been subdivided into zones. Area a had six zones, starting with zone A I nearest to the surface of the copper filter segment (this segment is absent in the micrographs of areas a and b because it sprang away during preparation of the thin section). The same order of zones was maintained in areas b—e, with the zones with the smallest number nearest to the filter segment (the segment(s) is visible in the micrographs of these areas because they were made from a polished block in which the copper filter segments remained during the grinding process). Area e had two filter segments, and zones with smaller numbers were therefore present twice. The zones with the higher numbers E IV and E V merged and the precipitates in them finalized the clogging process which occurred at the entrance of the water-tube filter between two filter segments.

Materials in areas a—e

All areas were analysed with EDXRA (energy dispersive X-ray analysis) which can detect chemical elements up to magnifications of $\times 10,000$

Fig.3. Schematic cross-section of the water-tube filter. Five areas (a—e) were distinguished. Each area contained zones in which the chemical elements are indicated. Areas a and b were located inside the tube, areas c and d externally, and area e between two filter segments in the clogged entrance of the tube. The numbers of figures that are given below have also been indicated behind the areas, e.g. area a (Fig.4).

Internal section of the tube with precipitates on Cu-filter segments

Clogging precipitates in entrance tube and between Cu-filter segments

area b (Fig. 5)

area a (Fig. 4)

area c (Fig. 6)

area d (Fig. 7)

area e (Fig. 8)

External section of the tube with precipitates on Cu-filter segments

area a (Fig. 4) details:

(S) Fe	(Zn)	zone AVI
S Fe Fe	Cu Cu Zn	zone AV
	Ca Ca	zone AIV
S Fe Fe	Cu	zone AIII
S Fe	Cu	zone AII
S Fe	Ca Cu	zone AI

area b (Fig. 5) details:

zone BV	(S) (Si) Fe	Zn Ca Fe Si Zn	void
zone BIII	S (Si) (Fe) Cu (Zn)		
zone BII	S (Si) (Fe) (Cu) (Zn)		
zone BI	S (Si) (Fe) Ca Cu (Zn)		

area c (Fig. 6) details:

zone CI	(S) Cu
zone CII	S Cu
zone CIII	S (Fe) Cu (Zn)
zone CIV	S (Fe) Cu (Zn)
zone CV	S (Fe) Cu (Zn)
zone CVI	S (Fe) Cu (Zn) (Si) (S) Fe (Zn)

area d (Fig. 7) details:

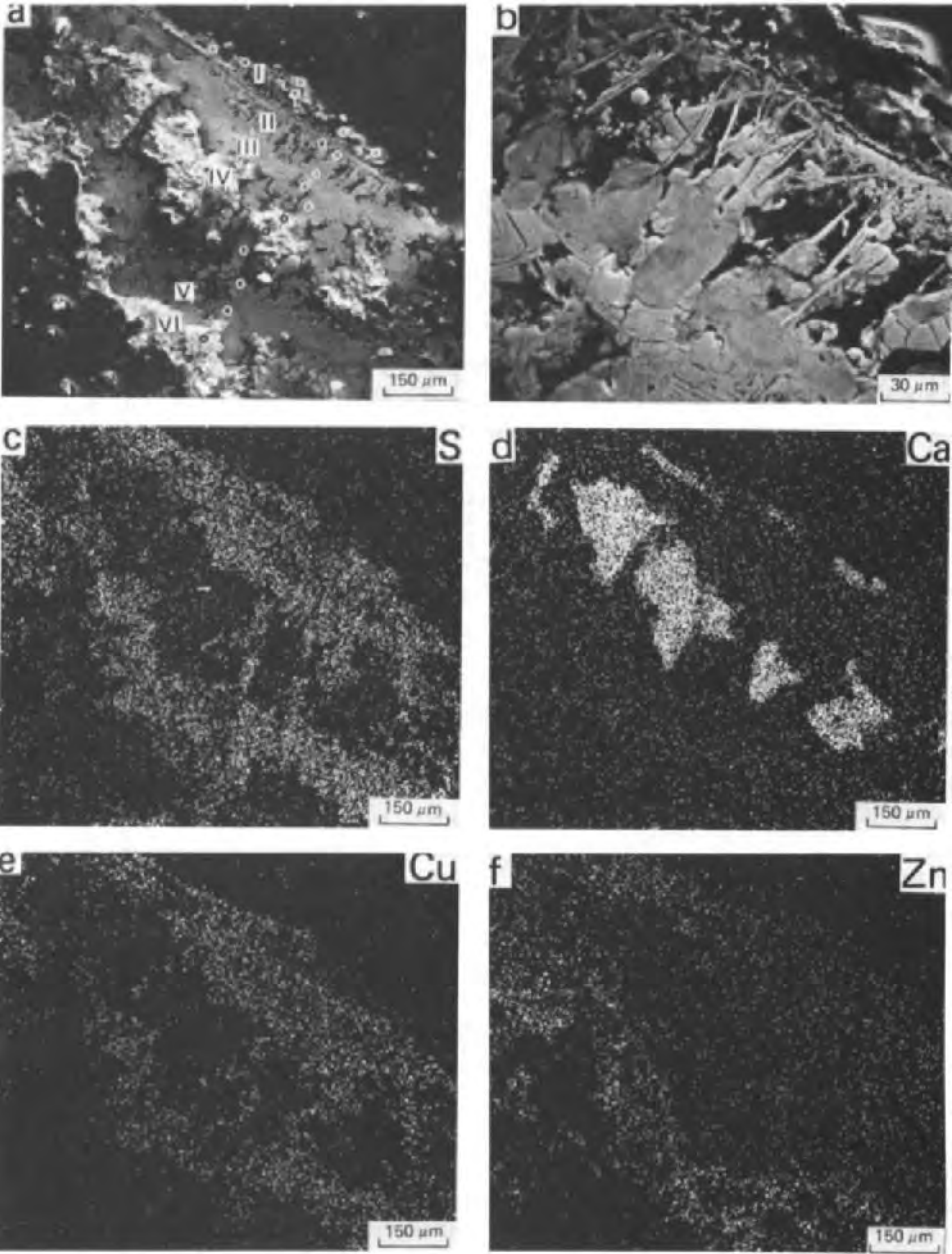
zone DI	
zone DII	S Cu
zone DIII	S (Fe) Cu
zone DIV	S (Fe) Cu (Zn)
zone D V	(S) Fe (Cu)
zone D VI	(S) Fe

area e (Fig. 8) details:

zone EI	(S) S Fe
zone EII	Cu Cu Cu (Zn)
zone EIII	Fe (Zn)
zone EIV	(S) (Fe) (Zn)
zone EV	Fe (Zn)

[Cu] copper represented in large quantities and locally in a zone
 (Cu) copper represented in small quantities and locally in a zone

(Bisdorf et al., 1975, 1976). Point analyses, which allow the detection of the heavier chemical elements in a spot with a diameter of 1 μm , and X-ray images, which give the distribution of the chemical elements in a micrograph and were of importance for the subdivision of the areas into zones, were



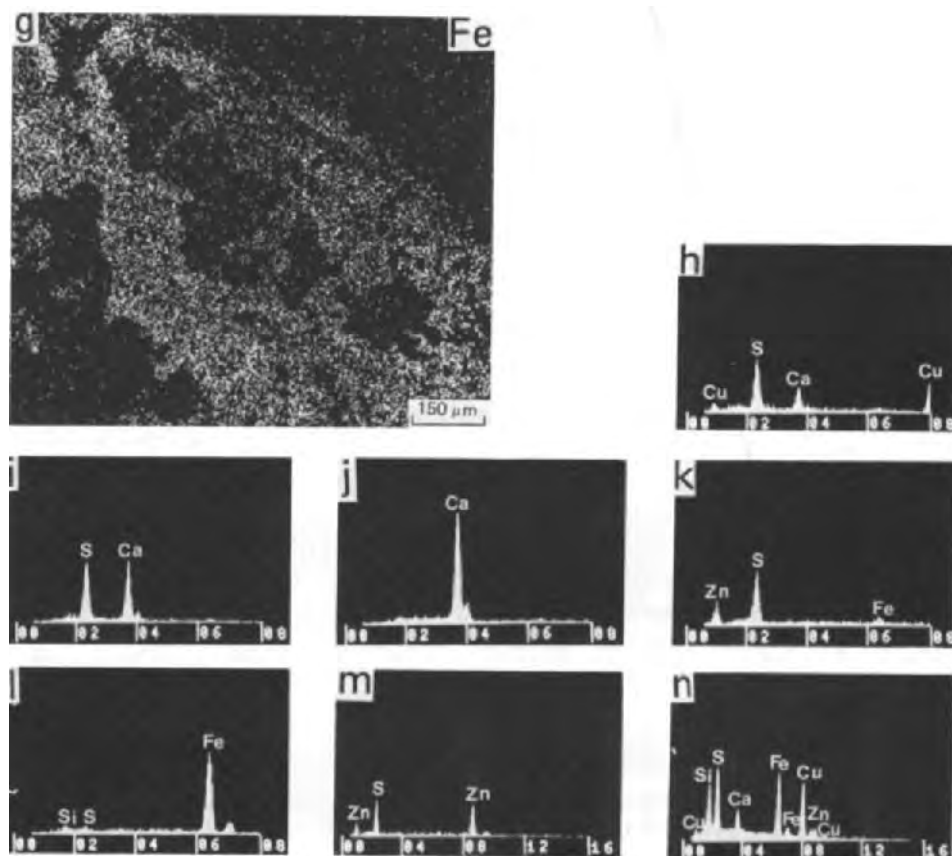


Fig.4. Backscattered electron scanning image (BESI) of area a with six zones (a). Circles in the micrograph indicate how a linear traverse was made using point analyses. Special attention was given to zone A I adjacent to the copper filter segment — this segment is absent because it sprang away during preparation of the thin section. Part of zones A I to A III of micrograph (a) has been enlarged in (b). X-ray images of S, Ca, Fe, Cu and Zn (c to g) give the distribution of chemical elements in micrograph (a). Point analyses (h to n) indicate a variety of chemical elements found in the zones of area a.

made. One relatively complete EDXRA analysis procedure has been included for area a (Fig.4), but some of the point analyses were omitted. A few remarks are given below about each of the zones in the different areas (cf. Fig.3) and the chemical composition of these zones is discussed.

Area a

Six zones were recognized in area a (Figs.3 and 4a). Some of the zones are clearly visible on the micrograph because they are white (Fig.4a). Another indication that zones exist is found in the distribution of chemical elements in the X-ray images (Fig.4, c–g) and in point analyses (Fig.4, h–n). The observations done with a light microscope were also of importance to establish zones and to determine the larger minerals.

Zone A I (Fig.4a) contained flakes of the copper filter segment (absent in this micrograph). Point analyses demonstrated that sulphur, copper, calcium and iron were present in this zone. The flakes themselves contained mainly copper and sulphur with some iron. XRD analyses of the materials close to the surface of the tube indicated that covellite (CuS) was present. This, and EDXRA measurements of flakes in other areas, suggest that the flakes consist of covellite on which iron hydroxide had sometimes precipitated. The calcium could form calcite (CaCO_3) and calcium and sulphur gypsum ($\text{CaSO}_4 \cdot 2\text{H}_2\text{O}$); measurements of oxygen were not done. The presence of calcite and gypsum, associated with the flakes, was confirmed by light microscopy.

An enlarged view of part of the zones A I to A III in Fig.4a is given in Fig.4b. Needle-shaped forms are present in zone A II and contain S, Fe and Cu. The rather massive material of zone A III, which extends into zone A II, contained the same elements but more sulphur and less copper occurred. The quantity of iron was rather small except for a few microareas. Most of these materials were poorly crystalline to amorphous. No determination of the compounds present could therefore be made by XRD analysis. SEM-EDXRA analysis could only provide an estimate of the relative quantities of the heavier chemical elements which were represented in the precipitates and flakes. Consequently, no quantitative analyses are given in this study.

Zone A IV contained calcite which was measurable as calcium by EDXRA and was determinable by light microscopy. The concentrations of calcium are indicated well in the X-ray image of Fig.4d. Zone A V also contained sulphur, iron and copper. One point analysis, however, indicated the replacement of copper by zinc. Zone A VI contained no copper and iron was the principal element. Some sulphur was also represented. Light microscopy and XRD analyses indicated that predominantly poorly crystalline iron hydroxides were represented in zone A VI.

Area b

Five zones were distinguished in area B (Figs.3 and 5). The zones were less easy to recognize than in area a. This can be illustrated by the inter-fingering of zones B III and B V. Zone B IV occurred adjacent to the void and followed a different direction from that of the other zones.

Zone B I includes several flakes of the original filter (absent in this micrograph). The elements zinc and silicon were added to sulphur, copper, iron and calcium found in the zone with flakes (zone A I) of area a. Calcite and gypsum were also present in zone B I. Zone B II contained the same elements as in zone B I with the exception of calcium. The amount of copper was somewhat less than in zone B I. The morphology of the components in zones B II (needles) and B III (an amorphous and massive precipitate) was different but the chemical elements found in them were the same.

Zone B IV was situated adjacent to a void and contained calcium, iron,

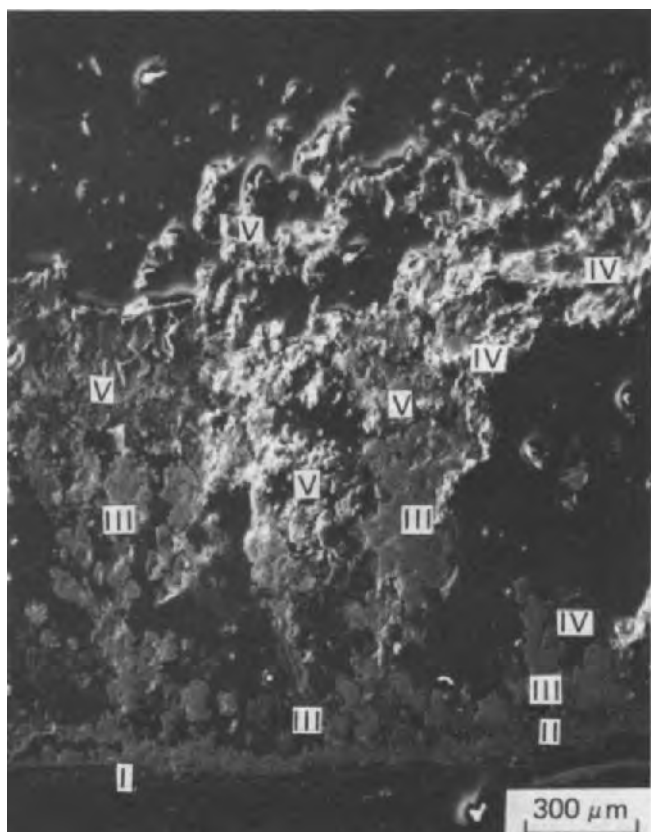


Fig.5. BESI of area b with five zones. The copper filter segment itself is absent (cf. explanation Fig.4). A relatively large gypsum crystal was found in zone B IV.

silicon and zinc. Calcite and gypsum were present. A relatively large gypsum crystal was also found. Zone B V contained silicon, sulphur, iron and zinc. Poorly crystalline iron hydroxides were mainly found in the outer part of zone B V which was close to the free flowing water mass inside the tube.

Comparison of areas a and b

A comparison of areas a and b inside the tube showed that copper was present closest to the wall of the filter segment. The reverse was the case with iron which reached the highest concentrations away from the wall of the tube near to the free flowing water. Both elements, however, occurred in most zones. Zinc was usually present in small quantities but formed a major element in zone A V. Sulphur was normally present in the zones nearest to the wall of the tube and became less abundant in zones away from this wall. The element Si was only found in small quantities in area b.

The flakes in zone B I were less corroded than in zone A I. Covellite was

represented in both zones and so were calcite and gypsum. Silicon and zinc were added in zone B I to the elements found in zone A I. Some elements were also added to the ones in zones A II and A III, but zones B II and B III had similar morphologies, i.e. needles in zones A II and B II and massive precipitate in zones A III and B III. Zone A IV with calcite and zone B IV with calcite, gypsum and elements such as iron, silicon and zinc, were not comparable. Zone B V was comparable with zones A V and A VI, especially the subzone with iron hydroxides nearest to the free flowing water inside the tube.

Area c

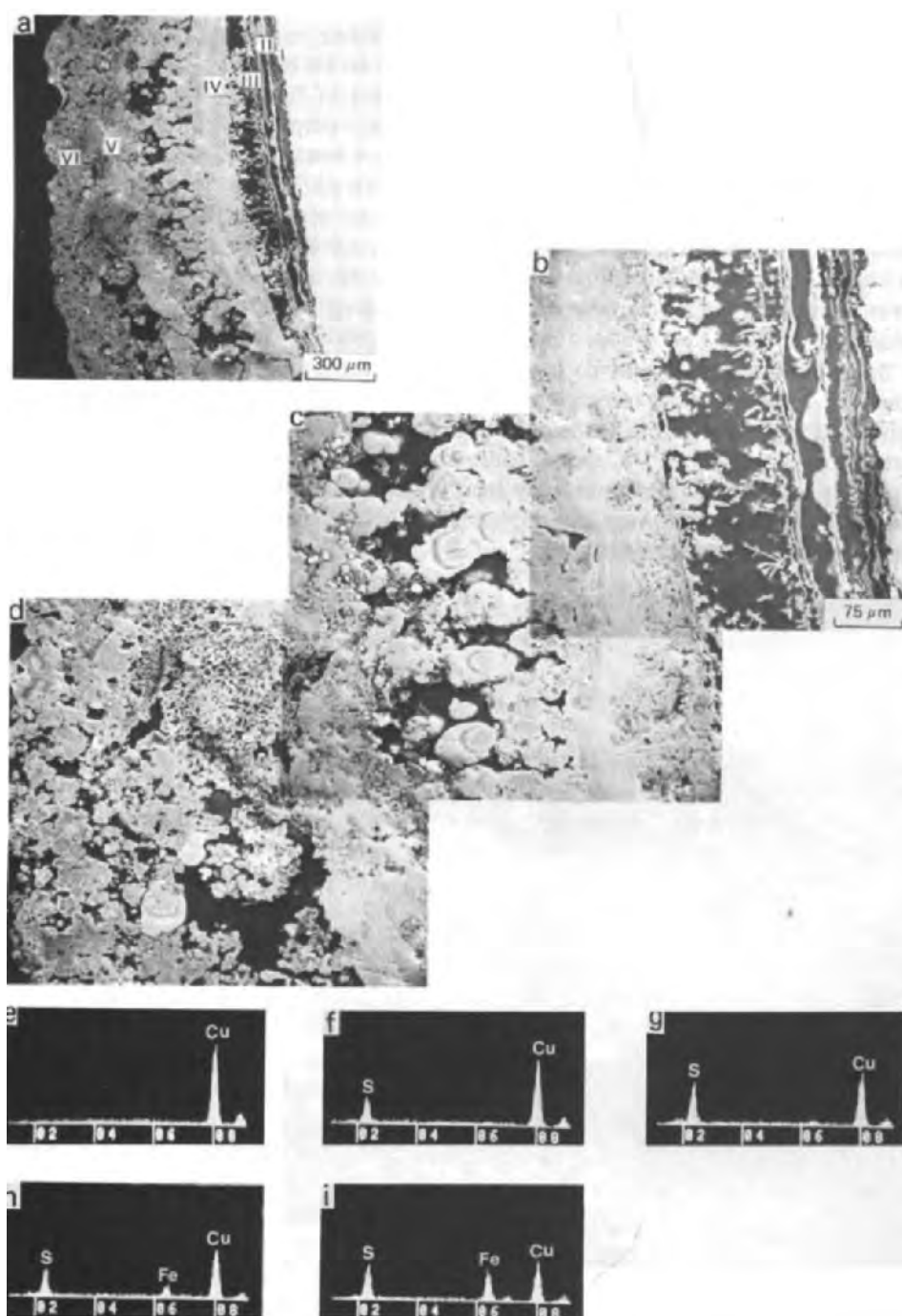
Area c contained six zones (Fig.3 and Fig.6a). The central part of Fig. 6a has been enlarged in Fig.6,b—d. The copper filter segment is now present, because submicroscopic work was done on a polished block in which the copper filter segment could be retained during the grinding procedure. As a consequence the process by which flakes were produced from the filter segment could be studied.

The corroded copper filter segment is represented by zone C I (Fig.3) and visible in Fig.6b. Other micrographs of this zone were presented in figs.9—13 of Bisdom et al. (1983a). The edge of the filter segment is indented. EDXRA measurements indicated that the filter only gave copper if analysed inside the segment away from the edges (Fig.6e). Analyses of the edge itself, often coloured whitish along a very small line, demonstrated a little sulphur together with copper (Fig.6f). It is not known whether this is already covellite.

Zone C II (Fig.6, a and b) was the zone with flakes derived from the filter segment. The continuation of the peeled off flakes is demonstrated well in Fig.6a. A more detailed view in Fig.6b indicates that the flakes can either stay rather straight over some length or become bent. Point analyses showed that the amount of sulphur had increased in the flakes (Fig.6g), compared to sulphur at the edge of the copper filter segment. It was assumed that covellite was present in the flakes.

Zone C III (Fig.6, a and b) can be compared to the zones with needles on the inside of the tube. The flakes have mainly disappeared and precipitates appear in quantity. Some iron appeared viz. nearest to the wall of the tube (Fig.6h). The outer part of this zone still contained copper in significant quantities together with sulphur and more iron (Fig.6i). The zones C III and C II were rather porous.

Fig.6. BESI of area c with six zones (a). The copper filter segment is represented here and in Figs.7 and 8, because submicroscopic work was done on a polished block. The middle part of (a) has been enlarged in (b) to (d). Point analyses (e) to (i) indicated that a little sulphur was present in the corroded edge of the filter (f) and that the amount of sulphur had increased in the flakes which were derived from the copper filter segment. Iron appeared in zone C III (cf. Fig.3) and was subsequently represented in all younger zones.



Zone C IV (Fig.6,a–c) contained a few rather massive layers on top of which grew forms in which concentric rings can be discerned. Similar forms and more or less dendritic patterns were found in figs.14–15 of Bisdom et al. (1983a). The precipitates contained iron, sulphur and copper. Zinc, which appeared in zone C III, was also present both in this zone and in the younger ones. The zinc could be present in small patches.

Zone C V (Fig.6,a, c and d) also seemed to start with a massive layer, which was not continuous. The composition of the precipitates is similar to those in zone C IV. This is also the case for the precipitates in the remainder of zone C V, some of the materials of which had a honeycomb structure.

Zone C VI (Fig.6,a and d) is the youngest zone in the precipitates with a position farthest away from the filter. A heterogeneous morphology was exhibited by the precipitates in which various pores occurred. Only the outermost zone of C VI had a somewhat different composition. The precipitates contained predominantly iron with small quantities of Si, S and Zn. The zone could be compared to zone A VI of area a inside the tube in which iron hydroxides occurred.

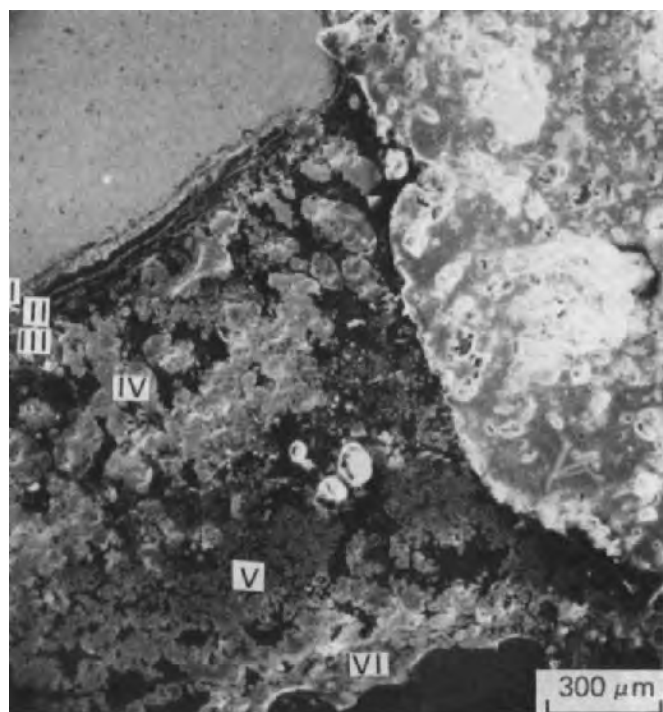


Fig.7. BESI of area d with six zones and a quartz pebble which is stuck in the opening of the filter. Only the youngest zones bend around the pebble.

Area d

Area d (Fig.7) contained six zones and a quartz pebble stuck into an opening of the filter. Only zones D IV and D V bent around the quartz pebble. The older zones stopped when they reached it. Emplacement of the quartz pebble is thought to have occurred at an early stage, possibly during emplacement of the tube or just after. It is also possible, however, that emplacement of the quartz pebble occurred during the deposition of zone D V; the first zone to bend around the pebble.

Zone D I shows the corroded edge of the filter segment and zone D II shows flakes derived from this segment. Sulphur and copper were present, starting with a little sulphur at the edge of the segment and more sulphur in the flakes. A relatively massive zone, part of which was not affected by corrosion, has broken away from the filter segment in zone D II. This massive band disintegrated into various flakes at some distance from the tube and in the same zone DII.

Zone D III, the zone with needles or finger-like outgrowths, occupied only part of the micrograph (cf. Fig.3). The more massive rings of zone D IV touched the flakes of zone D II in the other part of the micrograph. Sulphur, iron and copper were represented in zones D III and D IV. Zn was only measured in zone D IV. Zone D V contained sulphur, iron and copper. The precipitates were porous and a honeycomb structure was present in some of the materials. Zone D VI was more massive and contained iron and sulphur. The presence of iron hydroxide is probable.

Comparison of areas c and d

The comparison of both areas is rather easy because most of the zones can be recognized in areas c and d. One of the main differences is that zone D III is not continuous, whereas zone C III is. Also, zone C IV has a rather massive basis and this is not the case in zone D IV.

Corrosion of the tube was indicated by a little sulphur at the edge of the filter segment. The edge itself was frequently indicated by a whitish line which contained the sulphur when subjected to point analyses. The flakes were well developed in both micrographs.

The distribution of chemical elements indicated that copper was mostly present close to the tube and iron in the youngest zones away from the filter. Iron was not found in zones C I, C II, D I and D II. Sulphur was always present but least in zone C VI. It is envisaged that iron hydroxides were present in the external part of zone C VI and in zone D VI. Due to the work with a polished block, however, transmitted light microscopy could not be done. Identification of iron hydroxide was therefore mainly done by comparison with zone A VI. Zinc was present in zones C III to C VI of area c but only in zone D IV of area d.

Area e

Area e (Fig.8) covers the entrance of the tube between two copper filter segments, and therefore has a double set of zones (Fig.3). Precipitates have

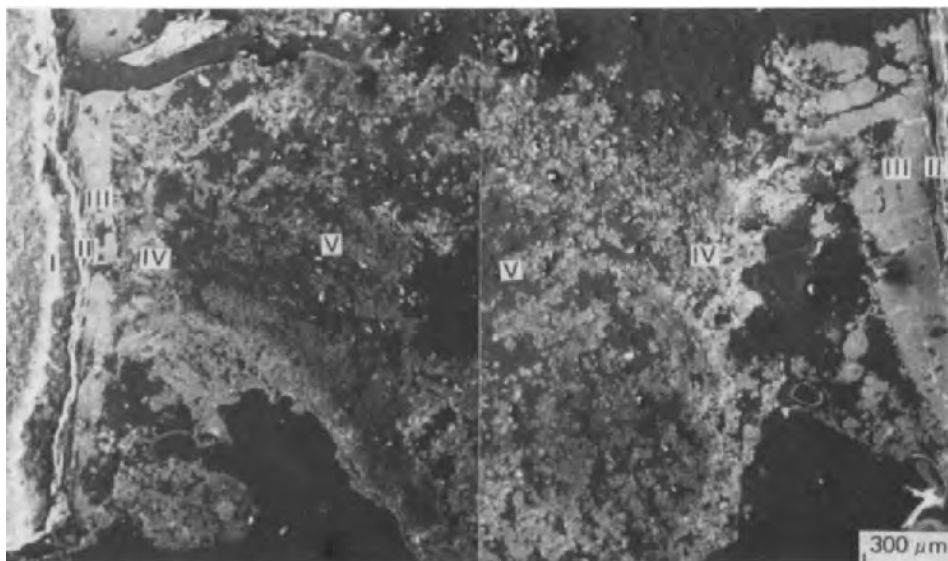


Fig.8. BESI of area e with five zones. The zones can be compared to those of other areas (cf. Fig.3). The youngest zones of precipitates on two filter segments merged and clogged the entrance of the tube.

clogged the entrance of the tube. Five zones could be distinguished, i.e. three related to each of the two filter segments and two which had merged together. Zones E I contained the edges of the corroding filter segments with some S and a high quantity of copper. Zones E II contained the flakes with more sulphur than copper. The massive zones E III were mainly deposited directly on top of zones E II without the zone with needle shapes. Zones E III contained sulphur, iron, copper and zinc. No well-developed concentric rings were found.

The central part of the entrance of the tube with zones E IV and E V, demonstrated a kind of arrested flow structure which has been drawn in Fig.3. Zone E IV contained sulphur, iron and zinc, and extended between the two E III zones from one segment to the other. Zone E V did not penetrate into the internal part of the tube. It extended into the external part of the tube and was surrounded on three sides by zone E IV. Zone E V contained less iron and more sulphur than zone E IV. Zinc was present in small quantities in both zones. Zone E V was porous if compared to zone E IV. The latter zone was denser and contained a few larger pores as well as small ones.

Comparison of area e with areas a to d

Zone E I is comparable to zones C I and D I. No equivalent to zone E I can be found on the internal part of the tube because no filter segment was represented after preparation of a thin section. Zone E II, however, is

equivalent to zones A I and B I with flakes and to zones C II and D II. The massive zone E III can be compared to zones A III and C IV, whereas less massive or dense precipitates were found in zones B III and D IV. Zones E IV and E V were similar in morphology and composition to zones A VI, B V and C VI.

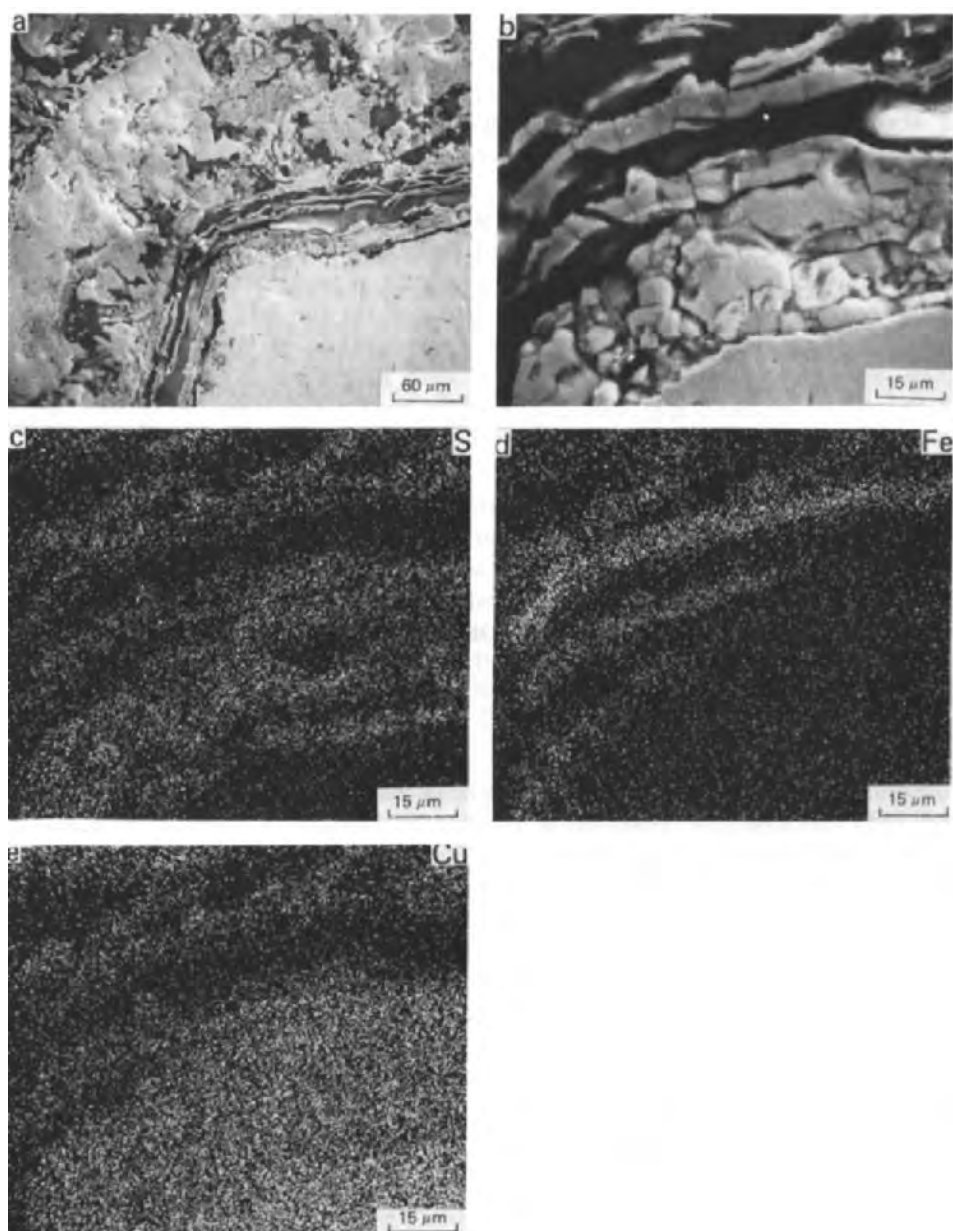


Fig.9. BES of the corroded corner of a copper filter segment, flakes and precipitates (a). The central part of (a) was enlarged (b) and X-ray images of sulphur (c), iron (d) and copper (e) were made (cf. text).

XRD analysis

XRD analysis demonstrated that covellite (CuS) was the principal constituent of the inner zones close to the filter segment, whereas iron hydroxide was the main constituent in the outer zones with the highest zone-numbers. Calcite (CaCO_3) and gypsum ($\text{CaSO}_4 \cdot 2\text{H}_2\text{O}$) were also determined. Siderite (FeCO_3), quartz (SiO_2) and sulphur (S) were also recognized. The identification of cuprite (Cu_2O), magnesium ferrite (MgFe_2O_4), chalcopyrite (CuFeS_2) and akageneite ($\beta\text{-FeOOH}$) was not certain. XRD analysis did not indicate compounds with zinc, although this element was represented above trace element quantities according to SEM-EDXRA analysis. It is therefore possibly present in an amorphous form.

Flake-development at the corner of a filter segment

An example of the development of flakes at the corner of a filter segment is given in Fig.9a. The images were made from the lower left corner of the copper filter segment which is situated on the left in Fig.3. No schematic drawing was made in this case. Only details of the inner zones are given. It is clearly visible that the zone with flakes bends around the corner of the filter segment and that the massive zone was deposited immediately on top of the flakes (Fig.9a).

A detail of the central part of Fig.9a is given in Fig.9b. X-ray images of the area in the latter micrograph were made of sulphur (Fig.9c), iron (Fig.9d) and copper (Fig.9e). The distribution of iron in Fig.9d indicated that this element was represented in the zone with flakes; similar to zones A I and B I with flakes inside the tube but different from zones C II, D II and E II with flakes because no iron was detected in these zones with EDXRA.

CONCLUSIONS

The study of precipitates on filter segments of a tube indicated a rather complex environment in which a variety of reactions have taken place. XRD and light microscopic analyses were able to identify a number of minerals in the precipitates which were predominantly comprised of amorphous and poorly crystalline materials. The latter precipitates could be analysed for their chemical elements by SEM-EDXRA and enlarged by SEM to observe the morphological detail.

Various zones were identified in areas a–e. Copper was represented in larger quantities close to the tube, both inside and outside. Iron was most represented in the youngest zones away from the filter segments. A similar distribution was found in the clogging precipitates at the entrance to the filter. Copper could occur in all zones and a little iron could be present in the flakes close to the tube. Usually, however, the flakes contained only copper and sulphur. These elements were also found by XRD analysis in covellite (CuS). The corrosion of the copper filter segments themselves was indicated by indented edges. A thin whitish line could often be observ-

ed along the edges. Point analyses indicated a little sulphur together with copper in this line. The amount of sulphur had increased in the flakes which were derived from the filter segments.

Sulphur was a very common element in most zones and probably formed a number of compounds with copper, iron and zinc. Only covellite was indentified, however, near to the tube and in the inner zones. Poorly crystalline to amorphous iron hydroxides occurred in the outer and youngest zones, both inside and outside the tube. Calcite and gypsum were also formed, i.e. only inside the tube, and in an environment which was constantly submerged according to the available well data.

The investigation of amorphous and poorly crystalline materials with SEM-EDXRA demonstrated the presence of various heavy elements and sulphur. To obtain additional information work should be done with EMA (electron microprobe analyzer) or SEM-WDXRA (scanning electron microscope — wavelength dispersive X-ray analyzer) — instruments not used in this study. If quantification of all elements, including trace elements, is also required, SIMS (secondary ion mass spectrometry) should be used (Bisdorn et al., 1977, 1983b; Henstra et al., 1980). The latter submicroscopic technique, however, is even more costly than the electron microscopic ones and can therefore only be applied if considered of prime importance for the success of a major project.

REFERENCES

- Bisdorn, E.B.A., 1983. In situ microanalysis of man-made precipitates in soil beneath a landfill and on the surface of a water-tube filter. In: R. Hallberg (Editor), *Environmental Biogeochemistry*. 5th International Symposium on Environmental Biogeochemistry, 1981, Stockholm. Ecological Bulletins, 35: 547—553.
- Bisdorn, E.B.A. and Jongerius, A., 1979. Onderzoek naar verstoppend materiaal in een waterleidingbuis m.b.v. lichtmicroscopie, REM-EDAX en röntgendiffractie (in Dutch). Report No. 1471. Netherlands Soil Survey Institute, Wageningen, 15 pp.
- Bisdorn, E.B.A., Henstra, S., Jongerius, A. and Thiel, F., 1975. Energy dispersive X-ray analysis on thin sections and unimpregnated soil material. *Neth. J. Agric. Sci.*, 23(4): 113—125.
- Bisdorn, E.B.A., Henstra, S., Hornsveld, E.M., Jongerius, A. and Letsch, A.C., 1976. Wavelength and energy dispersive X-ray microanalysis with EMA and SEM-EDXRA on thin sections of soils. *Neth. J. Agric. Sci.*, 24(4): 209—222.
- Bisdorn, E.B.A., Henstra, S., Jongerius, A., Brown, J.D., von Rosenstiel, A.P. and Gras, D.J., 1977. Light and heavy element detection in thin sections of soils with the ion microprobe mass analyzer (IMMA). *Neth. J. Agric. Sci.*, 25(1): 1—13.
- Bisdorn, E.B.A., Thiel, F., Volbert, B. and Jackman, J., 1983a. Variations in backscattered electron (BSE) images with a Scanning Electron Microscope (SEM) as applied to mineral grains and excrements in a podzol, to precipitates on a water-tube filter and to bauxite. *Geoderma*, 30: 93—116.
- Bisdorn, E.B.A., Henstra, S., Werner, H.W., Boudewijn, P.R., Knippenberg, W.F., Grefte, H.A.M. de, Gourgout, J.M. and Migeon, H.N., 1983b. Quantitative analysis of trace and major elements in thin sections of soils with the secondary ion microscope (Cameca). *Geoderma*, 30: 117—134.

- Henstra, S., Bisdorf, E.B.A., Jongerius, A., Morgan, A.E., Werner, H.W. and Grefte, H.A.M. de, 1980. Quantitative analysis on thin sections of soils by secondary ion mass spectrometry. In: P. Brederoo and V.E. Cosslett (Editors), *Electron Microscopy 1980. Proceedings of the 7th European Congress on Electron Microscopy including the 9th International Conference on X-ray Optics and Microanalysis*, The Hague. Seventh European Congress on Electron Microscopy Foundation, Leiden, 1980. Vol. 3. Analysis, pp. 224—225.
- Jongerius, A. and Heintzberger, G., 1975. Methods in soil micromorphology. A technique for the preparation of large thin sections. *Neth. Soil Surv. Inst. Wageningen, Soil Surv. Pap.*, 10: 48 pp.

APPLIED SUBMICROSCOPY AND IMAGE ANALYSIS

This Page Intentionally Left Blank

QUANTIMET 720 ANALYSIS OF POROSITIES IN BACKSCATTERED ELECTRON SCANNING IMAGES MADE WITH DIFFERENT PHOTO-TECHNIQUES

D. SCHOONDERBEEK¹, F. THIEL² and E.B.A. BISDOM¹

¹*Netherlands Soil Survey Institute, P.O. Box 98, 6700 AB Wageningen (The Netherlands)*

²*Technical and Physical Engineering Research Service, 6700 AJ Wageningen (The Netherlands)*

(Accepted for publication February 17, 1983)

ABSTRACT

Schoonderbeek, D., Thiel, F. and Bisdom, E.B.A., 1983. Quantimet 720 analysis of porosities in backscattered electron scanning images made with different photo-techniques. *Geoderma*, 30: 271–275.

Three photo-techniques were used to make backscattered electron scanning images (BESI) of the same area in a thin section of soil using a scanning electron microscope (SEM). Subsequent porosity analysis with an image analyzer (Quantimet 720) showed that different results could be obtained in a number of diameter classes while the total porosity was virtually the same, a phenomenon which may be related to beam instability of SEM. Under such conditions, one needs a dependable photo-technique in which soil constituents on a BESI micrograph can be compared with the same constituents on the display screen of SEM and Quantimet. Such a photo-technique is suggested and can be used to obtain a limited number of measurable BESI micrographs.

INTRODUCTION

Larger pores in thin sections can be measured and characterized by a combination of light microscopic and Quantimet techniques (Jongerius et al., 1972; Jongerius, 1974; Ismail, 1975; Bouma et al., 1977; Murphy et al., 1977). The image analyzer can analyse voids with diameters larger than 30 μm in structure photograms made with transmitted light. Smaller voids cannot be measured using this technique due to the thickness of a thin section which is usually about 30 μm or less.

Backscattered electron scanning images (BESI) can be used for the portrayal of microvoids and larger, because information is predominantly obtained from a thin layer at a depth of a few micrometres below the surface of a thin section (Bisdom and Thiel, 1981). BESI can therefore be used to measure both smaller and larger pores (Jongerius and Bisdom, 1981). In practice, pores smaller than 100 μm are measured on BESI by Quantimet. Larger pores can also be analysed in this way but it is more economical to do this using light microscopic and Quantimet techniques.

The present paper discusses the variation in porosity measurements with the Quantimet 720 on BESI made with different photo-techniques and with a SEM in which beam instability occurred. This study has been performed to obtain a dependable photo-technique which allows porosity analysis from a small number of BESI micrographs under such conditions.

MATERIALS AND METHODS

Backscattered electron scanning images were obtained using different photo-techniques from the same area in a thin section of a ploughpan developed in sandy loam of southwest Netherlands. BESI were made with a Jeol-JSM-35C scanning electron microscope equipped with a backscattered electron detector of the semi-conductor type containing two solid state detectors. BESI can be made on film, photographic paper, or both.

Quantimet 720 analysis of porosities in thin sections of soils is usually done from film negatives or positives. The input to the Quantimet of such film is done via a light microscope or an epidiascope. Photographic paper can be used as a control, to compare images from the film on the display screen of the Quantimet. In the present case, three different photo-techniques were used to obtain BESI on a film; with or without paper prints as a control.

The first photo-technique involved a 24 mm \times 36 mm negative from Ilford Pan F. No paper print was made. The second method used a 9 cm \times 12 cm positive and a paper print made from the small film negative obtained with the first technique. Polaroid 55 P/N film was used in the third technique in which a negative as well as a 9 cm \times 12 cm paper print was obtained. For the Quantimet measurements, the micrographs obtained with these three techniques from the same area in a thin section, were subdivided into a number of fields.

RESULTS

The area of which the porosity was studied by Quantimet is given in Fig. 1. The original magnification of the BESI micrograph, made with the third technique on Polaroid 55 P/N film, was \times 100. Such an enlargement is relatively low for submicroscopic work but is sufficient to include capillary pores which have a diameter of 30 μ m or less (Table I). If smaller pores are also of interest, larger magnifications can be made until a maximum is reached. The maximum magnification is strongly dependent on the type of material being investigated in the thin section and on the possibilities of the back-scattered electron detector system of the SEM used.

For measurements by Quantimet the area on BESI was subdivided into four fields on the small film negative of 24 mm \times 36 mm (first photo-technique) and into twenty-four fields on the positives and negative of 9 cm \times 12 cm (second and third technique). An average of all Quantimet measurements, done on BESI at \times 100 and with the three techniques, is given in

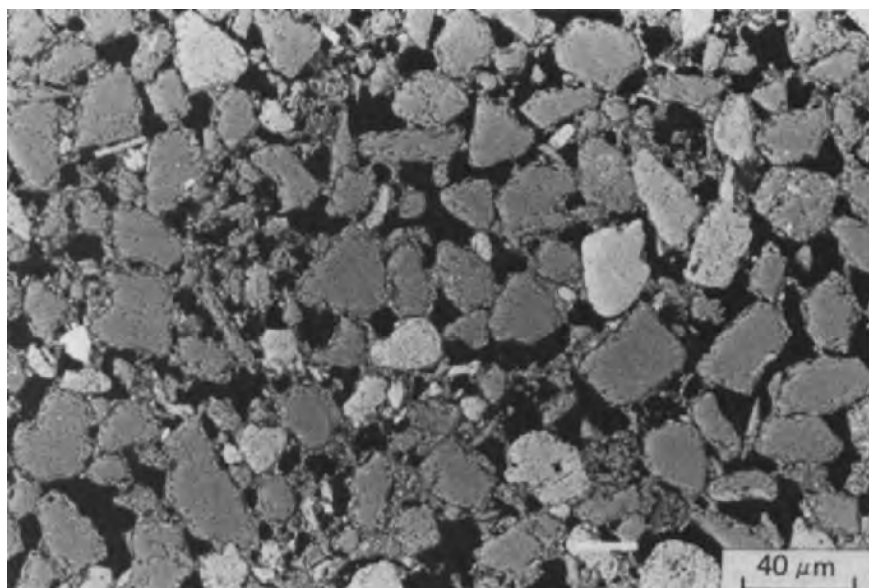


Fig. 1. BESI of a microarea in a ploughpan which was used to test different photo-techniques.

Table I. In this table seven pore diameter classes are presented together with their porosities and the total porosity of all the voids measured. The smallest pores analysed had a diameter of $0.3\ \mu\text{m}$, while the largest diameters were more than $100\ \mu\text{m}$.

Measurements of the porosity on the enlarged $9\ \text{cm} \times 12\ \text{cm}$ positive (second photo-technique) were different from the porosity measurements obtained with techniques one and three (Table I). The measured total porosity was 30.9% instead of 23.5% or 23.6%. This is a large difference which must be due to enlargement of the negative of $24\ \text{mm} \times 36\ \text{mm}$ to a positive of $9\ \text{cm} \times 12\ \text{cm}$. Apparently, the area occupied by black to grey colours increases significantly on the positive film during enlargement.

The total porosity on the $24\ \text{mm} \times 36\ \text{mm}$ negative film (photo-technique no. 1) is 23.5% and hardly differs from the total porosity measured with technique no. 3. Both techniques, however, show differences of porosities in a number of diameter classes. For example, from 3.0 to $6.0\ \mu\text{m}$ and 6.0 to $15.0\ \mu\text{m}$. Such differences in porosity measurements may be related to beam instability of the SEM which is being used.

If the Polaroid 55 P/N film of photo-technique no. 3 is used, we obtain simultaneously a paper print and a film negative of $9\ \text{cm} \times 12\ \text{cm}$. This paper print can be used directly to determine the quality of BESI and subsequently to control the detection and measurements by Quantimet 720. The result is that one has controlled Quantimet measurements from BESI that are of a good quality. Such control is not possible with technique no. 1 in which

TABLE I

Quantimet measurements on BESI ($\times 100$) of the porosity of the same microarea by three different photo-techniques

Photo-techniques	Diameter classes (μm)	Porosity (%)	Total porosity (%)
No. 1: 24 mm \times 36 mm negative — Ilford Pan F	0.30— 0.90 0.91— 3.00 3.01— 6.00 6.01— 15.00 15.01— 30.00 30.01—100.00 >100.00	0.1 0.9 3.7 2.6 7.0 8.3 0.9	23.5
No. 2: 9 cm \times 12 cm positive and paper print — enlargement of the small film negative obtained with photo-technique no. 1	0.30— 0.90 0.91— 3.00 3.01— 6.00 6.01— 15.00 15.01— 30.00 30.01—100.00 >100.00	0.1 2.0 9.0 1.8 10.0 8.0 0.0	30.9
No. 3: 9 cm \times 12 cm direct negative and paper print — Polaroid 55 P/N	0.30— 0.90 0.91— 3.00 3.01— 6.00 6.01— 15.00 15.01— 30.00 30.01—100.00 >100.00	0.1 0.6 5.1 0.9 6.7 8.9 1.3	23.6

only negatives are used. It was also demonstrated that enlarged positives or paper prints (9 cm \times 12 cm) of photo-technique no. 2, obtained from the 24 mm \times 36 mm negatives (photo-technique no. 1), did not give dependable porosity measurements. Consequently, we prefer to work with Polaroid 55 P/N film if a scanning electron microscope is used in which beam instability may occur.

CONCLUSIONS

If a SEM is used which, due to beam instability, can cause problems in the production of constant high quality micrographs, a controlling photo-technique should be used. Such control can be exerted by using a Polaroid 55 P/N film (photo-technique no. 3) in which both negative and paper print are 9 cm \times 12 cm. On the paper print, one can observe whether this BESI micrograph is of a good quality and compare it with what is visible on the display screen of the SEM. The same BESI paper print is subsequently used to check the image on the display screen, often called display, of the Quantimet 720.

Enlarged 9 cm \times 12 cm film and paper print (photo-technique no. 2), from a 24 mm \times 36 mm negative, did not give accurate porosity measure-

ments due to photographic processing. Quantimet measurements done on a small film negative (photo-technique no. 1) gave a similar total porosity measurement to the one found with the Polaroid 55 P/N film (photo-technique no. 3). Differences existed, however, in porosities of a number of diameter classes. Under such conditions, possibly due to beam instability, photo-technique no. 3 is preferred. Only a limited number of high quality BESI micrographs can be obtained with photo-technique no. 3. If a large quantity of BESI micrographs is required, equipment for beam stabilization is necessary in the SEM. Under such conditions, one can also work with photo-technique no. 1 using 24 mm \times 36 mm negatives of Ilford Pan F or another film.

REFERENCES

- Bisdom, E.B.A. and Thiel, F., 1981. Backscattered electron scanning images of porosities in thin sections of soils, weathered rocks and oil-gas reservoir rocks using SEM-EDXRA. In: E.B.A. Bisdom (Editor), *Submicroscopy of Soils and Weathered Rocks*. 1st Workshop of the International Working-Group on Submicroscopy of Undisturbed Soil Materials (IWGSUSM) 1980, Wageningen. Centre for Agricultural Publishing and Documentation (Pudoc), Wageningen, pp. 191–206.
- Bouma, J., Jongerius, A., Boersma, O., Jager, A. and Schoonderbeek, D., 1977. The function of different types of macropores during saturated flow through four swelling soil horizons. *Soil Sci. Soc. Am. J.*, 41 (5): 945–950.
- Ismail, S.N.A., 1975. Micromorphometric soil-porosity characterization by means of electro-optical image analysis (Quantimet 720). *Neth. Soil Surv. Inst. Wageningen, Soil. Surv. Pap.*, 9: 104 pp.
- Jongerius, A., 1974. Recent developments in soil micromorphology. In: G.K. Rutherford (Editor), *Soil Microscopy*. Proceedings of the 4th International Working-Meeting on Soil Micromorphology, Kingston, 1973. The Limestone Press, Kingston, Ont., pp. 67–83.
- Jongerius, A. and Bisdom, E.B.A., 1981. Porosity measurements using the Quantimet 720 on backscattered electron scanning images of thin sections of soils. In: E.B.A. Bisdom (Editor), *Submicroscopy of Soils and Weathered Rocks*. 1st Workshop of the International Working-Group on Submicroscopy of Undisturbed Soil Materials (IWGSUSM) 1980, Wageningen. Centre for Agricultural Publishing and Documentation (Pudoc), Wageningen. pp. 207–216.
- Jongerius, A., Schoonderbeek, D. and Jager, A., 1972. The application of the Quantimet 720 in soil micromorphology. *The Microscope*, 20: 243–254.
- Murphy, C.P. Bullock, P. and Turner, R.H., 1977. The measurement and characterisation of voids in soil thin sections by image analysis, Part I. Principles and techniques. *J. Soil Sci.*, 28 (3): 498–508.

This Page Intentionally Left Blank

THE CHARACTERIZATION OF MICROPOROSITY IN A PLOUGH PAN BY SUBMICROSCOPIC AND QUANTIMET TECHNIQUES

A. JAGER, O. BOERSMA and E.B.A. BISDOM

Netherlands Soil Survey Institute, P.O. Box 98, 6700 AB Wageningen (The Netherlands)

(Accepted for publication February 17, 1983)

ABSTRACT

Jager, A., Boersma, O. and Bisdom, E.B.A., 1983. The characterization of microporosity in a ploughpan by submicroscopic and Quantimet techniques. *Geoderma*, 30: 277–283.

Ploughpans are usually recognizable in thin sections because of their massiveness (density) when compared with adjacent parts of the soil. When pores can be measured in the ploughpan such massiveness can be documented and compared with the porosity of the underlying soil profile. Such measurements, however, concern only meso- and macropores when done by Quantimet on micrographs obtained with the light microscope. This is due to the thickness of the thin section and the necessity to work with transmitted light. The measurement of the smaller mesopores may also be problematic with the light microscopy—Quantimet technique.

The introduction of backscattered electron scanning images allows to obtain micrographs of a very thin layer and this made it possible to measure micro- and mesopores by Quantimet. If only small magnifications are used, macropores can also be measured.

In the present investigation, micro- and mesopores were quantified by a combination of backscattered electron and Quantimet techniques and the macropores by light microscopy and Quantimet. It was demonstrated that macro- and mesopores were less frequent in a ploughpan than outside, whereas capillary or micropores increased somewhat.

INTRODUCTION

Soil compaction leading to the formation of ploughpans (Fig. 1) is a significant problem in sandy loams of arable land from areas with river- and sea clays. It is usually caused by soil tillage when the soil is too wet. This may give puddling and compaction of the soil materials underneath the furrow to form a ploughpan. The soil compaction, however, is not only caused by machines under humid conditions but can also be influenced by the degree of structure stability which itself is, amongst other things, dependent on the clay and humus content. Field and micromorphological observations have also shown that intensive arable farming may lead to a decrease in the activity of soil organisms coupled with a degradation of soil structure.

The characterization of compaction in a soil can be done by a comparison of the porosities in compacted and looser parts of the same soil using light microscopic and Quantimet techniques (Jongerius et al., 1972, Jongerius,

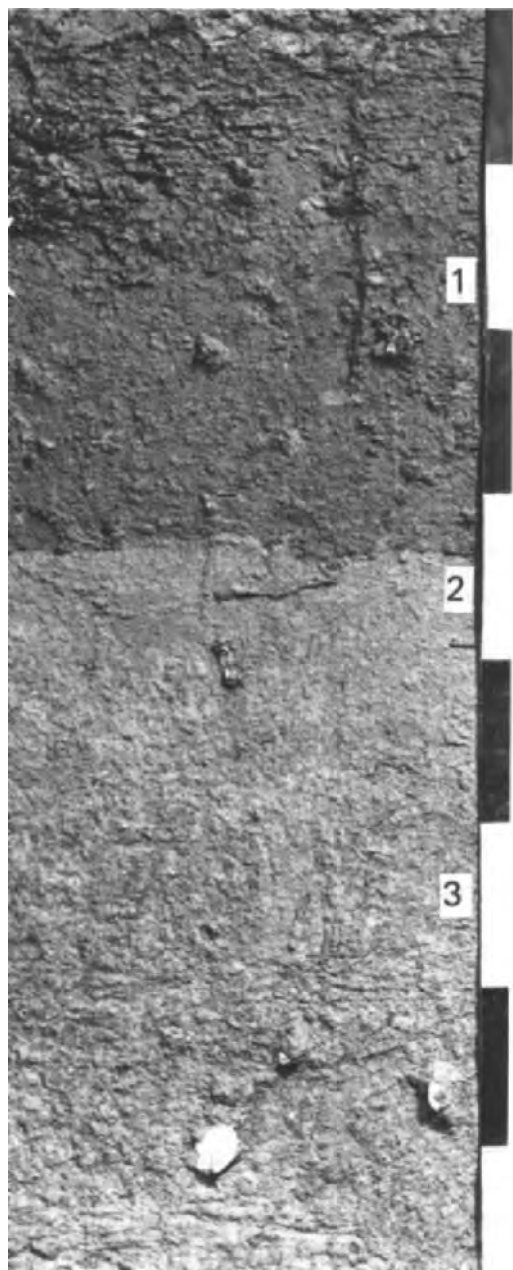


Fig. 1. Lacquer peel of sandy loam with a ploughed horizon (1), a ploughpan (2) and an undisturbed soil horizon with shells (3).

1974; Ismail, 1975). However, only pores with diameters larger than $30\text{ }\mu\text{m}$ can be analysed, because transmitted light is used and the thickness of a thin section frequently approaches this value. Consequently, only mesopores with diameters from $30\text{ }\mu\text{m}$ to $100\text{ }\mu\text{m}$ and macropores with diameters larger than $100\text{ }\mu\text{m}$ can be analysed. Micropores, capillary pores with diameters smaller than $30\text{ }\mu\text{m}$, need to be measured with a Quantimet on micrographs which are obtained with a submicroscopic technique.

MATERIALS AND METHODS

Backscattered electron scanning images (BESI) (Bisdom and Thiel, 1981) can be used to characterize micro-, meso- and macropores (Jongerus and Bisdom, 1981). With this submicroscopic technique, predominantly micropores and mesopores are studied by Quantimet. The instrument used was a Jeol-JSM-35C equipped with a backscattered electron detector of the semiconductor type comprising two solid state detectors. The smallest diameter of pores measured in this study was $3\text{ }\mu\text{m}$.

A Quantimet 720 image analyzer equipped with a light microscope and an epidiascope, was used to study negative film obtained with a scanning electron microscope (SEM). The film was the negative of Polaroid P/N which also provided paper prints. During Quantimet study of the negatives BESI were portrayed on the display screen and the porosity was measured.

BESI are obtained from a thin layer at predominantly some micrometres depth below the surface of the thin section. Backscattered electrons from nearer-to-surface parts of the thin section are also involved but the main image is obtained from a small depth in the thin section. The signal is derived from a thin layer which is a few micrometres thick. This layer is usually situated deeper in plastic-impregnated pores than in minerals. Such a thin layer allows Quantimet measurements of even very small pores, dependent on the magnification used to obtain BESI and the type of material which is analysed.

In the present study, both capillary pores (micropores) and mesopores were measured by Quantimet from BESI, while Quantimet and light microscopic micrographs were used to obtain porosity figures on macropores.

RESULTS

The characterization of porosities in ploughpans of sandy loams in the southwest of the Netherlands forms part of a survey in which compaction phenomena are studied on a number of farms. The aim of this porosity and structure study is to obtain information which can prevent structure deterioration and improve the structure of compacted soils. This has a direct effect on the growth of crops.

Ploughpans are usually easy to distinguish from the overlying ploughed layer and the underlying soil pedon if attention is paid to structure morphology (Fig. 1). When only a small amount of clay is present the ploughpan is

frequently rather massive (dense) without structure, or a weakly developed platy structure can be recognized. If the clay content increases, however, angular blocky structure elements are common. Most ploughpans are only a few centimetres thick, but thicknesses up to 15 cm were measured.

The ploughpan in soils with small amounts of clay usually affects water transport and root penetration more than one in soils with more clay. This is due to the usually massive structure of the former ploughpan which leads

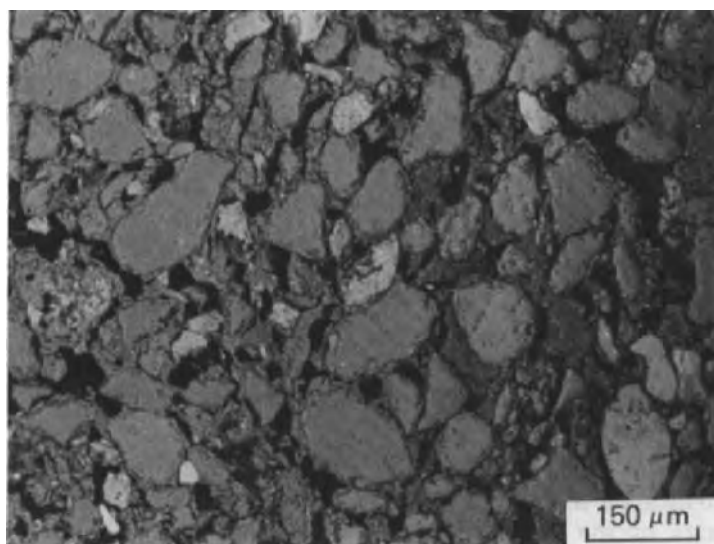


Fig. 2. Backscattered electron scanning image of a small part of the massive ploughpan.

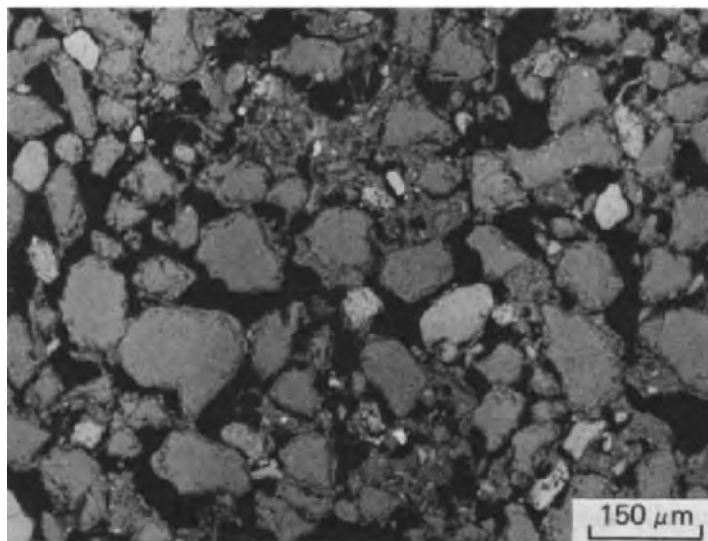


Fig. 3. BESI of a small part of the undisturbed and uncompacted soil horizon underneath the ploughpan.

to stagnation of superfluous rainwater and the formation of puddles in the furrows. Those developed in soils richer in clay usually have the possibility to form cracks due to swelling and shrinkage of the clay component. This will not be the case in winter when the soil is swollen but starts during spring. The result is that an angular blocky structure is formed in the ploughpan.

The present investigation was carried out to obtain BESI-Quantimet information on porosities present in the ploughpan itself and in the underlying more porous part of the soil. Microareas were selected in the massive ploughpan (Fig. 2) and in the undisturbed soil with a low clay content just underneath it (Fig. 3). BESI allowed portrayal of micro-, meso- and macropores. The latter, however, can be measured better with a combination of light microscopic and Quantimet techniques because this works faster and is accurate (cf. Jongerius and Bisdom, 1981). The results of porosity measurements both in the ploughpan and underneath it are given in Fig. 4. The differences in the porosity characteristics between the two are as follows.

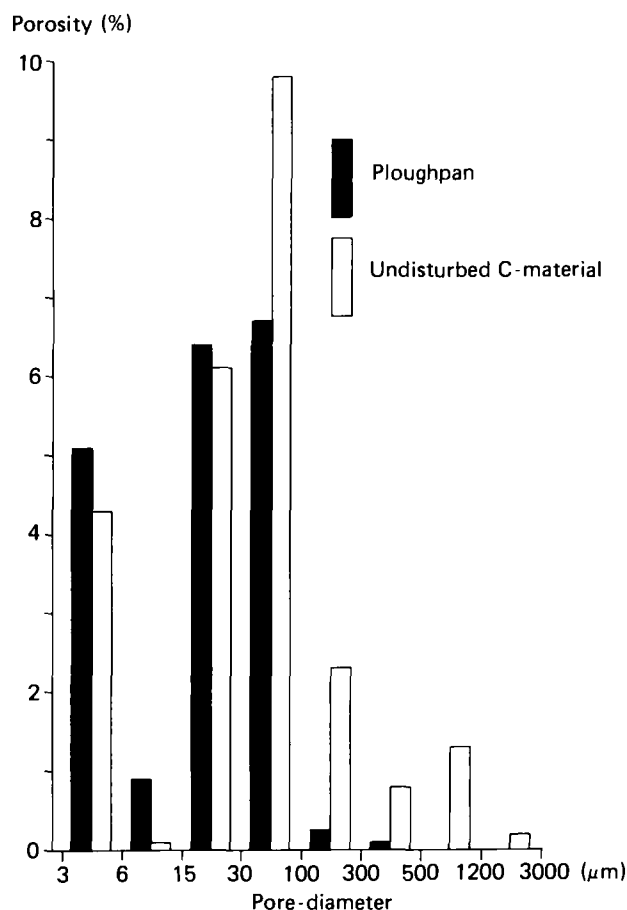


Fig. 4. Quantimet measurements of micro-, meso- and macropores from BESI of the ploughpan and the undisturbed horizon.

The undisturbed porous part underneath the ploughpan has macropores, whereas the largest macropores are absent in the ploughpan and the smaller macropores have significantly decreased in number. Consequently, most of the macropores are lost when a massive ploughpan is formed.

Mesopores with diameters of 30 μm to 100 μm also decrease in the ploughpan if compared with the underlying undisturbed soil. Micropores, in this case with diameters between 3 μm and 30 μm , are present in larger numbers in the ploughpan. Differences in numbers of micropores in the ploughpan and porous soil are, however, less pronounced than expected.

In the present investigation no attention was paid to differences in shapes of pores and it is, therefore, not yet known which changes in forms occur during the formation of a massive ploughpan in a sandy loam soil. The reason for this omission is that we would prefer to study the porosity of a larger number of ploughpans and underlying soil before figures are given on form changes of pores during the formation of different types of ploughpans.

CONCLUSIONS

The combination of backscattered electron scanning images and Quantimet measurements has allowed the study of capillary and larger pores. Macropores were measured using light microscopic and Quantimet techniques. It could be shown that virtually no macropores, pores with diameters larger than 100 μm , remained in the massive ploughpan. Mesopores also decreased in number, whereas the quantity of pores with diameters between 3 μm and 30 μm increased somewhat.

The present combination of light microscopic, submicroscopic and Quantimet techniques can be used to study a variety of compaction phenomena in soils by investigating porosity characteristics. It is important that capillary pores can also be measured. Pores with diameters less than 3 μm can be measured with the image analyzer if sufficient *BESI* are made at higher magnifications. The comparison of the figures on micro-, meso- and macropores will give information on changes in porosity characteristics when soil is compacted.

REFERENCES

- Bisdorn, E.B.A. and Thiel, F., 1981. Backscattered electron scanning images of porosities in thin sections of soils, weathered rocks and oil-gas reservoir rocks using SEM-EDXRA. In: E.B.A. Bisdorn (Editor), *Submicroscopy of Soils and Weathered Rocks*. 1st Workshop of the International Working Group on Submicroscopy of Undisturbed Soil Materials (IWGSUM) 1980, Wageningen. Centre for Agricultural Publishing and Documentation (Pudoc), Wageningen, pp. 191–206.
- Ismail, S.N.A., 1975. Micromorphometric soil-porosity characterization by means of electro-optical image analysis (Quantimet 720). *Neth. Soil. Surv. Inst., Wageningen, Soil Surv. Pap.*, 9: 104 pp.

- Jongerius, A., 1974. Recent developments in soil micromorphology. In: G.K. Rutherford (Editor), *Soil Microscopy. Proceedings of the 4th International Working-Meeting on Soil Micromorphology*, Kingston, 1973. The Limestone Press, Kingston, Ont., pp. 67—83.
- Jongerius, A. and Bisdorn, E.B.A., 1981. Porosity measurements using the Quantimet 720 on backscattered electron scanning images of thin sections of soils. In: E.B.A. Bisdorn (Editor), *Submicroscopy of Soils and Weathered Rocks. 1st Workshop of the International Working-Group on Submicroscopy of Undisturbed Soil Materials (IWGSUSM)* 1980, Wageningen. Centre for Agricultural Publishing and Documentation (Pudoc), Wageningen, pp. 207—216.
- Jongerius, A., Schoonderbeek, D. and Jager, A., 1972. The application of the Quantimet 720 in soil micromorphology. *The Microscope*, 20: 243—254.

This Page Intentionally Left Blank

THE DEVELOPMENT OF SOIL POROSITY IN EXPERIMENTAL SANDY SOILS WITH CLAY ADMIXTURES AS EXAMINED BY QUANTIMET 720 FROM BESI AND BY OTHER TECHNIQUES

J. CHRETIEN and E.B.A. BISDOM

I.N.R.A., Station de Science du Sol, 17 Rue Sully, 21034 Dijon (France)

Netherlands Soil Survey Institute, P.O. Box 98, 6700 AB Wageningen (The Netherlands)

(Accepted for publication February 17, 1983)

ABSTRACT

Chrétien, J. and Bisdom, E.B.A., 1983. The development of soil porosity in experimental sandy soils with clay admixtures as examined by Quantimet 720 from BESI and by other techniques. *Geoderma*, 30: 285–302.

For this study thin sections have been prepared of natural and artificial sands mixed with 20% and 40% clay. These and other samples had already been examined using soil physical and soil mineralogical methods for loose samples. Initial thin section studies, with the help of the light microscope alone, have been enlarged upon in this investigation using backscattered electron scanning images and an image analyzer (Quantimet 720). This allowed quantitative information to be obtained on the development of different types of soil porosity patterns using various clay admixtures. Information was also obtained on the influence the form of mineral grains had on the shape of pores in the mixtures of sand and clay. It was also possible to obtain quantitative information on the amount of clays and larger mineral grains in the thin sections. Much of the present data cannot be obtained automatically but must be manually controlled by using the image editor of the Quantimet. This type of work, however, may provide basic data which can subsequently be used to help explain various processes which occur in soils.

INTRODUCTION

The influence of the form of sand grains on porosity characteristics of sandy soils was studied under experimental conditions and in loose samples by Chrétien (1971) using soil physical and mineralogical methods. Work was done in the 100 μm to 160 μm sieve-fraction. The roundness and sphericity of individual grains were examined with the stereo-microscope and the results compared with porosity data from physical methods. These data, however, gave virtually no information on the packing of sand grains and the framework of sandy soils. The same negative result was obtained for the form and dimension of individual voids in natural and artificial sandy soils.

As a consequence, Chrétien (1979) decided to mix sands with certain

quantities of clay, viz. from 10 to 70% clay, and to prepare thin sections of these mixtures. Light microscopic observations of these thin sections revealed considerable differences in porosity patterns of the sands which were mixed with clay. If the sands were mixed with smaller amounts of clay, sand grains could exercise considerable influence on the types of pores which developed. Some observational insight was obtained in the distribution and arrangement of soil components, but no confirmative exact data could be obtained on the relation between shapes of soil components and porosity characteristics.

In the present study, backscattered electron scanning images (BESI) and an image analyzer were used to characterize soil components and soil porosity in sandy material mixed with 20% and 40% clay. The soil components consisted of artificial sand-sized materials, viz. marbles, and natural sand-sized mineral grains mixed with different percentages of the same clay.

MATERIALS AND METHODS

Eight sandy materials were used in the experiments by Chrétien (1979) and each of these were mixed with 10%, 20%, 30%, 40%, 50%, 60% and 70% clay. Two of the eight were artificial, viz. glass marbles with rounded forms and angular artificially crushed quartz. The glass marbles are called "Marbles" in this paper and the second sample "Bordeaux". All sands were of the sieve-fraction 100 μm to 160 μm . The six remaining sands were: Fontainebleau (marine and dune sands of the Tertiary Fontainebleau Formation), Saône (fluvatile sands from the recent terraces of the Saône), Serre (sands from the Trias in the forest of Serre), Morvan (sands from weathered granite of the Morvan Massive), Vivarais (sands from migmatite of the "Moyen-Vivarais" of France) and Maures (sands from weathered micaschist of the Maures Massive). These sand and clay mixtures are indicated in Fig. 1 (Chrétien, 1979).

Fontainebleau was comprised of rounded quartz. Saône consisted of slightly rounded quartz and feldspar. Serre had predominantly slightly angular quartz and feldspar. Morvan consisted of angular sands with quartz, feldspar and 10% mica. Vivarais had slightly rounded sands with quartz, feldspar and 20% mica. Maures was comprised of 70% lamellar material (mainly mica), and quartz and feldspar. Only light minerals which floated in a liquid with a specific gravity of 2.68, viz. quartz, K-feldspar and Na-feldspar, were studied. Heavy minerals were not examined because they were represented in insignificant quantities. The latter fraction also included iron-oxides and Ca-feldspar.

In the initial experiments (Chrétien, 1971), sands without clay admixtures were tested for roundness and sphericity with a stereo-microscope. Porosity and permeability were determined with methods that are commonly used in soil physics. In the experiments of 1979, Chrétien made thin sections of the sands which were now mixed with various quantities of clay. The

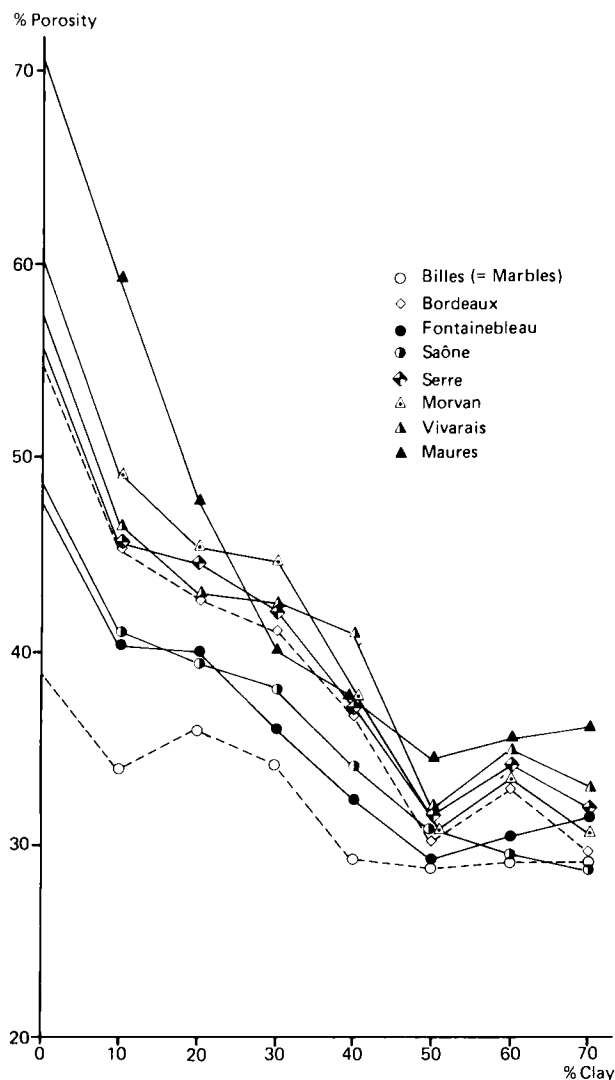


Fig. 1. Porosities of sands with increasing quantities of added clay as determined by soil physical methods.

clay consisted of a mixture of montmorillonite, illite and kaolinite with a little quartz according to X-ray diffraction analysis. Porosities were again studied with physical methods and individual pores observed with the light microscope. Some of the pore patterns were drawn from micrographs (these are in this study made with the light microscope) of thin sections. Loose materials were studied with the scanning electron microscope (SEM) and images (these are in this study made with SEM) made of various mixtures of sand and clay. In situ characterisation of pores remained problematic,

however, and it was decided that additional techniques were necessary.

Such techniques were possible using an image analyzer (Quantimet 720), and a scanning electron microscope (Philips SEM 505) equipped with four backscattered electron detectors. The Quantimet can be used to study pores with diameters larger than $30\text{ }\mu\text{m}$ on micrographs of thin sections (Jongierius, 1974, 1975; Jongierius et al., 1972 a, b; Murphy et al., 1977). If back-scattered electron scanning images (BESI) are made of thin sections (Bisdorn and Thiel, 1981), pores smaller than $30\text{ }\mu\text{m}$ can also be measured by Quantimet (Jongierius and Bisdorn, 1981).

RESULTS

The work by Chrétien (1971, 1979) on the relation between the form of soil components and porosity was started with only sandy material. This allowed certain results to be obtained which are discussed briefly below before the results of the experiments with sand and clay admixtures. This gives a basis for the results of the present study in which BESI are analyzed with the Quantimet 720 and used for porosity and mineral quantification.

Results of experiments on loose sands without clay admixtures

A number of conclusions were reached by Chrétien (1971) working with loose artificial and natural sands. The following characteristics were found for the sands. The density of the sands was often close to that of quartz, viz. 2.65. Maures (sands high in mica) had a density of 2.78. Plaquettes (an artificial sand consisting of platy and angular glass; not used in later experiments) had a density of 2.48.

The number of grains per gram was highest in the Maures sands with 750,000 and lowest for Marbles with 200,000. The specific surface in cm^2/g was smallest for Marbles with 126.4 and highest in Maures with 550.9. The weight of the sands was highest for Marbles and smallest in Maures. The weight differed in loosely packed sands (1.61 g/cm^3 for Marbles and 0.82 g/cm^3 for Maures) and compacted sands (1.74 g/cm^3 for Marbles and 1.25 g/cm^3 for Maures). The values for the other sands varied between these extremes.

The porosity of the sands differed significantly. Loosely packed Marbles had a porosity of 38.92% and compacted Marbles became 33.71%. Marbles had the lowest porosity values of the sands. The highest porosities were found in the highly micaceous Maures sands, viz. 70.35% when loosely packed and 55.11% when compacted.

Roundness and sphericity were determined for loose grains with the stereo-microscope and compared with the porosity figures of loosely packed sands. Marbles had the highest roundness and sphericity values and the lowest porosity, whereas Maures had a low roundness and the smallest

sphericity and porosity values. It could be demonstrated that the shapes of the sand grains formed a basic criterium which strongly influenced all other characteristics of the sands; including porosity. It was also found, however, that very little could be said about the relation between the form of the sand grains and the form of the pores or the manner of packing. Only in the case of Marbles could a possible relation between physically measured porosity values and packing be established. This was impossible for natural situations such as occur in sandy soils.

Results of experiments on loose sands with clay admixtures, of the study of thin sections and of SEM-observations of loose sands with clay admixtures

Loose sands with clay admixtures

During subsequent studies (Chrétien, 1979) clay was added to two artificial and six natural sands, to observe what happened with the forms of pores going from sands to clay with sand. Thin sections were prepared to give some insight into the form of pores by light microscopy. Soil physics methods were used to obtain figures on total porosity. Unhardened pieces of soil material were studied with SEM.

Porosities were found to decrease in the sands until 50% clay had been added (Fig. 1). The strongest decrease in porosity occurred for most sands during the addition of 10% clay and of 30% to 50% clay. Maures formed an exception with the largest porosity decrease below 30% clay admixture.

The curves in Fig. 1 demonstrate that Maures (mica plates) always have a higher porosity than Marbles, independent of the volume of added clay. The porosities of the rounded and slightly rounded sands of Fontainebleau and Sâone are slightly higher than for Marbles and are very similar. The more angular sands of Bordeaux, Serre, Morvan and Vivarais have again higher porosities and form a group of curves above Fontainebleau and Saône.

Only a selection, viz. Marbles, Saône, Morvan and Maures, are used as examples to discuss the results of these experiments. The decrease in porosity of the sands was largely due to the infilling of pores when 10% clay was added. The rounded sand grains of Marbles and Saône were embedded in clay and contacts between the grains became less if 10% to 30% clay was added. This was not the case with angular sand grains (Morvan) and mica-sands (Maures) in which the contacts between sand grains were maintained. As a consequence, with the addition of clay, mainly infilling of the pores took place in Morvan and Maures. The porosity in Maures decreased significantly due to a considerable decrease in specific surface. The addition of 30% to 50% clay gave predominantly a dislocation of sand grains. Above 50% clay admixture the contacts between individual sand grains were virtually lost and the grains no longer had a function in the support of a skeleton. Porosities of individual sands remained virtually the same and came close to one another (Fig. 1).

Sands with clay admixtures in thin sections

Light microscopic observations of thin sections gave information on the form, size and number of pores, the arrangement of sands and the distribution of clays. The investigation was done on sands with 20%, 40% and 70% clay admixtures.

The arrangement of sands, clay and pores in sands with a 20% clay admixture gave different types of packing. In Marbles, clay was present as rings around the marbles and formed bridges between them. In the other sands grain cutans predominated.

The porosity in the thin sections was studied by making micrographs of the sands with clay admixtures and drawing the pores in them (Fig. 2). In sands with 20% clay the pores of marbles were usually rounded and had regular forms. Similar, but somewhat more complicated forms were present in Saône; a sand with slightly rounded to rounded minerals. Maures, a highly micaceous sand, showed various complex and elongated forms of pores. The pores were often angular with their greatest length parallel to the mica platelets. Pores of Fontainebleau with rounded and slightly rounded grains were similar to those of Saône. A variety of frequently complicated forms of pores was found in Serre and Vivarais which contained angular grains.

The size of pores in sands with 20% clay was measured by taking their largest diameter. The diameters were given in four size classes: smaller than 50 μm , 50–100 μm , 100–200 μm and 200–500 μm . The studied sands of the analysed sieve-fraction, 100–160 μm , had predominantly pores between 50 μm and 200 μm . The number of pores varied between 29 and 37 in each micrograph (Fig. 2). An estimation of the total porosity was obtained by cutting areas occupied by pores free from the paper, determining their weight, and comparing the weight with that of the whole micrograph. Information on different size classes was also gathered in this manner. Marbles and Fontainebleau had the lowest porosity, Maures and Serre a somewhat higher porosity. Form alone, however, was not a determining factor for porosity characteristics because Saône and Vivarais did not demonstrate a relation between the form of sand grains and porosity.

In the clays of Marbles, with an addition of 40% clay, microcracks occurred. These microcracks were regarded by Fies (1978) and Chrétien (1979) as newly developed. This new type of porosity also demonstrated that the influence of sand grains and their forms on the porosity had decreased significantly. The elongated pores were more or less oriented. Saône and Maures showed a considerable number of larger pores.

Marbles, Saône and Maures were also examined in thin sections with 70% clay. Only microcracks were visible in all samples and the influence of sand grains on porosity had virtually ceased. A part of the microcracks, in sands with 70% and 40% clay, could have been formed artificially during sample preparation.

The results of the measurements of porosity in thin sections indicated

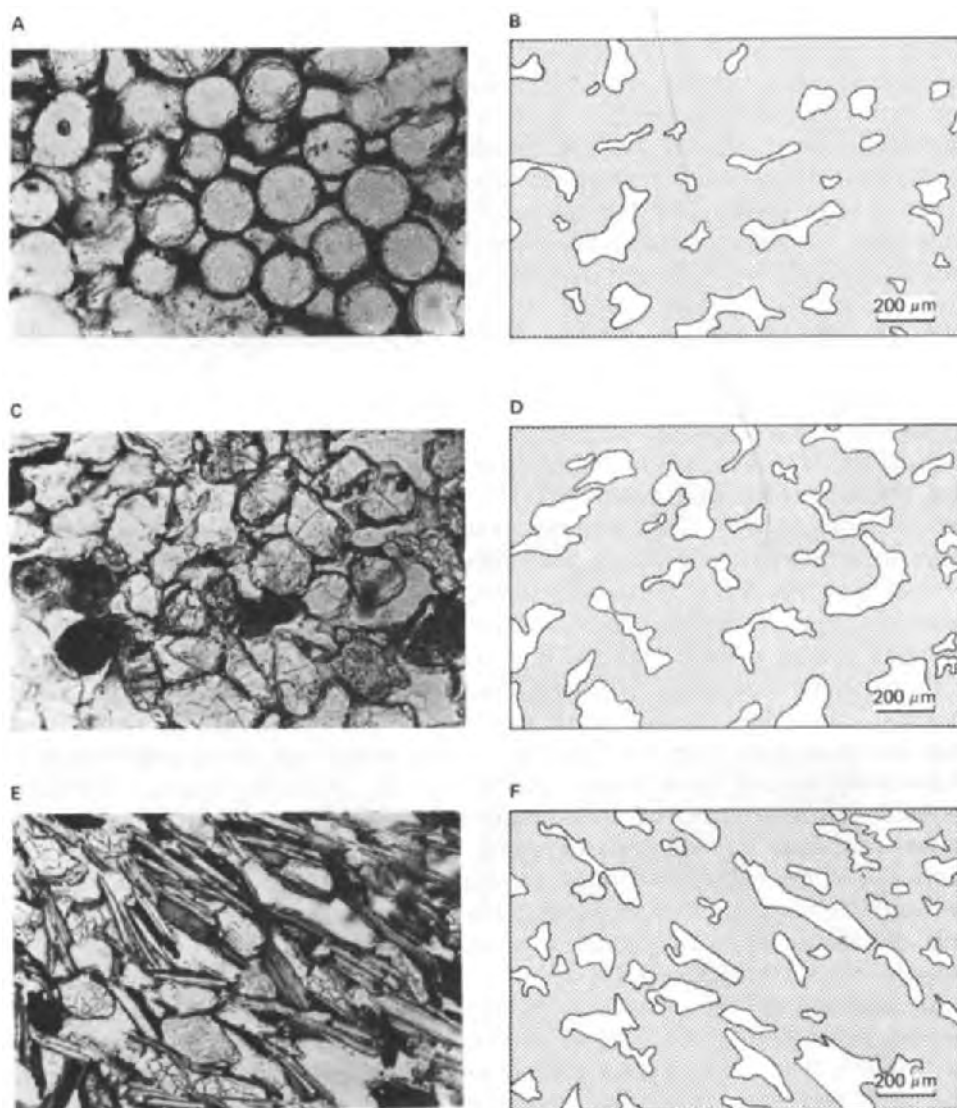


Fig. 2. Drawings of pores from light microscopic micrographs (plane polarized light) of sands mixed with 20% clay. Marbles (A, B), Saône (C, D) and Maures (E, F).

that the used method was not accurate (Chrétien, 1979). Drawing of pores from micrographs was rather arbitrary and positioning of the pores on the photos before they were drawn was sometimes difficult. Also, the number of pores selected in this manner is often too small to allow a statistical evaluation.

SEM-observations of loose sands with clay admixtures

SEM observations of loose sands with 30% and 70% clay need to be mentioned briefly at the end of this section. Sands with 30% clay had similar forms to those with 20% clay, viz. predominantly rounded pores in Marbles, mainly angular ones in Fontainebleau, and very irregular pores in Maures. Microcracks started to develop. Sands with 70% clay showed a continuous coating of the grains with clay in all samples. Micropores were still discernable in Maures but Marbles and Fontainebleau showed continuous infillings between the sand grains.

*BESI-Quantimet studies of sands with clay admixtures in thin sections**Measurement of porosities and minerals*

Backscattered electron scanning images (BESI) were made from thin sections of Marbles, Saône and Maures with 20% and 40% clay admixtures and analysed with the Quantimet 720 (Bisdom and Thiel, 1981; Jongerius and Bisdom, 1981). Two images were analysed of each sand with 20% clay. In sands with 40% clay, two images were analysed of Marbles, three of Saône and seven of Maures. Of these, two images were selected from each category giving three figures with four images each, viz. Marbles (Fig. 3), Saône (Fig. 4) and Maures (Fig. 5).

Porosity data could be obtained directly and automatically from BESI in most cases, but manual work with the image editor of the Quantimet was also necessary. The present study concentrated on the overall porosity characterisation of each image. A number of pores, however, continued beyond the boundary of individual images. This continuation of pores raises problems in the measurement of individual pores. Consequently more BESI micrographs should be made along linear traverses on a thin section to overcome this problem. This was not done in the present study, and consequently no individual pores were measured. This will be the subject of a forthcoming publication.

In addition to the measurement of the porosity attention was also paid to the measurement of coarser minerals and clays. The results are given in Table I. The average clay percentages measured in BESI were close to the 20% and 40% clay which was put into the sands. However, data of some images indicate that considerable deviation of these figures may occur locally in the thin sections.

A special study was done on the relation between the forms of pores and the forms of individual minerals. Drawings were made from BESI on transparent paper for this study. If a mineral bordered a pore, a line was drawn along the length of the contact. In some cases a thin clay cutan occurred on mineral grains and was also in contact with a pore. If this grain cutan was very thin and ran parallel to the surface of a mineral this surface was also considered as a contact zone.

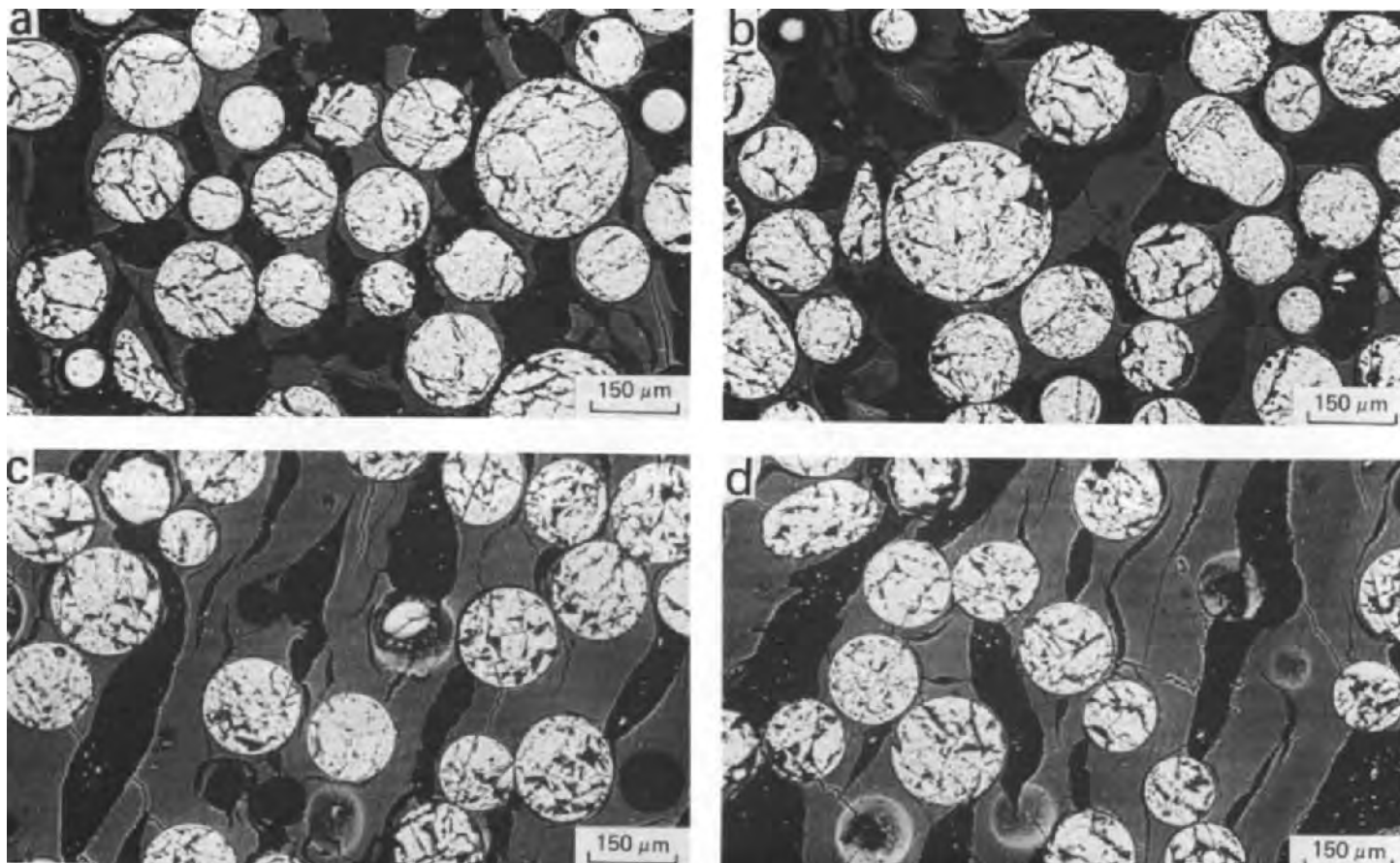


Fig. 3. Backscattered electron scanning images (BESI) of Marbles with 20% clay (a, b) and 40% clay (c, d) admixtures.

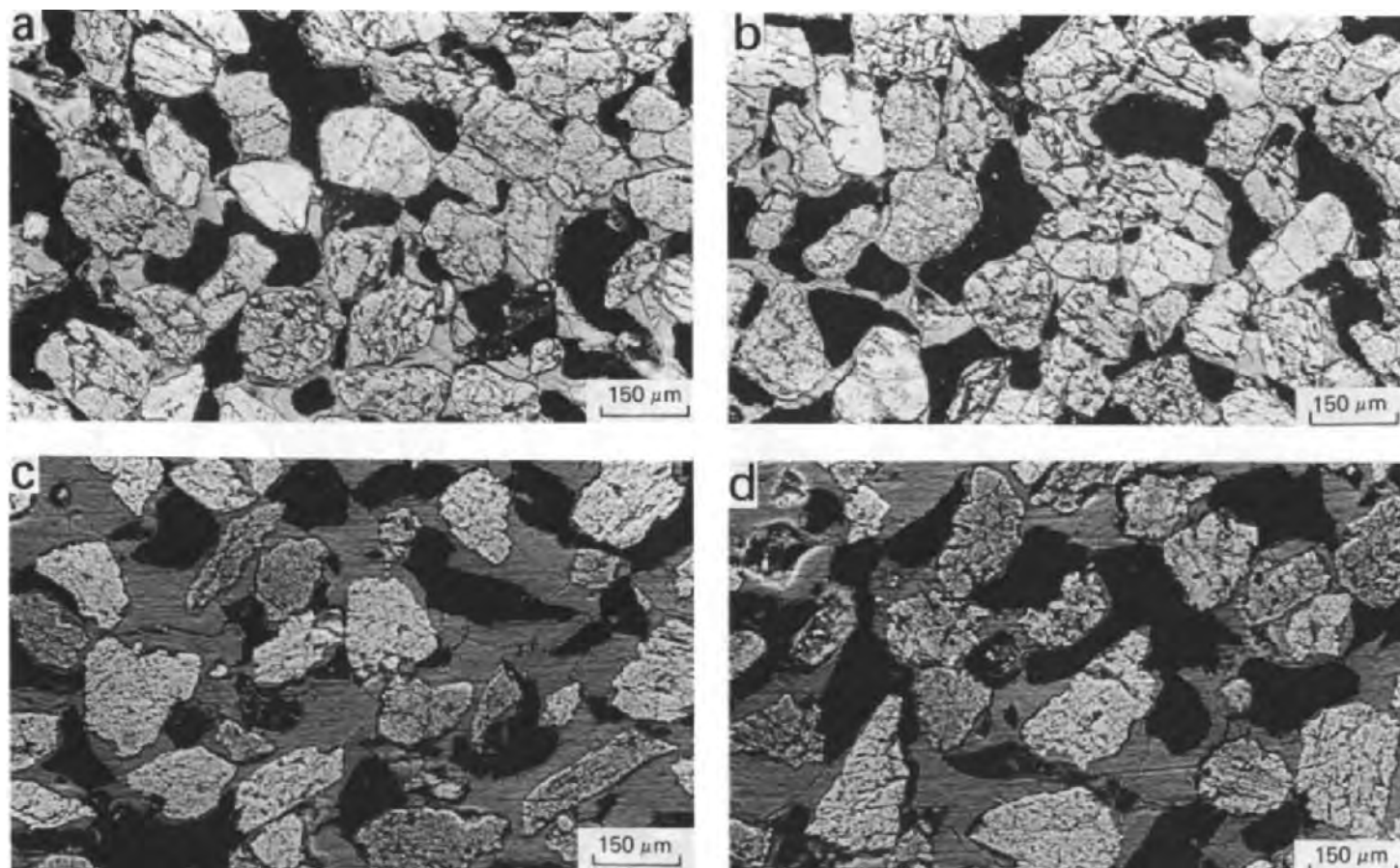


Fig. 4. BESI of Saône with 20% clay (a, b) and 40% clay (c, d) admixtures.

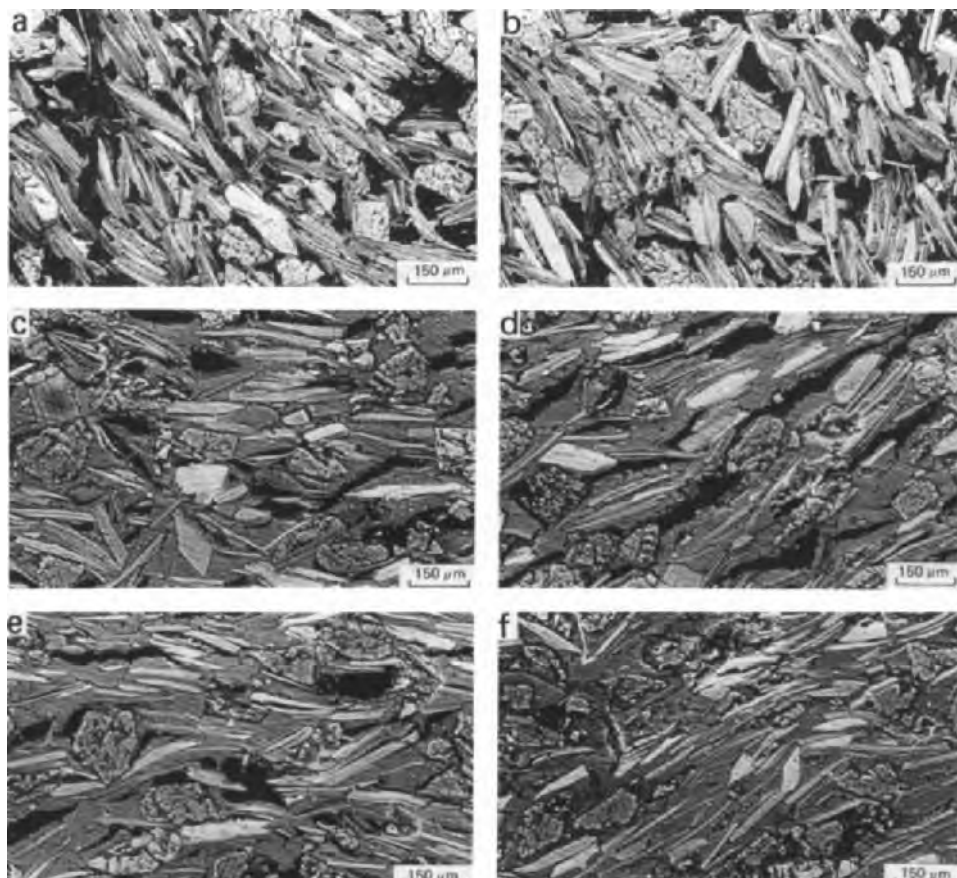


Fig. 5. BESI of Maures with 20% clay (a, b) and 40% clay (c–f) admixtures.

Porosity characteristics

Changes in porosity with increasing clay content. The porosity percentages of Marbles, Saône and Maures sands with 20% and 40% clay admixture are given in Table I. Marbles and Saône with 20% clay demonstrate virtually the same porosity percentages, whereas the difference is somewhat larger for Maures. Marbles with 40% clay show virtually the same results of measurements, while larger differences are found in the measurements of Saône and Maures. If average porosity percentages are taken, the changes are the following for sands with 20% and 40% clay admixtures, respectively 33.94 to 24.06 for Marbles, 28.04 to 25.69 for Saône, and 27.40 to 19.82 for Maures. These results indicate that the porosity of Saône decreased only slightly when 40% clay was added to the sand, whereas the loss in porosity was much larger for Marbles and Maures. The area occupied by pores in a thin section can also be given in μm^2 . Fig. 6 illustrates the trends which were discussed above.

TABLE I

Quantimet measurements of porosity, mineral percentages and clay percentages in BESI of Marbles, Saône and Maures with 20% and 40% clay admixtures*¹

Sample	Clay added to sands (%)	Porosity in thin section (%)	Coarser minerals in thin section (%)	Clay in thin section (%)
Marbles	20	35.46	45.69	18.85
Marbles	20	32.42	47.99	19.59
Marbles	40	24.41	38.99	36.60
Marbles	40	23.70	33.28	43.02
Saône	20	28.62	52.26	19.12
Saône	20	27.45	53.96	18.59
Saône	40	24.66	36.97	38.37
Saône	40	28.94	35.92	35.14
Saône	40	23.48	34.12	42.40
Maures	20	29.38	49.58	21.04
Maures	20	25.41	52.80	21.79
Maures	40	17.79	52.80	29.41
Maures	40	24.52	35.08	40.40
Maures	40	22.78	31.79	45.43
Maures	40	22.08	29.87	48.05
Maures	40	15.00	39.99	45.01
Maures	40	17.53	48.49	33.98
Maures	40	19.10	30.47	50.43

*¹ BESI magnification $\times 100$.

Pore patterns. Apart from the measurements indicated in Table I, attention was paid to area (A), perimeter (Pe), drawn perimeter (DPe) and horizontal projection (HPr) of the pores. These allowed some insight to be obtained into porosity characteristics of Marbles, Saône and Maures.

Pore patterns or void patterns were classified for clayey soils by Jongerius (1974) and Ismail (1975) at a smaller magnification. The same classification graph has been used in this study for sands mixed with 20% and 40% clay (Fig. 7). Void pattern classes of sandy soils (Ismail, 1975) have different class limits which are insufficiently determined at present. The net result is that data plotted in the classification graph of Jongerius (1974) correlate with different void patterns than those indicated on the graph.

Marbles with 20% clay are present in class 3.3 and shift to classes 2.2 and 3.2 when 40% clay is added. Smooth-walled vughs, interconnected vughs, channels and planes are present in Marbles with 20% clay. Special

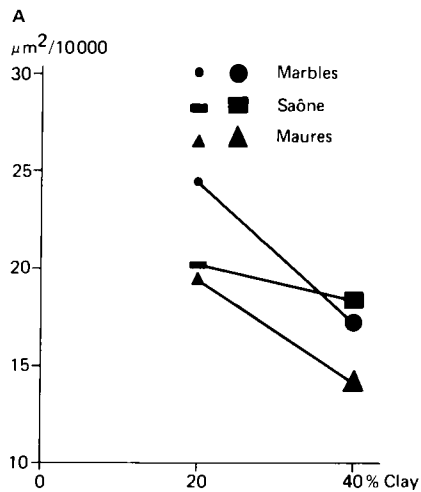


Fig. 6. Average area occupied by pores in BESI from three sands with 20% and 40% clay admixtures.

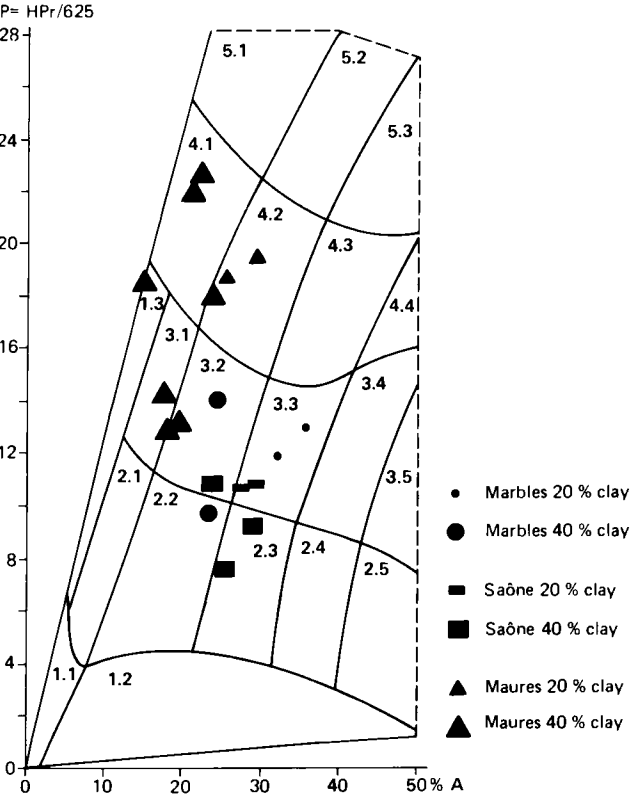


Fig. 7. Classification of pore patterns, for sands mixed with 20% and 40% clay, using the classification graph introduced in 1974 for clayey soils.

types of voids are vesicles which were formed between clay and marbles. Such vesicles can be connected with other types of pores. The porosity pattern of Marbles with 40% clay is strikingly different and consists predominantly of channels and planes. Vughs still occur, but become more elongated, and change into channels. Vesicles can still be discerned.

Saône with 20% clay (class 3.3) has predominantly vughs and interconnected vughs. Many vughs are smooth-walled. Planes, due to shrinkage of clay, are numerous and have a smaller diameter than planes of the Marble samples. These shrinkage-planes are also found in Saône with 40% clay (classes 2.3 and 3.2) and may interconnect vughs. The conformation of the walls of vughs and interconnected vughs has become somewhat more irregular with an increase of angular forms.

Maures with 20% clay (class 4.2) seem to have a considerable number of simple packing voids caused by the random packing of single mineral grains (micas, quartz and feldspars). Closer observation indicates, however, that clay coatings are also present in most pores. Vughs and interconnected vughs are the most predominant. Maures with 40% clay (classes 1.3, 3.1, 3.2, 4.1 and 4.2) demonstrate very large differences in pore patterns. Elongated voids (channels, joint planes, planes, interconnected vughs) are dominant. Some micrographs have oriented pores, others virtually lack larger pores.

Relation between the form of pores and the form of individual minerals. Perimeters of all pores in Marbles, Saone and Maures with 20% and 40% clay admixtures (Figs. 3–5) were measured on BESI by Quantimet. The procedure followed has been explained in the section “measurements of porosities and minerals” and the results of the measurements are given in Fig. 8.

The curves for the perimeter and drawn perimeter of Marbles and Saône show similar trends in Fig. 8, whereas this is not the case for Maures. The average drawn perimeter, when taken as a percentage of the average perimeter of all pores, is highest in clays with 20% clay, viz. 15.4% for Marbles, 21.9% for Saône and 24.4% for Maures. These figures become significantly lower for sands with a 40% clay admixture: 7.1% for Marbles, 16.4% for Saône and 4.3% for Maures. These data indicate that the addition of 20% clay has the greatest effect on Marbles, i.e. marbles occupy the smallest percentage of the walls of voids. If 40% clay is added, the role of Marbles is taken over by Maures with 4.3%. This means that even larger percentages of platy micas in the sample have ceased to influence the conformation of the walls of pores.

CONCLUSIONS

A series of experiments has been conducted over several years to obtain information on the relation between the shape of mineral grains, pore

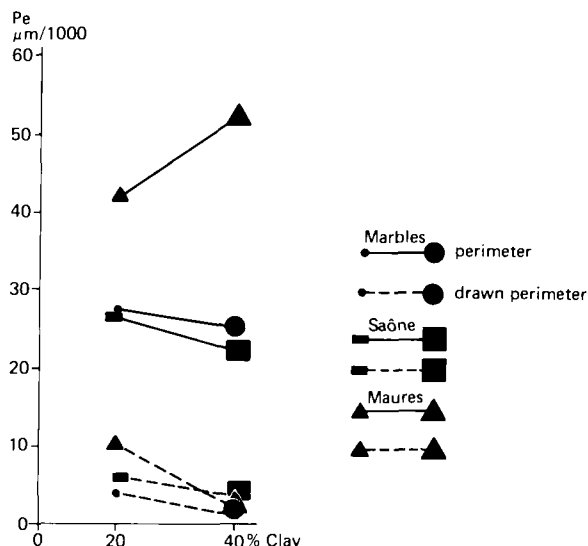


Fig. 8. Influence of predominantly sandy mineral grains on the conformation of the walls of pores.

patterns and the form of pores. The first experiments dealt with loose sands without clays using natural and artificial materials and conventional methods of soil physics and soil mineralogy. Significant new information was obtained (Chrétien, 1971). Secondly, clay was added in various quantities to the sands and thin sections were made. Light microscopy and the already mentioned methods were again not capable of giving a real answer to the same questions. Basically, porosity patterns and forms are too intricate to study in many cases unless image analyzer systems are available which can be used in combination with high quality micrographs made from thin sections. Micrographs made with the light microscope did not give sufficiently accurate information on the porosity and backscattered electron scanning images (BESI) therefore must be made with the scanning electron microscope.

In the present study BESI were measured with the Quantimet to investigate thin sections of sands with 20% and 40% clay admixtures (Figs. 3–5) and to obtain further information on the same questions. Magnifications of $\times 100$ were used to study the form of pores, pore patterns and mineral grains as a totality. The results of this investigation gave a number of new aspects. One of these was that porosity percentages measured with BESI-Quantimet methods (Table I and Fig. 6) are different from earlier results done with soil physical methods (Fig. 1). In Fig. 1 Maures has the highest porosity at 20% and 40% clay admixtures, followed by Saône and Marbles. Table I and Fig. 6 indicate, however, that the average porosities are smallest for Maures. Marbles with the lowest porosity (Fig. 1) has the highest porosi-

ty at 20% clay admixture according to BESI-Quantimet measurement results. Saône has a middle position at 20% clay and a somewhat higher porosity than Marbles at 40% clay admixture. Only the porosity values for Marbles with 20% and 40% clay come close to the physically determined ones in Fig. 1. Saône and Maures have much smaller porosity values according to Quantimet studies from BESI. Such differences in the results of physically determined porosity values and those given by BESI-Quantimet could possibly be explained by pointing out that the thin section method represents a two-dimensional area and not a three-dimensional volume. Another argument is that many thin sections should be measured, and a large number of fields in each thin section, to allow statistical evaluation of the variability in the distribution of various types of porosity in the studied samples. Also, at the present magnification of only $\times 100$ no detailed information is obtained on very fine pores, whereas this can be done using physical methods. However, the present BESI-Quantimet analysis of porosities in thin sections clearly indicates that a discrepancy exists between the results of this method and soil physical ones. Much more work is necessary to reach final conclusions on this subject but indications are that the BESI-Quantimet method may be of considerable help to soil physics as was demonstrated for heavy clay soils by Bouma et al. (1977, 1979) using light microscopic micrographs instead of BESI, smaller magnifications than the present ones, the Quantimet 720 and soil physical methods.

The relation between mineral grains and the form of pores was found by marking the surfaces of the voids occupied by mineral grains and measuring their length with the Quantimet. These measured perimeter data were subsequently compared with the total perimeters obtained from all pores. Due to a magnification of only $\times 100$ of BESI, done to obtain comparable results with earlier experiments, the relation between the surface of minerals and the form of very small pores could not be established with certainty. However, general trends were obtained for small and larger pores and these are of interest. The trends for perimeter and drawn perimeter (Fig. 8) were similar for Marbles and Saône. Some decrease in perimeter, influenced by the form of mineral grains, occurred going from a 20% to a 40% clay admixture. Maures had a completely different upward trend for the perimeter and a steeper downward slope for the dashed line of the drawn perimeter. The increase in perimeter occurred because long elongated pores and small pores with various shapes replaced vughs and interconnected vughs. The drawn perimeter of Maures, at 40% clay admixture, was situated between Saône and Marbles in Fig. 8. The presence of platy mica grains in Maures was therefore of no special significance any longer, whereas the micas still played a role at 20% clay admixture.

Pore pattern changes can be observed in micrographs but the Quantimet measurements are necessary to bring some type of order in the often intricate patterns. The classification chart (Fig. 7) was used and demonstrated a number of shifts in patterns going from sands with 20% to sands with

40% clay admixture. Marbles showed a variety of pore-types at 20% clay admixture, whereas predominantly channels and planes were left when 40% clay had been added. Saône showed only small differences for 20% and 40% clay admixtures, although angular forms in parts of the pore walls were discernable in sands with 40% clay. Maures had a significant number of simple packing voids at 20% clay admixture and showed a large variety of pore patterns at 40% clay admixture (Fig. 5).

The present results can be considered as preliminary because all sands with different percentages of clay added have not yet been studied with BESI-Quantimet. Also, a larger area of the thin section has to be studied along linear traverses to gain representative results. Larger magnifications of BESI will be necessary to obtain more detailed information on individual pore characteristics, especially of the smaller pores. Information can also be obtained on forms of larger mineral grains and on the place of clay accumulations. This will allow some insight into the development of fabric and structure of soils, especially if combined with detailed work on and experiments with soil porosity.

REFERENCES

- Bisdom, E.B.A. and Thiel, F., 1981. Backscattered electron scanning images of porosities in thin sections of soils, weathered rocks and oil-gas reservoir rocks using SEM-EDXRA. In: E.B.A. Bisdom (Editor), *Submicroscopy of Soils and Weathered Rocks*. 1st Workshop of the International Working-Group on Submicroscopy of Undisturbed Soil Materials (IWGSUSM) 1980, Wageningen. Centre for Agricultural Publishing and Documentation (Pudoc), Wageningen, pp. 191–206.
- Bouma, J., Jongerius, A., Boersma, O., Jager, A. and Schoonderbeek, D., 1977. The function of different types of macropores during saturated flow through four swelling soil horizons. *Soil. Sci. Soc. Am. J.*, 41 (5): 945–950.
- Bouma, J., Jongerius, A. and Schoonderbeek, D., 1979. Calculation of saturated hydraulic conductivity of some pedal clay soils using micromorphometric data. *Soil Sci. Soc. Am. J.*, 43(2): 261–264.
- Chrétien, J., 1971. Essai de caractérisation des sables en tant que squelette minéral du sol. *Ann. Agron.*, 22(6): 615–654.
- Chrétien, J., 1979. Etude expérimentale de la porosité de mélanges sables-argile. *Aspects micromorphologiques*. *Sci. Sol*, 4: 333–353.
- Fies, J.C., 1978. Porosité du sol: étude de son origine texturale. Thesis, Strasbourg, France.
- Ismail, S.N.A., 1975. Micromorphometric soil-porosity characterization by means of electro-optical image analysis (Quantimet 720). *Neth. Soil Surv. Inst., Wageningen, Soil Surv. Pap.*, 9, 104 pp.
- Jongerius, A., 1974. Recent developments in soil micromorphology. In: G.K. Rutherford (Editor), *Soil Microscopy, Proceedings of the 4th International Working-Meeting on Soil Micromorphology*, Kingston, 1973. The Limestone Press, Kingston, Ontario, Canada, pp. 67–83.
- Jongerius, A., 1975. Micromorphometric soil analysis by means of Quantimet 720. In: *Fortschritte der quantitativen Bildanalyse; Vorträge des IMANCO-Symposiums*, pp. 161–185.

- Jongerius, A. and Bisdorf, E.B.A., 1981. Porosity measurements using the Quantimet 720 on backscattered electron scanning images of thin sections of soils. In: E.B.A. Bisdorf (Editor), *Submicroscopy of Soils and Weathered Rocks*. 1st Workshop of the International Working-Group on Submicroscopy of Undisturbed Soil Materials (IWGSUSM) 1980, Wageningen. Centre for Agricultural Publishing and Documentation (Pudoc), Wageningen, pp. 207—216.
- Jongerius, A., Schoonderbeek, D., Jager, A. and Kowalinski, S., 1972a. Electro-optical soil porosity investigation by means of Quantimet-B equipment. *Geoderma*, 7(3/4): 177—198.
- Jongerius, A., Schoonderbeek, D. and Jager A., 1972b. Soil porosity characterization by means of electro-optical image analysis. In: *La Fertilidad Física de los Suelos*. Reports del Seminario Internacional, Sevilla, pp. 107—123.
- Murphy, C.P., Bullock, P. and Turner, R.H., 1977. The measurement and characterisation of voids in soil thin sections by image analysis, Part I. Principles and techniques. *J. Soil Sci.*, 28(3): 498—508.

THE CHARACTERIZATION OF THE SHAPE OF MINERAL GRAINS IN THIN SECTIONS OF SOILS BY QUANTIMET AND BESI

E.B.A. BISDOM and D. SCHOONDERBEEK

Netherlands Soil Survey Institute, P.O. Box 98, 6700 AB Wageningen (The Netherlands)

(Accepted for publication February 17, 1983)

ABSTRACT

Bisdom, E.B.A. and Schoonderbeek, D., 1983. The characterization of the shape of mineral grains in thin sections of soils by Quantimet and BESI. *Geoderma*, 30: 303–322.

Silt-sized mineral grains were analysed for their shapes or forms in thin sections of soils using backscattered electron scanning images (BESI) and an image analyzer (Quantimet 720). This work was done with an image-editor and required manual editing of the shape of mineral grains on the display screen of the Quantimet. Shape analysis of coarse and fine silt grains could thus be performed at magnifications of $\times 240$ and $\times 480$.

The shape of the mineral grains could be characterized by five parameters: area (A), perimeter (Pe), largest and smallest Feret's diameters (F_{max} and F_{min}), lobation ratio (Lr) and indentation ratio (Ir). A relation was found, however, between the A/Pe^2 ratio and the Lr and Ir ratios. Consequently, shape analysis of mineral grains can be done by measuring three of the five parameters, i.e. A , Pe and F_{max}/F_{min} . These parameters, however, are still not able to reproduce the shape of individual mineral grains and images of them therefore remain necessary.

Several of the 54 mineral grains were found to have different shapes but the same A/Pe^2 ratio. An explanation for this phenomenon is given by using a theoretical model in which two-dimensional forms change their shapes from a circle ($A/Pe^2 = 79$) to a line ($A/Pe^2 = 1$). Form separation of mineral grains with the same A/Pe^2 ratio can be done by using the F_{max}/F_{min} ratio.

The measurement of the shape of the mineral grains, the theoretical model and observation of the micrographs of the individual mineral grains, made it possible to draw a diagram with shape classes which can be used for shape classification purposes. Knowledge gathered in soil micromorphology on shape analysis of pores and soil aggregates has also been used to obtain boundaries of shape classes in the diagram. The present study is intended both as a proposal as to how two-dimensional shape classification can possibly be done, and as a work-model. The boundaries of the shape classes can easily be adjusted if data from forthcoming studies require it.

INTRODUCTION

Shape or form analysis of mineral grains in thin sections of soils, in contrast to shape analysis of pores (voids), has hardly been done. Virtually all our knowledge on shape analysis is derived from the study of pores in soils using transmitted light microscopy and an image analyzer (Jongorius, 1974; Ismail, 1975; Murphy et al., 1977; Bouma et al., 1977, 1979). Only pores

larger than 30 μm could be measured with this technique due to the thickness of a thin section which usually approaches this value. If backscattered electron scanning images (BESI) are used (Bisdom and Thiel, 1981), pores smaller than 30 μm can also be measured by an image analyzer (Jongerijs and Bisdom, 1981). Shape analysis of pores that are smaller and larger than 30 μm can thus be done with an image analyzer (Quantimet 720).

In the present investigation, the BESI-Quantimet technique could also be used for shape analysis of mineral grains; after establishing the magnifications to be used with Quantimet measurements, and after a procedure had been worked out to obtain measurable forms of the mineral grains. A more complicated objective, on which little knowledge was amassed during the study of the shape of pores, became apparent during the study of shape data on individual mineral grains. This objective was to find a way to indicate how the measured two-dimensional shapes are related to each other. A solution to this problem, based on the BESI-Quantimet technique, is presented in this study.

The insight into how two-dimensional forms can be related to each other, gave a better understanding of shape classification problems. This allowed the introduction of a simple classification with shape classes. It became apparent that the parameters which can be measured by Quantimet, cannot reproduce the actual forms of mineral grains. Images of the mineral grains therefore remain necessary.

In order to explain various matters associated with shape analysis, the more theoretical aspects of the present study and a theoretical model are discussed in the section on materials and methods together with technical details. Shape data of the measured mineral grains are presented in the section on results.

MATERIALS AND METHODS

SEM—Quantimet

The present study on the shape of mineral grains has been done with an image analyzer (Quantimet 720) using backscattered electron scanning images (BESI) made with a Jeol-JSM-35C scanning electron microscope (SEM). The SEM was equipped with a backscattered electron detector of the semiconductor type which contained two solid state detectors. BESI obtained with the BE-detector was of sufficient quality to allow shape analysis of minerals in thin sections of soils which consisted of thin layers of sandy, silty and clayey materials. Shape measurements were done with the image editor of the Quantimet, which meant that manual editing of the shape of mineral grains on the display screen of the image analyzer was necessary.

If BESI are used for shape analysis, a much thinner layer — predominantly just underneath the surface of the thin section and a few micrometres thick — is portrayed than is possible with transmitted light microscopy (Bisdom

and Thiel, 1981). This allowed the study of pores both smaller and larger than $30\text{ }\mu\text{m}$ by Quantimet (Jongierius and Bisdom, 1981). In the present study, both coarse and fine silt-sized grains were selected for shape analysis and several were smaller than $30\text{ }\mu\text{m}$ (Fig. 1). Shape analysis of pores smaller and larger than $30\text{ }\mu\text{m}$ had shown that the measured porosity could vary with the magnification of BESI. This indicated that attention has to be paid to magnifications of BESI used for shape analysis of mineral grains by Quantimet.

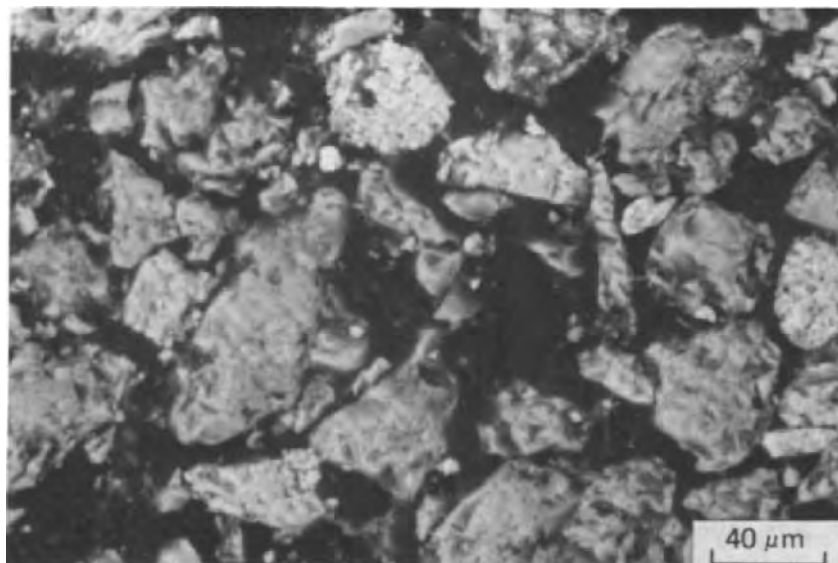


Fig. 1. Silt grains in stratified sandy soils of The Netherlands. 54 mineral grains were measured by Quantimet in this backscattered electron scanning image.

Image-editing of mineral grains and magnifications to be used for shape analysis

Initially, in order to obtain correct magnifications for shape analysis, Quantimet measurements were done from BESI on sand- and silt-sized mineral grains at $\times 120$, $\times 240$ and $\times 480$. It was found that most grains needed image-editing before shape measurements could be done. Many grains exhibited small dark grey to black areas internally. These small areas usually represented very shallow and somewhat deeper situated areas in the mineral grain and were called internal undeeep pores in Fig. 2A. These internal undeeep pores had to be excluded from measurements which concerned the external shape of mineral grains (Fig. 2B) and this was done with the image editor of the Quantimet.

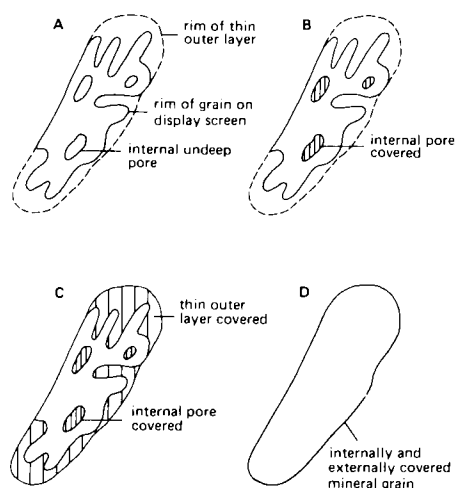


Fig. 2. Schematic illustration of the image-editing of a mineral grain. A. A grain as it appears on the display screen of the Quantimet. B. Covering of internal pores. C. Covering of the thin outer layer if the surface of the grain slopes down. D. Completely edited grain.

The second problem which had to be examined was the position of the boundary of the vague outer rim of several mineral grains (cf. Fig. 1). This can be explained using the data given in Table I. The two internally covered mineral grains, which were taken as an example, gave area and perimeter measurements which were different at the three magnifications. Image-editing of the periphery of the mineral grains was therefore necessary; a procedure which was called external covering (Fig. 2C). The results of measurements done on the same mineral grains as in Table I, but internally and externally covered, are given in Table II. What is measured is given in Fig. 2D. All area measurements were similar, but the perimeter at $\times 120$ magnification was different from those at $\times 240$ and $\times 480$. Consequently, ratios derived

TABLE I

Two internally covered mineral grains (the same as in Table II) measured at different magnifications

Mineral grain	Magnification	Area (A) (μm^2)	Perimeter (Pe) (μm)	$A/Pe^2 \times 1000$	Lobation ratio (Lr)
1	$\times 120$	631	224	12	2.53
1	$\times 240$	539	274	7	3.37
1	$\times 480$	517	364	4	4.54
2	$\times 120$	256	87	34	1.53
2	$\times 240$	243	103	22	1.89
2	$\times 480$	199	166	7	3.33

TABLE II

Two internally and externally covered mineral grains (the same as in Table I) measured at different magnifications

Mineral grain	Magnification	Area (A) (μm^2)	Perimeter (Pe) (μm)	A/Pe^2 $\times 1000$	Lobation ratio (Lr)
1	$\times 120$	698	153	30	1.64
1	$\times 240$	695	169	24	1.82
1	$\times 480$	687	167	24	1.81
2	$\times 120$	286	100	28	1.68
2	$\times 240$	312	121	21	1.96
2	$\times 480$	295	122	20	2.01

from these parameters, i.e. A/Pe^2 and the lobation ratio (Lr), were similar at $\times 240$ and $\times 480$ magnifications.

Finally, some explanation needs to be given as to why several mineral grains have vague outer boundaries. If a mineral has sharp edges, the outer rim will usually be the same on BESI and on the display screen of the Quantimet. However, many grains have sloping edges. These minerals have a rim which gradually becomes vague on BESI and vanishes if the surface of the grain is situated below the detection limit for backscattered electrons. This vague rim of the mineral grain has lighter to darker grey colours on BESI and it are these darker colours which may cause detection difficulties for the Quantimet if no help is given by the image-editor. The external covering of the mineral grain is done by comparison of the image on the display screen of the Quantimet with BESI. Shape analysis of mineral grains has thus become possible using the BESI-Quantimet technique. An example of the image-editing of three mineral grains is given in Fig. 3.

Theoretical aspects of shape measurements with the BESI-Quantimet technique

Parameters used for shape analysis

Five parameters have been used to characterize the shape of mineral grains, viz. area (A), perimeter (Pe), largest and smallest Feret's diameters (F_{max} and F_{min}), lobation ratio (Lr) and indentation ratio (Ir). Of these, the Feret's diameter is a diameter which can be measured in a horizontal, vertical and two diagonal directions. The largest and smallest Feret's diameters are indicated by F_{max} and F_{min} .

The lobation ratio or "Lappingsquotient" was mentioned by Kubiena et al. (1961) and used for shape analysis of pores and soil aggregates by Beckmann (1962). The latter author defined Lr as the ratio between the perimeter of the actual surface of a soil component and the circumference of a

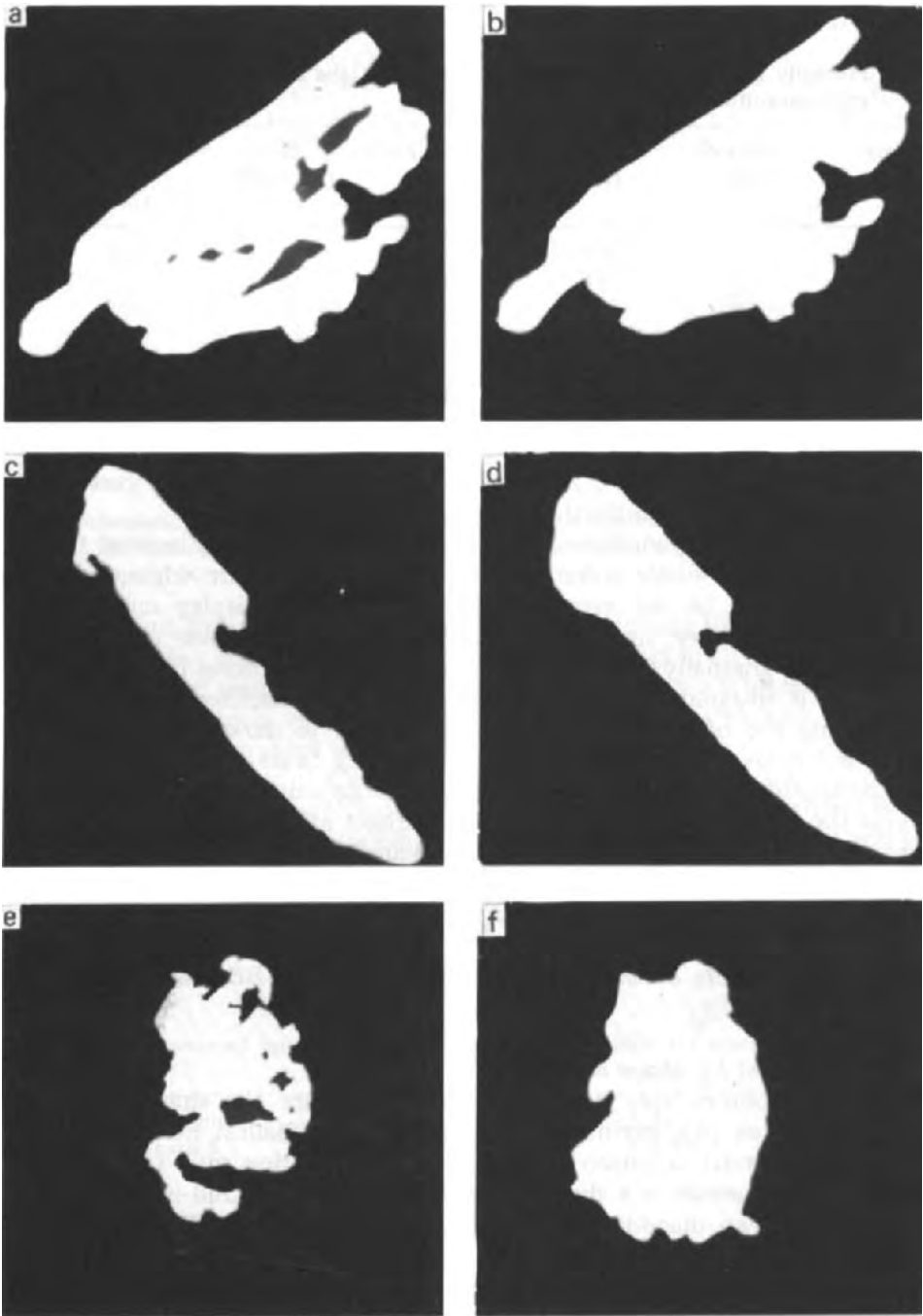


Fig. 3. Different steps in image-editing of three mineral grains. (a) A grain with shallow and discontinuous internal pores; a thin outer layer is not present. (b) Internally covered. (c) A second grain with a thin outer layer but without internal porosity. (d) Externally covered. (e) The third grain with internal pores and a thin outer layer. (f) Internally and externally covered mineral grain.

circle with the same area. Small values of Lr approach the form of a circle ($Lr = 1$), whereas larger values are associated with more lobate forms. The indentation ratio can be regarded as a ratio which is similar to the lobation ratio, whereby indentations are used instead of lobes.

The relation between area, perimeter and lobation ratio

The definition of the lobation ratio (Lr) allows this ratio to be related to the area (A) and perimeter (Pe) using the equation:

$$Lr = \sqrt{\frac{1}{4\pi \times A/Pe^2}}$$

This is a significant relation between Lr and A/Pe^2 ratios, because both have been used for shape analysis. Seven shape classes were defined by Beckmann (1962), using the lobation ratio and light microscopy for shape analysis of aggregates and pores (cf. Fig. 4). Three shape classes, which are not indicated in Fig. 4, were used to define the shape of pores (voids) by Quantimet (Jongerijs, 1974; Murphy et al., 1977; Jongerijs and Bisdorf, 1981). This was done by measuring the area and perimeter of the pores and by calculating the A/Pe^2 ratio used for shape analysis. Rounded voids had $A/Pe^2 \geq 40$, vughy voids ratios <40 and ≥ 15 , and planar and digitate voids ratios <15 .

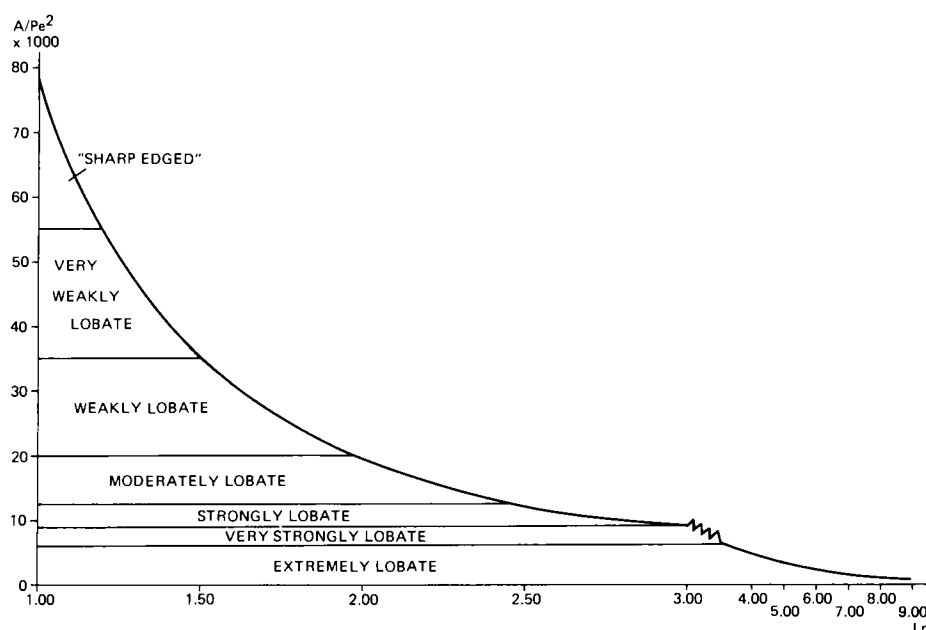


Fig. 4. Shape classes as defined by Beckmann (1962). These are based on the lobation ratio ("Lappungsquotient") and were related to area (A) and perimeter (Pe) determined by Quantimet (cf. text). "Sharp-edged" is indicated with inverted commas, because all measured mineral grains of this shape class had no sharp edges and were rounded.

If the two shape classifications are compared, there is little conformation of terms. A problem may even exist, because rounded voids had an $A/Pe^2 \geq 40$ and Beckmann indicated that "sharp-edged" forms were present with $Lr = 1.2$ to 1.0 , equivalent with A/Pe^2 ratios of 55 to 79. In view of this, it was necessary to have a closer look at the shapes of two-dimensional figures (forms) and how these are related to each other.

Shape analysis of two-dimensional figures

Due to the equation given above, Lr and A/Pe^2 ratios could be related to each other and the curve in Fig. 4 could be drawn. Shape analysis of mineral grains, which is discussed in the section on results, indicated that various grains with different forms can have the same A/Pe^2 ratio and are therefore plotted in the same point of the curve in Fig. 4 (cf. Fig. 9). To explain this phenomenon, a theoretical model was made in which two-dimensional forms change from a disc (circle) to a line (Figs. 5 and 6). Three horizontal sequences of forms with rounded and sharp edges are shown in Fig. 5, whereas forms with lobes and indentures were portrayed on a curve (a curve which suggests the curve in Fig. 4) in Fig. 6.

All figures start at the left with a disc that has an A/Pe^2 ratio of 79. This is the ratio for a disc with a circle as periphery. If the disc is hand-drawn, the perimeter becomes more irregular; the perimeter increases and the ratio may decrease to 74. The form of the disc can change in various ways (cf. Figs. 5 and 6) until a line is reached with an A/Pe^2 ratio of one. If this line is sufficiently thin and long enough, the ratio may even decrease below one. Hand-drawn lines are usually thicker, somewhat irregular and rather short. Consequently, the ratio can increase to about three for such hand-drawn lines. All other two-dimensional forms, if classified according to the A/Pe^2 ratio, are situated on the curve of Fig. 4 between the points which represent a circle ($A/Pe^2 = 79$, $Lr = 1$) and a line ($A/Pe^2 = 1$, $Lr = 9$).

Only a few figures have been drawn in Figs. 5 and 6, whereby the figures with lobes and indentations are found in Fig. 6. A/Pe^2 ratios are indicated below each figure and a special case is present in Fig. 5B, i.e. with the ratios of the central three figures. The first ratio is that of a disc with one line as a wing and the second ratio between brackets, of the disc with two wings. The addition of a second line to the disc gave a significant decrease in the A/Pe^2 ratios.

All ratios decrease from left to right in Figs. 5 and 6. It is interesting to note, that a few ratios are the same but represent different forms, e.g. the figures with an A/Pe^2 ratio of twelve of Figs. 5A, 5B and 6A. If these forms were plotted on the curve of Fig. 4 they would all be represented by the same point. A second example, with A/Pe^2 ratios of seven, is given in Figs. 5C and 6A. This point would be plotted below the point with a ratio of twelve on the curve of Fig. 4.

The above result indicates that, with the use of A/Pe^2 ratios for shape analysis, various forms (figures) can be represented by one point of the curve

in Fig. 4; except for the extremities of the curve occupied by the disc (circle) and line. To subdivide the figures of one point of the curve, other parameters than area, perimeter, or lobation ratio should be used. This can usually be done by measuring Feret's diameters, i.e. the F_{\max}/F_{\min} ratio.

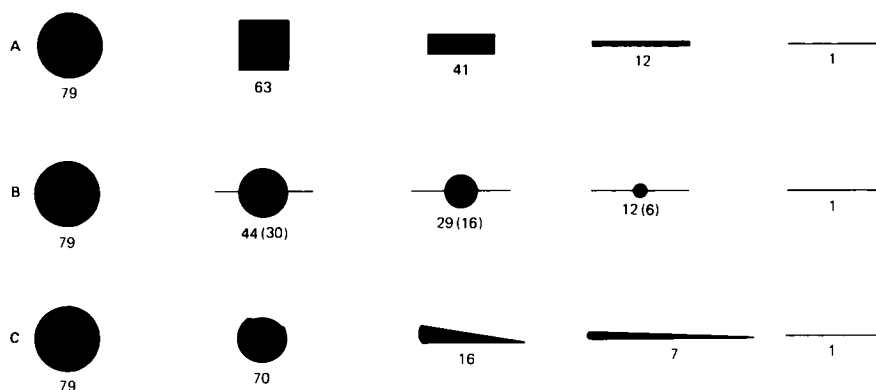


Fig. 5. From disc (circle) to line for two-dimensional forms with rounded and sharp-edged peripheries. The values of A/Pe^2 ratios are indicated underneath the figures. The two numbers in B, underneath three figures, represent the value of the A/Pe^2 ratio of a circle with one line and of a circle with two lines (between brackets).

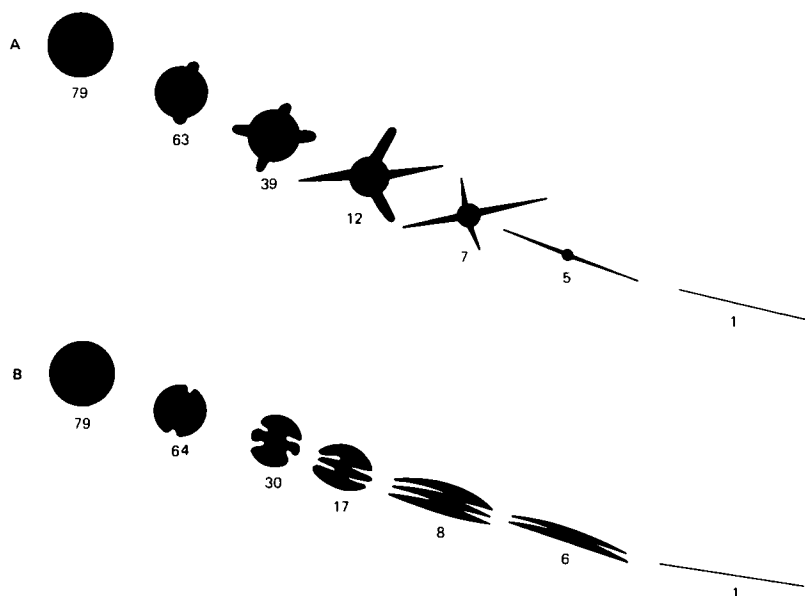


Fig. 6. From disc (circle) to line for two-dimensional figures with lobes (A) and indentures (B). The values of A/Pe^2 ratios are indicated underneath the figures.

Shape classification of two-dimensional figures

Shape classification of two-dimensional figures with A/Pe^2 ratios can be understood best if attention is paid to the periphery or perimeter of such forms. Small changes in the perimeter, rather than small changes in the area, will result in changes of the A/Pe^2 ratio. This increase in perimeter can be done in various ways (cf. Figs. 5 and 6). For example, in Fig. 5B, a disc can obtain a small ratio if sufficient lines (wings) are added to it. In Fig. 5B, the area of the disc was decreased simultaneously. However, the disc can also be maintained at the size of the left figure in Fig. 5B. By adding larger lines (wings) to the larger disc, the perimeter can be made to increase so much, that the disc shifts to the right of Fig. 5B. During such a shift, A/Pe^2 ratios can be arrived at which are equal to the ones associated with the smaller discs in Fig. 5B. In other words, one can shift a large disc with larger wings from the left to the right in Fig. 5B until it has the same A/Pe^2 ratio as a smaller disc with smaller wings. These two figures (forms) can then be plotted as one point in Fig. 4.

The above manipulation can also be done with other figures. In Fig. 5A, the first three figures are a disc, a square and a rectangle. The addition of lines (wings) to the disc can decrease the A/Pe^2 ratio to that of the square or rectangle and, if desired, even farther to the right in Fig. 5A. If lines are added to the square, the A/Pe^2 ratio can be brought above the rectangle and reach the same ratio. In this way, one has placed three figures at the place in which only the rectangle is visible in Fig. 5A, i.e. the rectangle itself, the square with wings, and the disc with longer wings. All three figures have an A/Pe^2 ratio of 41 and represent figures of the same point of the curve in Fig. 4.

The increase in perimeter of a certain figure can also be obtained by adding lobes (Fig. 6A) or indentations (Fig. 6B) to a central disc. Such lobes and indentations can have various forms and sizes. It is understandable, however, that a large number of very small lobes and indentations will increase the perimeter of a form more than is done by the addition of a few lobes with a large area. The consequence was already indicated above with the hand-drawn circle, that had an A/Pe^2 ratio of 74 instead of 79 for the ideally drawn circle (disc).

The lobe with a larger area can also change form towards a spine, e.g. the figures with A/Pe^2 ratios of twelve and seven in Fig. 6A. The longer and thinner the spine, the more it approaches the form of a line and thus the larger the perimeter and the smaller the area of the spine. By using this principle, one can move the figure with a ratio of twelve to the right in Fig. 6A. This is done by making the spines longer and thinner, whereby the core of the figure, a disc, can be maintained at the same size. In this way this figure can also obtain an A/Pe^2 ratio of seven instead of twelve. The result is that two different forms are found for a point on the curve of Fig. 4 with an A/Pe^2 ratio of seven.

The above examples should suffice to explain why so many two-dimensional figures (forms) can be represented by one point on the curve of Fig. 4 and how such forms are related to each other. The explanation on two-dimensional form-developments, using A/Pe^2 ratios, also explains why the use of names in shape classifications can only serve very specific objectives. If one point of the curve of Fig. 4 can represent many two-dimensional forms, this means that a whole shape class — which occupies a part of the length of the curve in Fig. 4 — represents an enormous number of forms. It also means that many unexpected shapes may in reality form a part of a shape class; forms which at first sight have no relation to each other.

The theoretical model for two-dimensional forms, in which A/Pe^2 ratios and lobation ratios have been used, together with the results of measurements of the 54 mineral grains (cf. section on results) and of shape analysis done of pores and soil aggregates in earlier micromorphological studies, gave the diagram in Fig. 7. This diagram is proposed as a working-model for two-dimensional shape classification of soil constituents in thin sections of soils. Only Roman numerals are given for shape classes. The only shape class-boundaries which are recognizable at this point of the paper, are the ones used in the study of pores (voids), i.e. $A/Pe^2 = 40$ and 15. The other boundary-ratios were mainly chosen after studying the shapes of 54 silt-sized mineral grains which are discussed in the next section. The shape classification of two dimensional forms (Fig. 7) is only a proposal which could be

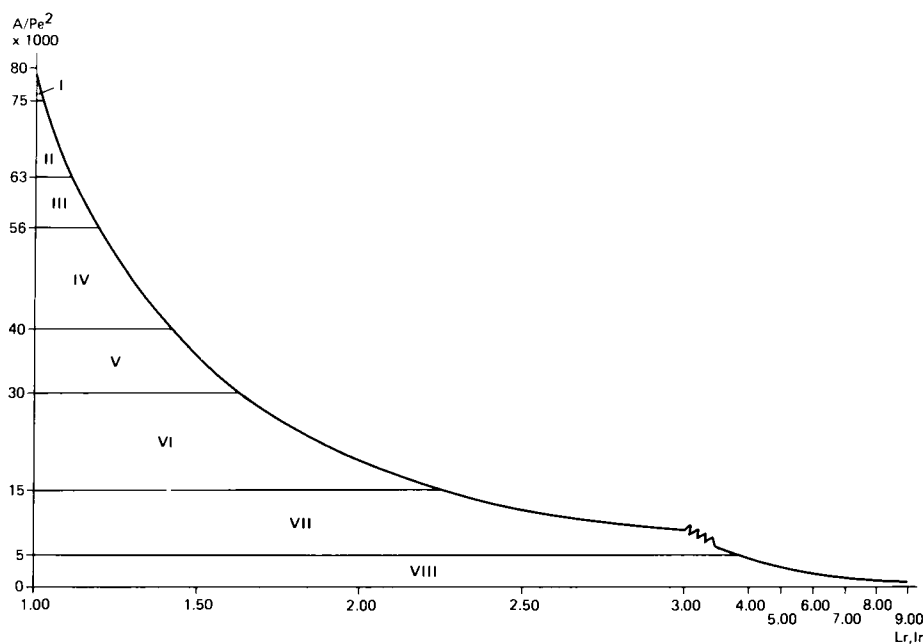


Fig. 7. Suggested shape classes for two-dimensional forms. The classes can be used for A/Pe^2 ratios alone, or in combination with lobation and indentation ratios.

used as a working-model until more data on shapes of soil constituents have been obtained.

RESULTS

Area and perimeter

54 silt-sized mineral grains were investigated in this study and their area and perimeter have been plotted in Fig. 8. Most grains demonstrated an increase in perimeter when the area increased. Jongerius (1974) used the A/Pe^2 ratio for the characterization of the shape of voids and the same is done here for mineral grains. The A/Pe^2 ratios of the 54 mineral grains have been plotted on the curve of Fig. 9, which is part of the curve of Fig. 4, because no ratios of silt grains fell into the other shape classes. Beckmann's names for shape classes have been indicated in Fig. 9.

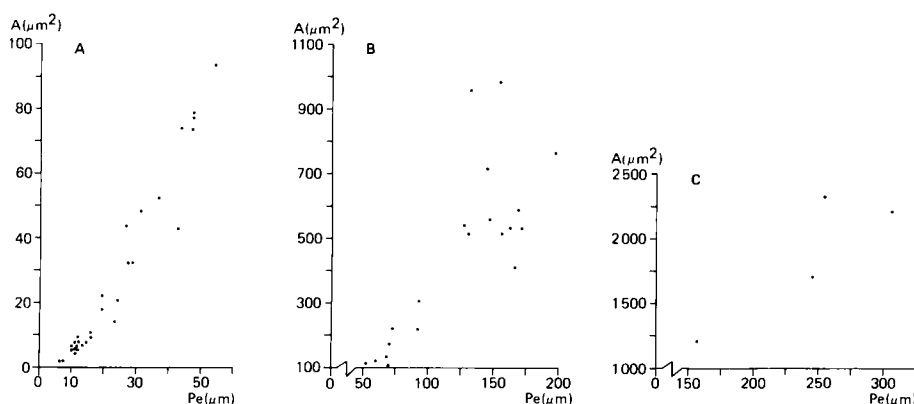


Fig. 8. The relation between area and perimeter is illustrated in diagrams A to C. The perimeter usually increases with area but there are exceptions.

The bar-scale at the top of Fig. 9 indicates in which area class each of the 54 mineral grains of Fig. 9 is situated. The numbers of the grains start at the left of the bar-scale and increase, together with the area, towards the right. The total number of grains in each area class can also be read. The largest number of mineral grains was measured in the area classes $5-10 \mu\text{m}^2$ and $500-1000 \mu\text{m}^2$. The numbers on the curve in the diagram indicate that larger and smaller grains can be present in each of the shape classes.

A number of representative micrographs of silt grains, from each of the shape classes in Fig. 9, is given in Fig. 10 and Fig. 11, e and f. The internally and externally image-edited grains of Fig. 10, a-d represent Beckmann's "sharp-edged" shape class, Fig. 10, e-h the very weakly lobate shape class, Fig. 10, i-l the weakly lobate shape class, and Fig. 11, e and f the moderately lobate shape class.

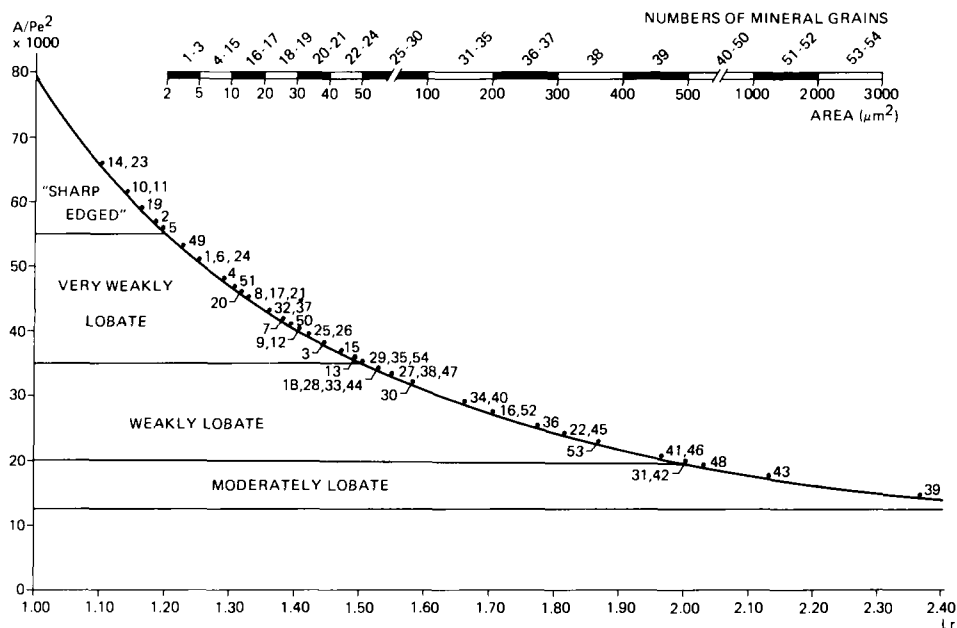


Fig. 9. Part of the diagram shown in Fig. 4 on a different scale. All measured mineral grains are indicated with a number which corresponds to the ones on the bar-scale. This bar-scale indicates to which area-class each number belongs.

Each of the mineral grains in Figs. 10 and 11 has a number. This is also given because it allows the use of Fig. 9. These are: 14 (Fig. 10a), 10 (Fig. 10b), 19 (Fig. 10c), 5 (Fig. 10d), 49 (Fig. 10e), 24 (Fig. 10f), 51 (Fig. 10g), 25 (Fig. 10h), 28 (Fig. 10i), 30 (Fig. 10j), 40 (Fig. 10k), 41 (Fig. 10l), 43 (Fig. 11e) and 39 (Fig. 11f).

A few remarks can be made concerning the shape of the silt grains and the names of shape classes given by Beckmann (1962). Rounded and egg-shaped minerals, which could be weakly lobate, were present in Fig. 10, a–d. These forms were not “sharp-edged”, as is the name of the shape class to which the silt grains belong. Sharp-edged grains and grains with lobes were present in Fig. 10, e–h; the very weakly lobate shape class. One grain in this class had larger lobes (cf. Fig. 10g) but most of the lobes were still weakly developed. One or more sharp edges were found on the periphery of most grains. Beckmann’s term weakly lobate seems difficult to apply to the shape of the mineral grains in Fig. 10, i–l. The lobes of the silt grains have become larger and several have an irregular form. Embayments are present and some of the mineral grains have indentations. Two representatives of the moderately lobate shape class (Fig. 11, e and f) had very different forms. Grain 11e demonstrates an increase in indentation and many lobes, whereas grain 11f is very elongated, weakly platy, with several smaller lobes.

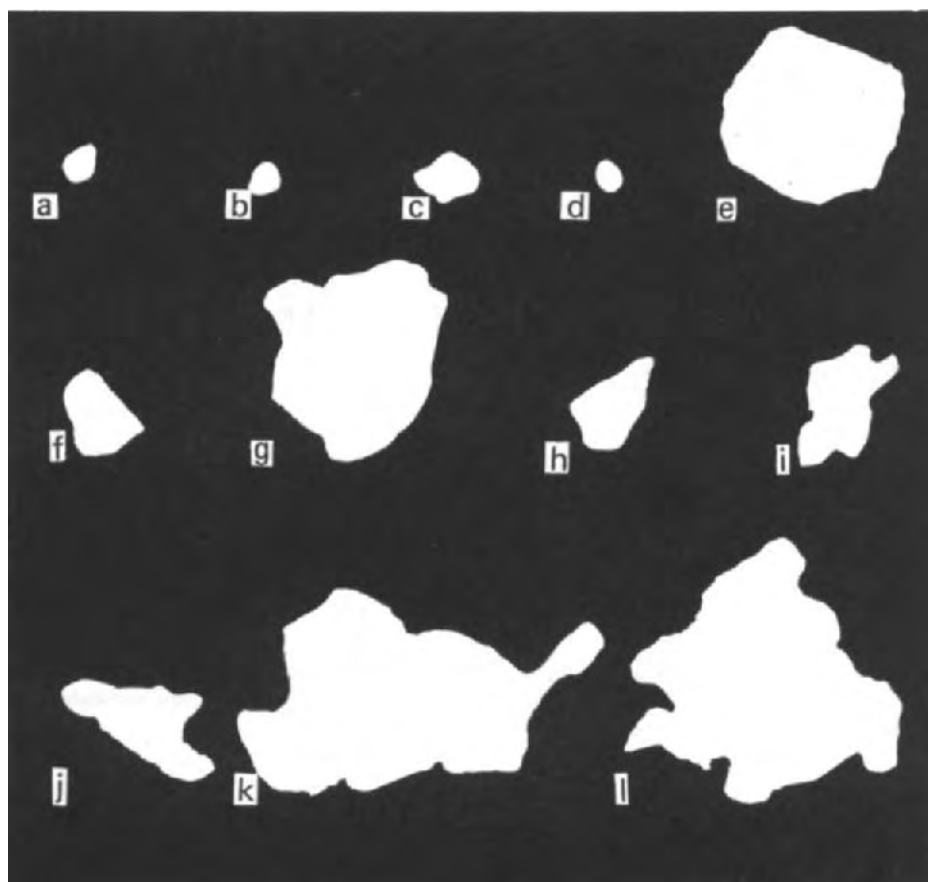


Fig. 10. Examples of shape classes in Fig. 9. Rounded to weakly lobated mineral grains in the “sharp-edged” shape class (a–d); sharp edges and lobes in the very weakly lobate shape class (e–h); and the latter forms and indentations in the weakly lobate shape class (i–l). Representatives of the moderately lobate shape class are present in Fig. 11, e and f.

Feret's diameters

The shape of most mineral grains can be characterized by using A/Pe^2 ratios, the lobation ratio and micrographs. There are grains, however, which have different shapes but the same A/Pe^2 or Lr ratio. Grains with these characteristics are shown in Fig. 11, a–d and data from measurements given in Table III. In such cases, one can introduce Feret's diameters (Jongerus and Bisdorf, 1981). The largest and smallest grain diameters can be determined together with those at angles of 45° and 135° . For shape analysis, the ratio between the largest Feret's diameter (F_{max}) and the smallest one (F_{min}) is taken.

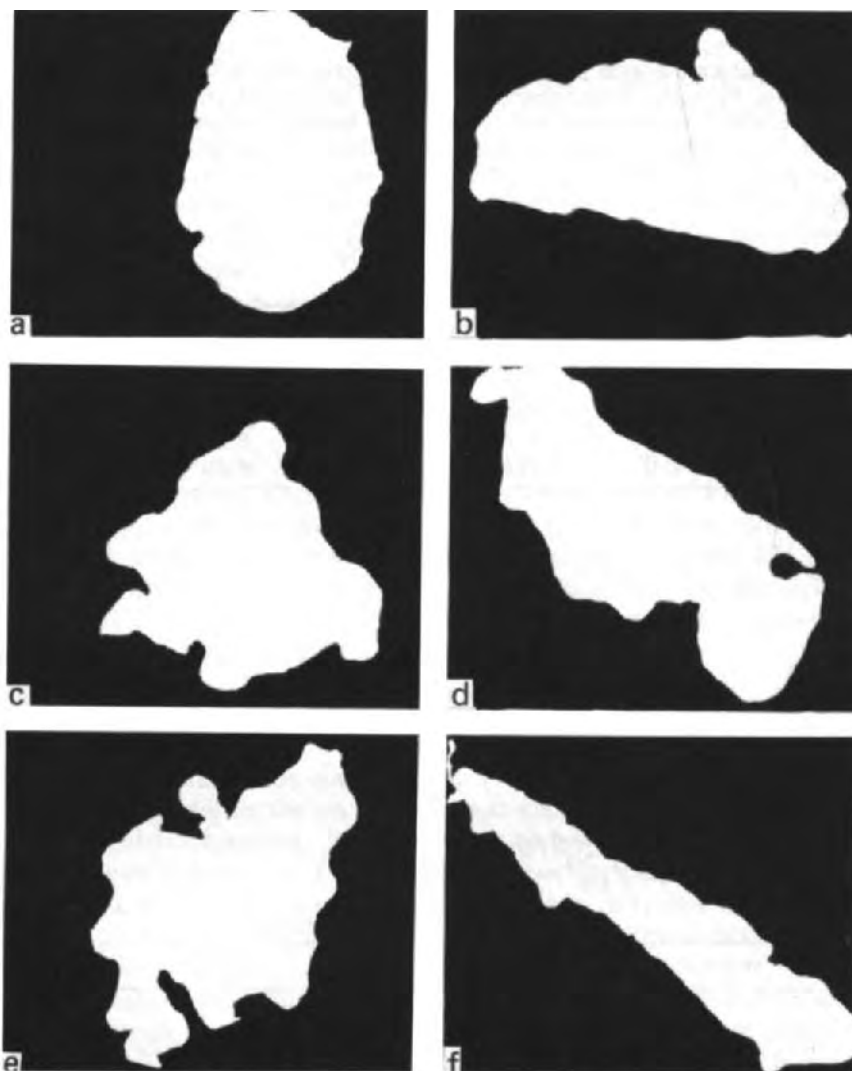


Fig. 11. Shapes of mineral grains in Table III. The F_{\max}/F_{\min} (the largest and the smallest Feret's diameter) ratio can be used to separate grain-pairs a and b or c and d; grains which have similar A/Pe^2 ratios but a different shape. F_{\max}/F_{\min} can also be used to separate elongated forms of mineral grains (f) from grains with a smaller Feret's ratio (e).

Grain-pair a and b in Fig. 11 has virtually the same A/Pe^2 ratio, i.e. 34 and 33 and L_r of 1.53 and 1.55 (Table III). If F_{\max}/F_{\min} is determined these are 1.49 and 1.72. The same can be done for grain-pair c and d of Fig. 11 (cf. Table III). Consequently, grains with a similar A/Pe^2 ratio could be separated from each other by using the ratio F_{\max}/F_{\min} .

TABLE III

Separation of mineral grains with virtually the same (grain-pairs a—b and c—d) A/Pe^2 ratios and Lr values by using F_{max}/F_{min} , the ratio of the largest and smallest Feret's diameter; grains e and f are minerals with the highest lobation values (smallest A/Pe^2 ratios) in Fig. 9, of which the elongated form of mineral f is well expressed in a high F_{max}/F_{min} ratio

Mineral grain code in Fig. 11	Mineral grain in Fig. 9	A (μm^2)	Pe (μm)	$A/Pe^2 \times 1000$	Lr	F_{max}/F_{min}
a	44	542	126	34	1.53	1.49
b	47	717	146	33	1.55	1.72
c	41	515	157	21	1.99	1.03
d	46	591	169	21	1.97	2.55
e	43	539	175	18	2.13	1.25
f	39	410	169	14	2.36	4.72

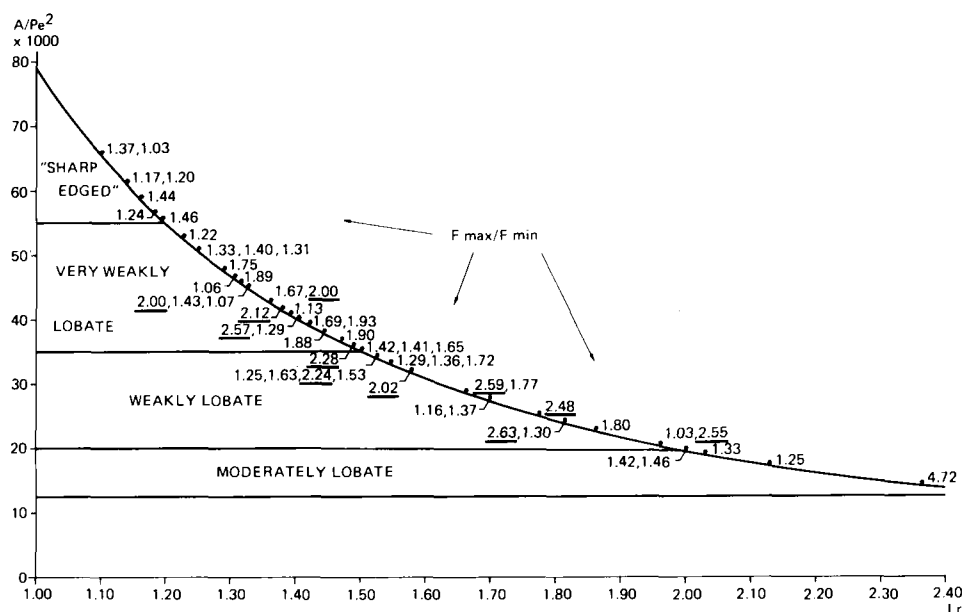


Fig. 12. F_{max}/F_{min} ratios of individual mineral grains; their position corresponds with that of the 54 mineral grains in Fig. 9. Ratios of 2.00 (suggested as a minimal ratio for elongated or platy forms) and higher are underlined.

Another possibility for using F_{max}/F_{min} , is to differentiate between elongated (platy) and rounded forms. An elongated grain is present in Fig. 11f and a more rounded one in Fig. 11e. The elongated grain has a ratio of 4.72, whereas the grain in Fig. 11e has only 1.25. Elongated forms of mineral grains in Fig. 11 seem to start in grain b with a ratio of 1.72. A better ex-

ample of an elongated form is found in grain d with a ratio of 2.55 and the best one in f with the very high ratio of 4.72. No elongated forms can be distinguished in Fig. 8, a, c and e with F_{\max}/F_{\min} of 1.49, 1.03 and 1.25. This seems to indicate that the ratio F_{\max}/F_{\min} can separate elongated mineral grains from the ones which are more rounded or quadrangular.

The next step was to observe all the micrographs of the 54 silt grains and to plot all F_{\max}/F_{\min} ratios in Fig. 12. It was found that elongated forms are clearly discernable at $F_{\max}/F_{\min} = 2.00$ and higher. This value is on the safe side and it may well be that a somewhat smaller value will be favoured in the future. The plotted ratios in Fig. 12 show that the F_{\max}/F_{\min} ratios of two and more may occur in all shape classes, except the one called "sharp-edged" by Beckmann (1962). The mineral grains in Fig. 12 have been plotted on the same curve and in the same points as in Fig. 9. The numbers of the points with F_{\max}/F_{\min} ratios can therefore be found in Fig. 9.

The first mineral grain with $F_{\max}/F_{\min} = 2.00$ occurred in Beckmann's very weakly lobate shape class. It is grain number 8 of Fig. 9. A second grain with number 37 had the same ratio, etc. Only the very elongated forms of minerals which were found in this study occur in Figs. 11f and 3d. Both grains, which are virtually platy, have $F_{\max}/F_{\min} > 4$, viz. 4.72 (Fig. 11f) and 4.22 (Fig. 3d). The rounded grains in Beckmann's "sharp-edged" shape class had an F_{\max}/F_{\min} of 1.46 or less (Fig. 12).

Shape classification of mineral grains and voids

The suggested shape classification (Fig. 7) has already been introduced as a working-model in the section on materials and methods together with the theoretical background. Two boundary-ratios of $A/Pe^2 = 40$ and 15 have already been included in Fig. 7 and are based on shape classification of voids. What has to be explained now is the reason why the other boundaries in Fig. 7 were suggested; these are mainly based on knowledge obtained in the present investigation.

For reasons which have already been explained, shape classes are indicated using Roman numerals. Class I has the upper boundary at $A/Pe^2 = 79$ ($Lr = 1.00$); this represents a circle (disc) which is smooth. The lower boundary was placed at $A/Pe^2 = 75$ ($Lr = 1.05$). This can be a circle with a somewhat irregular periphery, but also a polygon with a large number of angles. A regular polygon with eight angles has a ratio of about 75. Both rounded and sharp-edged forms can therefore be present. Very small lobes and indentations may also occur.

The lower boundary of class II was placed at $A/Pe^2 = 63$ ($Lr = 1.12$). This represents a square with sharp edges and other forms. The lobation ratio and the indentation ratio are still small and so are most lobes and notches of the mineral grains.

Class III has its lower boundary at $A/Pe^2 = 56$ ($Lr = 1.19$). This is a rectangle with a 1 : 2 ratio for the sides. It was chosen because it has $F_{\max}/$

$F_{min} = 2.00$. This point on the curve of Fig. 7 should represent the first elongated (somewhat platy) form on the curve. Rounded forms with smaller lobes and indentures were still dominantly represented in the investigated mineral grains.

Class IV is the first in which sharp-edged mineral grains have been found. The sharp edges could occupy a larger part of the periphery of the grains. Rounded forms had decreased significantly in the silt grains and were largely replaced by lobes of different sizes. Indentations were present but, as was the case with the first three classes, attracted less attention than the lobe-forms. The lower boundary of this shape class was placed at $A/Pe^2 = 40$ ($Lr = 1.41$); a boundary which is the upper limit of vughs and the lower one of more or less rounded voids. The first elongated mineral with $F_{max}/F_{min} = 2.00$ was observed in this shape class and had $A/Pe^2 = 45$.

Class V has a lower boundary at $A/Pe^2 = 30$ ($Lr = 1.63$). It is an arbitrary boundary between the ratios 40 and 15 in which vughy voids are present. The only reason is to obtain a smaller shape class. Indentations on mineral grains attracted attention for the first time. The indentations could have various sizes and forms. Lobes, some of them rather large, were also found. Elongated grains were present. Sharp edges could occupy several discontinuous and small parts of the periphery of mineral grains or one or more longer distances.

Class VI has a lower boundary which coincides with that of vughs, viz. $A/Pe^2 = 15$ ($Lr = 2.30$). Indentations and lobes have become somewhat more irregular than in class V. Indentations of mineral grains could cut deep into these. More grains than in class V were elongated and had an F_{max}/F_{min} ratio greater than two. Sharp edges seemed to occupy discontinuous and small parts of the periphery of the grains and fewer longer distances than in class V. Theoretically, however, platy forms with sharp edges can be present in this class.

Class VIII has been separated from the former class because, like class I, it voids from planar and digitate voids. The lower boundary of this class was placed at $A/Pe^2 = 5$ ($Lr = 3.99$). Platy forms are common, but star-shaped forms can also occur according to theoretical considerations explained in the section on materials and methods. Cracks with smooth or more irregular walls will fall into this class as long as they are thin. As soon as the crack is widened, to give a relatively large area, it will form part of class VI.

Class VIII has been separated from the former class because, like class I, it should represent some extreme forms which end as a line with an $A/Pe^2 = 1$ ($Lr = 8.92$). Long and thin platy forms are represented. Theoretically, however, a circle (disc) with one or more long to very long needles can also fall into this class. All forms with a very large perimeter, compared with the enclosed area, can be placed in this class.

CONCLUSIONS

Shape analysis of mineral grains in thin sections of soils can be done with BESI and Quantimet. Manual work with the image-editor of the Quantimet 720 is necessary to define the often complex peripheral forms of the grains. All silt grains which were represented in Fig. 1 were measured, except those which extended beyond the boundary of the backscattered electron scanning image. The magnifications which could be used for the shape analysis of the grains were $\times 240$ and $\times 480$. In the present case $\times 480$ was chosen because this allowed an easy internal and external covering of the mineral grains with the image-editor.

Area (A), perimeter (Pe) and Feret's diameters of 54 silt-sized mineral grains were measured. The lobation ratio (Lr) could be related to the A/Pe^2 ratio with a formula. The indentation ratio (Ir), if defined in the same way as the lobation ratio, can also be related to the A/Pe^2 ratio. A diagram was made of A/Pe^2 and Lr , and provisional shape classes were introduced. All forms of the measured mineral grains could be distinguished individually using A/Pe^2 and F_{max}/F_{min} . Reproduction of the shape of individual mineral grains is not possible with these parameters, however, and micrographs of each mineral therefore remain necessary.

Eight shape classes, the boundaries of which were based on knowledge obtained during former shape analysis studies of voids, the present investigation of silt-sized mineral grains and from a theoretical model, are given in Fig. 7. It was demonstrated with the theoretical model that all two-dimensional forms can be placed between two extremes, i.e. a circle ($A/Pe^2 = 79$) and a line ($A/Pe^2 = 1$). A number of examples was given in the theoretical model of the changes in forms with decreasing A/Pe^2 ratios. This allowed some understanding of the type of two-dimensional figures which can be expected in certain shape classes, i.e. in a certain range of A/Pe^2 ratios. Measurements also indicated that the same F_{max}/F_{min} ratios could occur in different shape classes and that these were therefore not specific for one shape class. The F_{max}/F_{min} ratio, however, can be used to separate elongated (planar forms) ($F_{max}/F_{min} \geq 2$) from other forms.

The present study has succeeded in relating different two-dimensional forms, based on A/Pe^2 measurements. Relatively few of the possible shapes were, however, encountered in the present investigation and consequently the suggested boundaries of the shape classes in Fig. 7 may have to be changed when more shape data become available during subsequent studies of soil constituents. It could be practical to introduce different boundaries for shape analysis of minerals, voids, soil aggregates, etc. However, this will not change the principle of two-dimensional shape analysis which has been discussed. The present shape study also indicates that shape analysis may require relatively large magnifications, due to the necessity of correct perimeter measurements of especially smaller soil particles and voids.

REFERENCES

- Beckmann, W., 1962. Zur Mikromorphometrie von Hohlräumen und Aggregaten im Boden. *Z. Pflanzenernähr., Düng. Bodenk.*, 99 (144): 129—139.
- Bisdorn, E.B.A. and Thiel, F., 1981. Backscattered electron scanning images of porosities in thin sections of soils, weathered rocks and oil-gas reservoir rocks using SEM-EDXRA. In: E.B.A. Bisdorn (Editor), *Submicroscopy of Soils and Weathered Rocks. 1st Workshop of the International Working-Group on Submicroscopy of Undisturbed Soil Materials (IWGSUSM) 1980, Wageningen*. Centre for Agricultural Publishing and Documentation (Pudoc), Wageningen, pp. 191—206.
- Bouma, J., Jongerius, A., Boersma, O., Jager, A. and Schoonderbeek, D., 1977. The function of different types of macropores during saturated flow through four swelling soil horizons. *Soil Sci. Soc. Am. J.*, 41(5): 945—950.
- Bouma, J., Jongerius, A. and Schoonderbeek, D., 1979. Calculation of saturated hydraulic conductivity of some pedal clay soils using micromorphometric data. *Soil Sci. Soc. Am. J.*, 43(2): 261—264.
- Ismail, S.N.A., 1975. Micromorphometric soil-porosity characterization by means of electro-optical image analysis (Quantimet 720). *Neth. Soil Surv. Inst., Wageningen, Soil Surv. Pap.*, 9: 104 pp.
- Jongerius, A., 1974. Recent developments in soil micromorphology. In: G.K. Rutherford (Editor), *Soil Microscopy. Proceedings of the 4th International Working Meeting on Soil Micromorphology, Kingston, 1973*. The Limestone Press, Kingston, Ont. pp. 67—83.
- Jongerius, A. and Bisdorn, E.B.A., 1981. Porosity measurements using the Quantimet 720 on backscattered electron scanning images of thin sections of soils. In: E.B.A. Bisdorn (Editor), *Submicroscopy of Soils and Weathered Rocks. 1st Workshop of the International Working-Group on Submicroscopy of Undisturbed Soil Materials (IWGSUSM) 1980, Wageningen*. Centre for Agricultural Publishing and Documentation (Pudoc) Wageningen, pp. 207—216.
- Kubiena, W., Beckmann, W. and Geyger, E., 1961. Zur Methodik der Photogrammetrischen Strukturanalyse des Bodens. *Z. Pflanzenernähr., Düng. Bodenk.*, 92(137): 116—126.
- Murphy, C.P., Bullock, P. and Turner, R.H., 1977. The measurement and characterisation of voids in soil thin sections by image analysis, Part I. Principles and techniques. *Soil Sci.*, 28 (3): 498—508.

POROSITY MEASUREMENTS AND FORM ANALYSIS OF MINERAL GRAINS IN THIN SECTIONS FROM OIL- GAS RESERVOIR ROCKS USING QUANTIMET 720 AND BESI

E.B.A. BISDOM¹, H.A. van ADRICHEM BOOGAERT², G. HEINTZBERGER¹,
D. SCHOONDERBEEK¹ and F. THIEL³

¹ *Netherlands Soil Survey Institute, P.O. Box 98, 6700 AB Wageningen (The Netherlands)*

² *Geological Survey of The Netherlands, 2000 AD Haarlem (The Netherlands)*

³ *Technical and Physical Engineering Research Service, 6700 AJ Wageningen (The Netherlands)*

(Accepted for publication February 17, 1983)

ABSTRACT

Bisdom, E.B.A., van Adrichem Boogaert, H.A., Heintzberger, G., Schoonderbeek, D. and Thiel, F., 1983. Porosity measurements and form analysis of mineral grains in thin sections from oil–gas reservoir rocks using Quantimet 720 and BESI. *Geoderma*, 30: 323–337.

Submicroscopic and image analyzer techniques have been applied for the measurement of the porosities of oil–gas–water reservoir rocks from thin sections. Backscattered electron scanning images (BESI) were made predominantly at low magnifications of $\times 30$ and $\times 60$. Porosity data from linear traverses were obtained and differences in porosities between two sandstone reservoirs and a carbonate reservoir were determined. A large number of the measured pores contained clayey material. The surface occupied by this material was subtracted from the apparent porosity measurements with the image editor of the Quantimet 720 to give the real porosity.

A sample from one of two sandstone reservoirs contained oil and could not be hardened using the common procedure for impregnation of the sample by a polyester resin. Gamma radiation was applied and hardening occurred in one weekend after 5 Mrad (50 kGy) had been absorbed. Hardening of this sample gave no problems, if the oil had been removed by monostyrene before a start was made with the impregnation process; such a sample was used for the present porosity study.

Form analysis was done of individual mineral grains using BESI and Quantimet. The grains were represented in a number of shape classes of a diagram used for shape classification. Form-separation of individual minerals was also possible.

INTRODUCTION

Earlier measurements of porosities in thin sections often used an integration ocular for point counting in conjunction with a light microscope. More recently, an image analyzer (Quantimet) has been introduced (Jongerijs et al., 1972). This allowed the measurement of the total area occupied by pores; especially in clayey soils. Subsequent investigations and more modern

equipment has allowed better in situ porosity analysis of soils (Jongerijs, 1974; Ismail, 1975; Murphy et al., 1977; Bouma et al., 1977, 1979). The analyses concerned pores larger than $30\text{ }\mu\text{m}$ in diameter. Due to the use of transmitted light and the thickness of the thin section, it was hardly possible to analyse pores with smaller diameters. Incident light gave no better results. Moreover, the study of sandy soils caused problems. Because of their orientation minerals could remain extinguished using crossed polarizers, or sufficient contrast could not be made between a number of minerals and the pores. Various light microscopic techniques were tested to see which could provide measurable porosities, by Quantimet. This was not successful and, consequently, other techniques had to be tried.

With the introduction of backscattered electron scanning images (BESI) (Bisdorn and Thiel, 1981) the above problem was solved. These images were of such high quality and could be taken at such a variety of magnifications, that pores with diameters smaller and larger than $30\text{ }\mu\text{m}$ (the smallest pore diameter measurable on micrographs made with transmitted light) could be measured by Quantimet (Jongerijs and Bisdorn, 1981). The latter paper gave examples of such Quantimet measurements on BESI for soils. In the paper by Bisdorn and Thiel (1981), examples of pores in BESI of soils, weathered rocks, and oil—gas reservoir rocks were given, but only the soil porosity was measured (Jongerijs and Bisdorn, 1981). The present study is primarily intended to give an example of measurements in oil—gas reservoir rocks. A special case was the presence of clays in many pores of the sandstone reservoirs. These, however, were also measured and subtracted from the total area of the pores to give the real porosity.

BESI were taken at a low magnification, because porosity measurements at smaller magnifications can cover a larger area in one micrograph and are therefore more economic. Contiguous micrographs were made along linear traverses.

Form analysis was done of 50 larger mineral grains which were easy to distinguish at a magnification of $\times 60$. Usually, and especially for smaller silt-sized mineral grains, good results are obtained if form analysis is done on BESI at $\times 240$ or $\times 480$ (Bisdorn and Schoonderbeek, 1983).

MATERIALS AND METHODS

Light microscopy

The thin sections for this study were obtained from core samples of two sandstone and one carbonate reservoirs. The first sample came from a Lower Cretaceous sandstone reservoir and from a depth of about 1300 m. The sample contained oil and comprised mainly well-sorted subangular quartz grains, deposited in a former beach ridge environment. The matrix contained a little clay, usually in small patches. No cement was present.

The second sandstone reservoir provided samples from depths above and

below a gas—water contact-level situated at about 3080 m depth. Physical measurements indicated about 10% porosity and a permeability of maximally 0.6 millidarcy. The Lower Permian sandstone consisted of predominantly well-sorted subrounded to rounded quartz with several grains of flint. The sands were deposited as aeolian sands in a desert environment. The matrix contained a small percentage of clay, which was partly fibrous. The cement consisted of quartz and dolomite. Most of the pores were filled with cement. Some of the dolomite in the pores was subsequently leached.

The third reservoir, an Upper Permian dolomite, gave a core sample from a depth of about 1950 m. The carbonate was originally an algal oolite which formed in a shallow marine to lagoon environment. The oolite was subsequently dolomitized. The leached centres of the ooides were either empty or filled with anhydrite and carbonate crystals. The latter crystals are coarser than those of the original rock.

SEM, BESI, Quantimet

Two scanning electron microscopes were used: a Philips SEM 505 and a Jeol-JSM-35C. The SEM 505 provided backscattered electron scanning images of contiguous microareas in a thin section which could be analysed with an image analyzer, the Quantimet 720. Magnifications were usually $\times 60$, and $\times 30$ was used in one case. Larger magnifications were also used to study the morphology of clays in the pores. Energy dispersive X-ray analysis (EDXRA), used for the measurement of chemical elements, was done with the JSM-35C.

If clay occupied a pore partly or completely, porosity measurements required the use of the image editor of the Quantimet. Such manual work was necessary, because the contrast of the clay with the pore on BESI was not sufficient to be measured automatically by Quantimet. The occurrence of clay on the display screen of the Quantimet was carefully checked and compared with the clay on BESI. The apparent porosity was the total area occupied by pores; with or without clay in the pores. The real porosity was obtained by subtracting, with the image editor, the area occupied by clay from the area occupied by the apparent porosity. If no clay was present the apparent porosity and the real porosity were identical.

The hardening of oil-containing sample by gamma radiation

The oil-containing sample, similar to the other core-samples in this study, was treated first with a polyester resin according to the method described by Jongerius and Heintzberger (1975). However, the sample did not harden in this manner. Recently, due to experiments done at the Netherlands Soil Survey Institute, hardening of the oil-containing sample succeeded by using deep-penetrating gamma radiation. This gamma radiation was obtained from a plate-shaped source in which a number of bars with Cobalt-60 were placed

in a rack. Each bar is able to provide 1000 Ci ($37 \cdot 10^{12}$ Bq) or more, depending on the type of installation.

The absorbed dose for this oil-containing sample was 5 Mrad (50 kGy). The treatment which worked best was the "train" principle whereby samples moved past the source a number of times with intermittent rest periods of an hour or more during which time they were not affected by radiation. Polymerization and hardening of the sample was thus performed in a weekend.

RESULTS

Oil-containing sandstone

A light microscopic micrograph of the oil-impregnated sample which was treated with gamma radiation is shown in Fig. 1. Some of the mineral grains show a relatively thick coating (grain cutan) of oil but most of the grains had thin skins of oil. Some of it was dissolved during and after the impregnation process. The impression is, however, that the micrograph gives a rather good picture of the in situ situation of the oil-containing rather loose sandstone.

The porosity, which represents the percentage of the total area of a micrograph that is occupied by pores, was measured by Quantimet from BESI of a thin section from which the oil had been removed using monostyrene (Fig.

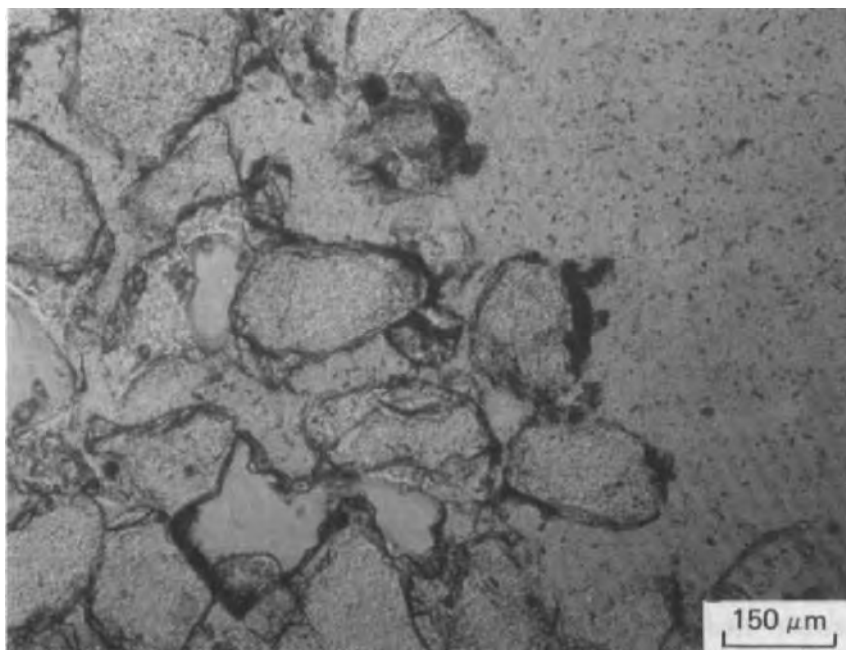


Fig. 1. Oil-impregnated sandstone. The oil is visible as thick and thin blackish coatings on some of the mineral grains. Plane polarized light.

2). Pores with or without clay were present in Fig. 2a, whereas no clay was found in Fig. 2b. Consequently, the real porosity could be measured in Fig. 2b, i.e. 21.17%. The apparent porosity was 24.95% in Fig. 2a. The real porosity was found by subtracting the percentage occupied by clay from the apparent porosity. The percentage of clay was 2.53% and the real porosity 22.42%.

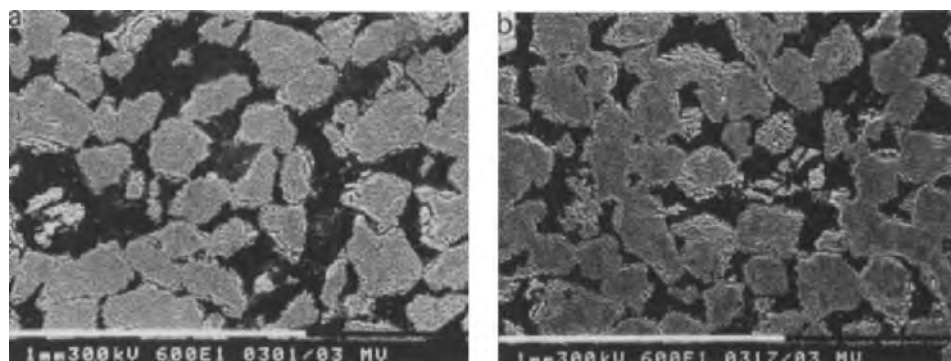


Fig. 2. Backscattered electron scanning images (BESI) of the same oil-containing sandstone as in Fig. 1. However, the oil was removed from the sample with monostyrene in order to demonstrate the real porosity. Micrograph a shows that clay patches occupy some of the pores whereas no clay could be detected in micrograph b. Porosity-values in text.

The central part of Fig. 2a and other areas of the micrograph have patches of light grey to dark grey clayey material. The central part of Fig. 2a was subsequently enlarged with the SEM 505 to a maximum of $\times 16,000$ (Fig. 3). The platy aspect of clay minerals in the packets became visible at the maximum magnification. The maximum magnification, at which the materials in the micrograph become vague, is dependent on the type of material and the possibilities of the instrument which is used.

The micrographs in Fig. 3 also indicate that the morphology of the clay changes at different magnifications. Only a few strings with clay packets are discernable in Fig. 3b but many become visible at higher magnifications. This indicates that the fine-grained clay in Fig. 3b has a similar morphology if the clay can be enlarged sufficiently. Another point is the appearance of micropores in the fine-grained clays of Fig. 3b at higher magnifications (Fig. 3d). This phenomenon was also found in soils where smaller pores could be measured at higher magnifications (Jongorius and Bisdom, 1981).

Sandstone reservoir with gas—water contact

The second sandstone reservoir, with the gas—water contact at about 3080 m, had a much smaller apparent and real porosity than the oil-impregnated one. Quantimet porosity measurements were done on sixteen micrographs, viz. twelve micrographs from two thin sections from the gas-contain-

ing part of the core at 3071 m and four micrographs of one thin section from the water-containing part of the reservoir at a depth of 3084 m. All micrographs were taken in a series of four and of contiguous microareas on the thin section (Figs. 4 and 5). Such an approach allows a continuous measurement of pores along linear traverses.

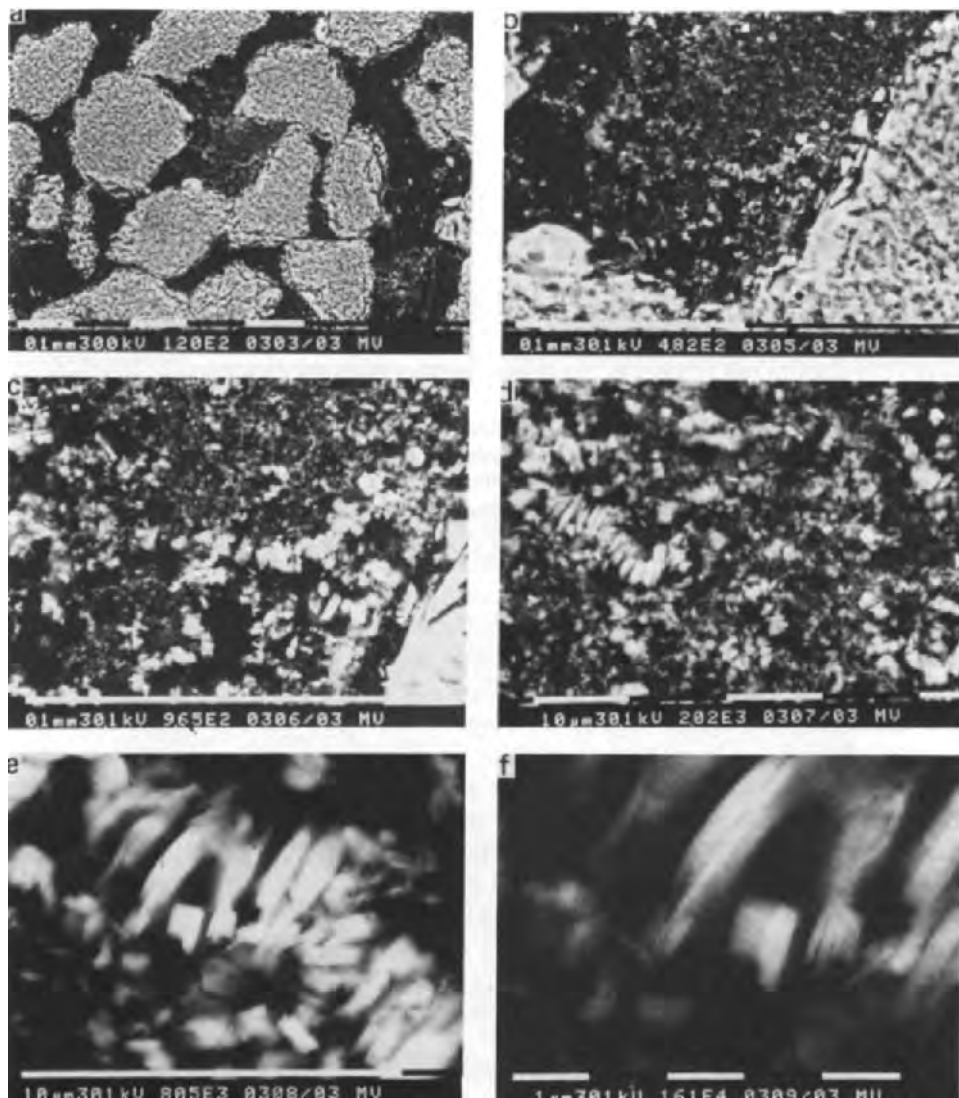


Fig. 3. Enlargements of the clay in the central part of Fig. 2a. A few strings of clay packets occur at low magnifications (b) and increase in number with higher magnifications (d). At a magnification of $\times 16,000$ individual clay platelets just start to appear in the clay packets.

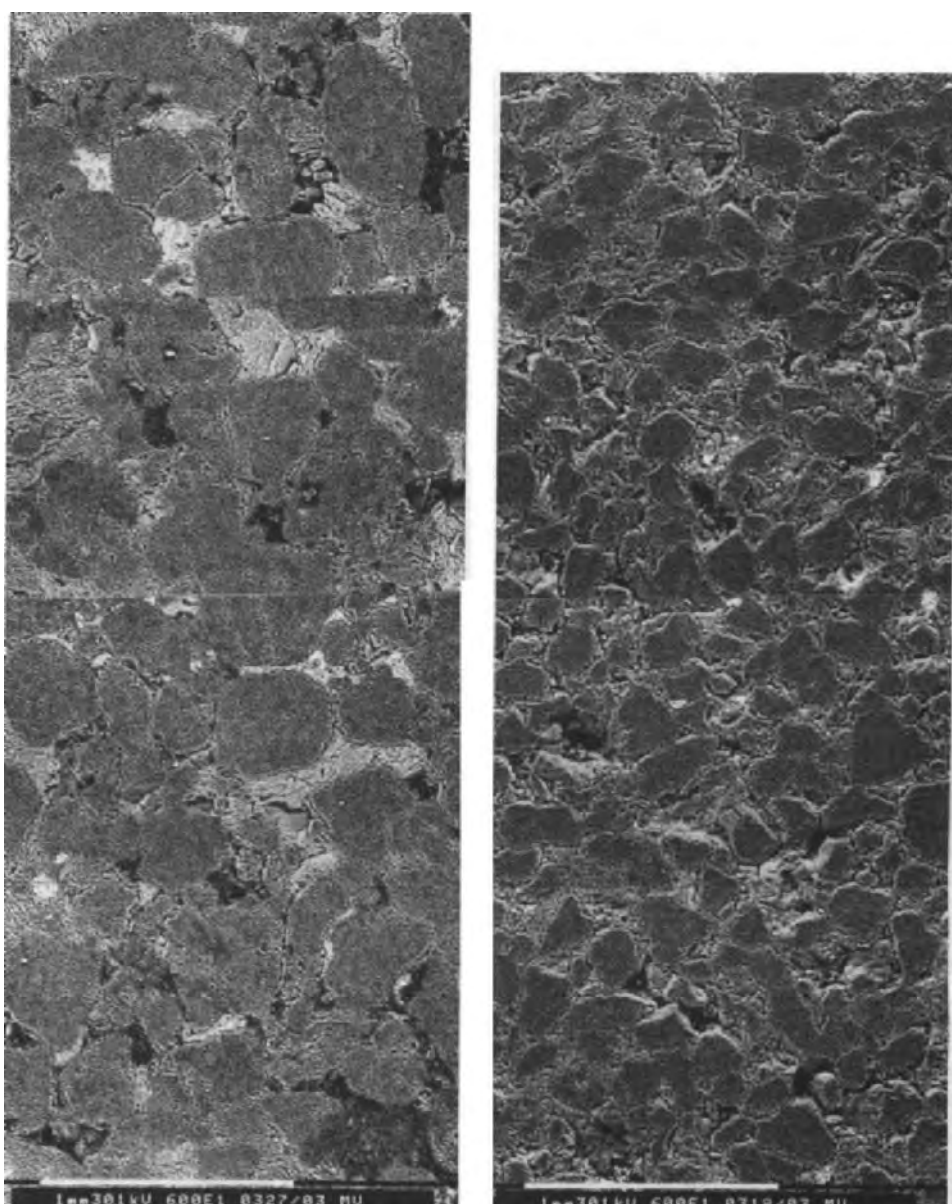


Fig. 4. Four contiguous BES-SEM micrographs of the gas-containing part of the second sandstone reservoir. Greyish to white colours represent predominantly dolomite. Individual mineral grains are discernable. Porosity-values in text.

Fig. 5. Four contiguous BES-SEM micrographs of the water-containing part of the second sandstone reservoir. The grains are smaller and less rounded than in Fig. 4. Porosity-values in text.

The twelve micrographs of the gas-containing part of the core had 9.12% apparent porosity as a maximum, followed by a value of 5.00% and up to 2.30% as a minimum. If the same micrographs are investigated for the real porosity the values were: 1.16%, 1.04% and 0.28% in the same order. This left 8.04%, 3.96% and 2.02% for the clay in the pores. The clay occupied, therefore, 87.39%, 79.20% and 87.82% of the apparent porosity. The smallest real porosity does not appear in these values. It was only 0.12%.

The four micrographs from the water-containing section (Fig. 5) of the core had apparent porosities of 1.07%, 2.24%, 3.27% and 3.13%. In the same order the real porosities were: 0.45%, 0.69%, 1.24% and 1.46%. The percentage of clay was: 0.62%, 1.55%, 2.03% and 1.67%. This gave 57.94%, 69.20%, 62.07% and 53.35% of the apparent porosity occupied by clay.

The above figures indicate that the apparent porosity of the gas-containing part of the core could be higher than that of the underlying water-containing section. The real porosity in all measured micrographs was always smaller than 1.79% and often even smaller than 1%. The clay occupied less volume of the pores in the water-containing part of the reservoir.

The morphology of the clay was studied at various magnifications with a JSM-35C (Fig. 6). The clay which was studied, was present in the gas-

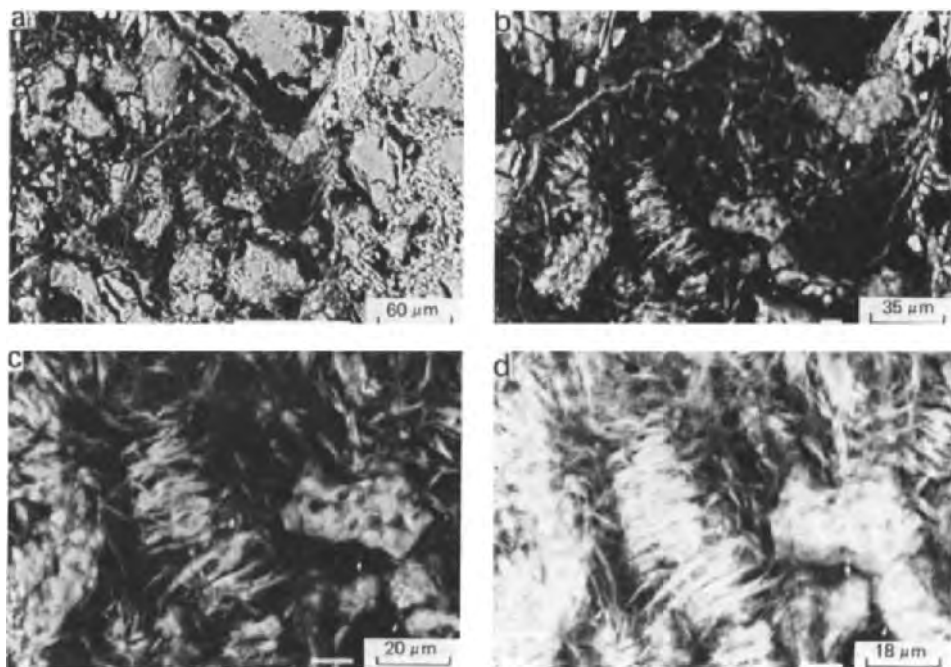


Fig. 6. BES-1 enlargements of fibrous clay in pores. Differences in exposure times of micrographs (c) and (d) give an idea of the distribution of the clay in the pore. Only a low microporosity is left.

containing part of the reservoir and was fibrous. Details are most visible at higher magnifications. It was also demonstrated that the type of detail in the micrograph can be changed by varying the conditions under which the micrograph is taken (Fig. 6, c and d). Such detailed information can be of importance at especially the lower magnifications of $\times 30$ and $\times 60$ used in this porosity study. It allows some insight into the real quantity of clay present in the pores and into the real porosities which can be expected. If necessary, porosity analysis can also be done at larger magnifications (Jongerius and Bisdom, 1981; Bisdom and Schoonderbeek, 1983).

Chemical elements were measured in the clay patches of the gas-containing section of the core (Fig. 7). The elements Na, Mg, Al, Si, S, Cl, K and Fe were present. These elements were interpreted to represent clay, dolomite and halite (Fig. 7, a and b). No Fe is visible in Fig. 7b because the scale has been changed with respect to Fig. 7a. An EDXRA measurement of somewhat impure halite is given in Fig. 7c. The measurements are point analyses at $\times 10,000$ magnification. This allows analysis of microareas of the clays in the pores. In this case, the occurrence of halite could be added to the light microscopic observations which indicated the presence of clay and dolomite.

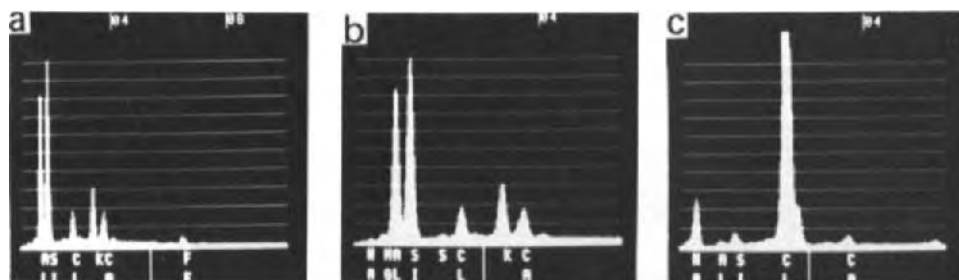
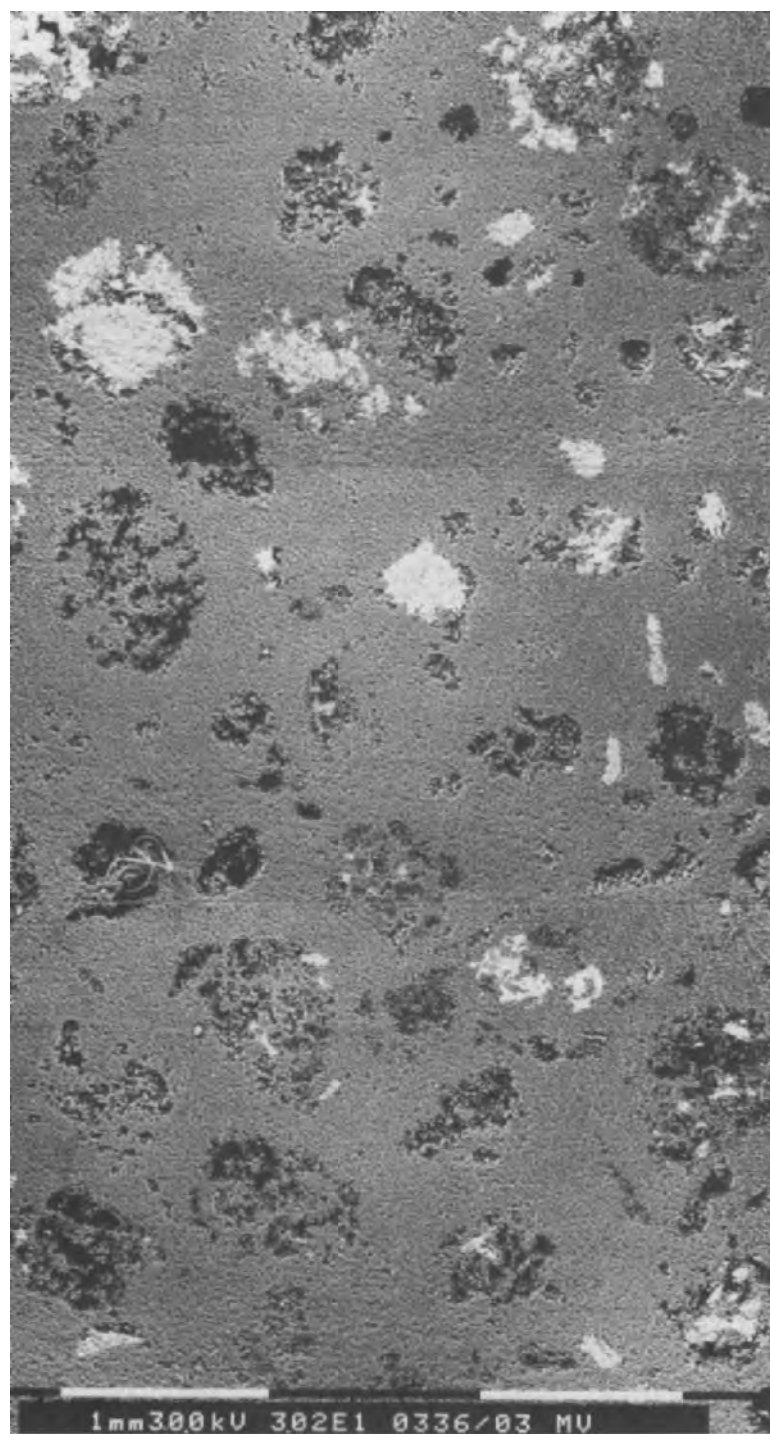


Fig. 7. Energy dispersive X-ray analysis of the fibrous clay in Fig. 6. Very small particles of dolomite and halite are associated with the fibrous clay (cf. text).

Dolomitized algal oolite reservoir

No clay was found in the examined pores of the dolomitized algal oolite. Consequently, porosities could be measured automatically by Quantimet and no image editing was necessary. Three micrographs are given in Fig. 8 and represent a linear traverse over a small part of the thin section. Anhydrite and carbonate, deposited in pores that occupy the leached centres of oolites, were not measured. If necessary, however, these minerals could be included in porosity measurements in a similar way to that done for clays. The real porosity in the upper micrographs was 5.24%, in the middle 6.59% and in the lower micrograph 9.13%. This real porosity was higher than that of the oil-gas containing sandstone reservoir but lower than measured in the oil-impregnated sandstone reservoir.



Area and perimeter of the pores in the three reservoirs

If the area and perimeter of the pores in the three reservoirs are measured, these data can be used to distinguish the different pores (Fig. 9). The diagram in Fig. 9A indicates that the pores of the dolomitized algal oolite have the largest perimeter and have an area which is somewhat comparable to that of the oil-containing sandstone. The larger perimeter of the pores in the carbonate reservoir is due to the inclusion of numerous small particles in the measurements.

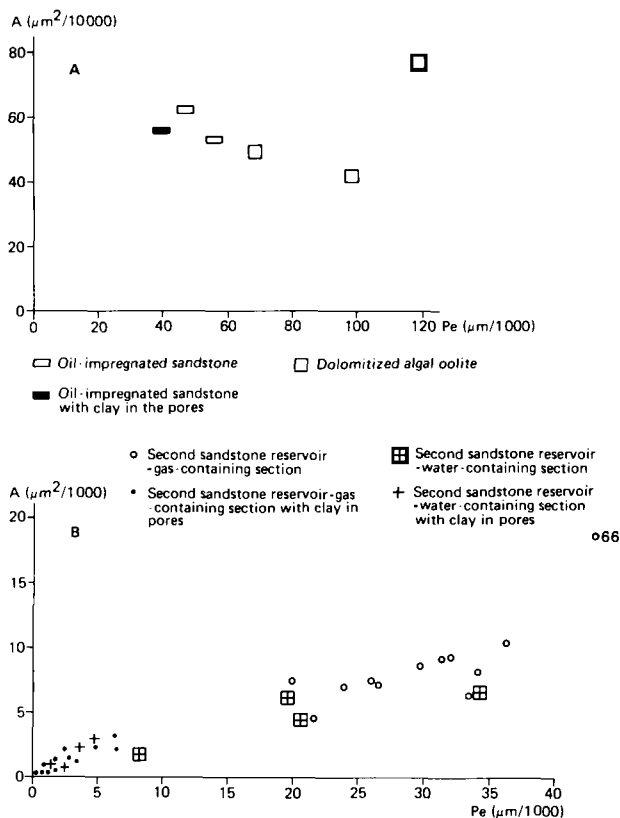


Fig. 9. Differences in area and perimeter measurements of pores from three reservoirs using BESI-Quantimet techniques. The first sandstone reservoir (oil-containing) and the carbonate reservoir (A) have a much higher real porosity than the second sandstone reservoir (B) with the gas–water contact. A differentiation was also made for the two sandstone reservoirs in area and perimeter measurements of pores with and without clay infillings.

Fig. 8. Three contiguous BESI micrographs of dolomitized algal oolite. The white colour in the leached centres of the ooides represents anhydrite and carbonate. Porosity-values in text.

The area and perimeter diagram of the sandstone reservoir with the gas—water contact is given in Fig. 9B. The area is much smaller than that of the oil-containing sandstone reservoir which is given in Fig. 9A. The horizontal and vertical scale of the diagram in Fig. 9B had to be adjusted to accommodate all measurements; especially those of the area and perimeter of the pores which provide the real porosity. It is clearly demonstrated that the latter had smaller areas and perimeters than the pores which gave the total porosity. No larger differences were found in area and perimeter measurements of clay-filled pores in the gas- and water-containing sections of the second sandstone reservoir (Fig. 9B).

Form characterization of individual mineral grains in sandstone reservoirs

Form analysis of individual mineral grains and pores has been described by Bisdorn and Schoonderbeek (1983). It was found during that study that shape analysis of the silt-sized grains was done best at magnifications of $\times 240$ and more. This allowed good observation of the grain boundaries on the display screen of the Quantimet and good comparison of such images with BESI micrographs. In this investigation, BESI were made at $\times 60$ of the two sandstone reservoirs. The mineral grains were sufficiently large to distinguish on BESI and consequently form (shape) analysis was done.

A total of 50 mineral grains was measured: 10 in the oil-containing sandstone, 30 in the gas-containing section of the second sandstone reservoir, and 10 in the water-containing section. No individual mineral grains were present in the analysed part of the dolomitized algal oolite and, consequently, no shape analysis could be done.

Form characterization of individual mineral grains is possible by using area (A), perimeter (Pe) and the largest and smallest Feret's diameters (F_{max} and F_{min}). Shape analysis is mainly based on the A/Pe^2 ratio which is related to the lobation ratio (Lr) and the indentation ratio (Ir) by formula and diagram (Bisdorn and Schoonderbeek, 1983). Eight shape classes were distinguished in that study using knowledge from porosity studies and shape analyses of mineral grains. It was also explained in the latter publication that the same point, on the curve which relates A/Pe^2 and Lr and Ir , may represent different forms. In such cases F_{max}/F_{min} ratios of the grains are usually different and can be used to distinguish forms with the same A/Pe^2 ratio.

The 10 grains, which have been measured in the oil-containing sandstone from which the oil has been removed (Fig. 2), had A/Pe^2 ratios between 32 and 47. They are numbered 1 to 10 in Fig. 10. The 30 grains of the gas-containing section of the second sandstone reservoir had A/Pe^2 ratios of 31 to 57 and have numbers 11 to 40 in Fig. 10. The 10 grains of the water-containing section of this reservoir had A/Pe^2 ratios of 41 to 55 and form the numbers 41 to 50 in Fig. 10. The minerals of the oil-containing sandstone reservoir were represented in shape classes IV and V; those of the gas-containing second sandstone reservoir in shape classes III to V; and of the

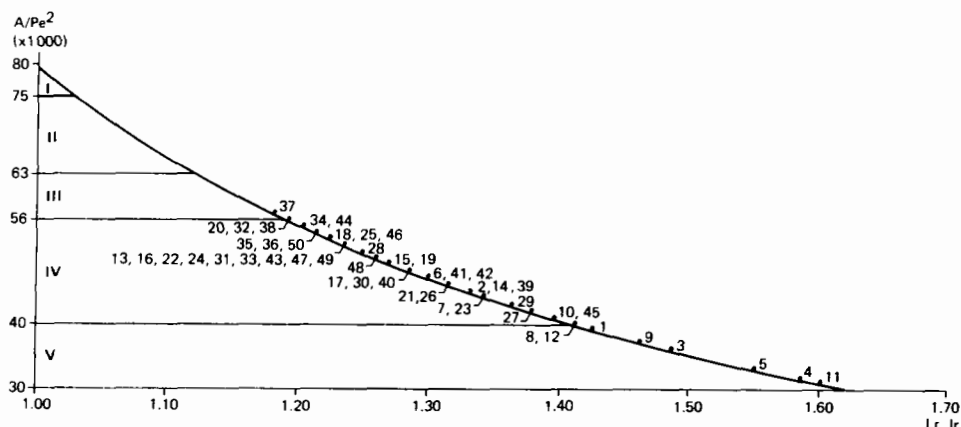


Fig. 10. Form characterization by Quantimet 720 of 50 mineral grains in BESI from two sandstone reservoirs. Area (A) and perimeter (Pe) measurements of individual grains were plotted on a curve which relates the A/Pe^2 ratios to the lobation (Lr) and the indentation (Ir) ratios.

water-containing part of the second sandstone reservoir in shape class IV. Not all the eight shape classes introduced by Bisdorn and Schoonderbeek (1983) are given in Fig. 10 and the horizontal scale was modified to accommodate all measurements from the two sandstone reservoirs. Most of the shape measurements by Quantimet occurred in class V and have A/Pe^2 ratios from 40 to 56.

The F_{max}/F_{min} ratios of the 50 mineral grains are presented in Fig. 11. They have the same place as in Fig. 10. It has been explained (Bisdorn and Schoonderbeek, 1983) that if $F_{max}/F_{min} = 2.00$ and higher, this usually

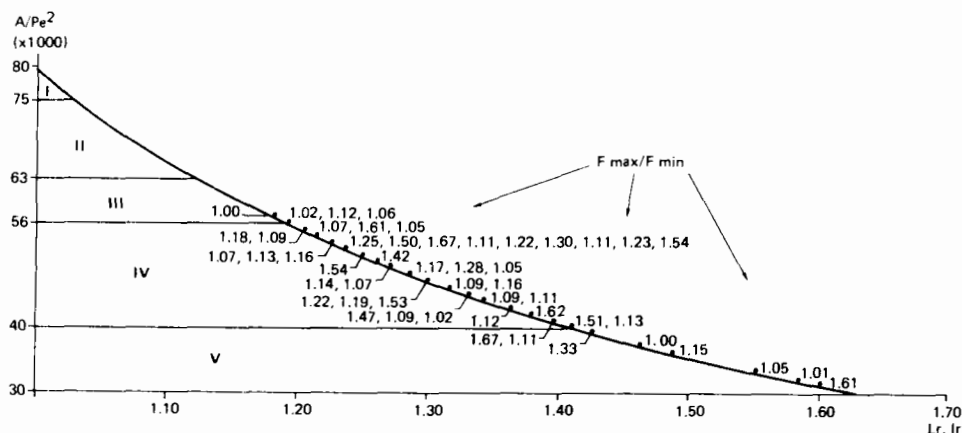


Fig. 11. The largest (F_{max}) and smallest (F_{min}) Feret's diameters indicated as a F_{max}/F_{min} ratio for each of the 50 mineral grains. The position of the grains is the same as in Fig. 10 (cf. text).

indicates elongated forms; the largest diameter of the grain or pore being double, or more, the size of the smallest diameter. In the present study, no elongated forms were encountered. The largest F_{\max}/F_{\min} ratio was 1.67 and the smallest 1.00. The F_{\max}/F_{\min} ratios in Fig. 11 were independent of the shape classes. Several of these ratios can be present in one point on the curve, indicating that a number of minerals with different shapes can have the same A/Pe^2 ratio.

CONCLUSIONS

The present study has demonstrated that porosity measurements can be done in thin sections from oil—gas—water reservoir rocks by using combined submicroscopic and Quantimet techniques. Low magnifications were used for practical reasons. Contiguous micrographs, at $\times 30$ and $\times 60$ magnifications, were made along linear traverses in various thin sections. Shape analysis was done of 50 mineral grains at magnifications of $\times 60$. These grains were so large that their forms were interesting to analyse at this low magnification. If the same measurements are done at higher magnifications, the perimeter will usually become larger. This will affect the A/Pe^2 ratio which will become smaller and a shift of the points will occur to the right on the curve which shows the relation between the A/Pe^2 ratios and the lobation (Lr) and indentation (Ir) ratios. This could mean that certain points on the curve shift from one shape class to another.

It has been found that the porosity characteristics of the two sandstone reservoirs and of the carbonate reservoir were rather easy to distinguish by using area and perimeter measurements of the pores. The presence of clayey material in many pores of the sandstone reservoirs caused an important problem. However, the area occupied by clay could be separated in the pore from the area without clay. In this way an accurate measurement of the porosity could be given. Porosity measurements of the oil-containing sandstone reservoir and of the carbonate reservoir were similar to the ones found by physical methods. The real porosity of the second sandstone reservoir with the gas—water contact, however, was smaller than indicated by physical methods. This was possibly due to the high quantity of clay in the pores; measurable by Quantimet and visible on BESI. Consequently, the real porosity was significantly lower than the apparent porosity. Physical measurements indicated, however, that the clay in the pores formed less of a flow-barrier than expected from the BESI-Quantimet data.

Of importance for the study of oil-containing samples is the possibility of being able to harden these with gamma radiation, i.e. usually 5 Mrad (50 kGy) or more, if polyester resin was used. The process is also much quicker and the hardening can take place in one weekend. A large number of soil samples of the Netherlands Soil Survey Institute and of the International Soil Museum, with hardening problems, were also treated in this manner and hardened. Consequently, it seems reasonable to assume that polyester resin-

hardening by gamma radiation can be an important preparation technique from now on and also for certain core samples.

REFERENCES

- Bisdom, E.B.A. and Thiel, F., 1981. Backscattered electron scanning images of porosities in thin sections of soils, weathered rocks and oil—gas reservoir rocks using SEM-EDXRA. In: E.B.A. Bisdom (Editor), *Submicroscopy of Soils and Weathered Rocks*. 1st Workshop of the International Working-Group on Submicroscopy of Undisturbed Soil Materials (IWGSUSM) 1980, Wageningen. Centre for Agricultural Publishing and Documentation (Pudoc), Wageningen, pp. 191–206.
- Bisdom, E.B.A. and Schoonderbeek, D., 1983. The characterization of the shape of mineral grains in thin sections of soils by Quantimet and BES1. *Geoderma*, 30: 303–322 (this issue).
- Bouma, J., Jongerius, A., Boersma, O., Jager, A. and Schoonderbeek, D., 1977. The function of different types of macropores during saturated flow through four swelling soil horizons. *Soil Sci. Soc. Am. J.*, 41(5): 945–950.
- Bouma, J., Jongerius, A. and Schoonderbeek, D., 1979. Calculation of saturated hydraulic conductivity of some pedal clay soils using micromorphometric data. *Soil Sci. Soc. Am. J.*, 43 (2): 261–264.
- Ismail, S.N.A., 1975. Micromorphometric soil-porosity characterization by means of electro-optical image analysis (Quantimet 720). *Neth. Soil Surv. Inst., Wageningen, Soil Surv. Pap.*, 9: 104 pp.
- Jongerius, A., 1974. Recent developments in soil micromorphology. In: G.K. Rutherford (Editor), *Soil Microscopy. Proceedings of the 4th International Working-Meeting on Soil Micromorphology*, Kingston, 1973. The Limestone Press, Kingston, Ont., pp. 67–83.
- Jongerius, A. and Bisdom, E.B.A., 1981. Porosity measurements using the Quantimet 720 on backscattered electron scanning images of thin sections of soils. In: E.B.A. Bisdom (Editor), *Submicroscopy of Soils and Weathered Rocks*. 1st Workshop of the International Working-Group on Submicroscopy of Undisturbed Soil Materials (IWGSUSM) 1980, Wageningen. Centre for Agricultural Publishing and Documentation (Pudoc), Wageningen, pp. 207–216.
- Jongerius, A. and Heintzberger, G., 1975. Methods in soil micromorphology. A technique for the preparation of large thin sections. *Neth. Soil Survey Inst., Wageningen, Soil. Surv. Pap.*, 10: 48 pp.
- Jongerius, A., Schoonderbeek, D. and Jager, A., 1972. The application of the Quantimet 720 in soil micromorphology. *The Microscope*, 20: 243–254.
- Murphy, C.P., Bullock, P. and Turner, R.H., 1977. The measurement and characterisation of voids in soil thin sections by image analysis, Part I. Principles and techniques. *J. Soil Sci.*, 28 (3): 498–508.

This Page Intentionally Left Blank

SUBJECT INDEX

- Aberdeenshire (Scotland), 162
- absorbed electron image, 11, 18
- absorption of pollutants by aragonite, 10
- accurate measurement of the porosity, 336
- acicular goethite, 223
- Adelaide (Australia), 237
- adhesion of soil particles to organic materials, 42
- adsorbed dose of radiation, 7
- aeolian transport, 215
- aerobic sludge, 37
- age gradient, 23
- aggradational sites, 215
- aggradational soils, 195
- aggregate destruction, 136
- aggregates, 25, 27, 195
- aggregation of iron and manganese, 192
- agricultural productivity, 59
- akageneite, 268
- Alberta (Canada), 233, 234, 235
- Alberta soils, 233, 235
- albic horizon, 188
- Alfisols, 188
- algal oolite, 325
- alimentary canals, 25
- allophane, 212, 213
- allophane-generating sites, 195
- allophane-like materials, 212
- allophane micro-aggregates, 213
- allophanic cement, 214
- alluvial deposits, 185
- alluvial soils, 179, 187, 193
- AlO, 32
- Al₂O₃, 206, 212
- alteration, 187, 193
- alteration of organic matter, 22
- alumina, 237
- aluminium, 7, 9, 11, 14, 18, 25, 30, 56, 59, 63, 85, 87, 123, 125, 126, 128, 155, 161, 163, 166, 167, 169, 171, 172, 175, 176, 190, 192, 214, 219, 220, 222, 225, 228, 230, 231, 241, 242, 331
- alumino-silicate plasma, 192
- Ambt Delden (The Netherlands) landfill, 4
- amorphous cement, 208, 212
- amorphous component 206, 207, 208, 212
- amorphous materials, 8, 9, 17, 18, 19
- amorphous substances, 9, 25
- amorphous to X-rays, 237
- amphiboles, 25
- anaerobic sludge, 37
- Andic Cryumbrepts, 196
- Andic Humitropepts, 196
- andosols, 195, 215
- Angola, 252
- anhydrite, 325, 331
- anion mass spectra, 31
- anisotropic backscattering, 97
- anisotropic inclusions, 201
- anisotropic mullgranic unit, 240
- Antwerp (Belgium), 179, 184
- apatite, 199
- apparent porosity, 323, 325, 327, 330, 336
- A/Pe² measurements, 321
- application of livestock effluents, 35
- application of manure, 36
- application of pig slurry, 35
- application of sewage sludge, 35, 36
- application of submicroscopic techniques in soil micromorphology, 146
- Aquod, 162
- arable farming, 277
- arable land, 277
- aragonite, 10
- area and perimeter measurements of the pores, 336
- area classes, 314
- area occupied by clay, 336
- area occupied by pores, 295
- area with intensive cultivation, 36
- area without clay, 336
- Argentina, 21, 23
- Argialboll, 188
- argillans, 192, 241
- argillic B horizon, 240, 242
- argillic horizons, 233
- Argillic Pelludert, 21
- argon, 119
- arrested flow structure, 266
- aseptic fabric, 23
- ashes, 196, 197
- atomic absorption spectroscopy, 5
- atomic contrast, 93
- Auger electron spectroscopy (AES), 130
- average drawn perimeter, 298
- backscattered electron detectors, 79, 93, 95, 150, 256

- backscattered electron detectors system, 79, 94
- backscattered electron images, 78, 79, 93, 172
- backscattered electron imaging, 80, 87
- backscattered electron method, 220
- backscattered electron (BSE) mode, 93
- backscattered electron scanning images (BESI), 9, 10, 18, 47, 48, 49, 51
- backscattered electron signals A or B, 95
- backscattered electron techniques, 277
- backscattered electrons (BE), 279, 307
- bacterial lysis, 27
- Banff (Canada), 235
- barite, 199
- bars with Cobalt-60, 325
- bauxite, 93, 94, 95, 114, 117, 118
- BE and SE techniques, 162
- BE detector, 220
- beach ridge, 324
- beach ridge development, 176
- beam stabilization, 275
- behaviour of heavy metals, 24
- Belgian Campine, 179
- BESI, 78, 79, 80, 87, 88, 93, 114, 219, 220, 227, 230, 256
- BESI methods, 299
- BESI micrographs, 274, 275, 334
- BESI paper print, 274
- BESI-Quantimet data, 336
- BESI-Quantimet information on porosities, 281
- BESIs, 155, 156
- BESI system, 272
- β -FeOOH, 268
- bimodal pore distribution, 252
- biogenic opal, 65, 70
- biolites, 201
- biological activity, 32, 43
- biological structures, 190
- black and brown cutanic materials, 9
- black and brown pollutants, 10
- black cutans, 8, 11, 14, 15, 17, 18, 19
- black spruce, 171, 176, 177
- blades of grass, 70
- bog iron ore, 78
- bog-ore profile, 180
- bombardment-induced light emission (BLE), 130
- bone fragments, 187, 190, 193
- bone tissue, 190
- Bordeaux (sands), 286, 289
- boron, 123
- boundaries of shape classes, 303
- breakthrough curves, 7
- break up of a crust, 39
- bright-field imaging, 83
- British Columbia (Canada), 56
- brown and black substance, 19
- brown cutans, 8, 9, 11, 15, 17, 18, 19
- BSE coefficient, 94
- BSE detectors, 95, 96, 104
- BSE images, 93, 94, 99, 110
- BSE-information in the secondary electron signal, 97
- BSE micrographs, 94
- BSE mode, 79, 80, 87, 93
- BSE signal, 93
- BSE technique, 80
- BSE(A) mode, 104
- BSE(A+B), 104
- BSE(A+B) images, 80, 104, 110
- BSE(A+B) imaging, 104
- BSE(A+B) mode, 80, 93, 96, 97, 99, 104, 114
- BSE(A-B) image, 97
- BSE(A-B) mode, 97
- BSE(B) mode, 104
- bulk chemistry, 1
- CaCO₃, 137, 139, 142, 172, 260, 268
- calcareous material, 171, 176
- calcareous dune sand, 2, 3, 5, 8
- calcareous nodules, 188
- calcite, 117, 122, 123, 124, 126, 127, 133, 172, 253, 261, 262, 268, 269
- calcium, 4, 9, 14, 18, 25, 59, 85, 123, 125, 126, 127, 135, 136, 137, 161, 166, 169, 171, 172, 175, 176, 190, 220, 253, 260
- calcium-dominated organans, 171, 177
- calcium oxalate crystals, 70
- calcium oxalates, 70
- ¹⁴C analyses, 176
- CaO, 123, 124, 207
- Ca₂O, 123
- Ca₂O₂, 123
- capillary pores, 51, 272, 277, 279, 282
- carbon, 57, 79, 94, 123, 139, 163
- carbonate, 8, 331
- carbonate crystals, 325
- carbon dating, 23
- carbonate reservoir, 323, 324, 333, 336
- CaSO₄ · 2H₂O, 260, 268
- cathodoluminescence, 115
- cathodoluminescence detection, 95
- cation mass spectra, 29
- ¹⁴C dating, 32
- cell structure, 25, 27
- cellular inclusions, 70

- cellulose fibers, 70
- cement, 324
- cement chemistry, 214
- cement formation, 213
- cement segregation, 214
- cementing constituents, 207
- cementing materials, 162, 166
- Chaco Deprimido (Argentina), 187, 188, 194
- chalcopryrite, 268
- changes in cultivated agricultural topsoils, 35
- changes in forms, 281, 321
- changes in illumination, 95
- changes in porosity with increasing clay content, 295
- changes in surface structure, 35
- channel-type pores, 46
- characterization of compaction in a soil, 277
- characterization of microporosity in a ploughpan, 277
- characterization of porosities, 279
- characterization of the shape of mineral grains in thin sections, 303
- characterization of the shape of voids, 313
- chemical bonding, 7
- chemical characteristics, 194
- chemical characterization, 212
- chemical features, 214
- chemical soil parameters, 195
- chemical stratification, 214
- chinone-hydroquinone systems, 31
- chlamydic component, 240
- chlamydic fabric sequence, 233, 240
- chlamydic sequence, 240
- chloride, 4
- chlorine, 9, 14, 18, 57, 69, 85, 207, 212, 331
- chromium, 123, 124, 207
- chromium oxide, 199
- clays, 117, 122, 125, 126, 127, 133, 159
- circulation of soil organic matter, 21
- clay, 117, 122, 125, 126, 127, 133, 159
- clay aggregates, 3, 5, 135, 142, 146, 248
- clay cutans, 25
- clay domains, 192
- clay fabric, 252
- clay-filled pores, 334
- clay fraction, 201
- clay illuviation, 25
- clay in the pores, 330, 336
- clay lamella, 43
- clay matrix, 32, 248, 252
- clay microaggregates, 3, 5, 135, 142, 146, 248
- clay orientation, 248
- clay particles, 25, 39
- clay particle configurations, 244
- clay platelets, 248
- clay with sand, 289
- cleavages, 10
- clogging precipitates, 268
- close-to-surface material in a thin section, 83
- clustering of spherules, 208
- coating of oil, 326
- coatings, 8, 18, 19
- Cobalt-60, 5, 325
- collapse of vesicles, 43
- collemboles (apterygote insects), 27, 28
- colloidal surfaces, 7
- Colombian andosol material, 215
- Colombian andosol profile, 195
- column experiments, 1, 2, 7, 18
- combination of BSE and SE detectors, 94
- combined submicroscopic and Quantimet techniques, 336
- compacted soils, 279
- compaction phenomena, 279
- comparison of porosities, 277
- composite particles, 195, 196, 198, 201, 206, 207, 208, 209, 211, 212, 214, 215
- composition of the cementing material, 59
- compost of aerobic sludge and the organic fraction of urban refuse, 37
- composition of the mineral grains, 59
- composition of the precipitates, 255, 264
- compost of anaerobic sludge and the organic fraction of urban refuse, 36, 37
- compression process, 248
- computerized X-ray spectrometer, 57
- concentration layer, 192
- concentration profiles, 188
- concentric and continuous bands, 19
- concretions, 190
- conductive elements, 70
- conductive vesicles, 70
- constituents of allophane, 212
- contact X-ray microradiography, 65
- contacts between the grains, 289
- contiguous microareas in a thin section, 325, 328
- contiguous micrographs, 324, 336

- continuum of fabric types, 233, 234
- contrast of the clay with the pore on
BESI, 325
- conventional radiography, 65
- copper, 1, 3, 4, 7, 8, 11, 14, 15, 17, 18, 19,
85, 253, 260, 261, 262, 264, 265, 266,
268, 269
- copper filter segments, 253, 256, 260,
262, 265, 268
- copper water-tube filter, 94
- co-precipitation of silica and alumina,
214
- core samples, 324, 325, 337
- corroded edge, 265
- corroded flakes, 261
- corrosion of a water-tube filter, 104
- corrosion of copper filter segments, 253,
268
- corrosion of the tube, 265
- covellite, 253, 260, 261, 262, 268, 269
- corundum, 199
- Cretaceous, 324
- cristobalite, 201
- critical point dried specimens, 244, 247
- critical point drying technique, 243, 244
- crust formation, 36, 39, 49, 51
- crusting problems, 35
- crusts of the mycelia, 231
- crystal splitting, 159
- crystalline constituents, 201
- crystalline phases, 213
- crystallites, 17
- crystals, 114
- crystal-vitric ashes, 197
- CuFeS_2 , 268
- Cu-filter, 104
- Culbin Forest (Scotland), 162, 163
- Culbin profile, 166
- cuneiform aggregates, 25
- CuO_2 , 268
- cuprite, 268
- curly stem-like halite, 149, 153, 154
- curly stem-like salt efflorescence, 149,
150
- CuS , 17, 18, 260, 268
- cutan development, 19
- cutan formation, 201
- cutan fragments, 212
- cutaneous siderite deposits, 183
- cutanic materials, 9, 17
- cutans, 187, 190, 191, 223
- cycle of sedimentation, 43, 49
- cytochemical methods, 21
- Dandi (India), 150
- Dandi series of soils, 158
- dark grains, 21, 32
- dark veins, 192
- decaying roots, 179
- decrease in perimeter, 300
- decrease in permeability, 136
- decrease in pores, 48
- decrease in porosity, 289
- decrease in specific surface, 289
- decomposing plant fragments, 27
- degradation of soil structure, 277
- degree of structure stability, 277
- dejections of enchytreids, 27
- dejections of collembolus, 27
- deleterious effect of potassium is less
than that of sodium, 142
- deleterious effects, 135, 142
- dendritic pattern, 110
- dense continuous network of clay
particles, 142
- density of a ploughpan, 277
- density of the sands, 288
- depositional crusts, 36
- depositional surface, 214
- depth information, 99
- depth of analysis with backscattered
electrons, 99
- depth profiling, 121
- destabilisation processes, 49
- detachment of clay from sand particles,
136
- detachment of soil constituents, 36
- detector efficiency, 79
- detector systems, 79, 96
- detrital grains, 182, 183
- development of flakes, 268
- development of soil porosity, 285
- developmental sequences of podzolic
soils, 171
- diatoms, 25, 27, 180, 185
- digitate voids, 309, 320
- difference between SE and BSE(A+B)
signals, 99
- differences in porosity patterns, 286
- differences in shapes of pores, 282
- different photo-techniques, 272
- different shape classes, 321
- differential absorbance of X-rays, 65,
66, 72
- differential chemical composition, 66
- diffuse cell structure, 27
- diminution during transport, 215

- diopside, 199
- direct imaging secondary ion microscope, 119
- discontinuous concentric rings, 10
- disintegrating flakes, 253
- dislocations, 10
- dispersed state, 37
- dispersion of clay microaggregates, 135
- dispersion of volcanic soil material, 215
- dispersion products, 208
- disruptive influence of clay aggregates (slurry features), 248
- dissolved clays, 212
- dissolved components, 212
- distribution images, 192
- distribution of features, 190
- distribution of various types of porosity, 300
- dolomite, 325, 331
- dolomitized algal oolite, 331, 333, 334
- dolomitized oolite, 325
- dominant fabric sequence, 234
- drawing of pores, 290, 291
- dune sands, 286
- duoplasmatron iron source, 119
- duripans, 56
- dynamic relationships within fabric sequences, 234
- earth-consuming organisms, 27
- earthworm burrows, 65
- earthworms, 237
- Eastern Cordilleras (Colombia), 197
- ECON windowless detector, 256
- EDAX system, 220, 256
- edges of the corroding filter segments, 266
- EDXRA, 219, 222, 229, 231, 256, 260, 268
- EDXRA analysis, 85, 259
- EDXRA measurements, 88, 177, 219, 222, 223, 260, 262
- EDXRA spectra, 59, 61, 62, 175
- EDXRA system, 104
- effects of potassium on soil structure, 142
- effects of sodium on soil structure, 142
- effects of soil crusts, 35
- effects of wetting and drying of the soil, 49
- electron beam, 57
- electron energy-loss spectrometry (EELS), 130
- electron microprobe analysis (analyzer) (EMA), 1, 7, 8, 11, 17, 18, 78, 85, 115, 118, 132, 198
- electron microprobe analysis (EMP), 130
- electron microprobe techniques, 195
- electron microscopy, 55, 75, 188
- electron multiplier, 121
- electron probe micro-analyses (EPMA), 206
- electron spectroscopy for chemical analysis (ESCA), 130
- electronic partition functions, 122
- electro-optical image analysis, 35, 36
- elemental distribution images, 188
- elemental microanalysis, 187
- elongated mineral grains, 319
- eluviated horizon, 240, 242
- EMA, 185, 235, 269
- enchytreids (small earthworms), 27, 28
- encrustation of mycelia, 229, 231
- encrustation of tubular features, 231
- energy-dispersive spectroscopy (spectrometer) (EDS), 162, 190
- energy dispersive X-ray analysis (EDX), 130
- energy dispersive X-ray analyzer (analysis) (EDXRA), 25, 163
- engineering and urban uses, 59
- engineering behaviour, 248
- engineering soil microfabric, 247
- engineering soils, 243
- Entre Rios Province (Argentina), 22
- erosional products, 215
- estimation of the total porosity, 290
- etched specimens, 57
- exchangeable potassium percentage (EPP), 135, 139, 141, 146
- exchangeable sodium, 150
- excrements, 93, 96, 99, 114
- exfoliated and weathered pieces of the copper tube, 104
- experimental columns, 2, 3, 7, 8, 17
- experimental plots, 36, 37, 43, 49
- experiments with soil porosity, 301
- external covering of mineral grains, 306, 307, 321
- externally image-edited grains, 314
- fabric analyses, 94, 215
- fabric of small undisturbed lumps, 195
- fabric of the composite particles, 198
- fabric sequences, 233, 234, 235, 240, 242
- fabrics, 57, 59, 87, 234, 237, 240, 242, 243, 248, 252
- faecal pellets, 25, 27
- farming rotations, 36
- fatty acids, 2, 7

- faunal activity, 21, 23, 25
- faunal excrements, 176
- feather-like gypsum, 159
- fecal pellets, 235
- FeCO_3 , 268
- feldspars, 62, 73, 172, 201, 286, 298
- FeO , 31, 206, 212
- FeO_2 , 31
- Fe-oxihydrates, 179
- ferrallitization, 229
- ferrallitization processes, 219
- fertilizer, 231
- fertilizer application, 136
- FeS , 15, 17, 18
- fibre optics, 95
- fibrous clay, 330, 331
- Fife (Scotland), 162
- final stage of accumulation, 214
- fine-lamellated amorphous substance, 27
- fine structure of soil fabric, 72
- flakes of the copper filter segment, 260
- flint, 325
- fluvial sands, 286
- fluvio-lacustrine deposit, 196
- f-matrix, 233, 234, 235, 241, 242
- f-members, 233, 234, 235, 237, 240, 241, 242
- Fontainebleau Formation, 286
- Fontainebleau (sands), 286, 289, 290, 292
- form analysis of individual mineral grains and pores, 334
- form changes of pores, 282
- form of individual voids, 285
- form of pores, 289, 290, 298, 299, 300
- form of sand grains, 285, 289
- form separation of mineral grains, 303
- formation of a clay enriched layer, 136
- formation of a massive ploughpan, 282
- formation of an impeded clay layer, 140
- formation of an impeded layer, 136
- formation of an impermeable layer, 146
- formation of ploughpans, 277
- formation of puddles in the furrows, 281
- formation of vesicles, 43
- forms of mineral grains in thin sections of soils, 303
- forms with a very large perimeter, 320
- fossilization, 229
- fragipan horizons, 55, 59
- fragipan prism, 59
- fragipans, 56, 61, 62, 63
- fragmentation of organic matter, 25
- fragmic fabric sequence, 233
- fragmoidic, 234
- fragmoidic porphyric, 234
- freezing of wet soil, 139
- frozen sample, 139
- fulvic acids, 7
- fungal hyphae, 229, 231
- fungal sclerotium, 32
- fungus filaments, 25, 27
- fungus lysis, 27
- fungus mycelium, 27
- furrows, 43, 277, 281
- galena, 15, 17, 18
- gamma radiation, 1, 2, 5, 6, 323, 325, 326, 336, 337
- Gandolfi camera, 180
- gas reservoir rocks, 94, 323
- gas-water contact, 327, 334, 336
- gel-like material, 201
- generation of (SE-BSE) signals, 97, 99
- genetic process, 171
- gibbsite crystals, 95, 114
- gilgai relief, 22, 32
- glacially derived detrital material, 196
- glauconites, 190, 203
- Glasgow (U.K.), 248
- glass, 201, 212
- glass contents, 197
- glass marbles, 286
- glass phases, 213
- glassy fragments, 196
- glauconite, 183
- goethans, 223
- goethite, 80, 179, 181, 185, 222, 223, 230, 254
- goethite coatings, 181
- goethite fibres, 181, 185
- goethite needles, 179
- gold, 37, 172, 180
- granitic, 233, 234
- granitic sequence, 235
- granitic sequence of fabric, 233
- granoidic, 234
- granoidic porphyric, 234
- grasses, 65
- grazing incidence, 118
- greenhouse agriculture, 136
- greenhouse soils, 136
- Guasca (Colombia), 195, 196
- Gujarat (India), 149, 150
- gypsum, 149, 156, 159, 253, 260, 262, 268, 269

- Halaquepts, 149, 150
 halomorphic soils, 188
 halite, 149, 151, 153, 154, 157, 158, 159, 199, 331
 halite crusts, 159
 hard bog-ore, 183
 hardening of oil-containing sample by gamma radiation, 325
 hardening of samples, 2, 6
 HC measurement system, 137, 139
 HCO_3^- , 32
 heavy-metal contamination, 1
 heavy-metal sulphides, 17
 heavy-mineral composition, 211
 heavy minerals, 197, 198, 213, 286
 hematite, 199, 222, 230
 heterogeneous crust, 49
 heterogeneous mixture of black and brown cutanic material, 8
 HgCl_2 , 137
 high acceleration voltages, 114
 high energy ion scattering (HEIS), 130
 high mass resolving power, 119, 123, 125
 highly micaceous Maures sands, 288
 high primary electron energies, 99
 high-resolution electron micrographs, 212, 213
 high resolution films and plates, 66
 high resolution images, 66
 high-resolution transmitting microscope, 237
 highly birefringent plasma, 59
 hollow spherules, 213
 honeycomb structure, 264, 265
 H_2O_2 , 212
 holes in the thin section, 57
 homogenisation, 32
 horizon, 163
 Hosmer soil (U.S.A.), 59
 Hudson Bay Lowlands of Ontario (Canada), 171, 177
 humic acids, 7
 humic material, 163
 humic podzols, 171, 172, 176, 177
 humifying fragments of organic matter, 28
 humo-ferric-podzol, 171
 humod, 162
 humus-iron cementation, 163
 humus-form, 25
 hydrogen, 94, 118, 123, 124, 129, 132, 171, 172, 176
 hydromorphic soils, 193
 hydrous aluminosilicates, 212
 idiomorphic shapes, 201
 illite, 22, 135, 139, 140, 287
 ilmenite, 199
 image analyzer, 271, 279, 282, 286, 288, 303, 304, 323, 325
 image contrasts, 66, 73
 image-edited grains, 314
 image-editing, 331
 image-editing of mineral grains, 305
 image editor, 285, 292, 303, 304, 305, 321
 image of the surface of a thin section, 114
 imaging of precipitates, 104
 imaging of the surface, 110
 imaging with backscattered electrons, 83
 imaging of the topography, 97
 impact of raindrops, 36, 43
 impeded drainage, 135
 improved water infiltration, 42
 ion microprobe mass analyzer (IMMA), 118, 119
 in situ analysis of chemical elements, 19
 in situ characterisation of pores, 287
 in situ investigation of unhardened soil crusts, 36
 in situ investigation of unhardened soil peds, 36
 in situ microchemical analysis, 48
 in situ microchemical element analysis, 115
 in situ microchemical information, 231
 in situ microchemical investigation of all chemical elements, 118
 in situ microchemistry, 133
 in situ porosity analysis, 324
 in situ research of thin sections, 133
 in situ shadow images, 65
 increase in porosity, 42
 indentations, 309, 310, 312, 315, 319, 320
 indentations on mineral grains, 320
 indented edges, 268
 India, 149
 Indian benchmark soils, 149
 Indonesian volcanic soils, 196
 infilling of pores, 289
 infiltration rate, 38
 influence of the form of mineral grains on the shape of pores, 285
 influence of the form of sand grains on porosity characteristics, 285
 information depth, 97

- infrared spectroscopy study, 63
- input solution, 4
- instability of aggregates, 36
- instrumental techniques for bulk, thin film and microanalysis, 119
- intensity of primary beam, 66
- intensity of radiation, 66
- intensity of transmitted radiation, 66
- intensity of X-rays, 70
- intensity ratios, 66
- intensive cultivations, 36
- inter-aggregate porosity, 252
- intergrade fabrics, 242
- interlayer adsorption on illite, 141
- internal matrix, 203
- internal standard method, 122
- internally covered mineral grains, 306, 321
- internally image-edited grains, 314
- interpretation of soil processes, 22
- intra-aggregate porosity, 252
- investigate the effects of potassium on the permeability of soils 136
- ion images, 117, 118, 121, 122, 123, 125, 126
- ion microscopy (microscope) 11, 114, 117, 118, 119, 122, 125, 132, 133, 231
- ion optical column, 119
- ion scattering spectrometry (ISS), 130
- ion spectra, 117
- ion thinning technique, 77
- iron, 1, 3, 4, 7, 8, 9, 11, 14, 17, 18, 19, 25, 28, 29, 30, 31, 56, 59, 63, 66, 85, 87, 94, 110, 124, 161, 163, 166, 167, 169, 176, 190, 192, 193, 201, 214, 219, 220, 222, 223, 225, 228, 230, 231, 241, 242, 253, 260, 261, 262, 264, 265, 266, 268, 331
- iron-coated organic material, 78, 79, 80, 85
- iron-coated organic matter, 77
- iron-coated peaty material, 87
- iron compounds, 192
- iron hydroxides, 80, 253, 260, 261, 262, 264, 265, 268
- iron-manganese nodule, 29
- iron nodules, 219, 220, 221, 223, 225, 227, 228, 230, 231
- iron oxide nodules, 66
- iron oxides, 201, 286
- iron oxihydrates, 185
- iron sulphide (mackinawite), 15, 17, 18
- isobanded granoidic intergrades, 237
- isotropic amorphous brown cutanic materials, 9
- isotropic cement, 212
- isotropic component, 201, 215
- isotropic inclusions, 201
- Israel, 136
- Italy, 35, 36, 49
- iunctic, 233, 234
- iunctic porphyric, 234
- iunctic sequence, 233
- jadeite, 199
- James Bay Lowlands of Ontario (Canada), 171, 177
- joint planes, 298
- joints, 203
- kaolinite, 22, 123, 139, 225, 287
- K-feldspar, 286
- kinds of soils, 192
- laboratory columns, 2
- lagoon environment, 325
- Laguna de Fuquene area (Colombia), 197
- land spreadings of pig slurry, 42
- landfill, 1, 2, 3, 7, 10, 18
- landscape dynamics, 196
- Lappungsquotient, 307
- large variety of pore patterns, 301
- laser analysis, 231
- laser beam, 118, 130
- laser-induced ions, 29
- laser-induced mass spectra, 21, 29
- laser microprobe analysis (LMP), 130
- laser microprobe mass analysis (analyzer) (LAMMA), 11, 29, 115, 117, 130
- laser milling, 118
- laser optical emission spectrometry (LOES), 130
- lateritic soils, 219, 231
- lateritization processes, 219, 231
- lathlike crystallites, 183
- lathlike crystals, 184
- lavas, 162, 166
- layering of the goethite, 181
- leachates, 3, 4, 7
- leachates with fatty acids, 3
- leachates without fatty acids, 3, 4
- leached centres of ooides, 325, 331
- leaching product of fertilizer, 231
- lead, 1, 3, 4, 7, 8, 11, 14, 18, 19
- lead sulphide (galena), 17, 18
- length of the contact, 292

- levels in an andosol profile, 195
- lichen vegetation, 177
- light concentrates, 209
- light microscopic investigations, 19
- lighter elements, 155
- light-mineral compositions, 211, 213
- light-mineral fractions, 195, 213
- light-mineral spectra, 201
- limestone fragments, 172
- linear traverses, 117
- limonite, 179
- lithium, 123
- lithorelicts, 65, 66, 73, 240
- livestock effluents, 36, 37
- LM SEM mode, 83
- lobate forms, 309
- lobation ratio, 303, 307, 309, 311, 313, 316, 321, 336
- local thermal equilibrium model, 121
- Loch Leven (Scotland), 161, 162
- Lochend coatings, 169
- Lochend Farm (Scotland), 161, 162
- Lochend material 161, 166, 169
- Lochend profile, 169
- loess, 59
- loess derived Hosmer soil (U.S.A.), 59
- loessoid sediments, 188
- long elongated pores, 300
- loose sands, 289, 299
- loose sands with clay admixtures, 289
- low energy ion scattering (LEIS), 130
- low hardness of saline material, 159
- low magnification (LM) scanning mode, 83
- low temperature ashing (LTA), 57
- low-temperature ashing technique, 162
- Lower Cretaceous sandstone reservoir, 324
- Lower Permian sandstone, 325
- Luanda (Angola), 252
- mackinawite (iron sulphide), 15, 17, 18
- macroenvironmental mineral equilibria, 179, 185
- macropores, 73, 277, 279, 281, 282
- macroporosities, 93
- mafic rocks, 207
- magnesium, 4, 25, 123, 124, 125, 126, 128, 135, 136, 137, 153, 163, 172, 176, 190, 214, 331
- magnesium ferrite, 268
- major and trace elements, 117, 118, 122
- Malaysia, 219, 223
- manganese, 4, 7, 28, 29, 30, 31, 66, 192, 193
- man-made precipitates, 254
- manure, 36
- manure on an organic carbon basis, 37
- Marbles, 288, 289, 292, 295, 296, 298, 299
- marine alluvium, 149, 150
- marine clay, 248
- mass numbers, 29, 31, 32, 121, 122, 123
- mass resolution, 119
- mass spectra, 29, 31, 121
- mass spectrograms of ions, 29
- mass spectrometer, 119
- mass spectrometric methods (SSMS or SIMS), 129
- mass spectrometry, 29
- mass spectroscopy, 29
- massive crusts, 149, 151, 157
- massive ploughpan, 279, 280, 281, 282
- massive structure, 280
- material and topographic contrast in soil material, 95, 96
- material contrast, 95, 96, 104, 114
- mathematical models, 19
- matrichlamydic, 240
- matrichlamydic fabrics, 240
- matriplectic, 240
- matriplectic fabrics, 240
- matriplectic porphyric, 240
- matrix, 206, 211
- matrix-dependent fitting parameter, 122
- Maures (sands), 286, 288, 289, 290, 292, 295, 296, 298, 300, 301
- Maures Massive (France), 286
- maximally ground thin sections, 88
- measured total porosity, 273
- measured two-dimensional shapes, 304
- measurement of the shape of mineral grains, 303
- measurements of porosities and minerals, 292, 298
- measurements of porosity, 273, 292
- mechanism of crust formation, 36, 37
- mesopores, 277, 279, 281, 282
- metal sulphides, 18
- methanogenic phase, 4, 18
- methods for bulk analysis, 129
- methods of macro-, micro-, or ultra-microanalysis, 129
- MFD system, 93
- MgFe₂O₄, 268
- micaceous Maures sands, 288
- micas, 196, 286, 298
- micaschist, 286
- microanalysis, 187, 191, 206

- microareas, 85, 95, 223, 228, 230, 231, 260, 331
- microchemical analysis, 185, 215, 219
- microchemical detail, 85
- microchemical differences, 11
- microchemical information, 88, 94, 231
- microchemical submicroscopic techniques, 179
- microchemistry, 18, 79, 118
- microcracking, 244
- microcracks, 10, 42
- microcrystalline materials, 9, 18
- microcrystallites, 17
- micro-environmental conditions, 214
- microenvironments, 179, 185, 213
- microfabric, 114, 233, 234, 240, 247
- microfabric anisotropy, 248
- microfabric character, 247
- microfabric features, 247
- microfabric of engineering soils, 243
- microlayers, 37, 39, 43, 49
- micromorphological model, 213
- micromorphological research, 115
- micro-organisms, 27
- microporosities, 93
- micropores, 277, 279, 281, 282, 292, 327
- microprobe, 166, 192, 237
- microprobe analyses, 237
- microradiography of thin sections, 65
- microscopic fabric analysis, 215
- microscopic organic features, 21
- microstructure of the crust, 37
- microstructures, 27, 114, 180, 181
- microtechniques, 130
- microthickness differences, 87
- microvariations in chemical elements in a cutan, 12
- microvariety, 85
- microvoids, 271
- migmatite, 286
- mineral aggregates, 28
- mineral compositions, 209
- mineral phases, 214
- mineral spectra, 209
- mixed brown and black cutanic materials, 9
- mixing of organic and mineral materials, 25
- mixture of ashes and non-volcanic material, 196
- mixture of depth and surface information, 99
- mixtures of sand and clay, 285, 287
- MnO, 31
- MnO₂, 31
- mobile organic substances, 176
- moder, 233
- moderately lobate shape class, 314, 315
- molar ratios, 206, 207
- Mollic Cryoboralf pedon, 240
- Mollisols, 188
- monochromatic X-ray source, 66, 68
- monomorphic grain coatings, 163
- monomorphic organic coatings, 161, 169
- montmorillonite, 287
- Morayshire (Scotland), 162
- morphology of clays in pores, 325
- Morvan (sands), 286, 289
- Morvan Massive (France), 286
- Moyen-Vivarais (France), 286
- mull, 25
- mull f-members, 235
- mull layers, 233, 237
- mullgranic, 235, 237
- mullgranic fabric types, 235, 237
- mullgranic fabrics, 237
- mullgranic type, 237
- mullgranic units, 237
- mullgranoidic, 235
- mullgranoidic fabric type, 235
- mullgranoidic porphyric, 235
- mullgranoidic porphyric intergrade, 235
- mullgranoidic porphyric types, 237
- multichannel analyzer, 220
- multi-element analysis, 129
- multi-function-detector (MFD), 93, 94
- muscovite, 240
- mycelium, 27, 219, 229, 231
- Na₂CO₃, 212
- names of shape classes, 315
- names in shape classifications, 313
- Na₂O, 207
- Natraqualf, 188
- natric horizons, 188
- Natrustalf, 188, 189
- negative ion spectra, 122
- negative secondary ions, 119
- negative spectra, 32
- neocutans, 191
- neosesquan, 192
- Nete Valley (Belgium), 179, 184
- New Brunswick soils (Canada), 56
- New Orleans (U.S.A.), 244
- NH₄, 136
- Nicaragua, 181
- nickel, 1, 3, 4, 7, 8, 9, 11, 14, 15, 17, 18, 19, 69, 206, 212, 214
- NiS, 17, 18
- nitrogen, 94

- nodules, 25, 30, 65, 66, 219, 227, 228, 230
- number of minerals with different shapes, 336
- optical emission spectrometry (OES), 129, 130
- oil-gas containing sandstone reservoir, 331
- oil-gas reservoir rocks, 94, 323, 324
- oil-impregnated sample, 6, 326
- Old Red sandstone, 162
- olivine, 199
- ooides, 325
- oolite, 325
- opal phytolites, 201
- opaline bodies, 180
- Ontario (Canada), 171
- opening of the filter, 265
- optical transmission microscopy (OTM), 55, 56, 59, 63
- optically anisotropic materials, 201
- optically isotropic materials, 195, 201
- organans, 171, 172, 175, 176, 177
- organic compounds, 29, 30, 31
- organic constituents, 59
- organic fertilizer, 48
- organic matter, 56, 59, 73, 77, 78, 87, 104
- organic matter of very high residence time, 32
- organic soil constituents, 25
- organic tissue, 104
- organically treated crust, 49
- organically treated plots, 48, 51
- organo-mineral complexes, 25
- orientation of minerals, 324
- orthoclase, 199
- orthogranic fabric types, 240
- orthogranic type, 242
- ortstein horizons, 56
- ortstein soils, 172
- OTM examination, 59
- OTM photographs, 63
- oxygen, 94, 260
- packing, 289, 290
- packing of sand grains, 285
- packing of single mineral grains, 298
- palladium, 172
- palygorskite, 123
- papules, 61, 63
- parent glass fragments, 213
- parent materials, 214, 215
- Paris Basin, 169
- particle induced X-ray emission (PIXE), 130
- PbS, 15, 17, 18
- peaty materials, 83
- pedal fabric, 248
- pedogenic mechanisms, 194
- pedogenic trends, 235
- pedogenically generated 233, 234
- pedorelics, 206, 212, 213, 215
- pedorelicts, 240
- pedotubules, 203
- Pelludert, 32
- Pelludert (Argillic), 21, 22
- percentage of clay, 325, 327, 330
- percolate, 4, 19
- perimeter diagram, 334
- perimeter measurements, 334
- perimeter of pores, 48, 298, 333
- peripheral forms, 321
- periphery of mineral grains, 306, 320
- permeability 286, 325
- Permian dolomite, 325
- Permian sandstone, 325
- Petrocalcic Xerochrept, 117, 122
- petrological microscope, 198, 209
- phosphate adsorption capacity of allophane, 212
- phosphatic material of biological origin, 189
- phosphatic nodules, 187
- phosphorus, 85, 161, 166, 169, 188, 190, 214
- photo-techniques, 271, 272, 273, 274, 275
- phyllosilicates, 201
- physical measurements, 325
- physical methods, 285, 287
- physically determined porosity values, 300
- physicochemical information on the behaviour of metals in columns during experiments, 7
- phytoliths, 180, 185
- pig hairs, 39
- pig slurry, 36, 37, 39, 42, 48, 49
- pipe, 253
- place of clay accumulations, 301
- planosols, 187, 188, 192
- plant debris, 25, 27, 32
- plant remains, 176
- Plaquettes (sands), 288
- platy structures, 37, 42, 51
- plectic, 234

- plectic porphyric, 234
- plectic porphyric intergrade fabrics, 242
- pleistoplasmatic related distribution, 237
- Pliocene gravels, 163
- plots treated with anaerobic sludge and urban refuse, 48
- plots treated with organic debris, 48
- ploughed layer, 279
- ploughpan (plowpan), 272, 277, 279, 280, 281, 282
- PO_2 , 31
- PO_3 , 31
- P_2O_5 , 206, 207
- Po area (Italy), 36
- podzolic soils, 171
- podzolization, 242
- podzols, 93, 94, 96, 104, 114, 161, 162, 163, 169
- polluted heavy-metal-containing solutions, 19
- polluted precipitate, 1, 2, 8
- polyhedral aggregates, 25
- polyvalent cations, 176
- poor stability of soil aggregates, 36, 43, 46
- poorly crystalline materials, 8, 9, 17, 18, 19, 253, 260, 268, 269
- pore diameter, 324
- pore diameter classes, 273
- pore distribution, 252
- pore pattern changes, 300
- pore patterns, 287, 296, 298, 299, 301
- pore structure, 65
- pores and soil aggregates, 313
- pores in sands, 290
- porosimetry, 248
- porosities of individual sands, 289
- porosity, 223
- porosity analysis, 271, 272, 324, 331
- porosity and mineral quantification, 288
- porosity and structure study, 279
- porosity changes, 36, 51
- porosity characterisation, 292
- porosity characteristics, 47
- porosity in the thin section, 290
- porosity measurements, 47, 272, 273, 274, 275, 281, 323, 324, 325, 331, 336
- porosity patterns, 298, 299
- porosity percentages, 295, 299
- porous microstructure, 180, 181
- porous zones, 262, 266
- porphyric, 234, 235, 240
- porphyric fabrics, 235, 242
- porphyric types, 234, 237, 242
- portrayal of materials and porosities, 94
- positive ion spectra, 122
- positive secondary ion spectra, 122, 123
- positive secondary ions, 119
- positive spectra, 32
- potassium, 4, 9, 14, 18, 59, 63, 123, 124, 125, 135, 136, 137, 141, 155, 163, 166, 172, 190, 192, 219, 223, 231
- potassium adsorption ratios (PAR), 135, 137, 140
- potassium effects on soil permeability, 136
- potassium enriched soils, 135
- potassium fixation properties, 139
- precipitate on a corroded copper filter, 110
- precipitates on a water-tube filter, 93, 114
- precipitates on filter segments, 268
- precipitates which clogged a water-tube filter, 253
- precipitates which clog the filter of a water tube, 96
- precipitation of pollutants, 10
- preferential adsorption, 7
- preparation of ultrathin sections, 88
- primary ion energy, 119
- primary ions, 119
- primary volcanic minerals, 212
- protozoa, 27
- Province of Antwerp (Belgium), 179, 184
- pseudo sands, 196
- pseudotopography, 97
- puddles, 43
- puddling and compaction of soil materials, 277
- pyrite, 179, 185
- pyrite framboids, 179, 184, 185
- pyrolysis of soil materials, 29
- pyroxenes, 197, 201
- quantification, 73, 94
- quantification of trace and major elements, 117
- quantification of trace elements, 11
- quantification of trace elements in thin sections, 132
- Quantimet analysis of porosities in BESI, 271
- Quantimet measurements, 47, 48, 51, 272, 273, 275, 279, 282, 300, 304, 324
- Quantimet methods, 299

- Quantimet porosity measurements, 327
 Quantimet techniques, 271, 277, 281, 282
 quantitation of pores, 35
 quantitative analysis, 121, 122, 127
 quantitative microchemical analysis, 117
 quantitative microspot analysis, 121
 quantitative SIMS analysis, 127
 quantity of clay in the pores, 336
 quantity of pores, 282
 quartz, 62, 66, 73, 96, 163, 166, 172, 175, 201, 213, 214, 237, 268, 287, 298, 324, 325
 Quaternary, 22
- radiating aggregates, 184
 radiating goethite fibres, 181
 radiation, 66, 68, 69
 radiation source, 6
 radiography, 65, 68
 radiography film, 66
 raindrop impact, 36, 37, 49
 real porosity, 323, 324, 325, 327, 330, 331, 334, 336
 real quantity of clay, 331
 redox buffer, 4
 redox potential, 4
 reduction in HC in sodic sandy soils, 136
 reclamation of polluted soils, 11
 reduction in the average pore size, 142
 reduction of elongated pores, 48, 51
 reduction of the number of cracks, 48
 Rehovot (Israel), 136, 140, 141
 related distribution, 233
 related distribution patterns, 242
 relation between the form of sand grains and porosity, 290
 relation between the form of soil components and porosity, 288
 relation between the forms of pores and the forms of individual minerals, 290
 replacement of clay by calcite, 133
 reservoirs, 333
 residence times of organic matter, 22
 restricted micro-environments, 213
 retention of heavy metals, 7
 reticulated platelets, 191
 rhodonite, 199
 rhombohedral crystals, 183
 river clays, 277
 rock fragments, 195, 196
 root exudates, 237
 root penetration, 280
 root tissues, 31
- rosette-like aggregates of gypsum prisms, 159
 roundness and sphericity values, 288
 rubber trees, 219, 231
 Rutherford backscattering spectrometry (RBS), 130
- Sabana de Bogotá (Colombia), 195, 197, 215
 Sabana Formation, 196
 salic horizons, 157
 saline soils, 6
 salt-affected soil series, 149, 150
 salt-affected soils, 159
 salt crusts, 158
 salt crystals, 153
 salt efflorescence, 149, 150, 151, 158
 San Francisco (U.S.A.), 244
 sand and clay admixtures, 288
 sand and clay mixtures, 286
 sands with clay admixtures, 290
 sandstone reservoirs, 323, 324, 327, 331, 334, 335, 337
 sandstones, 242, 326, 334
 sandwich grids, 29
 sandy loams of arable land, 277
 sandy soils with clay admixtures, 285, 296
 Saône (sands), 286, 289, 290, 292, 295, 298, 299, 300, 301
 saturated hydraulic conductivity of heavy clays, 47
 scanning Auger microprobe (SAM), 130
 scanning electron micrographs of soils, 161, 163, 166
 scanning electron microscopy (microscope)-energy dispersive X-ray analysis (analyzer) (SEM-EDXRA), 1, 7, 8, 11, 14, 17, 18, 21, 25, 26, 28, 35, 36, 55, 56, 57, 59, 63, 77, 78, 83, 87, 118, 132, 176, 219, 221, 223, 230, 235, 241, 253, 260, 268, 269
 scanning electron microscope (microscope)-wavelength dispersive X-ray analysis (analyzer) (SEM-WDXRA), 1, 7, 8, 11, 17, 18, 85, 118, 132, 185, 269
 scanning transmission electron microscope (microscopy) (STEM), 2, 18, 77, 78, 79, 83, 85, 87, 114, 130, 230
 scanning transmission electron microscope (microscope)-energy dispersive X-ray analysis (analyzer) (STEM-EDXRA), 2, 7, 8, 11, 18, scintillators, 95, 97

- scintillators (A+B), 96, 104
- Scottish podzols, 162
- sea clays, 277
- SE-BSE image, 97
- SE-BSE mode, 93, 104, 110, 114
- SE-BSE signals, 99
- SE-detector, 94
- SE images, 80, 97, 99, 104
- SE mode, 93, 104
- SE- signal, 97
- SE techniques, 162
- seasonal compaction, 237
- second generation ion microscope, 132
- second generation SIMS instruments, 119
- second sandstone reservoir, 334
- secondary electron images (SEI), 11, 18, 37, 39, 42, 51, 57, 78, 156, 191
- secondary electron images (SEIs), 155, 156
- secondary electron (SE) images, 80
- secondary electron (SE) detector system, 115
- secondary electron (SE) micrographs, 94
- secondary ion currents, 121
- secondary ion emission, 121
- secondary ion imaging, 123
- secondary ion mass spectrometry (SIMS), 29, 94, 121, 129, 130, 269
- secondary ion microscope (microscopy), 117
- secondary ion optics, 119
- secondary ions, 118, 119, 132
- sedimentary processes, 242
- sedimentation cycle, 43
- sedimented clay lamella, 43
- SEM-EDXRA analysis, 230, 260, 268
- SEM-EDXRA investigation, 77, 78, 79, 83, 110, 114, 115
- SEM-EDXRA mode, 115
- SEM-EDXRA studies, 253
- SEM equipment, 162
- SEM examination, 163
- SEM instruments, 77, 78
- SEM microanalysis, 169
- SEM micrograph montages, 247
- SEM micrographs, 65, 70, 142, 241, 247
- SEM microscopy, 65
- SEM mode, 79, 83, 87, 88
- SEM observations, 135, 139, 142, 161, 243, 244, 248, 252
- SEM pictures, 150
- SEM techniques, 65
- SEM stubs, 163
- SEM studies, 142, 162
- semi-arid parts of Gujarat (India), 149
- semi-quantitative analyses, 11
- semi-quantitative microchemical analysis, 11
- separation of different contrasts in soil material, 95, 96
- sequences of fabric, 242
- Serre (France), 290
- sesquioxide accumulations, 192
- sesquioxides, 32, 190, 191, 192
- sesquioxidic nodules, 187
- sesquioxidic segregations, 188
- sewage sludges, 36, 37, 39, 46, 48
- shadowing effects, 256
- shadowing or topographic effects, 96
- shape analysis, 303, 304, 305, 309, 310, 313, 321, 334, 336
- shape analysis of aggregates and pores, 309
- shape analysis of coarse and fine silt grains, 303
- shape analysis of mineral grains, 334
- shape analysis of minerals, 321
- shape analysis of minerals in thin sections of soils, 304
- shape analysis of pores, 303, 304, 305
- shape analysis of pores and soil aggregates, 303, 307
- shape analysis of soil aggregates, 321
- shape analysis of voids, 303, 321
- shape class-boundaries, 313
- shape classes, 303, 304, 309, 313, 314, 315, 319, 320, 323, 334, 335, 336
- shape classification of two-dimensional forms, 313
- shape classification of voids, 319
- shape classifications, 303, 310, 313, 319
- shape data of individual mineral grains, 304
- shape groups of pores, 48
- shape measurements, 305, 335
- shape of individual mineral grains, 303, 321, 334
- shape of mineral grains in thin sections, 303
- shape of voids, 309
- shapes of pores, 282, 285, 304, 309
- shapes of sand grains, 289
- shapes of soil components, 286
- shapes of two-dimensional figures, 310
- shearing, 248
- shear zone, 248
- shell fragments, 10, 11, 19
- short living organic matter, 32
- shortage of manure, 36

- shrinkage cracks, 181
- shrinkage fissures, 181
- siderite, 179, 180, 181, 183, 185, 268
- siderite deposits, 183
- siderite spherulites, 182, 183, 184
- signal mixing, 95
- signals A+B give material contrast, 95
- signals A-B give topographic contrast, 95
- silicified cell wall elements, 70
- silica, 214
- silicon, 9, 11, 14, 18, 25, 30, 56, 57, 59, 62, 63, 85, 87, 123, 124, 125, 126, 128, 155, 163, 166, 167, 172, 175, 176, 190, 192, 214, 219, 220, 222, 223, 228, 229, 231, 241, 261, 262, 331
- silty clay crust, 46
- silver, 37
- SIMS analysis, 119
- SiO₂, 32, 206, 212, 268
- SiO₃, 32
- Si X-ray signal, 163
- size classes, 290
- size of pores, 290
- size of pores in sands, 290
- skins of oil, 326
- slickensides, 32
- sludges, 37
- slurry, 248
- slurry features, 248
- small-scale sedimentation processes, 43, 49
- smectite, 22
- sodic clay soils, 136
- sodic soils, 193
- sodium, 4, 25, 57, 123, 124, 125, 135, 136, 150, 155, 159, 163, 172
- soft bog-ore, 182, 183, 184, 185
- soil aggregates, 191, 215
- soil column, 214
- soil compaction, 277
- soil components, 10
- soil crust, 51
- soil deterioration, 141
- soil fabrics, 198, 233
- soil fauna, 25
- soil faunal activity, 237
- soil horizon, 25, 27
- soil humic acid, 7
- soil lumps, 212
- soil management, 135
- soil matrix, 23, 28, 29
- soil microfabric, 243
- soil mineralogical methods, 285
- soil mineralogy, 136
- soil mixing, 32
- soil nodules, 190
- soil organic matter, 7, 21, 29
- soil permeability, 135, 136
- soil physical methods, 285, 299
- soil physics, 286, 289, 299, 300
- soil porosity, 285, 286, 301
- soil porosity patterns, 285
- soil protection measures, 2
- soil structure, 146, 277
- soil tillage, 277
- soils of the Dandi series (India), 159
- solodic soils, 188
- solodised soils, 187
- solodised solonetztes, 192
- soluble salts, 5
- sources of organic matter, 36
- Spain, 122
- spark source mass spectrometry (SSMS), 117, 119, 129, 130
- specimen's topography, 97
- spectra, 21, 29, 31, 32
- spectrometer, 163
- spherules, 208, 213
- spodic B horizons, 169
- spodic horizons, 233
- stabilization of microaggregates, 141
- stagnation of superfluous rainwater, 281
- STEM-EDXRA analysis, 87
- STEM-EDXRA investigation, 77, 79, 83
- STEM-EDXRA micrographs, 78, 85, 87, 88
- STEM-EDXRA mode, 115
- STEM images, 83
- stem-like halite, 158
- STEM mode, 79, 83, 87
- STEM mode of operation, 83
- STEM transmission mode of operation, 83
- step scan analysis, 122, 125
- step scanning of samples, 121
- stereomicroscope, 37, 247
- stereophotography, 252
- stereoscan, 163, 180
- straw fragments, 39
- strings with clay packets, 327
- strongly cemented horizon, 161, 163
- structural crusts, 36, 37
- structural model of allophane, 213
- structure and fabric analysis of soil materials in thin sections, 94
- structure deterioration, 279
- structure of compacted soils, 279
- structure of organic matter grains, 32
- structure stability, 277

- study of capillary and larger pores, 282
- study of pores, 305
- study of the morphology of clays in pores, 325
- subcutaneous siderite spherulites, 183
- suberin-like material, 32
- submicroscopic analyses, 114, 188, 253
- submicroscopic characterisation, 187
- submicroscopic data, 151
- submicroscopic imaging, 47
- submicroscopic investigations, 19, 27
- submicroscopic methods, 21, 22
- submicroscopic observations, 149
- submicroscopic study, 231
- submicroscopic techniques, 2, 18, 49, 51, 66, 83, 117, 128, 146, 150, 185, 187, 194, 235, 237, 269, 277, 279, 282, 323, 336
- submicroscopic visualisation, 49
- submicroscopic work, 262
- submicroscopical analysis, 17, 18
- submicroscopy, 1, 2, 7, 8, 17, 18, 21, 80, 93, 114, 149, 155, 159, 256
- subpolyhedral microaggregates, 27
- subtracting the signal of two scintillators, 97
- Sueva (Colombia), 196
- sulfur, 176
- sulphate, 4, 7
- sulphate reducing bacteria, 7
- sulphides, 7
- sulphides of heavy metals, 7
- sulphur, 7, 8, 9, 11, 14, 17, 18, 32, 110, 156, 166, 169, 212, 253, 260, 261, 262, 264, 268, 269, 331
- Sunshine Basin (Canada), 235
- suppression of the BSE-information in the secondary electron signal, 97
- surface crusts, 36, 42, 48, 49, 153
- surface sealing, 43
- surface structure, 35
- Surinam, 94, 110
- synthetic landfill leachate, 4
- tantalum, 118, 122
- TEM-EDXRA mode, 79, 94, 95
- TEM mode, 87
- tephra, 196
- Tertiary, 286
- terraces, 286
- The Hague (The Netherlands), 253
- The Netherlands, 2, 94, 279
- thecamoebae, 25, 27
- theoretical model, 303, 304, 310, 313, 321
- thin film analysis, 119, 129
- thin section studies, 285
- three-dimensional distribution, 129
- three-dimensional electron optical data, 55
- three-dimensional morphological detail, 162
- Timorin (Israel), 136, 140, 141
- Timorim calcium soil, 142
- titanium, 25, 31, 123, 124, 125, 155, 163, 214, 223, 228, 231
- todorokite (complex manganiferous material), 191
- total area, 323, 325, 326
- total area of the pores, 324
- total porosity, 48, 51, 271, 273, 334
- trace and major elements, 95, 123
- trace elements, 117, 118, 123, 128, 133, 149, 150, 153, 162, 163
- translocated humic material, 163
- translocation of fine particles, 36
- transmission electron energy loss spectrometry (TEELS), 130
- transmission electron microscope (microscopy) (TEM), 18, 27, 77, 78, 79, 85, 88, 130, 230
- transmission electron microscope-energy dispersive X-ray analysis (TEM-EDXRA), 77, 79, 85, 87, 88
- transmission mode, 77, 83
- transmitted electrons, 78
- transmitted light images, 57
- transmitted-light microscopy, 75
- transmitted secondary electrons, 77
- transport of organic and mineral particles, 25
- transport of polluted materials in soils, 2, 19
- treated crusts, 51
- treated plots, 47, 48, 51
- treatment with pig slurry, 35, 49
- treatment with sewage sludge, 35, 49
- treatment with urban refuse, 35
- Trias, 286
- Tropeptic Haplarthox, 219
- tube-containing iron nodules, 219
- tubular features, 219, 221, 223, 229
- turbostratic, 248
- turbostratic nature of the random fabric zones, 248
- turbostratic zones, 248
- turbulent array of parallel oriented clay platelets, 248
- TV-rate images, 96
- two-dimensional distribution, 129

- two-dimensional figures, 310, 312, 313
- two-dimensional form-developments, 313
- two-dimensional forms, 303, 304, 310, 313, 321
- two-dimensional optical data, 55
- two-dimensional shape analysis, 321
- two-dimensional shape classification, 303
- two-dimensional shapes, 304
- two stage critical point drying technique 244
- types of crusts, 36
- types of packing, 290
- types of pores, 286, 298
- types of voids, 298
- Typic Cryochrept, 235
- Typic Fragiudult, 59
- Typic Humaquept, 78

- Ultisol, 181
- ultrafabric, 88
- ultramafic rocks, 207
- ultramicroscopic observations, 187
- ultrastructure, 88
- ultrathin sections, 77, 78, 85, 87, 88, 115
- uncovered thin sections, 154, 159
- uncultivated soils, 150
- undisturbed samples, 172
- undisturbed soil, 281, 282
- undisturbed soil samples, 39, 135, 149, 151
- unhardened soil materials, 37, 51, 150, 161
- untreated crust, 49, 51
- untreated plots, 51
- untreated soil, 42
- Upper Old Red Sandstone, 162
- Upper Permian dolomite, 325
- uranium, 129
- Ustochrepts, 150

- Van der Waal's forces, 39
- variability in structure, 43
- variety of compaction phenomena, 282
- vegetative material, 70
- Vertic Xerochrept, 35, 36, 37, 39, 42, 48, 49, 51
- vertical changes in cement chemistry, 214
- Vertisols, 21, 22, 25, 29
- vesicles, 43, 46, 70, 298
- visualisation of pores, 35
- Vivarais (France), 286
- Vivarais (sands), 289, 290
- vivianite, 179, 180, 181, 182, 183, 185

- void patterns, 296
- void systems, 25, 114
- voids, 17, 18, 19, 25, 65, 66, 75, 87, 149, 150, 153, 154, 155, 159, 242, 260, 271, 273, 321
- volcanic ashes, 195, 196, 197, 213, 237
- volcanic glass, 195, 213
- volcanic minerals, 212, 213
- volcanic origin, 213
- volcanic soils, 6, 195
- volume of the pores, 330
- volumetric shrinkage, 244
- vughy porphyric, 235
- vughs, 298, 300, 320

- wall of the filter segment, 261
- water-containing part of the reservoir, 328, 330
- water-containing section of a reservoir, 324
- water-tube, 255
- water-tube filter, 253, 256
- wavelength dispersive spectroscopy (WDS), 162
- wavelength dispersive X-ray analysis (analyzer) (WDXRA), 114
- wavelength dispersive X-ray spectrometer, 163, 188
- WDS system, 166
- WDXRA, 188, 190, 193
- weathered granite, 286
- weathered micaschist, 286
- weathered minerals, 28
- weathered rocks, 94, 324
- weathering, 230
- weathering component, 237
- weathering of calcareous material, 171
- weathering of kaolinitic clay, 231
- weathering products, 206
- wet chemical analysis, 18, 119, 129, 231
- wet chemical bulk analysis, 128
- wet chemical data, 118
- wet chemical methods, 119
- wet chemical techniques, 128
- wet chemistry, 1, 117, 129
- western coastal states of India, 150
- white radiation, 68
- Windyhills (Scotland), 162, 163
- Windyhills profile, 166

- X-ray detector, 172
- X-ray diffraction (XRD), 5, 15, 18, 70, 123, 253
- X-ray diffraction analysis, 287
- X-ray diffraction equipment, 68

- X-ray diffraction pattern, 237
- X-ray equipment, 65, 75
- X-ray fluorescence spectrometry (XRF), 129, 130
- X-ray generator, 68
- X-ray images, 11, 76, 122, 156, 172, 175, 220, 228, 258, 259, 260, 268
- X-ray microanalysis, 166, 169
- X-ray microcamera, 237
- X-ray microradiograph (micro-radiography), 70, 75
- X-ray microradiograph technique, 66
- X-ray pattern, 201
- X-ray photoelectron spectroscopy (XPS), 130
- X-ray powder analysis, 201
- X-ray projection radiography, 66, 68
- X-ray radiography, 65
- X-ray source, 68, 69, 70
- X-ray spectra, 163, 166, 167
- X-ray spectrometer (spectrometry), 57, 129
- X-ray transmission, 70
- X-ray transparent sheet, 69
- X-ray tube voltages, 68
- X-ray tubes, 68
- X-rays, 57, 65, 66, 166, 237
- XRD, 231, 235
- XRD analysis, 17, 18, 162, 169, 180, 255, 260, 268
- XRD techniques, 17, 225, 253
- Yagur (Israel), 136, 140, 141
- Yerua series (Argentina), 22
- Yerua soil, 32
- ZAF-corrections, 199
- Zaire, 223
- zinc, 1, 3, 4, 7, 8, 11, 14, 15, 18, 19, 253, 260, 261, 262, 264, 265, 266, 268
- ZnS, 17, 18
- zonal arrangement, 214
- zonal development, 213
- zones of silification, 70
- zone with flakes, 268